DIRECT DESIGN OF REINFORCED CONCRETE SKEW SLABS

by

Laila Mahmoud Abd El-Hafez

A Thesis Submitted for the Degree of

Doctor of Philosophy

Department of Civil Engineering

University of Glasgow

September, 1986

By the name of "God" the Compassionate, the Merciful.

To my Parents

ACKNOWLEDGEMENTS

The author records her deep debt of gratitude to Professor H. B. Sutherland, Head of Civil Engineering Department, for the facilities provided for this work.

The work described in this thesis was carried out in the Department of Civil Engineering at the University of Glasgow under the general direction of Professor A. Coull whose help and interest is gratefully acknowledged.

I wish to express my indebtedness to my supervisors, Dr.P. Bhatt and Dr. D. R. Green for their valuable guidance and advice throughout the work.

Grateful thanks are also to:

Dr. P. D. Arthur and Dr. D. V. Phillips for their interest and useful discussions.

The Structural Laboratory staff, especially Late Mr J. Love, Mr I. Todd, Mr A. Burnett, Mr. J. Thomson, Mr. J. Coleman and B. Thornton for assisting in the experimental work.

The computer staff of the Civil Engineering Department, especially Mr. G. Irving for his advice and help.

The staff members of Glasgow University Computing Service in particular Mr. D. Fildes for his help in some matters relating to programmming.

Many friends whose help and advice will never be forgotten.

Finally, my thanks are reserved for my family for their boundless patience and continual encouragement throughout the years.

SUMMARY

This thesis presents the results of an experimental and theoretical study of reinforced concrete skew slabs designed using the elastic stress fields in conjunction with the yield criterion for reinforced concrete slabs. The elastic stress field is obtained from finite element program using uncracked stiffness and the yield criterion adopted is given by

$$(M^*_x - M_x + M^*_\alpha \cos^2\alpha)(M^*_\alpha \sin^2\alpha - M_y) - (M_{xy} + M^*_\alpha \sin\alpha \cos\alpha)^2 = 0$$

where M_x, M_y and M_{xy} are the elastic applied bending and torsion moments normal to the x and y axis at the ultimate load. M^*_x and M^*_α are the ultimate flexural moment capacities of the section normal to the x and skew axis respectively and α is the angle of skew between x and α axis.

The experimental work was conducted on a "large scale" skew slabs. The models included slabs of uniform thickness and ribbed slabs. The major parameters were the angle of skew and the arrangement of steel in the slab viz orthogonal or skew directions.

The theoretical work was done using the nonlinear finite element program based on the isoparametric Mindlin element. In order to allow for the development of cracks through the thickness, the "layer approach" was adopted. Nonlinear effects due to the yielding of steel, cracking and crushing of concrete were included. A

nonlinear finite element program was used to study the spread of yielded zones in the slab, the effect of fixing the direction of crack at its first appearance, prediction of the true deflection at working loads from the elastic deflection at working loads and a careful study of the yield criterion itself.

The results show that the design procedure adopted is viable but care has to be taken to ensure that punching shear failure does not occur at obtuse corners.

CONTENTS

NOTATION

a' The depth from the compression face to the neutral axis.

A The area of a rigid region.

A_i The Equivalent area of steel of i^{-th} layer.

A_{ctx}, A_{cty} The effective concrete areas in tension per unit width in the x and y direction.

A_n The equivalent area of steel normal to the crack.

A_s Area of steel in the Longitudinal direction

a_x, a_y The spacing of cracks in the x and y directions.

A_α Area of steel in the α direction.

a Maximum cracks spacing.

b The section breath.

b_s Body forces.

$[B]$ Strain matrix.

$[B_f]$ Strain matrix associated with flexural deformation.

$[B_P]$ Strain matrix associated with plane stress deformation.

$[B_s]$ Strian matrix associated with shear deformation.

C Shear strain coefficient.

C_1, C_2 Coefficients for the tension stiffening.

D The flexural stiffness per unit width.

$[D]$ Elasticity matrix.

$[D']$ The instantaneous elasticity matrix.

$[D_c]$ The elasticity matrix related to inplane stresses for cracked concrete

$[D_e]$ Rigidity inplane matrix for steel layer.

$[D_p]$ Elasticity matrix related to inplane stresses.

$[D_s]$ Elasticity matrix related to transverse shear stresses.

$[D]^*$ Rigidity inplane matrix for cracked concrete.

d	The effective depth.
d_n	Depth to the neutral axis.
d_{zi}	The thickness of i^{-th} layer
E	Young's modulus.
E_c	Young's modulus of concrete.
E_s	Young's modulus of steel.
E_x, E_y	Young's modulus in X and Y directions in an isotropic plate.
E_{x1}	Young's modulus in the lateral plane.
f_b	Bond stress.
f_{bb}	Bearing stress.
f_c	Compressive stress in concrete at seviceability.
f_c	Compressive strength of concrete.
$f_{c'}$	Cylinder compressive strength of concrete.
f_{cu}	Cube compressive strength of concrete.
f_d	Equivalent biaxial compressive strength of concrete.
F_i	The steel force per unit width of i^{-th} layer.
f_i	The stress in i^{-th} layer of steel inclined an angle α_{ni} to direction normal to the crack direction.
F_n	The resolved steel force per unit length in the. n-direction.
f_{co}	Discontinuity stress.
f_n	The stress in the equivalent area of steel normal to the crack.
f_r	Modulus of rupture.
f_s	The tensile stress in the steel.
$f_{s'}$	The compressive yield stress in the steel.
f_y	The yield strength of the steel.
f_x	The x-steel stress.
f_α	The α-steel stress.

$\{F\}$ Vector of nodal forces in the cartesian coordinate system.

$\{F'\}$ Vector of nodal forces in the local coordinate n,t.

G Shear modulus.

h Plate thickness.

H' The strain hardening parameter for steel.

I Moment of inertia.

I_{cr} Moment of intertia of a cracked section.

I_g Gross moment of inertia of uncraked section.

I_{eff} Effective moment of inertia of a section.

[J] Jacobian matrix.

$[J]^{-1}$ Inverse of Jocobian Matrix.

K_a The tranverse shear stiffness for cracked section.

K_b Constant to account for the distribution and surface Charactesistic of bars for the bond stress.

K Coefficient depends on the slab shape, load patterns and support condtion

[k] Stiffness matrix.

$[K]^e$ Stiffness matrix related the local axes.

K_4, K_5 Coefficients depend upon the probability of exceedence.

L_x The length of the slab.

m Ratio between tensile and compressive strengths of concrete.

M Bending moment at any stage of loading.

M_{cr} Cracking moment.

M_x, M_y, M_{xy} Applied moment component at a point in cartesian coordinates.

M_x^*, M_α^* Design moments in x, α direction respectively.

M_{90}^* Design moment in y direction.

M_n^* The yield strength of the section at the yield line.

M_n, M_t, M_{nt} Applied moment components at a point in local

coordinate system n,t.

M_u, M_v, M_{uv} Applied moment components at a point in u, v coordinates system.

N_x, N_y, N_{xy} Inplane forces at a point in the Cartesian coordinate system.

P The applied load.

P_{cr} Cracking load.

$P_{\delta L}$ Service deflection load.

P_y First yield load.

P_u Ultimate load.

q The load intensity.

Q_x, Q_y Shear force components in cartesian coordinate.

Q_x, Q_x', Q_y, $Q'y$ The shear force acting on the sides of the element.

R_c Cover ratio.

S The loaded surface area.

$\{S\}$ Stress vector.

S_x, S_y The effective shear moduli in the x and y directions.

$[T_b]$ The transformation matrix for boundray condition.

[T] The transformation matrix for cracks.

ΔU The total internal potential energy.

ΔV The total external potential energy.

v The volume of the plate.

u, v, w The displacements at point in the plate with coordinates (x, y z).

u_0, v_0, w_0 The displacements at the plane reference plane.

w Crack width.

v_a The transverse shearing force for cracked section.

w_{max} Maximum crack width.

W The total load acting on the element.

x, y, z Rectangular cartesian coordinates.

x, y, z Distances along x, y, z respectively.

x_1 Depth of stress block.

z The level at a point in x,y cartesian system of coordinates.

z_i The distance from the reference plane to the layer centre.

α Angle of skew.

α_i The angle between the x-direction and the i^{-th} layer

α_{ni} The angle between the normal to the crack and α_i^{-th} steel layer.

β Shear retention factor.

γ Shear shape factor.

γ_{xz}, γ_{yz} Shear strain compoments in the cartesian coordinates.

γ_{nz}, γ_{tz} Shear strain compoments in the local coordinates n,t.

$\{\delta\}$ Nodal displacement vector in the cartesian coordinates.

$\{\delta'\}$ Nodal displacement vector in the local coordinates n,t.

Δ Shear displacement.

ϵ_f The ficitious strain

ϵ_c The current strain.

$\epsilon_n, \epsilon_t, \epsilon_{nt}$ Strain components in n,t coordinate.

$\epsilon_x, \epsilon_y, \epsilon_{xy}$ Strain components in cartesion coordinates.

ϵ_i The strain in the direction of an ith layer of reinforcement at angle α_i to the n- direction.

ϵ_m The strain at any depth from the compression face.

ϵ_p The peak strain

ϵ_{erf} Recorded strain at the previous converged configuration.

ϵ_y The steel yield strain.

$\Delta\epsilon$ The incremental strain in the steel.

ϵ The strain vector.

ϵ_0 The vector of initial strains

ξ, ς Nondimensional local coordinate system.

θ Angle of principal plane.

θ_{cr} The angle of crack with related to X-axis.

θ_x, θ_y The rotations of the normal in the xz and yz planes respecively.

θ_n, θ_t The rotations of the normal in the nz and tz planes respectively.

ν Poission's ratio.

ν_b Shear resistance of the slab.

ν_d Shear stress at design load.

ν_{bAn} Shear resistance of the beam considering effective steel area.

ν_{bAs} Shear resistance of the beam considering longitudinal area of steel.

ν_s Shear stress.

ν_u Shear stress at ultimate load.

τ_x, τ_y The transverse shear rotations in the xz and yz plane. respectively.

ρ_x, ρ_y Steel ratios in the X and Y direction.

ρ_α Steel ratio in the α direction.

$\{\sigma\}$ The stress vector.

$\{\sigma_0\}$ The initial stress vector.

σ Stress at a point.

σi The incremental stress.

σ_{oct} The octahedral normal streee.

σ_n The normal stress.

σ_p The peak stress.

σ_x, σ_y, σ_{xy} Stress components in cartesian coordinates. (note; τ_{xy} has the same meaning of σ_{xy})

σ_1, σ_2 The principal stresses.

τ_{xy}, τ_{xz}, τ_{yz} The shear stresses in xy, xz, yz planes respectively.

Φ Bar diameter.

Φ_x Bar diameter in the x diretion.

Φ_α Bar diameter in the α direction.

CHAPTER ONE

INTRODUCTION

Reinforced concrete skew slabs find extensive application in bridges and possible application in building floor systems. Present designs of reinforced concrete slabs are based on limit state concepts so as to ensure that the structure satisfies the prescribed "limit state" requirements. Accordingly, two limit state criteria have to be satisfied by such designs viz: the ultimate limit state and the serviceability limit state. Most of the existing methods of slab design are based on limit analysis concepts and concentrate exclusively on the ultimate limit state. Thus the main concern of these methods is the ultimate load for the slab, with empirical rules (e.g. span/depth ratio....etc.) to ensure satisfactory performance at the serviceability limit state.

Apart from the code rules, the general design methods available are:

(a) Yield Line method: In this method, a number of collapse mechanisms compatible with the edge conditions of the slab are used to derive the limit load. The true collapse load corresponds to the collapse mechanism giving the least load. This method provides an upper bound to the ultimate load.

(b) Hillerborg's Strip method: In the simple version of this method, a torsionless stress field, which is in equilibrium with the externally applied load, is used to calculate the necessary strength at various points in the

slab. This method provides a lower bound to the ultimate load.

(c) Elastic stress fields: Another lower bound approach to slab design, which is called direct design method and used extensively in UK bridge design practice, is to use an elastic moment field in conjunction with the slab's yield criterion to design the slab.

The basic requirement by this approach is to satisfy the equilibrium and the yield conditions. For slabs the equilibrium equation to be satisfied (see section (2.2.3.1)) is

$$\frac{\partial^2 M_x}{\partial x^2} - 2\frac{\partial^2 M_{xy}}{\partial x \partial y} + \frac{\partial^2 M_y}{\partial y^2} = -q \qquad (1.1)$$

where (M_x, M_y, M_{xy}) are the moment components at any point on the slab and q is the lateral load. By adopting linear elastic moment-curvature relationships, (section (2.2.2) Eqn (1.1) can be transformed to

$$\frac{\partial^4 w}{\partial x^4} + 2\frac{\partial^4 w}{\partial x^2 \partial y^2} + \frac{\partial^4 w}{\partial y^4} = \frac{q}{D} \qquad (1.2)$$

where w the lateral deflection and D is the isotropic flexural stiffness of the plate.

The solution to the Eqn (1.2) results in a set of elastic stresses (M_x, M_y, M_{xy}) in equilibrium with external loads.

The yield criteria for skew slabs (section (3.3)) is given by

$$(M^*_x - M_x + M^*_\alpha \cos^2_\alpha)(M^*_\alpha \sin^2_\alpha - M_y) - (M_{xy} + M^*_\alpha \sin\alpha \cos\alpha)^2 = 0.0 \qquad (1.3)$$

where M^*_x and M^*_α are the ultimate flexural moment capacity of the section normal to x and α skew axis respectively. α is the skew angle between the x and α axis clockwise positive (from x axis).

For given (M_x, M_y, M_{xy}), the values of M^*_x and M^*_α are calculated so as to satisfy the yield criterion Eqn (1.3).

This results in a possible lower bound approach to the design of reinforced concrete slabs.

The object of the present study is to critically examine both experimentally and by numerical studies based on nonlinear finite element analysis, the behaviour of the skew slabs designed by direct design procedure. Attention will be focussed on the behaviour of the slab at the two important limits. Apart from the ultimate load, the aspects of behaviour which will be studied in detail are:

(i) Spread of yielding in the slab.

(ii) Calculation of the "working load" deflection from the initial elastic deflection.

(iii) Possbilty of shear failure at obtuse corner.

(iv) Effect of fixing the direction of crack in the slab.

The aim of this work is to produce a fully "verified" general design procedure for the design of reinforced concrete skew slabs.

CHAPTER TWO

LITERATURE REVIEW

2.1 INTRODUCTION

Reinforced concrete slabs are relatively thin structural elements, whose main function is to resist loads acting normal to their plane. Slabs are used as floors and roofs of buildings, as walls in tanks and buildings and as bridge decks. The design criteria to be satisfied reflects the different types of loading and the main functions of the slab. The design criteria for reinforced concrete slabs is based on elastic and plastic behaviour. The purpose of this Chapter is to discuss the background to these criteria and some basic aspects of the nonlinear analysis of reinforced concrete slabs.

2.2 ANALYSIS AND DESIGN OF REINFORCED CONCRETE SLABS

2.2.1 Introduction

In this section, the manner in which slab theories and design methods have developed is summarised. The behaviour of linearly elastic thin plates loaded perpendicular to their plane was investigated by Lagrange (1) using differential equation of plate bending. The first method of dealing with rectangular plates was developed by Navier (1). He used a double fourier series to transform the differential equation into a series of algebraic equations. Use of a single trigonometric series to represent loading which, greatly facilitated progress, was proposed by Levy (1). An excellent survey has been

presented by Timoshenko and Woinowsky - Krieger (1). Unfortunately as slabs become more complex and more representative of actual slabs, it becomes more and more difficult to find suitable deflection functions which satisfy the boundary conditions. Due to this difficulty, approximate numerical methods were developed for analysis of complex slabs. The first method to meet with widespread success was the method of finite differences (1), (2) and (12). In this approach, the differential equations are replaced by algebraic expressions linking deflections at a grid of stations. The solution procedure involved the setting up and solving a set of linear simultaneous equations. This approach was used by Robinson (3) to study the behaviour of simply-supported skew bridge slabs under concentrated load. Morley (12) also investigated a uniformly loaded, simply supported rhombic slabs for a range of skew angles from 0 to 60^{o} degrees. Major developments were made in finite difference methods when large sets of simultaneous equations were solved using digital computer. In the last three decades, the finite element method has been developed (4,5) which is particularly suitable for automatic computation. This method has been used extensively in this work and further details are given Chapter Four.

The development of mathematical theory of plasticity leads to the development of theory of limit analysis. This theory enabled the collapse loads of perfectly plastic bodies to be calculated as upper and lower bounds to true collapse load.

A well-known method of obtaining upper bounds for slabs is Johansen's yield line theory. On the other hand a lower bound method which was developed for the direct design of slabs is the strip method of Hillerborg (7). Another lower bound design method is to use an elastic moment field in conjunction with the yield criterion for reinforced concrete slabs. This is the method used in this study and will be discussed in detail in Chapters three and five.

2.2.3 ELASTIC METHOD OF ANALYSIS

In this section two theories of elastic plate behaviour viz; classical plate theory and Mindlin plate theory will be discussed. In the classical plate theory, it is assumed that shear deformation and inplane effects due to restraints at the boundaries can be ignored. This theory is suitable for thin slabs in which the lateral deflection is sufficiently small compared to the slab thickness. Mindlin plate theory (63) allows for transverse shear deformation effects to be included and can be used for both thin and thick slabs.

2.2.3.1 Equilibrium

Considering the equilibrium of forces acting on the slab element shown in Fig. (2.1), with dimensions dx and dy in the x and y directions respectively and thickness t in z direction. The following equilibrium equations can be derived.

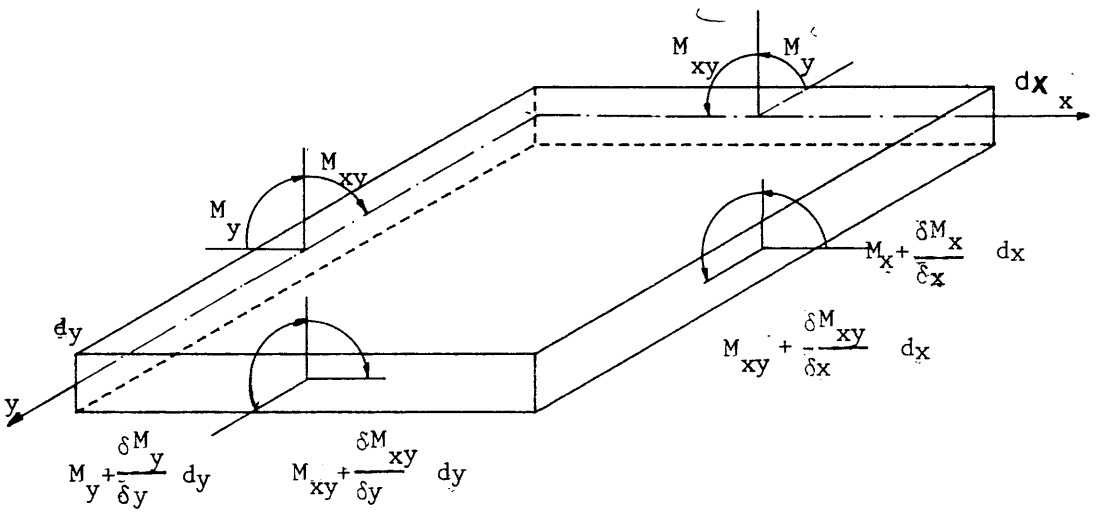

(a) Moments per unit length

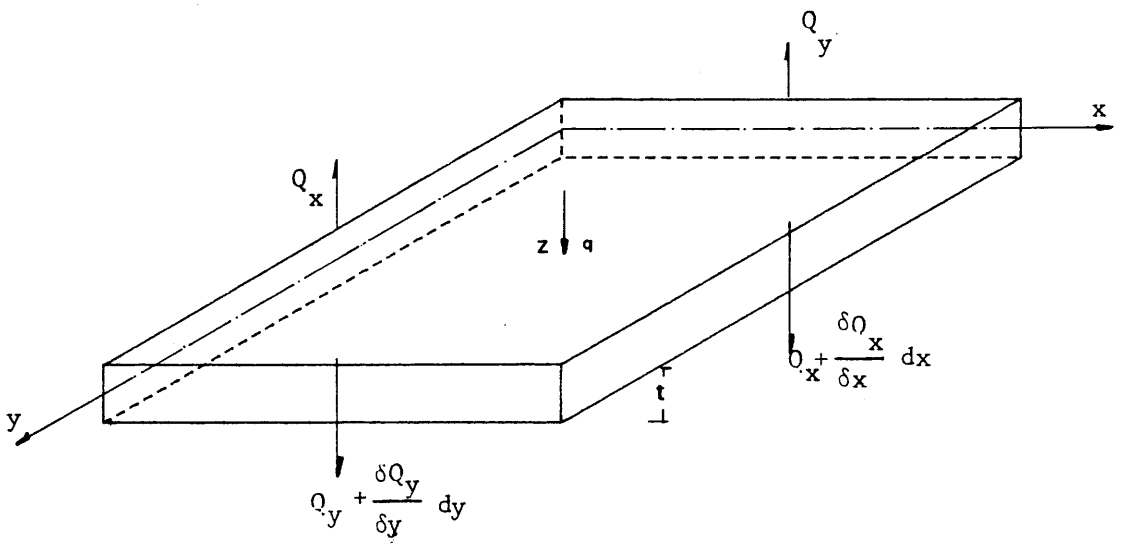

(b) Shear forces per unit lenght

Fig. (2.1) Equilibrium of slab element

$$\frac{\partial Q_x}{\partial x} + \frac{\partial Q_y}{\partial y} + q = 0.0$$

$$-\frac{\partial M_x}{\partial x} + \frac{\partial M_{xy}}{\partial x} + Q_x = 0.0 \qquad (2.1)$$

$$-\frac{\partial M_y}{\partial y} + \frac{\partial M_{xy}}{\partial y} + Q_y = 0.0$$

where q is the normal loading intensity, $q = q(x,y)$

Q_x and Q_y are the shearing forces per unit length along x and y directions respectively

M_x, M_y and M_{xy} are the bending moment per unit length along x and y direction and torsional moment respectively

By eliminating Q_x and Q_y from the three equations, they can be combined in to one equation as

$$\frac{\partial^2 M_x}{\partial x^2} - 2\frac{\partial^2 M_{xy}}{\partial x \partial y} + \frac{\partial^2 M_y}{\partial y^2} = -q \qquad (2.2)$$

Eqn (2.2) is known as the plate equilibrium equation.

2.2.3.2 Stress-Strain Relationship

In case of classical plate theory the following assumptions are usually made;

(a) The material obeys Hooke's law.

(b) The deflection is small relative to the slab thickness.

(c) The direct stress normal to the middle surface can be ignored.

(d) Plane section remain plane before and after bending. Therefore the strains due to displacement at any level z are given by;

$$\varepsilon_x = -z\frac{\partial \Theta_x}{\partial x} \quad , \quad \varepsilon_y = -z\frac{\partial \Theta_y}{\partial y} \quad \text{and} \quad \varepsilon_{xy} = -z\left(\frac{\partial \Theta_x}{\partial y} + \frac{\partial \Theta_y}{\partial x}\right) \tag{2.3a}$$

where ε_x, ε_y and ε_{xy} are the inplane strains at level z at a point in x,y cartesian system of coordinates. It should be noted that in the classical plate theory the rotations (θ_x and θ_y) of normals to neutral axis can be related to the lateral displacement (w) as follows

$$\theta_x = \frac{\partial w}{\partial x} \quad , \quad \theta_y = \frac{\partial w}{\partial y} \tag{2.3b}$$

On the other hand in Mindlin's plate theory in which the lateral deflection, w and the rotation θ_x, θ_y are treated as independent variables, reference to Fig. (2.2) shows that

$$\Theta_x = \frac{\partial w}{\partial x} + \psi_x \quad , \quad \Theta_y = \frac{\partial w}{\partial y} + \psi_y \tag{2.4a}$$

The inplane strains are given by

$$\varepsilon_x = -z\frac{\partial \Theta_x}{\partial x} \quad , \quad \varepsilon_y = -z\frac{\partial \Theta_y}{\partial y} \quad \text{and} \quad \varepsilon_{xy} = -z\left(\frac{\partial \Theta_x}{\partial y} + \frac{\partial \theta_y}{\partial x}\right) \tag{2.4b}$$

where ψ_x and ψ_y are the average rotation due to the transverse shear effects in the x and y directions respectively.

The stresses are related to the strains by

$$\begin{Bmatrix} \sigma_x \\ \sigma_y \\ \sigma_{xy} \end{Bmatrix} = \begin{vmatrix} E_x & E_{x1} & 0 \\ E_{x1} & E_y & 0 \\ 0 & 0 & G \end{vmatrix} \begin{Bmatrix} \varepsilon_x \\ \varepsilon_y \\ \varepsilon_{xy} \end{Bmatrix} \tag{2.5}$$

where E_x, E_y, G and E_{x1} are independent material constants which are needed to define the elastic properties of the plate.

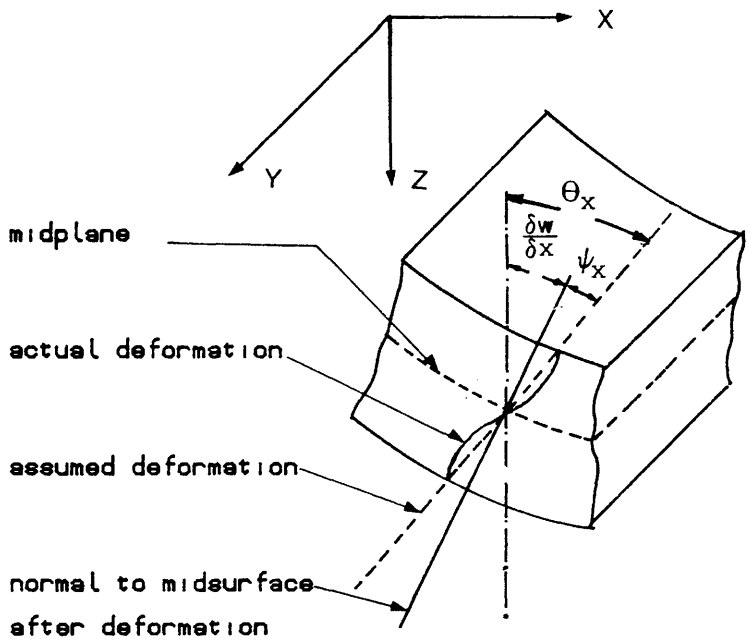

Fig. (2.2) Cross-section deformation of Mindlin plate

The moments (bending and torsional) are given by

$$\begin{Bmatrix} M_x \\ M_y \\ M_{yy} \end{Bmatrix} = \int_{-t/2}^{t/2} \begin{Bmatrix} \sigma_x \\ \sigma_y \\ \sigma_{xy} \end{Bmatrix} z\,dz \qquad (2.6)$$

For classical plate theory, moments can be written as follows:

$$\begin{Bmatrix} M_x \\ M_y \\ M_{xy} \end{Bmatrix} = \int_{-t/2}^{t/2} \begin{vmatrix} E_x & E_{x1} & 0 \\ E_{x1} & E_y & 0 \\ 0 & 0 & G_{xy} \end{vmatrix} \begin{Bmatrix} -\frac{\partial^2 w}{\partial x^2} \\ -\frac{\partial^2 w}{\partial y^2} \\ 2\frac{\partial^2 w}{\partial x \partial y} \end{Bmatrix} z\,dz \qquad (2.7)$$

or

$$\begin{Bmatrix} M_x \\ M_y \\ M_{xy} \end{Bmatrix} = \begin{vmatrix} D_x & D_{x1} & 0 \\ D_{x1} & D_y & 0 \\ 0 & 0 & D_{xy} \end{vmatrix} \begin{Bmatrix} -\frac{\partial^2 w}{\partial x^2} \\ -\frac{\partial^2 w}{\partial y^2} \\ 2\frac{\partial^2 w}{\partial x \partial y} \end{Bmatrix} \qquad (2.8)$$

where $D_x = \frac{E_x t^3}{12}$, $D_y = \frac{E_y t^3}{12}$, $D_{xy} = \frac{Gt^3}{12}$ (2.9)

and $D_{xI} = \frac{E_{x1} t^3}{12}$

For Mindlin plate theory, moments and shearing forces can be written as follows:

$$\begin{Bmatrix} M_x \\ M_y \\ M_{xy} \end{Bmatrix} = \begin{vmatrix} D_x & D_{x1} & 0 \\ D_{x1} & D_y & 0 \\ 0 & 0 & D_{xy} \end{vmatrix} \begin{Bmatrix} -\frac{\partial \theta_x}{\partial x} \\ -\frac{\partial \theta_y}{\partial y} \\ \frac{\partial \theta_x}{\partial y} + \frac{\partial \theta_y}{\partial x} \end{Bmatrix} \qquad (2.10)$$

$$\begin{Bmatrix} Q_x \\ Q_y \end{Bmatrix} = \begin{vmatrix} S_x & 0 \\ 0 & S_y \end{vmatrix} \begin{Bmatrix} \theta_x - \frac{\partial w}{\partial x} \\ \theta_y - \frac{\partial w}{\partial y} \end{Bmatrix} \qquad (2.11)$$

where S_x and S_y are the effective shear moduli in the x and y directions respectively. For an isotropic material $S_x = S_y = 5Et^3/12\ (1+\ \nu)$.

Substitution of Eqns (2.8) in Eqn (2.2) ,leads to the following fourth-order partial differential equation of classical plate theory, in the x, y cartesian system

$$D_x \frac{\partial^4 w}{\partial x^4} + 2\ (D_1 + 2D_{xy}) \frac{\partial^4 w}{\partial x^2 \partial y^2} + D_y \frac{\partial^4 w}{\partial y^4} = q \qquad (2.12a)$$

introducing the notation, $H = D_1 + 2D_{xy}$

we obtain

$$D_x \frac{\partial^4 w}{\partial x^4} + 2H \frac{\partial^4 w}{\partial x^2 \partial y^2} + D_y \frac{\partial^4 w}{\partial y^4} = q \qquad (2.12b)$$

For isotropic plates:

$$E_x = E_y = \frac{E}{(1-\nu^2)}, \quad E_{x1} = \frac{E}{(1-\nu^2)} \quad \text{and } G = \frac{E}{2(1+\nu)}$$

and Eqn (2.12a) reduces to

$$\frac{\partial^4 w}{\partial x^4} + 2 \frac{\partial^4 w}{\partial x^2 \partial y^2} + \frac{\partial^4 w}{\partial y^4} = \frac{q}{D} \qquad (2.12c)$$

where E and ν are the values of Young's modulus and Poisson's ratio. Eqn (2.12c) can be solved in simple cases by analytical methods and in more complicated cases by numerical methods of finite differences and finite elements. In the analytical procedures, the deflections of the plate are represented by either a double infinite fourier series (Navier solution) or by single infinite fourier sine series (Levy's solution). A detailed account of such methods can be found in text books on plate theory (1,2).

(a) Oblique Coordinates

When considering skew plates, it is useful to rewrite Eqn (2.12c) with the oblique angle equal to the skew angle of the plate α .

Consider the oblique axis set (u,v) which is related to cartesian set (x,y), Figs (2.3a) and (2.3b) by

$$x = u + v \sin \alpha \quad \text{and} \quad y = v \cos \alpha$$

or (2.13)

$$u = x - y \tan \alpha \quad \text{and} \quad v = y \sec \alpha$$

Using this transformation, the moments in the oblique system are related to the cartesian system as follows:

$$\begin{aligned} M_u &= \sec \alpha (M_x + M_y \tan \alpha - 2 M_{xy} \tan \alpha) \\ M_v &= M_y \sec \alpha \\ M_{uv} &= M_{xy} + M_y \tan \alpha \end{aligned} \tag{2.14}$$

The moment-curvature relationships in terms of the oblique coordinate Fig. (2.3) can be written for an isotropic plate as follows:

$$\begin{aligned} M_u &= \frac{t^3}{12} \left(A_{11} \frac{\partial^2 w}{\partial u^2} + A_{12} \frac{\partial^2 w}{\partial v^2} - A_{13} \frac{\partial^2 w}{\partial u \partial v}\right) \\ M_v &= \frac{t^3}{12} \left(A_{12} \frac{\partial^2 w}{\partial u^2} + A_{22} \frac{\partial^2 w}{\partial v^2} - A_{23} \frac{\partial^2 w}{\partial u \partial v}\right) \\ M_{uv} &= \frac{t^3}{12} \left(-A_{13} \frac{\partial^2 w}{\partial u^2} - A_{23} \frac{\partial^2 w}{\partial u \partial v} + A_{33} \frac{\partial^2 w}{\partial u \partial v}\right) \end{aligned} \tag{2.15}$$

and shearing forces as

$$\begin{aligned} Q_u &= \frac{t^3}{12} \left(- A_{11} \frac{\partial^3 w}{\partial u^3} - 3 A_{13} \frac{\partial^3 w}{\partial u^2 \partial v} - (A_{12} + 2A_{33}) \frac{\partial^3 w}{\partial u \partial v^2} - A_{23} \frac{\partial^3 w}{\partial u^3}\right) \\ Q_v &= \frac{t^3}{12} \left(- A_{31} \frac{\partial^3 w}{\partial u^3} - (A_{21} + 2 A_{33}) \frac{\partial^3 w}{\partial u^2 \partial v} - 3 A_{23} \frac{\partial^3 w}{\partial v^3}\right) \end{aligned} \tag{2.16}$$

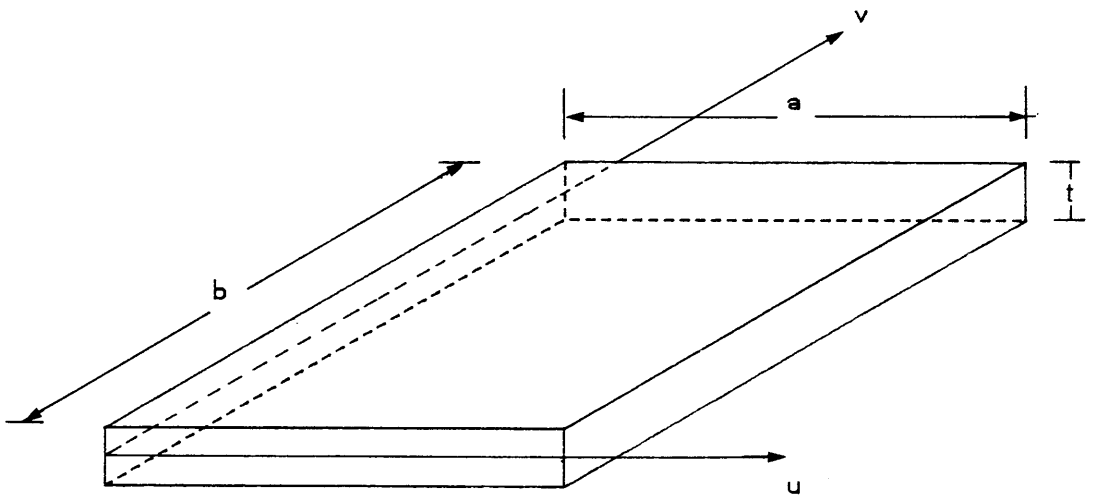

(a) Slab dimension

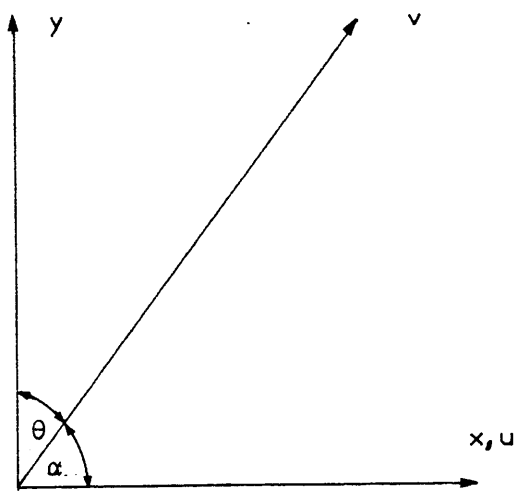

(b) The oblique axis system

Fig. (2.3) Skew slab in the oblique system of coordinate

where

$$A_{11} = E_x \cos\alpha + 2(E_{x1} + 2G) \sin\alpha \tan\alpha + E_y \sin\alpha \tan^3\alpha$$

$$A_{22} = E_y \sec^3\alpha$$

$$A_{33} = G \sec\alpha + E_y \tan^2\alpha \sec\alpha$$

$$A_{12} = E_{x1} \sec\alpha + E_y \tan^2\alpha \sec\alpha$$

$$A_{13} = (E_{x1} + 2G) \tan\alpha - E_y \tan^3\alpha$$

$$A_{23} = -E_y \tan\alpha \sec^2\alpha$$

The governing differential equation in terms of oblique coordinates can be written for the case of an isotropic plate as follows:

$$\nabla^2\nabla^2 w = \frac{q}{D} \qquad (2.17)$$

where

$$\nabla^2 = \sec^2\alpha \left[\frac{\partial^2}{\partial u^2} - 2 \sin\alpha \frac{\partial^2}{\partial u \partial v} + \frac{\partial^2}{\partial v^2}\right]$$

Analytical solutions to this equation have been found for some of the simpler loading arrangements and boundary conditions by using the series type solution or the strain energy method (10) (13).

(b) The series type solution

Quintan (10) assumed the displacement in the form of double infinite trigonometric series. By the introduction of certain functions called root functions and boundary functions, this double series can be transformed into a single infinite series. This, he claimed, will handle any of the simple boundary conditions and loading patterns. Unfortunately, no results have been published for this method. In 1964 Kennedy and Huggins (11) published a method for solving a skew plate simply supported on two opposite edges and elastically supported at the other two

edges under the action of a uniform load. The displacement was assumed as a single infinite fourier series. Results were obtained for a range of angles of skew 15 to 75 degrees and the aspect ratio (length/breadth) in the range of 0.7 to 2.0. It was noticed that the convergence deteriorated with increasing angle of skew.

(c) Strain energy solution

The concept of strain energy solution for plates was developed by Ritz (1) based on the principle of minimization of total potential. The strain energy stored in an isotropic skew plate is given by

$$U = \frac{D \sec \alpha}{2} \int_0^a \int_0^b [(\nabla^2 w)^2 + 2(1-\nu)\sec^2 \alpha \left(\frac{\partial^2 w}{\partial u^2} \cdot \frac{\partial^2 w}{\partial v^2} - \left(\frac{\partial^2 w}{\partial u \partial v}\right)^2\right)] du dv \qquad (2.18)$$

The work done by the external forces during the deflection of the plate is given by

$$V = \cos \alpha \int_0^a \int_0^b q.w \, du \, vu - \int_s \left(M_n \frac{\partial w}{\partial n} - Q_n.w - M_{ns} \frac{\partial w}{\partial s}\right) ds \qquad (2.19)$$

where a and b are the sides of the plate, M_n the normal moment, M_{ns} the tangential moment and Q_n the force in the n direction.

The principle of virtual displacements states that for equilibrium, the change in strain energy is equal to the external work done by the forces during the displacement.

$$\Delta U = \Delta V \qquad (2.20)$$

where U and V obtained by applying variational calculus to Eqns (2.18) and (2.19).

If a function is assumed for the deflected surface of the plate, then by substitution into Eqn (2.20) a solution can be found.

Using this form of solution, Morely (12) solved the problem of a swept cantilever plate under the action of a uniform load. Using Eqn (2.18) and assuming that the stress resultants and load could be taken as functions of one of the coordinate, Coull (13) solved the problem of a uniformly loaded skew plate with two sides simply supported and the other two free. Coull (14) extended this work to include the effect of line loads parallel to the supports by using Macaulay's method of brackets to allow for discontinuity. This artifice also enabled him to analyse continuous skew slab by treating the internal supports as line loads. He concluded that in order to obtain a convergent solution to the problem, only the first two terms of a more general power series for the oblique bending moment in the direction of span need be employed. To obtain better accuracy, the method may be extended by assuming more terms in the series used, but only at the expense of a greater difficulty of solution of the resulting equations.

2.2.3 NUMERICAL SOLUTION

Under this group, three methods are considered viz; finite differences, finite element and grillage analogy.

2.2.3.1 Finite Difference Method: In the finite differences method, a slab is first covered by a grid work of stations. Where possible a regular grid of equally spaced stations is employed (1) using rectangular or skew co-ordinates mesh. In applying this method, the derivatives in the differential equation (2.12b) are replaced by linear algebraic expressions, having deflections at stations as variables. A linear equation representing the differential equation is formed at each station for which there is an unknown deflection. Together they constitute a set of linear simultaneous equations, whose solution provides the values of deflections at the stations. The deflections at the nodes are used to form approximate expressions for curvatures etc. to determine moments and shear forces. The derivation of the method and its application in case of skew slabs, can be found in (1), (2), (12), (15). The method has been largely superseded by the finite element method.

2.2.3.2 Finite Elements Method: A slab to be analysed by finite element is first modelled by an assembly of discrete elements of simple geometric shape. In the most popular approach, a displacement field is assumed over each element in terms of values of displacement at prescribed nodal points (16). In an alternative approach, moment fields are assumed over elements and displacements are assumed on the boundaries of the element. The method of virtual work is used to form a set of linear simultaneous equations called stiffness

equations. An isoparametric element (17) based on Mindlin plate theory (63) has been used in this study and further details will be given in Chapter Four.

2.2.3.3 Grillage Analogy: Analysis of a grillage of beams by the stiffness method is a relatively straightforward and economic process. To predict the behaviour of a slab by grillage analysis, it is first necessary to specify the properties and layout of the component beams. The accuracy of a solution is largely dependent on the accuracy of this structural modelling. For a skew slab bridge deck, for example, members are positioned parallel to the abutments and free edges. Solution of the stiffness equations provides the joint deflections and rotations. The equivalent plate bending moments and shear forces are usually calculated from the interpretation of the concentrated bending and torsional couples at ends of each grillage member. The application of this method of analysis to bridge decks can be found in (18).

2.2.4 PLASTIC METHOD OF ANALYSIS AND DESIGN (78)

Because of the nonlinearity of the material properties of reinforced concrete resulting from the tensile cracking of concrete and plastification of steel, redistributions of moments and shears away from the elastic values occur. This is possible only if the slab sections are sufficiently ductile so that the sections continue to deform at constant moment. This section

discusses some of the popular plastic methods as applied to reinforced concrete plates.

2.2.4.1 Yield Line Theory

Yield line theory is an upper bound method of flexural analysis of under-reinforced slabs. For purposes of analysis, a collapse mechanism is assumed at ultimate load such that

(a) The moments at the plastic hinges are equal to the ultimate moments of resistance of the section.

(b) The collapse mechanism is compatible with the boundary conditions.

A collapse mechanism, defined by a displacement at a particular point, is used and this permits the corresponding displacements at load points and the rotations at the yield lines to be determined from the geometry. The work done by the loading is equated to the energy dissipated at the yield lines. To simplify the calculations, it is assumed that the deformations are confined yield lines only, and that the segments of slab between them remain rigid. With these assumptions the work equation simplifies to.

$$\sum_{i=1}^{n_1} \int_s M_n^* \, \theta_n \, d_s = \sum_{i=1}^{n_2} q \, \delta \, dA \qquad (2.21)$$

where n_1 is the number of yield lines, θ_n is the rotation of the couples M_n^* which is the ultimate moment of section at yield line, n_2 is the number of rigid, flat segments, q is load intensity, δ is displacement at the point of

application of q, s is the distance measured along a yield line and A is the area of a rigid region. Detailed descriptions of the theory and applications are given in Park and Gamble (6).

The main advantage of yield line theory is that it requires relatively simple calculations. Its greatest use is in assessing the strength of existing slabs, although it can be used as a design method. The difficulty of this method in design is that an engineer must use imagination and experience to ensure that all likely failure models have been investigated. Although it is a theoretical upper bound method and thus results in an overestimation of the true collapse load of a slab, many factors such as membrane force effect, strain hardening of steel, etc. contribute to the actual collapse load being greater than the the theoretical ultimate load and thus leading to a 'safe' design. Morley (22) extended conventional yield line theory by considering mechanisms which involve yield lines in which both rotations and displacements normal to the yield line occur. The rotations and displacements can be obtained from considerations of the geometry of a displaced slab. More details are given in Park (6). However, these methods rely heavily on an assessment of the in-plane restraint provided and this is extremely difficult to determine for actual structures. Although the yield line theory applies to any shape of slab, any load and any edge conditions, it is restricted in practice to slabs of constant thickness, uniformly reinforced in each of two mutually perpendicular or skew directions. The method does not give any information on the best steel

distribution within the slab and does not give any information about the general behaviour of the slab w.r.t crack width and deflection.

2.2.4.2 The Lower Bound Method

The lower bound method postulates a distribution of moments in the slab system at the ultimate load such that:

(a) The equilibrium conditions are satisfied at all points of the slab system.

(b) The yield criterion defining the strength of the slab sections is not exceeded any-where in the slab system.

(c) The boundary conditions are complied with.

The ultimate load is calculated from the equilibrium equation and the postulated distribution of moments. For a given slab system the lower bound method gives an ultimate load which is either equal to or less than the true ultimate load.

The methods based a lower bound approach to the ultimate load include

(a) Hillerborg's simple and advanced strip method

(b) Strong bands method

(c) Strip deflection method

(d) Direct design approach

2.2.4.2.1 Hillerborg's simple and advanced Strip Method (23)

In any lower bound design method, a designer is free to choose any moment distribution that he wishes provided that it satisfies the slab equilibrium equation:

$$\frac{\partial^2 M_x}{\partial x^2} + \frac{\partial^2 M_y}{\partial y^2} - 2\frac{\partial^2 M_{xy}}{\partial x \partial y} = -q \qquad (2.22)$$

Hence it is permissible to put $M_{xy} = 0.0$ throughout the slab, so that Eqn (2.22) reduces to

$$\frac{\partial^2 M_x}{\partial x^2} + \frac{\partial^2 M_y}{\partial y^2} = -q \qquad (2.23)$$

If it is now decided to divide the load q into a component $q\alpha$ carried in the x-direction and $(1-\alpha)q$ in the y-direction, Eqn (2.23) can be split into two equilibrium equations:

$$\frac{\partial^2 M_x}{\partial x^2} = -\alpha q \quad \text{and} \quad \frac{\partial^2 M_y}{\partial y^2} = -(1-\alpha)q \qquad (2.24)$$

It is emphasised that the chosen value of α can, and in general, does, vary over a slab.

It is usual to choose $\alpha = 0.0$ (all of the load carried in the Y-direction), $\alpha = 0.5$ (the load is shared equally between the x- and y-direction) or $\alpha = 1.0$, (all of the load carried in the x- direction).

In general, it is first necessary to decide upon the positions of the lines which divide the slab into regions of different load distribution direction. These lines are referred to as load dispersal lines or discontinuity lines. A designer is free to choose any load dispersal, and any discontinuity lines that he wishes. However, it is sensible to choose load dispersals which result in the load being transmitted to its nearest support. Moreover, Hillerborg (23) has suggested that it is preferable to take the load a relatively long distance to a built-in support than a relatively short distance to

a simple support. Thus, for discontinuity lines emanating from a corner, he suggested the positions shown in Fig. (2.4)

Equations (2.24) are the equilibrium equations for beams running in the x- and y- directions. Hence a two dimensional slab design problem has been reduced to a one -dimensional beam problem (or strip).

Hillerborg's strip method is illustrated by considering the design of a skew slab with two parallel edges simply supported and the other edges free as shown in Fig. (2.5a), to resist a uniformly distributed load of 0.01 N/mm.

For the slab under consideration, two distributions are considered Figs (2.5a) and (2.5b). In the first case, a system of beams are running in the skew direction, gives a system of statically determinate beams. The second system is similar to the first one with a strong diagonal beam A1-A2 Fig. (2.5c).

Considering distributions (2.5a) and (2.5b) only in the case Fig. (2.6a) the reaction distribution is very different from the elastic distribution, because skew slab transmits a considerable portion of loading to the obtuse corners and the strips must reflect the true slab action. In the second distribution when a strong beam is considered, the distribution of the reaction is similar to the elastic solution using finite element, but different in value depending on the stiffness of the strong beam (the dimension of the considered strong beam is given in

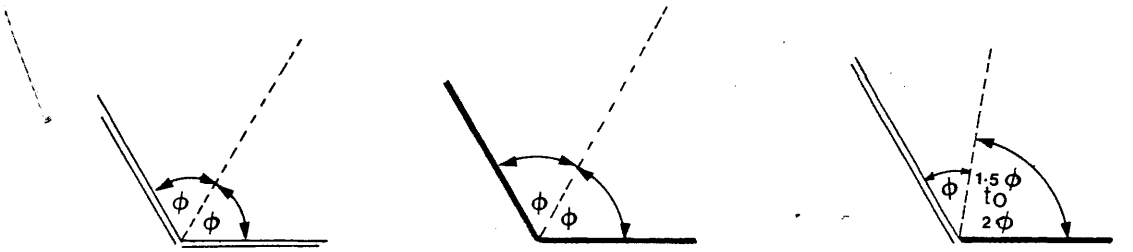

Load discontinuity line

Simply supported

Fixed

Fig. (2.4) Load discontinuity lines at a corner

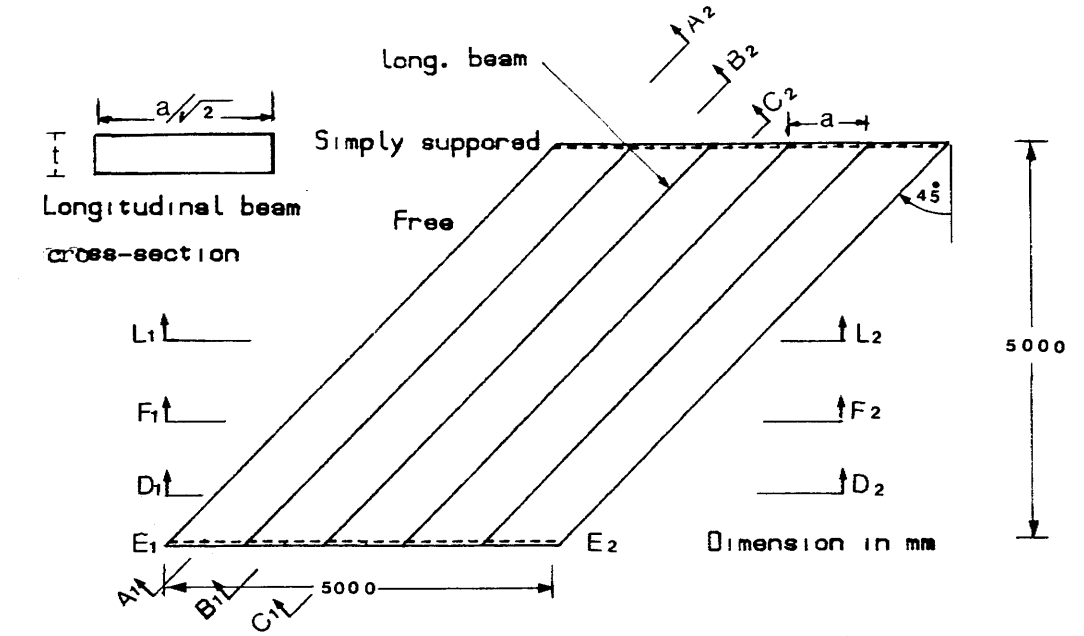

(a) Longitudinal beams system (simple strip method)

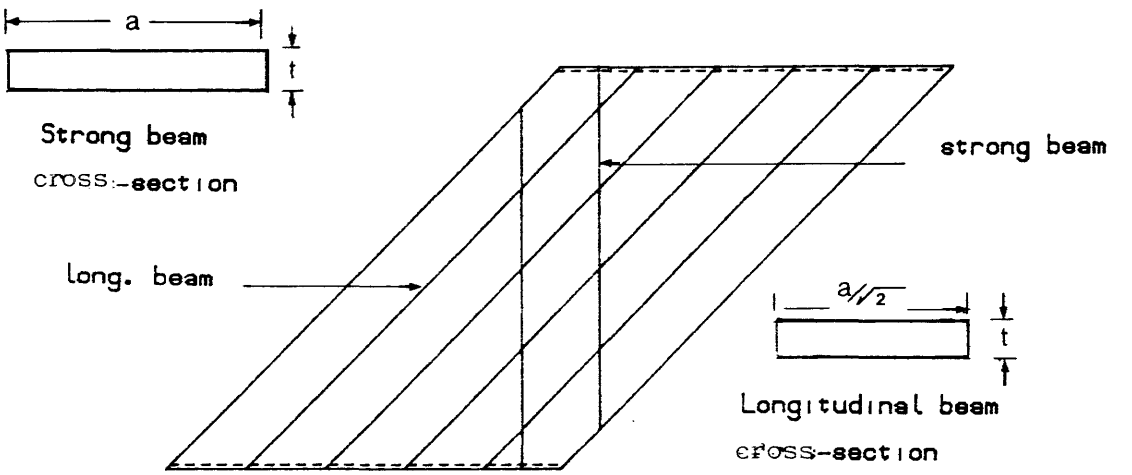

(b) Longitudinal beams with strong beam (simple strip method)

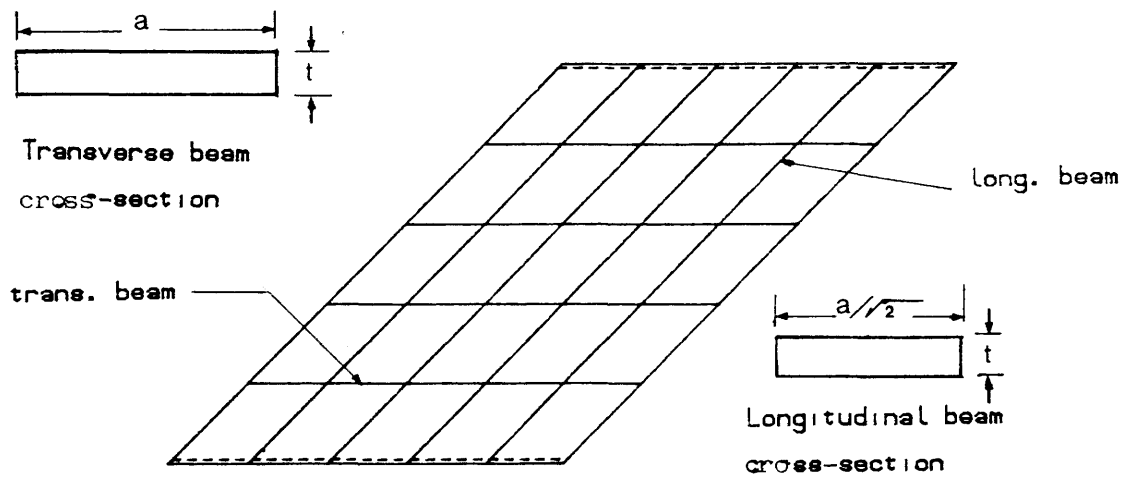

(c) Longitudinal beams with transverse beams

Fig. (2.5) SKEW PLATE UNDER UNIFORM LOAD

Fig. (2.5b)). The envelopes of longitudinal moment M at different sections are given in Figs (2.6b), (2.6c) and (2.6d). It can be seen from these curves that the moment distribution due to the first distribution is in considerable error compared with the finite element solution and that the effect of the strong beam improves the solution.

It can be seen from this example that the use of the simple strip method is not at all straightforward. One needs to think carefully about the system of beams which will be best suited to reflect the behaviour of skew slabs.

However if the correct solution is obtained, reinforcement must be provided to fit exactly the strip moments. Wood and Armer (111) have critically examined the strip method and concluded that it leads to an exact solution, with coincidental upper and lower bounds, if the reinforcement is provided to fit exactly the strip moments. However, Fernando and Kemp (25) have since shown that Wood and Armer's conclusion is not necessarily true, although it is extremely difficult to find practical situations in which it is not true.

One important drawback of the strip method is that, in pursuit of simple solution, the designer may choose stress distributions which depart far from those required for a good serviceability behaviour i.e. widely different from linear elastic solution. Such a distribution will seriously impair the function of the

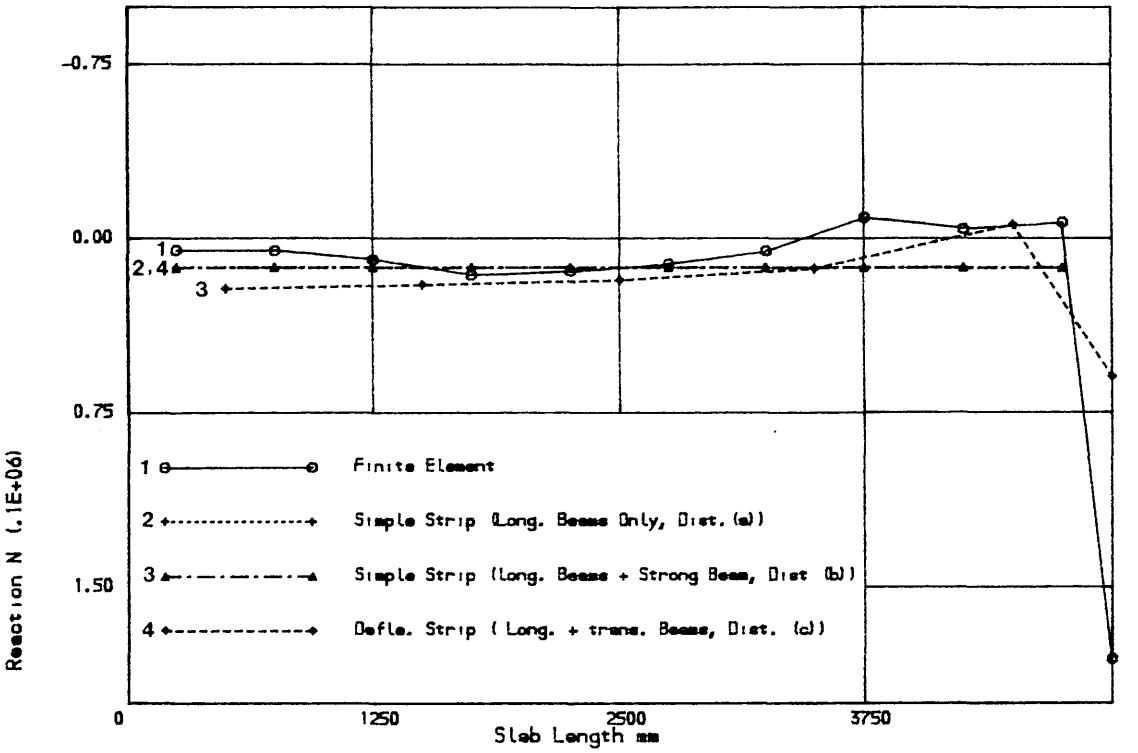

Fig. (2.6a) Reaction envelopes for skew slab at edge E1-E2

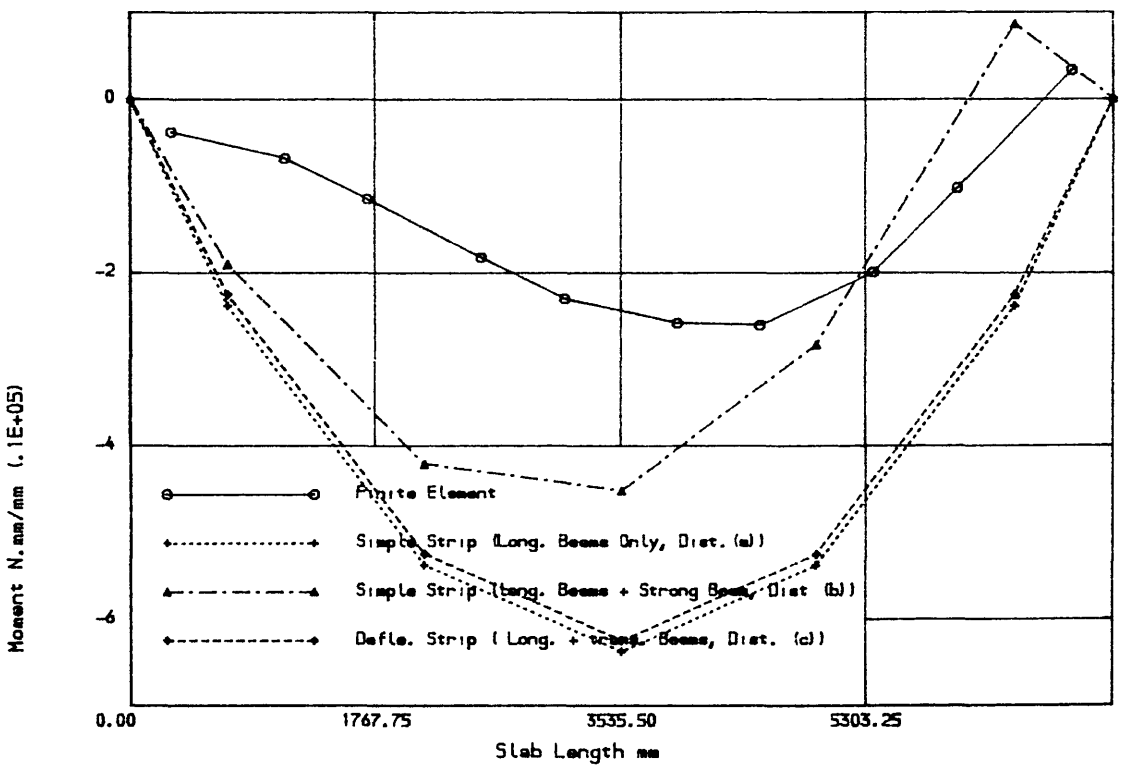

Fig. (2.6b) Moment envelopes for skew slab at section A1-A2

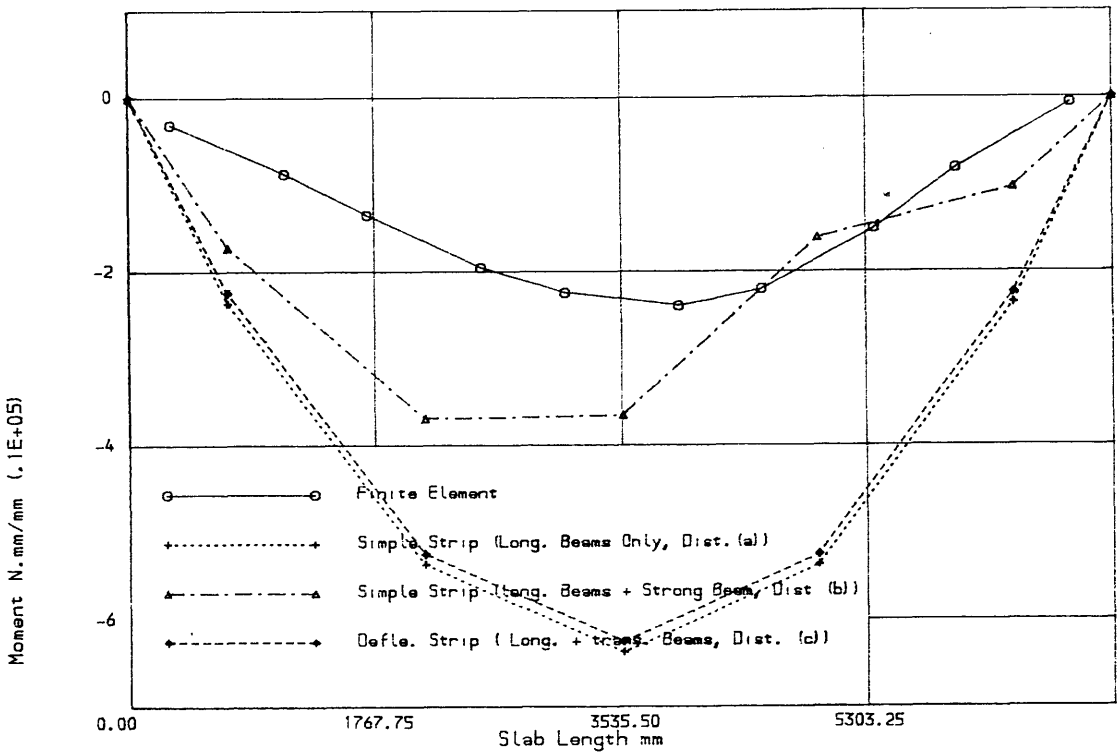

Fig. (2.6c) Moment envelopes for skew slab at section B1-B2

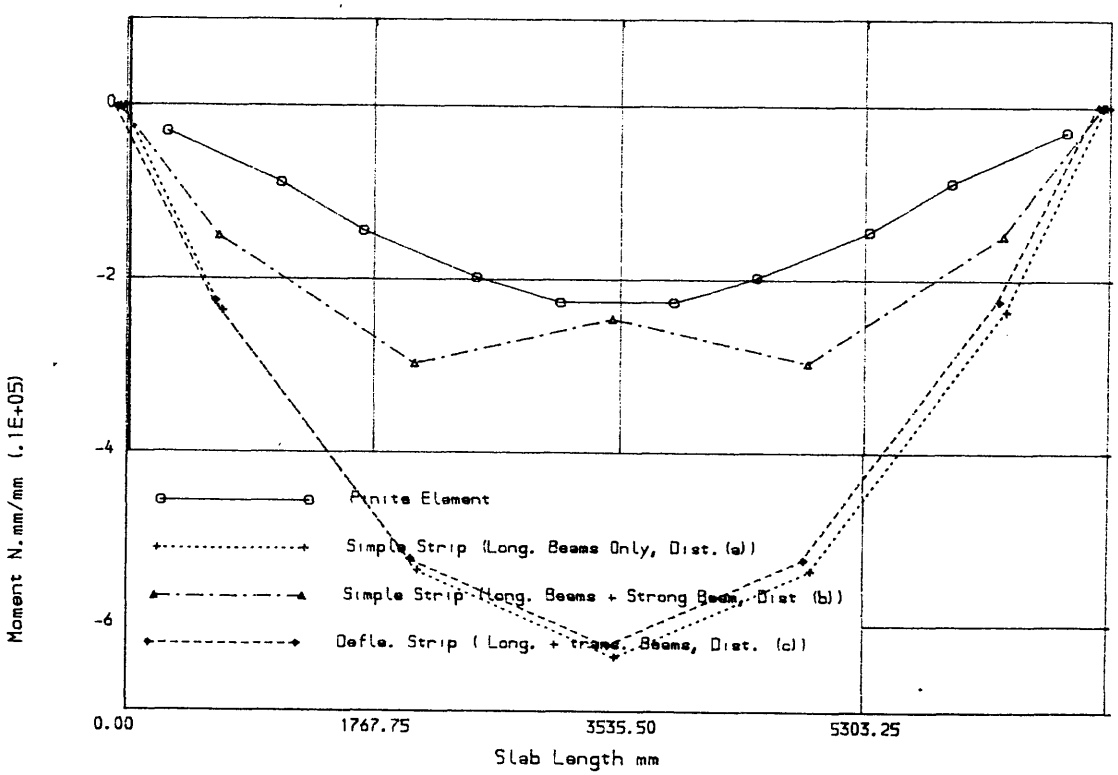

Fig. (2.6d) Moment envelopes for skew slab at section C1-C2

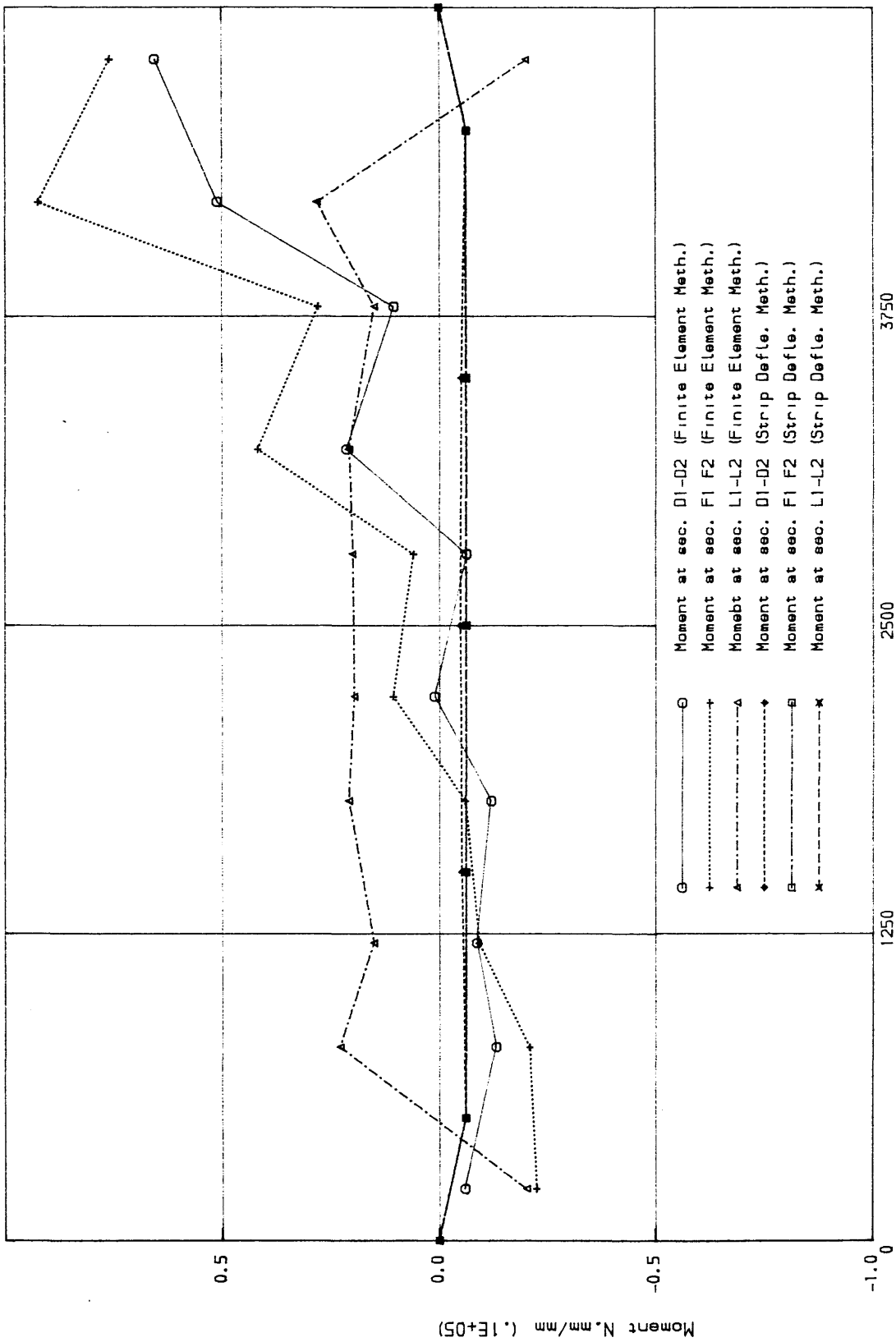

Fig. (2.6f) Transverse moment envelopes for skew slab

slab at early stages of loading.

The simple strip method as described cannot be applied to concentrated loads. In order to deal with concentrated loads, Hillerborg (24) introduced load distribution elements which essentially transform the concentrated load to a uniformly distributed load. A slab is divided into elements bounded by lines of zero shear force and zero twisting moment. A bending moment distribution is then chosen such that zero shear forces occur along the element boundaries. Hence, the chosen moment distribution must result in maximum sagging or hogging moment at the elements boundaries. The three types of element which can be used to divide the slab of Fig. (2.7a) are illustrated in Fig. (2.7b) and described below:

Type 1: Rectangular shape, in which the load is dispersed in one direction and which is supported along one edge.

Type 2: Triangular shape, in which the load is dispersed in one direction and which is supported along one edge.

Type 3: Rectangular shape, in which the load is dispersed in two directions and which is supported at one corner.

The Type 3 element transforms the concentrated load to a uniformly distributed load and permits one-way strip action to be considered in the type 1 and type 2 elements. Further details can be found in (26).

2.2.4.2.2 Strong Bands Method

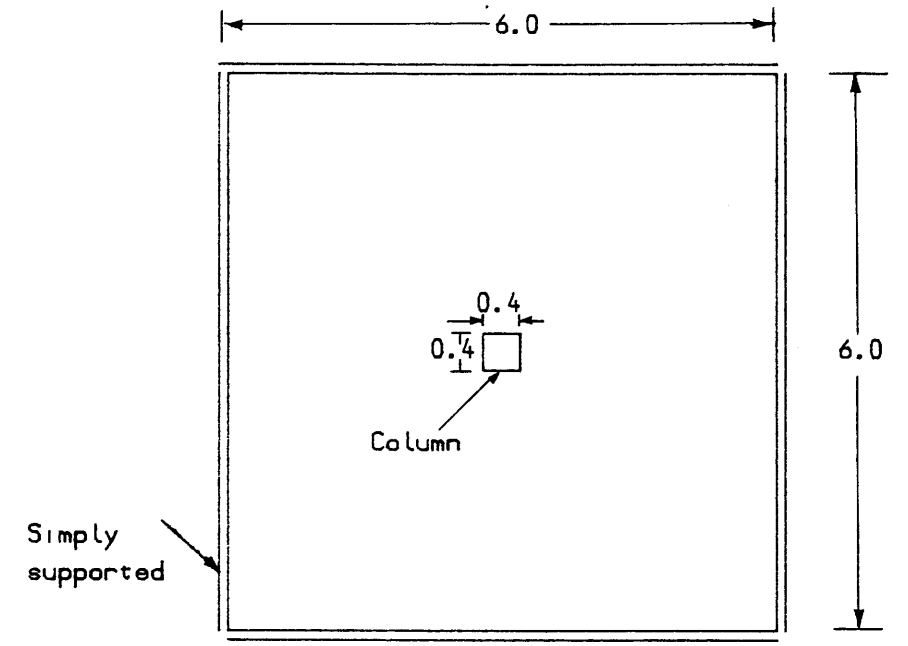

Design ultimate load = 10 KN/m Dimension in m

(a) Concentrated load example

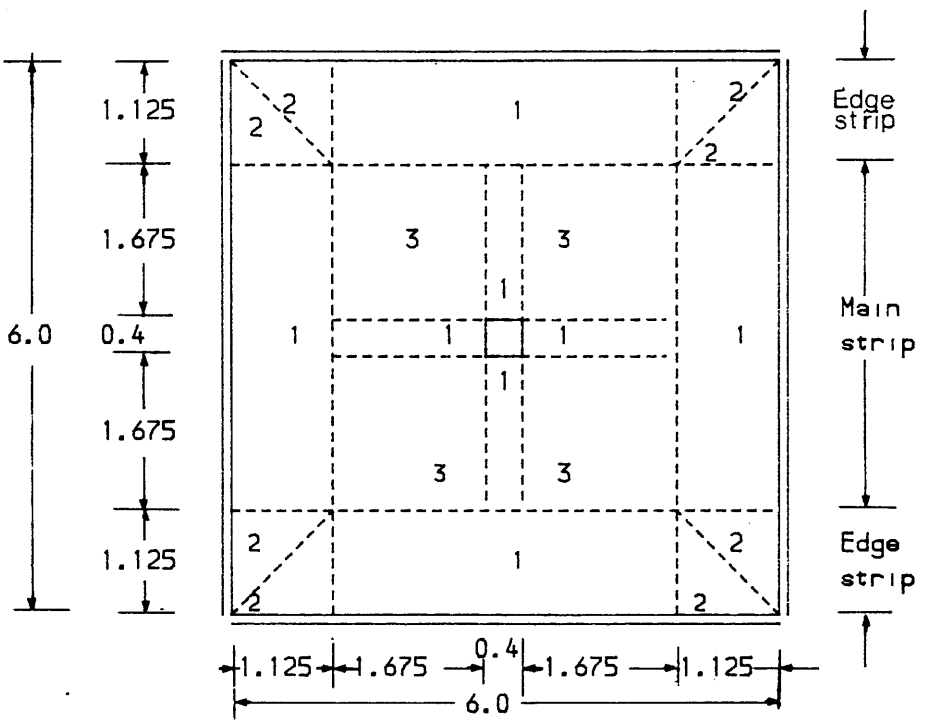

(b) Element division

Fig. (2.7) Advanced strip method

Because of the difficulties of Hillerborg's derivation of the moment fields for the Type 3 element, Wood and Armer (111) have proposed the use of strong bands of reinforcement within a slab. These act as beams which transfer the concentrated load to the supports or to be rest of the slab.

For example, for the slab given in Fig. (2.7a) the two sets of strong bands shown in Fig. (2.8) could be adopted to carry the load to the supports. This figure also shows the directions in which the load is assumed to be carried in the various parts of the slab.

A local set of bands over the columns is first considered Fig. (2.8b). The columns support the short, narrow strong bands which provide a uniform reaction over the centre 1.5 m square of slab. The central square of slab supports the strong bands of Fig. (2.8a), which, in turn, support strips in the outer parts of slab. The designer is free to choose the widths of the latter strong bands and to choose either the moment distributions in the strips and strong bands or the reactions between the various intersecting strips and strong band. It is emphasised that the moment distribution obtained is dependent on the assumptions of strips widths made by the designer.

Kemp (112) has pointed out that a drawback of the strong band approach is that it is difficult to choose suitable widths for the strong bands. If the band widths are chosen to be too narrow, then the reinforcement is heavily concentrated over the narrow band. Although a

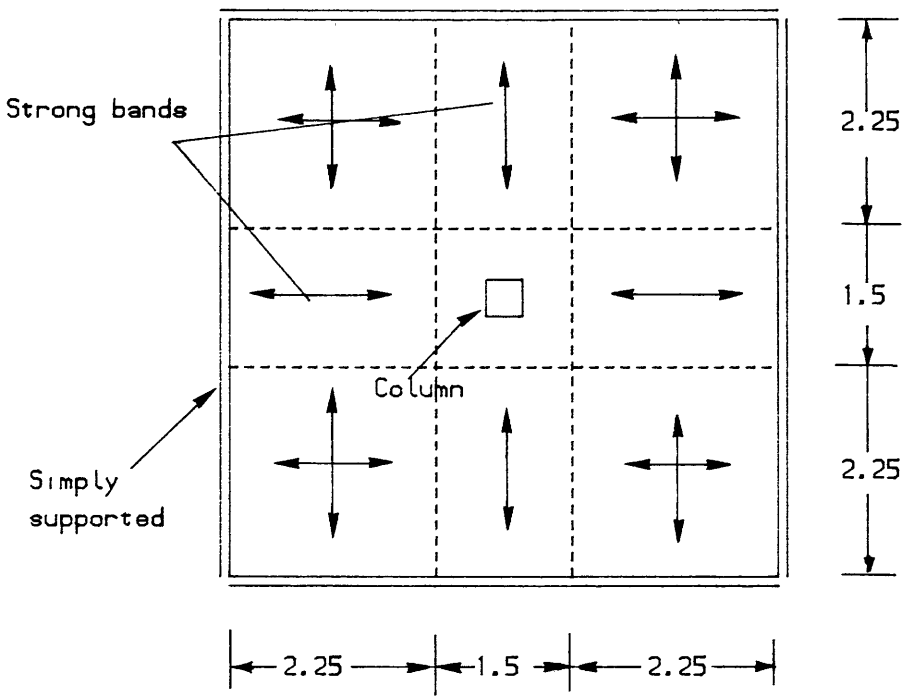

Design ultimate load = 10 KN/m Dimension in m

(a) General

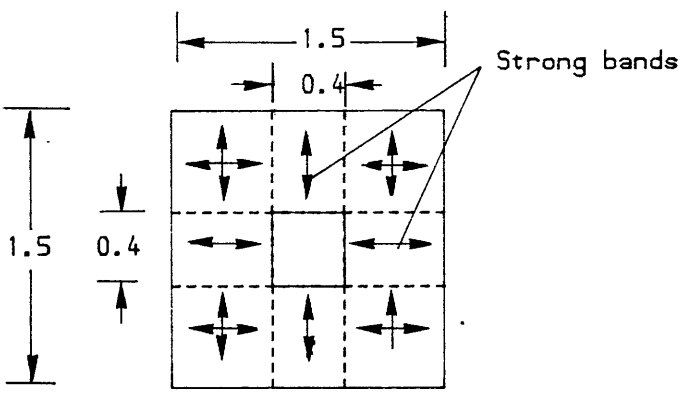

(b) Local strips

Fig. (2.8) Strong bands

satisfactory reinforcement arrangement will be achieved from the strength viewpoint, excessive cracking or deflection could occur at working loads because of the large amounts of moment redistribution required. In order to overcome this problem, and to make more efficient use of areas of a slab outside the strong bands, Kemp (112) proposed a method of design based upon chosen distributions of shear force. This is in contrast to the chosen distributions of loading which are used in the conventional strip method.

A slab is first divided into rectangular elements whose sides are parallel to the reinforcement directions. In common with the simple strip method, it is assumed that there are no twisting moments on the sides of the element. Such an element is shown in Fig. (2.9) together with the total load (W) acting on the element and the shear forces (Q_x, $\grave{Q}_x$, Q_y, $\grave{Q}_y$) which act on its sides. The vertical equilibrium equation of the element is

$$(Q_x - \grave{Q}_x) + (Q_y - \grave{Q}_y) = W \qquad (2.25)$$

The principle of the method is simply to choose shear forces on the sides of the element which satisfy this equilibrium equation. In this way, a shear force distribution throughout the slab is obtained. From the shear force distribution, the bending moments may be calculated. Fig. (2.10) shows one possible shear force distribution throughout the slab under consideration in Fig. (2.7a).

2.2.4.2.3 Strip Deflection Method

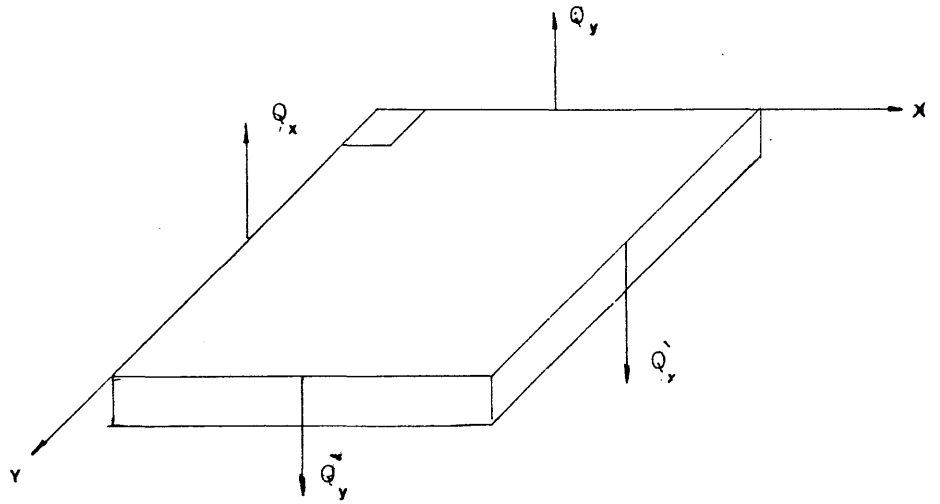

Fig. (2.9) Shear forces on slab element

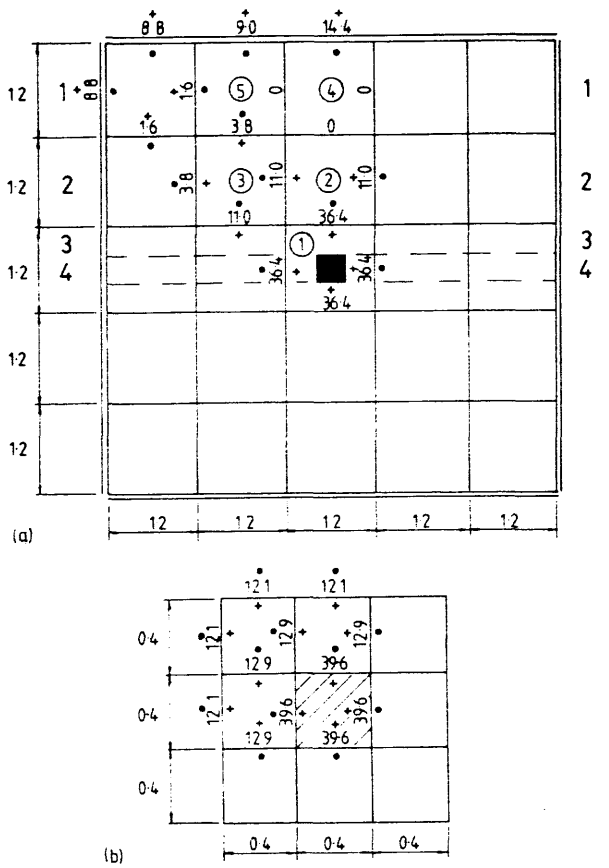

+ Shear force acts upward on the external boundary of the element

• Shear force acts downward on the external boundary of the element

Fig. (2.10) Elements and shear forces (KN) for shear distribution:
(a) Stage 1 mesh (b) Fine mesh for centre squre of Stage 1 mesh

As mentioned in section (2.2.4.2.1)it is possible when using the simple strip method to choose any value of load distribution parameter which in the hands of a bad designer can lead to an unexceptable design. Fernando and Kemp (27) have proposed the strip deflection method to overcome this difficulty.

In this method a slab is first divided into orthogonal/skew strips parallel to the reinforcement directions to form a set of rectangular, square or skew areas. The intensity of loading on each area is assumed to be uniform but can vary from area to area. In the simple strip method, a designer would choose the amount of load, q_x, carried in the X-direction and for equilibrium, the amount of load, q_y, carried in the Y-direction in then $(q - q_x)$. In the strip deflection method, a value of q_x is not chosen, but q_x and q_y are determined such that there is compatibility of elastic deflections at intersection point of the strip centre lines. The elastic deflections can be determined using elastic beam theory (because the twisting moments are assumed to be zero) in terms of the unknown loads q_x and $q_y = (q - q_x)$ and appropriate flexibility coefficients which are independent of loading, but depend on the geometry and boundary conditions of the problem. Once the load distributions is known, the shear forces and bending moments can be determined. In this method, increasing the number of strip improves the accuracy, but at the expense of increasing the number of simultaneous equations to be solved.

It is interesting to note that the Rankine-Grashof method of slab design the CP110 (30) is a special case of the general strip deflection in which a single strip is considered in each direction. Fernando and Kemp (27) have pointed out the similarity between the strip deflection method and the analysis of a slab as a grillage with zero torsional stiffness. This has been used to solve the same example in Fig. (2.5a) by considering the distribution of the strips in Fig. (2.5c), using the programme package FLASH (20).

The envelopes of the reactions and the moments at different section are given in Figs (2.6a), (2.6b), (2.6c) and (2.6d) and (2.6e). There is not much difference between the simple one way strips and the strip deflection method for the example under consideration thus emphasising the importance of torsion in skew slabs.

It may be useful to use grillage analysis to predict the behaviour of a skew plate, but it is necessary to specify the properties and layout of the component beams. The accuracy of solution is largely dependent on the aptness of this structural modelling. Solution of the stiffness equations provides the joint deflections and rotations. Bending moments are usually calculated from the interpretation of the concentrated bending and torsional couples at ends of each grillage member. Engineering judgement is needed at this stage to minimise the introduction of further errors in the estimations of these moments and forces.

Fig. (2.11) shows two types of grillage fromework for the slab under consideration (Fig. (2.5 a) , the choice is dependent on the reinforcement arrangement. In Figs (2.12a), (2.12b), (2.12c) and (2.12d) show the comparison of the reaction and bending moments for the grillage analysis and the finite element method. It can be seen that grillage analysis results compare well with finite element solution specially when the grillage fromewok was orthogonal as shown in Fig. (2.11b).

In practice, according to CP110 (30), torsional reinforcement is normally added at a corner contained by edges over only one of which the slab is continuous as a certain percentage of the midspan reinforcement. Hago (9) carried out a design of a series of a uniformly loaded rectangular slabs with various boundary condition and aspect ratios, by this following two approaches:

1- Using the simple strip method (torsionless analysis) to provide reinforcement to resist the normal moment components M_x and M_y. The torsional stress component Mxy was ignored and in addition torsion steel was provided, using the CP 110.

2- Using direct design method (9) (torsion analysis) to provide reinforcement to resist the three moment components M_x, M_y and M_{xy}.

Based on a comparison of the total reinforcement volume he concluded the torsional analysis is at least 10% more economical than the torsionless analysis.

2.2.4.5 Direct Design Approach

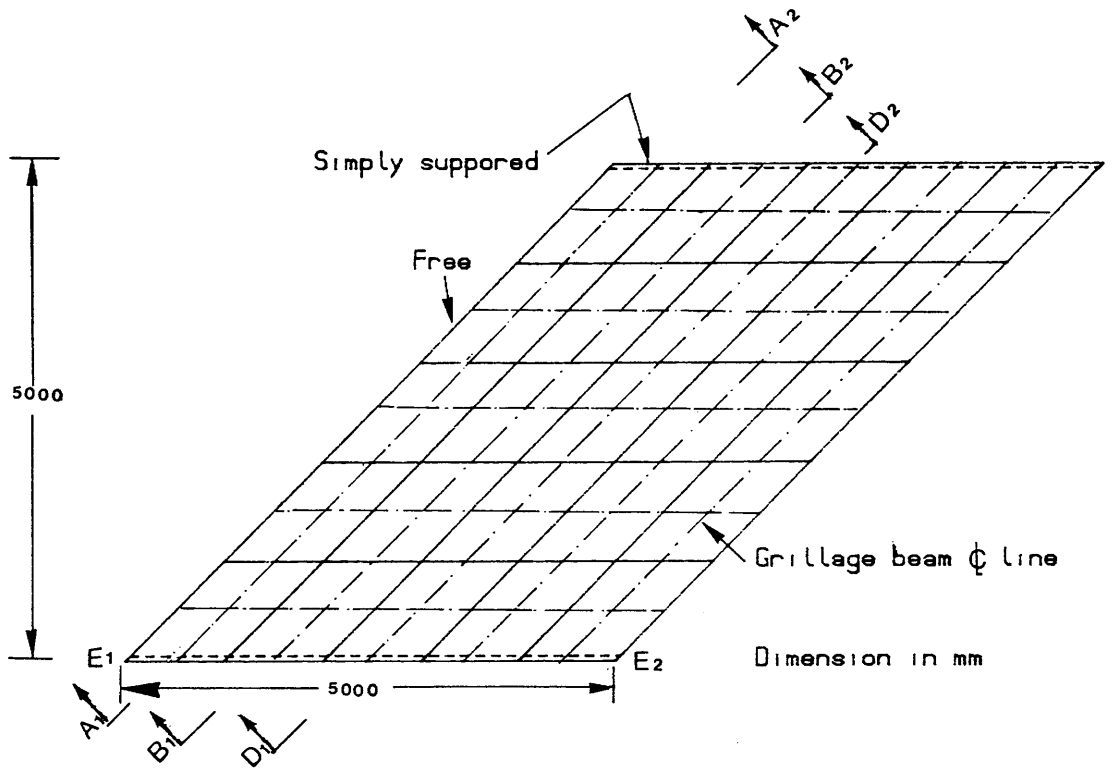

(a) The steel distribution parallel to the edges

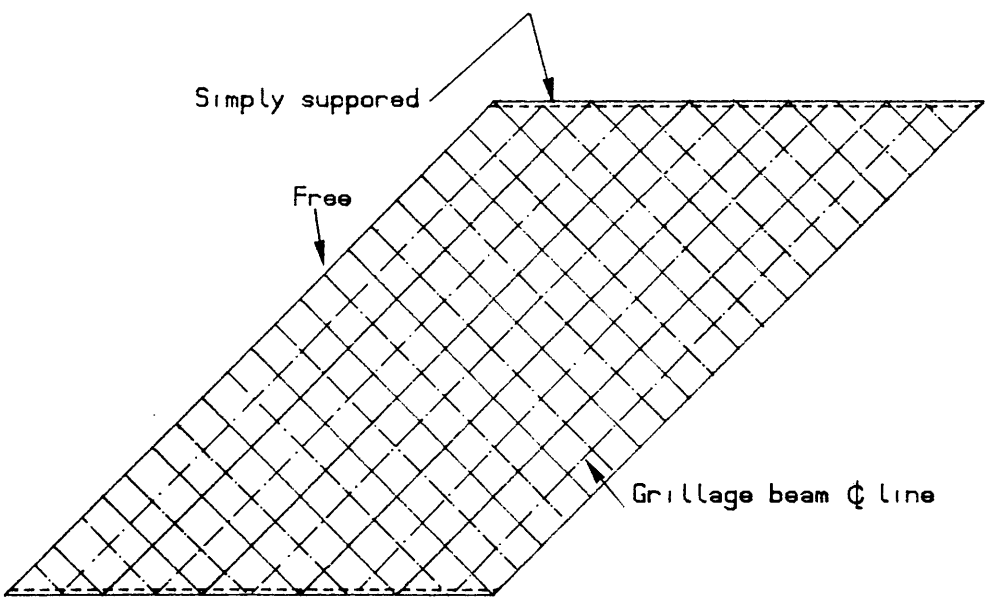

(b) The steel distribution parallel and orthogonal to the free edge

Fig. (2.11) Grillage distribution

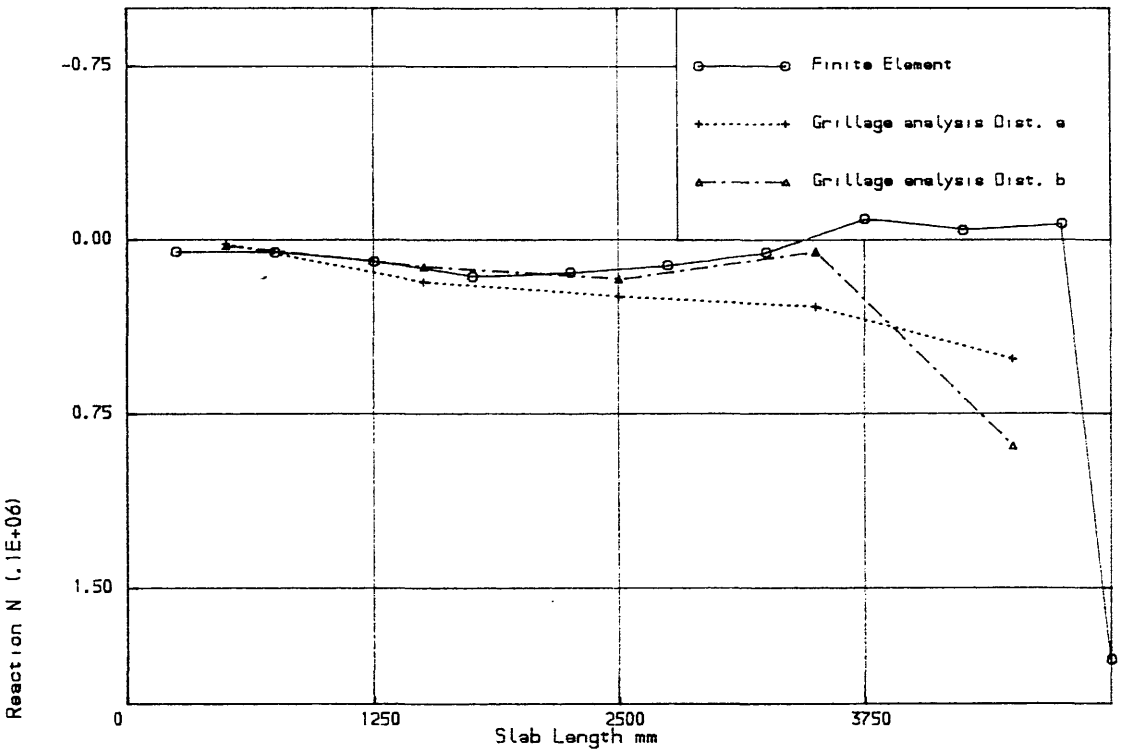

Fig. (2.12a) Reaction envelopes for skew slab at edge E1-E2

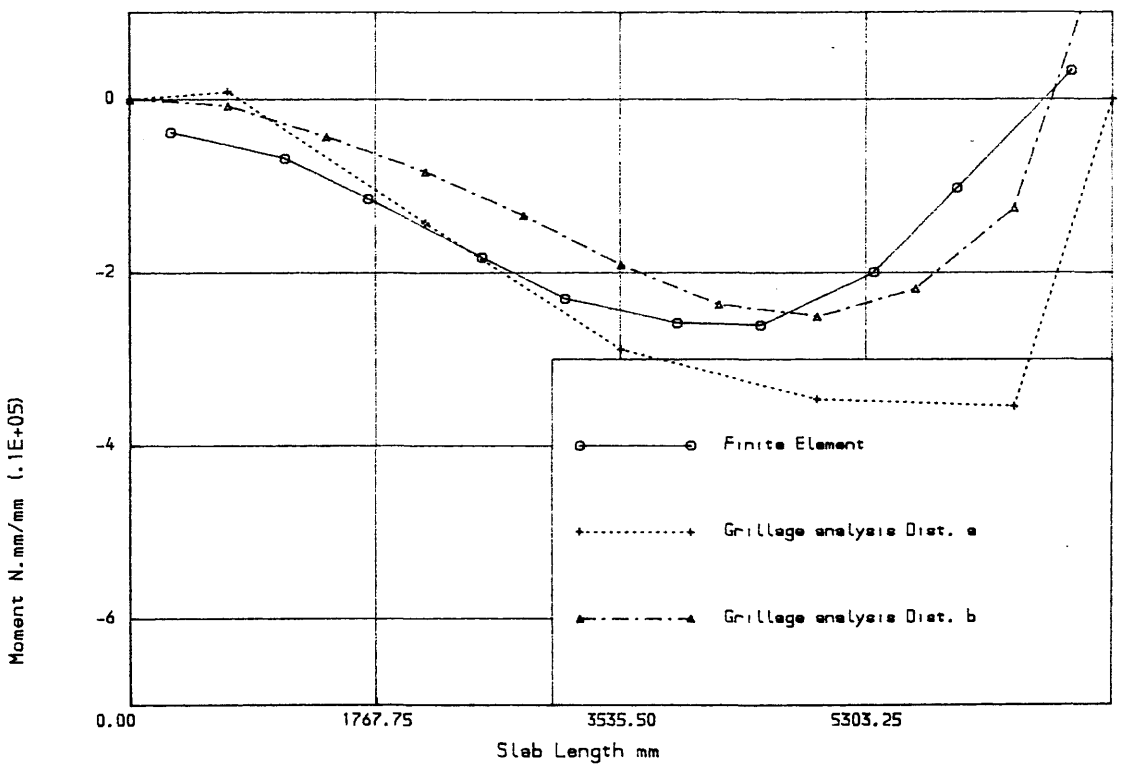

Fig. (2.12b) Moment envelopes for skew slab at section A1-A2

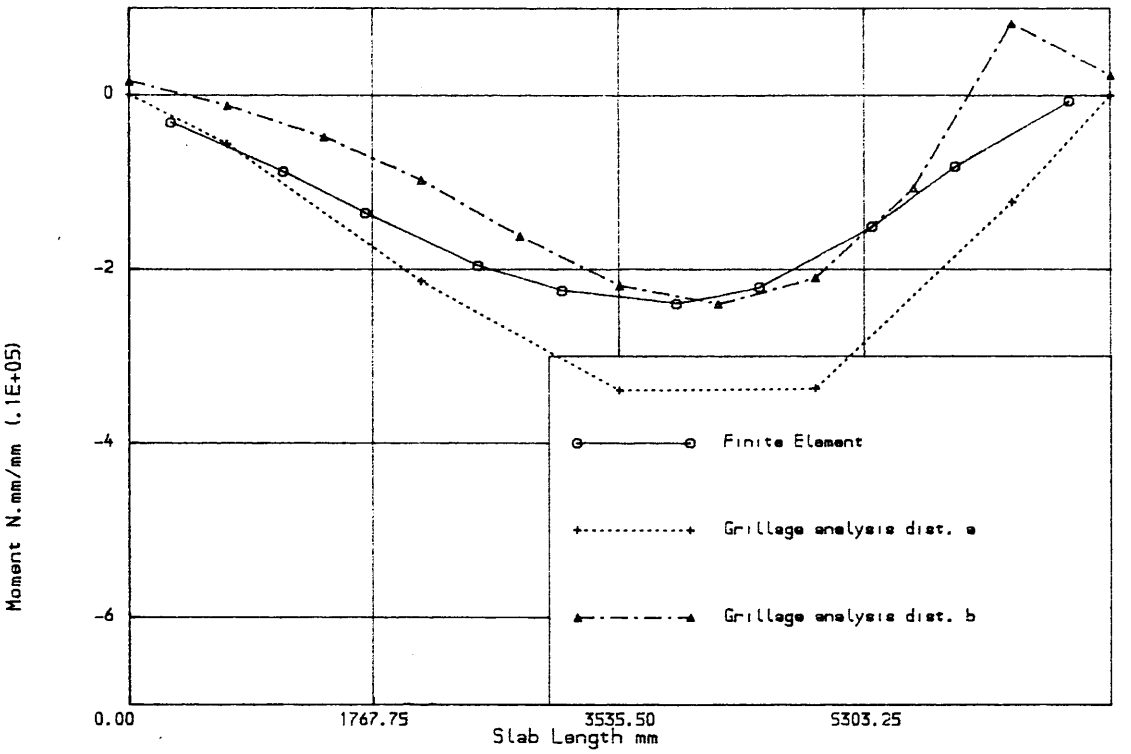

Fig. (2.12b) Moment envelopes for skew slab at section B1-B2

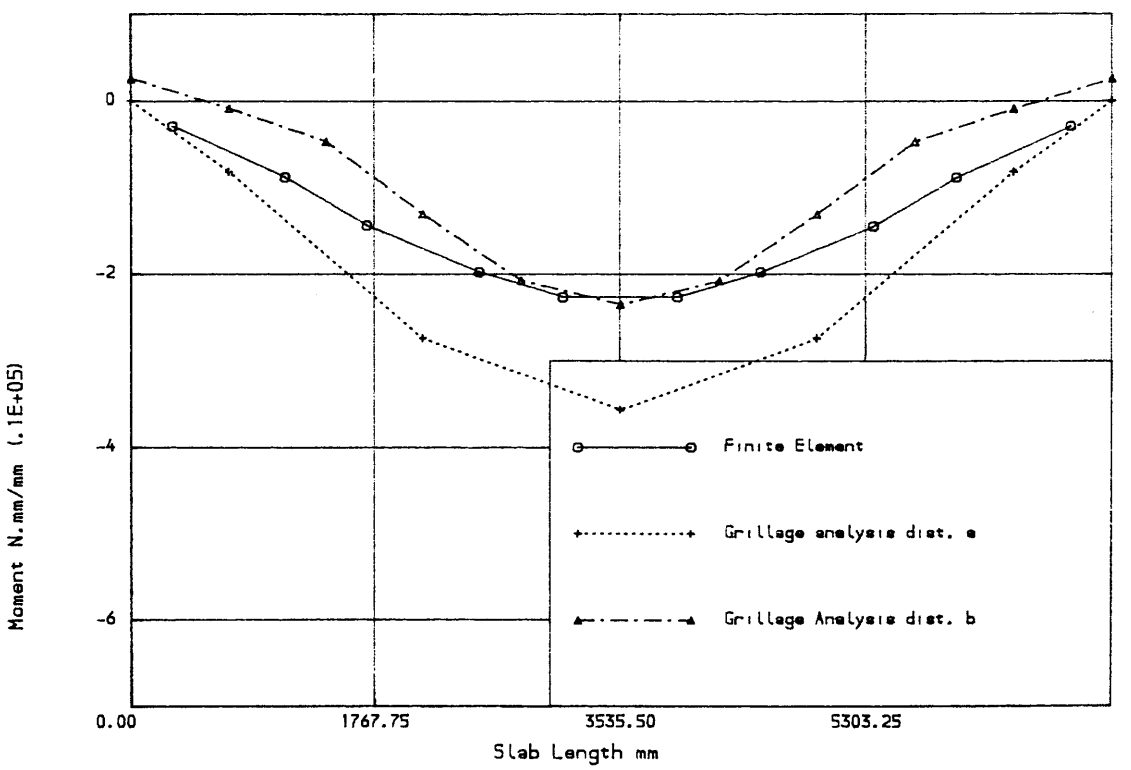

Fig. (2.12d) Moment envelopes for skew slab at section C1-C2

This approach unlike the pure upper bound (yield line) and pure lower bound (Hillerborg's strip method) considers serviceability and ultimate load behaviour of a under-reinforced slab. In this method an elastic stress field and a yield criteria for slab is used to design the slab. The approach was first proposed by Hillerborg (23) and later reconsidered and restarted by Wood (75), for the case of orthogonal steel. Nielsen (76) has also presented equations for the optimum design of orthogonal steel. Subsequently Armer (77) derived equations for the case in which the steel lies in predetermined skew directions. Hago (9) used this approach to design and test 'large scale' orthogonally reinforced rectangular slabs and beam slab model with various boundary conditions. He carried out an experimental and theoretical work to check this approach. He concluded that the Direct Design approach provides designs with good service and ultimate behaviour with a reserve strength at least 10% above the design loads. The basic idea of this approach and the derivation for the general case of angle of skew will be considered in Chapter Three.

2.3 DESIGN AND ANALYSIS FOR SERVICEABITILY LIMIT STATE

2.3.1 Introduction

It is essential that all structures should be designed so that they possess not only adequate strength but also they behave in a satisfactory manner under all load conditions (i.e at limit states). Satisfactory

behaviour at working loads is generally considered in terms of cracking, deflection and vibration characteristics. Each of these characteristics is a function of stiffness and working load stress levels (in particular steel stress levels). It is important to consider the effects of both applied forces and applied deformation (e.g. shrinkage and temperature movements) on serviceability limit state. The following discussion is limited to deflections and cracks due to applied load only.

The European and American design codes (8) and (32) of practices generally ensure that the material stresses in reinforced concrete slabs are not excessive at the serviceability limit state and thus specific stress limitations are not generally given in codes. However, the British bridge code BS 5400 (BSI, 1978) does give stress limitations, because this code does not require crack widths to be checked under all possible load combinations.

Because concrete cracks under sustained loading, determination of the displacements of a reinforced concrete slab, even under working loads, strictly requires a non-linear analysis. Suitable methods will be reviewed in section (2.4), and one of these methods will be given in detail in Chapter Four. However, such analyses are in general too expensive for design office. Hand calculation methods are often used to estimate the curvatures, in order to calculate deflections or crack widths. Such calculation can be based on the elastic

moment field calculated by using uncracked section properties. The determination of moment/curvature relationships will be considered before considering the various serviceability criteria.

2.3.2 Moment-Curvature Relationships

Fig. (2.13) shows the bilinear moment-curvature relationship. The curvature is given by

$$\frac{1}{r_b} = \frac{M}{I_{cr} E_c} \qquad (2.26)$$

where $1/r_b$ is the curvature

M the moment under consideration

E_c the long-term elastic modulus (in this study the short-term elastic modulus is considered), the short term elastic modulus is given by

$$E_c = 4.73 \sqrt{f'_c} = 4.25 \sqrt{f_{cu}} \ \text{kN/mm}^2 \qquad (2.27)$$

where f'_c is the cylinder strength (N/mm^2)

and f_{cu} is the cube strength

I_{cr} is the second moment of area of the cracked section. Ignoring concrete in the tension zone overestimates the true curvature because of the stiffening effect of concrete in tension between cracks. The following two approaches, adopted in practice, are presented.

(a) Effective secant stiffness

Branson (31) has proposed, from considerations of short-term beam deflection data, the use of the effective secant stiffness illustrated in Fig. (2.13). The short-

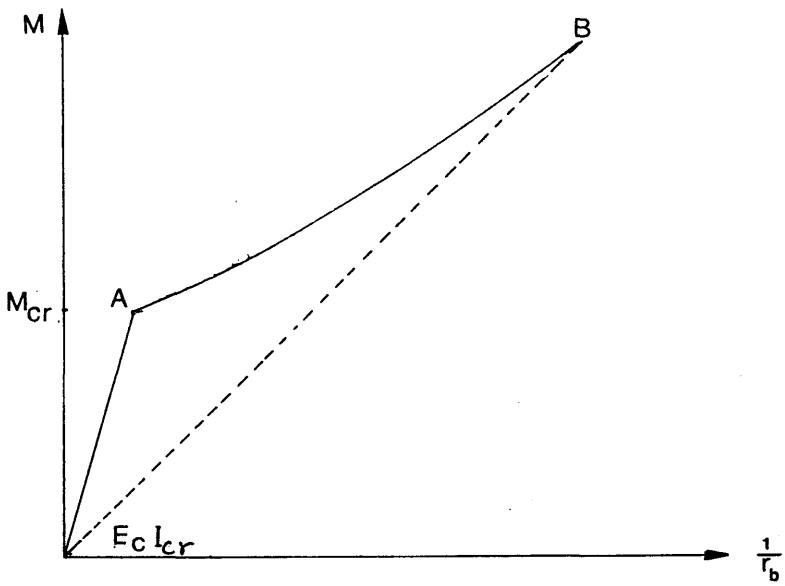

Fig. (2.13) Effective secant stiffness

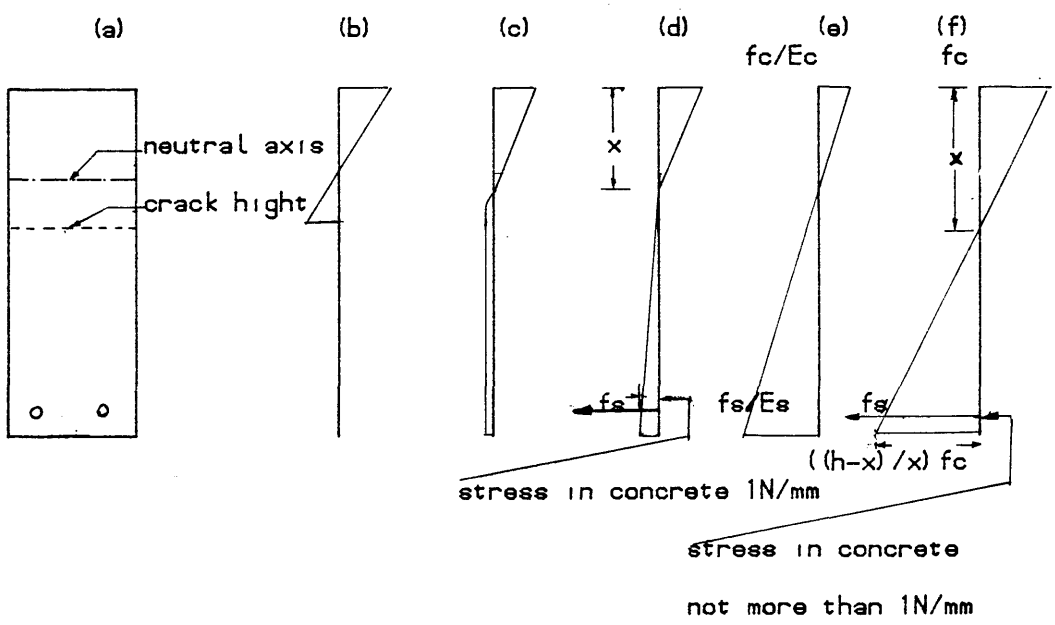

Fig. (2.14) Concrete flexural stresses, (a) cracked section (b) at crack (c) between cracks (d) average (e) strains (f) section not cracked

term elastic modulus of concrete is given by Eqn (2.27). The effective second moment of area (I_{eff}) is given by

$$I_{eff} = \left(\frac{M_{cr}}{M}\right)^3 I_g + \left[1 - \left(\frac{M_{cr}}{M}\right)^3\right] I_{cr} \qquad (2.28)$$

where M is the moment under consideration, M_{cr} is the cracking moment, I_g is the second moment of area of the uncracked transformed section and I_{cr} is the second moment of the cracked transformed section.

This approach was adopted by the American Building Code ACI (32) and the American Bridge code Committees (33).

(b) Effective tensile concrete stress

The distributions of flexural stress in concrete at a crack and mid-way between cracks are shown in Figs (2.14b) and (2.14c). The average effect of the variation in tensile stress distributions can be considered by assuming the triangular distribution of "average" effective stress shown in Fig. (2.14d) with an effective stress (f_e = 1N/mm) specified (21) at the centroid of the tension reinforcement. The curvature can be obtained from the relationships

$$\frac{1}{r_b} = \frac{f_c}{xE_c} = \frac{f_s}{(d-X)E_s} \qquad (2.29)$$

where x is the neutral axis depth, f_c and f_s are the stresses in concrete and reinforcement respectively.

Assessment of stresses and the neutral axis depth can be found by a trial-and-error approach (21). This

approach is adopted for deflection calculations in CP 110 (30) and BS 5400 (34).

2.3.3 Deflection

In design, it is usual to comply with the specified deflection criteria by limiting span to depth ratio. However, in exceptional cases, it may be necessary to calculate deflection and to ensure that they are less than the specified value. The deflection of a slab under a simple loading can be calculated from a formula of the type:

$$\delta = \frac{kWL^2}{D} \qquad (2.30)$$

where K is a coefficient which depends on the slab shape, load patterns and support boundary conditions, W is the total loading, L is the span and D is the flexural stiffness per unit width. It is necessary to determine K and D.

Values of coefficient K in Eqn (2.30) have been given by Timoshenko (1) for some cases of rectangular slabs and for others can be calculated by finite element method.

If the slab is uncracked, then D is given simply by $Et^3/ 12(1-\nu^2)$, ν is Poisson's ratio . However, after cracking, D is given approximately by the effective cracked stiffness (E_cI_{eff})at a particular section which is calculated with tension stiffening allowed for by the method described in Section (2.3.2).

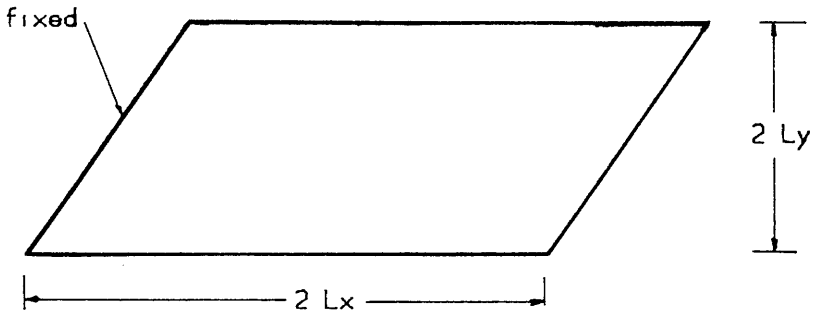

Fig. (2.15) Fixed slab under uniformly-distributed load

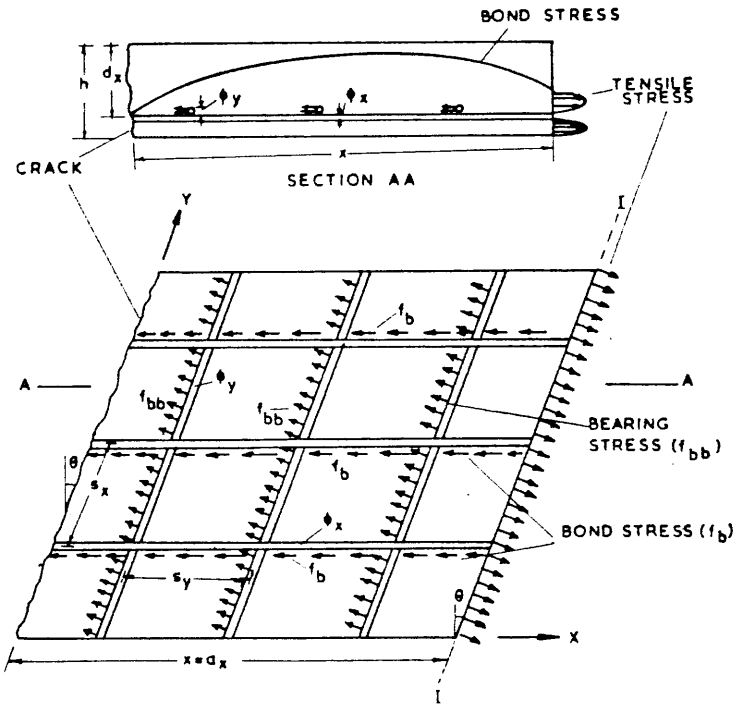

Fig. (2.16) Cross-Section of slab showing the distribution of bond stress, tensile stress and plane of reinforcement along X and Y directions

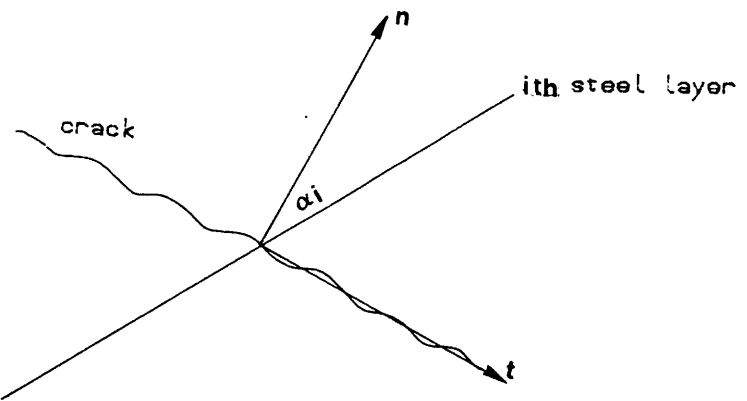

Fig. (2.17) Cracked slab

For restrained reinforced concrete skew slabs under uniform load Desayi and Prabhakara (35) proposed a method for estimating the short-time deflection. The method is developed in three stages.

The first stage considers the elastic behaviour of the slab up to cracking load. The deflection at centre of a skew slab is calculated on the basis of the solution available for elastic skew plates (32) as

$$\delta = \frac{\alpha P L_x^4}{E_c I_g} \qquad (2.31)$$

where I_g the gross second moment of area

E_c the modulus of elasticity of concrete

P the intensity of uniformly-distributed load

α is a constant for fixed skew plate based on the ratio and skew angle and is obtained from Table 1, Page 352 of (19)

L_x is the slab length. See Fig. (2.15).

Eqn (2.31) is valid up to a load $P = P_{cr}$, where P_{cr} is the intensity of load corresponding to the first cracking of concrete and can be calculated using;

$$P_{cr} = \frac{M_{cr}}{BL_x} \qquad (2.32)$$

in which $M_{cr} = f_r I_g/h$

where B is dependent on the aspect ratio and angle of skew. See Ref (35) Page 354.

f_r is the modulus of rupture of concrete

h the distance of extreme tensile fiber from centroid of concrete section.

In the second stage, after cracking up to the yield

line collapse load, the following equation is used to calculate the deflection.

$$\delta = \alpha \frac{P L_x}{k E_c I_e} \qquad (2.33)$$

where K is constant dependent on the aspect ratio, skew angle and material properties of the slab. See Ref (35) Page 8810. This result covers skew angles of 15^o, 30^o and 45^o degrees, aspect ratio of 1.5 and coefficients of orthotropy ranging from 1.222-2.136. is constant as given above.

I_{eff} is the cracked moment of inertia given by

$$I_{eff} = I_g \left(\frac{P_{cr}}{P}\right)^3 + \left[1 - \left(\frac{P_{cr}}{P}\right)^3\right] I_{cr} \qquad (2.34)$$

where P and I_g are defined above, P_{cr} is the cracking load and I_{cr} is the second moment of area of the cracked section.

Eqn (2.34) for effective moment of inertia I_{eff} is similar to the one in Ref (31) for beams and one way slabs. Here the moment terms are replaced by load intensity terms so the deflection can be calculated for any given load intensity.

In the third stage the deflection is calculated at the yield load by taking the effect of membrane force into consideration. The method is simple and starightforward for the first and second stages but is complicated for the third stage. As deflection calculation at this stage has little practical significant, it is not discussed.

2.3.4 Cracking

The problem of predicting the maximum crack width is very complex. Due to its stochastic nature, The assessment of crack widths is made using empirical equations derived following statistical approach. Two theories deal with the prediction of crack widths in the structural members.

(a) The slip theory assumes that the crack widths depend on the amount of bond slip in reinforcement and the crack widths are normally expressed in terms of steel stresses.

(b) The No slip theory considers the crack widths to be effectively zero at the face of reinforcing bar and the crack widths are expressed in terms of strains in concrete.

The No slip theory of cracking in reinforced concrete slabs has been developed by Beeby (114). Beeby (42) proposed the following design formula:

$$W = \frac{K4 \; a_{cr} \; \varepsilon_m}{1 + K_5 \left(\frac{a_{cr}-c}{h-x}\right)} \qquad (2.35)$$

where h is the overall slab depth, x is the neutral axis depth calculated ignoring tension stiffening, a_{cr} crack spacing, c the concrete cover and K_4 and K_5 are coefficients which depend upon the probability of crack width exceeding a give value. For the 20% level adopted in building and bridge practice, $K_4 = 3$, $K_5 = 2$ (Beeby (115), whilst for the 5% level adopted in the water-retaining code, the value of K_4 and K_5 are 4.5 and 2.5 respectively Clark (110).

ε_m is the strain calculated using the following equation

CP110 (30)

$$\varepsilon_m = 0.0007\, bh\, (a' - x)\, A_s\, f_s\, (h-x) \qquad (2.36)$$

where a' is the depth of the crack from the compression face,

A_s is the steel area, f_s the steel yield strength and h and x as given above.

Clark (110) has shown that Eqn (2.35) can be applied to slabs in which the principal stresses do not coincide with the reinforcement direction. In such cases, the crack width calculation should be carried out in the principal moment direction by using the equivalent areas of reinforcement discussed in section (2.3.5), and a should be measured perpendicular to the reinforcing bars most nearly aligned to the principal moment direction.

Beeby (38) investigated cracking in one-way slab and concluded that the no slip theory gives better prediction of crack widths than the slip theory. He also found that crack width and spacing are both linearly related to the distance from the point where the crack is measured to surface of the nearest bar.

For a Two-way slab Nawy (39) and and Orenstein (40) have proposed the following formula (in SI units):

$$w = K f_s \sqrt{(\phi\, s_o/\rho)\, (h-x)(d-x)} \qquad (2.37)$$

where K is a coefficient which depends on the loading and boundary conditions of slabs, ϕ is the diameter of bars perpendicular to the cracks under consideration, ρ is the effective steel ratio of these bars and s_o is the spacing of orthogonal bars (i.e. those parallel to the cracks). Thus, it is implied that cracks always form perpendicular

to bars, which is not necessarily true.

The reason for the spacing (s_o) of bars parallel to cracks being a parameter in Eqn (2.37) is that the equation was derived from tests on slabs reinforced with welded mesh. The location of the welded intersection influenced the crack patterns. It should be noted that Park and Gamble (6) have shown that Eqn (2.37) can grossly over-estimate crack widths when the transverse bar spacing (s_o) is large. However, when reinforcing bars are used, the spacing of the transverse bars is unlikely to influence significantly the crack spacing (114), (110).

Desayi and Kulkarni (41) also did extensive work on two way reinforced concrete slabs, and Prabhakara (42) extended the work to cover skew slabs subjected to uniformly distributed loading. Assuming the reinforcement is laid along the direction x and y Fig. (2.16) the spacing of cracks formed in the x-direction (a_x) is

$$a_x = \frac{K_t f_t A_{cty}}{\pi(\phi_x/S_x) k_b f_b \cos\theta + (\phi_y/S_y) f_{bb}} \qquad (2.38)$$

similarly the spacing of the cracks formed in the Y-Direction (a_y) is

$$a_y = \frac{k_t f_t A_{cty}}{\pi(\phi_x/S_x) K_b f_b \cos\theta + (\phi_x/S_x) f_{bb}} \qquad (2.39)$$

where A_{ctx} and A_{cty} are effective concrete areas in tension per unit width in the X and Y directions respectivly, and it can be calculated as follows;

$$A_{ctx} = 2(h-d_x)-A_{sx}$$

$$A_{cty} = 2(h-d_y)-A_{sy}$$

where h total depth of slab.

f_t tensile strength of concrete

ϕ_x, ϕ_y bar diameters in direction x and y

f_b bond stress

f_{bb} bearing stress

S_x, S_y spacing between bars in directions x and y

θ the angle of skew and is equal zero for orthogonal steel

K_b and K_t are constants

A_{sx}, A_{sy} area of reinforcement per uint width in the x and y directions respectivly

The maximum crack width is then estimated at any stage of loading from

$$W_{max} = a_{max}\, \epsilon_s\, R_c \qquad (2.40)$$

where a_{max} is the crack spacing at $M = M_{cr}$ and ϵ_s is the strain in the steel, R_c cover ratio $= (h-d_n)/(d-d_n)$ and d, d_n effective and neutral axis depths respectively

Test results have indicated that constants K_b = 1.0, f_{bb} =0.5 f_t, f_b =f_{ub} M/M_p and, f_{ub} = the ultimate bond stress can be taken from CP 110 (30) section(3.11.6). M, M_p are the applied ultimate moments in the direction of reinforcement.

The method estimates cracks widths with reasonable accuracy. One good aspect of the method is that it is independent of the type of loading and the aspect ratio of slab. The method is established for rectangular, square and skew slabs with skew angles of 15^o, 30^o, 45^o and with simply supported slabs or fixed support conditions

2.3.5 Stresses and Strains in Skew Bending

The BS 5400 code of practice (34) states that it is necessary to check cracks widths in highway brides under HA loading for loading combinations. This means that there is an indirect check on the reinforcement stress. It is desirable to ensure that the steel remains elastic under all serviceability conditions so that cracks which open under the application of occasional loading will close when the loading is removed.

The stresses, strains and curvature of a slab subjected to one way bending in the reinforcement direction are determined by straight forward application of conventional modular ratio theory, with the inclusion of tension stiffening when appropriate. However, in general, the principal stresses, strains and curvatures in a slab do not coincide with the reinforcement directions. It is then difficult to check accurately the stresses, strains and hence the curvature of a slab under general state of stress. Clark (34) has suggested the following approximate procedure for determining stresses:

i- Assume the section to be uncracked and calculate the four principal extreme fiber stresses caused by stress resultants due to the applied service loads.

ii- Where a principal tensile stress exceeds the appropriate limiting value of tensile strength of concrete, assume that cracks form perpendicular to the direction of that principal stress.

iii- Consider each set of cracks in turn and calculate an

equivalent area of reinforcement perpendicular to these cracks. (see step vi)

iv- Using the equivalent area of reinforcement, calculate the stresses in the direction perpendicular to cracks by using modular ratio theory.

v- If the calculated stress in the equivalent area of reinforcement is f_n, then calculate the stress in an i-th layer of reinforcement, inclined at an angle α_i to direction perpendicular to the cracks, from $f_i = \delta f_n$. The stress transformation factor δ is discussed below, after the factors determining the equivalent area of reinforcement normal to a crack have been considered.

vi- The calculation of equivalent area of reinforcement (step iii above) is explained by considering a point in a cracked slab Fig. (2.14) where the average direct and shear strains, referred to axes perpendicular and parallel to a crack are ε_n, ε_t, ε_{nt}.

The strain in the direction of an ith layer of reinforcement at angle α_i to the n-direction is given by

$$\varepsilon_i = \varepsilon_n \cos^2 \alpha_i + \varepsilon_t \sin^2 \alpha_i - \gamma_{nt} \cdot \sin \alpha_i \cos \alpha_i$$

Assuming only axial strains in the reinforcement, the steel stress is

$$f_i = E_s \varepsilon_i$$

where E_s is the elastic modulus of steel. If the steel area per unit width is A_i, the steel force per unit width is given by

$$F_i = A_i f_i$$

if N such layers of steel are considered, the total

resolved steel force per unit length in the n- direction is

$$F_n = \sum_{i=1}^{N} F_i \cos^2\alpha_i$$

$$= E_s \sum_{i=1}^{N} A_i (\varepsilon_n \cos^4\alpha_i + \varepsilon_t \sin^4\alpha_i - \gamma_{nt} \sin^2\alpha_i \cos^2\alpha_i)$$

The force F_n can also be considered in terms of an equivalent area (A_n) of reinforcement per unit width in the N-direction. Thus $F_n = A_n E_s \varepsilon_n$. Hence, by comparison with the previous equation,

$$A_n = \sum_{i=1}^{N} A_i(\cos^4\alpha_i + \frac{\varepsilon t}{\varepsilon_n} \sin^2\alpha_i \cos^2\alpha_i - \frac{\gamma_{nt}}{\varepsilon_n} \sin\alpha_i \cos^3\alpha_i \qquad (2.40)$$

It is reasonable, at the serviceability limit state to assume that the n- and t- directions will very nearly coincide with the principal strain directions. Thus γ_{nt} = 0, and the third term in the brackets of the above equation can be ignored.

There are now three cases to consider for a slab not subjected to significant tensile inplane stress resultants.

1- If the slab is cracked on one face only and in one direction only, $\varepsilon_n >> \varepsilon_t$ and the expression A_n can be taken as

$$A_n = \sum_{i=1}^{N} A_i \cos^4\alpha_i \qquad (2.41)$$

2- If the slab is cracked in two directions on the same face then ε_t will be the same sign as ε_n . If ε_t is again taken to be zero, the calculated value of A_n will be less than the true value. It is thus conservative to use Eqn

(2.41).

3- If the slab is cracked in two directions on opposite faces, ϵ_t will be of opposite sign to ϵ_n and could take any value. The precise value of ϵ_t/ϵ_n to adopt is then very difficult to determine directly, although some guidance is given by McNeice (45). Little error is involved in adopting the above method for An when the reinforcement is inclined at less than 25 to the direction perpendicular to the cracks. In slabs subjected to varying load patterns, the crack direction may not coincide with the principal strain direction of the load case under consideration. For such circumstances, it may be necessary to include γ_{nt} in an iterative procedure. This method is simple and straightforward and it is not dependent on the type of loading, but it is necessary to to carry out elastic analysis to find the stress resultants due to the applied loads. The stress transformation factor (δ), referred to previously should be taken as $\cos^2\alpha_i$.

2.4 NONLINEAR ANALYSIS

2.4.1 Introduction: Of the two methods used for analysis of slabs viz linear elastic analysis and plastic analysis,the first method is concerned with working load behaviour and the second method is concerned with behaviour at ultimate load. Neither approach provides information on structural behaviour in the intermediate range between the two limits.

Analysis to predict slab behaviour under a

prescribed load history requires nonlinear analysis which can be done using finite difference or finite element methods.

The finite difference method has been used to analyse plates by Bhaumik et al (43) and May et al (44) using the Tresca and Von Miss criteria. In this work the nonlinear analysis will be carried out using the finite element method.

2.4.2 Non-linear Analysis by Finite Element Method

To account for the nonlinearity due to cracking of concrete, yielding of steel and plastic flow under compressive stress in concrete, two basically different approaches have been used to obtain constitutive relations for use in finite element method. The first is a modified flexural rigidity approach in which an overall moment curvature relation reflecting the various stages of material behaviour is assumed. The second approach is based on idealized stress-strain relations for concrete and steel together with some assumption regarding compatibility of deformation between the constituent materials.

2.4.2.1 Macroscopic Models: In this model, concrete is assumed to be homogeneous and initially isotropic. Before cracking of concrete the reinforcement contributes little to moment of resistance (45).

In this case, material behaviour is linear elastic with the initial elastic matrix derived in the normal way

(4).

At the onset of cracking in the element, the stiffness of the element starts to decrease. The new stiffness at any stage of loading can be derived from the moment curvature diagram shown in Fig. (2.18), Jofriet and McNiece(45) used bilinear relationship of Beeby (38) before and after cracking

$$EI = E_c I_g \qquad \text{prior cracking} \qquad (2.42)$$

$$\grave{EI} = \grave{E_c} I_{cr} \qquad \text{after cracking} \qquad (2.43)$$

where $\grave{E_c} = 0.57 E_c$

Yielding of steel is not considered and thus any information about ultimate behaviour is not available.

Macroscopic models were also used by Bell and Elms (46, 47). In their model, the behaviour is idealised by a four stage moment curvature relationship, Fig. (2.18). Using the square yield assumption several intermediate loading surfaces were defined as shown in Fig.(2.19). The point on the moment-curvature curve corresponding to each surface is established and using the relative change of rigidity, the stiffness of an element satisfying a yield criterion is appropriately modified. Cook (6) has used a direct iteration procedure in the analysis in which the structure is solved successively under the load while stiffnesses are changed until equilibrium is reached. The use of moment curvature relationship is an extension of the elementary theory of bending in which the behaviour of concrete is not investigated in detail but only treated grossly in the tensile and compressive zones along two principal directions. Furthermore, if reinforcement

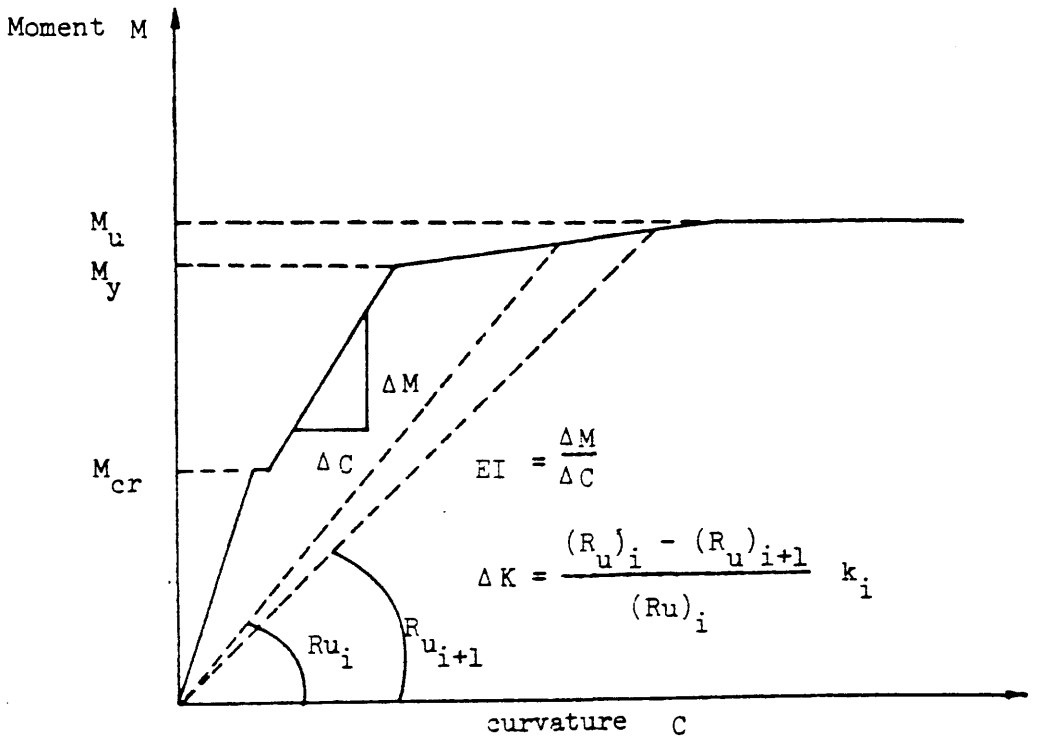

Fig. (2.18) Moment-curvature relationship for under-reinforced section

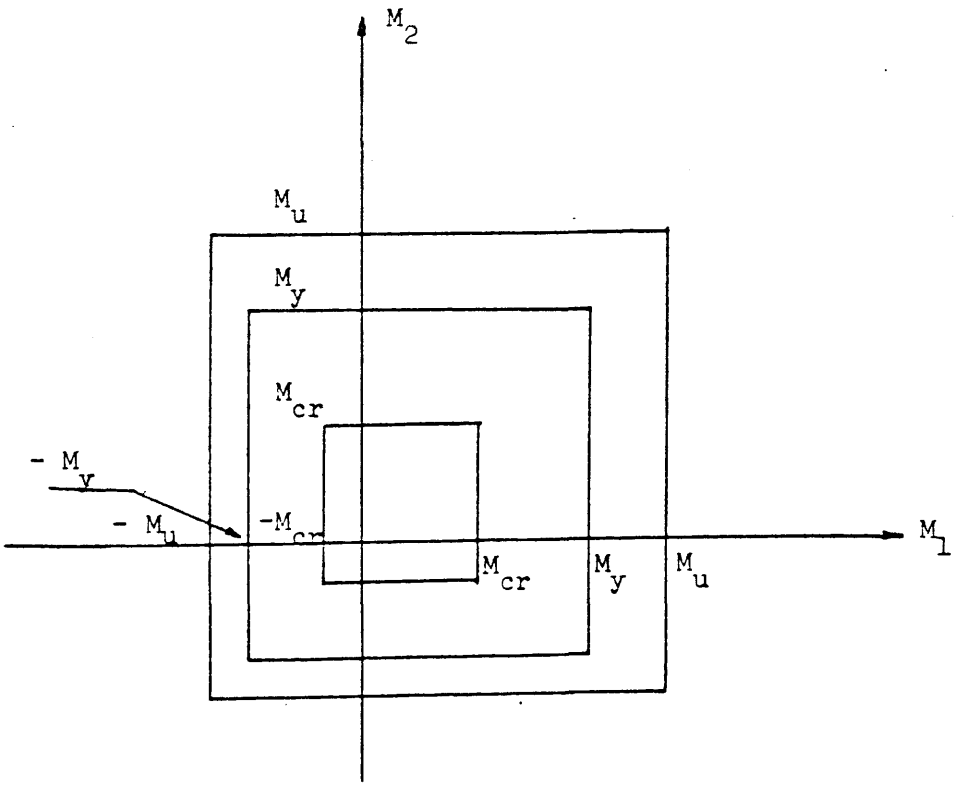

Fig. (2.19) Square yield surface

patterns vary, several moment-curvature may be needed for a single analysis. Load enhancement due to biaxial effects and the effects of constraint in the plane of structure are both neglected. Recent developments in these models involve the use of numerically integrated, high order elements for discretization, so that the variability of material properties within the element can be traced (49). Although all these models do not reflect the true variation of stress through the slab depth, the response can in most cases be predicted in a satisfactory manner (45).

2.4.2.2 Microscopic models

In this method, an attempt is made to simulate the spread of cracking over the depth of the element. The element is divided into a number of layers each of which may become plastic, or crack separately. Each layer is assumed to be in a state of plane stress and a linear strain variation over the depth of the slab is assumed based on the small deflection theory. As the number of layers is increased, this model provides a more realistic representation of the gradual spread of cracking over the depth of the element. In order to adjust the stresses and to evaluate stiffness characteristics of a layer, the constitutive relationships have to be defined according to the material state in that layer. This aspect will be considered in Chapter Four.

2.4.2.3 Review of Layer Finite Element Models

Layered approach is used widely with various types of elements. The first element used by Wegmuller (50) is a rectangular element with three degree of freedom (θ_x,θ_y ,w). The element ignores inplane effects, and thus assumes a fixed position for the middle plane of plate, such an assumption would be restricted only to problems in which membrane forces are negligible or there is little shift in neutral axis position.

For bending problems, as the cracking progresses deeper into the slab depth, the neutral axis shifts from its initial position towards the compression face. The layer approach has been used to solve this problem by taking the effect of membrane stresses into considerations. This of course requires additional inplane degrees to be incorporated in the element derivation. Wegmuller (51), Hand (52), Johanarry (53), Cope (54) and Hago (9) have used a rectangular element with five degrees of freedom (u,v,w, θ_x, θ_y) at each node. Hago (9) and Hand (52) have shown that inplane boundary conditions have a large effect on computed load deflection response. Cope and Rao (54) also studied this effect on fixed slabs and concluded that the neglect of inplane boundary has greater effects than relaxing of the restraints due to flexural boundary conditions.

Dotreppe et al (55) attempted to reduce computational effort by using a reduced bending stiffness model (similar to Wegmullter (50)). He assumed that membrane forces are zero and the bending stiffness was derived accordingly. Using this method the failure load of

a simply supported slab was underestimated by 10 %. This underestimate is interpreted as being due to the neglect of the inplane stresses. However, the assumption cannot be applied to problems in which there are inplane restraints. Abdel Rahman (56) used selective integration, 9 node, Hethos element based on Mindlin theory with five nodal degrees of freedom (u, v, w, θ_x, θ_y). He concluded that the use of initial stress method in the nonlinear analysis of reinforced concrete plates with coarse convergence tolerance may result in an overestimation of failure loads.

2.4.2.4 Modeling of Reinforcement

In developing a finite element model of reinforced concrete, at least three possible representations of reinforcement, Fig. (2.21), have been used:

1- An embedded representation: The reinforcing bar is considered to be an axial member built into the isoparmetric element such that its displacements are consistent with those of the element (66), (65).

2- A discrete representation: Axial force Members or bar links, may be used with two degrees of freedom at the nodes . Alternatively beam element may be used assumed to be capable of resisting axial force, shear, and bending, in this case three degrees of freedom are assigned at each end. This representation of steel has the limitation that the steel bars have to be along lines joining the predetermined nodes (66)

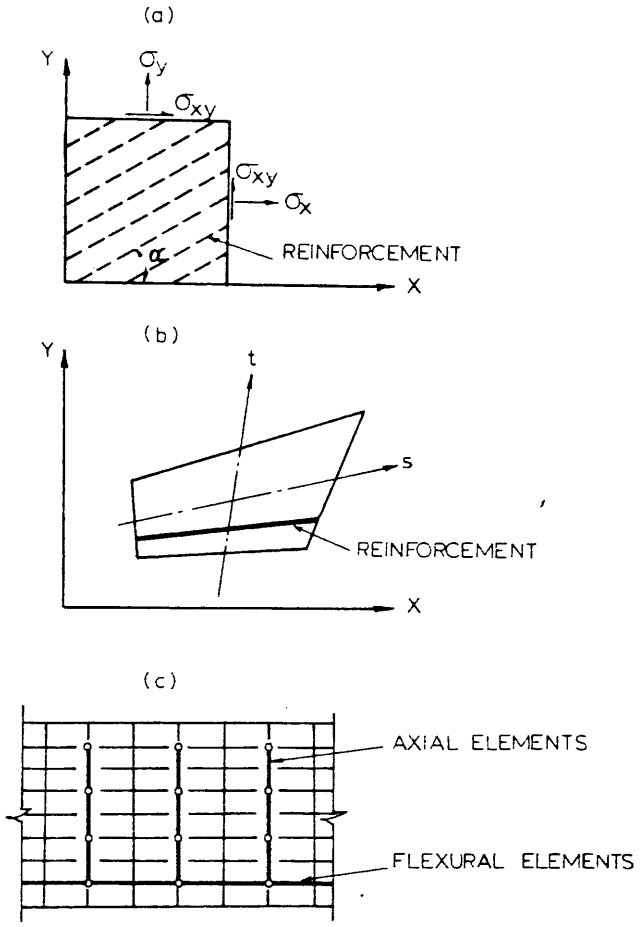

Fig. (2.20) Alternate representations of steel (a) distributed (b) embedded (c) discrete

3- Smeared model: The steel is assumed to be distributed over the concrete element with a given orientation angle. Perfect bond must be assumed between the concrete and steel and the steel is expected to resist stresses in the original bar direction only. For layered finite element analysis the smeared model is usually adopted. The steel layer is assumed to be elastic- plastic in both tension and compression with or without strain hardening. Bond slip is sometimes represented by reducing the modulus of steel (67). Details of layered element stiffness formulation will be given in Chapter Four.

2.4.3 The Observed Behaviour of Concrete

The main purpose of this section is to provide an initial description of some aspects of observed concrete behaviour, which will be useful in establishing the constitutive relationships of concrete under uniaxial and biaxial states of stress which result from in-plane stress states. It is important to note that discussions are limited to problems involving short term monotonic loading in which the effects of creep and cyclic loading can be neglected. The discussion is limited to the following aspects.

(a) Stress/strain relationship for concrete.

(b) Tension stiffening of cracked concrete

(c) Shear transfer in concrete

This will provide the necessary background for the later description of the constitutive modelling of the reinforced concrete flexural system in Chapter Four.

2.4.3.1 Stress-Strain relationship for Concrete

Concrete contains a large number of microcracks due to shrinkage especially at the interfaces between coarse aggregate and mortar even before any load has been applied. This property is decisive for mechanical behaviour of concrete. The propagation of these microcracks during loading contributes to the nonlinear behaviour of concrete at low stress level and causes volume expansion near failure. A typical stress strain relationship for concrete subjected to uniaxial compression in shown in Fig. (2.21a). The stress-strain curve has a linear-elastic behaviour up to about 30% its maximum compressive strength fc. For stresses above this point, the curve shows a gradual increase in curvature up to about 0.75fc to .90f_c where upon it bends more sharply and approaches the peak point at f_c. Beyond this peak the stress-strain curve has a descending part until crushing failure occurs at some ultimate strain (73). The behaviour of concrete in biaxial state of stress is dependent on the state of stress (70,71). Fig. (2.22) shows the stress-strain relationships of concrete under biaxial-compression. A maximum strength increase of approximately 25% is achieved at a stress ratio σ_1/σ_2 = 0.5 and the increase is only about 16% at equal biaxial-compression state (σ_1/σ_2 =1). Under biaxial compression-tension Fig. (2.23), the compressive strength decreases almost linearly as the applied tensile stress is increased. Under tension, the strength in biaxial state is almost the same as that of unaixial tensile strength (see Fig. (2.24))

The initial modulus of elasticity of concrete is

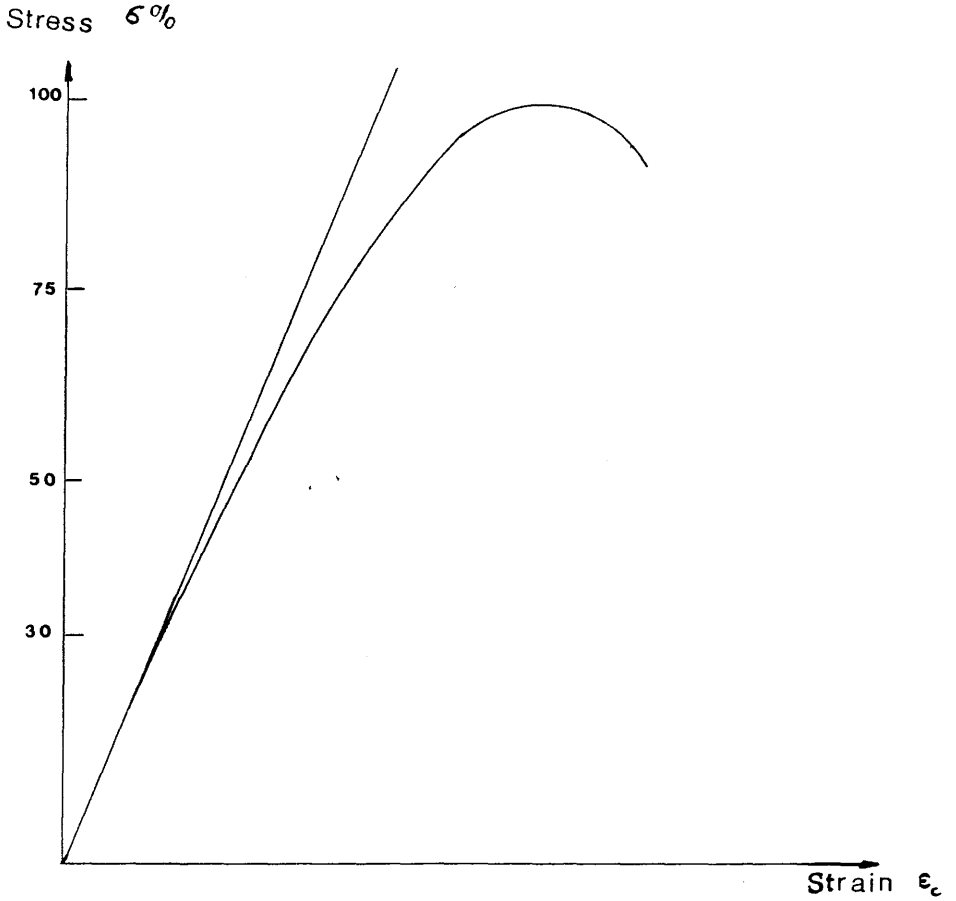

Fig. (2.21a) The stress-strain curve for uniaxial compression

Curve	Aggregate		Age, in mo
	Type	Size, in	
1	Granite	$\frac{3}{8}$ - $\frac{3}{16}$	2
2	Gravel	$\frac{3}{8}$ - $\frac{3}{16}$	2
3	Gravel	$\frac{3}{16}$ - B.S.7	3
4	Gravel	$\frac{3}{8}$ - $\frac{3}{16}$	2
5	Gravel	$\frac{3}{8}$ - $\frac{3}{16}$	1

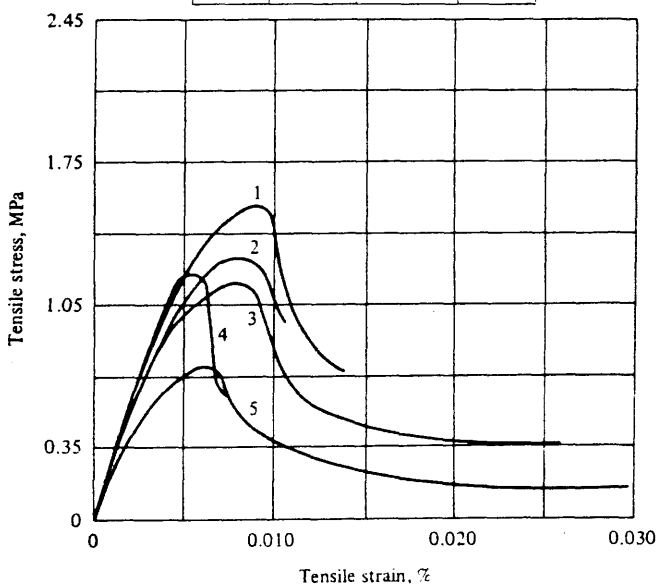

Fig. (2.21a) The stress-strain curve for uniaxial tension

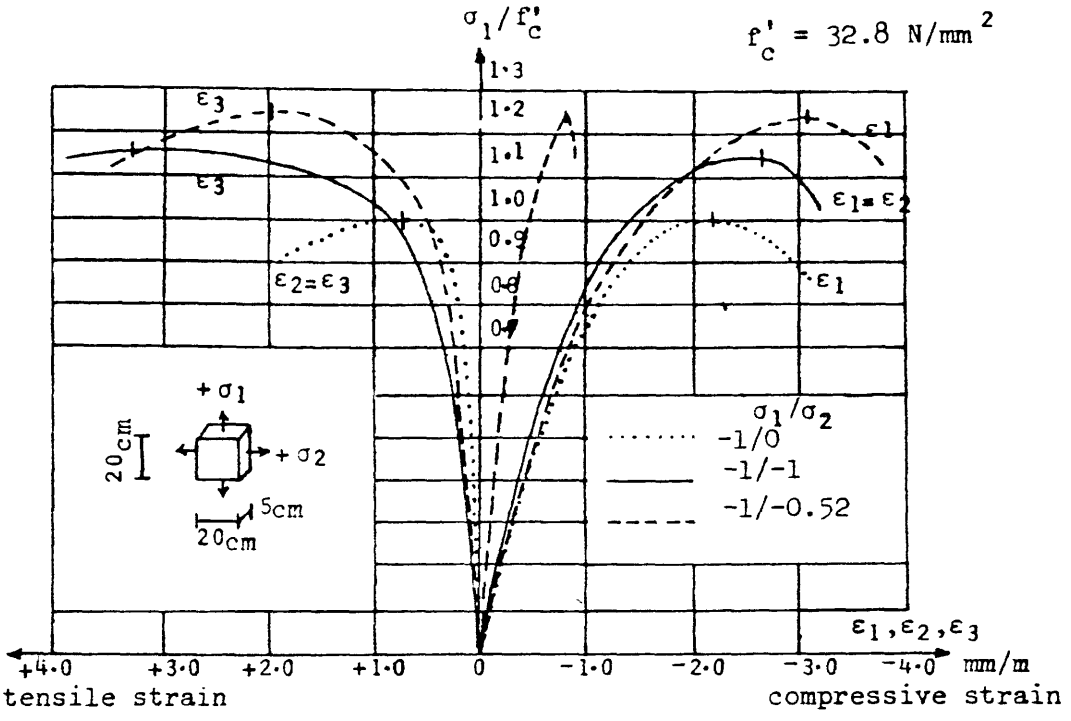

Fig. (2.22) Stress-strain relationships of concrete under biaxial-compression test (48)

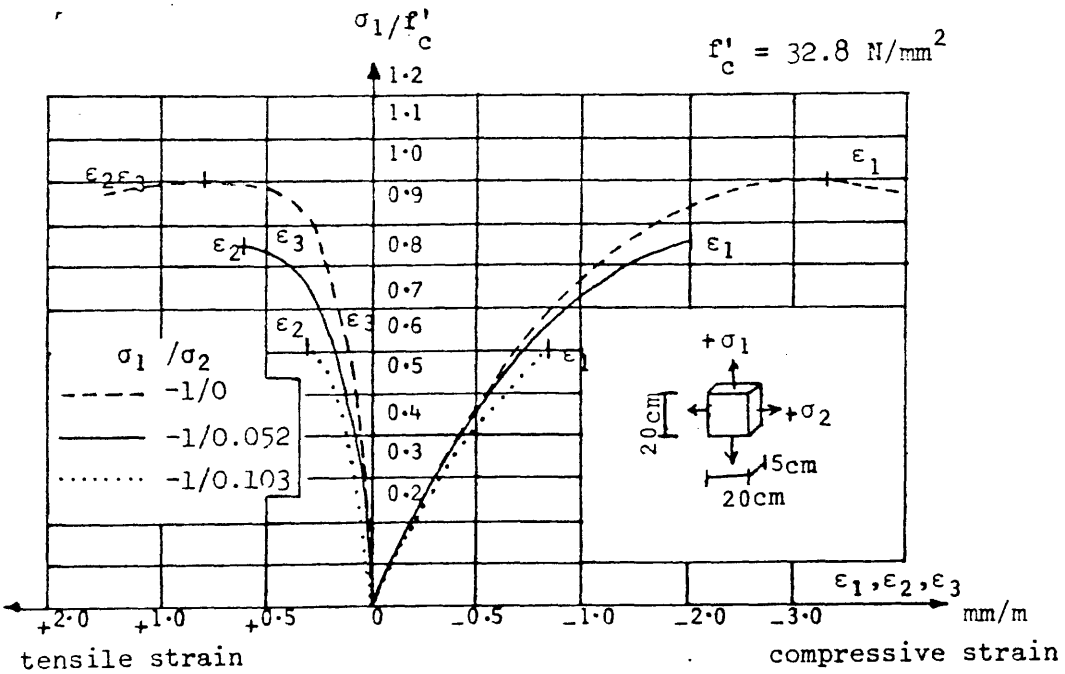

Fig. (2.23) Experimental stress-strain curves for biaxial tension-compression (48)

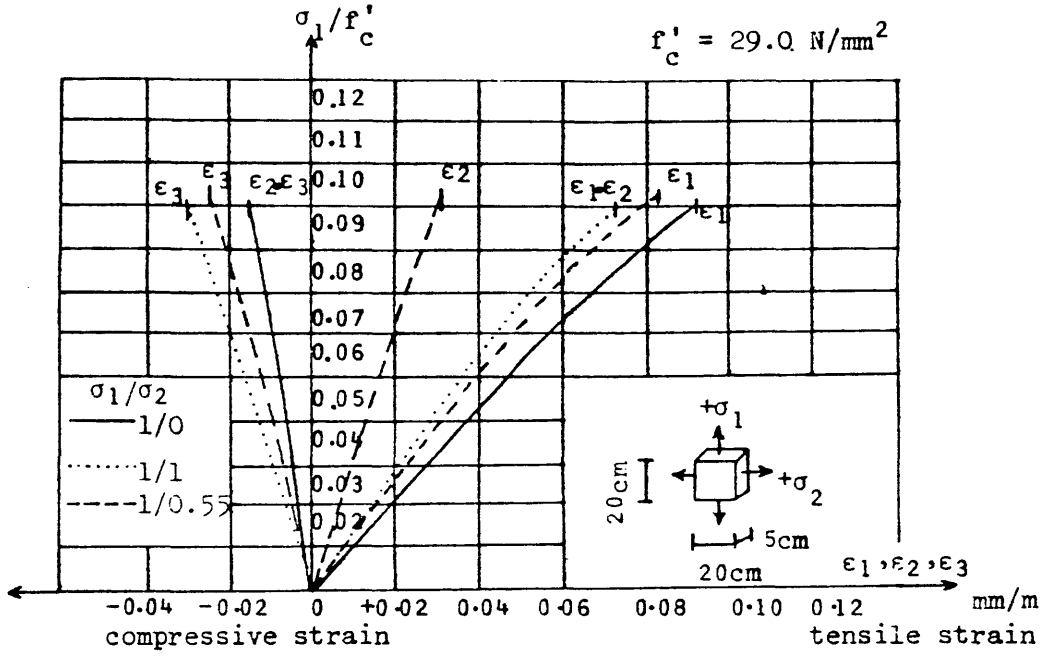

Fig. (2.24) Experimental stress-strain curves for biaxial tension (48)

highly dependent on the compressive strength. The initial modulus of elasticity E_c can be calculated with reasonable accuracy from the empirical formula (American Concrete Institute, 1977) (32)

$$E_c = .17058\ W\ f_c^{`}\ N/mm^2 \qquad (2.44)$$

Where W is the unit weight of concrete in (KN/m^3) and $f_c^{`}$ is the uniaxial compressive cylinder strength of concrete in (N/mm^2).

Poisson's ratio ν for concrete under uniaxial compressive loading is in the range of 0.15 to 0.22 with a representative value of 0.2. Under a uniaxial loading the ratio remains constant until approximately 80% of f_c at which stress the apparent Poisson's ratio begins to increase. For mathematical modelling, a value of of 0.19 (59) or 0.15 (53,9) has been extensively used.

Fig. (2.21b) shown the stress-strain curves for uniaxial tension. All are nearly linear up to a relatively high stress level. The ratio between uniaxial tensile and compressive strength may vary considerably but usually lies in the ranges of 0.05 to 0.1. The modulus of elasticity under uniaxial tension is somewhat higher and Poisson's ratio somewhat lower than in uniaxial compression. Liu et al (68) proposed the following mathematical relation for a biaxial stress-strain curve of concrete:

$$\sigma = \frac{A + B\ E_c\ \varepsilon}{(1 - \nu\alpha)(1 + C\varepsilon + D\varepsilon^2)} \qquad (2.45)$$

where σ, ε stress and strain in concrete, E_c, ν Young's

modulus and Poisson's ratio for concrete respectively, ratio of the principal stresses in concrete and A, B, C and D are constant and can be found from the following conditions

1. For $\varepsilon = 0.0$, $\sigma = 0.0$
2. For $\varepsilon = 0.0$, $\frac{\partial \sigma}{\partial \varepsilon} = E(1 - \nu\alpha)$
3. For $\varepsilon = \varepsilon_p$, $\sigma = \sigma_p$
4. For $\varepsilon = \varepsilon_p$, $\frac{\partial \sigma}{\partial \varepsilon} = 0.0$.

where σ_p and ε_p are the peak stress and peak strain in biaxial compression, respectively.

Substituting these in Eqn (2.44) and introducing the secant modulus at peak stress $E_{se} = \frac{\sigma_p}{\varepsilon_p}$,We have

$$\sigma = \frac{E_c \varepsilon}{(1-\nu\alpha)(1 + \frac{1}{(1-\nu\alpha)} \frac{E_c}{E_{se}} - 2)(\frac{\varepsilon}{\varepsilon_p}) + (\frac{\varepsilon}{\varepsilon_p})^2)} \qquad (2.46)$$

ε_p where is the plastic strain, and $\varepsilon_p = 0.0025$ for biaxial compression.

This equation was further investigated by Tasuji et el (69) and was found to represent the behaviour of concrete in both tension and compression.

4.3.4.2 Tension Stiffening of Cracked Concrete

Cracking is of prime importance in nonlinear behaviour of reinforced concrete elements. When a principal stress exceeds the tensile strength of concrete f_t , a crack forms in a direction normal to the direction of the offending principal stress.

Fig. (2.25) (36) shows the physical situation in

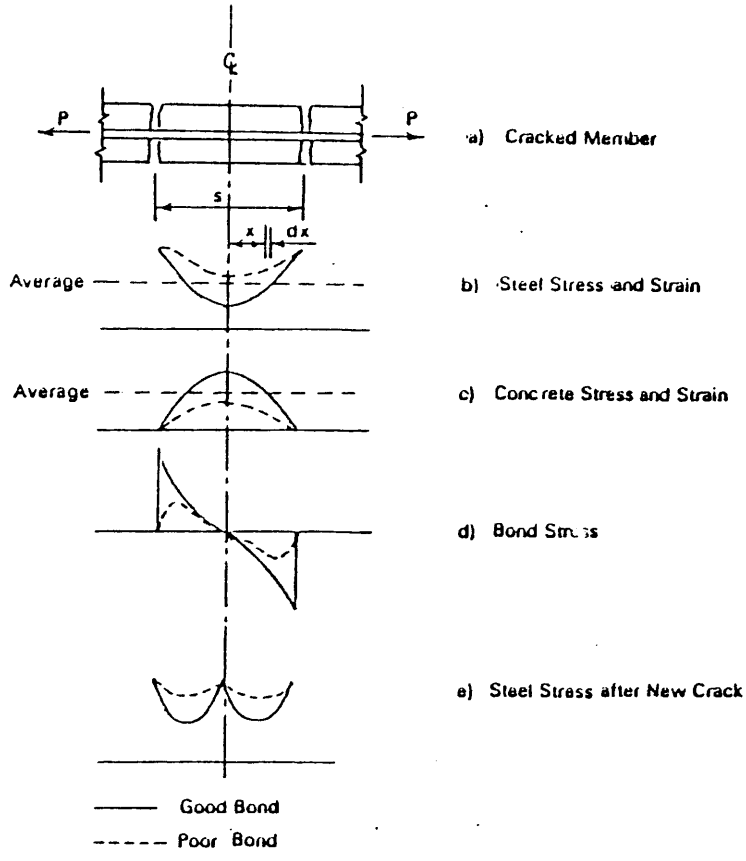

Fig. (2.25) Stress distribution in cracked reinforced concrete

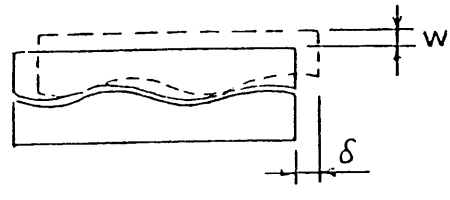

Fig. (2.26) Crack displacement

the vicinity of a crack in a reinforced concrete tension member. Fig. (2.26) indicates that at a crack the full load is carried by the reinforcement only, whereas between the cracks the load is shared between steel and concrete. This ability of concrete between cracks to share the tensile load with the reinforcement is termed tension stiffening. Thus while the concrete stress is zero at cracks, the average stress over a cracked region is not zero.

However as the load is increased and the stress in the concrete between cracks reaches the ultimate strength, then the concrete will rupture and a further crack forms between the main cracks. Therefore, the average concrete stress over the cracked region will progressively decrease with loading.

Apart from stress level, other factors affecting tension stiffening of concrete are the bond characteristics, the tensile strength of concrete, the crack spacings and the bar sizes and arrangements of bars. Some of these factors have been investigated by Clark and Cranston (58). These factors will be discussed in Chapter Four Section (4.5.2).

2.4.3.3 Shear Transfer in Cracked Concrete

The cracked surfaces of concrete are usually rough and irregular. When a force V is applied at a crack, both a tangential sliding δ and a normal displacement w result as shown in Fig. (2.27). When the normal displacement is

restrained by reinforcing bars crossing the crack, axial tensile stresses will develop in the reinforcement, which will then induce vertical compressive stresses in concrete. The resistance to sliding will then be provided by frictional force generated by the vertical compressive stresses in the concrete. This mechanism of shear transfer in cracked concrete is called the interface shear transfer mechanism (59). Apparently, the initial crack width is the primary variable affecting this mechanism. FenwicK and Pauley (60) performed direct shear tests which permitted the transfer of pure shear stresses across the precracked shear plane, while the crack width was held at a constant value. The following shear stress-displacement equation was proposed for the crack width and the concrete strength ranges employed:

$$v_a = (\frac{467}{c} - 8410)(0.0225\sqrt{f'_c} - 0.409)(\Delta - .0436c) \quad (2.47)$$

where v_a = interface shear stress transferred across crack (psi), c = initial crack width (in.), f_c = concrete compressive strength (psi) and Δ = shear displacement (in.)

Houde and Mirza (61) performed direct shear tests on precracked concrete blocks cracked along the shear plane with the initial crack width was set to a predetermined value. For the range of crack widths tested (0.002 in. to 0.02 in.) Houde and Mirza suggested the following shear stress-displacement relationship:

$$v_a = 57 (\frac{1}{c})^{3/2} \Delta (psi) \quad (2.48)$$

in which V_a is expressed in psi and c in in. An expression for the shear stiffness of cracked concrete K_a can be obtained by differentiating Eqn (4.48) with respect to Δ :

$$k_a = 57 \left(\frac{1}{c}\right)^{3/2} \text{ (psi)} \qquad (2.49)$$

AS is to be expected the shear stiffness of specimen decreased with increasing crack width. The following equation obtained from a regression analysis of the experimental results was proposed by Pauley and Loeber (72).

$$v_a = 73.0 + 50.9 \times 10^3 (\Delta)^2 \quad \text{psi} \qquad (2.50)$$

Pauley and Loeber (72) conclude that aggregate size, reinforcement ratio, bar size and concrete compressive strength are less important factors.

Fig. (2.27) Shows the relationship between the mean shear stress-shear displacement relationships considering the above mentioned three equations, by assuming the initial crack width is 0.3mm, concrete compression stress 40 N/mm^2 and the shear displacement ranges form 0.03 mm to 0.3 mm.

These curves revealed that the proposed Eqn (2.47) by Pauley and Loeber (72) is close to Eqn (2.48) by Houde and Mirza (61) although the second one does not depend on f_{cu}. Values predicted by Eqn (2.50) which is dependent only on the shear displacement are widely different from the values given by Eqns (2.47) and (2.48)

Another important mechanism of shear transfer in

cracked concrete is the dowel action of reinforcing steel. This mechanism develops when reinforcing bars, particularly those of larger diameters, cross a crack subject to shearing displacements. A significant part of shear force may be transmitted by dowel action in the bars (62). The main factors influencing the dowel behaviour are the dimensions of concrete cover around the bar, the presence of stirrups, the bar size and its yield strength and tensile strength of concrete.

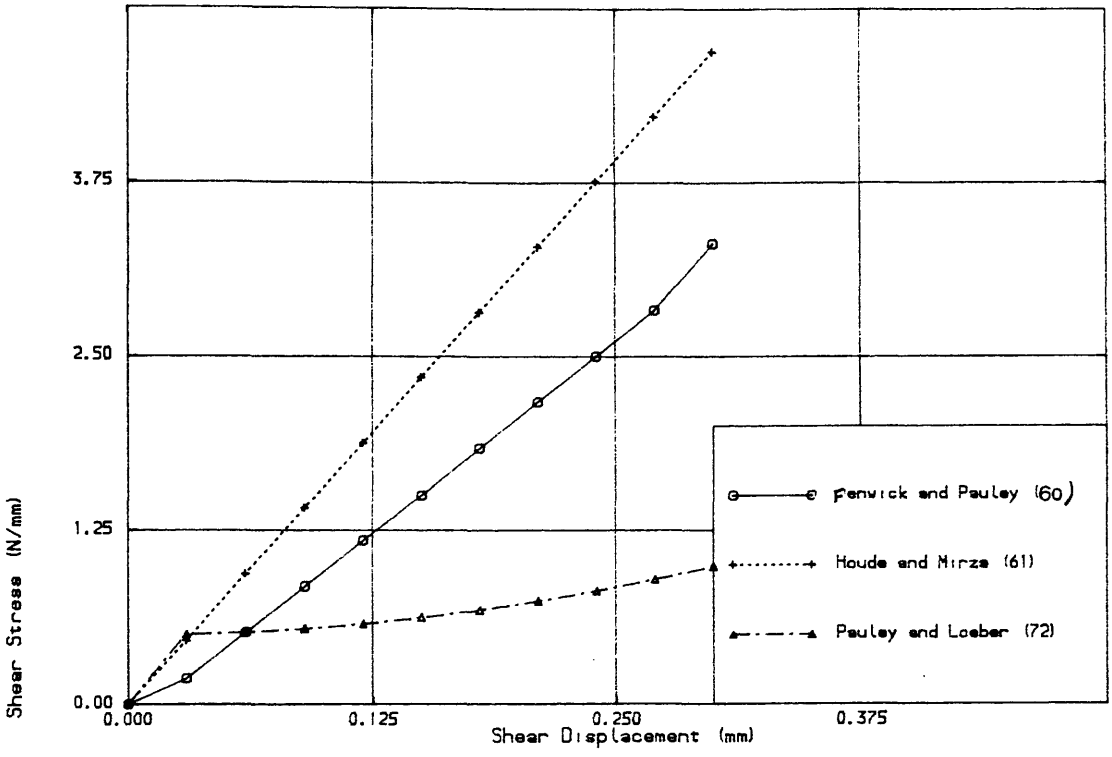

Fig. (2.27) The mean shear stress-shear displacement relationships for constant crack width for different authors

CHAPTER THREE

DESIGN OF REINFORCED CONCRETE SLABS

3.1 Introduction

In Chapter two the various methods available for the design of reinforced concrete slabs have been discussed. Most of these methods concentrate exclusively on ultimate loads. The direct design approach based on the theory of plasticity and on realistic understanding of material behaviour both at service and ultimate load will be examined in detail with particular reference to skew slabs.

In this chapter the following parameters will be discussed;

(a) The basic assumptions and terminology of the rigid-plastic theory of slabs.

(b) The direct design approach.

(c) The derivation of orthogonal and skew reinforcement design equations.

(d) The rules for placing steel reinforcement.

(e) Designing for membrane forces.

(f) Designing for combined bending and membrane forces.

3.2 THEORY OF PLASTICITY IN SLAB DESIGN

Assuming unlimited ductility, the correct solution to the ultimate load has to satisfy the following conditions of theory of plasticity:

1- The equilibrium condition: The internal stresses must

be in equilibrium with externally applied loads.

2- The yield criterion: The stress state must be such that the yield criteria for combined 'stresses' is not violated.

3- The mechanism condition: Under the ultimate load sufficient plastic regions must exist to transform the structure into a mechanism.

It is often not possible to find a design procedure satisfying the three conditions. Existing methods of design are either:

(a) An upper bound method which satisfies only conditions 3 by assuming a suitable collapse mechanism. Such a method is unsafe in that it provides a value of collapse load which is either greater than or equal to the true collapse load. The yield line method of reinforced concrete slabs is of this nature.

or (b) A lower bound method which satisfies conditions 1 and 2 by assuming a suitable stress field. This method is safe in that it provides a value of collapse load which is either less than or equal to the true collapse load. The various procedures based on Hillerborg's strip method falls into this category.

3.3 THE YIELD CRITERION

The yield criterion for a material is a mathematical description of the combinations of stresses which would cause yield of the material. In other words it is a relationship between applied stresses and strength.

The yield criterion for a slab element subjected only bending and twisting moments (M_x, M_y, M_{xy}) can be

written as

$$F(M_x, M_y, M_{xy}, M^*_x, M^*_y) = 0.0 \qquad (3.1)$$

where M^*_x and M^*_y are the uniaxial flexural strength of the slab in x and y directions respectively. The derivation of such yield criterion will be considered in this section. Consider the slab element Fig. (3.1) under the moment field M_x, M_y, M_{xy} per unit width. The sign convention adopted is that the direction of moments as shown in Fig (3.2) are positive. The following simplifying assumptions are:

(a) Bar diameters are small in comparison with the slab depth and bars can carry stress only in the direction of their original axes. Accordingly, kinking of bars across a yield line and dowel action are not considered.

(b) The concrete can carry no tensile stress.

(c) The slab is under-reinforced so that ductile failures occur.

(d) Membrane forces do not exist. It is acknowledged that the co-existence of such forces with flexural fields will considerably enhance or reduce the resisting moment of the slab depending on whether they are compressive or tensile, respectively. Such a case of mixed membrane forces and moments fields will be discussed in section (3.6).

For generality it is assumed that the skew reinforcement is at an angle α to the x- reinforcement measured clockwise from x axis Fig. (3.3).

The basic idea is that, if at any point P in a slab as shown in Fig. (3.3), a line with normal n and

tangentral direction t is examined then the normal moment M_n must not exceed the value M^*_n, in which M^*_n is the moment of resistance that the reinforcement in the slab could develop in direction n. This is therefore a normal moment criterion which is tested in every direction (76), (92).

Taking the normal to the yield line at an angle α to the x- axis, and considering the equilibrium of the element in Fig. (3.3), we have

$$M_n = M_x \cos^2\theta + M_y \sin^2\theta - 2 M_{xy} \sin\theta \cos\theta \qquad (3.2)$$

$$M_t = M_x \sin^2\theta + M_y \cos^2\theta + 2 M_{xy} \sin\theta \cos\theta \qquad (3.3)$$

$$M_{nt} = (M_x - M_y) \sin\theta \cos\theta + M_{xy}(\cos^2\theta - \sin^2\theta) \qquad (3.4)$$

Johansen's stepped criterion of yield in case of skew reinforcement Fig. (3.4), can be used to express the moment of resistance as follows.

$$M^*_n = M^*_x \cos^2\theta + M^*_\alpha \sin^2(\theta-\alpha) \qquad (3.5)$$

$$M^*_t = M^*_x \sin^2\theta + M^*_\alpha \cos^2(\theta-\alpha) \qquad (3.6)$$

Therefore, when designing the steel, the resistance to normal moment should be checked in every direction. Accordingly

$$M^*_n - M_n \geq 0 \qquad (3.7)$$

substituting (3.2) and (3.5) in (3.7) we have

Excess strength =

$$(M^*_x - M_x + M^*_\alpha \cos^2\alpha)\cos^2\theta + (M^*_\alpha \sin^2\alpha - M_y)\sin^2\theta +$$

$$2(M_{xy} + M^*_\alpha \sin\alpha \cos\alpha) \sin\theta \cos\theta \geq 0.0$$

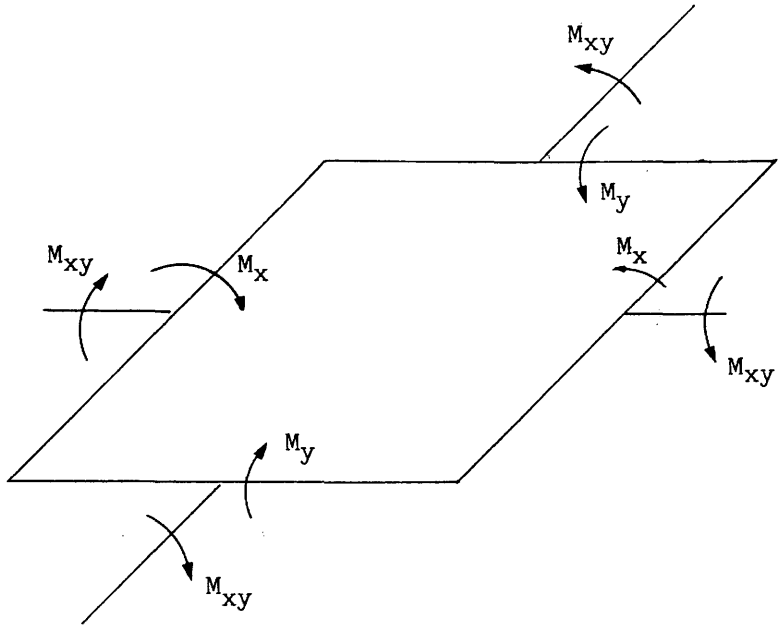

Fig. (3.1) Notation for moments on an element (positive as shown)

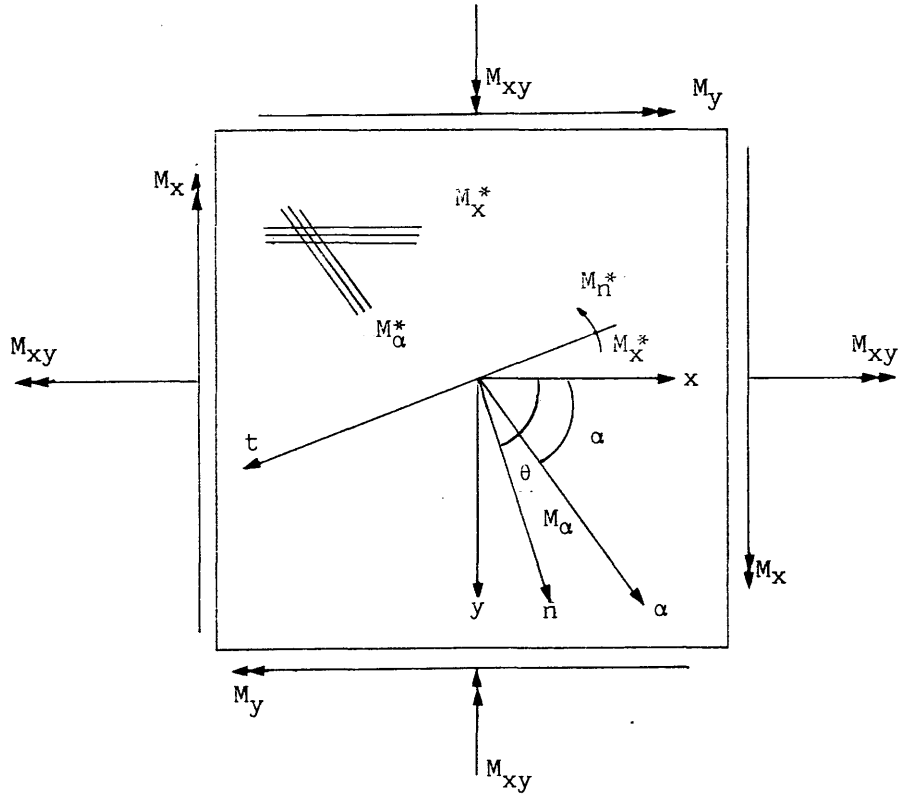

Fig. (3.2) Element with skew reinforcement

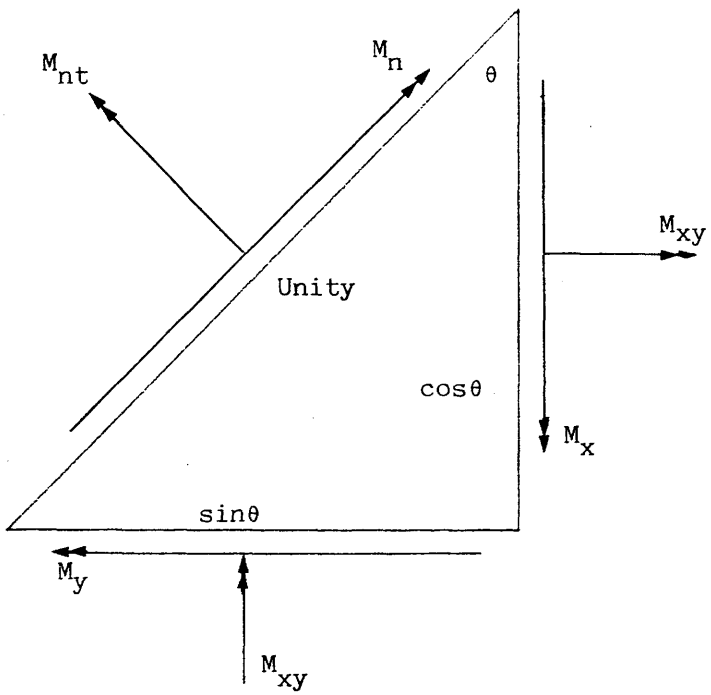

Fig. (3.3) Equilibrium of a slab element under moment field

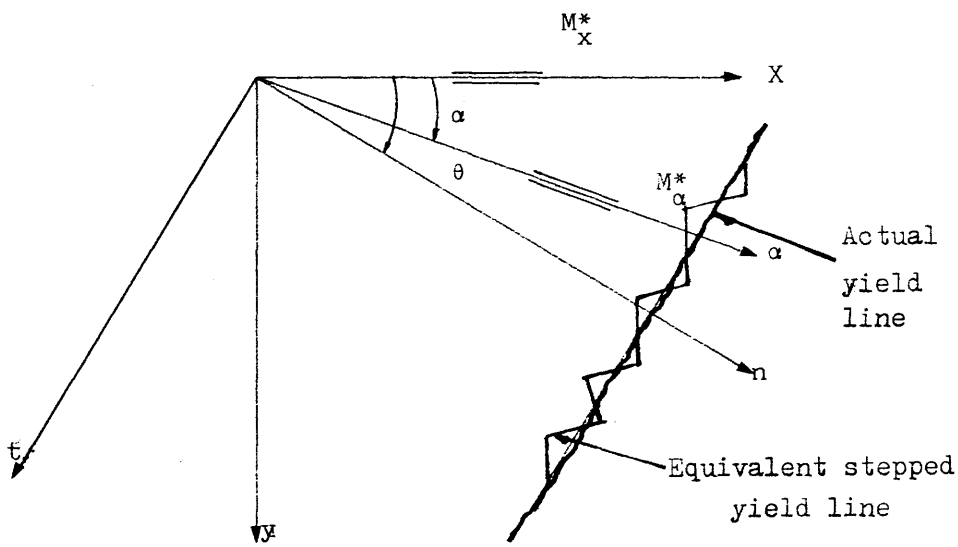

Fig. (3.4) Idealized yield line (Johansen's stepped yield criterion)

or

$$A \cos^2\theta + B \sin^2\theta + 2\,C \cos\theta \sin\theta \geq 0.0$$

where

$$A = M^*_x - M_x + M^*_\alpha \cos^2\alpha$$

$$B = M^*_\alpha \sin^2\alpha - M_y$$

$$C = M_{xy} + M^*_\alpha \sin\alpha \cos\alpha$$

dividing by $\cos\theta$ and putting $k = \tan\theta$

$$A + Bk^2 + 2\,Ck \geq 0.0 \qquad (3.8)$$

For optimum steel, excess strength must be a minimum.

$$Bk + C = 0.0 \text{ and since } B > 0.0 \text{ i.e. } M^*_\alpha > \frac{M_y}{\sin\alpha^2}$$

or

$$k = -C/B \qquad (3.9a)$$

by substituting the values of B and C in equation (3.9a) we get

$$k = \frac{-(M_{xy} + M^*_\alpha \sin\alpha \cos\alpha)}{(M^*_\alpha \sin^2\alpha - M_y)} \qquad (3.9b)$$

This gives the orientation of the plane of minimum resistance of skew steel. For the special case of orthogonal steel $\alpha = 90$ then

$$k = -\frac{M_{xy}}{M^*_{90} - M_y} \qquad (3.9c)$$

Substituting Eqn (3.9a) in Eqn (3.8) and using equality sign for minimum resistance, then

$$A + B\,(-C/B)^2 + 2C\,(-C/B) = 0.0$$

$$AB - C^2 = 0.0 \qquad (3.10)$$

Substituting the value of A and B in Eqn (3.10) we get

$$(M^*_x - M_x + M^*_\alpha \cos^2\alpha)(M^*_\alpha \sin^2\alpha - M_y) - (M_{xy} + M^*_\alpha \sin\alpha \cos\alpha)^2 = 0.0 \qquad (3.11a)$$

Eqn (3.11a) is the yield criterion for skew reinforced concrete slabs.

The yield criterion of orthogonal steel case for $\alpha = 90$ is given by

$$(M^*_x - M_x)(M^*_{90} - M_y) - M^2_{xy} = 0.0 \qquad (3.11b)$$

Which is the same equation arrived at by Save (81), Nielsen (91), Lenchow and Sozen (80), Kemp (79).

This has been confirmed for orthogonal steel case by works of Lenschow and Sozen (80), Cardenes and Sozen (82), Lenkei (83), and Jain et al (84). Morley (85) has shown that an explicit yield criterion can only be obtained if it is assumed that the concrete had an infinite compressive strength. The reason for this is that, with finite concrete compressive strength, the neutral axis depth and hence the lever arm of the steel vary with direction and consequently the moments of resistance do not transform according to Mohr's circle. This means that the transformations in Eqns (3.2), (3.3) (3.5) (3.6) are only true for a slab of infinite concrete compressive strength, when the neutral axis obviously lies at the surface of the slab, and in which the lever arm of steel is its effective depth. Hence M^*_x, M^*_α are the moments, about the extreme surfaces of the steel forces. This lever arm is greater than the true lever arm in the

actual slab of finite concrete compressive strength and thus leads to an overestimation of the strength of the slab. Thus, Since Eqn (3.11a) form the exact yield criterion for a slab of infinite concrete compressive strength, they will give an upper bound on the yield criterion of a slab with the same steel arrangement but with finite concrete compressive strength. However in most practical situations, the error is very small.

For yield of steel at top surface of the slab, a similar procedure to the one just described for positive yield can be applied . If the top steel layer are laid in X and α directions to provide the resisting moments M^*_x and M^*_α respectively, then the yield condition with negative steel can be written as

$$(\bar{M}^*_x + M_x - \bar{M}^*_\alpha \cos^2\alpha)(\bar{M}^*_\alpha \sin^2\alpha + M_y) - (M_{xy} - \bar{M}^* \sin\alpha \cos\alpha)^2 = 0.0 \qquad (3.12a)$$

If $\alpha = 90$ for orthogonal steel case, the yield criterion is given by

$$(\bar{M}^*_\alpha + M_x)(\bar{M}^*_{90} + M_y) - M^2_{xy} = 0.0 \qquad (3.12b)$$

where both M_x and M_y are negative moments.

3.4 THE DIRECT DESIGN APPROACH

The proposed design approach is very simple and straightforward. The method satisfies the three conditions of theory of plasticity as discussed below.

3.4.1 The Equilibrium Condition

In general it is very difficult to find moment fields (other than elastic moment fields) which satisfy the equilibrium equation (2.2). Elastic moment fields based upon uncracked stiffness using finite element method will be used to design slabs at ultimate limit state because elastic solutions are easily determined for most structures and prior knowledge of the reinforcement is not required.

3.4.2 The Yield Condition and Design Equations

The yield condition will be satisfied if the strength at any point is made equal to or greater than the applied stresses, as can be seen in Eqns (3.11) and (3.12) for bottom and top steel. An elastic analysis of the slab under the ultimate load by the finite element provides the stress resultants M_x, M_y, M_{xy} for laterally loaded plates. Using these moments in the yield criterion, the design equations can be derived.

3.4.3 Design of Skew Reinforcement

(a) Positive moment fields:

Referring to Eqn (3.11a):

$$M_x^* = \frac{(M_{xy} + M_\alpha^* \cos\alpha \sin\alpha)^2}{M_\alpha^* \sin^2\alpha - M_y} + M_x - M_\alpha^* \cos^2\alpha \qquad (3.13)$$

The total amount of steel at any point is proportional to

$$M_x^* + M_\alpha^* = \frac{(M_{xy} + M_\alpha^* \cos\alpha \sin\alpha)^2}{M_\alpha^* \sin^2\alpha - M_y} + M_x + M_\alpha^* (1 - \cos^2\alpha) \qquad (3.14)$$

So that for a minimum steel

$$\frac{d(M_x^* + M_\alpha^*)}{d(M_\alpha^*)} = 0.0 \qquad (3.15)$$

From Eqns (3.14) and (3.15) we get

$$M^*_\alpha = \frac{M_y \pm \sqrt{M_y^2 \cos^2\alpha + 2 M_y M_{xy} \cos\alpha \sin\alpha + M_{xy}^2 \sin^2\alpha}}{\sin^2\alpha}$$

simplifying

$$M^*_\alpha = \frac{M_y}{\sin^2\alpha} \pm \left(\frac{M_y \cos\alpha + M_{xy} \sin\alpha}{\sin^2\alpha}\right)$$

since $$M^*_\alpha > \frac{M_y}{\sin^2\alpha}$$

$$\therefore \quad M^*_\alpha = \frac{M_y}{\sin^2\alpha} + \left| \frac{M_y \cot\alpha + M_y}{\sin\alpha} \right| \qquad (3.16)$$

referring to Eqn (3.13)

$$M^*_x = M_x - M^*_\alpha \cos^2\alpha + \frac{M_{xy} + M^*_\alpha \sin\alpha \cos\alpha}{M^*_\alpha \sin^2\alpha - M_y} \qquad (3.17)$$

since $$M^*_\alpha = \frac{M_y}{\sin^2\alpha} + P$$

where $$P = \left| \frac{M_x + M_y \cot\alpha}{\sin\alpha} \right|$$

substituting the value of M^*_α in Eqn (3.17) we get

$$M^*_x = M_x + \frac{(M_{xy} + M_y \cot\alpha)^2 + P(M_y \cos^2\alpha + 2M_{xy} \sin\alpha \cos\alpha)}{P \sin^2\alpha}$$

substituting the value of P we get

$$M^*_x = M_x + M_y \cot\alpha^2 + 2M_{xy} \cot\alpha + \left| \frac{M_{xy} + M_y \cot\alpha}{\sin\alpha} \right| \qquad (3.18)$$

For orthogonal steel $\alpha = 90$ the two Eqns (3.16) and (3.18) will be reduced to

$$M^*_x = M_x + |M_{xy}| \qquad (3.19)$$

$$M^*_{90} = M_y + \left| M_{xy} \right| \qquad (3.20)$$

(b) Negative moment fields

For negative steel at the top of the slab, similar procedure to the one just described for positive steel can be applied using the negative yield criterion. The corresponding Eqns to (3.16) and (3.18)

$$M^*_x = M_x + 2M_{xy} \cot \alpha + M_y \cot^2\alpha - \left| \frac{M_{xy} + M_y \cot \alpha}{\sin \alpha} \right| \qquad (3.21)$$

$$M^*_\alpha = \frac{M_y}{\sin^2\alpha} - \left| \frac{M_{xy} + M_y \cot \alpha}{\sin \alpha} \right| \qquad (3.22)$$

For $\alpha = 90$ the case will be reduced for the case of orthogonal steel, which can be written as follows

$$M^*_x = M_x - \left| M_{xy} \right| \qquad (3.23)$$

$$M^*_{90} = M_y - \left| M_{xy} \right| \qquad (3.24)$$

(c) Mixed moment fields

For Positive moment fields if $M^*_\alpha = 0.0$ then from yield criterion Eqn (3.11)

$$M^*_x = \frac{-M^2_{xy}}{M_y} + M_x$$

since $M^*_x > M_x$

$$M^*_x = M_x + \left| \frac{M^2_{xy}}{M_y} \right| \qquad (3.25)$$

If $M^*_x = 0.0$ then from yield criterion Eqn (3.11b)

$$M^*_\alpha = \frac{M_x M_y - M^2_{xy}}{M_x \sin^2\alpha + M_y \cos^2\alpha + 2M_{xy} \sin \alpha \cos \alpha}$$

rearranging

$$M^*_\alpha = \frac{M_y}{\sin^2\alpha} - \frac{(M_{xy} + M_y \cot \alpha)^2}{\sin^2\alpha (M_x + 2M_{xy} \cot \alpha + M_y \cot^2\alpha)}$$

since $M^*_\alpha > \frac{M_y}{\sin^2\alpha}$

$$\therefore \quad M^*_\alpha = \frac{1}{\sin^2\alpha}\left[M_y + \left|\frac{(M_{xy} + M_y \cot\alpha)^2}{(M_x + 2M_{xy}\cot\alpha + M_y \cot^2\alpha)}\right|\right] \qquad (3.26)$$

For orthogonal steel $\alpha = 90$

$$\therefore \quad M^*_{90} = M_y + \left|\frac{M^2_{xy}}{M_x}\right| \qquad (3.27)$$

For negative moment fields considering the negative yield criterion and following the same procedure the corresponding expressions for negative steel are:

$$M^*_x = M_x - \left|\frac{M^2_{xy}}{M_y}\right| \quad \text{where} \quad M^*_\alpha = 0.0 \qquad (3.28)$$

$$M^*_\alpha = \frac{1}{\sin^2\alpha}\left[M_y - \left|\frac{(M_{xy} + M_y \cot\alpha)^2}{M_x + 2M_{xy}\cot\alpha + M_y \cot^2\alpha}\right|\right] \qquad (3.29)$$

where $M^*_x = 0.0$

For $\alpha = 90$ The corresponding Eqn (3.29) is

$$M^*_{90} = M_y + \left|\frac{M^2_{xy}}{M_x}\right| \qquad (3.30)$$

3.4.3.1 Rules For Placing Skew Reinforcement

Given the stress field (M_x, M_y, M_{xy}) with angle of skew equal α at any point on the slab, the reinforcement in the x and α directions will be placed according to following rules:

(a) Bottom steel

(1) Compute the design moments M^*_x and M^*_α from Eqns (3.16) and (3.18).

(2) If $M^*_x < 0$, then set $M^*_x = 0.0$ and calculate M^*_α from

Eqn (3.26). If $M^*_\alpha < 0$, then $M^*_x = M^*_\alpha = 0.0$.

or

(3) If $M^*_\alpha < 0$, then set $M^*_\alpha = 0$ and calculate M^*_x from Eqn (3.25). If $M^*_x < 0$, then $M^*_x = M^*_\alpha = 0.0$.

or

(4) If both M^*_x and $M^*_\alpha > 0.0$ then adopt the calculated values as the design moments.

or

(5) If both M^*_x and $M^*_\alpha < 0.0$ then $M^*_x = M^*_\alpha = 0.0$

(b) Top Reinforcement:

(1) Compute the design moments M^*_x and M^*_α from Eqns (3.21) and (3.22).

(2) If $\bar{M}^*_x > 0$, then set $\bar{M}^*_x = 0.0$ and calculate $\bar{M}^*_\alpha$ from Eqn (3.29). If $\bar{M}^*_\alpha > 0$, then $\bar{M}^*_x = \bar{M}^*_\alpha = 0.0$.

or

(3) If $\bar{M}^*_\alpha > 0$, then set $\bar{M}^*_\alpha = 0$ and calculate $\bar{M}^*_x$ from Eqn (3.28). If $\bar{M}^*_x > 0$, then $\bar{M}^*_x = \bar{M}^*_\alpha = 0.0$.

or

(4) If both $\bar{M}^*_x$ and $\bar{M}^*_\alpha < 0.0$ then adopt the calculated values as design moment.

or

(5) If both $\bar{M}^*_x$ and $\bar{M}^*_\alpha >$ the $\bar{M}^*_x = \bar{M}^*_\alpha = 0.0$

For the bottom, if $M^*_x = M^*_\alpha = 0.0$ then the minimum steel may be provided according the code of practice. For the top if $\bar{M}^*_x = \bar{M}^*_\alpha = 0.0$ then the mimimum steel may be provided according the code of practice.

3.4.3.2 Multiple Loading Cases

The above rules apply only when the slab is

subjected to a moment field resulting from a single load case. In practice, many slabs and particularly bridge decks are subject to multiple loading cases. The reinforcement must then be proportioned to satisfy the multiple moment triads (M_{xi}, M_{yi}, M_{xyi}) i = 1,...., No. of load cases. For multiple loading cases, the problem can be attacked in the following steps.

1- Using the design equations in section (3.5), For each case of loading i, calculate the corresponding M^*_{xi}, $M^*_{\alpha i}$.

2- Calculate the Maximum of all the M^*_{xi} and $M^*_{\alpha i}$ taking into consideration all the load cases. let these be M^*_{xmax}, $M^*_{\alpha max}$.

Evidently if we use these as the design moments, then a safe design will result but not necessarily an optimum design. So we move towards an optimum design as follows.

3- Assume that in the x direction we provide $M^*_{x\ max}$, but in the α direction we provide $M^*_{\alpha i}$ so a to satisfy the yield criteria. In each case $M^*_{\alpha i}$ is given by

$$M^*_{\alpha i} = \frac{1}{\sin^2\alpha}\left| M_y + \frac{(M_{xy} + M^*_{\alpha i} \sin\alpha \cos\alpha)^2}{(M^*_{xmax} - M_x + M^*_{\alpha i} \cos^2\alpha)} \right| \qquad (3.31)$$

Calculate the maximum of all these $M^*_{\alpha i}$, let that be M^*_{emax}. Evidently, a safe design is produced if we use M^*_{xmax} in conjunction with the $M^*_{\alpha emax}$ determined so as to satisfy the yield criteria.

4- A similar procedure to 3 above can be done using Eqn (3.32), if we choose $M^*_{\alpha max}$ as the design moment in direction and calculate the M^*_{xi} for each load so as to

satisfy the yield criteria and choose the maximum of all the M^*_{xi} to determine the design moment in the x direction, let that to be $M^*_{\alpha emax}$. The M^*_{xi} in each case is given by

$$M^*_{xi} = M_x - M^*_{\alpha\,max}\cos^2\alpha - \frac{(M_{xy} + M^*_{\alpha max}\sin\alpha\cos\alpha)^2}{M^*_{\alpha\,max}\sin\alpha - M_y} \qquad (3.32)$$

(5) Therefore a better design is to choose.

(6) We can stop at this stage but we can improve on this by assuming that other combinations are possible and use a simple search technique to get the smaller of two sets of design moments Viz;

$(M^*_{xmax} + M^*_{\alpha max})$ or $(M^*_{\alpha\,max} + M^*_{xemx})$ This can be done by examining the feasible design region as shown in Fig. (3.8). For each load case check if the design moment at the grid points is a better minimum. If it is not, reject it. If it is a better minimum, then check to see if it violates the yield criteria. If it does, reject it, if not see at which grid pint we can get a minimum of (M^*_x + M^*_α). This gives us the optimum design moments.

The above procedure is adopted for positive steel, the same procedure can be used for negative steel, in which case, the minimum replaces the maximum in the above steps. A similar procedure has been explained by Kemp (86).

3.4.3 3 Design of Reinforcement For Membrane Forces

Table (3.1) summarizes the expressions for the areas of reinforcement, principal stresses in concrete and

the angle of the major principal concrete stress to x axis for each case derived by Clark (37). Fig. (3.6) shows the sign convention of the applied stresses. Fig. (3.7) shows the directions of reinforcement and principal stresses in concrete. . The following symbols are used in Tables (3.1) and (3.2) and Fig (3.7):

A_x, A_y and A_α reinforcement areas per unit length in the x, y and α directions respectively.

f_c yield stress of concrete as shown in Fig. (3.5).

f_s and f'_s tension and compression steel yield stresses.

σx, σy and τxy in-plane direct and shear stresses per unit length.

θ orientation of major principal concrete stress to x axis

ρ_x, ρ_y and ρ_α are the reinforcement ratios in the x,y and directions respectively.

σ_1, σ_2 principal concrete stresses

$$\sigma_{xf} = \sigma_x - f_c$$

$$\sigma_{yf} = \sigma_y - f_c$$

$$B = \sqrt{1 - \frac{4}{f_c^4}\,(\tau_{xy} + \sigma_y \cot\alpha)(\tau_{xy} + \sigma_{yf} \cot\alpha)}$$

When $\alpha = 90$ we have the case of orthogonal reinforcement, and The expressions in table (3.1) reduce to these given in table (3.2)

3.4.3.4 Design For Combined Bending and Membrane Forces

The stress sextad in this case becomes (N_x, N_y, N_{xy}, M_x, M_y, M_{xy}), and to design for all the six

components, a filled sandwich model in Fig. (3.9) is used (37, 87,90). In such an approach, all six stress resultants are resolved into a set of inplane stress resultants acting at the outer shells of the sandwich. Fig. (3.11) shows such an element, whereas Figs (3.10) and (3.11) show the resolution of these forces and how they are all lumped at the level of the reinforcements. The basic assumption behind such methods is that the reinforcement will be centrally positioned in the outer shells of the element. Further to simplify the problem for designers, it is best to assume that

$$Z_x = Z_y = Z_{xx}$$

$$X_x = X_y = X_{xx}$$

$$Y_x = Y_y = Y_{xx}$$

where Z_{xx} is some reasonable average value of the distance between the top steel layer and bottom steel layer (or between the compression zone and tension zone if one steel layer has been used and Xxx, and Yxx are some reasonable average values of the distances of the steel layers form the middle plane of the plate (89).

When all stress resultants are summed up as membrane forces at the reinforcement level, the problem reduces to the problem of designing for membrane forces only and equations described in the previous section can then be used.

3.4.3 The Mechanism Condition

The elastic stresses under the ultimate load calculated by the finite element method will be used to calculate the design moments using the design equations

derived above.

Because the necessary resistance is made equal to the calculated stress at every point in the slab, it is anticipated that all slab parts will attain their ultimate strength under the design load. Accordingly, with the minimum amount of redistribution, every point will turn into a plastic region at the design load, thus converting the slab into a mechanism.

3.4.3.1 Ductility

The Classical Plasticity assumes that the available ductility is infinite. Reinforced concrete by its very nature has limited ductility. Because the design process tries to achieve almost simultaneous yield of all the sections, the ductility demand made all sections which yielded early are minimized.

3.5 Conclusion

The rules set out in this chapter provide either an optimum reinforcement or a close upper bound to the minimum reinforcement in concrete slabs. These rules will ensure that the yield criteria are nowhere exceeded and the most portions of the slab will yield converting the structure into a mechanism at ultimate load. The conditions of equilibrium and boundary conditions will be satisfied by the stress field obtained from a finite element program. It has been assumed in the derivation of the design equations that concrete can carry no tension. The effect of this assumptions on the service load and the

ultimate load will be discussed in detail in chapter five

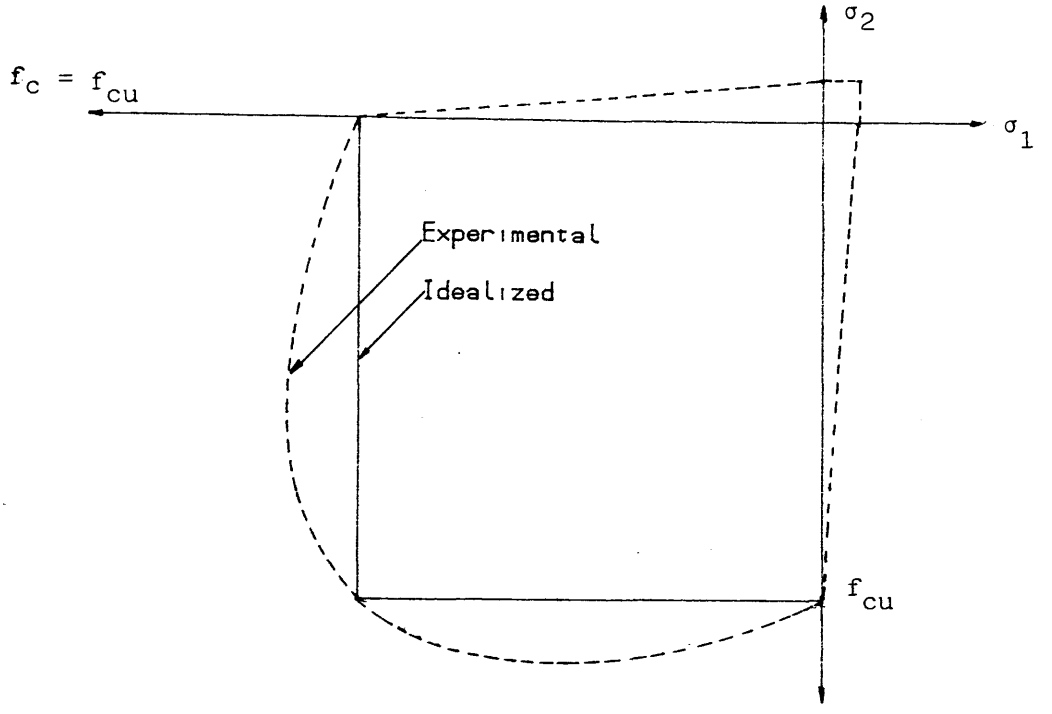

Fig. (3.5) Yield criterion for concrete in plane stress

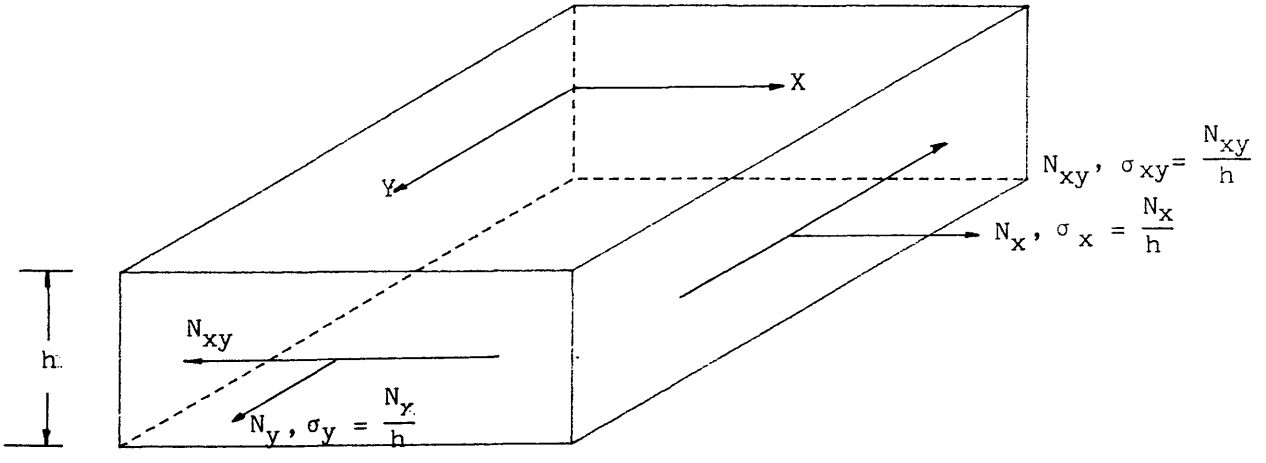

Fig. (3.6) Sign convention for direct and shear inplane forces per unit length

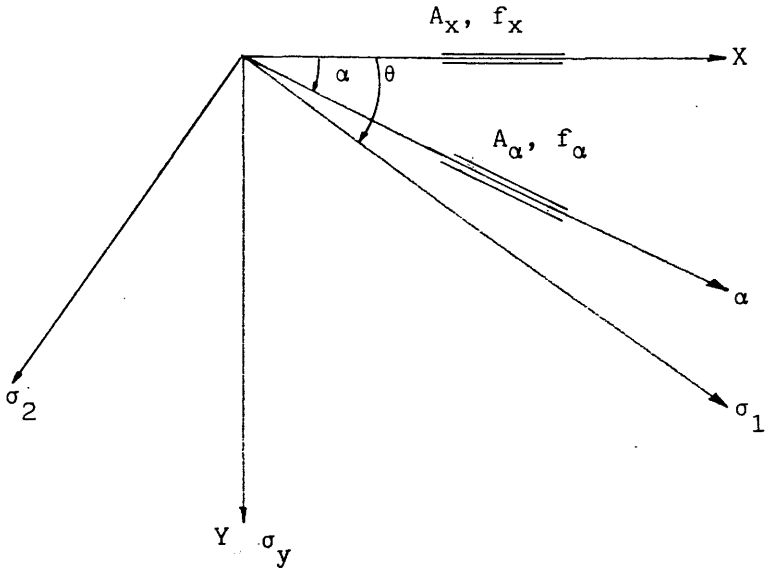

Fig. (3.7) Directions of reinforecement and principal stresses in concrete

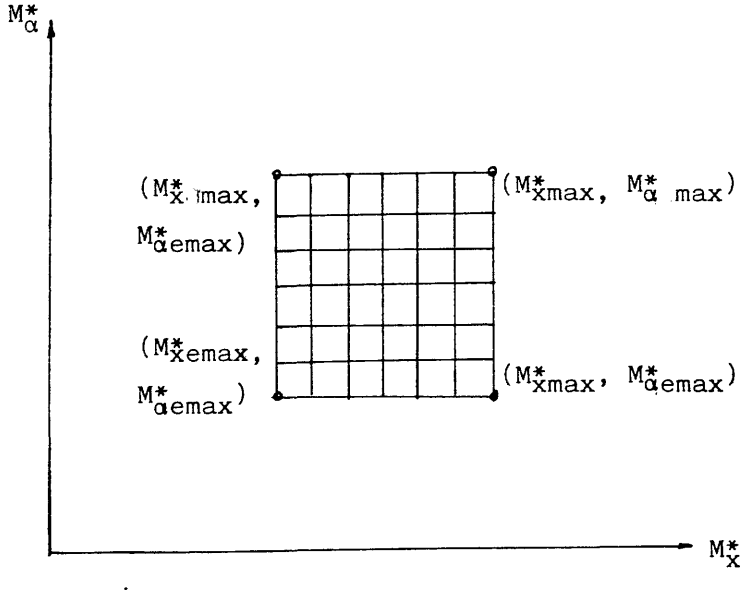

Fig. (3.8) Simple search technique

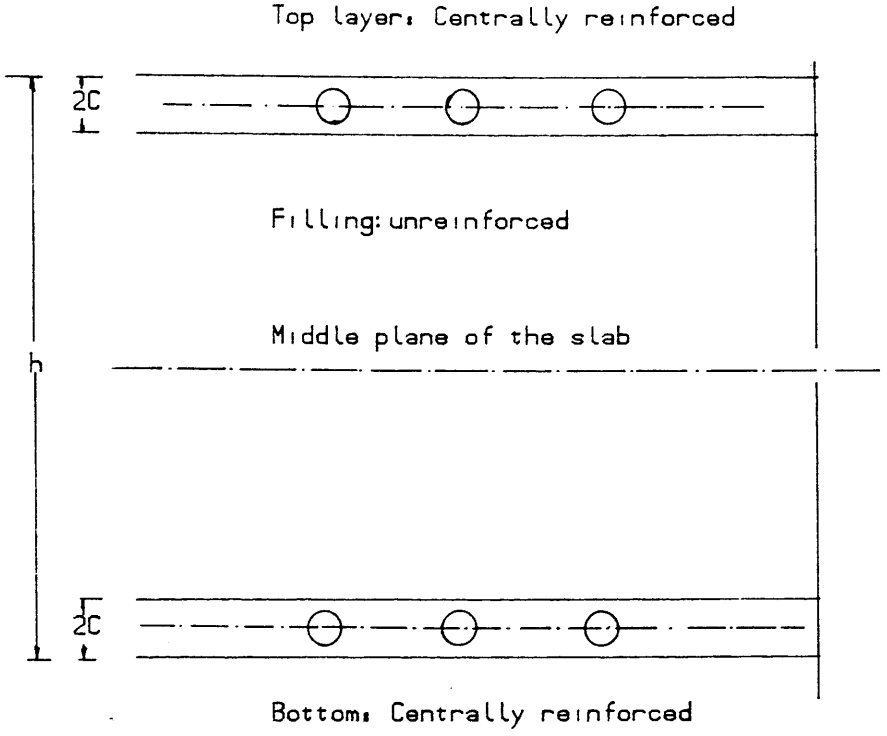

Fig. (3.9) Filled sandwich model

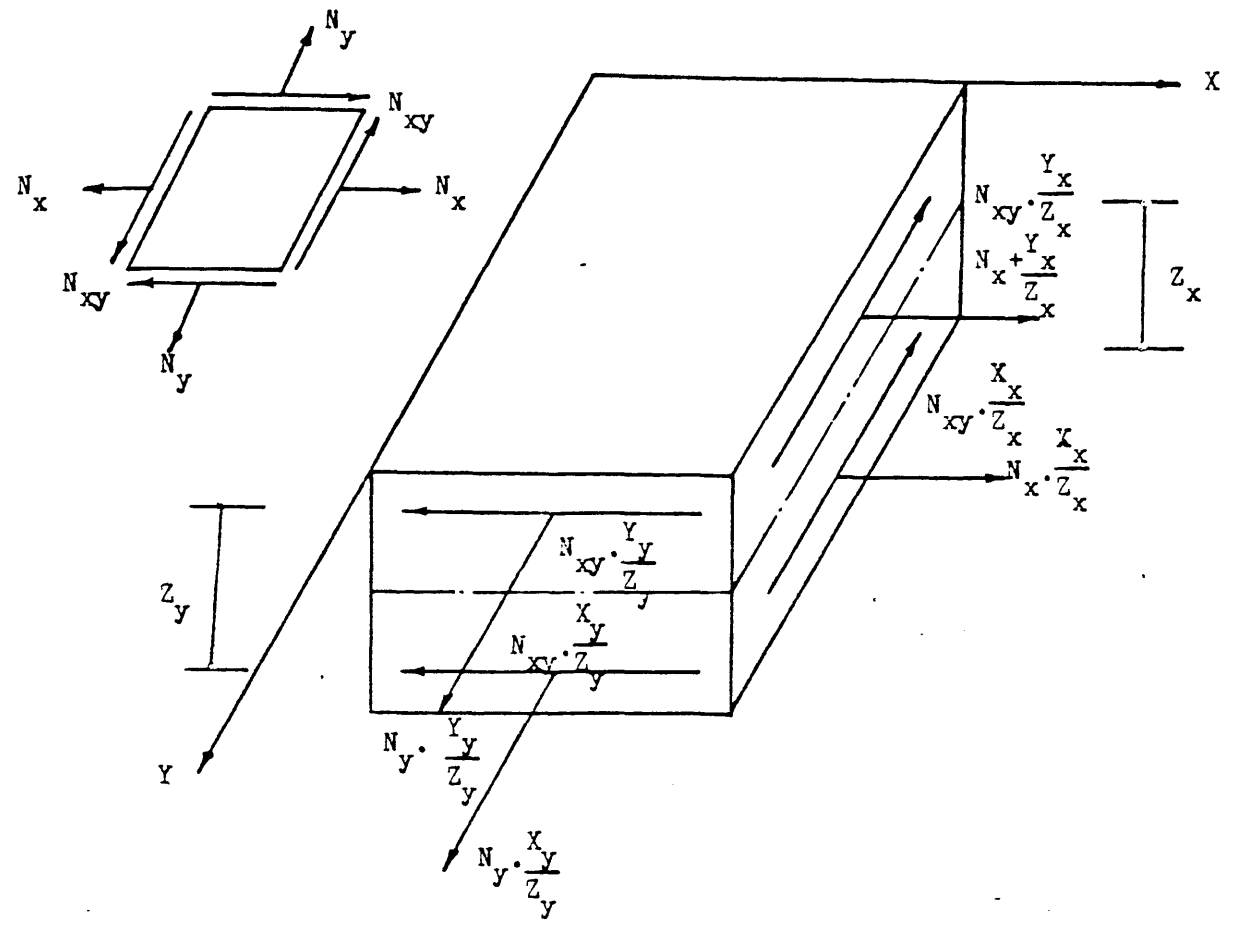

Fig. (3.10) Membrane stress resultants on a filled sandwich element

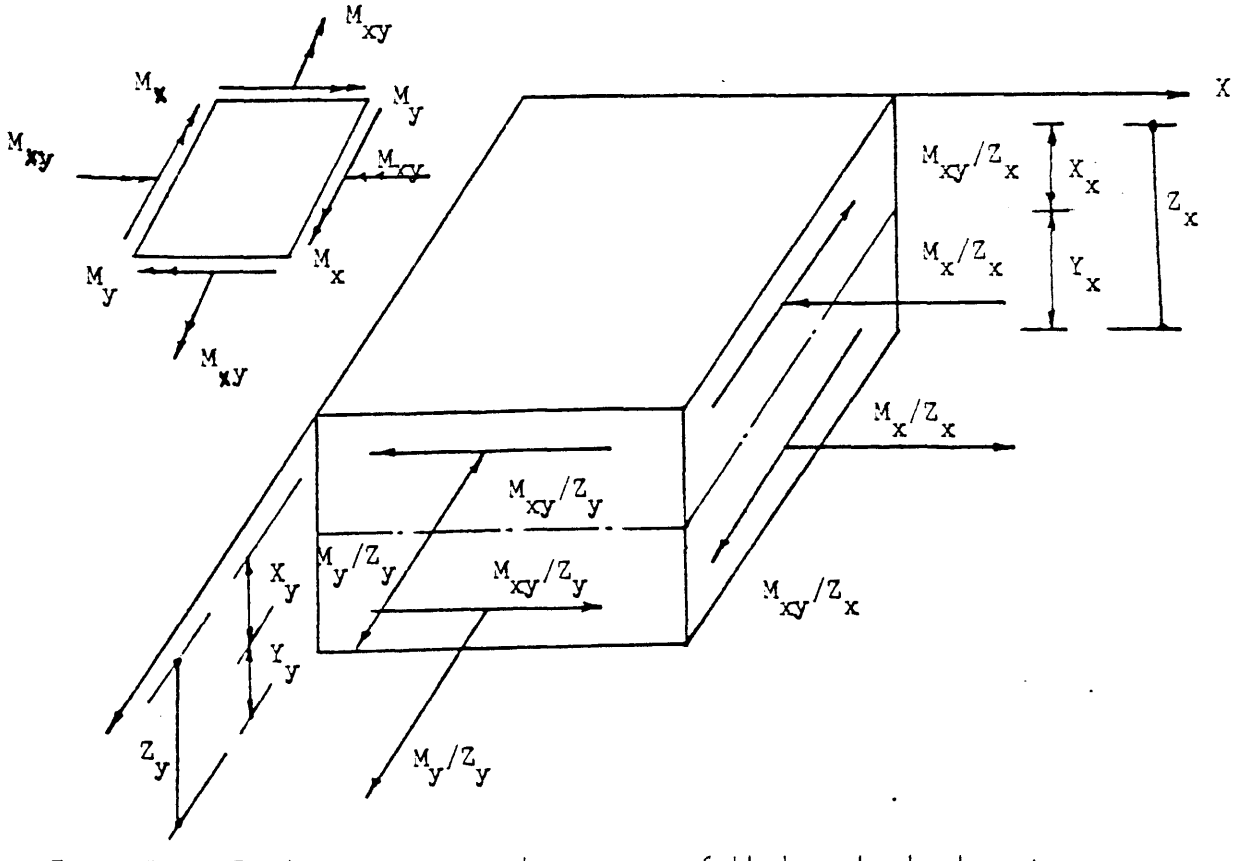

Fig. (3.11) Bending stress resultants on a filled sandwich element

Table (3.1) **Design equations for skew reinforcement.**

Case	ρ_x	ρ_α	σ_1	σ_2	$\tan\theta$
1	$\frac{1}{f_s}\left(\sigma_x + 2\tau_{xy}\cot\alpha + \sigma_y\cot^2\alpha + \left\lvert\frac{\tau_{xy} + \sigma_y\cot\alpha}{\sin\alpha}\right\rvert\right)$	$\frac{1}{f_s}\left(\sigma_y\operatorname{cosec}^2\alpha + \left\lvert\frac{\tau_{xy} + \sigma_y\cot\alpha}{\sin\alpha}\right\rvert\right)$	0	$-2(\tau_{xy} + \sigma_y\cot\alpha)(\cot\alpha \pm \operatorname{cosec}\alpha)$	$-(\cot\alpha \pm \operatorname{cosec}\alpha)$
2	0	$\frac{\operatorname{cosec}^2\alpha}{f_s}\left(\frac{\sigma_x\sigma_y - \tau_{xy}^2}{\sigma_x + 2\tau_{xy}\cot\alpha + \sigma_y\cot^2\alpha}\right)$	0	$\frac{(\sigma_x + \tau_{xy}\cot\alpha)^2 + (\tau_{xy} + \sigma_y\cot\alpha)^2}{\sigma_x + 2\tau_{xy}\cot\alpha + \sigma_y\cot^2\alpha}$	$\frac{\sigma_x + \tau_{xy}\cot\alpha}{\tau_{xy} + \sigma_y\cot\alpha}$
3	$\frac{1}{f_s}\left(\sigma_x - \frac{\tau_{xy}^2}{\sigma_y}\right)$	0	0	$\sigma_y + \frac{\tau^2 xy}{\sigma_y}$	$\frac{\tau_{xy}}{\sigma_y}$
4	$\frac{1}{f_s'}\left(\sigma_{xf} + 2\tau_{xy}\cot\alpha + \sigma_{yf}\cot^2\alpha - \left\lvert\frac{\tau_{xy} + \sigma_{yf}\cot\alpha}{\sin\alpha}\right\rvert\right)$	$\frac{1}{f_s'}\left(\sigma_{yf}\operatorname{cosec}^2\alpha - \left\lvert\frac{\tau_{xy} + \sigma_{yf}\cot\alpha}{\sin\alpha}\right\rvert\right)$	$f_c + 2(\tau_{xy} + \sigma_{yf}\cot\alpha)(-\cot\alpha \pm \operatorname{cosec}\alpha)$	f_c	$-(-\cot\alpha \pm \operatorname{cosec}\alpha)^{-1}$
5	0	$\frac{\operatorname{cosec}^2\alpha}{f_s'}\left(\frac{\sigma_{xf}\sigma_{yf} - \tau_{xy}^2}{\sigma_{xf} + 2\tau_{xy}\cot\alpha + \sigma_{yf}\cot^2\alpha}\right)$	$f_c + \frac{(\sigma_{xf} + \tau_{xy}\cot\alpha)^2 + (\tau_{xy} + \sigma_{yf}\cot\alpha)^2}{\sigma_{xf} + 2\tau_{xy}\cot\alpha + \sigma_{yf}\cot^2\alpha}$	f_c	$-\left(\frac{\tau_{xy} + \sigma_{yf}\cot\alpha}{\sigma_{xf} + \tau_{xy}\cot\alpha}\right)$
6	$\frac{1}{f_s'}\left(\sigma_{xf} - \frac{\tau_{xy}^2}{\sigma_{yf}}\right)$	0	$\sigma_y + \frac{\tau_{xy}^2}{\sigma_{yf}}$	f_c	$-\frac{\sigma_{yf}}{\tau_{xy}}$
7	$\frac{1}{f_s}\left[\sigma_x + \tau_{xy}\cot\alpha - \frac{f_c}{2}(1-\beta)\right]$	$\frac{1}{f_s'}\left[\sigma_y - \tau_{xy}\cot\alpha - \frac{f_c}{2}(1+\beta)\right]$	0	f_c	$\frac{\tau_{xy} + \sigma_y\cot\alpha - \frac{f_c}{2}(1+\beta)\cot\alpha}{\sigma_y\cot^2\alpha + \tau_{xy}\cot\alpha + \frac{f_c}{2}(1+\beta)}$
8	$\frac{1}{f_s'}\left[\sigma_x + \tau_{xy}\cot\alpha - \frac{f_c}{2}(1+\beta)\right]$	$\frac{1}{f_s}\left[\sigma_y - \tau_{xy}\cot\alpha - \frac{f_c}{2}(1-\beta)\right]$	0	f_c	$\frac{\tau_{xy} + \sigma_y\cot\alpha - \frac{f_c}{2}(1-\beta)\cot\alpha}{\sigma_y\cot^2\alpha + \tau_{xy}\cot\alpha + \frac{f_c}{2}(1-\beta)}$
9	0	0	$\frac{\sigma_x + \sigma_y + \sqrt{(\sigma_x - \sigma_y)^2 + 4\tau_{xy}^2}}{2}$	$\frac{\sigma_x + \sigma_y - \sqrt{(\sigma_x - \sigma_y)^2 + 4\tau_{xy}^2}}{2}$	$\frac{\sigma_x - \sigma_y - \sqrt{(\sigma_x - \sigma_y)^2 + 4\tau_{xy}^2}}{2\tau_{xy}}$

NOTES: Case 1: alternative sign is the same as that of $(\tau_{xy} + \sigma_y\cot\alpha)$.
Case 4: alternative sign is the same as that of $(\tau_{xy} + \sigma_y\cot\alpha)$.

Table (3.2) **Design equations for orthogonal reinforcement.**

Case	ρ_x	ρ_y	σ_1	σ_2	$\tan\theta$
1	$\frac{1}{f_s}(\sigma_x + \lvert\tau_{xy}\rvert)$	$\frac{1}{f_s}(\sigma_y + \lvert\tau_{xy}\rvert)$	0	$-2\lvert\tau_{xy}\rvert$	$-\frac{\tau_{xy}}{\lvert\tau_{xy}\rvert}$
2	0	$\frac{1}{f_s}\left(\sigma_y - \frac{\tau_{xy}^2}{\sigma_x}\right)$	0	$\sigma_x + \frac{\tau_{xy}^2}{\sigma_x}$	$\frac{\sigma_x}{\tau_{xy}}$
3	$\frac{1}{f_s}\left(\sigma_x - \frac{\tau_{xy}^2}{\sigma_y}\right)$	0	0	$\sigma_y + \frac{\tau_{xy}^2}{\sigma_y}$	$\frac{\tau_{xy}}{\sigma_y}$
4	$\frac{1}{f_s'}(\sigma_{xf} - \lvert\tau_{xy}\rvert)$	$\frac{1}{f_s'}(\sigma_{yf} - \lvert\tau_{xy}\rvert)$	$f_c + 2\lvert\tau_{xy}\rvert$	f_c	$-\frac{\tau_{xy}}{\lvert\tau_{xy}\rvert}$
5	0	$\frac{1}{f_s'}\left(\sigma_{yf} - \frac{\tau_{xy}^2}{\sigma_{xf}}\right)$	$\sigma_x + \frac{\tau_{xy}^2}{\sigma_{xf}}$	f_c	$-\frac{\tau_{xy}}{\sigma_{xf}}$
6	$\frac{1}{f_s'}\left(\sigma_{xf} - \frac{\tau_{xy}^2}{\sigma_{yf}}\right)$	0	$\sigma_y + \frac{\tau_{xy}^2}{\sigma_{yf}}$	f_c	$-\frac{\sigma_{yf}}{\tau_{xy}}$
7	$\frac{1}{f_s}\left[\sigma_x - \frac{f_c}{2}(1-\beta)\right]$	$\frac{1}{f_s'}\left[\sigma_y - \frac{f_c}{2}(1+\beta)\right]$	0	f_c	$\frac{2\tau_{xy}}{f_c(1+\beta)}$
8	$\frac{1}{f_s'}\left[\sigma_x - \frac{f_c}{2}(1+\beta)\right]$	$\frac{1}{f_s}\left[\sigma_y - \frac{f_c}{2}(1-\beta)\right]$	0	f_c	$\frac{2\tau_{xy}}{f_c(1-\beta)}$
9	0	0	$\frac{\sigma_x + \sigma_y + \sqrt{(\sigma_x-\sigma_y)^2 + 4\tau_{xy}^2}}{2}$	$\frac{\sigma_x + \sigma_y - \sqrt{(\sigma_x-\sigma_y)^2 + 4\tau_{xy}^2}}{2}$	$\frac{\sigma_x - \sigma_y - \sqrt{(\sigma_x-\sigma_y)^2 + 4\tau_{xy}^2}}{2\tau_{xy}}$

CHAPTER FOUR

THE FINITE ELEMENT METHOD

4.1 INTRODUCTION

In the previous chapter, the rules have been established for designing the reinforcement in concrete slabs for a given moment triad. The moment triad is obtained by elastic analysis using a finite element program. In this chapter, the finite element method will be described which will be used not only to calculate the elastic moment fields but also to carry out a detailed nonlinear analysis of the slab. Some examples demonstrating the accuracy of the finite element program will also be given.

4.2 Finite Element Formulation

As the standard procedure of finite element analysis is well known it is not described in detail here, but in order to define terms a brief review of the method is included. This is done with particular reference to the formulation of the Mindlin plate bending element.

4.2.1 Discretisation by Finite Elements

In any continuum, the actual number of degrees of freedom is infinite and unless a closed form solution is available, an exact analysis (within the assumptions made) is impossible. For any numerical approach an approximate solution is attempted by assuming that the behaviour of the continuum can be represented by a finite number of

unknowns. In the finite element method, the continuum is divided into a series of elements of simple geometric shape which are connected at a finite number of points known as nodal points. This process is known as discretisation. In the finite element displacement method, the displacement is assumed to have unknown values only at the nodal points and the variation within any element is described in terms of the nodal values by means of interpolation functions. Thus

$$\delta = N\,\delta^{e} \tag{4.1}$$

where N is a matrix of interpolation functions termed the shape functions and δ^{e} is vector of nodal displacements of the element. For structural applications, the derivation of the governing equilibrium equations is commonly based on the principle of virtual work given by.

$$\int \delta\varepsilon^{T}\,\sigma\,dv \;-\; \int \delta u^{T}\, b_{S}\, dA \;-\; \int_{\Gamma} du^{T}\, t\, d\Gamma \;=\; 0.0 \tag{4.2}$$

where ε, σ, b, t and are the strain vector, the stress vector, the body forces per unit volume, the surface tractions and the virtual displacements, respectively. Considering plate bending:

The body forces $b_S = (b_x,\ b_y,\ b_z,\ M_x,\ M_y)^{T}$

The tractions $t = (t_x,\ t_y,\ t_z,\ t_{mx},\ t_{my})^{\Gamma}$

and virtual displacement $\delta^{u} = (\delta_u, \delta_v, \delta_w, \delta\theta_x, \delta\theta_y)^{\Gamma}$

integrations are carried over the volume v of the plate and loaded surface area Γ.

The first term on the left hand side of Eqn (4.2)

represents the internal strain energy; and the second and third terms are respectively the work contributions of the body forces and distributed surface loads.

In the finite element representation, if strain-displacement relationships together with the linear stress-strain relationships are substituted into the virtual work expression Eqn (4.2) then the following system of linear equations can be obtained

$$k\delta - F = 0.0 \tag{4.3}$$

$$\text{where the stiffness matrix } k = \int_v B^T D B \, dv \tag{4.4}$$

$$\text{the equivalent nodel forces, vector } F = \int_v N b \, dv + \int_s Nq \, ds \tag{4.5}$$

where b the body forces per unit volume,

q the applied surface tractions

B is the strain matrix generally composed of derivatives of shape functions

D is linear elastic or elasto-plastic material stress strain matrix as will be shown in section (4.3.4)

4.3 Mindlin Plate Formulation

4.3.1 Introduction

Finite elements based on Mindlin's assumptions have one important advantage over elements based on classical thin plate theory. Mindlin plate elements require only C(0) continuity. The displacements considered are inplane displacements u and v the lateral displacement w and the independent nodal rotations θ_x and θ_y. However, elements

based on classical thin plate theory require (C_1) continuity; in other words $\partial w/\partial x$ and $\partial w/\partial y$ as well as u, v and w must be continuous across element interfaces. The Mindlin plate element is simpler to formulate than classical plate theory and has the added advantage of being able to model shear- weak as well as shear-stiff plate. Consequently if transverse shear deformation needs to be included, then it is automatically modeled with Mindlin elements. The eight node isoparametic element node (17) using layered representation is used in the present study.

4.3.2 Basic assumption

The plate thickness is divided into a finite number of layers parallel to the middle plane of the plate as shown in Fig. (4.1). Each layer is assumed to resist inplane stresses and transverse shear stress. The stress at the mid depth of the layer is assumed that to be representative of the stress in the whole layer. In otherwords variation of the stress through the thickness of the layer is ignored. Mindlin's formulation takes into account transverse shear deformation and is based on the following assumptions:

i- The normal to the reference surface before deformation remains straight but not necessarily normal to the reference surface after deformation. See Fig. (4.2).

ii- Stresses normal to reference surface are negligible, irrespective of the type of loading.

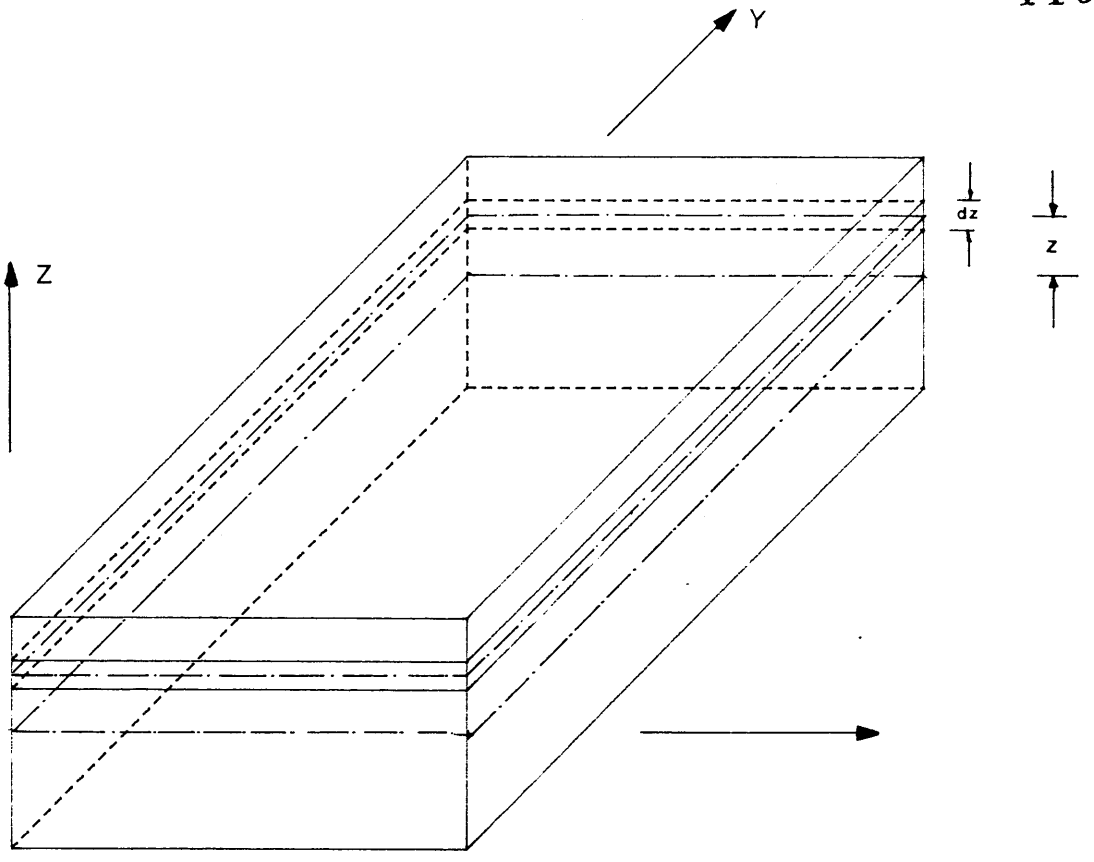

(a) Layer idealistion

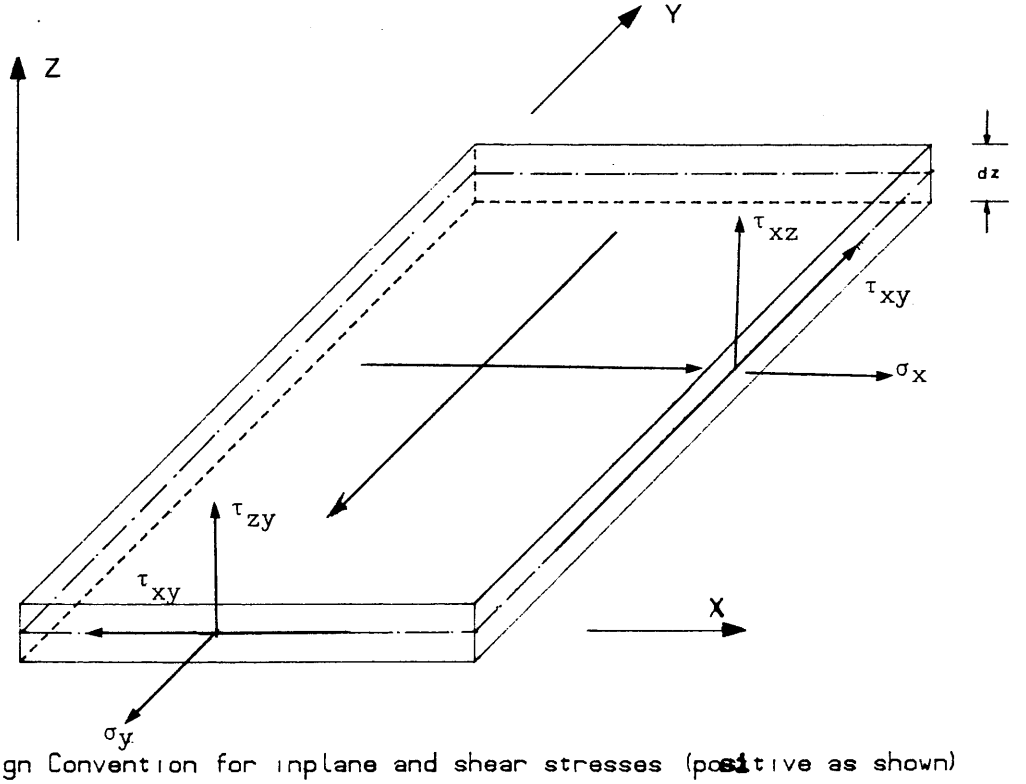

(b) Sign Convention for inplane and shear stresses (positive as shown)

Fig. (4.1) Layered plate model

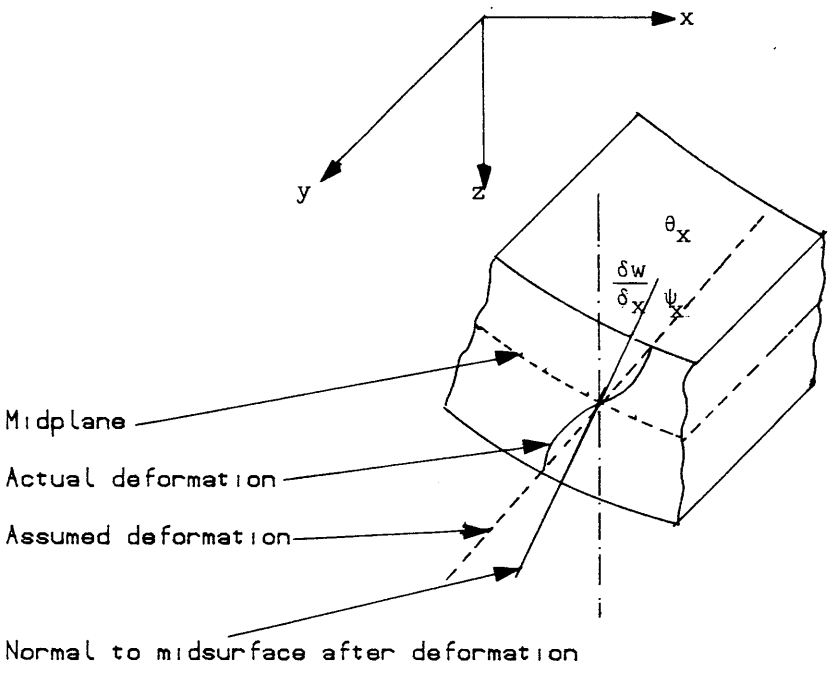

Fig. (4.2) Cross-section deformation of Mindlin plate

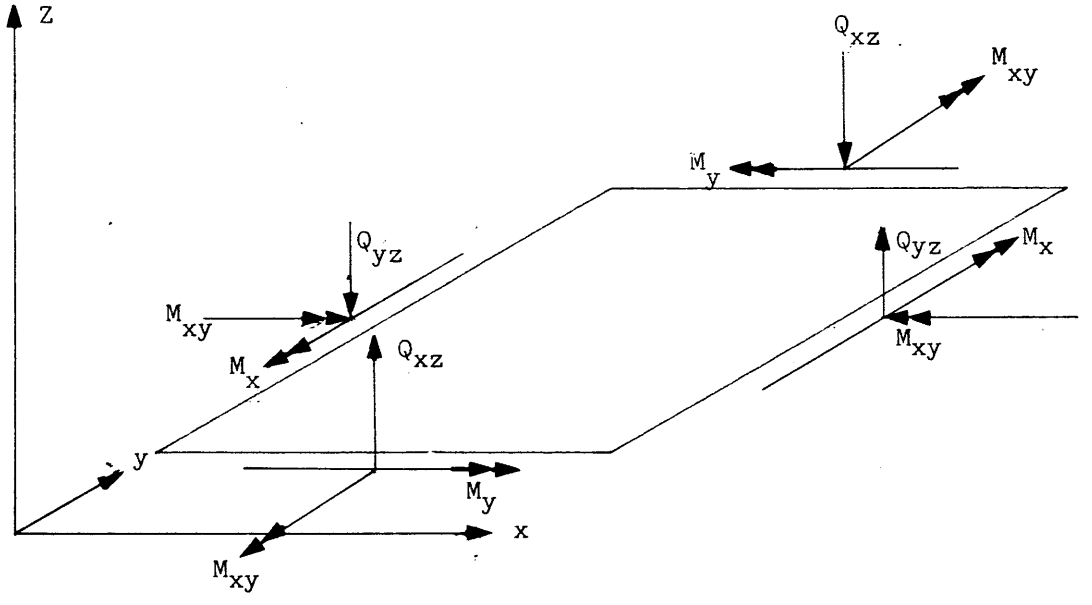

Fig. (4.3) A typical Mindlin plate (positive as shown)

4.3.3 Displacement representation for the element

Using Mindlin's assumptions, displacements u, v, and w at any point in the plate with coordinates (x, y, z) can be expressed as

$$\begin{Bmatrix} u(x, y, y) \\ v(x, y, z) \\ w(x, y, z) \end{Bmatrix} = \begin{Bmatrix} u_o\,(x,y) - z\,\theta_x(x, y) \\ v_o\,(x,y) - z\,\theta_y(x, y) \\ w_o\,(x,y) \end{Bmatrix} \qquad (4.6)$$

where u_0, v_0, and w_0 the displacement at the plate reference surface in the x , y and z directions respectively θ_x and θ_y, are the rotations of the normal in xz and yz plane respectively. See Fig. (4.2) for sign convention.

4.3.4 Shape Functions

Using the finite element idealistion, the displacement vector at any point in a eight node isoparametric element based on Mindlin plate element is given by the expression

$$\begin{Bmatrix} u^e \\ v^e \\ w^e \\ \theta^e_x \\ \theta^e_y \end{Bmatrix} = \sum_{i=1}^{8} \begin{bmatrix} N^e_i & 0 & 0 & 0 & 0 \\ 0 & N^e_i & 0 & 0 & 0 \\ 0 & 0 & N^e_i & 0 & 0 \\ 0 & 0 & 0 & N^e_i & 0 \\ 0 & 0 & 0 & 0 & N^e_i \end{bmatrix} \begin{Bmatrix} u^e_i \\ v^e_i \\ w^e_i \\ \theta^e_{xi} \\ \theta^e_{yi} \end{Bmatrix} \qquad (4.7)$$

where N^e_i is the shape function of at node i given in terms of the local coordinates (ξ, ζ) and $(u, v, w, \theta_x$

, θ_y) is the vector of nodal displacement at node i Following standard isoparametric formulation, the coordinate values x (ξ , ζ) and y (ξ , ζ). at any point within the element Fig. (4.4) ,may be defined by the expressions

$$X(\xi,\eta) = \sum_{i=1}^{8} N_i\,(\xi,\eta).X_i$$

and

$$Y(\xi,\eta) = \sum_{i=1}^{8} N_i\,(\xi,\eta).Y_i \qquad (4.8)$$

where (x_i, y_i) are the coordinates of node i, (ξ ,ζ) is the natural coordinate system which permits the use of elements with curvilinear shapes. $N_i(\xi,\zeta)$ are the two dimensional quadratic shape functions given by Zienkiewicz (16) as follows. Referring to Fig. (4.4)

For corner node i = 1, 3, 5, 7

$$N_i = {}^{1}/_{4}\,(1+\xi\xi_i)\,(1+\eta\eta_i)\,(\eta\eta_i - 1) \qquad (4.9)$$

For midside node i = 2, 4, 6, 8

$$N_i = \xi_i^2\,(1+\xi\xi_i)\,(1-\eta^2) + \frac{\eta_i^2}{2}\,(1+\eta\eta_i)\,(1-\xi^2) \qquad (4.10)$$

4.3.5 Strain-Displacement Relationship

In the two dimensional analysis based on the Mindlin plate bending and plane stress assumption, the strain displacement relationship may be written as:

$$\varepsilon_x = \frac{\partial u}{\partial x} - z\frac{\partial \theta_x}{\partial x}$$

$$\varepsilon_y = \frac{\partial v}{\partial y} - z\frac{\partial \theta_y}{\partial y}$$

$$\varepsilon_{xy} = \frac{\partial u}{\partial y} + \frac{\partial v}{\partial x} - z\left(\frac{\partial \theta_x}{\partial y} + \frac{\partial \theta_y}{\partial x}\right) \qquad (4.11)$$

$$\gamma_{xz} = C\left(\frac{\partial w}{\partial x} - \theta_x\right)$$

$$\gamma_{yz} = C\left(\frac{\partial w}{\partial y} - \theta_y\right)$$

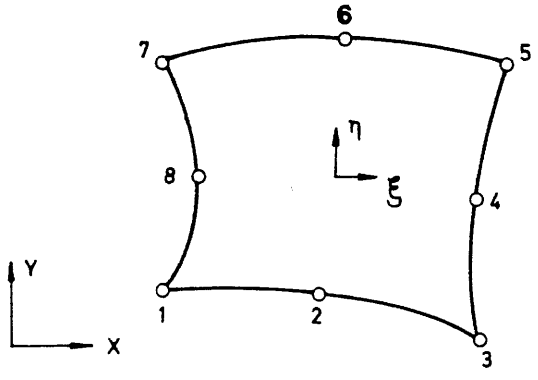

Fig. (4.4) Parabolic isoparametric plate bending element

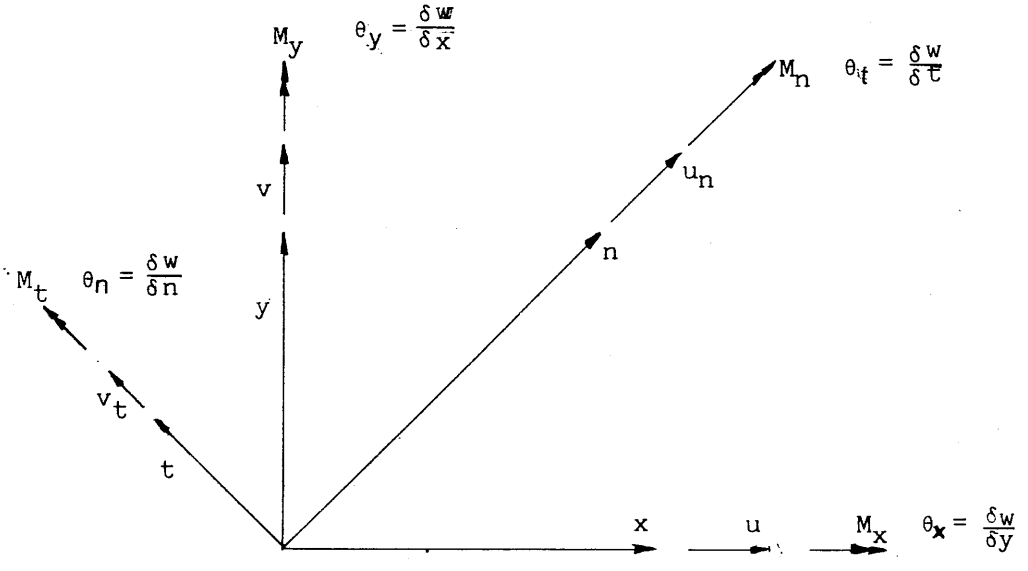

Fig. (4.5) Local directed boundary conditions

in which ε_x , ε_y and ε_{xy} are the inplane strains components. γ_{xz}, and γ_{yz} are the transverse shear strain components. z is the distance from the reference plane to the layer centre, as shown in Fig. (4.1a) and C is shear strain coefficient which depends on shape of cross-section. This is assumed to be equal 1.0 (93) . Eqns (4.11) may be written in matrix form as follows

$$\begin{Bmatrix} \varepsilon_x \\ \varepsilon_y \\ \varepsilon_{xy} \\ \gamma_{xz} \\ \gamma_{yz} \end{Bmatrix} = \begin{bmatrix} \frac{\partial}{\partial x} & 0 & 0 & -Z\frac{\partial}{\partial x} & 0 \\ 0 & \frac{\partial}{\partial y} & 0 & 0 & -Z\frac{\partial}{\partial y} \\ \frac{\partial}{\partial y} & \frac{\partial}{\partial x} & 0 & -Z\frac{\partial}{\partial x} & 0 \\ 0 & 0 & \frac{\partial}{\partial x} & -1 & 0 \\ 0 & 0 & \frac{\partial}{\partial y} & 0 & -1 \end{bmatrix} \begin{Bmatrix} u \\ v \\ w \\ \theta_x \\ \theta_y \end{Bmatrix} \qquad (4.12)$$

Using the finite element idealisation we can write

$$\begin{Bmatrix} \varepsilon_x \\ \varepsilon_y \\ \varepsilon_{xy} \\ \gamma_{xz} \\ \gamma_{yz} \end{Bmatrix} = \sum_{i=1}^{8} \left[\begin{array}{ccc|cc} \frac{\partial N_i^e}{\partial x} & 0 & 0 & -Z\frac{\partial N_i^e}{\partial x} & 0 \\ 0 & \frac{\partial N_i^e}{\partial y} & 0 & 0 & -Z\frac{\partial N_i^e}{\partial y} \\ \frac{\partial N_i^e}{\partial y} & \frac{\partial N_i^e}{\partial x} & 0 & -Z\frac{\partial N_i^e}{\partial y} & -Z\frac{\partial N_i^e}{\partial x} \\ \hline 0 & 0 & C\frac{\partial N_i^e}{\partial x} & -CN_i^e & 0 \\ 0 & 0 & C\frac{\partial N_i^e}{\partial y} & 0 & -CN_i^e \end{array}\right] \begin{Bmatrix} u_i \\ v_i \\ w_i \\ \theta_{xi} \\ \theta_{yi} \end{Bmatrix} \qquad (4.13a)$$

or simply $\{\varepsilon\} = \sum_{i=1}^{8} B_i \{\delta_i\}$ (4.13b)

where B is the 5X5 matrix in Eqn (4.13b) which contains the cartesian derivatives of the shape functions.

B_i can be written as follows

$$B_i = \left[\begin{array}{c|c} B_{pi} & B_{fi} \\ \hline 0 & B_{si} \end{array}\right] \qquad (4.14)$$

B_{pi} is the strain matrix associated with plane stress deformation

B_{fi} is the strain matrix associated with the flexural deformation

B_{si} is the strain matrix associated with the shear deformation

4.3.6 Cartesian Derivatives of Shape Functions

In the above expressions, the cartesian derivatives of shape functions may be obtained using the chain rule of partial derivatives:

$$\frac{\partial N_i}{\partial x} = \frac{\partial N_i}{\partial \xi} \cdot \frac{\partial \xi}{\partial x} + \frac{\partial N_i}{\partial \eta} \cdot \frac{\partial \eta}{\partial x}$$

and (4.15)

$$\frac{\partial N_i}{\partial y} = \frac{\partial N_i}{\partial \xi} \cdot \frac{\partial \xi}{\partial y} + \frac{\partial N_i}{\partial \eta} \cdot \frac{\partial \eta}{\partial y}$$

Using the standard isoparametric formulation (16), the Jacobian matrix J may be obtained as

$$J = \begin{bmatrix} \frac{\partial x}{\partial \xi} & \frac{\partial y}{\partial \xi} \\ \frac{\partial x}{\partial \eta} & \frac{\partial y}{\partial \eta} \end{bmatrix} = \sum_{i=1}^{8} \begin{bmatrix} \frac{\partial N_i}{\partial \xi} . x_i & \frac{\partial N_i}{\partial \xi} . y_i \\ \frac{\partial N_i}{\partial \eta} . x_i & \frac{\partial N_i}{\partial \eta} . y_i \end{bmatrix} \qquad (4.16)$$

The inverse of J is given by expression

$$[J]^{-1} = \begin{bmatrix} \frac{\partial \xi}{\partial x} & \frac{\partial \eta}{\partial x} \\ \frac{\partial \xi}{\partial y} & \frac{\partial \eta}{\partial y} \end{bmatrix} = \frac{1}{\det j} \begin{bmatrix} \frac{\partial y}{\partial \eta} & - \frac{\partial y}{\partial \xi} \\ \frac{\partial x}{\partial \eta} & \frac{\partial x}{\partial \xi} \end{bmatrix} \qquad (4.17)$$

The cartesian derivatives of the shape functions can thus be calculated from (4.13) and (4.15) , which will be used for the calculation of the strain matrix B. The discretized element volume in the isoparametric formulations is given by

$$dv = (dx.dy)dz = (\det J \, d\xi \, d\eta) \, dz \qquad (4.18)$$

4.3.7 Stress-Strain Relationship

For linear analysis of uncracked concrete and in the absence of initial stresses and strains, the stress-strain relationship may be written in the form

$$\{\sigma\} = [D] \{\varepsilon\} \qquad (4.19)$$

D is the elasticity matrix which takes the form

$$[D] = \frac{E}{(1-\nu^2)} \begin{vmatrix} 1 & \nu & 0 & 0 & 0 \\ \nu & 1 & 0 & 0 & 0 \\ 0 & 0 & \frac{(1-\nu)}{2} & 0 & 0 \\ 0 & 0 & 0 & \frac{(1-\nu)}{\gamma} & 0 \\ 0 & 0 & 0 & 0 & \frac{1+\nu}{\gamma} \end{vmatrix} \qquad (4.20a)$$

E is Young's modulus of elasticity, ν is poisson ratio and γ is the shear shape factor, usually taken = 1.2.

The matrix D can be written as follows

$$[D] = \begin{vmatrix} D_{pi} & 0 \\ 0 & D_s \end{vmatrix} \qquad (4.20b)$$

where D_p is related to the inplane stresses and D_s is related to the transverse shear stresses.

4.3.8 Element Stiffness Matrix and Force Vectors

All the information required to evaluate the element stiffness matrix K have has given above so that from Eqn (4.4) the element stiffness matrix can be written as

$$K = \sum_{i=1}^{n} \{ \iint B^T D B \, dx \, dy \} \, dz_i \qquad (4.21)$$

where dzi is thickness of ith layer, n is the total numbers of layers, B is the strain matrix and D is the elasticity matrix depending on the type of material and the state of stress (steel or concrete, elastic or plastic).

Numerical integration may be used to evaluate the stiffness matrix given by the above expression and Gauss-Legendre integration rules are chosen to carry out the integration over the element area. The reduced integration has been adopted to avoid locking. Constraints imposed by shear strain energy terms existing in the total potential energy, lead to the deterioration of the stiffness matrix and overstiff results are obtained when limiting span/depth situations are approached. Further details are given in Section (4.6).

Contributions from element e to the consistent force F are written as

$$F = \int N^T \, q \, dx \, dy \qquad (4.22)$$

Where q is the element surface force vector. Numerical integration is used to calculate the above integral.

4.3.9 Stress Resultants

The inplane forces (N_x, N_y, N_{xy}), flexural moments (M_x, M_y, M_{xy}) and shearing forces (Q_x, Q_y) can be written as follows

$$\{S\} = \begin{Bmatrix} N_x \\ N_y \\ N_{xy} \\ M_x \\ M_y \\ M_{xy} \\ Q_x \\ Q_y \end{Bmatrix} = \sum_{i=1}^{n} \begin{Bmatrix} \sigma_x \\ \sigma_y \\ \tau_{xy} \\ z_i\sigma_x \\ z_i\sigma_y \\ z_i\tau_{xy} \\ \tau_{xz} \\ \tau_{yz} \end{Bmatrix} dz_i \qquad (4.23)$$

4.3.10 Boundary Conditions

As the finite element formulation has displacement components (u, v, w, θ_x, θ_y) at the nodes as variables, displacement boundary conditions can be imposed. To allow representation of curved or inclined boundary supports (94), the variables at nodes on such edges are changed to (u, v, w, θ_n, θ_t) Fig. (4.5). Using well known contragredience rules;

$$\begin{Bmatrix} P_n \\ P_t \\ P_z \\ M_n \\ M_t \end{Bmatrix} = T^T \begin{Bmatrix} P_x \\ P_y \\ P_z \\ M_x \\ M_y \end{Bmatrix} \quad ; \quad \begin{Bmatrix} u \\ v \\ w \\ \theta_x \\ \theta_y \end{Bmatrix} = T \begin{Bmatrix} u_n \\ v_t \\ w \\ \theta_n \\ \theta_t \end{Bmatrix} \qquad (4.24)$$

where (P_n, P_t, P_z, M_n, M_t) and (P_x, P_y, P_z, M_x, M_y) are the vectors of the nodal force and nodal couples related to the local axes n,t and the global axes x,y respectively

and T the transformation matrix is given by;

$$T_b = \begin{bmatrix} \cos\theta & -\sin\theta & 0 & 0 \\ \sin\theta & \cos\theta & 0 & 0 \\ 0 & 0 & 1 & 0 \\ 0 & 0 & \cos\theta & -\sin\theta \\ 0 & 0 & \sin\theta & \cos\theta \end{bmatrix} \quad (4.25)$$

The element stiffness matrix K is transformed to

$$K^e = T^T K T \quad (4.26)$$

before assembly

4.4 MODELING OF THE MATERIAL

4.4.1 Introduction

Uniaxial and biaxial stress-strain relationships for different materials and the corresponding yield criteria are required in the layered finite element model. Stress-strain relationships for concrete were discussed in Chapter Two Section (2.4.3.1). In this Section representation of cracking and the failure criteria for concrete are discussed.

4.4.2 Cracking of Concrete

In any well designed under-reinforced concrete structure, the cracking of concrete and tensile yielding of steel reinforcement are the major sources of nonlinearity. In general, two main approaches have been used to model concrete cracking viz. the discrete and the smeared crack representation.

(i) In the discrete crack representation, a crack is

modeled by the physical separation of the structure on the two sides of the crack. This may be achieved in finite element analysis by separating the element on each side of the crack using additional nodes as shown in Fig. (4.7). Difficulties encountered in changing the topology of the mathematical model and the requirement of cracks to occur along predefined element side directions restrict the use of discrete crack models.

(ii) In the smeared crack system Figs (4.8) and (4.9), which has been adopted in the present work, cracking is modeled by altering the value of the coefficients in the material property matrix associated with a direction normal to the crack. The smeared crack model is more popular than the discrete crack model (95) because of ease of adoption in numerical work.

4.4.3 THE YIELD CRITERION

A multi-linear fit for the yield surface of Fig. (4.10) can be obtained in terms of the octahedral shear stress of the form (53)

$$\tau_{oct} = a - b \quad \sigma_{act} = 0.0 \tag{4.27}$$

where τ_{act} is the octahedral shear stress given by

$$\tau_{oct} = \frac{\sqrt{2}}{3} (\sigma_x^2 + \sigma_y^2 - \sigma_x \sigma_y + 3 \tau_{xy}^2)^{\frac{1}{2}} \tag{4.28}$$

and σ_{act} is the octahedrai mean normal stress given by

$$\sigma_{oct} = \frac{1}{3} (\sigma_x + \sigma_y) \tag{4.29}$$

a, and b are constants to be determined from experiments.

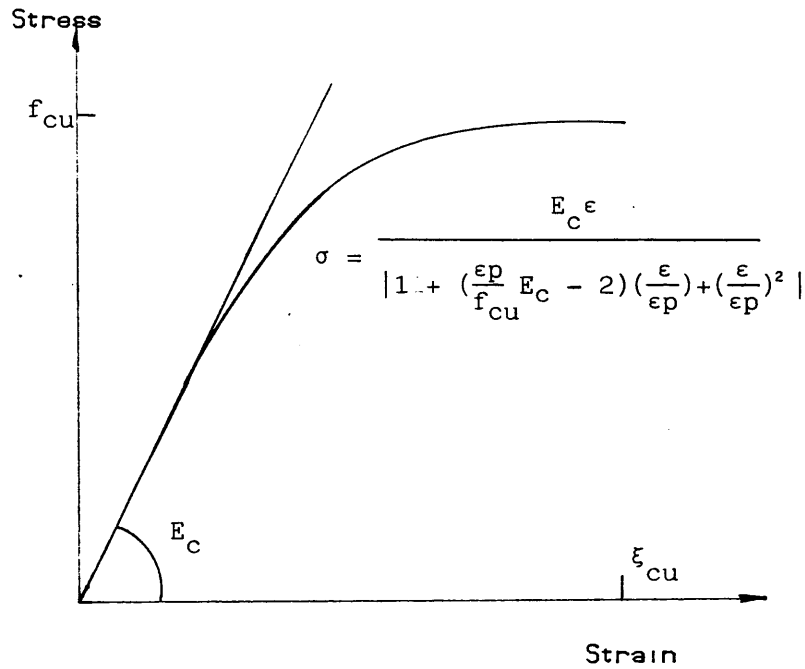

Fig. (4.6) Stress-Strain relationship for concrete in compression

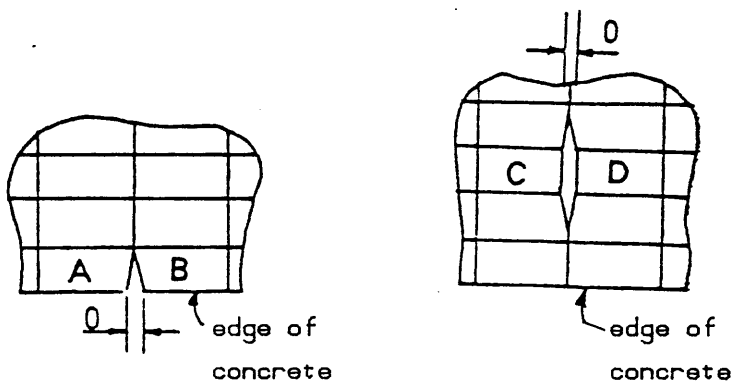

(a) Exterior (b) Interior crack

Fig. (4.7) Development of discrete cracks

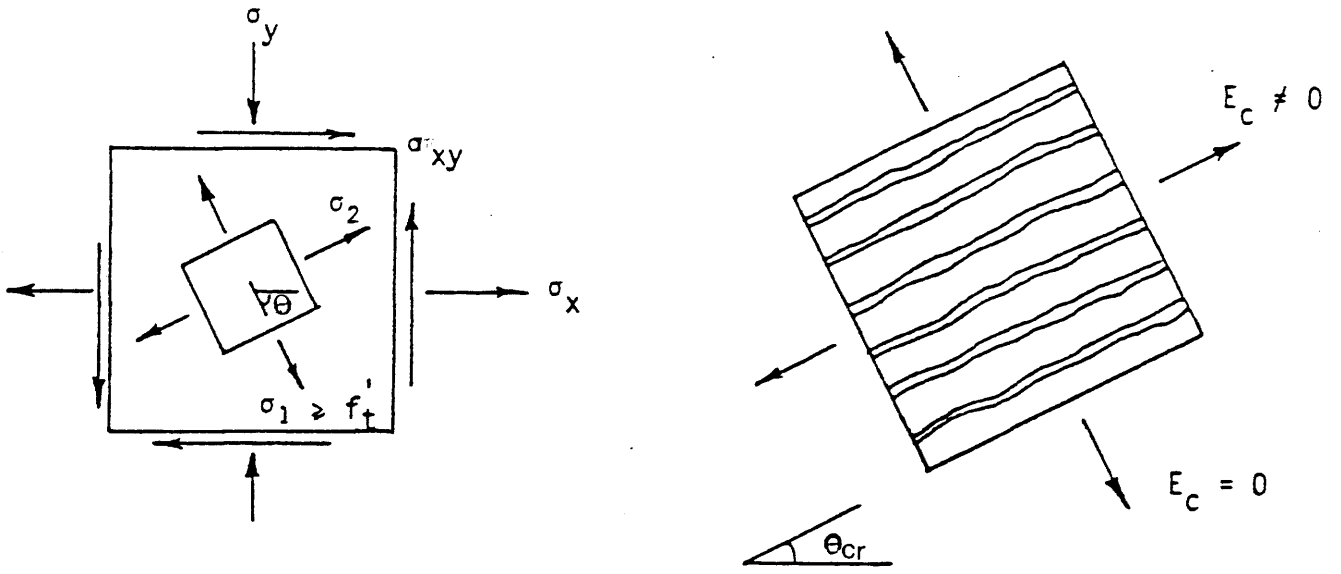

(a) Crack formation

(b) Crack representation

Fig. (4.8) Smeared single crack

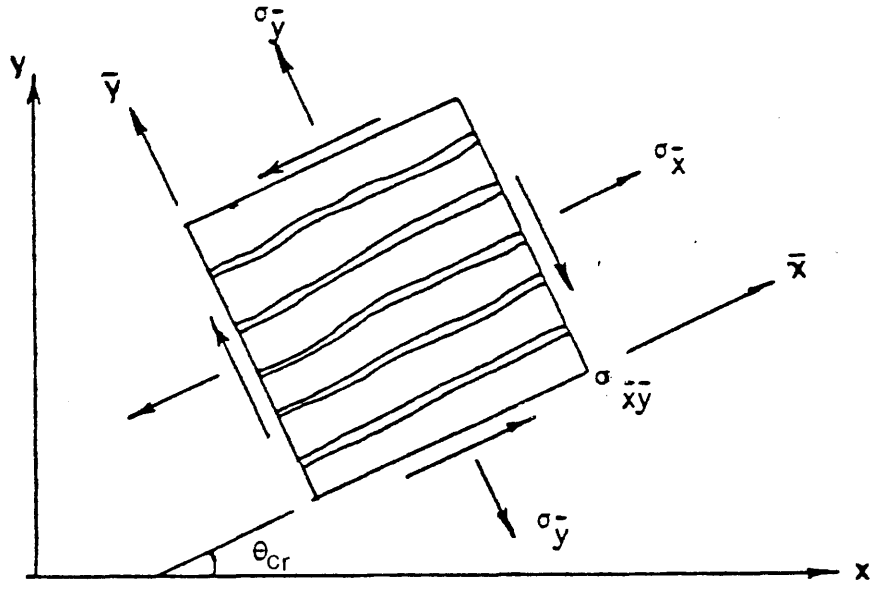

Fig. (4.9) Local coordinates for cracked concrete

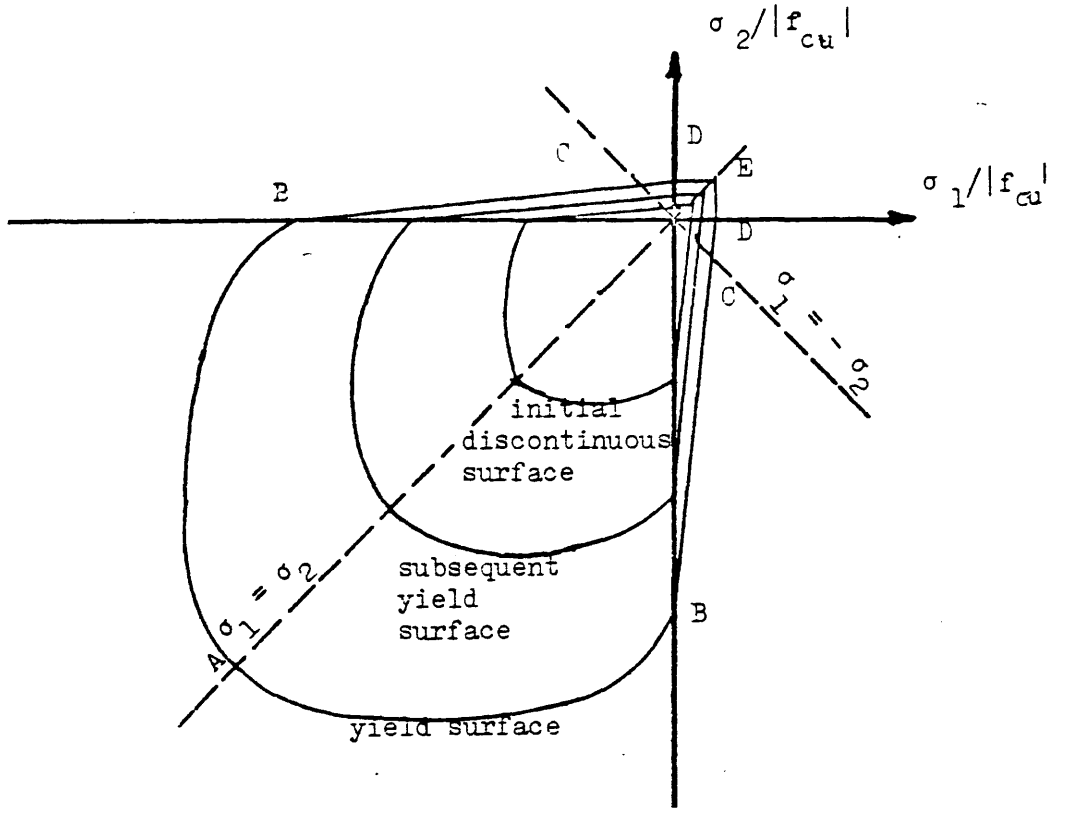

Fig. (4.10) "Zoning" the yield surface - initial and subsequent loading surfcaes

Taking f'_c as the uniaxial compressive strength of concrete, f_d as the equivalent compressive strength under biaxial compression, assumed to be 1.16 f'_c and m = f_t/f'_c, constants a and b in Eqn (4.27) can be established as follows:

(a) compression yielding:

(i) for uniaxial compression $\tau_{oct} = \frac{\sqrt{2}}{3} f_c$ and $\sigma_{oct} = -f_c/3$ then by (4.27)

$$\frac{\sqrt{2}}{3} f_c = - b + \frac{f_c}{3} + a \qquad (4.30)$$

(ii) for biaxial compression $\tau_{oct} = \frac{\sqrt{2}}{3} f_d$ and the σ_{oct} is $-2f_d/3$, then

$$\frac{\sqrt{2}}{3} fd = - 2b \frac{fd}{3} + a \qquad (4.31)$$

Solving for a and b, the yield criterion is give by

$$\frac{\tau_{oct}}{fc} + (0.1714 \frac{\sigma_{oct}}{fc} - 0.4143 = 0.0 \qquad (4.32)$$

(b) Tension-Compression

Using the same procedure, it can be shown that

$$\frac{\tau_{oct}}{fc} + \sqrt{2} (\frac{1-m}{1+m}) \frac{\sigma_{oct}}{fc} \frac{2\sqrt{2}}{3} \frac{m}{1+m} = 0.0 \qquad (4.33)$$

(c) Tension-Tension

Since there is no increase in ultimate tensile strength due to biaxial stressing, the simple circular interaction Eqn (4.34) is sufficient to represent the yield criteria in tension-tension zone.

$$(\sigma_1/f_t) + (\sigma_2/f_t) - 1 = 0.0 \qquad (4.34)$$

where $\sigma 1$ and $\sigma 2$ is the principal stresses.

4.5 DETAILS OF THE MATERIAL MODEL ADOPTED

Before describing the particular constitutive model used in this study, it is important to note that it is assumed that transverse shear stress does not affect the nonlinear behaviour except when the concrete crushes i.e that the stiffensses of the concrete equal zero in all direction is became zero.

4.5.1 Elastic Analysis

In the LAYER program, each layer is assumed to be in a state of plane stress. A layer is also assumed to be of one material whose properties are represented at the Gauss points.

Under plane stress assumptions, the stress-strain relation-ships of an isotropic elastic concrete layer is given by

$$\begin{Bmatrix} \sigma_x \\ \sigma_y \\ \tau_{xy} \end{Bmatrix} = \frac{E_c}{1-\nu^2} \begin{bmatrix} 1 & \nu & 0 \\ \nu & 1 & 0 \\ 0 & 0 & \frac{1-\nu}{2} \end{bmatrix} \begin{Bmatrix} \varepsilon_x \\ \varepsilon_y \\ \varepsilon_{xy} \end{Bmatrix} \qquad (4.35)$$

in which E_c is the modulus of elasticity and ν is Poisson's ratio of concrete.

4.5.2 Nonlinear Analysis-Stress Strain Relationship

1- The elastic analysis of composite material is used to find the stresses and strains for each layer at each Gauss point.

The principal stresses and strains can be

calculated and the state of stress can be checked with respect to the yield criterion i.e whether it is compression-compression or compression-tension or tension-tension type of yielding. The yield surface in Fig. (4.10) can be divided into four regions symmetrical about the $\sigma_1 = \sigma_2$ axis:

i- Biaxial compression failure AB

ii- Cleavage failure - BC.

iii- Failure under combined tension - DE

iv- Failure under tension compression stresses -CD

4.5.2.1 Biaxial Compression Failure: It was mentioned in Chapter Two that an initial linear elastic behaviour for concrete under compression is limited only to small load range up to 30% of the ultimate capacity. Beyond this range, some plastic action is involved. Accordingly, two approaches can be defined to deal with the stress-strain relationship of concrete under compressive forces:

(a) Perfect and work-hardening plasticity

(b) Representation of a given stress-strain relationship using curve fitting method

(a) Perfect and Work Hardening Plasticity: In compression, concrete can flow like a ductile material on the yield surface, before it reaches its crushing strain. To account for its limited plastic flow ability before crushing, a perfectly plastic model can be introduced. The complete stress-strain relationship is developed in three parts: (1) before yield, (2) during plastic flow, and (3) after fracture.

Before yield, a linear elastic model can be used. during the plastic flow, a yield surface is needed to define the onset of yield. The famous von Mises criterion defined in terms of an effective stress as

$$f = \frac{\sqrt{2}}{3} (\sigma_x^2 + \sigma_y^2 - \sigma_x\sigma_y + 3\tau_{xy}^2)^{\frac{1}{2}} - f'_c \qquad (4.36)$$

where f'_c is the uniaxial compressive strength of concrete. Eqn (4.36) has been used by many investigators (48,96,97).

To construct the stress-strain relationship in the plastic range, the normality of plastic strain increment vector ($d\varepsilon_i^p$) is directed normal to the yield surface f (σ_i). This condition may be expressed mathematically in the following form

$$\Delta\varepsilon_i^p = \lambda \frac{\delta f}{\delta \sigma_i} \qquad (4.37)$$

in which λ is a positive scalar proportionality constant. The onset of fracture can be defined using a crushing surface, analogous to (4.37) and expressed in terms of strains (97). After fracture, concrete is assumed to loose all its strength.

One disadvantage of this approach is that it excludes the effect of the mean normal stress and hence the observed plastic volume increase or dilatancy of concrete near failure is not included. This may lead to stiff predictions (53).

(b) Representation of a Given Stress-Strain-Curve using Curve fitting Method: Various empirical stress-strain equations expressed in terms of their respective

principal stress and strain values have been established by fitting curves to large amounts of biaxial test data (68), (99) (100) and (101). This was discussed in Chapter Two section (2.4.3.1). The following equation has been adopted in this work

$$\sigma_i = \frac{E\varepsilon_i}{(1-\alpha\nu)\left(1 + \frac{1}{(1-\nu\alpha)}\left(\frac{\varepsilon_p}{\sigma_p} E_c - 2\right)\frac{\varepsilon_i}{\varepsilon_p} + \left(\frac{\varepsilon_i}{\varepsilon_p}\right)^2\right)} \qquad (4.38)$$

where σ_i and ε_i stress and strain in the principal stress direction

σ_p , ε_p = experimentally determined values of maximum principal stress and corresponding strain, for compression $\varepsilon_p = 0.0025$ and $\sigma_p = f_{cu}$

ν is the poisson's ratio

α is the ratio of the principal stress in orthogonal direction to principal stress in direction considered.

E_c initial tangent modulus in uniaxial loading

Eqn (4.38) can be used to describe the stress-strain behaviour of concrete in biaxial compression up to peak strain equal to 0.0025 (peak strain). Beyond peak, the equation ceases to be valid due to the strain softening of concrete. In this work the softening of concrete is neglected by assuming perfectly plastic behaviour. Due to the fact that the major effect on the response of under-reinforced flexural members is due to cracking, post-peak behaviour of concrete in compression can be safely ignored.

For the numerical procedure adopted in this study, Eqn (4.38) is incrementally linearized during the

monotonic loading. This is usually done by using intermediate loading surfaces after Bell and Elms (47), and Chen et al (88). Such surfaces are shown in Fig. (4.10). The first loading surface corresponds to the initial discontinuity in the stress-strain diagram. Subsequent loading surfaces are assumed to have the shape of the limiting yield surface. Accordingly, the intermediate surfaces will be represented by equation (4.35) but with an intermediate strength fcc replacing the ultimate strength fc. An empirical form for f_{cc} has been suggested by Johanry (53)as

$$f_{cc} = f_{co} - f_t + f_t\ (E_c/E_i)$$

subject to $f_{co} = 0.5\ f_c$. E_c is the initial modulus. E_i is the instantaneous modulus. In this research Ei is computed using Eqn (4.38) for $\varepsilon_i < .0025$ and Eqn (4.39) if $0.0025 > \varepsilon_i < 0.0035$

$$E_i = f_{cu}/\varepsilon_i \qquad (4.39)$$

where f_{cu} the concrete compression strength and ε_i is the principal strain. The discontinuity stress f_{co} is assumed to be equal $0.5\ f_{cu}$ (53).

4.5.2 Cleavage Failure

The term cleavage failure is used to describe a state of failure which is intermediate between splitting and crushing. In this study cleavage failure is accounted for by using Eqn (4.33) for the compression-tension zone to check the failure. The modulus of elasticity is updated according to the state of stress using Eqns (4.38) and (4.39) as for compression-compression failure.

4.5.3 Cracking Model

The main feature of the present cracking model may be summarized as follows:

i- different crack directions are allowed for each layer,

ii- tension stiffening and shear retention are included,

iii- cracks are allowed to open or close during the load increment.

iv- cracking in one or two directions is allowed.

vi- Variable crack direction is allowed.

In checking for principal tensile stress, two approaches are possible as follows;

(a) Fixed crack direction analysis: In this analysis, the direction of the first crack is fixed as determined by the principal tensile stress direction at the time the principal tensile stress is equal to the tensile strength of concrete. It should be appreciated that in this method, matrix D is modified such that the stiffness perpendicular to the crack is zero, thus ensuring tensile stresses are maintained at zero value perpendicular to the fixed crack planes. However because of the fact that shear stress is allowed to act at the cracked surfaces, this procedure allows tensile stress to build up in directions other than the crack direction.

(b)"No-Memory" crack direction analysis: In the analysis, checking for the principal tensile stress is carried out in direction determined by the current state of stress. The material matrix D is never altered.

The cracking of concrete takes place when the stress at a point satisfies the biaxial either in

tension-tension zone or tension-compression zone.

In the tension-tension zone, concrete is assumed to crack if the yield criterion in Eqn (4.34) is violated. The crack direction is taken as being normal to the maximum offending principal stress direction. Two orthogonal cracks may form if both the principal stresses exceed the tensile strength at the same time.

Under tension-compression states of stress, cracking of concrete takes place if the yield criteria using Eqn (4.33) with $f_c = f_{cu}$ is violated. The crack direction in this case is assumed to be normal to the tensile principal stress. On further loading, concrete which has already cracked in one direction may also crack in another direction, which must be at an angle of at least 30 to the first crack direction (if non-orthogonal cracks were considered). Otherwise, if the concrete is subjected to high compressive stresses parallel to the crack direction, yielding and subsequent crushing of concrete may occur. Eqns (4.38) and (4.39) used to calculate the instantaneous modulus Ei, according to the state of stress.

Crack direction; The inclination w.r.t x axis of the principal stresses is calculated from

$$\tan 2\theta = \frac{-2\,\tau_{xy}}{\sigma_x - \sigma_y} \qquad (4.40)$$

the angle θ given by the above equation lies between -45° and 45°, therefore the actual crack direction θ_{cr} is determined as follows with respect to the x-axis:

(a) Calculate the principal stresses using the following

standard expression

$$\sigma_{1,2} = \frac{\sigma_x + \sigma_y}{2} \pm \sqrt{\left(\frac{\sigma_x - \sigma_y}{2}\right)^2 + \tau_{xy}^2} \qquad (4.41)$$

(b) calculate the normal stress associated with the angle using the following standard expression

$$\sigma_n = \sigma_x \cos^2\theta + \sigma_y \sin^2\theta + 2\,\tau_{xy} \sin\theta \cos\theta \qquad (4.42)$$

(c) compare the values of the principal stresses, (σ_1, σ_2) with the normal stress n:

i- if $\sigma_n = \sigma_1$ the angle of crack $\theta_{cr} = \theta$

ii- if $\sigma_n = \sigma_2$ the angle of crack $\theta_{cr} = \theta + 90$

(I) Singly cracked concrete

The cracked concrete is treated as an orthotropic material with the axes of orthotropy parallel and normal to the crack direction. The Poisson effect is neglected due to the lack of interaction between the two orthogonal directions after cracking and the modulus of elasticity of concrete is reduced to zero normal to the crack direction. Thus, the total stresses at the onset of cracking are given with respect to the local coordinate system x, y (shown in Fig. (4.11)

$$\begin{Bmatrix} \sigma_x \\ \sigma_y \\ \tau_{xy} \end{Bmatrix} = \begin{bmatrix} E_c & 0 & 0 \\ 0 & 0 & 0 \\ 0 & 0 & \beta G \end{bmatrix} \begin{Bmatrix} \varepsilon_x \\ \varepsilon_y \\ \gamma_{xy} \end{Bmatrix} \qquad (4.43)$$

Where E_c is the modulus of elasticity of concrete

β is the shear-retention factor for concrete ($0 < \beta < 1$), the choice of suitable value for this factor is discussed later

G is the shear modulus of concrete

The second diagonal term (diagonal term assumed with the direction normal to the crack)in the above matrix may then be updated if the tension stiffening is used.

(II) Doubly-Cracked Concrete

In the present work, concrete is allowed to crack in two directions . The following possibilities are allowed for.

(i) In the previously uncracked concrete, smeared cracks in two orthogonal directions develop when both the principal stresses are tensile and exceed the tensile strength of concrete. In this case the stress- strain relationship is given by:

$$\begin{Bmatrix} \sigma_x \\ \sigma_y \\ \tau_{xy} \end{Bmatrix} = \begin{bmatrix} 0 & 0 & 0 \\ 0 & 0 & 0 \\ 0 & 0 & \beta G \end{bmatrix} \begin{Bmatrix} \varepsilon_x \\ \varepsilon_y \\ \gamma_{xy} \end{Bmatrix} \qquad (4.44)$$

The first two diagonal terms w.r.t the the cracks directions in the above matrix may then be updated if the tension stiffening is considered.

(ii) On further loading of the singly cracked concrete, another set of smeared cracks may form when the stress state produces a tensile principal stress which exceeds the tensile strength of concrete, as shown in Fig. (4.11). In this case, the second set of cracks is be assumed orthogonal to the first and Eqn (4.44) can be used.

In order to transform the stresses in singly or doubly-cracked concrete which are defined with respect to

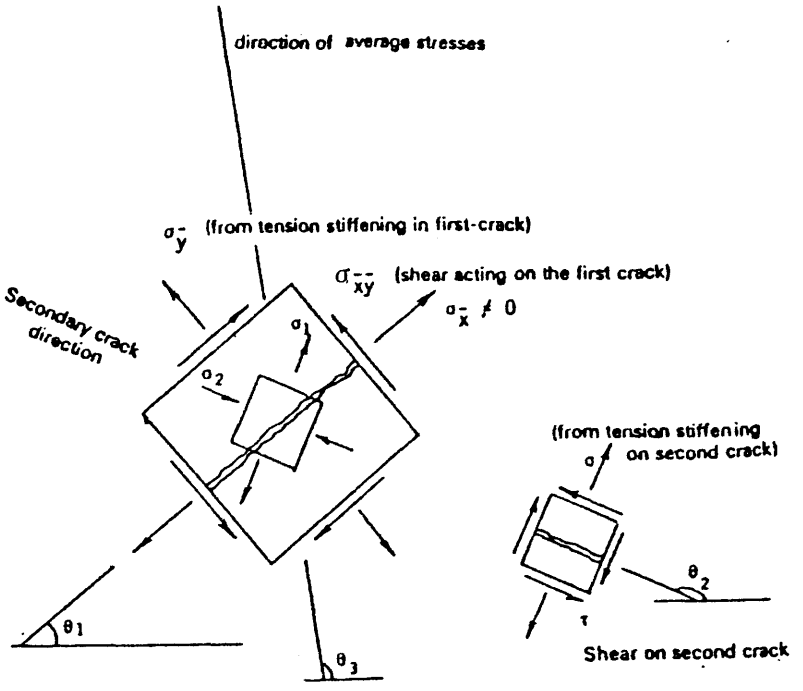

Formation of secondary crack

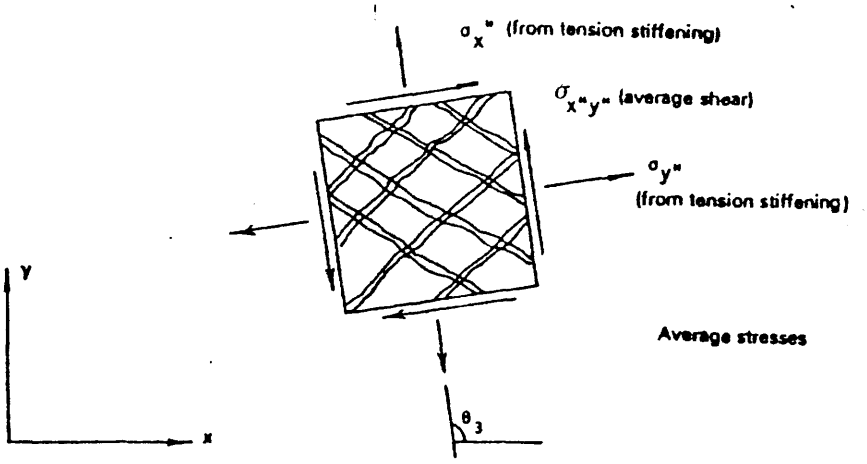

Fig. (4.11) Stresses in doubly-cracked concrete

the axes of orthotropy into global coordinate system, the standard procedure for transformation can be used as follows

$$D^* = T^T D_c T \tag{4.45}$$

where

$$T = \begin{bmatrix} C^2 & S^2 & SC \\ S^2 & C^2 & -SC \\ -2SC & 2SC & C^2-S^2 \end{bmatrix} \tag{4.46}$$

where $C = \cos\theta_{cr}$, $S = \sin\theta_{cr}$ and θ_{cr} is the angle of crack measured from the x-axis to the crack direction in the anticlockwise direction and D_c matrix is the material property in the local axes of orthotropy and is dependent on whether concrete is singly or doubly cracked and is given by Eqns (4.43) and (4.44). The final actual stresses referring to the global (x, y) coordinate systems can be obtained using Eqn (4.47).

$$\{\sigma\} = D^* \{\varepsilon\} \tag{4.47}$$

(c)- Tension Stiffening

The results for beams and one-way spanning slabs with differing steel ratios (102), have shown that the effect of tension stiffening decreases with an increase in the steel ratio and steel strain. The results suggest that tension stiffening can be ignored for steel ratio above .015 and for steel strains greater than about .0016 (Tor bar was used for the test specimens).

The form of the tension stiffening which is adopted in the present work is the same as that given by

(102). With reference to Fig. (4.12):

$$\begin{aligned}
&\text{Zone I} && \varepsilon_{cr} < \varepsilon \leq C_1\ \varepsilon_{cr} && \sigma = (2 - \frac{\varepsilon}{\varepsilon_{cr}})\ ft \\
&\text{Zone II} && \varepsilon_{cr} < \varepsilon \leq C_2\ \varepsilon_{cr} && \sigma = \frac{(2 - C_1)}{(C_2 - C_1)} (C_2 - \frac{\varepsilon}{\varepsilon_{cr}})\ ft \\
&\text{Zone III} && \varepsilon > C_2\ \varepsilon_{cr} && \sigma = 0
\end{aligned} \qquad (4.48)$$

Where f_t tensile strength of concrete and ϵ_{cr} equal cracking strain (0.0001)

The coefficients $C_1 = 1.3$ and $C_2 = 15$ were derived empirically to ensure good predictions for slabs and beams (102). Use of tension stress strain curves of this shape have been shown to give good correlation with test data for beams subjected to a gradually increasing load and with different steel ratio (103), (109).

Tension stiffening is dependent on many factors:

i- The tension stiffening effect in concrete is reduced with increasing distance from the steel reinforcement and increase in steel strain.

ii- Since in the smeared crack representation the cracked concrete is averaged over a certain distance, the tension stiffening is mesh dependent. As the mesh is refined, the effect decreases until it vanishes for elements of theoretically infinitesimal size.

iii- It must be noted that the inclusion of the tension stiffening in concrete by considering the average concrete stress over a certain distance results in a lower steel stress over the same distance as shown in Fig. (4.13). Therefore the maximum steel stress is underestimated by approximated 10% (the value is dependent on the value of the cracking strain, steel yield strain

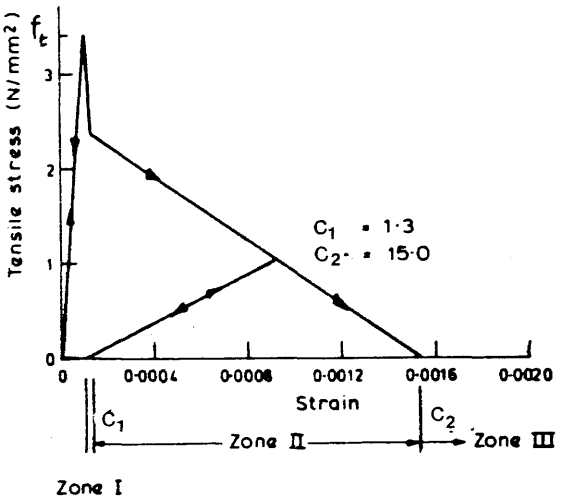

Fig. (4.12) Concrete tensile stress-strain curve

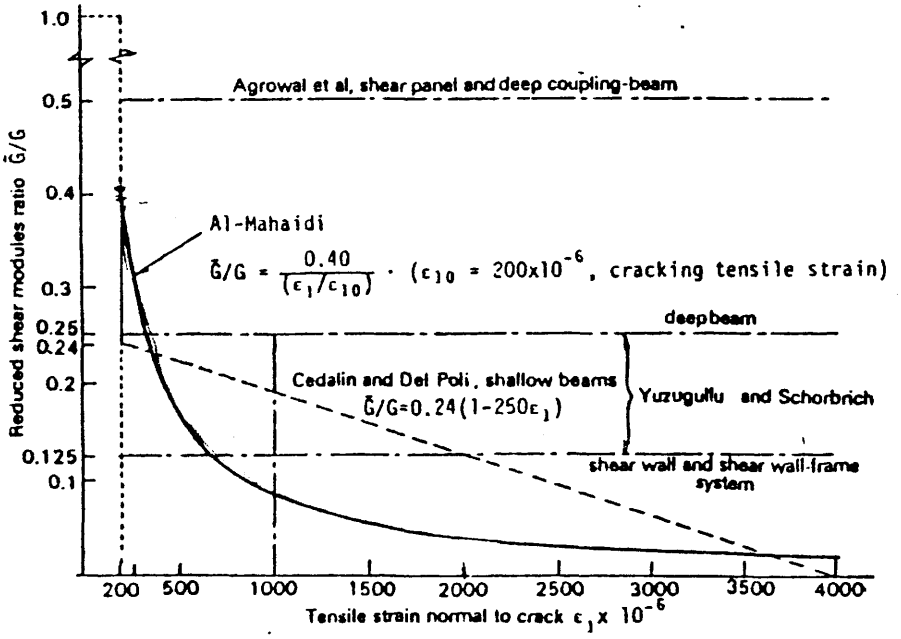

Fig. (4.13) Comparison of different expressions proposed for the reduced shear stiffness of concrete

and the value of coefficients C_1 and C_2 in Eqn (4.48)). If the cracked concrete stresses become equal to zero before the steel yields, then the ultimate load will not be affected by the tension stiffening. On the other hand tension stiffening may over-estimate the ultimate load if the yielding of steel takes place before the stresses in cracked concrete reach the zero-value.

(d) Shear Retention

Due to their rough nature, cracked concrete faces are capable of transmitting shear forces across cracks by friction. This force will induce normal stresses due to dilation which tend to stiffen the cracked concrete. In order to take the shear stiffness of concrete into account, a reduced shear modulus G equal to BG is retained in the stress-strain matrix as given in Eqn (4.43) and (4.44). This is equivalent to introducing a number of springs parallel to the crack direction to represent the effect of aggregate intrelock and to some extent the dowel action, but excluding taking the normal stresses resulting from friction. Hand et al (52) proposed the reduced shear modulus approach to overcome some numerical difficulties. They used a constant value of B throughout the analysis. Later, Cedolin and Poli (104) used B which decreases linearly with a fictitious strain normal to the crack (which represents the crack width). Al-Mahaidi(66) has also suggested a hyperbolic variation of G with the fictitious strain normal to the crack, as shown in Fig. (4.14). In the present work Eqn (4.49) due to the Al-Mahaidi (66) has been used.

$$B = \frac{0.4}{(\varepsilon_f / \varepsilon_{cr})} \qquad (4.49)$$

where ε_{cr} concrete cracking strain=(E_c/f_t) and ε_f is fictitious strain normal to the crack and is given by Eqn (4.50).

$$\epsilon_f = \epsilon_x \sin^2\theta_{cr} + \epsilon_y \cos^2\theta_{cr} - \epsilon_{xy} \sin\theta_{cr} \cos\theta_{cr} \qquad (4.50)$$

where ε_x, ε_y and ε_{xy} are the inplane strains and θ_{cr} is the angle of crack as it is given above.

(e) Partial and Full Closing of Cracks

In order to improve the realism of the present cracking model, the possibility of crack closing either partially or fully is considered . This behaviour may take place due to the redistribution of stresses during an iteration or upon further loading. In the present work, the possibility of cracking of a concrete layer is re-examined within each iteration until the numerical solution converges within the permissible convergence tolerances. After convergence, the direction of any cracking is fixed and orthotropic behaviour is assumed as explained before.

Previously formed Concrete cracks are also allowed to open or close partially or fully. Fig. (4.15) shows different possible crack configuration considered in this work. The fictitious strain normal to the crack direction (Eqn (4.50) is used to assess the state of the cracks in the cracked concrete. If this strain has a negative value, then the crack is assumed to be fully closed and the modulus of elasticity E_c is retained in a direction

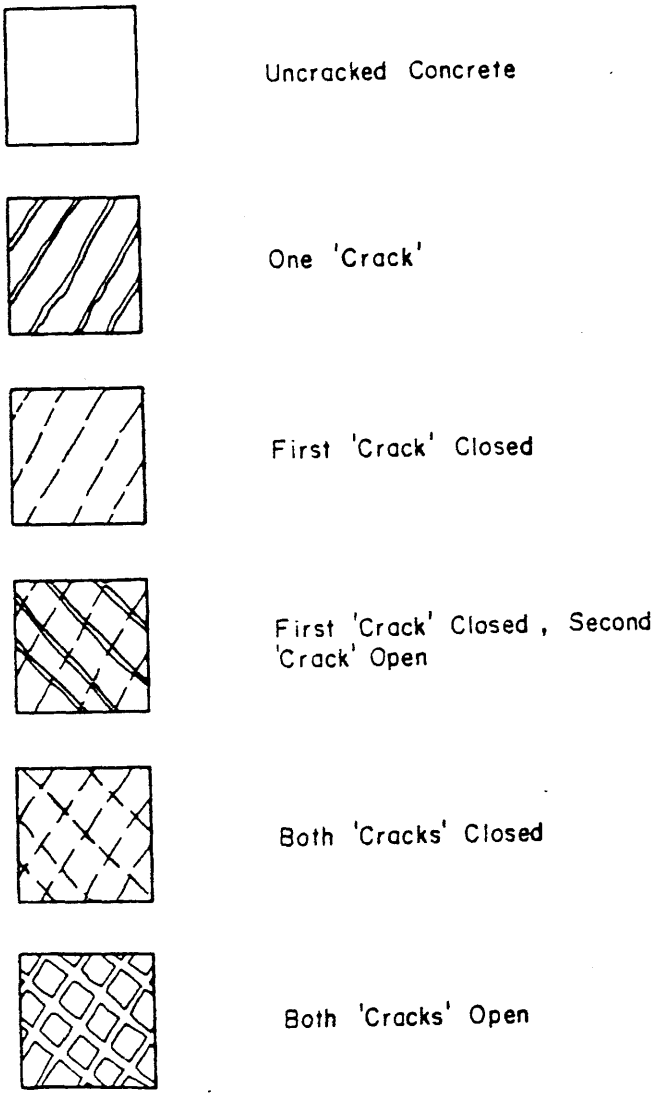

Fig. (4.14) Possible crack configurations

normal to the crack. However, the Poisson effect is ignored. If the current fictitious strain (ϵ_f) normal to the crack direction is decreasing, but still positive, partial closing of the crack is assumed. This situation may take place when the current strain ϵ_c is less than the strain ϵ_{ref} recorded at the previous converged configuration as in Fig. (4.12). In this case the stress normal to the crack (6) is calculated from:

$$\sigma = \frac{\sigma_{erf}}{\epsilon_{erf}} \epsilon_c \qquad (4.51)$$

in which σ_{erf} is the interpolated stress, cosserponding to the strain ϵ_{erf}.

4.5.4 Modeling of Steel Behaviour

In the present model, the steel reinforcement is smeared into equivalent steel layer with uniaxial properties. In contrast to concrete, the mechanical properties of steel reinforcement are well known (105). The typical stress-strain curve for steel reinforcing bar, loaded monotonically in tension, is shown in Fig. (4.15). The stress-strain curves of steel are assumed to be identical in tension and compression Fig. (4.16). The uniaxial stress-strain curve of steel is idealized in the present model to the form shown in Fig. (4.16). An elastic-plastic behaviour with possible strain hardening is assumed. Since steel bars can be oriented at any angle to global x-y axis, the layer behaviour is first described in the local axes direction, and then transferred to global axes. The transformations into global direction is

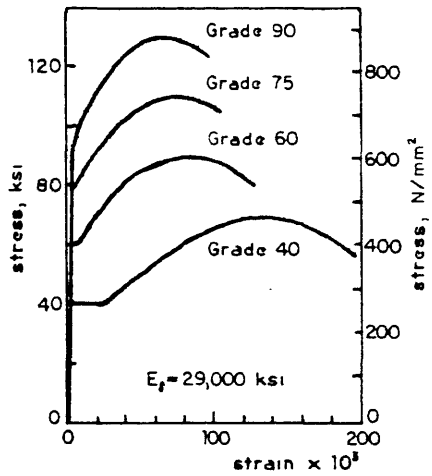

Fig. (4.15) Typical stress-strain curves for steel reinforcing bars

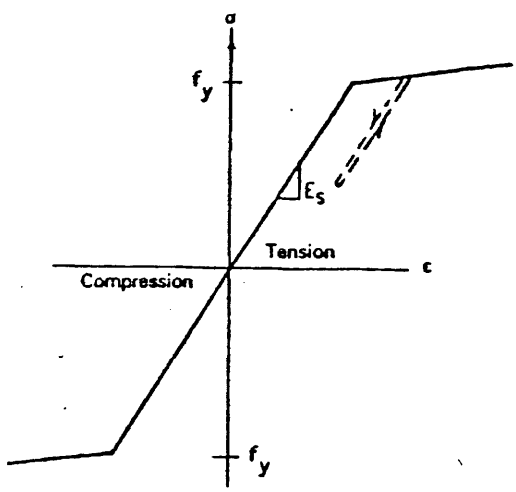

Fig. (4.16) Idealised stress-strain curve for steel

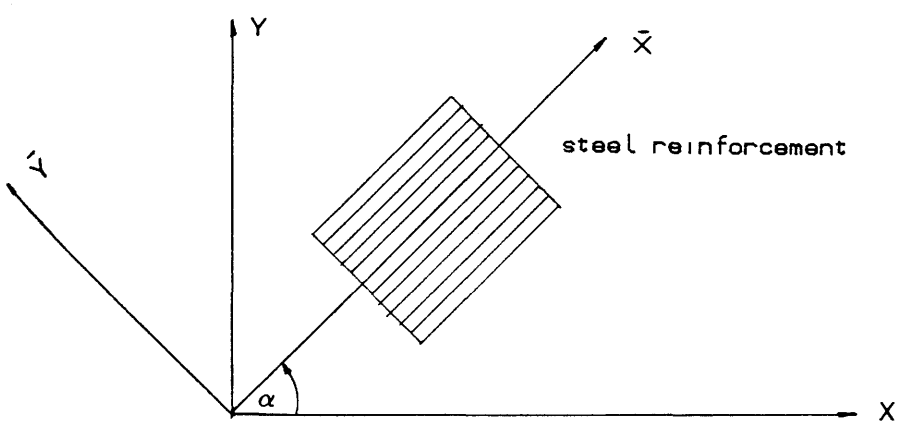

Fig. (4.17) Steel in the general direction

carried out using transformation matrix which depends on the angle between the local (x', y') and global coordinate (x, y), using the standard procedure of transformation

$$D_e = E_s \begin{bmatrix} c^4 & c^2s^2 & c^3s \\ s^2c^2 & s^4 & cs^3 \\ s\,c^3 & c\,s^3 & c^2\,s^2 \end{bmatrix} \qquad (4.52)$$

where $C = \cos\alpha$, $S = \sin\alpha$, α is the angle of inclination as in Fig. (4.17) and E_s is the modulus of elasticity of steel.

The incremental elastic stress-strain relationship is given by

$$\Delta\sigma = E_s\,\Delta\varepsilon \qquad (4.53)$$

When the uniaxial steel stress reaches its yield value f_y, the incremental elastic-plastic stress-strain relationship takes the form:

$$\Delta\sigma = E_s\left(1 - \frac{E_s}{(E_s + \grave{H})}\right)\Delta\varepsilon \qquad (4.54)$$

in which $\grave{H}$ is the strain hardening parameter for steel.

4.6 PRACTICAL IMPLEMENTATION OF MINDLIN ELEMENT (94) (106) (107)

In this study, 2x2 Gauss rule was used for both shear and bending terms to develop the 8-node isoparametric element which showed good performance was adopted with assuming constant representation for the shear force within the element (93). Since the study was not concerned with the extreme range of span/depth ratio,

troubles due to locking etc were not encountered.

4.7 NONLINEAR SOLUTION TECHNIQUES

The solution of nonlinear problems by the finite element method is usually attempted by one of three techniques:

a- Incremental (step-wise procedure)

b-Iterative (Newton-Rhaphson method)

c-Increment-Iterative (mixed procedure)

The general basis of each method is similar. The nonlinear stiffness equation (Eqn (4.55)) are solved by a succession of linear approximations. The different methods of applying these load-displacement paths influence the final solution. More details can be found in references (57), (108).

4.7.1 Increment Method

The basis of the increment method is the subdivision of the total applied load vector into small load increments, which do not necessarily need to be equal. During each load increment the equation:

$$F = K\delta \qquad (4.55)$$

is assumed to be linear, i.e. a fixed value of K is assumed using material data existing at the end of the previous increment. Nodal displacements can then be obtained for each increment and these are added to the previously accumulated displacements. The process is repeated until final the load is reached.

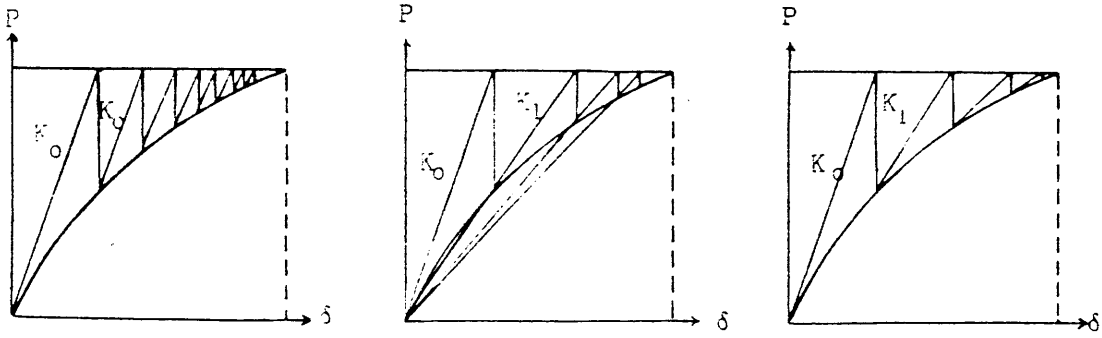

constant stiffness procedure

variable stiffness procedure

Secant Modulus Approach

variable stiffness procedure

Tangent Modulus Approach

(a) Iteration process

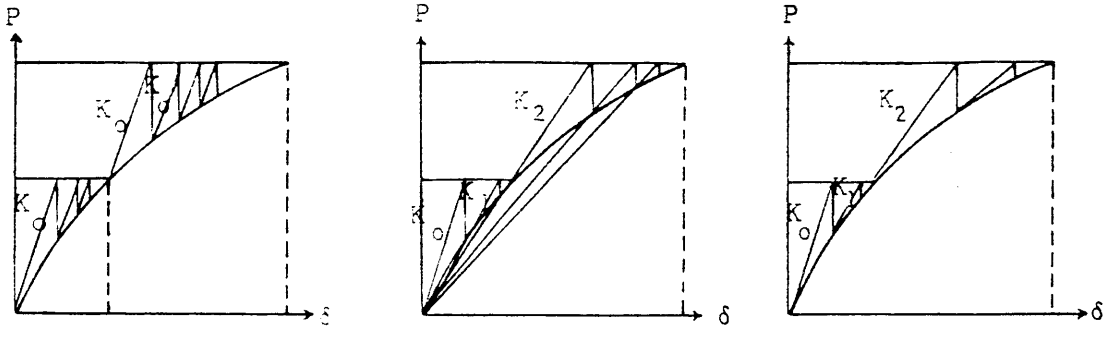

constant stiffness procedure

variable stiffness procedure

Secant Modulus Approach

variable stiffness procedure

Tangent Modulus Approach

(b) Mixed procedure

Fig. (4.18) Basic Procedure for nonlinear solution

The accuracy of this procedure depends on the increment size, smaller increments producing greater better accuracy at the expense of increased computational effort. A modification of this method is to apply half the load increment and to calculate a new structural stiffness corresponding to the total stresses at this value. The updated stiffness matrix is then utilized to compute an approximation for the full load increment. The incremental method in its original and modified form does not take into account the force redistribution during the application of the incremental load.

4.7.2 Iteration Method

In the iteration method, the full load is applied in one increment. Stresses are evaluated at that load according to the material law. This gives equivalent forces which may not be equal to the external applied forces, i.e. equilibrium is not necessarily satisfied. The portion of the total load that is not balanced is calculated as the difference between the total applied load vector and internal nodal forces calculated using the allowable stresses in the element. These are the unbalanced nodal forces which are then used to compute an additional increment of displacements and hence new stresses, which give rise to a new set of equivalent nodal forces. This process is repeated until equilibrium is reached to a certain degree of accuracy. When this stage is reached the total displacement is calculated by

summing the increment in displacement due to all the iterations.

There are many variations of this basic process and the solution accuracy and efficiency depends in many ways on the method used for computation of the stiffness matrix and the unbalanced nodal forces, Fig (4.18a).

(a) Computation of Unbalanced nodal forces

The process called the initial stress method (16), is adopted in this work and can be explained as follows. Let the stress-strain relationships to be

$$\sigma = [D]\{\varepsilon\} + \{\sigma_o\} \qquad (4.56)$$

where σ_o is the initial stress vector and D is the elasticity matrix.

Assuming $\sigma_o = 0$ initially, Eqn (4.55) is solved with an appropriate D matrix and strain ϵ_A, to obtain a certain level of stress σ_{A1} where

$$\{\sigma_{A1}\} = [D]\{\varepsilon_A\}$$

The stress which should have occurred is:

$$\{\sigma_{A2}\} = [\bar{D}]\{\varepsilon_A\}$$

where $\bar{D}$ is instantaneous elasticity matrix

The difference between the stresses:

$$\sigma_o = \{\sigma_{A2}\} - \{\sigma_{A1}\} \qquad (4.57)$$

is used as initial stress in Eqn (4.56), and equivalent unbalanced nodal forces {f} are calculated from:

$$\{f\} = -\int_v P_v^T \sigma_o \, dv \qquad (4.58)$$

The forces are removed by applying them to the structure

to obtain a correction to δ . This process is repeated until σ_0 becomes negligible.

(b) Method of Computing Element Stiffness Matrix

Generally either the stiffness matrix can remain constant or can be varied throughout a solution. In the constant stiffness method the initial linear stiffness is used at every stage in the analysis. Since calculating the new stiffness matrics and fully solving the equations is an expensive operation, this method has economic advantages because the stiffness is calculated only once. Also a symmetric positive definite matrix will exist. Its main disadvantage is that it usually requires a large number of iterations to achieve the desired accuracy, especially when cracking of concrete and yielding of reinforcement has occurred. Some acceleration processes have been suggested but the use of these techniques have not always met with success (64,65).

In the variable stiffness method, a Newton-Raphson method or its modified version is adopted. In the full Newton Raphson method the tangential stiffness matrix is updated Fig (4.18a) and a completely new system of equations is solved in each iteration. This process can be very expensive particularly if relatively small load increments have to be used. The procedure sometimes may lead to unsatisfactory results due to the approximation of the material law, numerical integration, convergence tolerance etc.

To overcome this difficulty some modification of

the full Newton-Raphson algorithm is made by updating the stiffness matrix only occasionally for each increment and maintaining the same matrix for successive iterations until convergence is a achieved, Fig (4.18a).

4.7.3 Mixed Method

In this method, a combination of the incremental and iterative process is used. The load is applied in increments and the solution at that load is obtained iteratively until equilibrium is satisfied to a prescribed accuracy.

The constant stiffness procedure base on the initial stiffness approach with either the secant modulus or the tangent modulus can be used. Fig (4.18b) shows the different methods of the mixed procedure.

4.8 Procedure Used in This Work

A modified version of the mixed procedure is used in this work. The modified Newton-Rhapson (16) approach is used to evaluate the stiffness matrix . In the variable stiffness approach which is used for the most of the analysis, the stiffness matrix is updated at the beginning of the second iteration and after the application of the incremental load in the first iteration, so that the nonlinear effects are reflected more accurately in the stiffness matrix. As the modified Newton-Rhapson method involves fewer stiffness calculations than the full Newton-Rhapson approach, economies in computation are

gained. However, to compensate for this a large number of iterations is required for convergence, particularly if there is a significant loss of stiffness in the system during a load increment due to cracking of concrete or yielding of steel. In this work the solution is accelerated by updating the stiffness at iteration eleven, if it is found difficult to attain the prescribed convergence. This algorithm gives satisfactory results for reasonable computational effort. As an additional economy measure, only the stiffness of the layer where yielding has occurred within the element is updated and added to the element stiffness using a direct access file.

4.8.1 Convergence Criteria

It is important in the incremental-iterative solution strategy that the solution obtained at the end of each iteration is checked to see whether it has converged to within convergence tolerance or whether it is diverging. The convergence criteria, usually used for nonlinear structural analysis are based on either displacement or on out-of-balance forces norm and sometimes on internal strain energy. In the present work, convergence is based on out-of balance force norm because it indicates directly how well equilibrium requirements are met (108). Since it is difficult and expensive to check the decay of residual forces for every degree of freedom, some overall evaluation of convergence is preferable. This is achieved by using the force norms as follows

$$\frac{\sum_{i=1}^{N} (F_{u,i}^{r})^{0.5}}{\left| \sum_{i=1}^{N} (R_i)^2 \right|^{0.5}} \times 100 \leq \text{Toler.} \qquad (4.59)$$

where N is the total number of nodal points of nonzero displacement in the structure. r denotes the iteration number , $F_{u,i}$ is the residual force at the ith displacement and R_i is the total external applied load at the ith displacement.

It must be noted here that in the formulation adopted for Mindlin plate element, stresses are separated into inplane stresses and transverse shear stresses. The inplane stresses are adjusted according to the current material law, while the stress-strain relationships for transverse shear stresses are kept constant except when the concrete is crushed where all the stresses are removed.

4.8.2 Frontal Equation Solution Technique

The simultaneous equation solving routine plays a major role in the efficiency of finite element programs. This is particularly true in the nonlinear finite element programs because a lot of processing time is used in solving and resolving the stiffness equations. In the present work a version of the frontal solution will be used. It was originally introduced by Irons (29) and subsequently modified by Hinton and Owen (5). The main idea of the frontal solution is to assemble the equations and eliminate the variables at same time. More details can

be found in (29).

4.8.3 Analysis Termination Criteria

The analysis program must be provided with some means of detecting the collapse of the structure. The failure of a structure takes place when no further loading can be sustained. This is indicated in the nonlinear solution by successively increasing displacement increments at each iteration. The growth of displacement increments results in the lack of convergence of nonlinear solution. The value of maximum deflection may be used as a criterion to stop the analysis at failure. When the maximum deflection reaches a certain specified value the analysis is terminated and the load at that point is taken as ultimate load. In this work the maximum deflection measured in the experiment is taken as ultimate deflection.

4.8.4 Basic Steps in The Method Used

1- Apply an increment of load Δf_i and calculate the first estimate of the incremental displacement

$$\Delta\{\delta_i\} = [K]^{-1} \{\Delta f_i\}$$

where K can be the initial elastic stiffness, or the tangential stiffness based on the conditions prevailing at the start of the increment.

2- Calculate the increment in strains and stresses

$$\varepsilon_i = \int [B]^T \Delta \{\delta_i\}$$

$$\sigma_i = [D] \{\varepsilon_i\}$$

3- Calculate the total displacement, strains and stresses by adding the incremental values to the previous values.

$$\delta_i = \delta_{i-1} + \Delta \delta_i$$

$$\varepsilon_i = \varepsilon_{i-1} + \Delta \delta_i$$

$$\sigma_i = \sigma_{i-1} + \Delta \sigma_i$$

4- Check the stress state against the relevant intermediate or final yield criteria. If any criterion is violated, the stresses are brought back to the yield surface.

5- Find the equivalent nodal forces due to σ_i ,which is inside the yield surface. Calculate the out of balance force

$$\Delta f_{ui} = \int B \sigma_i \, dv - f_i$$

where f_i is the total external load.

6- Check to see if the force norm satisfy the convergence criterion. If it does, then apply a new load increment and repeat steps from (1) to (6). If not, apply the residual force (Δf_{ui}) and calculate the corrective displacement ($\Delta \delta_i$) caused by them from

$$\Delta \delta_i = [K]^{-1} \Delta \{f_{ui}\}$$

return to step (2) and repeat the process until the convergence conditions are satisfied.

4.9 NUMERICAL APPLICATION

The object of this section is to demonstrate the reliability of the developed computer program LAYER and to conduct some selected numerical experiments. The basic

premise is that if over a wide range of experimental problems this model can produce an accurate prediction for the general behaviour (deflections, cracking loads, yielding loads and ultimate load), the program can then be used to predict the behaviour of similar. i.e. flexure dominated problems.

4.9.1 A Square Simply Supported Slab Under a Central Point Load

The slab is 1830.mm square and simply supported along the edges. The thickness of the slab is 14[illegible]9 mm with isotropic reinforcement ratio of 0.99%. The slab was tested under a central point load by Portland Cement Association and was analysed by Doterppe et al (55). The material properties used are:

f_{cu} = 47.7 N/mm^2 Ft = 3.8 N/mm^2

$_c$ = 24580. N/mm^2 E_s = 206850 N/mm^2

h = 139.7 mm t = 144.3 mm

A 4X4 element mesh is used over a symmetric quarter of the plate as shown in Fig (4.19). The depth of the slab is represented by 10 concrete layers and 2 smeared steel layers.

In the nonlinear solution, the combined algorithm is adopted in which the stiffness is updated at 2^{-nd} and 11^{-th} iterations, with the maximum number of iterations limited to 20. A convergence force tolerance of 5% was adopted. The average number of iterations to reach the specified convergence tolerance varied from 2 to 10. The increment load was .05 of experiment failure load.

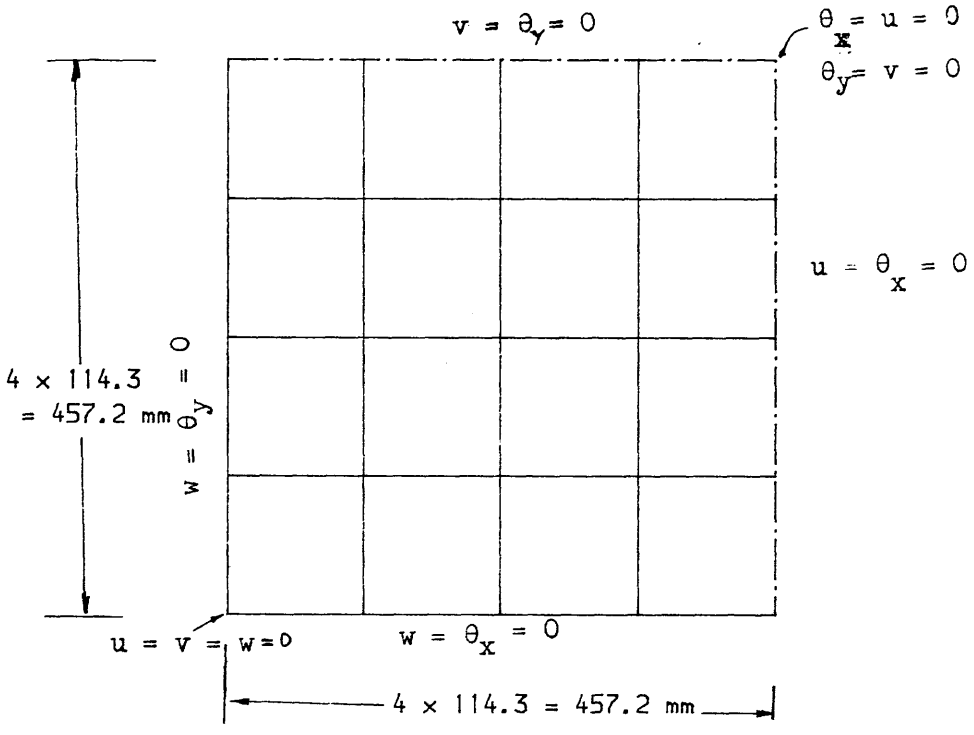

Fig. (4.19) Mesh idealisation for a simply supported slab under central load

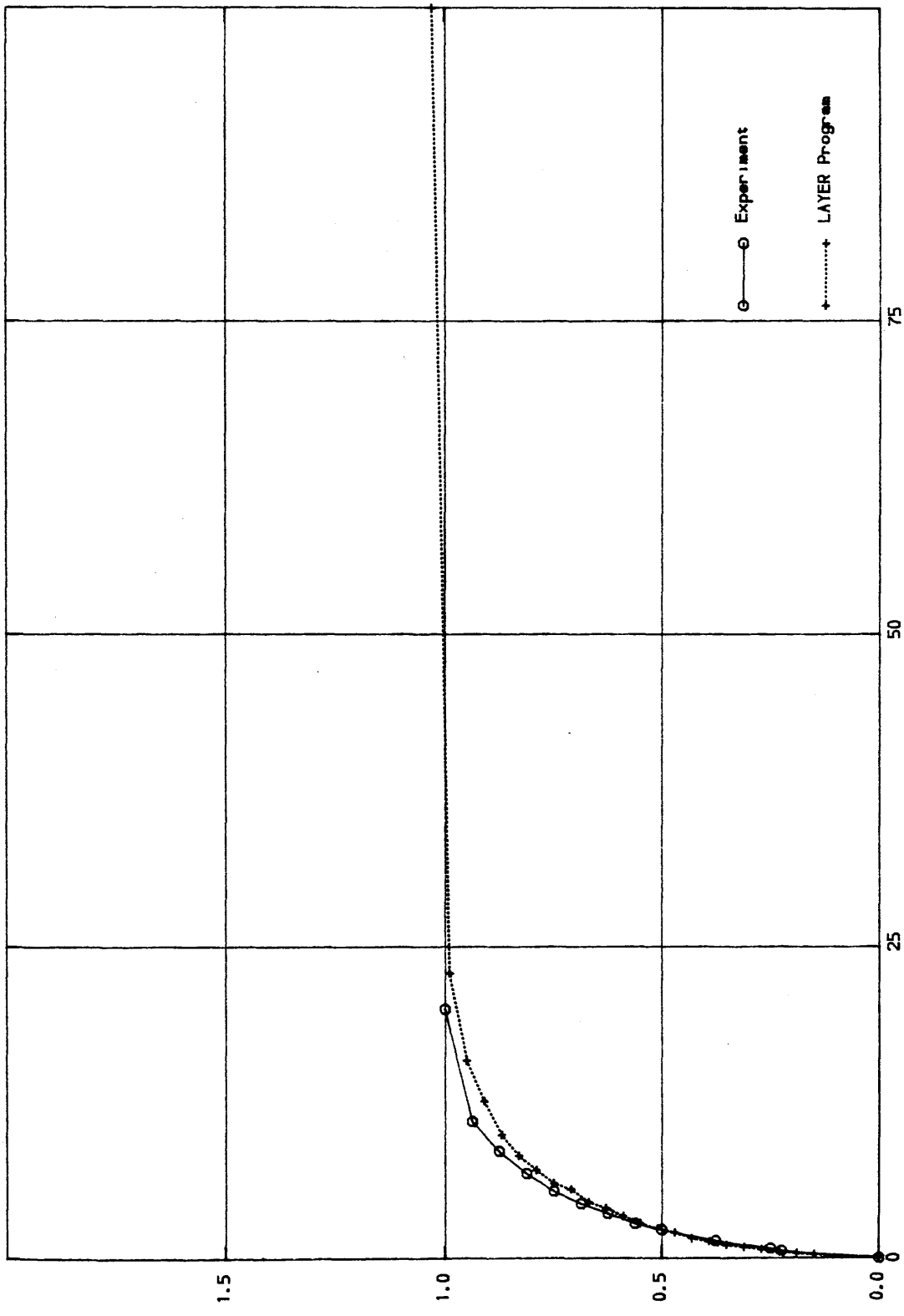

Fig. (4.20) Load-Central deflection curve for Dotreppe's slab

Fig (4.20) shows the excellent agreement between load-central deflection obtained experimentally and that obtained numerically without considering tension stiffening. the calculated ultimate load was 1.03 times the experimental failure load.

4.9.2 Hago's Slabs

Two of the five slabs tested by Hago (9) were chosen for analysis. These slabs have various degrees of orthotropy of reinforcement. Hence their analysis allows the effect of the amount of steel reinforcement to be tested as well different types of support conditions. These slabs were used to study the effect of the number of concrete layers, load increment size and tension stiffening on the numerical solution.

(a) Simply Supported Slab

The slab is 2100x2160 mm square and is simply supported along each edge to give 1900x1960 mm spans. The thickness of the slab is 100 mm, with orthotropic reinforcement as shown in Figs (4.21a,b). The slab was loaded with four-point-load system as shown in Fig (4.24d). The material properties used are as follows.

f_{cu} = 44.2 N/mm^2 $\quad$ f_t = 3.4 N/mm^2

E_c = 21500.N/mm^2 $\quad$ f_y = 460. N/mm^2

E_s = 214000. N/mm^2

Taking advantage of symmetry, only one quarter of the plate using 2x2 element mesh, as shown in Fig (4.21c) was analysed. The element size is dictated by the

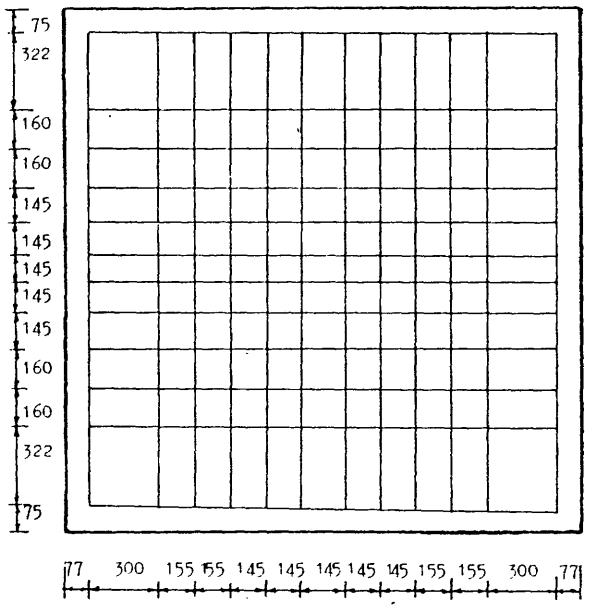

(a) Bottom steel

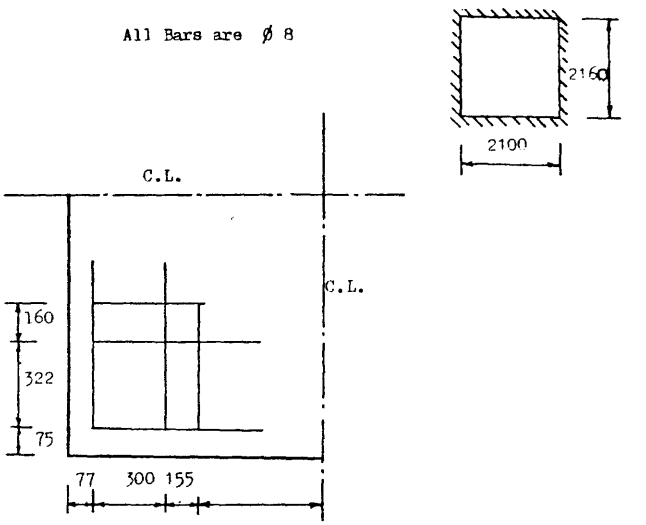

(b) Top steel

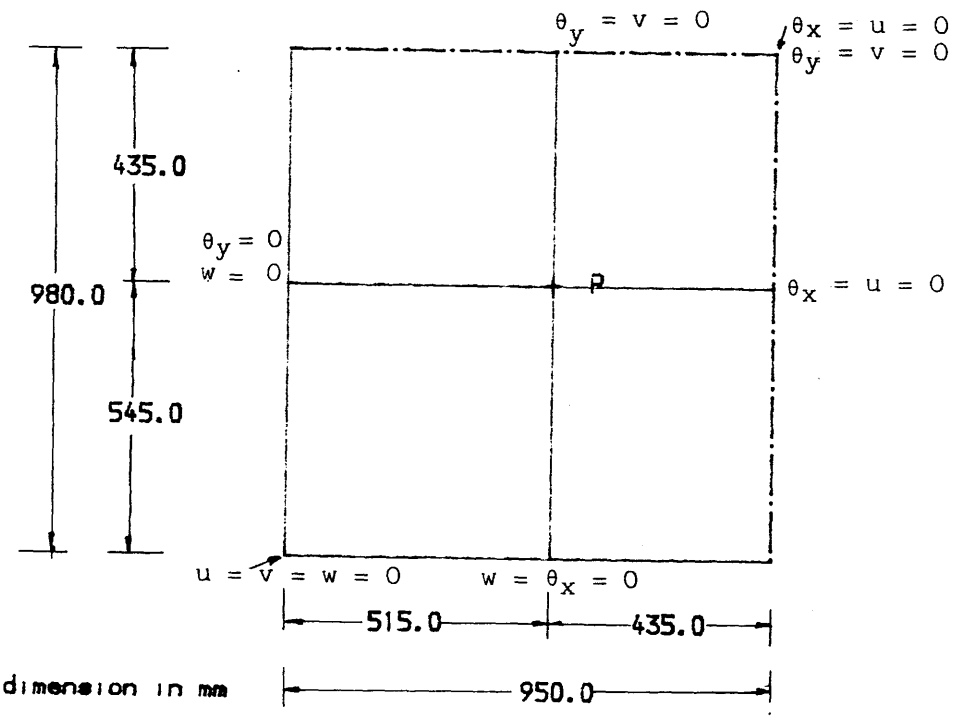

(c) Finite element idealisation

Fig. (4.21) Details of Hago's model three

idealization of the steel reinforcement. Three different idealizations for the concrete cross section have been used to study the effect of the number of layers. The convergence tolerance of 10% was adopted and this was reduced to 5% near the failure. The idea behind the reduced convergence tolerance near the failure is that, as explained in Section (4.8.1), the convergence is measured by the out-of-balance forces related to the total applied forces and at failure this percentage may be small but the out-of-balance force are large. Fig (4.22) shows the excellent agreement between the load-central deflection curves obtained experimentally and theoretically. There was some deviation from the experimental results for the stage between the first crack and the yielding of the steel.This may be due to the effect of the tension stiffening (the effect of the tension stiffening will be included in the next example). The theoretical failure load was 1.02 experimental failure load.

(i) Number of concrete layers

Four, six and eight concrete layers have been used to represent the cross-section of the plate. Load-central deflection curves are illustrated in Fig (4.23). Theoretically, if more layers are used, the nonlinear behaviour of the concrete is more accurate. However from the results presented in Figs (4.23) only small differences can be noted between the deflections obtained for the different number of layers. As expected the general trend is that a more flexible solution is obtained

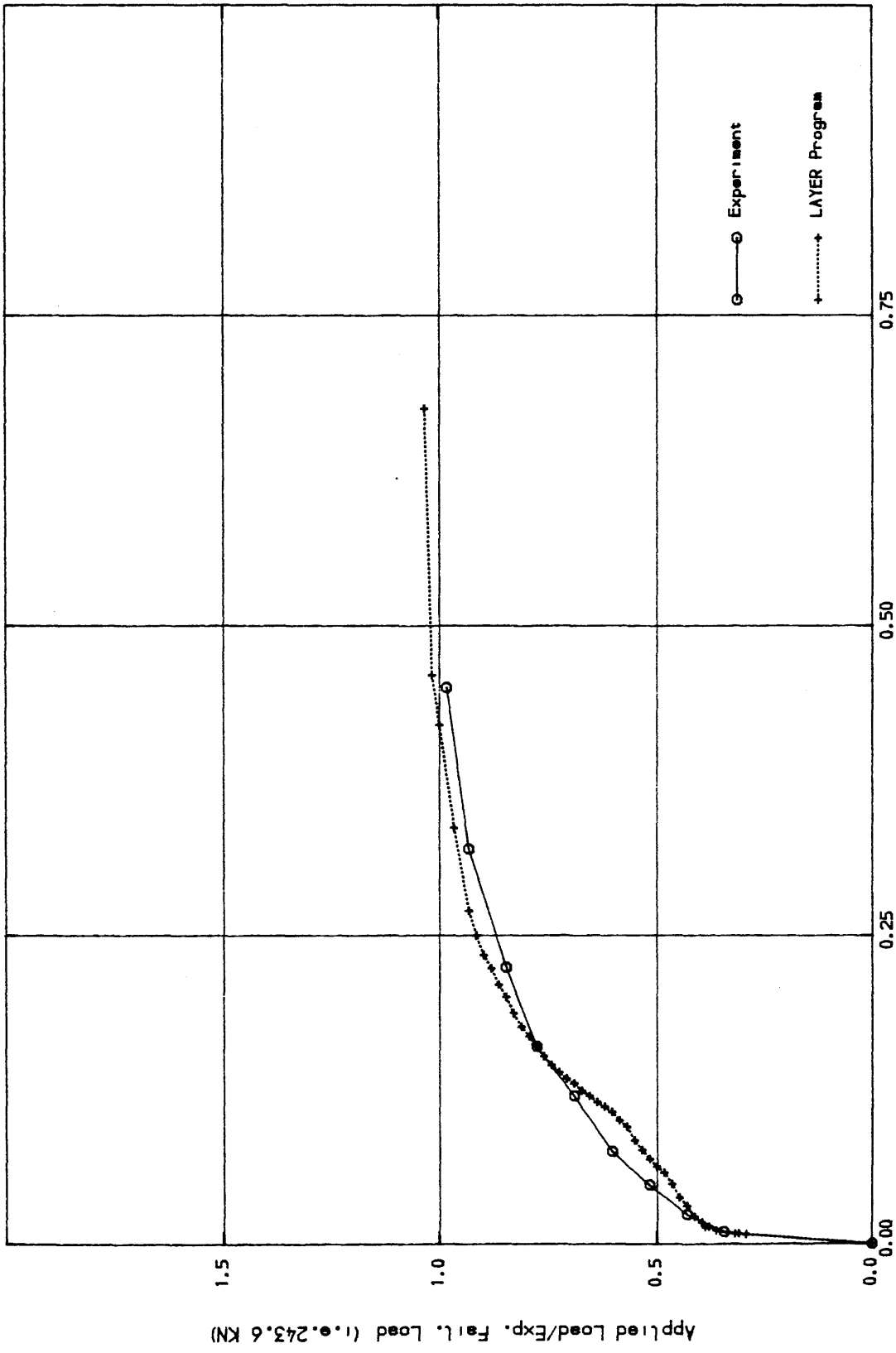

Fig. (4.22) Load-Central Deflection curve for Hago's model three

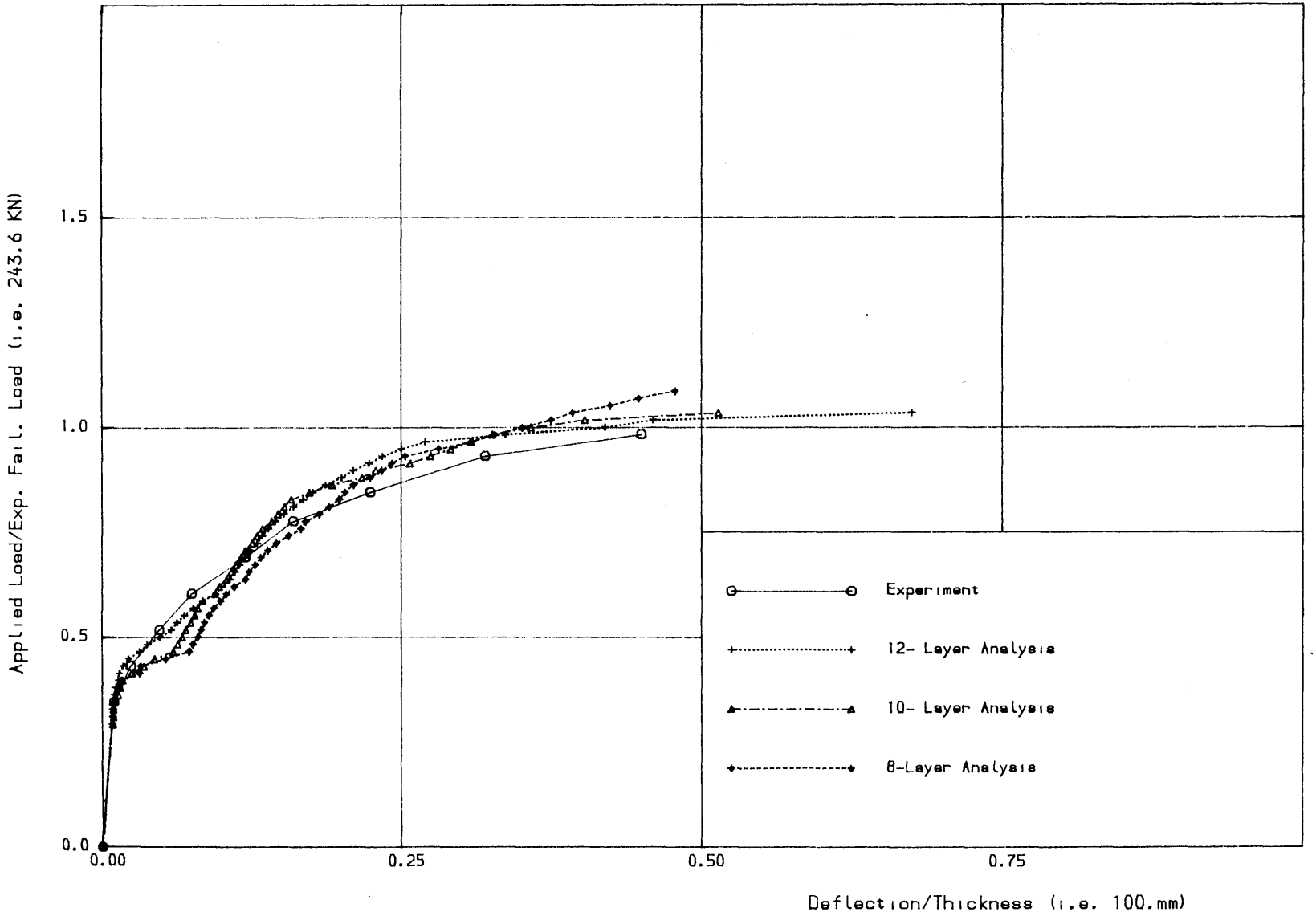

Fig. (4.23) Load-Central deflection curve for Hago's model three for different numbers of layer (inc. size = 0.05 Pcr.)

when a larger number of layers is used.

Comparisons of the solution time in all the cases show that the cost of analysis is only slightly influenced by the number of layers used in the analysis (the time decreases by 5% as the number of layer decreases by two). It is therefore concluded that the results are not sensitive to the number of concrete layers and that a total of 8 layers is sufficient, specially if there are two steel layers at top and two steel layers at bottom.

(ii) The load increment size

In order to keep costs down, it is important to apply small load increment only for highly nonlinear parts of the solution, e.g. the onset of cracking in concrete structures. Large load increments may be used whenever nonlinearity is not pronounced. Fig (4.24) shows the results of load-central deflection for the same slab using different sizes of load increments. It is clear that the predictions are slightly improved with a reduced size of load increment. However there is not much difference in the calculated results between load increment sizes for values of $0.05P_{cr}$, $0.1P_{cr}$ and $0.15P_{cr}$, where P_{cr} is the cracking load. It was decided that in the present work to use load increment size of $0.15\ P_{cr}$ for the highly nonlinear parts and to use a load increment of $0.25\ P_{cr}$ at the less sensitive situations.

b- Slab with two adjacent sides simply supported and one corner on column support

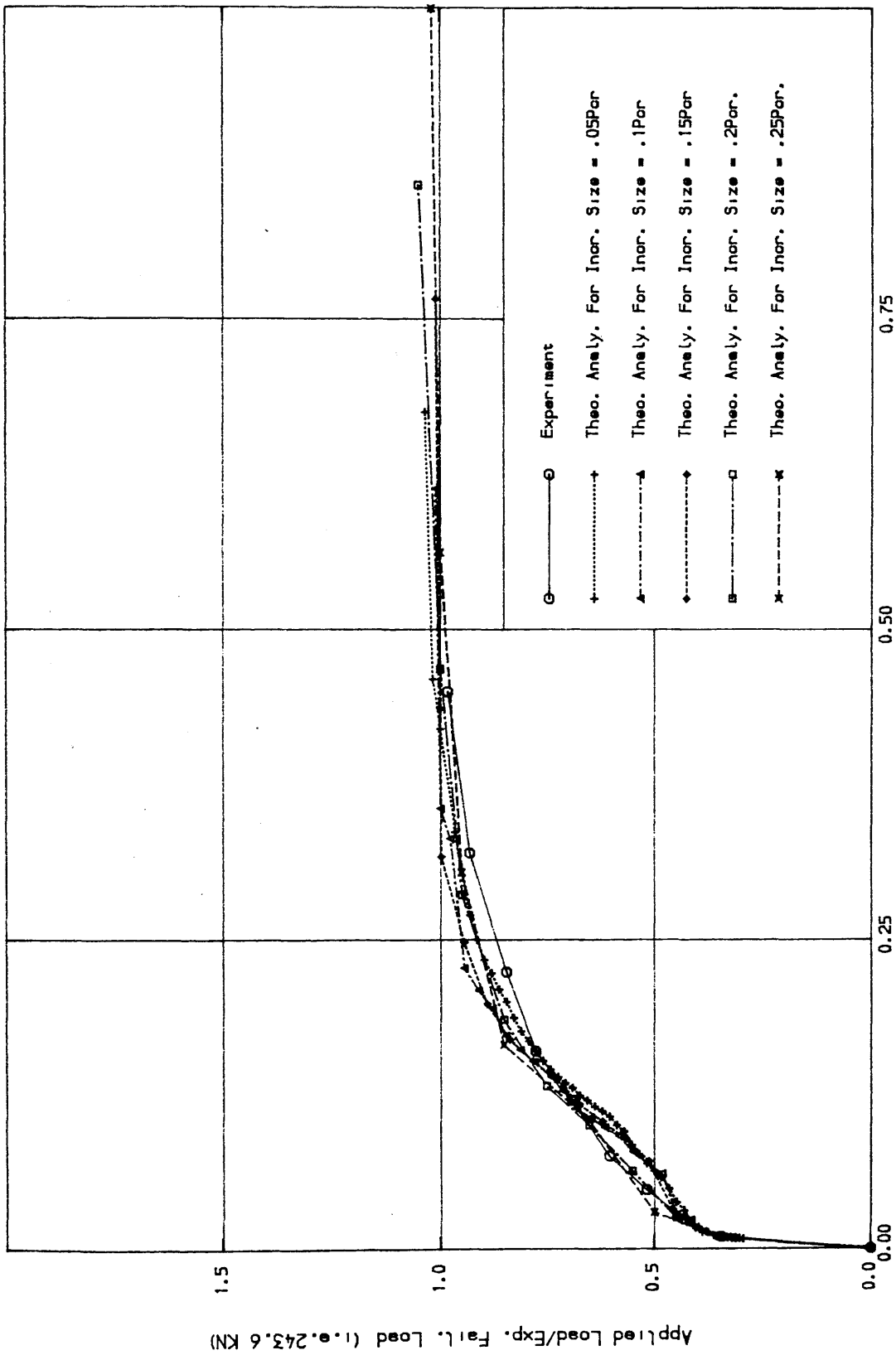

Fig. (4.24) Load-Central deflection for Hago's model three for different load increment

The slab is 2100x2160mm square and is simply supported along two adjacent sides only and pinned at the opposite corner to give a effective dimensions of 1960x1900 mm as shown in Fig (4.25). The thickness of the slab is 100 mm with orthotropic reinforcement as shown in Figs (4.25a) and (4.25b). The slab was loaded with two points loads as shown in Fig (4.25c). The following material properties are given in reference (9)

$f_{cu} = 37.3\ N/mm^2$ $\quad f_t = 2.97\ N/mm^2$

$c = 20400.N/mm^2$ $\quad f_y = 473\ N/mm^2$

$E_s = 214000.\ N/mm^2$

The slab was analysed, using 5X5 element mesh as shown in Fig. (4.26). The element size was chosen to suit on the system of loading and the arrangement of the steel reinforcement. The cross section was divided into 6 concrete layers and 4 steel layers where top and bottom steel are presented and 8 concrete layers and 2 steel layers where bottom steel only is presented. In the nonlinear solution, the combined algorithm is adopted in which the stiffness is updated at 2^{-rd} and 11^{-th} iterations, with the maximum number of iteration limited to 20. A convergence tolerance of 0.8% was adopted and was reduced near failure to 2%. In Fig (4.27) comparisons are presented for the load-deflection curves at position A (this is the critical point in the slab) obtained experimentally and those obtained in the present study ignoring tension stiffening and using two different tension stiffening curves viz (C_2 = 15.0 and C_2 = 25.0) in Eqn (4.48). It is noted from these comparisons that the

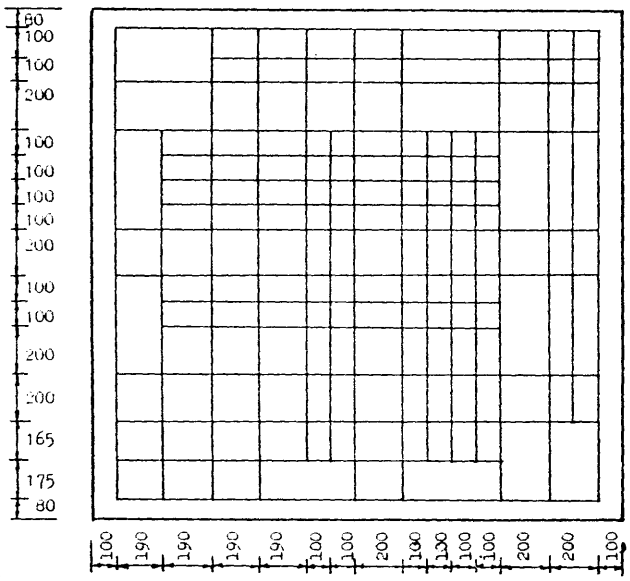

(a) Bottom steel reinforcement

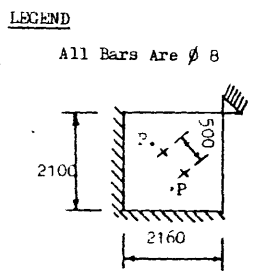

(c) Loading system

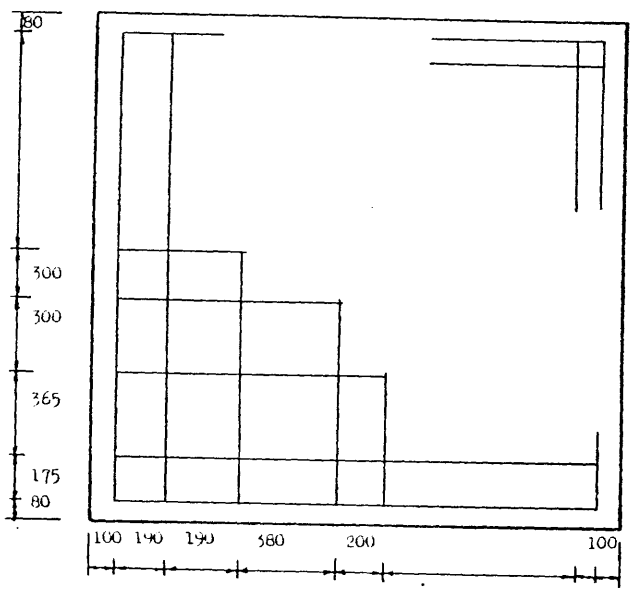

(b) Top steel reinforcement

Fig. (4.25) Details of Hago's Model four

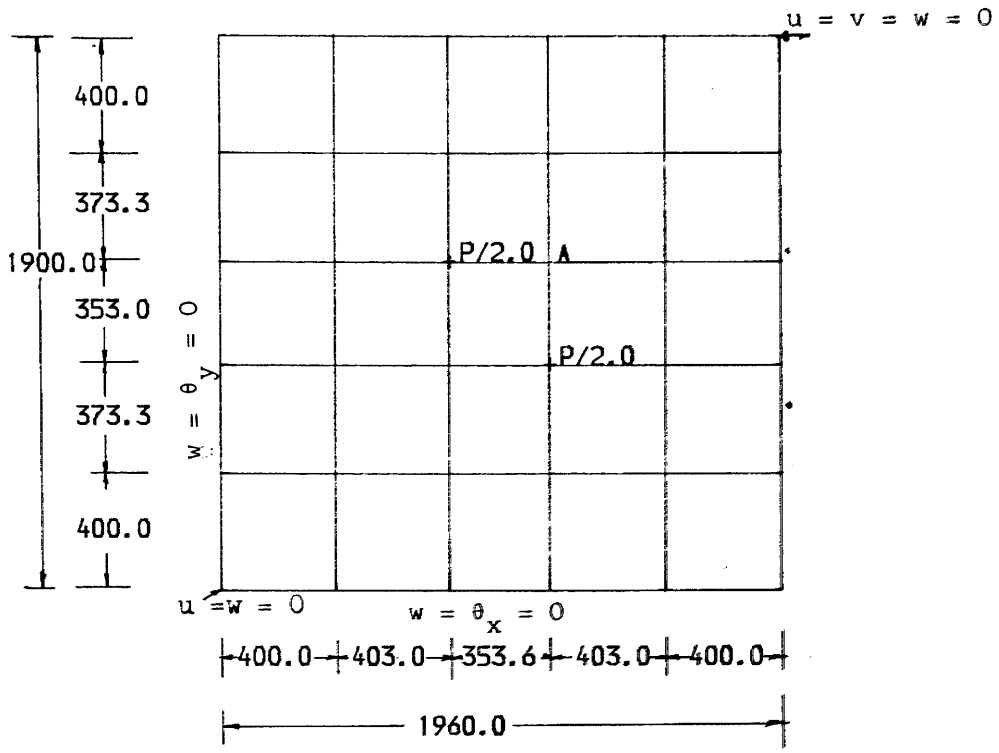

Dimension in mm

Fig. (4.26) Mesh idealistion of Hago's model four

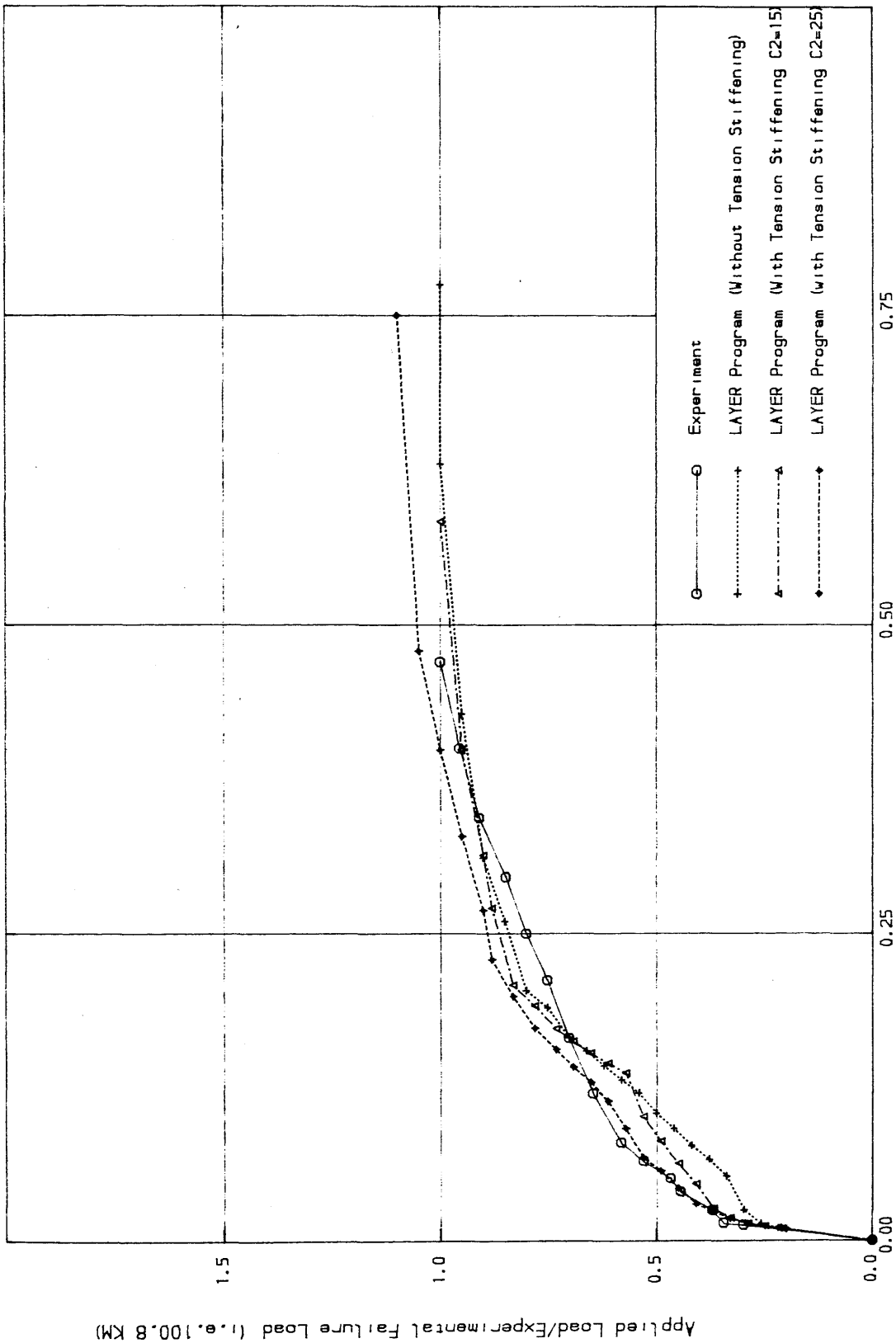

Fig. (4.27) Load-Deflection curve for Hago's model four at point A,
(see Fig. (4.26))

predicted results compare well with the experiment in all cases. However, better comparisons are obtained from using tension stiffening C_2 =15 (the factor C_2 determines the length of the descending branch). This result improved (especially at the serviceability limit) when C_2 = 25 but the predicted failure load was 10% higher than the experimental failure load. In Table (1) the initial cracking load, yielding load and failure load obtained experimentally are compared with those obtained numerically.

Table (1) Comparisons of the Initial Cracking Load and the Yielding Load

Stage of loading	Hago Experimental	Present study		
		with ten.		without ten
		C_2 = 15	C_2 = 25	
	kN	kN	kN	kN
Cracking load	35.1	25.2	25.2	25.2
Yielding load	90.	80.64	88.7	75.60
failure load	100.8	100.8	110.88	100.8

Obviously, the load at which the steel yields is affected by the tension stiffening and so also the ultimate load. It was noted that when tension stiffening with C_2 = 15 was used the average concrete strain $C_2 \varepsilon_{cr}$ (ε_{cr} is the cracking strain of the concrete) at which the cracked concrete is not allowed to carry stress normal to the crack direction is less than the strain at which the steel reinforcement started to yield. However when the tension stiffneing with C2 = 25 is used, the average

concrete strain $C_2 \varepsilon_{cr}$ is greater than the strain at which the steel reinforcement starts to yield.

4.9.3 Simply Supported T-Beam

This example was chosen to demonstrate the ability of the present model to analyse stiffened plates. This beam was tested and analysed by Rao (as reported by Hago (9)) using a combination of beam elements for the web of the beam and plain stress element for the flanges. The structural details and loading of the beam are shown in Fig (4.28a). The following material properties are given by Hago (9):

$_c$ = 35000. N/mm^2 $\quad E_s$ = 200000 N/mm^2

f_{cu} = 48. N/mm^2 $\quad f_t$ = 4.8 N/mm^2

ν = 0.2 $\quad f_y$ = 340. N/mm^2

By taking advantage of symmetry, one half of the beam was analysed using 4x3 elment mesh as shown in Fig (4.28b). The flange concrete section is divided into 5 concrete layers and 2 smeared steel layers. The web element is divided into 10 concrete layers and 2 top and 2 bottom smeared steel layers. The combined algorithm is used for the nonlinear analysis and a force convergence norm of 5% tolerance is adopted.

In Fig (4.29) the load-central span deflection curves for analysis by Rao, Hago and the present study for different value of ft are shown. The correlation is very good between the experiment and analytical curve for the present study. The analysis predicts a higher cracking

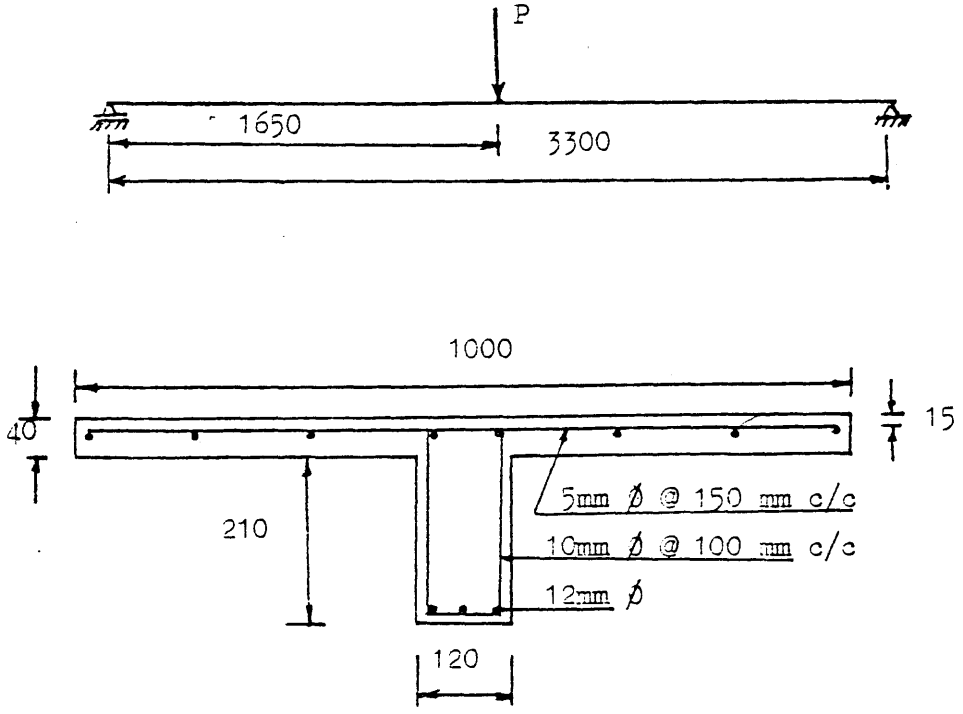

(a) Geometry and details of the reinforcement

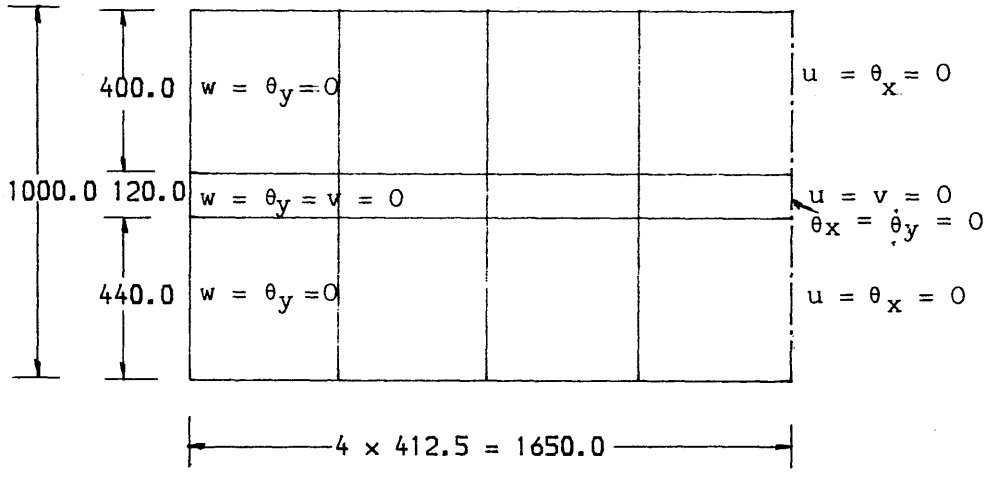

dimension in mm

(b) Finite element idealisation

Fig. (4.28) Details of Rao's T-Beam

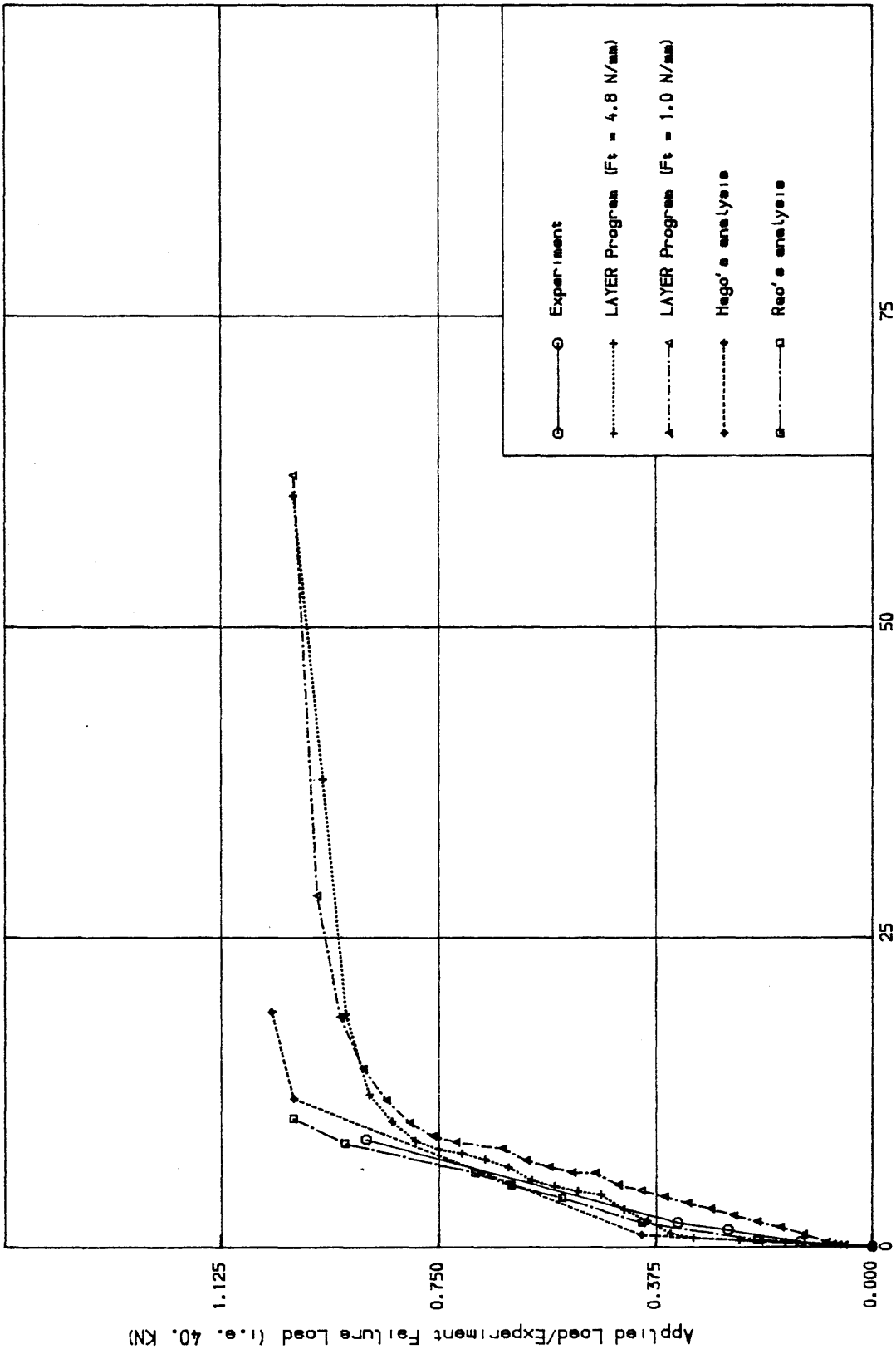

Fig. (4.29) Load-Central deflection curve for Rao's T-Beam (B1)

load of 13.6 KN as compared with actual cracking load of 9 KN. The failure occurs by yielding of the reinforcement at the middle span under loads equal to the experimental failure load. In his analysis Rao (as reported by Hago (9)) also obtained very much higher cracking load than the experimental value. He suggested that the low value of experimental cracking load could be due to the beam being already cracked prior to test, and suggested the value of 0.96 N/mm^2 for tensile strength. This value has been used in the present analysis as shown in Fig (4.29) giving a cracking load as 3.2 KN. The new value of f_t did not effect the ultimate load. When Rao (as repoted by Hage (9)) used the tensile strength equal to 0.96 N/mm^2 in his analysis, the behaviour was very flexible and he was not able to predict the ultimate load correctly. The experimental cracking load can be reached if a value of 2.2 N/mm^2 is used for tensile strength of concrete.

2.8.3 Hayes's Slab-Beam System

In this example, a square integral beam-slab is chosen from a series of tests conducted by Hayes (28). The edge beams were simply supported at the corners.

The plan and cross-section of the slab-beam are shown in Fig (4.30a). By taking advantage of biaxial symmetry, only one quarter of the slab is analysed using 5X5 element mesh as shown in Fig. (4.30b).

For the nonlinear solution, a combined algorithm is adopted ignoring tension stiffening. The load increment

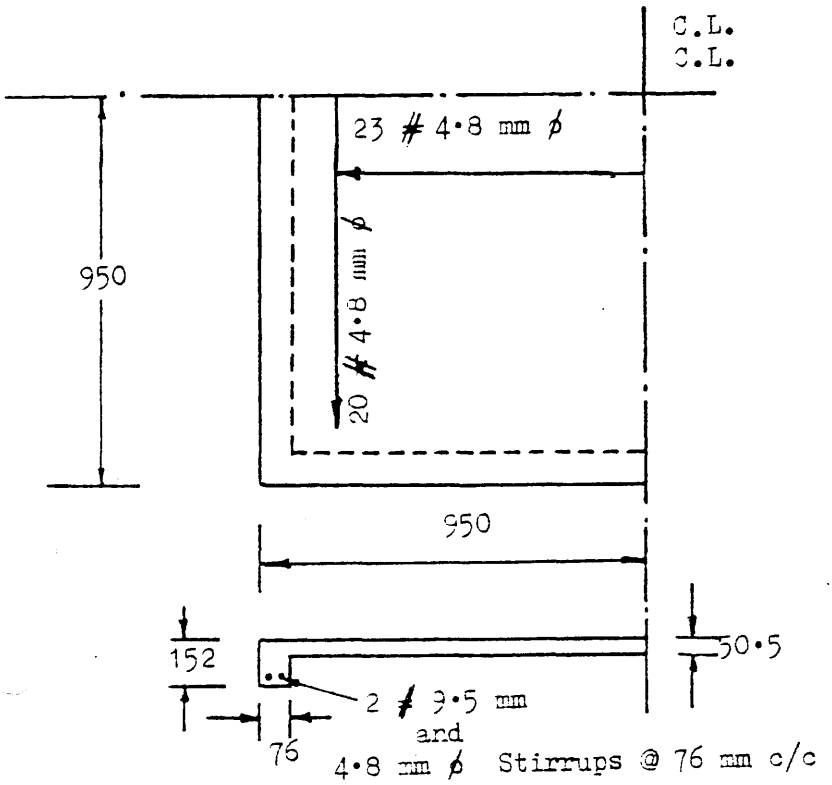

(a) Geometry and details of the reinforecement

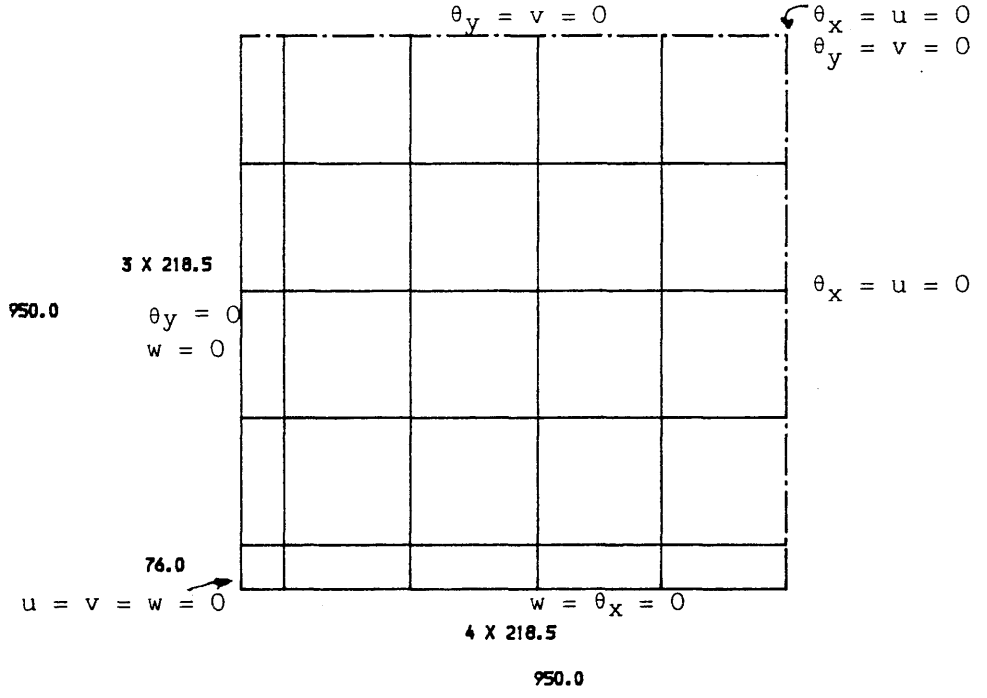

Dimension in mm

(b) Finite element idealisation

Fig. (4.30) Details of Hayes' s slab-beam system

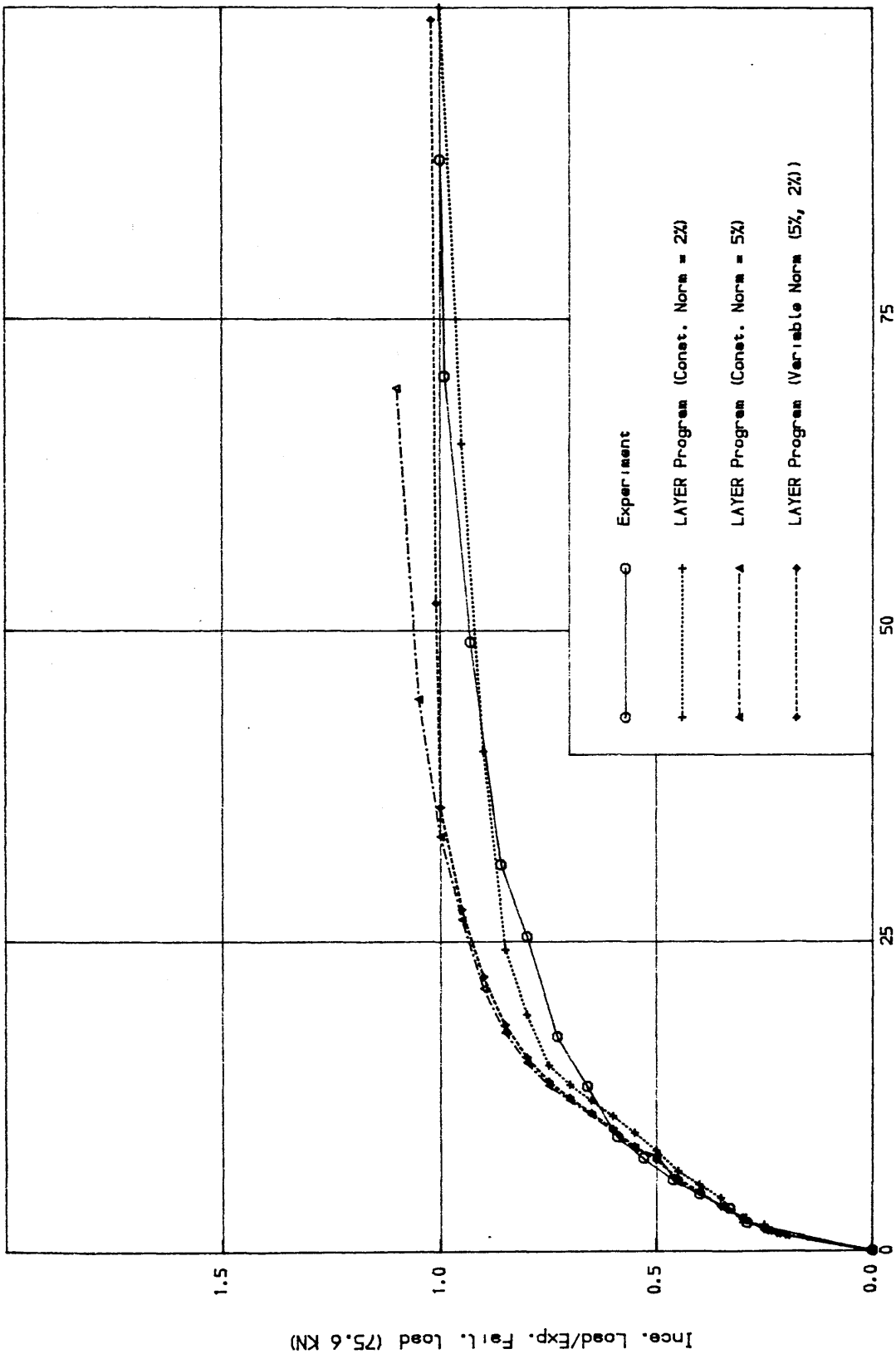

Fig. (4.31) Load-Central deflection curve for Hayes's slab

was 0.05 times experiment failure load. Fig (4.31) shows the load-central deflection curves obtained experimentally and those obtained in the present study using three different tolerance levels (constant norm of 5% and 2% and variable norm of 5% and 2%). It can be noted that the predicted results compare very well with the experiment results for all values of convergence tolerance. The three analysis predict the first cracking of the beam at a load 5.2 KN/mm^2 which is equal to the experimental cracking load. In the post cracking range and up to 80% of the ultimate load, only an average of 5 to 11 iterations are needed to achieve 2% tolerance and 3-8 iterations are needed for 5% tolerance. First yield of steel was detected at the centre of the supporting beams at 1.05 of the experimental steel yield load. The maximum number of iterations to achieve the specified tolerance level was increased by 30% when the tolerance was decreased from 5% to 2%. The 5% convergence tolerance level was used for most of the problems analysed in this work.

4.10 Conclusions

i- The proposed computational model is capable of providing a good prediction of the overall behaviour of reinforced concrete slabs, both plane and stiffened systems failing in flexure.

ii- The predicted behaviour and the cost of analysis are not significantly influenced by the number of concrete layers adopted and a total of 8 concrete layers is sufficient for all practical situations.

iii- The deflection values are sensitive to the value used for tensile strength of concrete and are much less influenced by the value of compressive strength.

iv- The deflections values are sensitive to amount of tension stiffening adopted especially at service load. However the tension stiffening is itself affected by many factors such as bar spacing, mesh size, the type of assumed curve to represent the tension stiffening and the convergence tolerance etc so that it is difficult to suggest values to be adopted in numerical analysis.

v- The deflections and the ultimate failure load are affected to a certain extent by the value of the convergence tolerance. 5% tolerance is recommended to be used and at the failure stage this tolerance should be reduced to 2%.

vi- A value of ($\beta = .4/(\varepsilon_f / \varepsilon_{cr})$) for the retention factor of concrete is recommended.

vii- A load increment of 0.15 P_{cr}. size can be used for highly nonlinear parts (onset of cracking and af failure) and way be increased up to 0.25P_{cr}. wherever nonlinearity is not too great.

CHAPTER FIVE

DIRECT DESIGN EQUATIONS - A CRITICAL STUDY

5.1 INTRODUCTION

In chapter four, a reliable finite element program was described. In this chapter, the direct design procedure described in chapter three will be critically examined using the finite element program. Only the uniform state of stress (inplane or flexural) will be examined. The procedure adopted is as follows:

i- The geometric details, materials properties and the design loads are used as input data for the program. The program performs an elastic analysis of the slab using the initial uncracked concrete section properties. At the specified ultimate design load, the stress distribution (N_x, N_y, N_{xy}) for inplane case or (M_x, M_y, M_{xy}) for plate bending case is calculated.

ii- For inplane stresses case, Clark's (37) equations given in chapter three are used to calculate the required areas of steel.

iii- For plate bending case, the design equations of Wood and Armer (77) described in chapter three, are used to calculate the required resisting moments. Using the limit state theory (Appendix A), the steel areas required to resist the design moments are calculated.

The main object of the critical study is to study the behaviour of the slab element when skew reinforcement is used. An additional object is to study the effect of tensile strength of concrete on the predicted behaviour.

For this purpose, a full incremental nonlinear analysis is performed by considering two different methods as follows;

(a) In the first method called the fixed crack analysis, the crack direction remains fixed and depends on the direction of the principal tensile stress at the loading state when the principal tensile stress equals the tensile strength of concrete. In addition, if there are two cracks, they are expected to be orthogonal. As has been explained in chapter four, the procedure involves the modification of the material stiffness matrix to allow for orthotropic properties of concrete after the concrete has cracked. Because of the fact that due to the aggregate interlock, shear stress is permitted on the cracked planes, there is a possibility of tensile stresses building up in directions other than the crack directions. As is well know (Gupta and Akbar (98.)), in reinforced concrete the direction of the initial and final cracks do not coincide. The assumption of fixed crack directions evidently involves errors in the analysis.

(b) In the second method called **No-Tension** analysis, the principal tensile stress is brought back to zero at every stage of the analysis. No modification in the material stiffness matrix is involved in this type of analysis. In addition the method accords with the assumption normally made in design of not relying on the tensile strength of concrete.

5.2 THEORETICAL DEVELOPMENT

It may be useful for the understanding of the stress distribution after cracking (either by using fixed crack analysis or **No-Tension** analysis) to establish the equilibrium condition at different stages of loading. Consider the skew reinforced plane stress element under N_y only shown in Fig. (5.1a). Let N_{1c} and N_{2c} be the principal stresses (assumed tensile) in the concrete Fig. (5.1b) . The equivalent stress distribution in the x,y system is given by

$$N_{xc} = N_{1c} \cos^2\theta + N_{2c} \sin^2\theta \qquad (5.1)$$

$$N_{yc} = N_{1c} \sin^2\theta + N_{2c} \cos^2\theta \qquad (5.2)$$

$$N_{xyc} = (N_{1c} - N_{2c}) \sin\theta \cos\theta \qquad (5.3)$$

where N_{xc}, N_{yc} and N_{xyc} are inplane stresses in the concrete and θ is the inclination of the principal stress N_{1c} to x-axis as shown in Fig. (5.2b).

(i) Before cracking

The following equilibrium equations are valid

$$N_{xyc} + N_{\alpha s} \sin\alpha \cos\alpha = 0.0 \qquad (5.4)$$

$$N_{yc} + N_{\alpha s} \sin^2\alpha = N_y \qquad (5.5)$$

$$N_{xc} + N_{xs} + N_{\alpha s} \cos^2\alpha = 0.0 \qquad (5.6)$$

where $N_{\alpha s}$ and N_{xs} are the stresses in the α -steel and x-steel respectively and α is the angle of inclination of α-steel to the X-axis as shown in Fig. (5.2a)

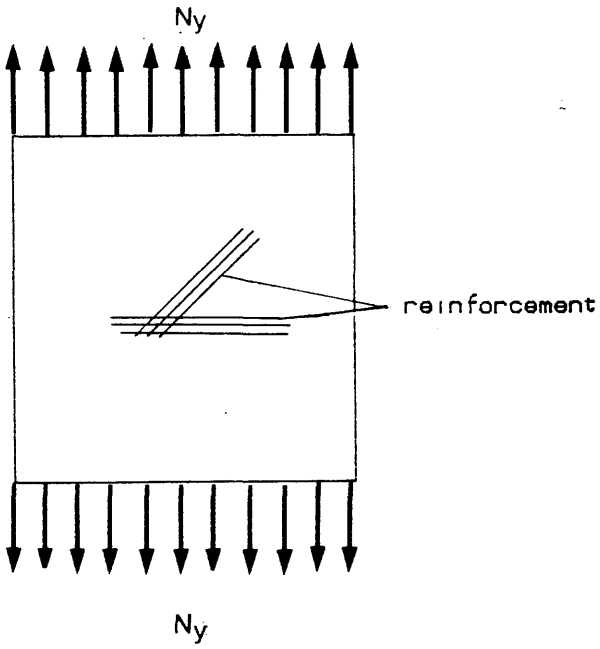

(a) Skew reinforcement

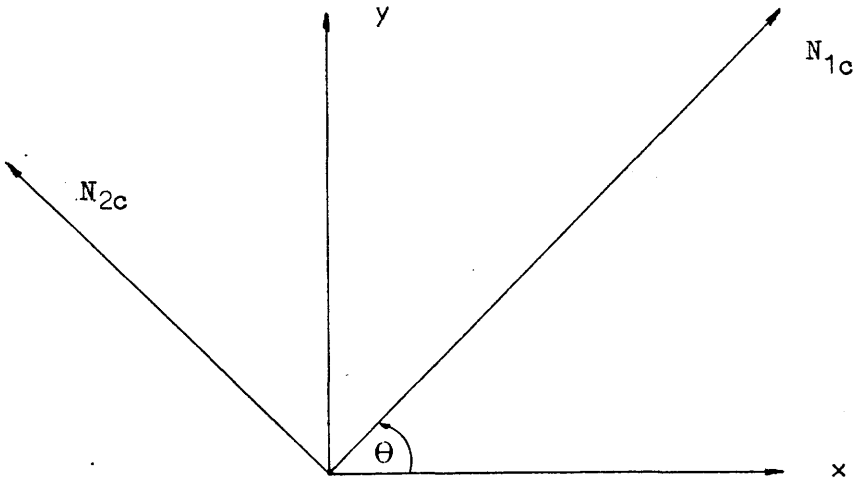

(b) Principal stress direction

Fig. (5.1) Element under plane stress

Before cracking, obviously $N_{\alpha s}$ and N_{xs} are practically zero, therefore $N_{xc} = N_{xyc} = 0.0$ (5.7)

$N_{yc} = N_y = N_{1c}$, $\theta = 90$ and $N_{2c} = 0.0$

i.e Initial crack is parallel to x-axis

(ii) After cracking

(a) In fixed crack analysis

$N_{yc} = 0.0$ because this is the stress normal to initial crack. However N_{yc} is not a principal stress because shear stress is assumed to act on the cracked plane. From the equilibrium equations we have;

$$N_{\alpha s} = N_y / \sin^2\alpha \tag{5.8}$$

$$N_{xyc} = -N_{\alpha s} \sin\alpha\cos\alpha = -N_y \cot\alpha \tag{5.9}$$

$$N_{xc} + N_{xs} = -N_{\alpha s} \cos^2\alpha = -N_y \cot^2\alpha \tag{5.10}$$

If it is assumed that the principal tensile stress N_{1c} in concrete is inclined at θ_1 to the x- axis, then since N_{yc} is held to 0.0

$$\therefore \quad N_{1c} \sin^2\theta_1 = -N_{2c} \cos^2\theta_1$$

i.e $$N_{2c} = -N_{1c} \tan^2\theta_1$$

$$\therefore \quad N_{xyc} = (N_{1c} - N_{2c}) \sin\theta_1 \cos\theta_1 = -N_y \cot\alpha$$

$$\therefore \quad N_{xyc} = N_{1c} (1 + \tan^2\theta_1) \sin\theta_1 \cos\theta_1$$

$$= N_{1c} \tan\theta_1 \tag{5.11}$$

$$\therefore \quad N_{1c} = -N_y \cot\alpha \cot\theta_1 \tag{5.12}$$

$$N_{2c} = N_y \cot \alpha \tan \theta_1 \qquad (5.13)$$

note that if $\tan\theta_1 > 0.0$ then, $N_{2c} > 0.0$, therefore there is the possibly of a second crack but not orthogonal to the first one.

Since $N_{xc} = N_{1c} \cos^2 \theta_1 + N_{2c} \sin^2 \theta_1$

$$N_{xc} = N_y \cot (- \cos^3 \theta_1 / \sin \theta_1 + \sin^3 \theta_1 / \cos \theta_1)$$

$$= -2 N_y \cot \alpha \cot 2\theta_1 \qquad (5.14)$$

from Eqn (5.10)

$$N_{xc} + N_{xs} = - N_y \cot^2 \alpha$$

$$N_{xs} = -N_y \cot^2 \alpha + 2 N_y \cot \alpha \cot 2\theta_1$$

$$= -N_y \cot \alpha (\cot \alpha - 2 \cot 2\theta_1) \qquad (5.15)$$

unless $\cot \alpha < 2 \cot 2\theta_1$ in Equ (5.15), x - steel (N_{xs}) will be is compression.

(b) Concrete as No-Tension analysis

In **No-Tension** analysis, any tensile stresses in concrete will be reduced to zero as assumed by Clark (37). For this particular case of loading, N_{1c} will be always tension, N_{2c} will be compression and the angle of principal stress θ will be different from 90^o depending on the angle of skew. When N_{1c} is reduced to zero, the equivalent stresses in concrete will be as from Eqns (5.1) to (5.3) assuming that $N_{1c} = 0$.

$$N_{xc} = N_{2c} \sin^2 \theta \qquad (5.16)$$

$$N_{yc} = N_{2c} \cos^2 \theta \qquad (5.17)$$

$$N_{xy} = - N_{2c} \sin \theta \cos \theta \qquad (5.18)$$

The equilibrium equations at any stage of loading are given by

$$N_{2c} \sin\theta \cos\theta + N_{\alpha s} \sin\alpha\cos\alpha = 0.0 \quad (5.19)$$

$$N_{2c} \cos^2\theta + N_{\alpha s} \sin^2\alpha = N_y \quad (5.20)$$

$$N_{2c} \sin^2\theta + N_{xs} + N_{\alpha s} \cos^2\alpha = 0.0 \quad (5.21)$$

Since there are four unkowns Viz N_{2c}, $N_{\alpha s}$, N_{xs}, θ additional equation is needed for a solution. The additional equation is obtained by optimizing the steel i.e

$$\frac{d\,(N_{\alpha s} + N_{xs})}{d\tan\theta} = 0.0 \quad (5.22)$$

Solving Eqns (5.15) to (5.22) leads to

$$\tan\theta = -\cot\alpha \pm \operatorname{cosec}\alpha \quad (5.23)$$

$$N_{xs} = N_y \cot^2\alpha + |N_y \cot\alpha/\sin\alpha| \quad (5.24)$$

$$N_{\alpha s} = N_y \operatorname{cosec}\alpha + |N_y \cot\alpha/\sin\alpha| \quad (5.25)$$

$$N_{c2} = -2\,(N_y \cot\alpha)(\cot\alpha \mp \operatorname{cosec}\alpha) \quad (5.26)$$

5.3 FIXED CRACK ANALYSIS

In fixed crack analysis, once the first crack occurs, its direction is held fixed. A second crack is checked at right angles to it at any time (more details in section (4.5.3) chapter four). The concrete tensile strength is taken as 0.08 of concrete compressive strength and the shear retention factor B is taken according to;

$$\beta = .4(\varepsilon_f/\varepsilon_{cr}) \text{ and } \beta \geq .1 \quad (5.27)$$

where ε_{cr} is the tensile cracking strain

ε_{n} is the fictitious strain normal to the crack at the stage of loading under consideration

The combined algorithm is adopted in which the stiffness is updated at 2nd and 11th iteration, with the maximum number of iteration limited to 20. Convergence tolerance is taken at 1% for angles of skew equal to 90^{o} and 75^{o} and 5% for angles of skew equal to 60^{o} and 45^{o} respectively. The reason for adopting coarse convergence at small angle of skew is that it was found very difficult to attain the 1% tolerance for angles of skew equal to 60^{o} and 45^{o}.

5.4 CONCRETE AS NO TENSION MATERIAL ANALYSIS

In **No-Tension** analysis, the concrete tensile strength is assumed to be zero to reflect the design assumptions. In this analysis, initial tangent stiffness approach is adopted as explained in section (4.7) (unless of course if the steel yields or concrete crushes when variable stiffness procedure is adopted).

As in fixed crack analysis, the convergence tolerance is taken as 1% for angles of skew 90^{o} and 75^{o} and 5% for angles of skew 60^{o} and 45^{o} respectively. The maximum number of iterations is limited to 150. This convergence tolerance was changed in some cases as will be explained later at the appropriate place.

5.5 ANALYSIS for Unit Stress

Four cases of constant stress have been considered viz;

(a) Inplane tensile axial load N_y

(b) Inplane shear load N_{xy}

(c) Pure bending moment M_y

(d) Pure torsion moment M_{xy}

For each case of loading, four slabs were considered. The slabs were identical except in reinforcement arrangement. Four angles of skew viz 90°, 75°, 60° and 45° as shown in Fig. (5.1) were studied. Table (5.1) gives the details of slabs examined.

5.6 RESULTS

5.6.1 Introduction

Tables (5.2) to (5.5) summarize the result for the cases considered. The results of Load-Deflection (or displacement), Load-Steel Stresses and Load-Maximum Concrete Compressive Stress are plotted for fixed crack analysis and **No-Tension** analysis for each case of loading in Fig. (5.2) to Fig. (5.39). Also for **No-Tension** analysis, the initial angle of crack (the false angle at the first iteration), the final angle of crack (the true angle at the final iteration) and the residual tensile stress in concrete after the specified convergence tolerance has been achieved, are plotted for the case of 75° skew for inplane load N_y.

5.6.2 Discussion of the Results

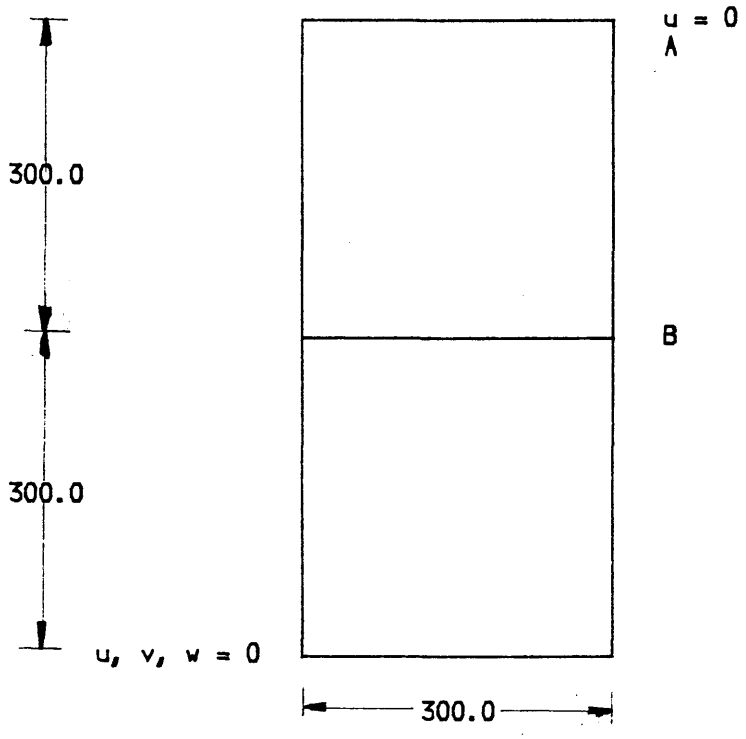

Note: For pure inplane case all w, Θ_x, Θ_y are constrained every-where

(a) Finite element idealisation for pure bending case

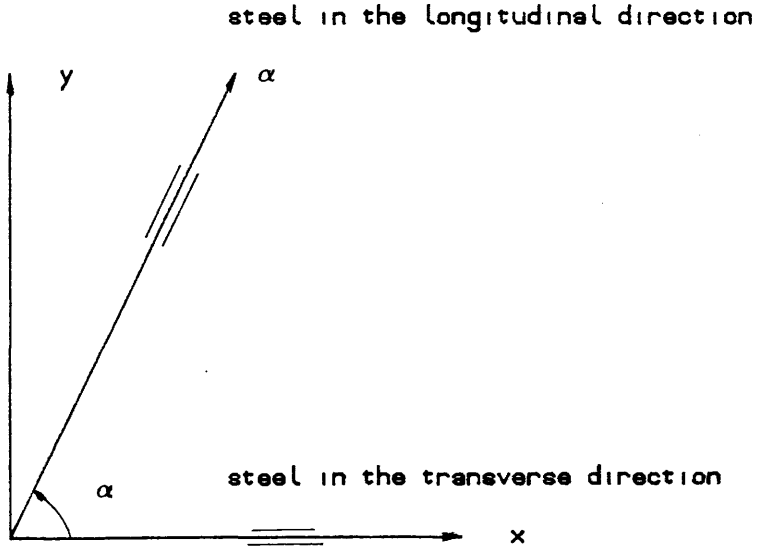

(b) Steel arrangment

Fig. (5.2) Details of tested slab element

Table (5.1) The Load Cases and Their Design Areas of Steel.

Angle of Skew	Pure tensile inplane N_y			Pure inplane N_{xy}			Pure M_y			Pure M_{xy}				
	Design Load N/mm	Steel mm^2/mm		Design Load N/mm	Steel mm^2/mm		Design Moment N.mm/mm	Steel mm^2/mm		Design Moment N.mm/mm	Steel mm^2/mm			
		Long. α	Trans. X		Long. α	Trans. X		Long. α	Trans. X		Bottom Long. α	Bottom Trans. X	Top Long. α	Top Trans. X
90^o	1000.0	2.667	Zero	1000.0	2.667	2.667	10000.0	.3228	Zero	10000.0	.3228	.3228	.3228	.3228
75^o	1000.0	3.6	.9312	1000.0	2.762	4.1898	10000.0	.44015	.1106	10000.0	.3345	.516	.3345	.1589
60^o	1000.0	5.33	2.667	1000.0	3.079	6.158	10000.0	.666	.3228	10000.0	.37447	.7771	.75	Zero
45^o	787.0	7.165	5.065	787.0	2.968	7.166	7870.0	.916	.6307	7870.0	.3604	.916	.2524	Zero

Note: The design load of 45^o is reduced to ensure ductile failure.

E_c = 24700 N/mm^2, f_{cu} = 38 N/mm^2, f_t = 2.85 N/mm^2, E_s = 170500 N/mm^2, f_{sy} = 375 N/mm^2, thickness = 100 mm

5.6.2.1 Inplane tensile load N_y

Results are presented in Table (5.2) and Figs (5.3) to (5.11). In general it was noticed that in **No-Tension** analysis, after the longitudinal steel had yielded, the rate of convergence was very slow. Also it was noted that as the angle of skew decreases, the rate of convergence became slow. This is quite logical because as the angle of skew decreases, shear stresses in concrete increases so as to be in equilibrium with the shear stress component of the α- steel. This shear stress produces tensile stress in addition to the tensile stresses in concrete due to external loading. In other words, the forces to be redistributed increase but because of the use of the initial tangential stiffness this has to be absorbed by the concrete. Due to this convergence problem, the convergence tolerance was increased to 5% for angles of skew 60^{o} and 45^{o}.

(a) Steel stress in the longitudinal direction

Table (5.2) and Figs (5.3) and (5.4) show that as the angle of skew decreased, in fixed crack analysis the steel in general did not yield. However in the case of **No-Tension** analysis the steel always yielded.

(b) Steel stress in transverse direction

Fig. (5.5) shows that for fixed crack analysis, for angle 75^{o} the steel carried a zero stress. For angles 60^{o} and 45^{o} the steel was in compression. This unexpected behaviour is because in fixed crack analysis, once a crack forms it is assumed that the direction of the crack remains constant throughout subsequent load increment.

This in general is not true. This incorrect angle is responsible for the incorrect redistribution of stresses in the subsequent load increment and as was shown previously in Eqn (5.15), the stress level in the transverse steel became compressive.

In **No-Tension** analysis, Fig. (5.7) shows that the transverse steel carries a considerable tensile stresses (the steel for 75° angle carries 0.97 Fy at ultimate load and the steel for angle 60° yield).

(c) Load-Maximum compressive stress in concrete.

Fig. (5.7) and Table (5.2) show that in fixed crack analysis, for angles 60° and 45°, concrete is crushed by reaching maximum compression strain before reaching the ultimate compressive strength. This is because after concrete has cracked in two orthognal directions the stiffnesses in these directions are reduced to zero and only the reduced shear stiffness is affected (see section (4.5.3) for more details). Therefore the strain in concrete is not related to the strength but in the analysis, the restriction on the maximum compressive strain comes in to operation.

In **No-Tension** analysis, Fig. (5.8) shows that as the angle of skew decreases, the compressive stresses increases.

(d) Ultimate load

Referring to Table (5.2) and load Vs displacement

curves in Fig. (5.9), in fixed crack analysis, the ultimate load for angle 90° is equal to the design load and the failure was due to yielding in the steel. It can also be seen that when the angle of skew is decreased, the ultimate load becomes higher than the design load for 75° angle, but for 60° and 45° angles the ultimate load is lower than the design load. In fact the failure load in fixed crack analysis was dependent on the appearance of the second crack which is dependent on the tensile strength of concrete and the shear retention factor B. For skew angle equal to 75°, the second crack appeared at a load of 1.3 design load and at that increment, the steel yielded due to the redistribution of the tensile stress. For angles 60° and 45°, the second crack appeared earlier (at 0.7 and 0.51 of the design load respectively) leading to the maximum compression strain in concrete reaching the limit value of crushing strain (0.0035). This was due to the effect of inplane shear strain as will be presently explained. In this analysis the first crack did not close but a second crack formed when the skew angle was different from 90°. It may appear that there is a contradiction between the appearance of the second crack and the loading case which is an uniaxial state of stress. But it has been shown in section (5.2) Eqn (5.13) from the equilibrium condition that after the first crack was formed, there was a possibility for the tensile stresses to build up in a direction which was not necessarily orthogonal to the first crack direction but was dependent on the angle of principal stresses (θ_1), the angle of skew (α) and the load level as shown in Eqn

(5.15).

For **No-Tension** analysis, Table (5.2) shows that the ultimate loads for angles 75^{o} and 60^{o} were slightly higher and for 45^{o} slightly lower than the design load. This was due to the limited number of iterations viz 150 which was insufficient to achieved proper convergence. It was found that for an angle of 45^{o} it was very difficult to get converged result after the steel yielded. In all cases, the failure occurred by yielding of the steel. Fig. (5.10) shows the load displacement at point A (see Fig. (5.2)) relationship for different angle of skew considering no-tension analysis. It showed that as the angle of skew decreased, the structure became more flexible and the failure was due to yielding of steel and not due to crushing of concrete.

(e) The effect of the angle of steel on the angle of crack

Fig. (5.11a) shows for the 75^{o} angle case, the effect of the skew reinforcement on the crack direction. It can be seen that at the initial load stages, the angle of crack at the beginning of iteration (incorrect orientation) is very different from the final angle of crack at the end of iteration (correct orientation). It can be seen also that at later load stages the initial angle of crack is closer to the final angle of crack. When the final angle of crack was compared with the angle of principal stress calculated using Eqn (5.23) it was found that at the initial stage of loading there was not much difference between the two values (see Fig. (5.11a). In the later load stages it was found there a large

Table (5.2) Comparison Between Fixed Crack and Concrete as No-tension Analysis For N_y Case.

Angle of Skew	Load at yield of α-steel/ design load		Load at yield of X-steel/ design load		Max-compression stress at ultimate load/f_{cu}		Ultimate load/ design load	
	Fixed crack analysis	No-tension analysis	Fixed crack analysis	No-tension analysis	Fixed crack analysis	No-tension analysis	Fixed crack analysis	No-tension analysis
90^o	1.0	1.01	No steel	No steel	0.0	0.0	1.0	1.01
75^o	1.3	1.1	-	*	0.12	0.2	1.3	1.1
60^o	-	0.9	-	1.1	Crushing	0.62	0.7	1.1
45^o	-	0.63	-	-	Crushing	0.98	0.51	0.89

- The steel did not yield.

* At 1.1 design load the transverse steel for angle 75 carries 0.97 f_y.

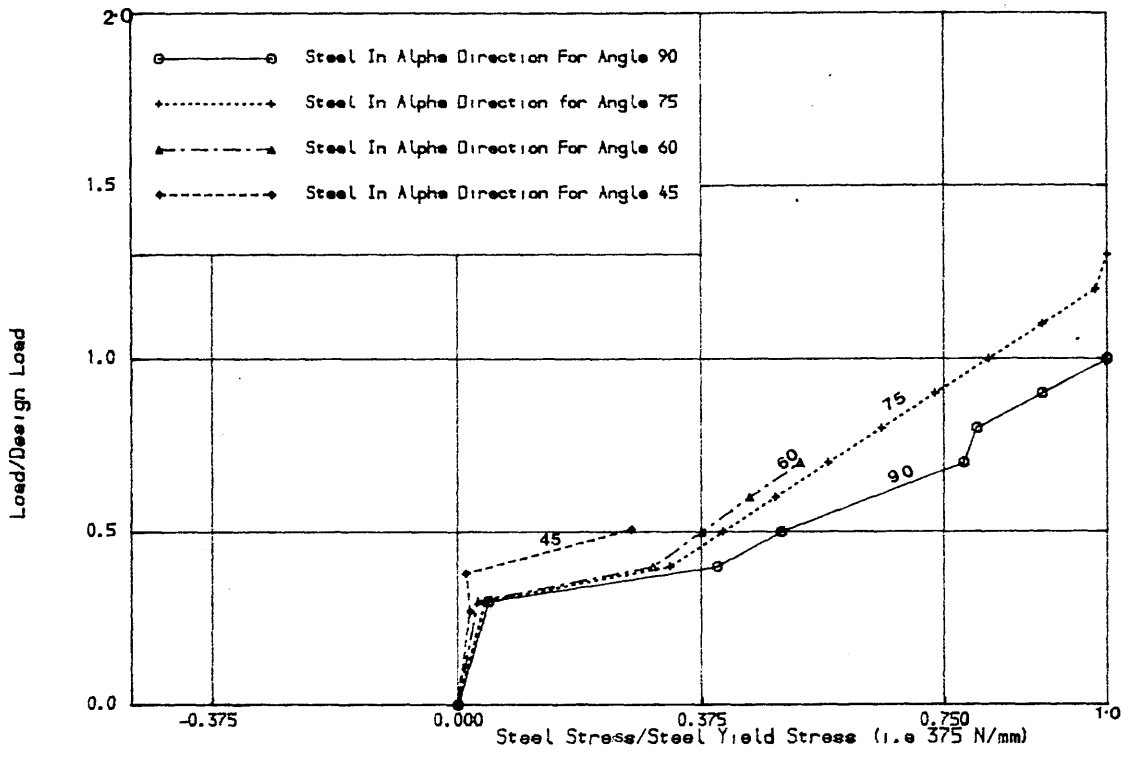

Fig. (5.3) Load-Longitudinal steel stress for pure Ny case for different angles of skew considering fixed crack analysis

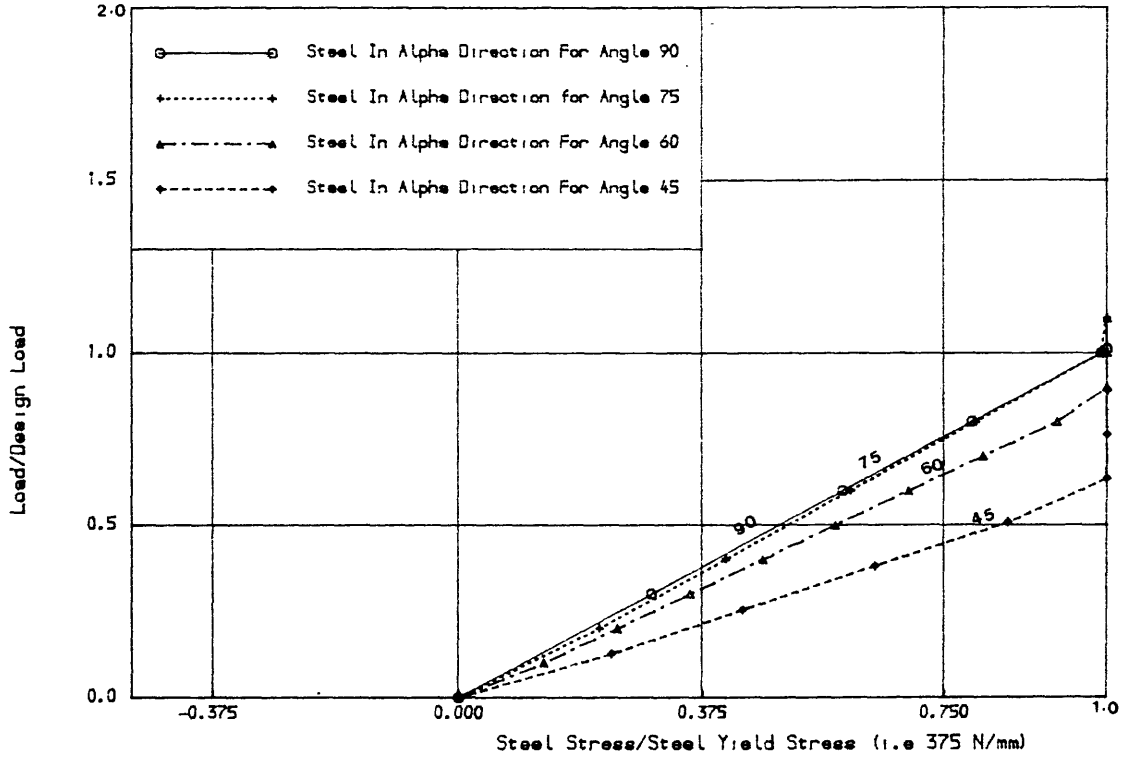

Fig. (5.4) Load-longitudinal steel stress for pure Ny case for different angles of skew considering no-tension analysis

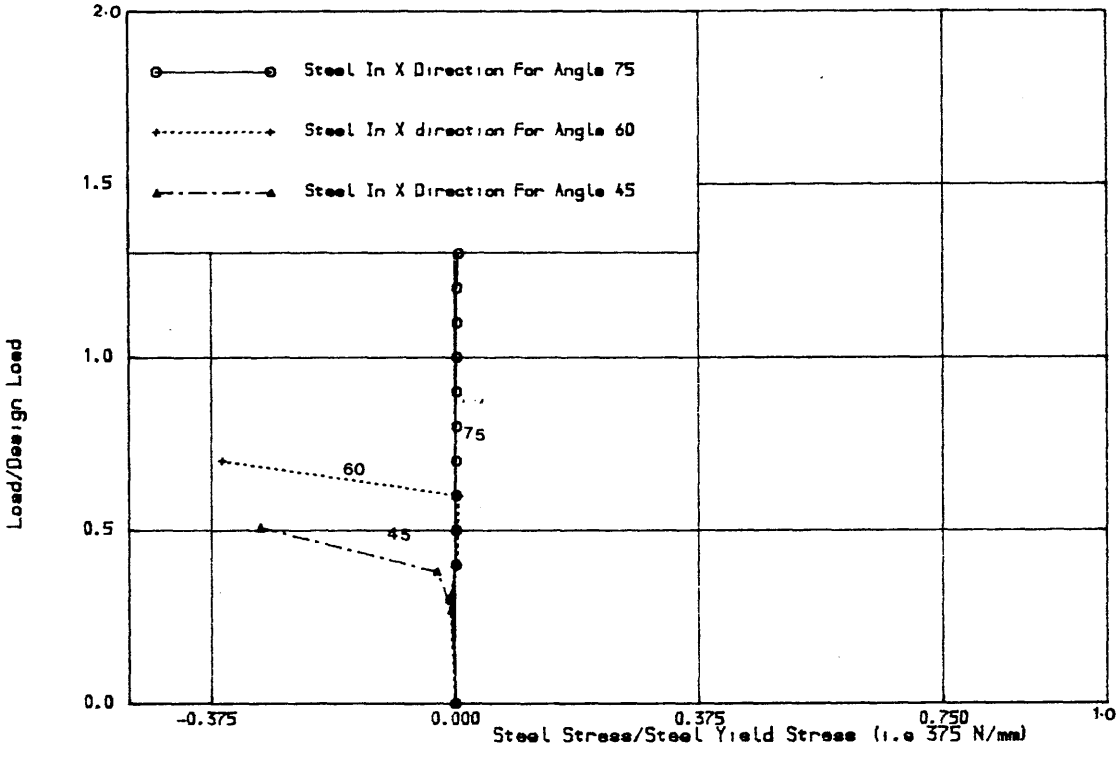

Fig. (5.5) Load-Transverse steel stress for pure Ny case for different angles of skew considering fixed crack analysis

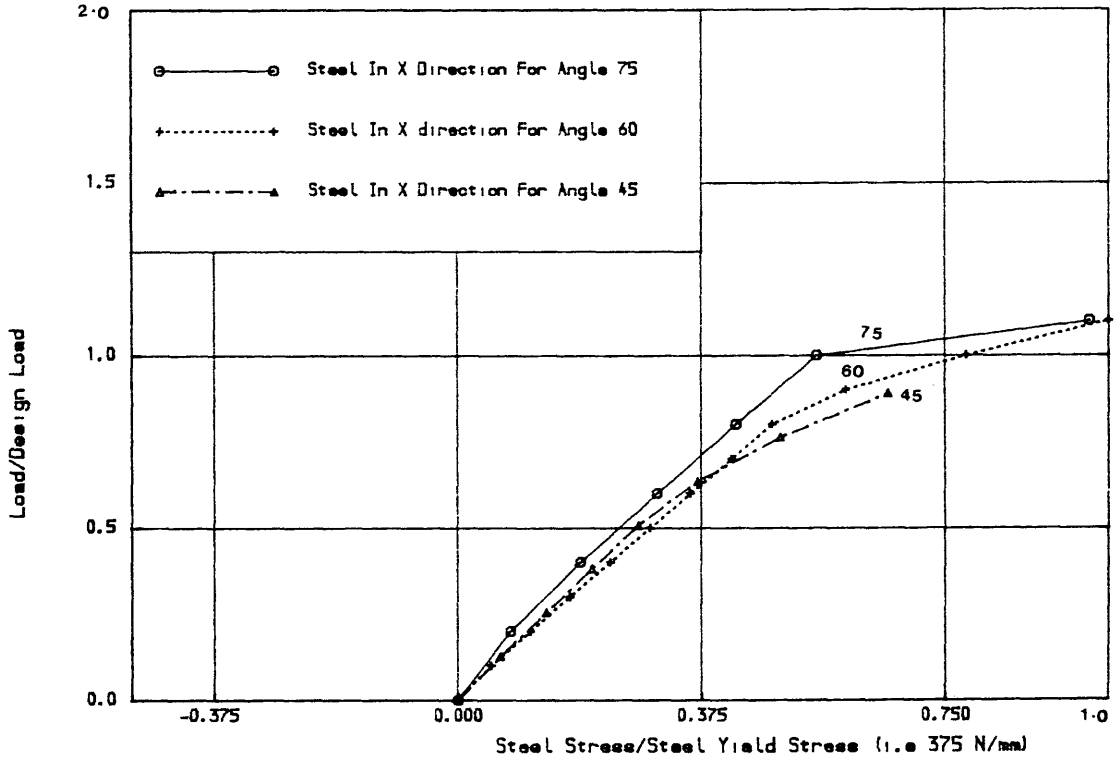

Fig. (5.6) Load-Transverse steel stress for pure Ny case for different angles of skew considering no-tension analysis

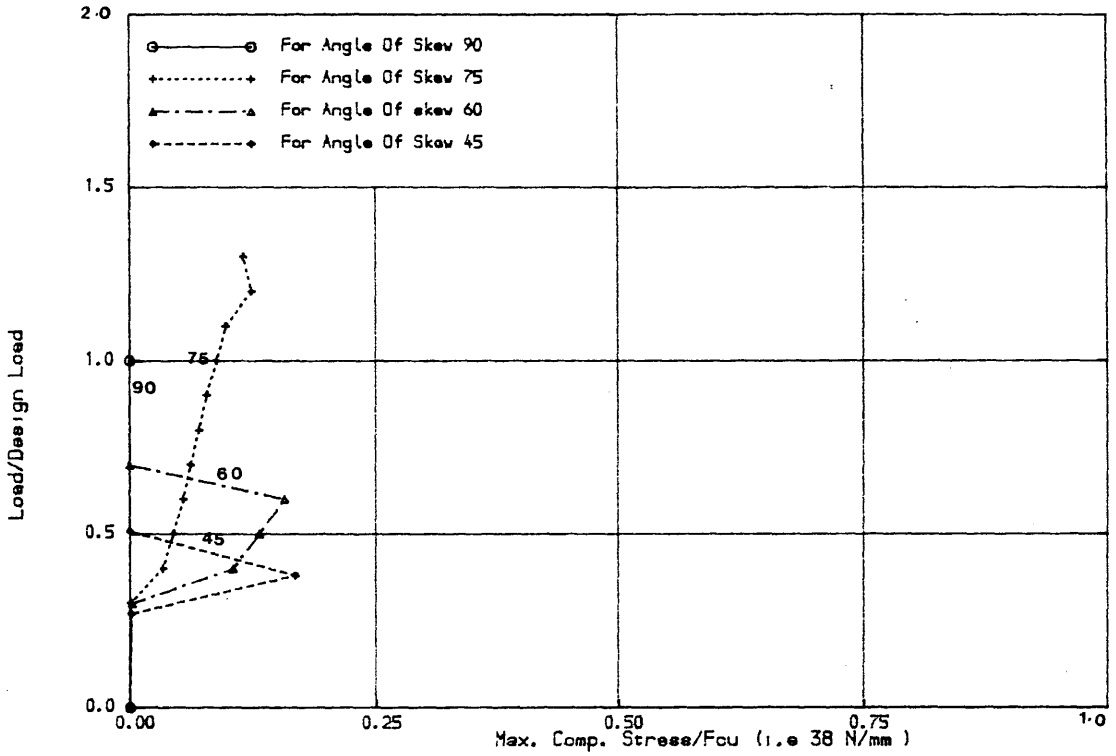

Fig. (5.7) Load-Max. compression stress for pure Ny case for different angles of skew considering fixed crack analysis

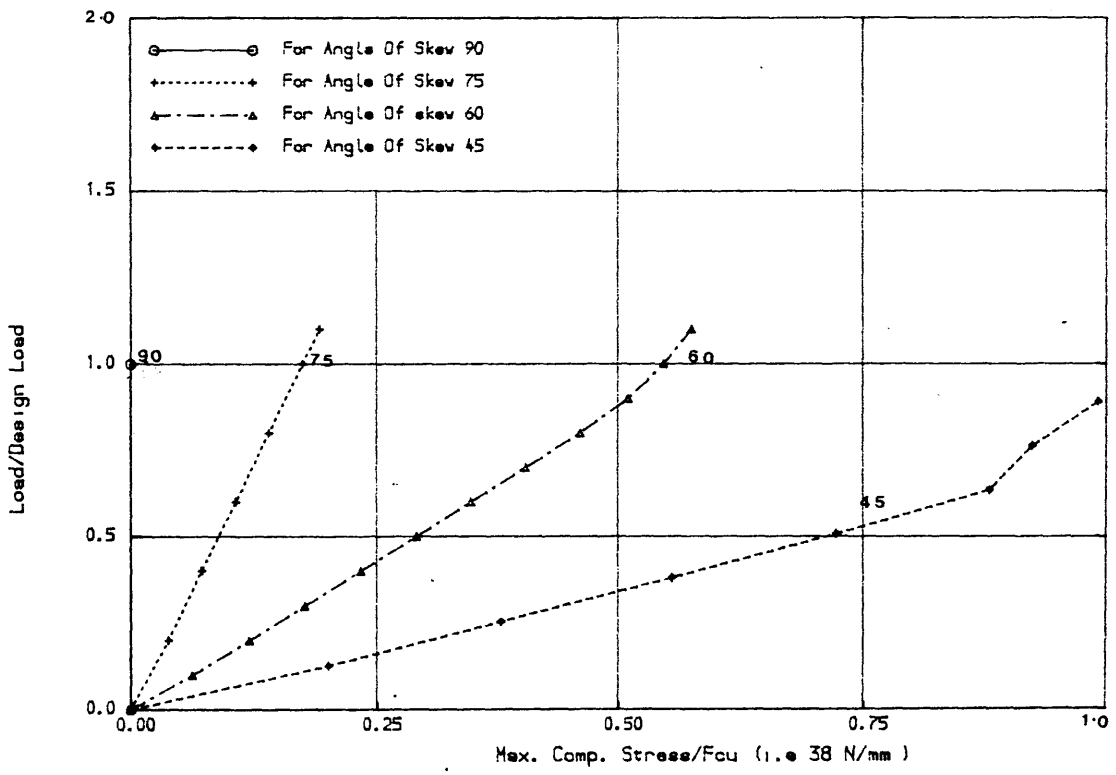

Fig. (5.8) Load-Max. compression stress for pure Ny case for different angles of skew considering no-tension analysis

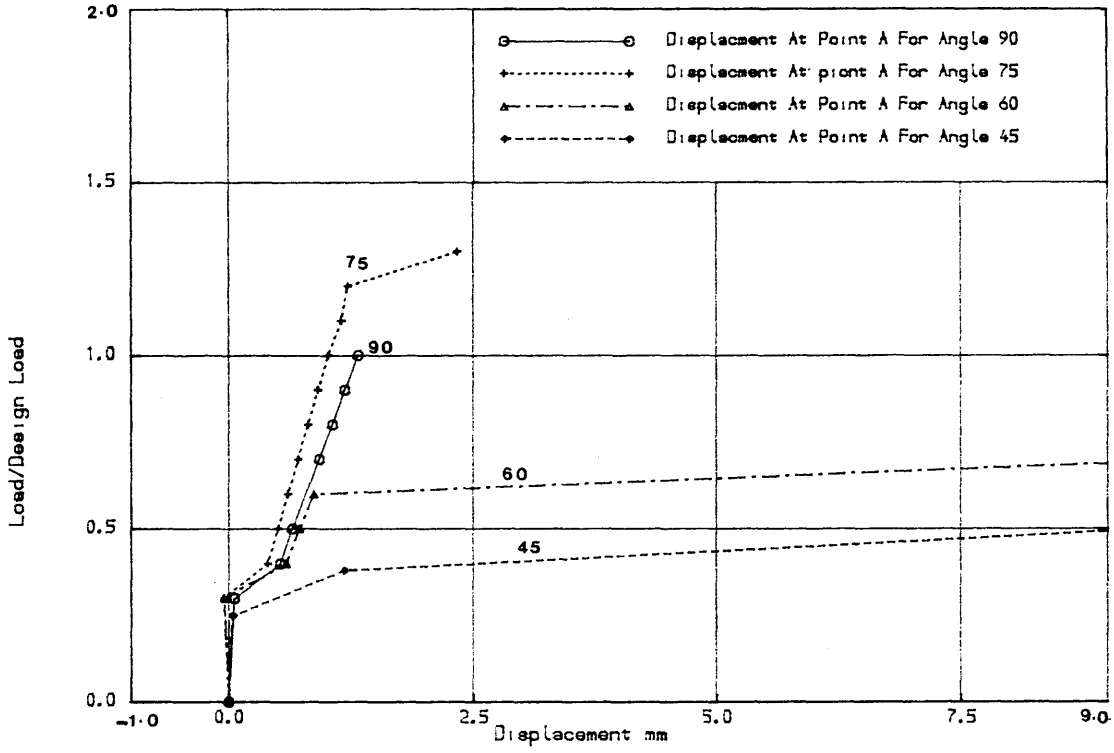

Fig. (5.9) Load-Displacement (V) for pure Ny case for different angles of skew considering fixed crack analysis

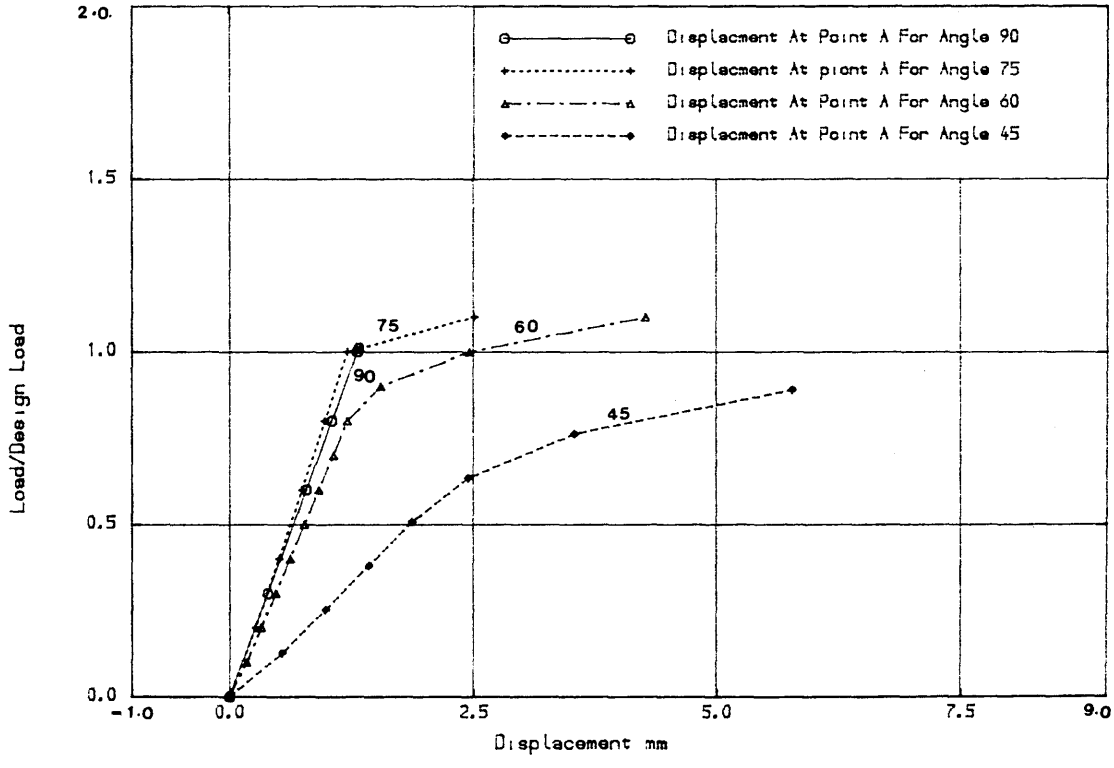

Fig. (5.10) Load-Displacement (V) for pure Ny case for different angles of skew considering no-tension analysis

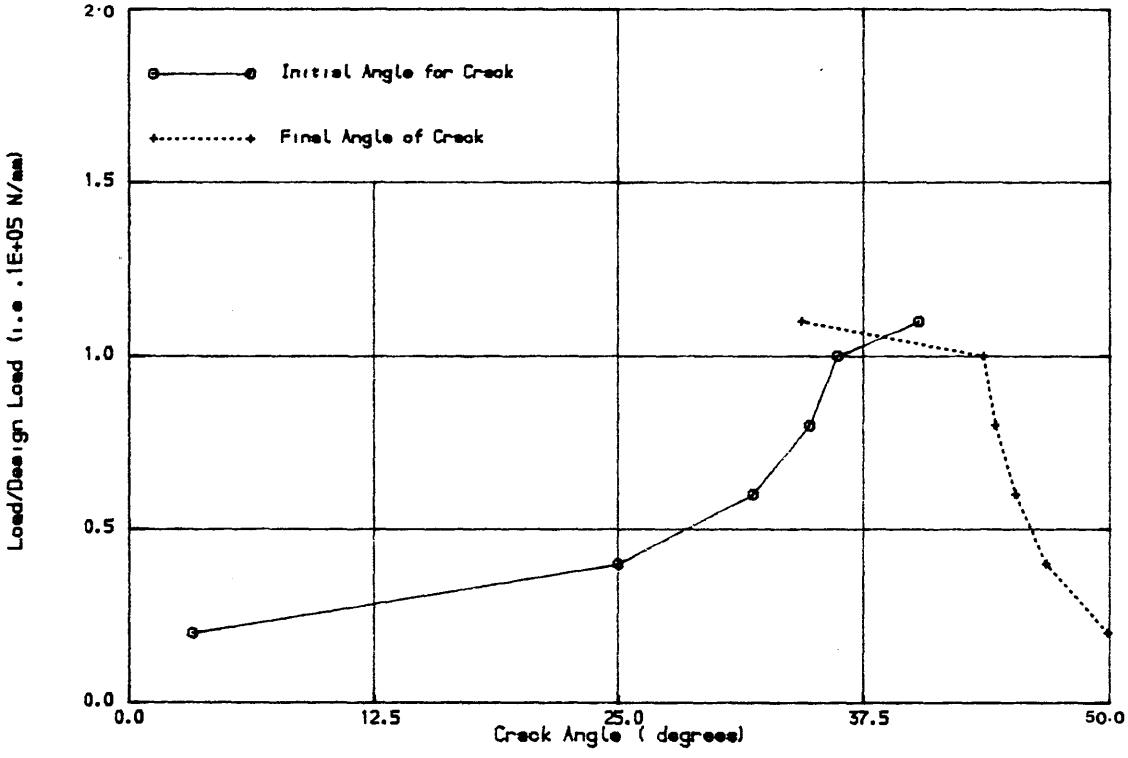

Fig. (5.11) Load-Crack direction for pure Ny case for angle of skew equal 75.0 degrees considering no-tension analysis

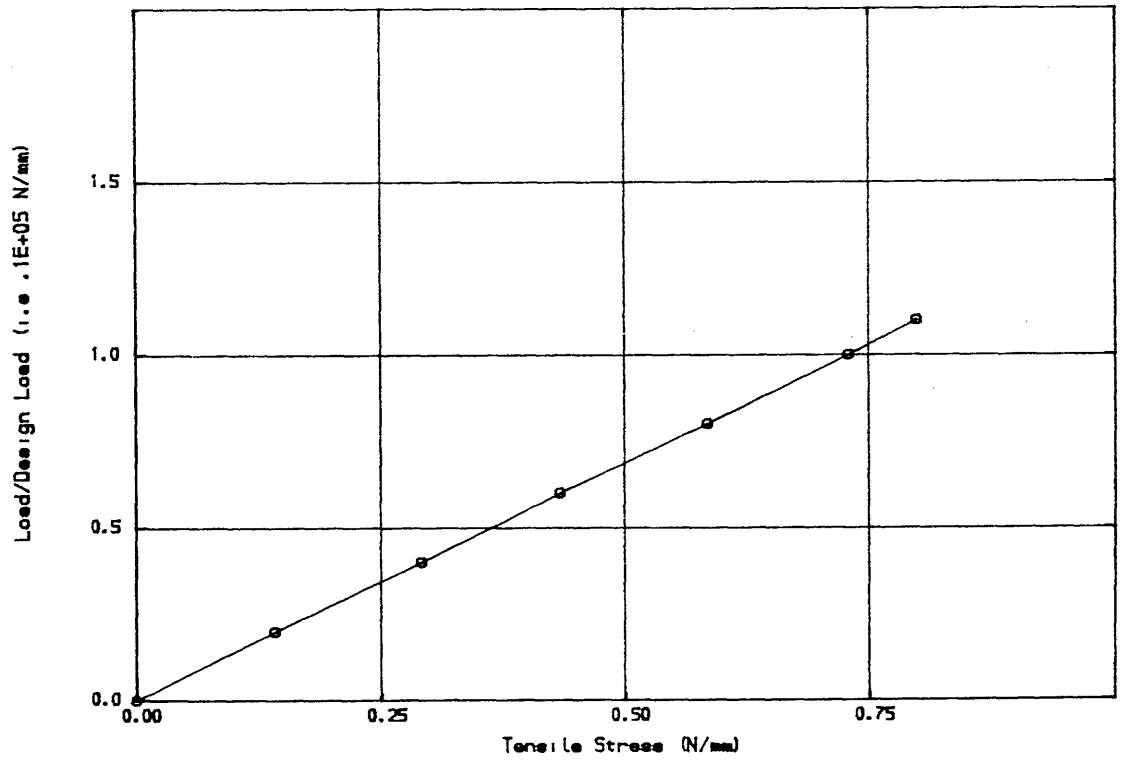

Fig. (5.11b) Load-Tensile stress in concrete for pure Ny case for angle of skew equal 75.0 degrees considering no-tension analysis

difference between the two values. This is due the effect of the tensile stresses which did not redistribute because of either the specified convergence tolerance or the maximum number of iteration as shown in Fig. (5.11b).

5.6.2.2 Inplane Shear stresses N_{xy}

The results are shows in Table (5.3) and Figs (5.12) and (5.19). From these results it can be seen that:

(a) The steel stress in the longitudinal direction

Table (5.3) and Fig. (5.12) show that in the case of fixed crack analysis, the steel yielded in tension for angles 90^{o}, 75^{o} , for 60^{o} steel yielded in compression and the load at yield decreased as the angle of skew decreased. For angle 45^{o}, the steel carried considerable compressive stress (0.9 Fy at failure). However in no tension analysis, Fig. (5.13) shows that the steel always yielded and the yield load decreased as the angle of skew decreased.

(b) The stress in the transverse direction

Table (5.3) and Figs (5.14) and (5.15) show that as the angle of skew decreased, in fixed crack analysis the steel in general did not yield. However in the case of **No - Tension** analysis, the steel for angles 90^{o} and 75^{o} yielded, while for angles 60^{o} and 45^{o} steel did not yield but still carried considerable tensile stresses (the stresses in the steel at failure are 0.85 and 0.73 of Fy for angles 60^{o} and 45^{o} respectively).

(c) The Maximum-Compressive stresses in concrete

Table (5.3) and Figs (5.16) and (5.17) show that in the case of fixed crack analysis, for angles 90° and 75° the concrete carried a considerable compressive stress and for angles 60° and 45° concrete crushed before it reached f_{cu}, for reasons explained in section (5.6.2.1 c).

In the case of **No-Tension** analysis Fig. (5.17), the compressive stress in concrete increased as the angle of skew decreased.

(d) Ultimate Load

Figs (5.18) and (5.19) and Table (5.3) show that in fixed crack analysis, for angles 90° and 75° the ultimate loads are equal to 1.0 and 1.05 of the design load respectively and the failure is due to yielding of steel. For angles 60° and 45° the ultimate loads are 0.7 and 0.5 of the design load respectively and the failure was caused by crushing of concrete. The ultimate load and the type of failure for angles 60° and 45° were dependent on the tensile strength of concrete and the shear retention factor β, see section (5.6.2 d). In the case of **No-Tension** analysis, the ultimate load decreased as the angle of skew decreased.

In **No-Tension** Fig. (5.19) shown that as the angle of skew decreased the structural became more flexible. It was noticed during the analysis that the ultimate load for angles 90° and 75° was very sensitive to the norm of convergence tolerance. When the norm of convergence

Table (5.3) Comparison Between Fixed Crack and No-tension Analysis for N_{xy} Case.

Angle of Skew	Load at yield of α-steel design load		Load at yield of X-steel design load		Max-compression stress at ultimate load/f_{cu}		Ultimate load/ design load	
	Fixed crack analysis	No-tension analysis	Fixed crack analysis	No-tension analysis	Fixed crack analysis	No-tension analysis	Fixed Crack analysis	No-tension analysis
90^{o}	1.00	1.02	1.02	1.02	0.56	0.56	1.0	1.02
75^{o}	.9	0.9	-	1.05	0.77	0.76	1.04	1.05
60^{o}	.7	0.8	-	-	Crushing	0.92	0.7	1.00
45^{o}	-	.51	-	-	Crushing	0.92	0.5	.89

- The steel did not yield

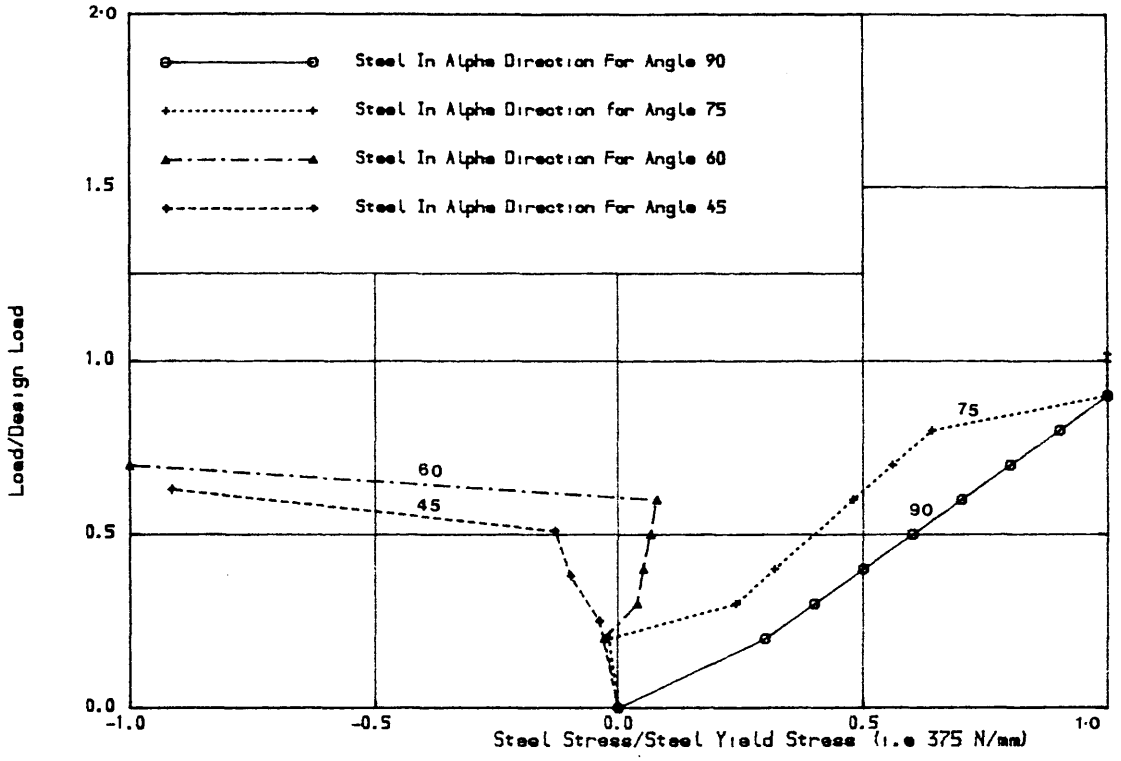

Fig. (5.12) Load–Longitudinal steel stress for pure Nxy case for different angles of skew considering fixed crack analysis

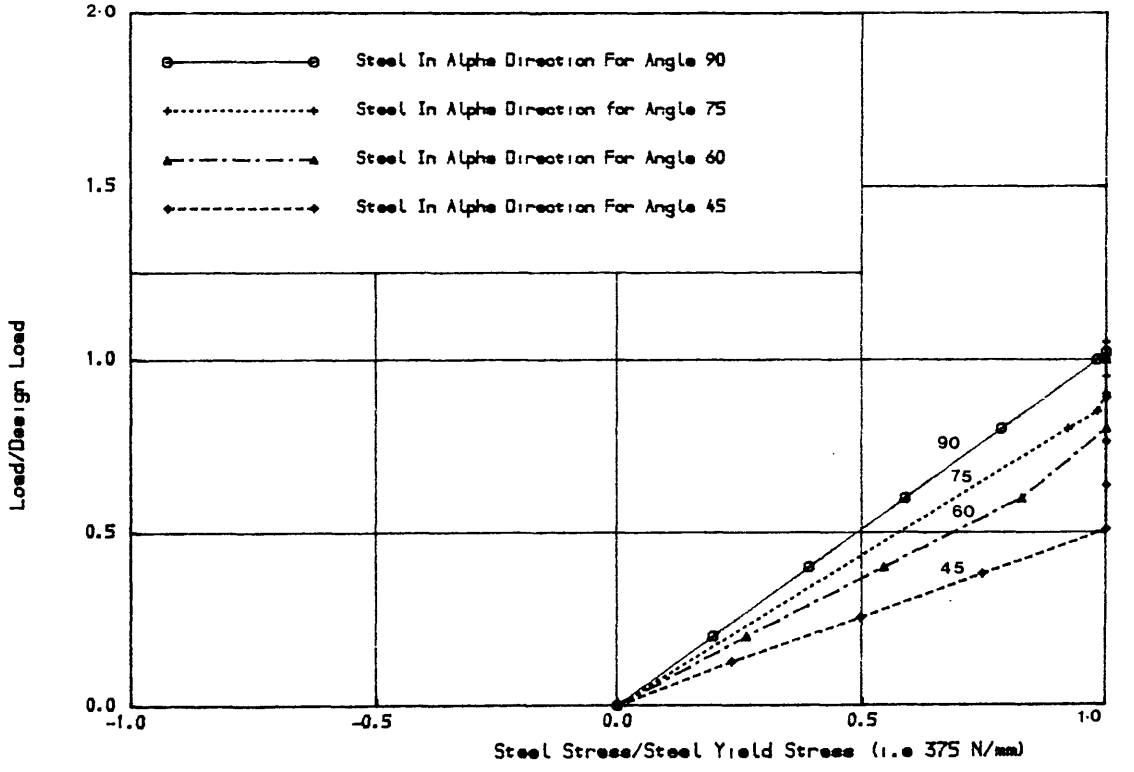

Fig. (5.13) Load–Longitudinal steel stress for pure Nxy case for different angles of skew considering no-tension analysis

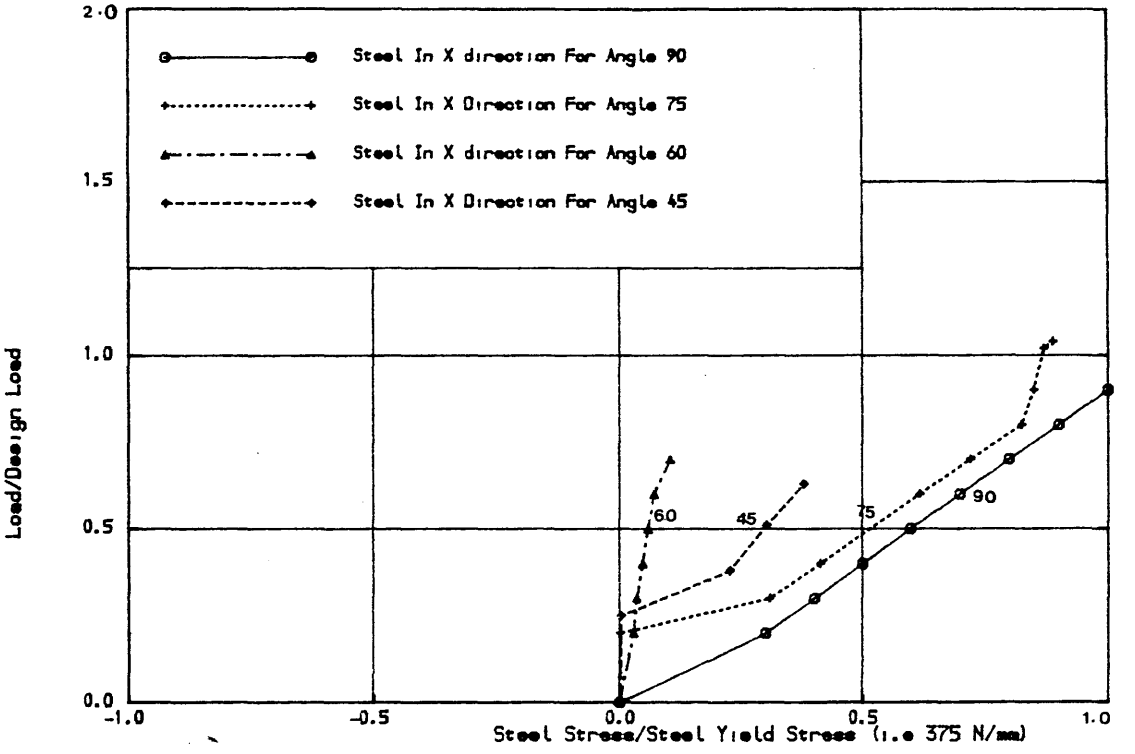

Fig. (5.14) Load-Transverse steel stress for pure Nxy case for different angles of Skew considering fixed crack analysis

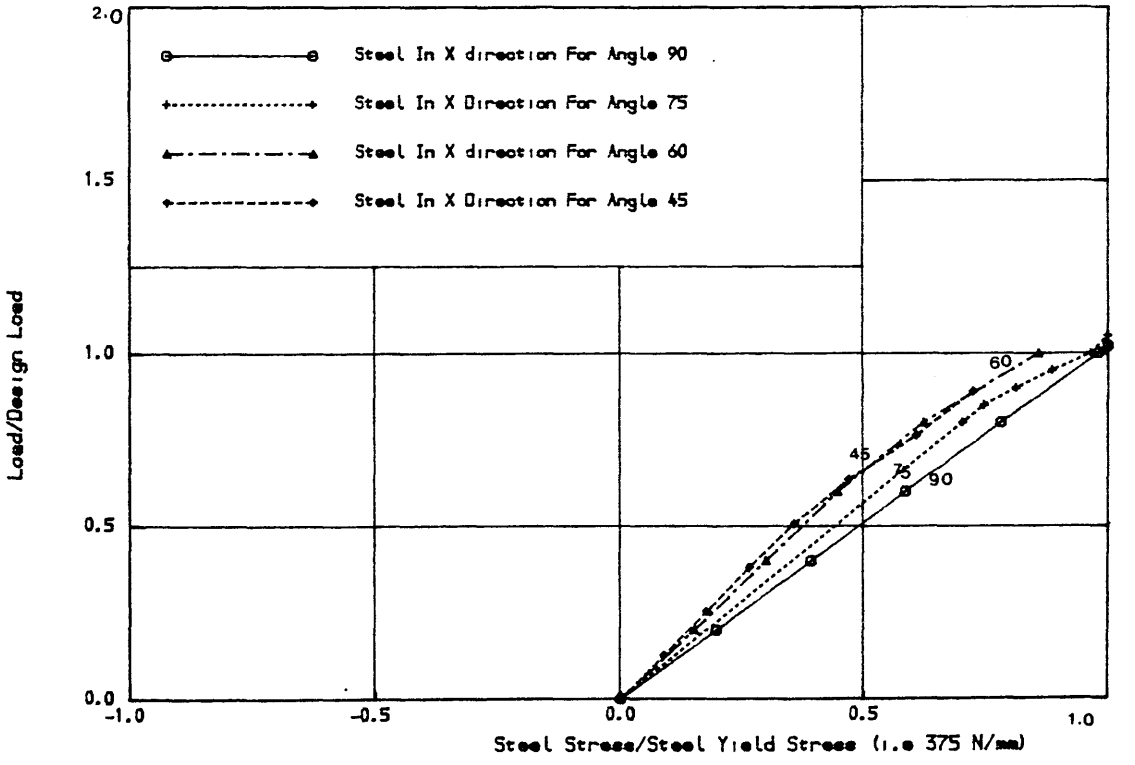

Fig. (5.15) Load-Transverse steel stress for pure Nxy case for different angles of skew considering no-tension analysis

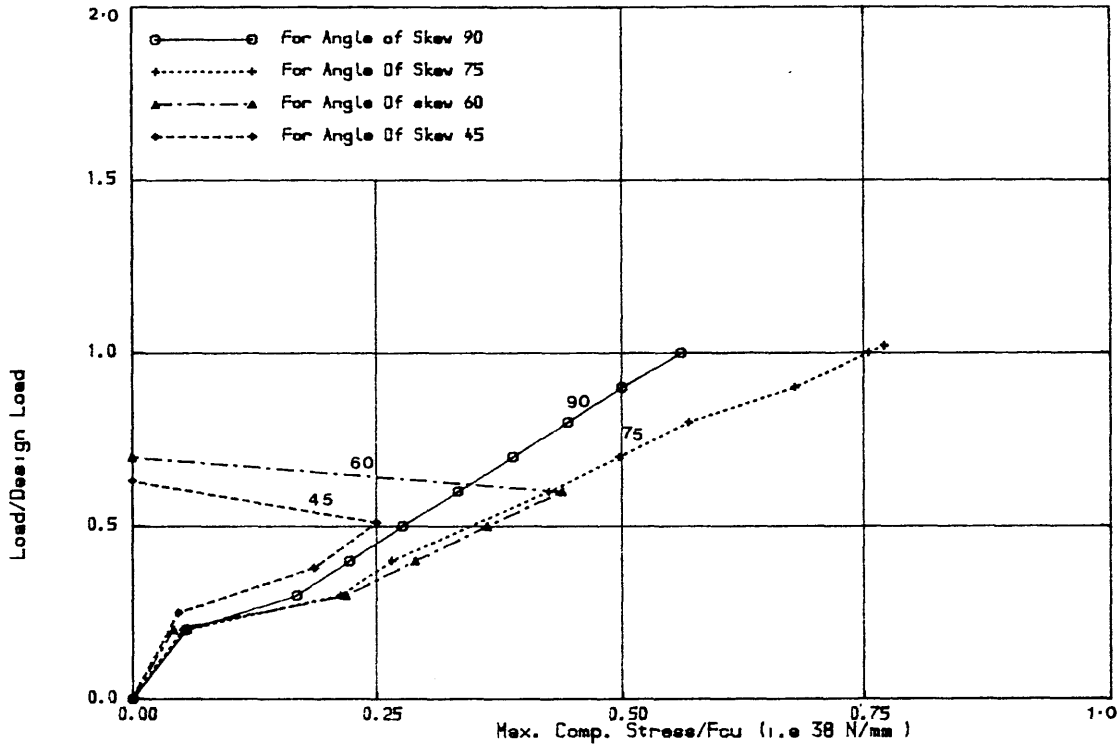

Fig. (5.16) Load-Max. compression stress for pure Nxy case for different angles of skew considering fixed crack analysis

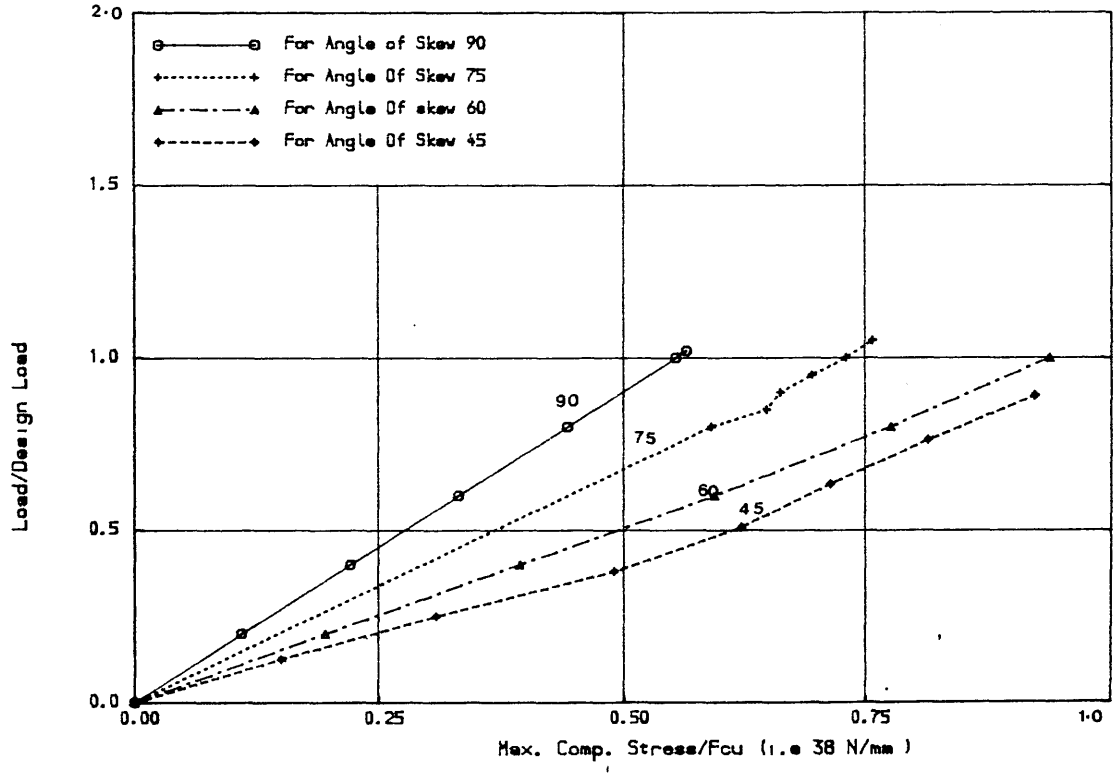

Fig. (5.17) Load-Max. compression stress for pure Nxy Case for different angles of skew considering no-tension analysis

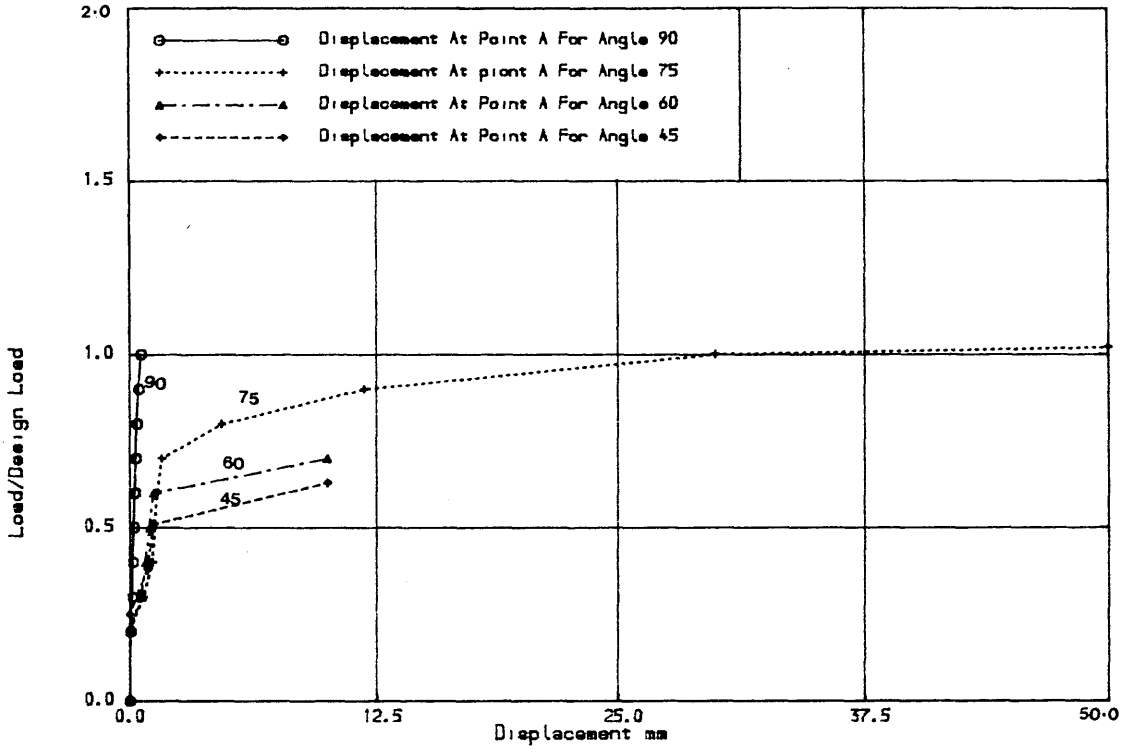

Fig. (5.18) Load-Displacement (v) for pure Nxy case for different angles of skew considering fixed crack analysis

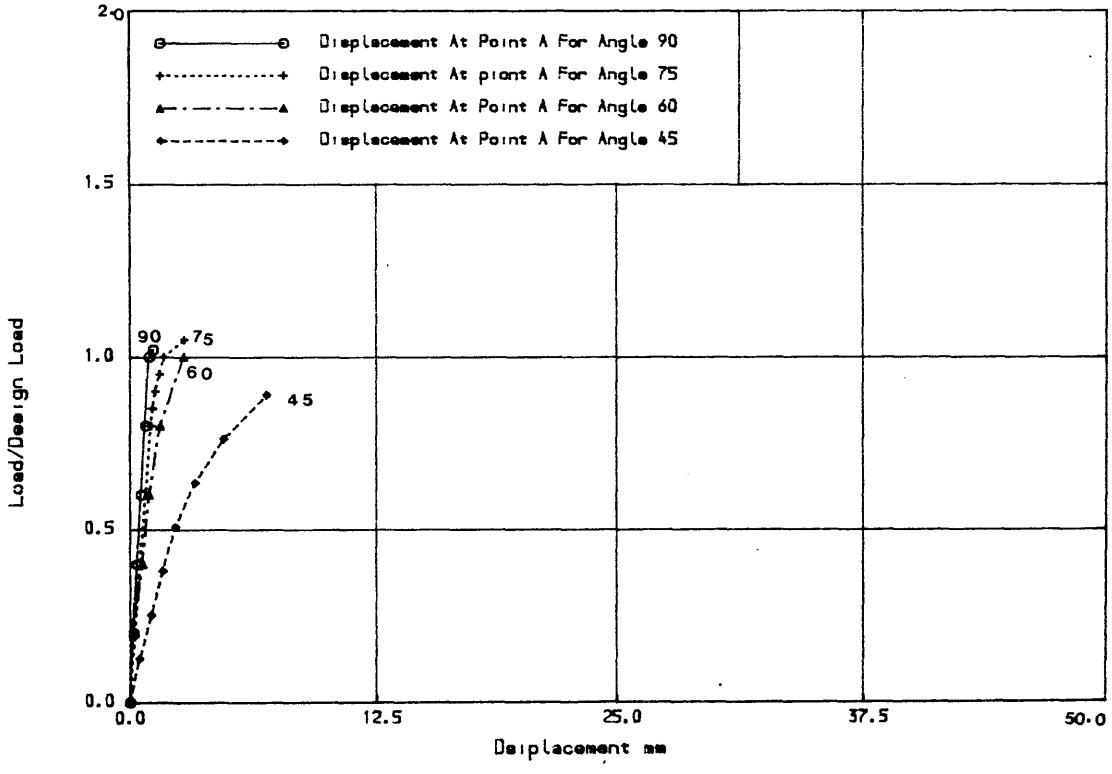

Fig. (5.19) Load-Displacement (v) for pure Nxy case for different angles of skew considering no-tension analysis

tolerance was 5%, the ultimate load for angles 75° and 60° were 1.6 and 1.5 design load respectively.

5.6.2.3 Pure Bending M_y

The results are presented in Table (5.4) and Fig. (5.20) to Fig. (5.28). Before the discussion of the results, it should be noted that it was evident during the analysis that the ultimate load for the M_y case is highly sensitive to the norm of the convergence tolerance and the number of iterations. For the M_y case to reach the similar norm of residual force for inplane case N_y, the number of iterations was very much smaller than that for the inplane N_y case. It can be seen from the results that:

(a) The steel stress in the longitudinal direction

Table (5.4) and Figs (5.20) and (5.21) show that in fixed crack analysis, for angles 90° and 75° the steel yielded while for angles 60° and 45° the steel did not yield. However in **No-Tension** analysis the steel always yields and that the yield load decreases as the angle of skew decreases.

(b) The steel stress in the transverse direction

Table (5.4) and Figs (5.22) and (5.23) shown that in fixed crack analysis, the steel carried practically zero stresses. However in **No Tension** analysis, the steel for angles 90° and 75° yielded and for the other angles steel carried a considerable tensile stress (for angles 60° and 45° the steel carried 0.97 and 0.76 of the yield

strength respectively).

(c) The Maximum-Compression stress in concrete

Table (5.4) and Fig. (5.24) shows that for angles 90^{o} and 75^{o} the concrete carries significant stresses but does not crush, but for angles 60^{o} and 45^{o}, the failure occurs by crushing in concrete due to reaching its compressive strain because of the presence of two orthogonal cracks. In the case of **No-Tension** analysis, Fig. (5.25) shows that as the angle of skew decreases the maximum compressive stress increases.

(d) The ultimate load

Table (5.5) and Fig. (5.26) show that for angle 90 the ultimate load is equal to the design load and the failure is due to yielding in the steel. For angles 75^{o} and 60^{o}, the ultimate load is greater than the design load whereas for angle 45^{o}, the failure load is less than the design load. As was explained before, in fixed crack analysis the failure load is dependent on the tensile strength of concrete and the shear retention factor B. In the case of **No Tension** analysis, Fig. (5.27) shows that the failure load for angles 90^{o}, 75^{o} and 60^{o} is greater than the design load and for angle 45^{o}, it is less than the design load. In all cases, the failure is caused by the yielding of steel. In fact, for angle 45^{o} after the longitudinal steel yields, it is very difficult to reach the specified norm of residual force and this probably is the reason why the ultimate load is much smaller that the design load.

Table (5.4) Comparison Between Fixed Crack and No-tension Analysis For M_y Case.

Angle of Skew	Load at yield of α -steel/ design load		Load at yield of X-steel/ design load		Max-compression stress at ultimate load/f_{cu}		Ultimate load/ design load	
	Fixed crack analysis	No-tension analysis	Fixed crack analysis	No-tension analysis	Fixed crack analysis	No-tension analysis	Fixed crack analysis	No-tension analysis
90^{o}	1.0	1.15	No-steel	No-steel	.28	.24	1.0	1.15
75^{o}	1.35	1.15	-	1.15	.38	0.30	1.35	1.15
60^{o}	-	.8	-	-	Crushing	0.32	1.3	1.15
45^{o}	-	0.51	-	-	Crushing	0.48	0.85	.76

- The steel did not yield.

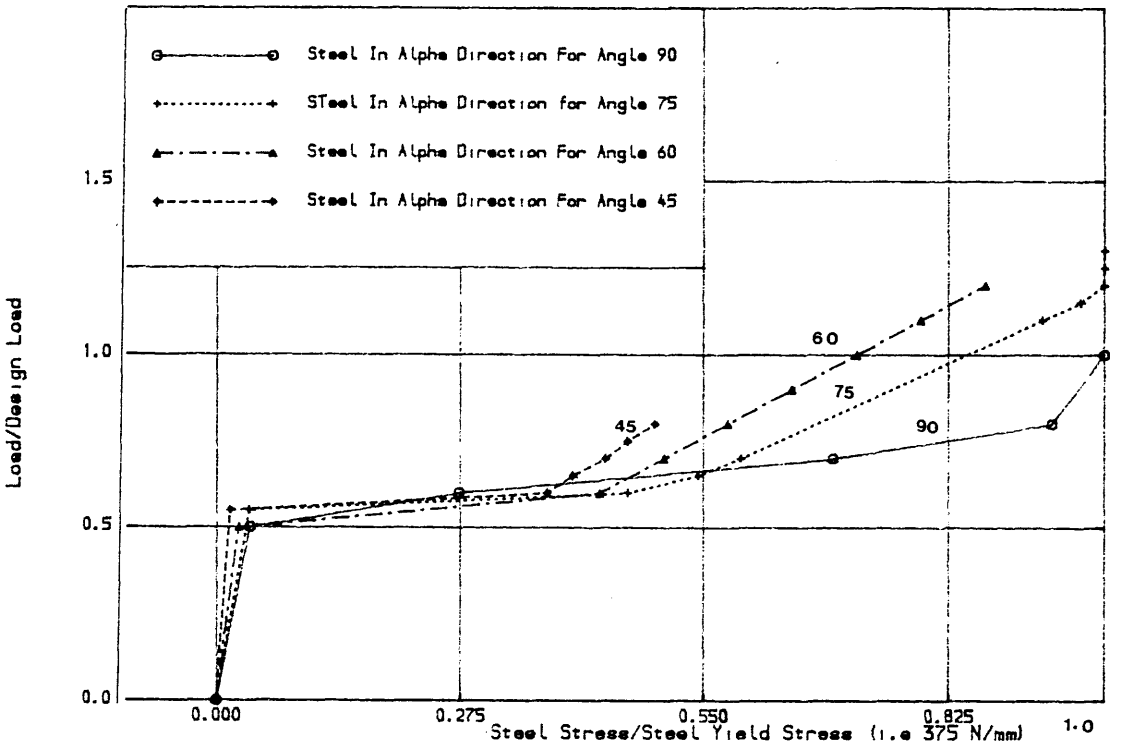

Fig. (5.20) Load-longitudinal steel stress for pure My case for different angles of skew considering fixed crack analysis

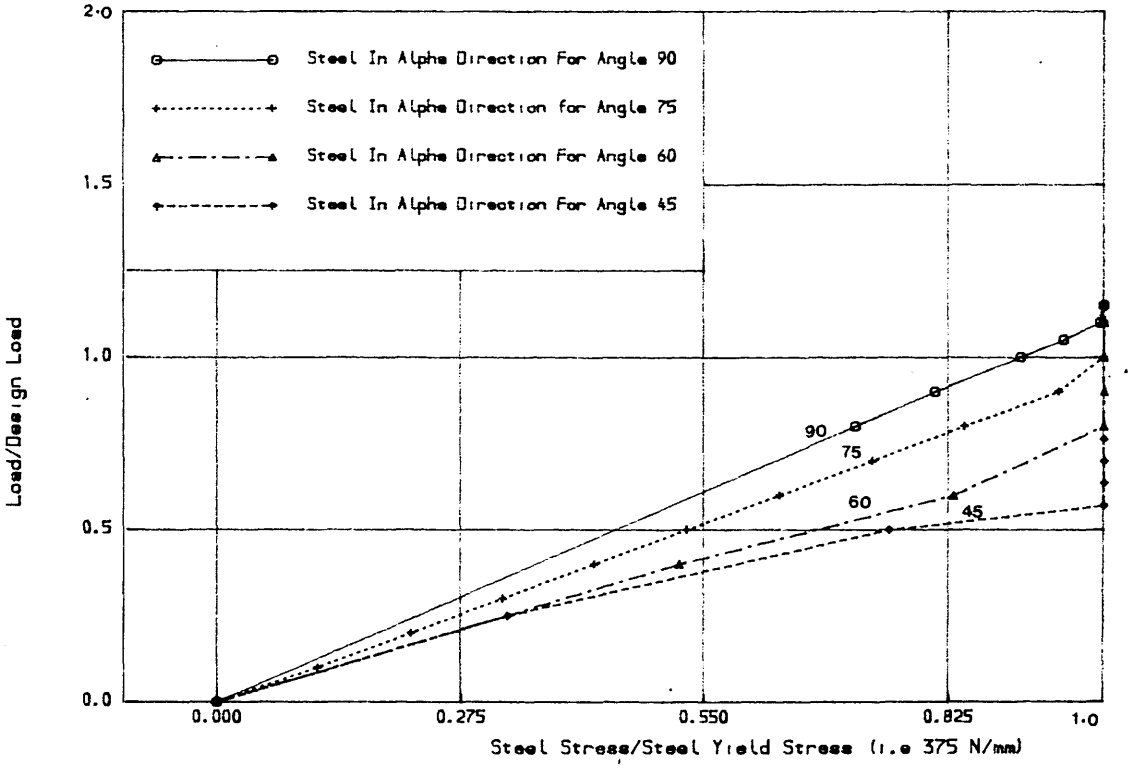

Fig. (5.21) Load-longitudinal steel stress for pure My case for different angles of skew considering no-tension analysis

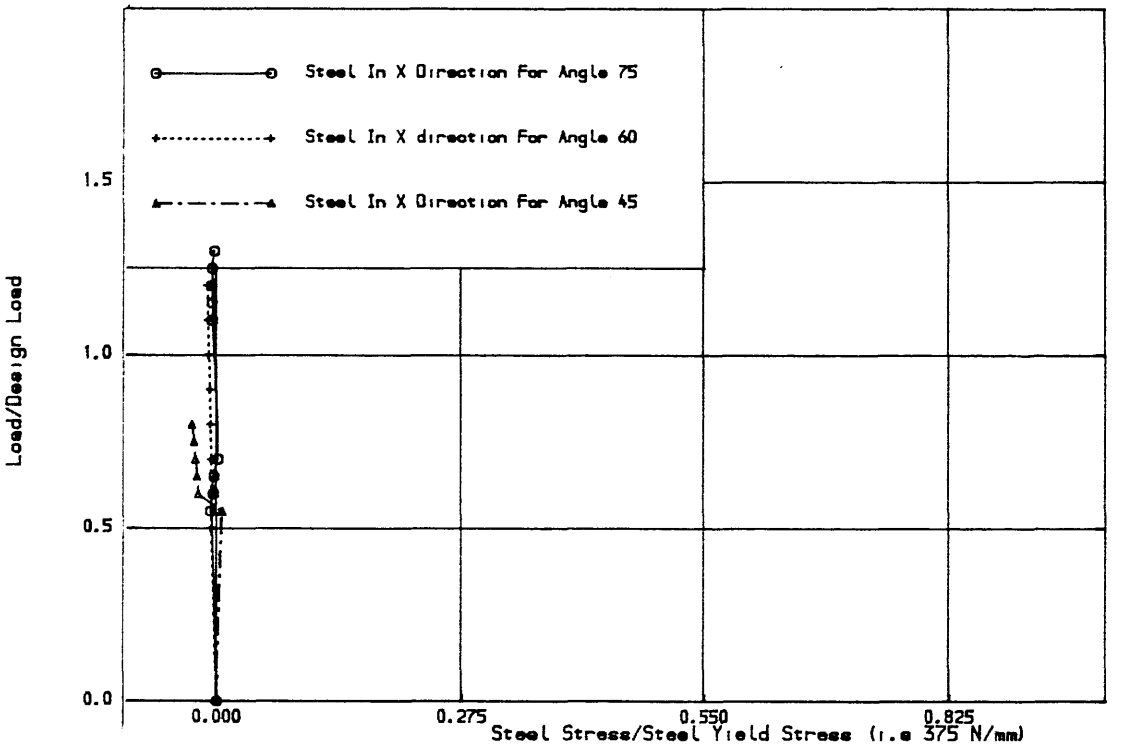

Fig. (5.22) Load-Transverse steel stress for pure My case for different angles of skew considering fixed crack analysis

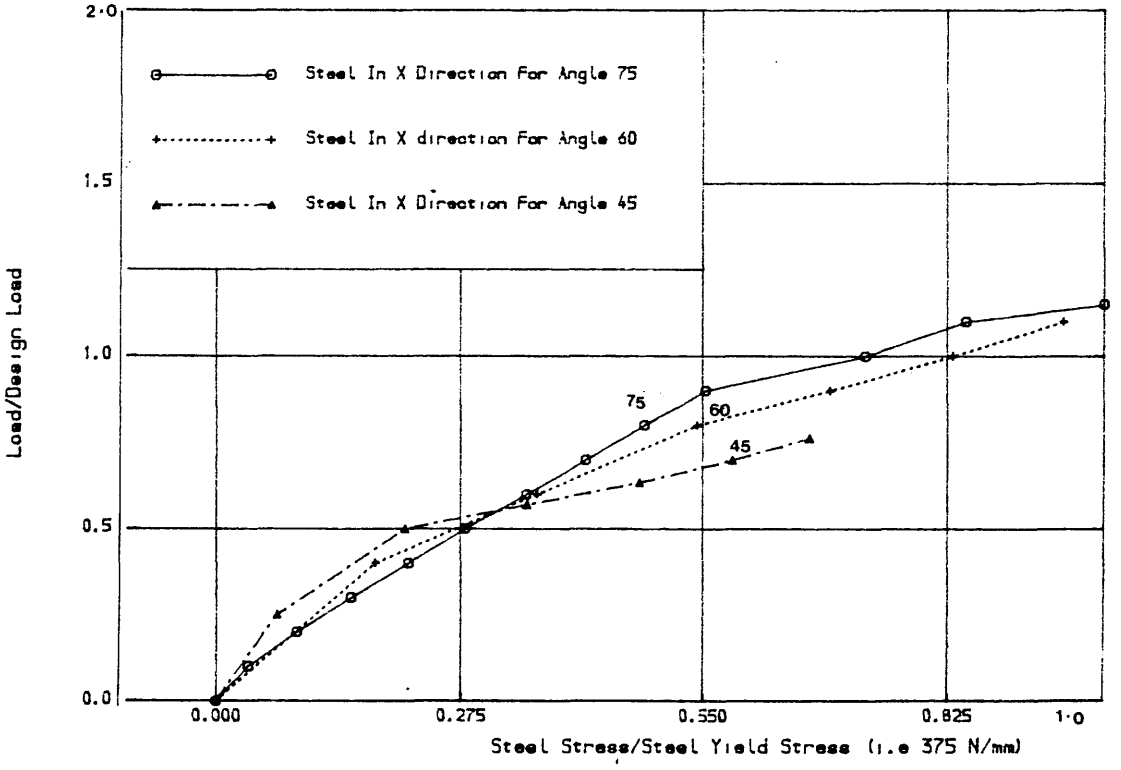

Fig. (5.23) Load-Transverse steel stress for pure My case for different angles of skew considering no-tension analysis

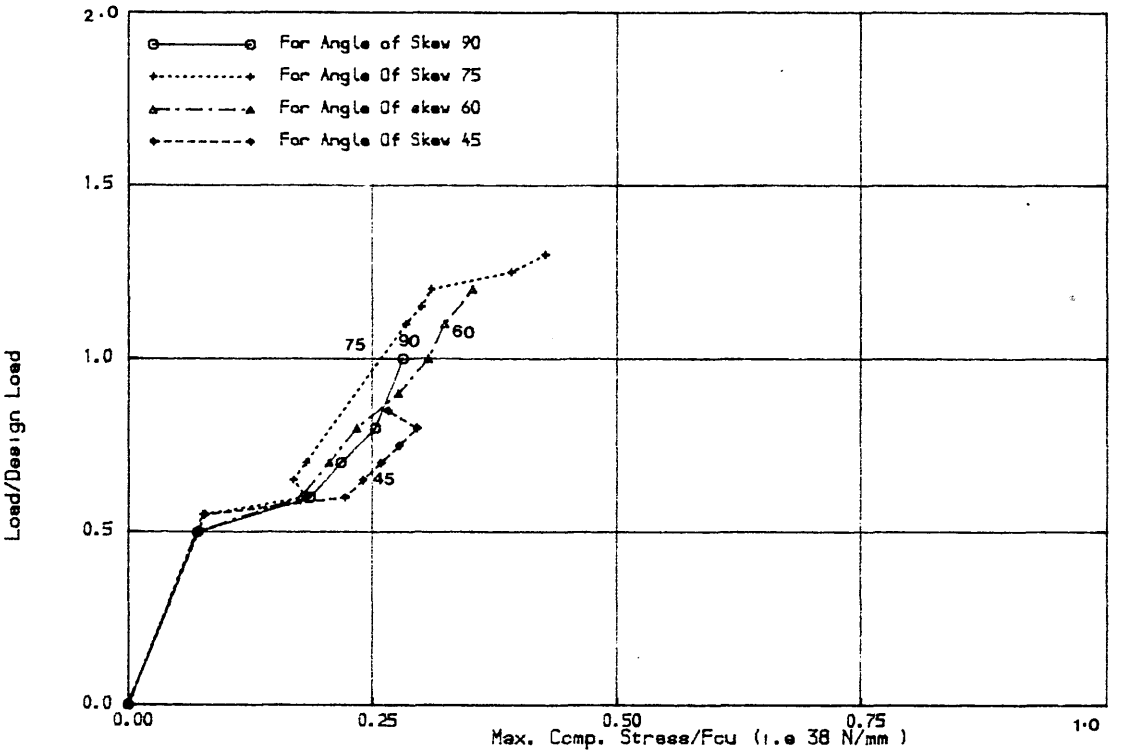

Fig. (5.24) Load-Max. compression stress for pure My case for different angles of skew considering fixed crack analysis

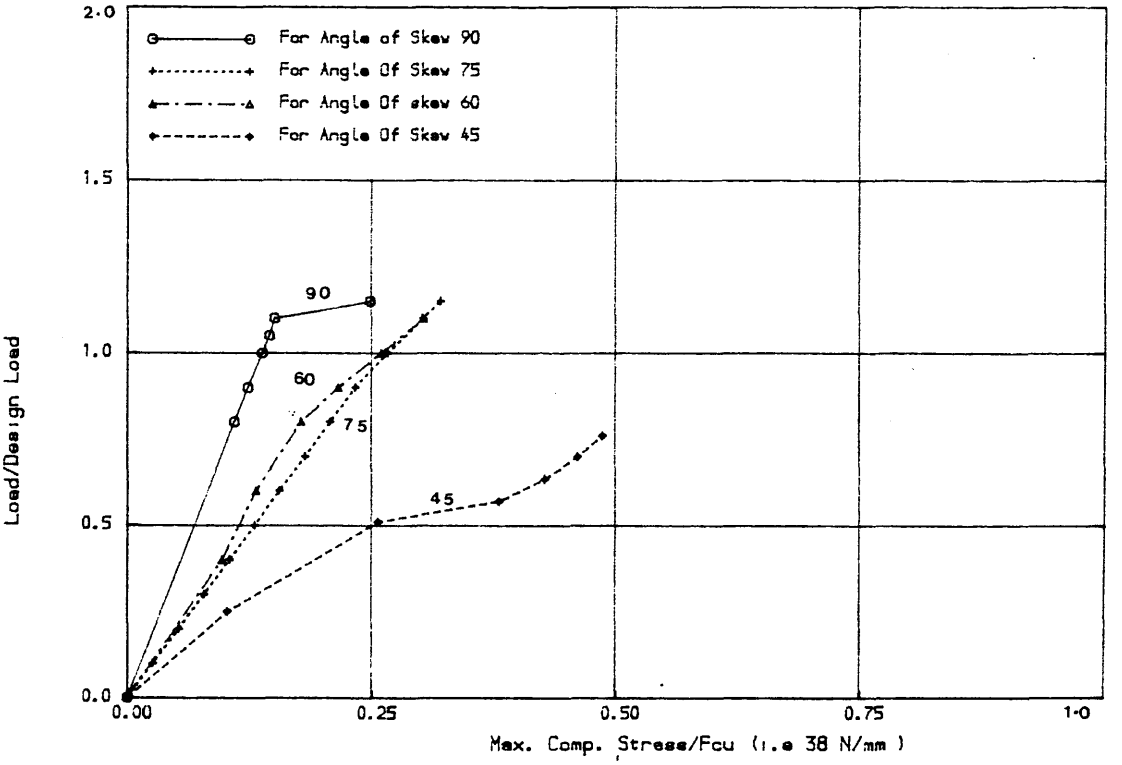

Fig. (5.25) Load-Max. compression stress for pure My case for different angles of skew considering no-tension analysis

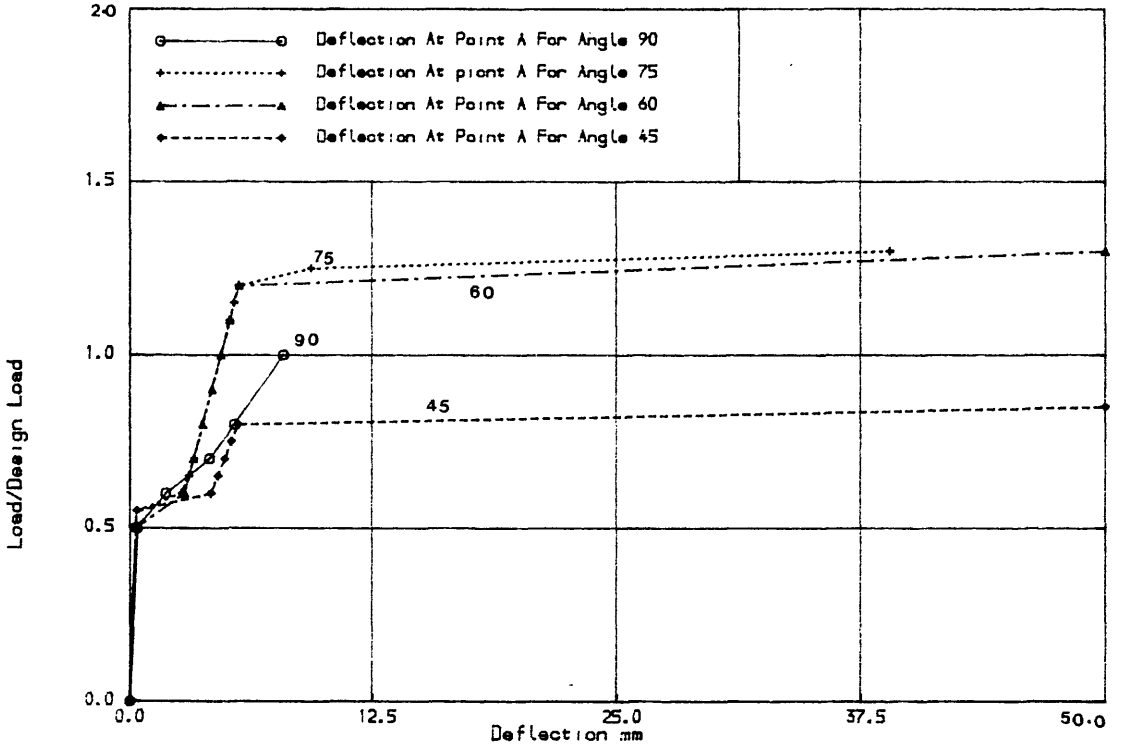

Fig. (5.26) Load-Deflection for pure My case for different angles of skew considering fixed crack analysis

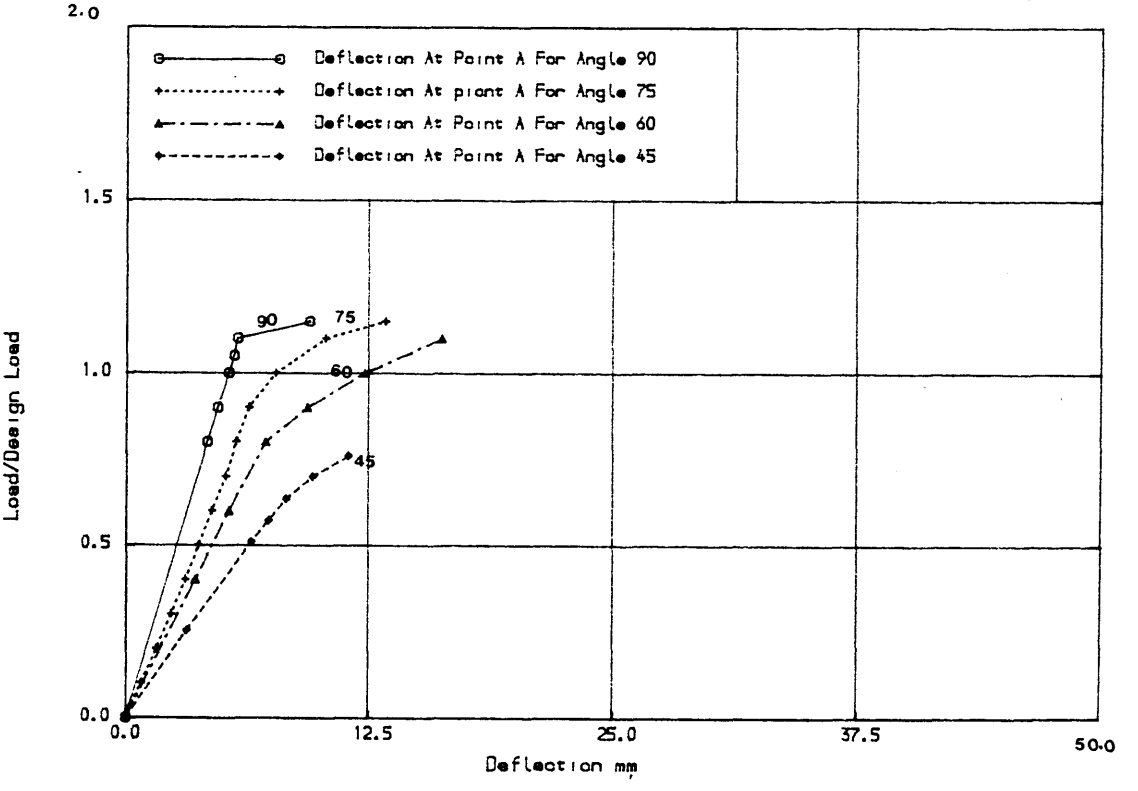

Fig. (5.27) Load-Deflection for pure My case for different angles of skew considering no-tension analysis

5.6.4 Pure torsional moment M_{xy}

The results are presented in Table (5.5) and Fig. (2.28) to Fig. (5.39).

(a) The steel stress in the longitudinal direction

Table (5.5) and Fig. (5.28) to (5.31) show that as the angle of skew decreases, in fixed crack analysis the top steel yields for all angles except for angle 45°. But for bottom steel, yielding takes place only for angles 90° and 75°. However in the case of the **No-Tension** analysis, Figs (5.29) and (5.31) show that the top and bottom steel always yield. Also these Figs show that the bottom longitudinal steel yields early as the angle of skew decreases. The yield load was 0.9 for longitudinal and transverse top and bottom steel, which is less than the yield load for fixed crack analysis. This will be discussed in section (5.6.2.4 d).

(b) The steel stress in the transverse direction

Table (5.5) and Figs (5.32) and (5.34) shown that in fixed crack analysis, for 90° and 75° angles the top and bottom steel yielded, the bottom steel does not yield for angles 60° and 45°. It should be noted that in theory no top steel was required for 60° and 45° cases.

In the case of **No-Tension** analysis, Fig. (5.33) shows that as the angle of steel decreases, the top transverse steel always yields. However as can be seen from Fig. (5.35) as the angle of skew decreases, the stress in the bottom transverse steel decreases and the

steel does not yield for angles 75°, 60° and 45°.

(c) The Maximum compressive stress in concrete

Table (5.5) and Fig. (5.36) show that as the angle of skew decreases, in fixed crack analysis the concrete in general fails by crushing before it reaches the compressive strength. However in the case of **No-Tension** analysis Fig. (5.37), as the angle of skew decreases the the maximum compression stress in concrete increases.

(d) Ultimate Load

Table (5.5) and Fig. (5.38) show that the ultimate load for all angles of skew is slightly higher than the design load. Except in the 90° angle case, the failure is caused by crushing of concrete. In the **No-Tension** analysis, Fig. (5.39) shows that as the angle of skew decreases the structure becomes more flexible. It may be surprising that the ultimate load in the case of 90° angle of skew is only 0.9 of the design load. This case was solved twice, in the first solution the convergence tolerance was 1% and this gave ultimate load of 1.5 design load. when the convergence tolerance limit was reduced to 0.1% the ultimate load of 0.9 of the design load. This is the reult presented in Fig. (5.39). This means that the ultimate load in case of pure torsion is sensitive to the convergence tolerance adopted. Another important reason is that when no tension analysis is considered, constant stiffness was used unless the concrete crushed or steel yielded when variable stiffness analysis is used. In fixed crack analysis,in general the core disintegrates because

Table (5.5) Comparison Between Fixed Crack and No-tension Analysis for Pure M_{xy} Case.

Angle of Skew	Load at yield of α-steel/ design load				Load at yield of X-steel design load				Max-compression stress at ultimate load/f_{cu}		Ultimate load/ design load	
	Fixed crack analysis		No-tension analysis		Fixed crack analysis		No-tension analysis		Fixed crack analysis	No-tension analysis	Fixed crack analysis	No-tension analysis
	Top	Bottom	Top	Bottom	Top	Bottom	Top	Bottom				
90^{o}	1.05	1.05	0.9	0.9	1.05	1.05	0.9	0.9	.63	.27	1.05	.9
75^{o}	1.05	1.05	0.8	0.8	1.05	1.05	0.7	-	Crushing	.68	1.05	.9
60^{o}	1.00	-	0.7	0.7	No Steel	-	No Steel	-	Crushing	.42	1.0	0.85
45^{o}	1.1	-	0.64	.64	No Steel	-	No Steel	-	Crushing	0.5	1.1	.87

- The steel did not yield.

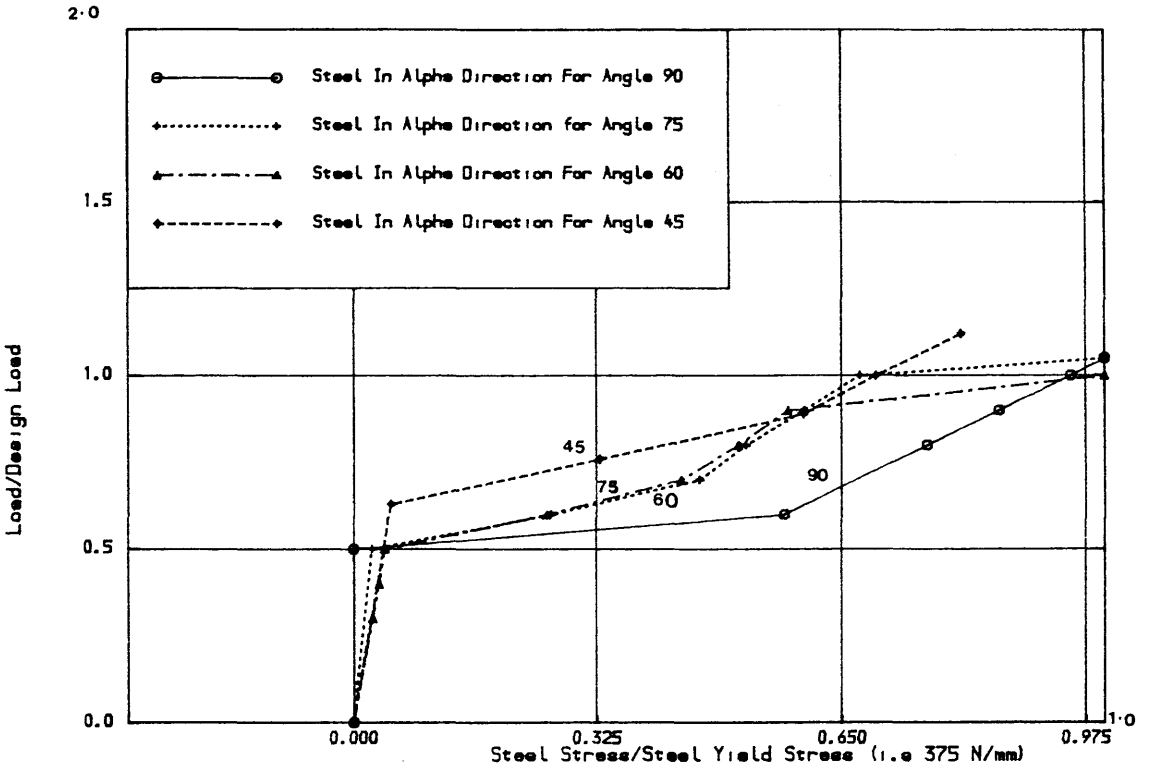

Fig. (5.28) Load-Top longitudinal steel stress for pure Mxy case for different angles of skew considering fixed crack analysis

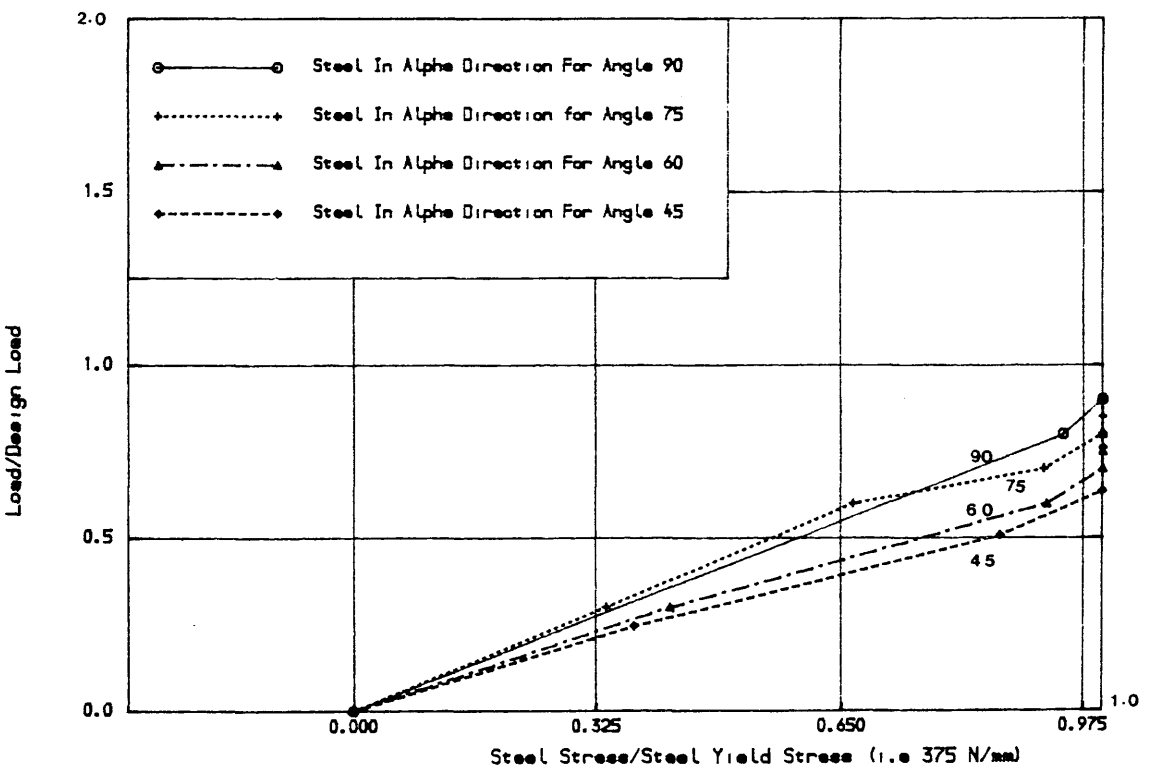

Fig. (5.29) Load-Top longitudinal steel stress for pure Mxy case for different angles of skew considering no-tension analysis

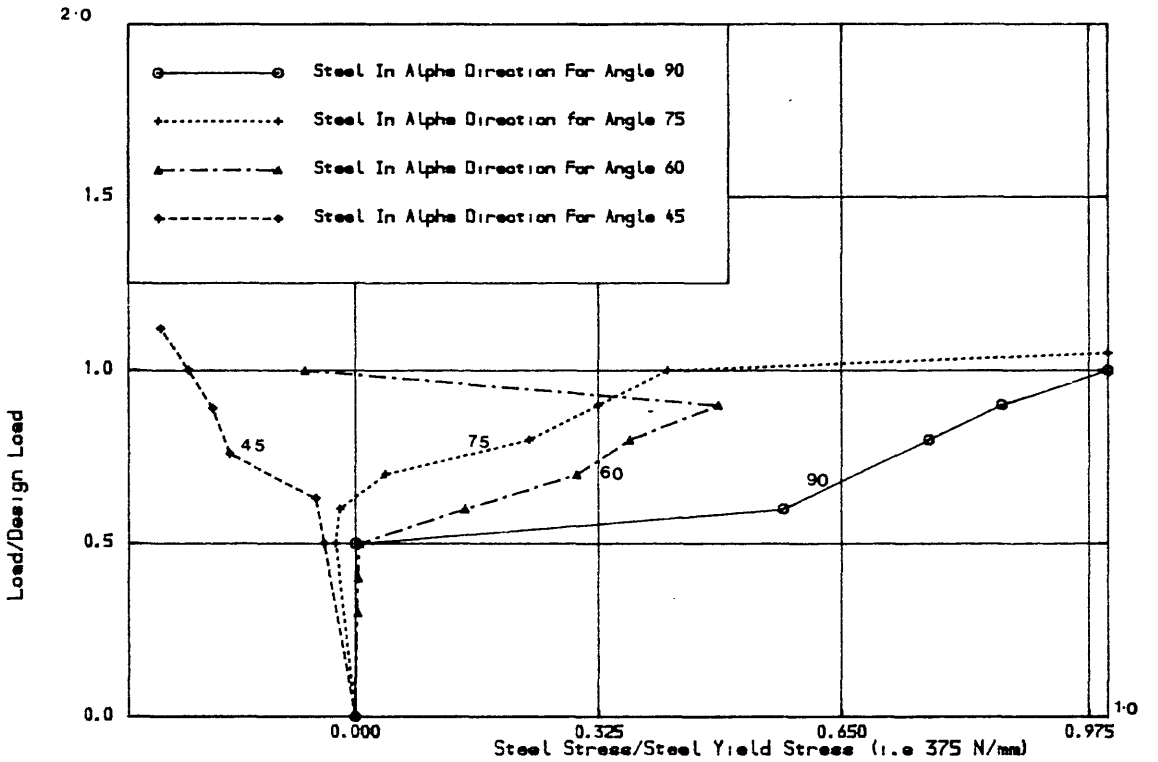

Fig. (5.30) Load-Bottom Longitudinal steel stress for pure Mxy case for different angles of skew considering fixed crack analysis

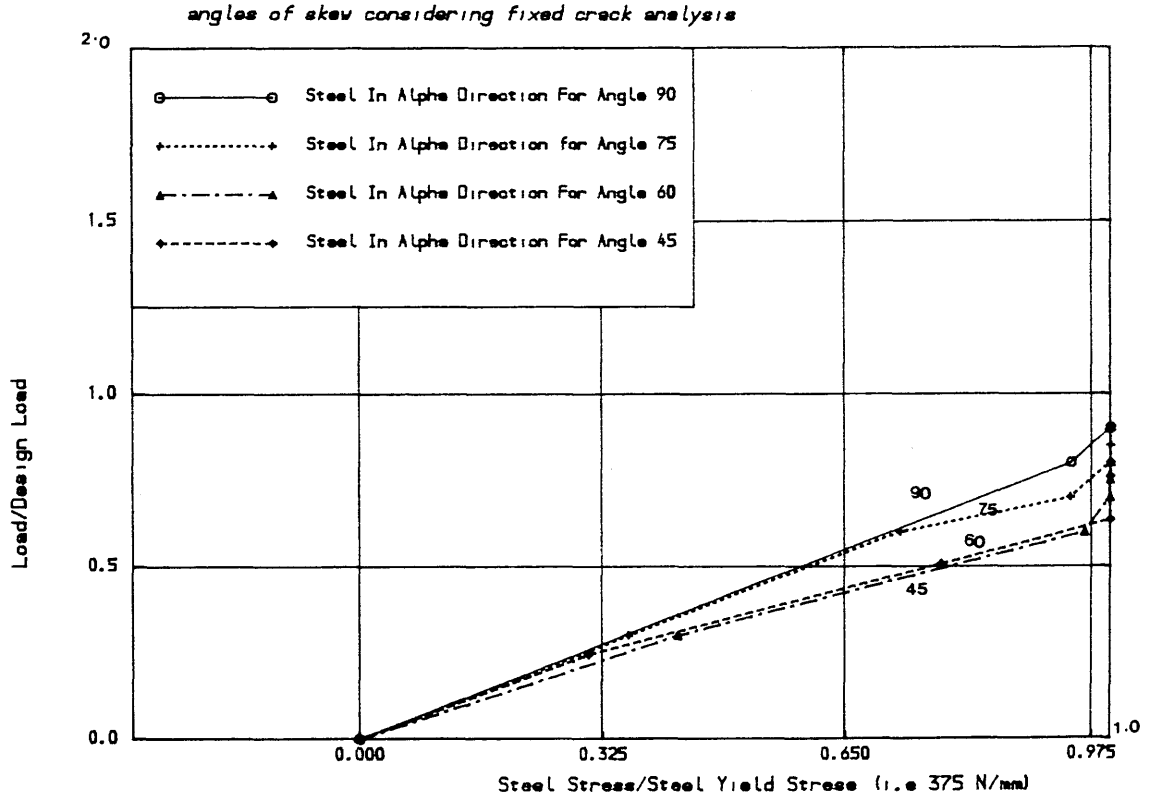

Fig. (5.31) Load-Bottom longitudinal steel stress for pure Mxy case for differen angles of skew considering no-tension analysis

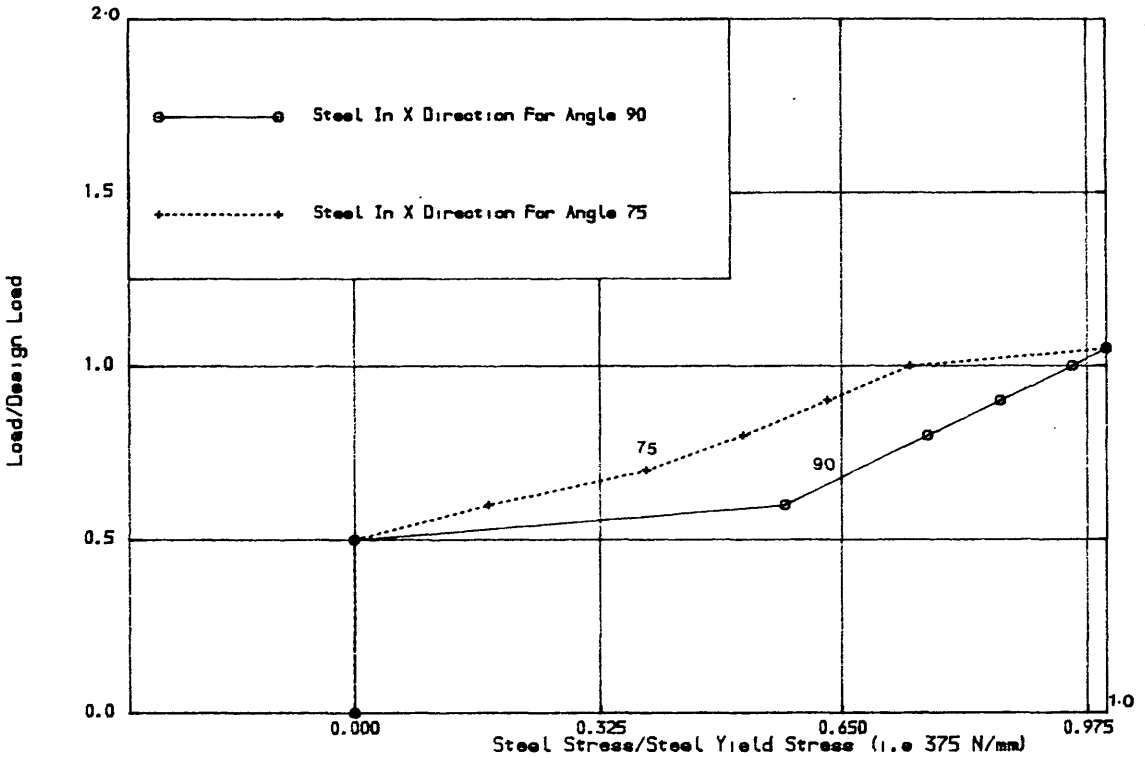

Fig. (5.32) Load-Top transverse steel stress for pure Mxy case for different angles of skew considering fixed crack analysis

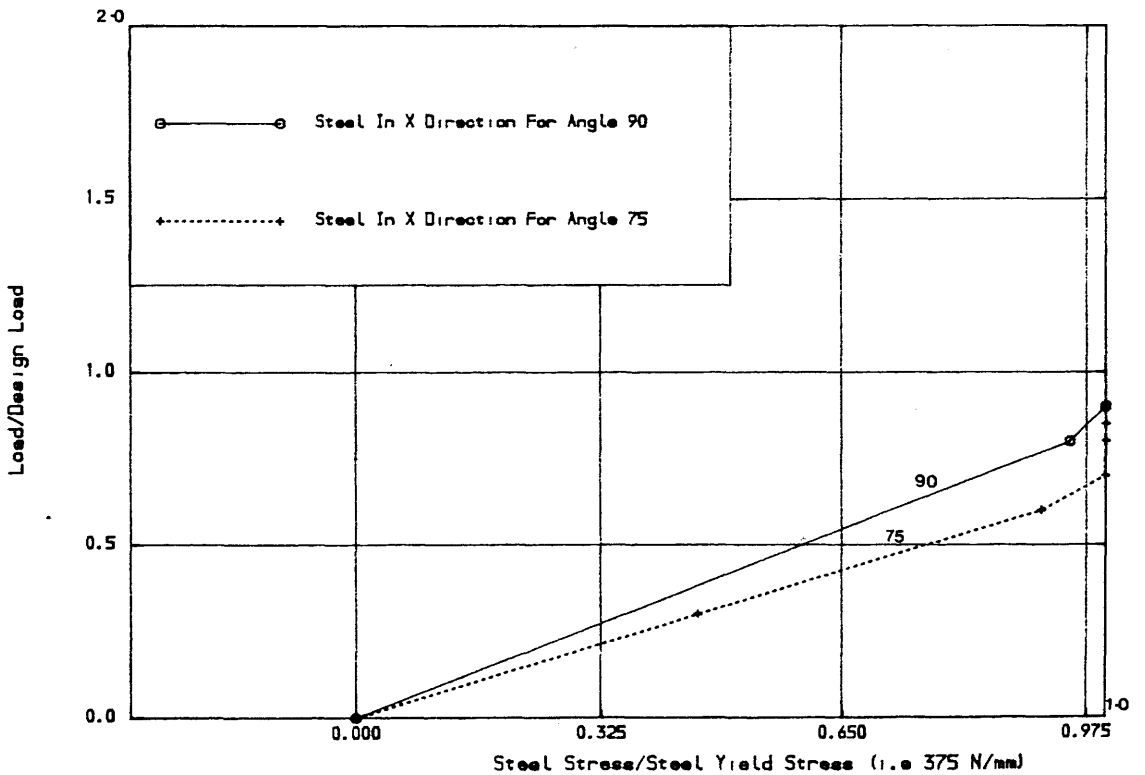

Fig. (5.33) Load-Top transverse steel stress for pure Mxy case for different angles of skew considering no-tension analysis

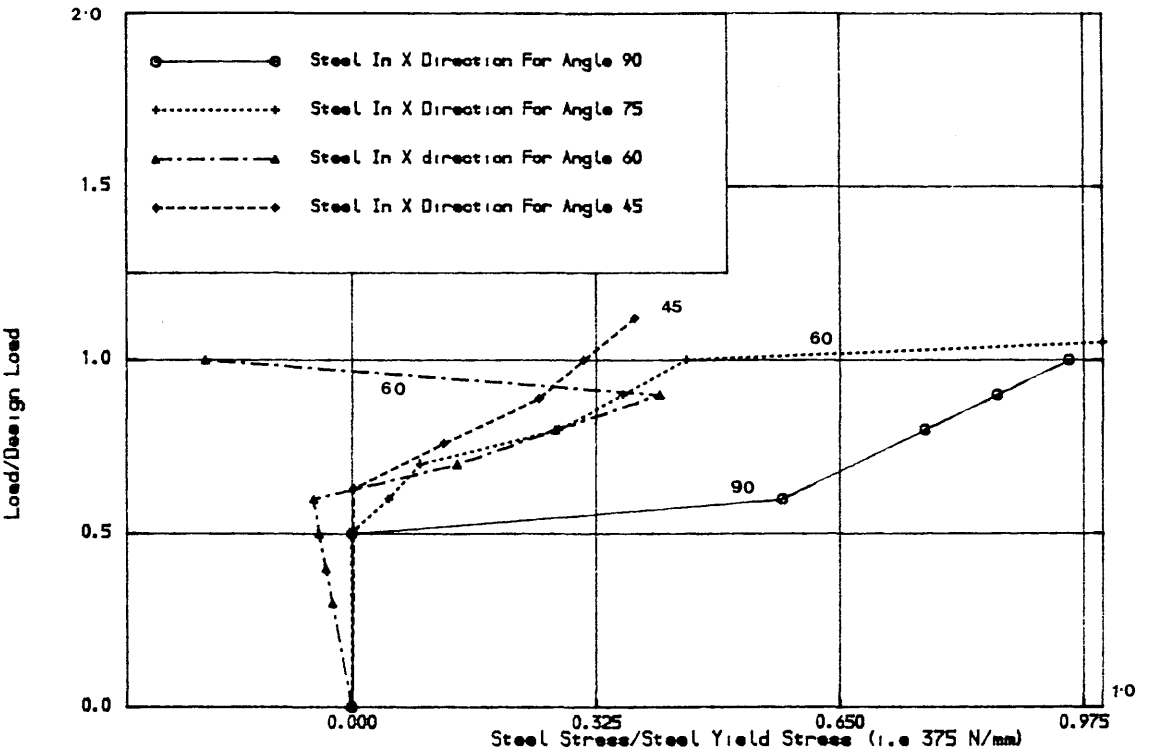

Fig. (5.34) Load–Bottom transverse steel stress for pure Mxy case for different angles of skew considering fixed crack analysis

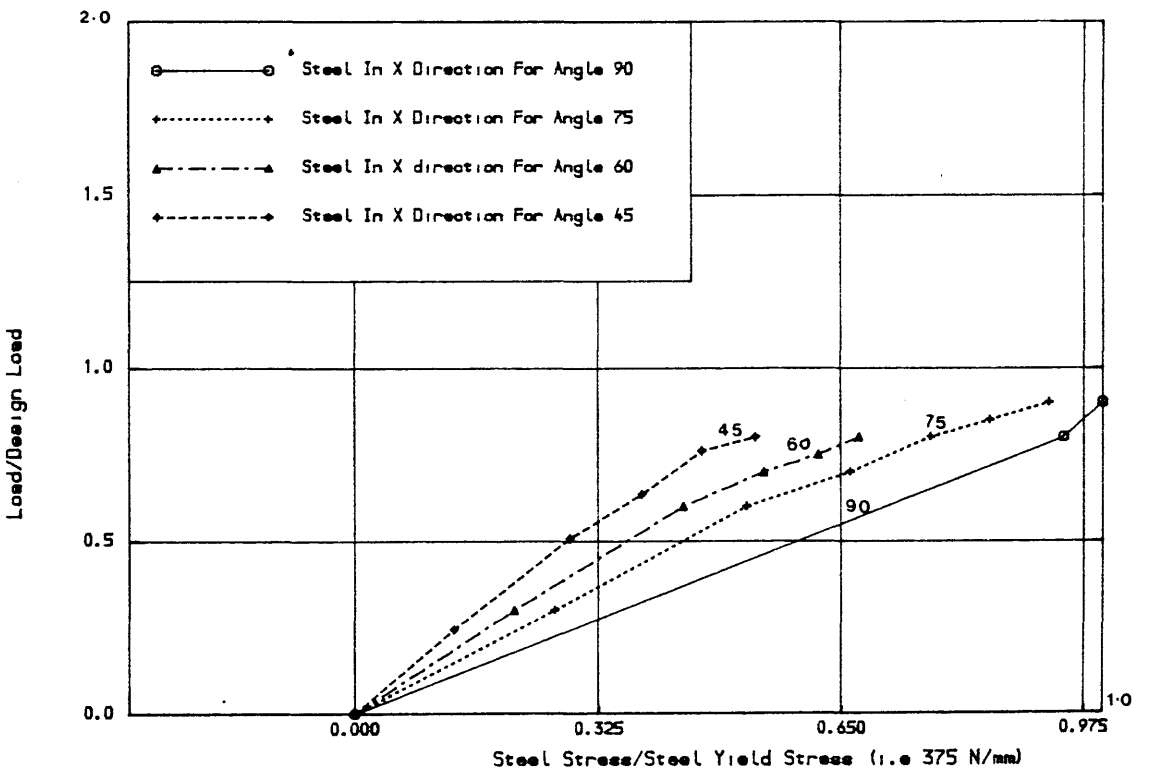

Fig. (5.35) Load–Bottom transverse steel stress for pure Mxy case for different angles of skew considering no-tension analysis

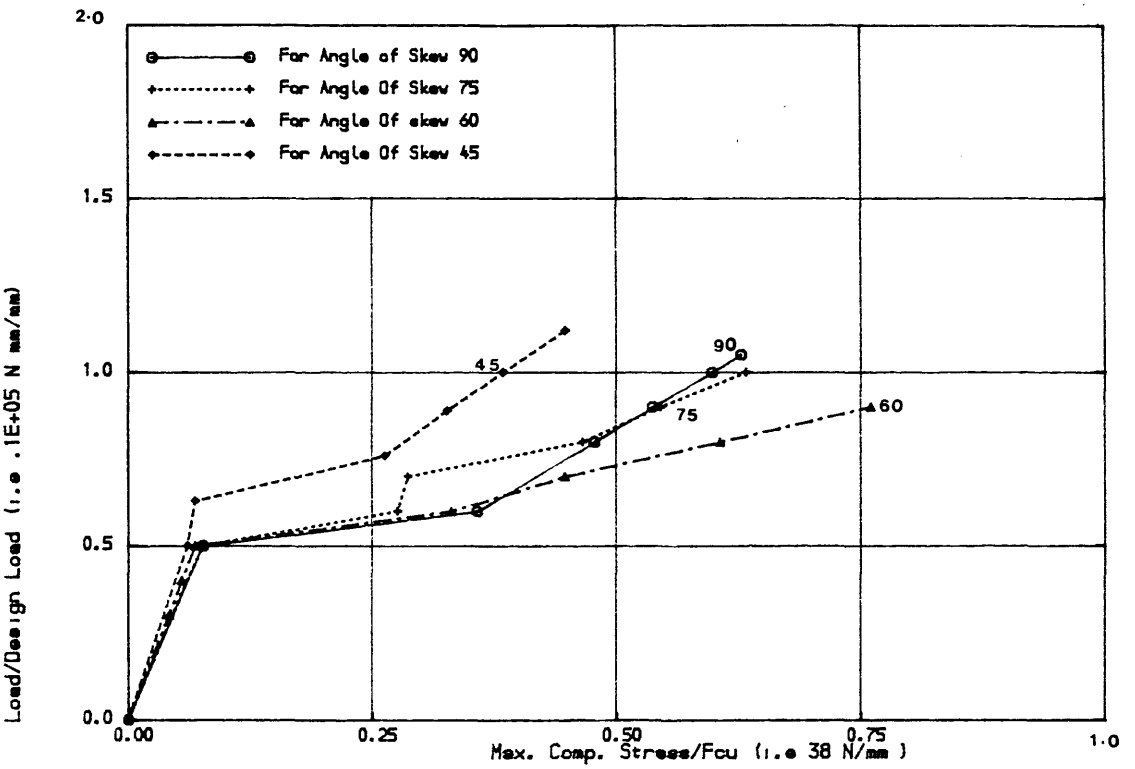

Fig. (5.36) Load-Top max. compression stress for pure Mxy case for different angles of skew considering fixed crack analysis

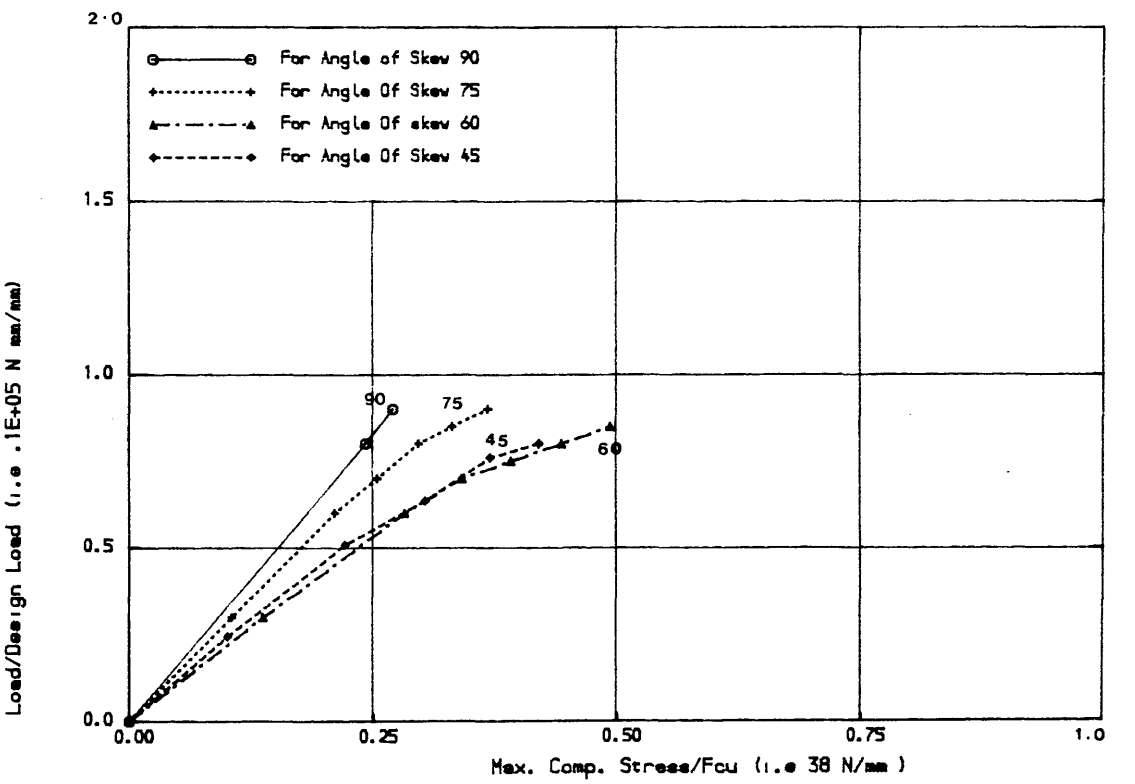

Fig. (5.37) Load-Top max. compression stress for pure Mxy case for different angles of skew considering no-tension

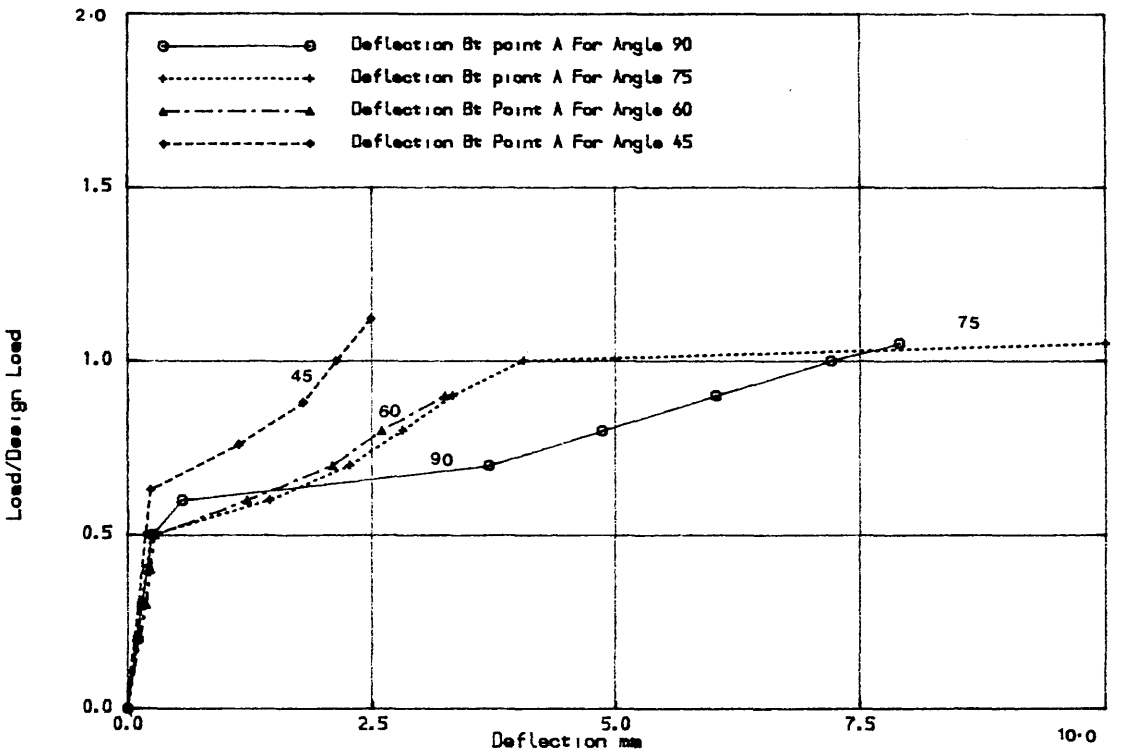

Fig. (5.38) Load-Bottom deflection for pure Mxy case for different angles of skew considering fixed crack analysis

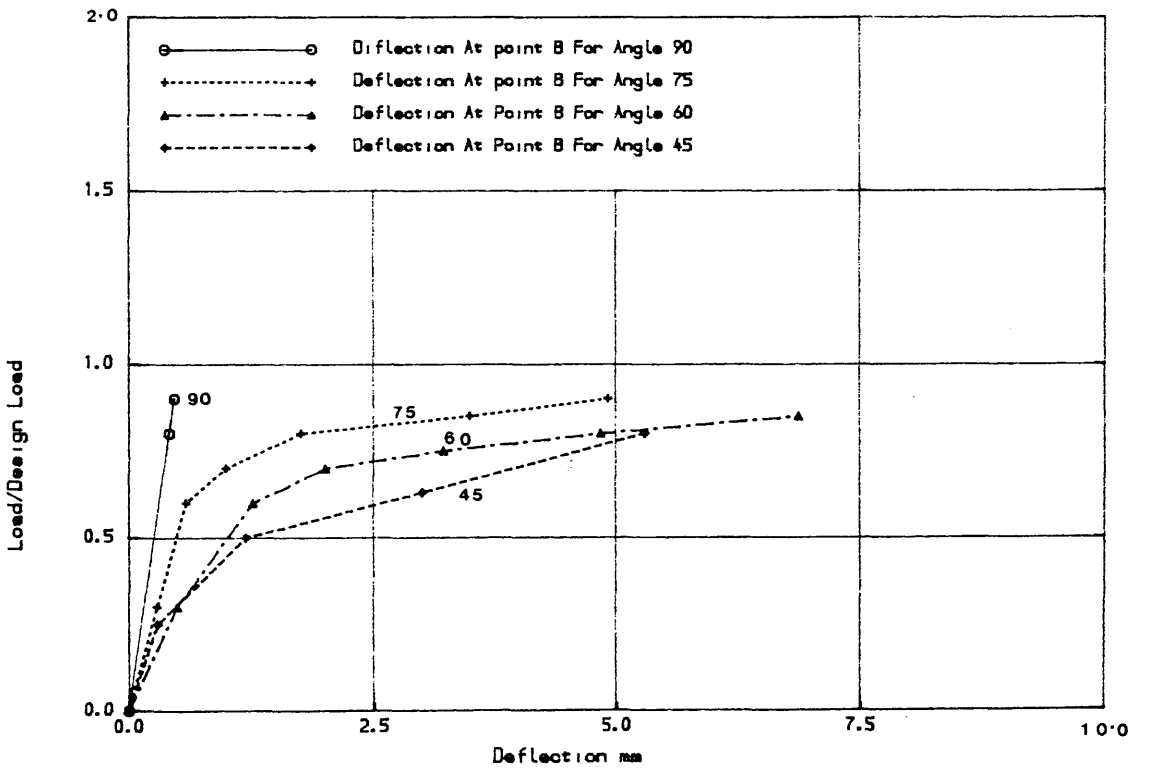

Fig. (5.39) Load-Bottom deflection for pure Mxy for different angles of skew considering no-tension analysis

of two orthogonal cracks. In **No-Tension** analysis, because of the initial tangential stiffness, this was not allowed and hence the core carried stress. This results in smaller stresses in the outer fibers of concrete and allows the steel to carry large stresses to maintain equilibrium. When angle 90° is considered the core completely disintegrated because of the orthogonal cracking leaving only the outer concrete and steel layer to carry the stresses. Because the core did not disintegrate in the case of **No-Tension** analysis, the stress at the outer fibers of concrete is underestimated while the stress in the steel is overestimated thus reducing the flexural capacity of the section.

5.7 Conclusions

1-Fixed crack analysis may be suitable when the orthogonal reinforcement case is used and may be misleading in the case of skew reinforcement.

2- Shear retention factor is an important parameter when skew reinforcement is considered.

3- Concrete as **No-Tension** material analysis reflected the the design assumptions and helped to understand the short comings of fixed crack analysis. behaviour.

4- As the angle of skew decreases the structure becomes more flexible and it is therefore important to check for serviceability. In **No-Tension** analysis tensile stress in concrete is assumed to be zero and this affects the serviceability calculation.

5-Theoretical investigation substantiates the validity of

the direct design method as a lower bound approach for slab of different angle of skew except when the angle decreases to 45^{o}. In the case of 45^{o} angle, the theoretical ultimate load is up to 20% less than the design load depending on the type of loading. More discussion about 45^{o} angle of skew will be given in Chapters Seven and Eight.

CHAPTER SIX

EXPERIMENTAL SETUP, MATERIAL AND INSTRUMENTATION ADOPTED

6.1 INTRODUCTION

The theory given in Chapter Three for the direct design of skew slabs is subjected to experimental verification by testing reinforced concrete skew slabs. Large scale skew slabs with different angles of skew and with different arrangements of steel were tested The loading rig from a previous work (9) was used with minor modification. The slabs satisfied the recommended span/depth ratios as given in section (3.3.8) of CP 110. Except for model six, the support condition consisted of two free opposite edges and the other two edges simply supported. For model six, which was ribbed skew plate, only the longitudinal ribs were simply supported at these ends. This Chapter describes:

(a) Design method and steel layout for the models.

(b) Loading rig and instrumentation used.

(c) Determination of the material properties of concrete and steel.

In all, six slabs were tested. Table (6.1) gives the details of the slabs tested. It should be noted that the angle of skew is measured anticlockwise from the support edge to the free edge (see Fig (6.15a)).

6.2 THE METHOD OF DESIGN

6.2.1 Flexural Reinforcement

The initial uncracked stiffness was used to obtain the elastic stress distribution under the ultimate loading,

TABLE (6.1) Tested Slabs - Designation and Dimensions

Model No.	Support Condition	Loading System	Angle of skew	Dimensions in mm	Steel arrangement	
					Longitudinal Steel	Transverse Steel
1	For all slabs, two parallel edges were free and other they were simply supported except the last model the longitudinal Beams only were simply supported.	Indirect four point load	120°	1945 x 2425 x 100	Parallel to the free edge	Parallel to the supported edge
2		Indirect two point load	60°	1945 x 2425 x 100	Parallel to the free edge	Parallel to the supported edge
3		Direct four point load	45°	2000 x 2970 x 100	Parallel to the free edge	Parallel to the supported edge
4		Direct four point load	45°	2000 x 2970 x 100	Orthogonal to the supported edge	Parallel to the supported edge
5		Direct four point load	45°	2000 x 2970 x 100	Parallel to the free edge	Orthogonal to the free edge
6 *		Direct four point load	45°	2000 x 2970 x 100	Parallel to the longitudinal ribs	Parallel to the transverse ribs

* ribbed slab, (see fig. (6.12.1)).

using the finite element program described in Chapter Four. The design equations, as given in Chapter Three, were used to evaluate the moment of resistance required to design the steel. The steel required was obtained according to limit state theory adopted by CP110 with material safety factors taken as unity. Full details are given in Appendix A.

6.2.2 The Shear Reinforcement

Since the obtuse corner supports provide maximum reaction, there is a possibility of punching shear failure at these corners. In addition, steep moment gradient occur in the obtuse corner regions. When shear resistance of the slab at the design load was calculated by using CP 110 (30) rules for slabs, it was found that no shear reinforcement was required. The reaction at the obtuse corner from the linear analysis at the design load was considered as a shearing force. This shearing force was considered as the sum of the three nodel reactions of the element which represent the obluse corner as shown in Fig. (6.1). The shear stress is calculated using CP110 (30) equation,

$$v_s = \frac{V}{bd} \qquad (6.1)$$

where V is the shear force, b the width under consideration and is taken as the length of the element in the direction of the support and d is the effect depth of the slab and is taken 0.85 of the thickness

The steel ratio which is involved in the calculation of the shear resistance is taken as the ratio of longitudinal steel in the width b (see Fig. (6.1)).

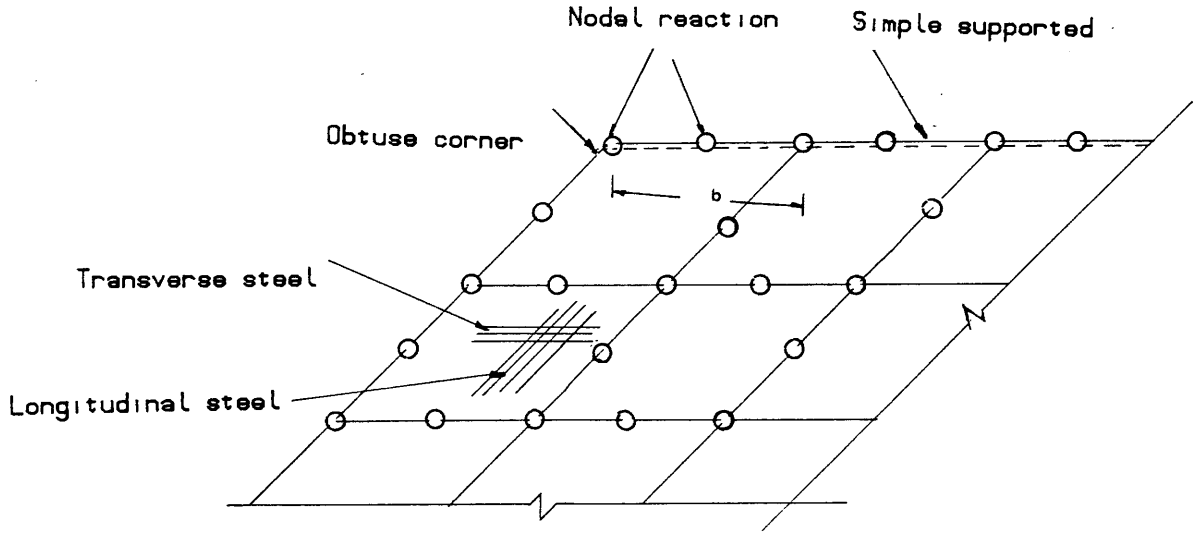

Fig. (6.1) Estimation of the reaction at the obtuse corner

Unfortunately because the experimental failure load was greater than the theoretical design load, shear failure occurred in the first and fifth models. More details about the cause of this type of failure and how it can be avoided is given in section (8.2.2.7) Chapter Eight.

6.2.3 The Steel Distribution

The design procedure adopted results the continuously varying reinforcement in the slab. Replacement of this continuously varying steel area by discrete reinforcing bars results in discrepancies between the steel theoretically required and that which is provided. Depending on the severity of the variation, the following procedures can be used to replace the continuously distributed steel areas by discrete reinforcing bars.

(a) If the variation of the distributed steel area is not severe from point to point, these areas can be averaged over a certain width. The total steel area is then obtained by multiplying the average value by the corresponding width and this which can then be replaced by discrete bar.

(b) If the variation of the distributed steel areas is severe from point to point over a certain width, the total steel was then obtained by multiplying the value at each point by the corresponding width. The required area of steel will be varied in steps by using welding to connect bars of the required diameter.

Fig. (6.2.1) to Fig. (6.6.2) show the design and the provided area of steel for each model. Table (6.2) shows the total volume of design steel and total volume of steel

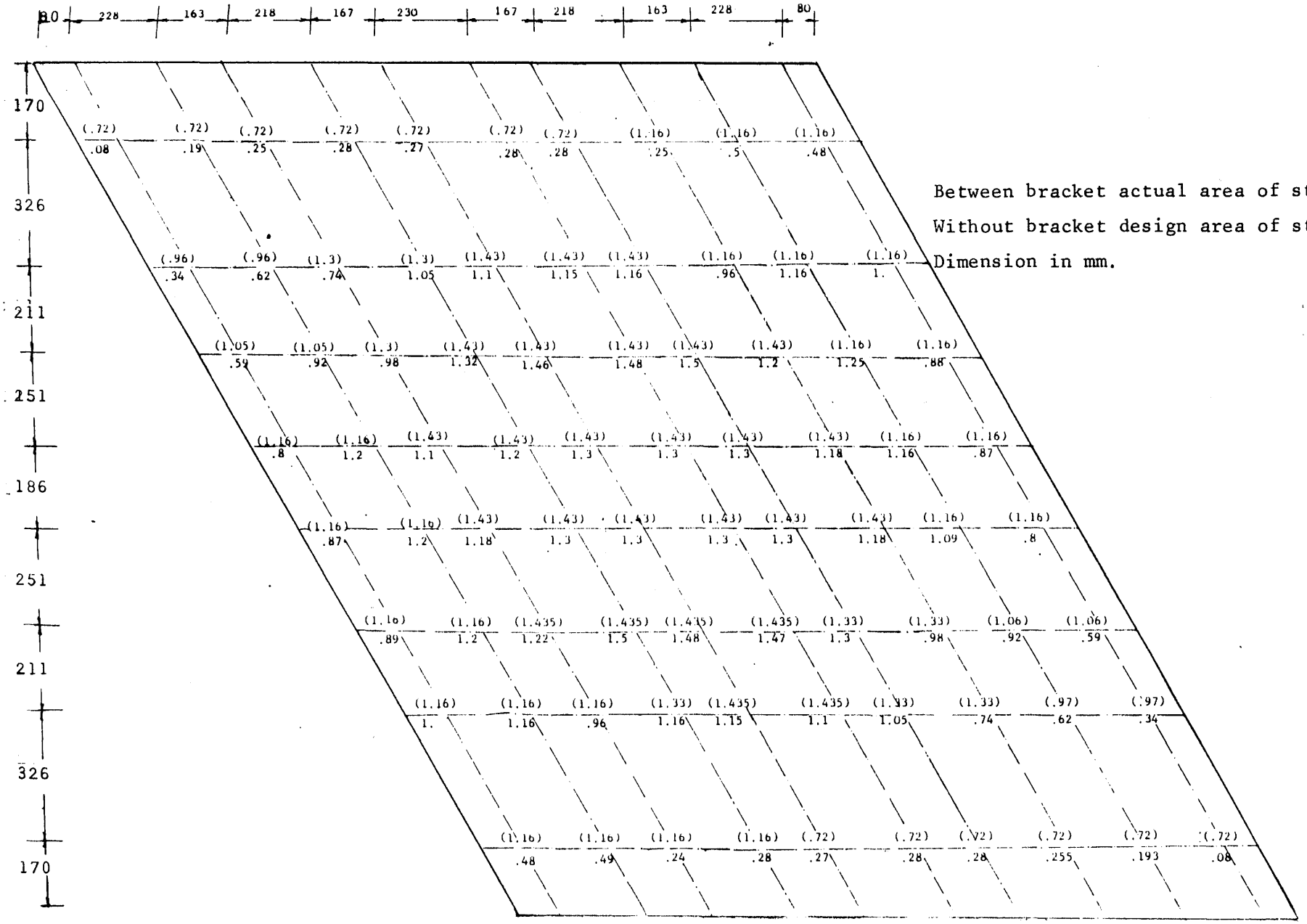

Fig.(6.2.1) MODEL SKEW SLAB NO.(1) Bottom Longitudinal area of steel per unit width (mm^2/mm)

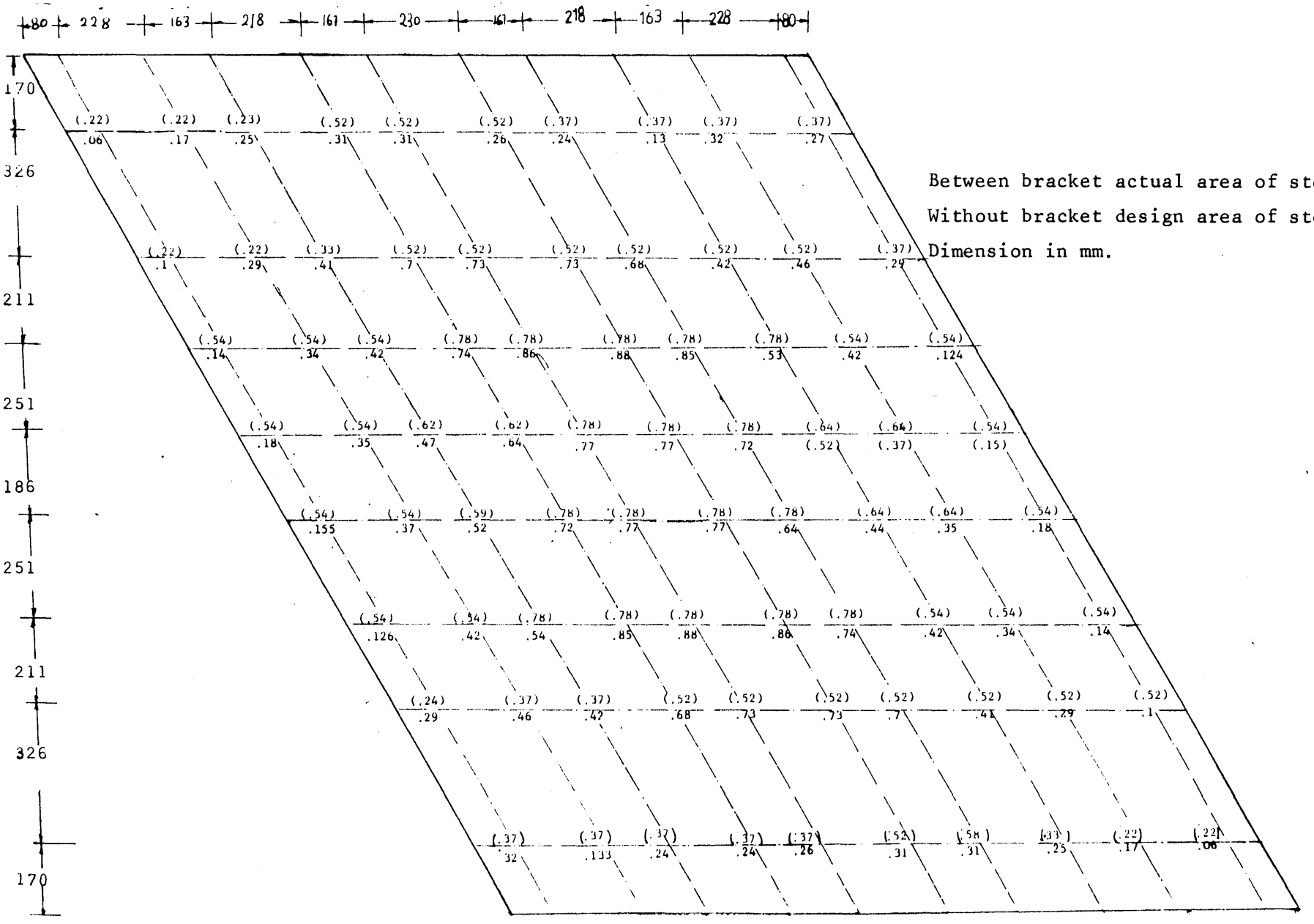

Fig.(6.2.2) MODEL SKEW SLAB NO.(1) Bottom Transverse area of steel per unit width mm^2/mm)

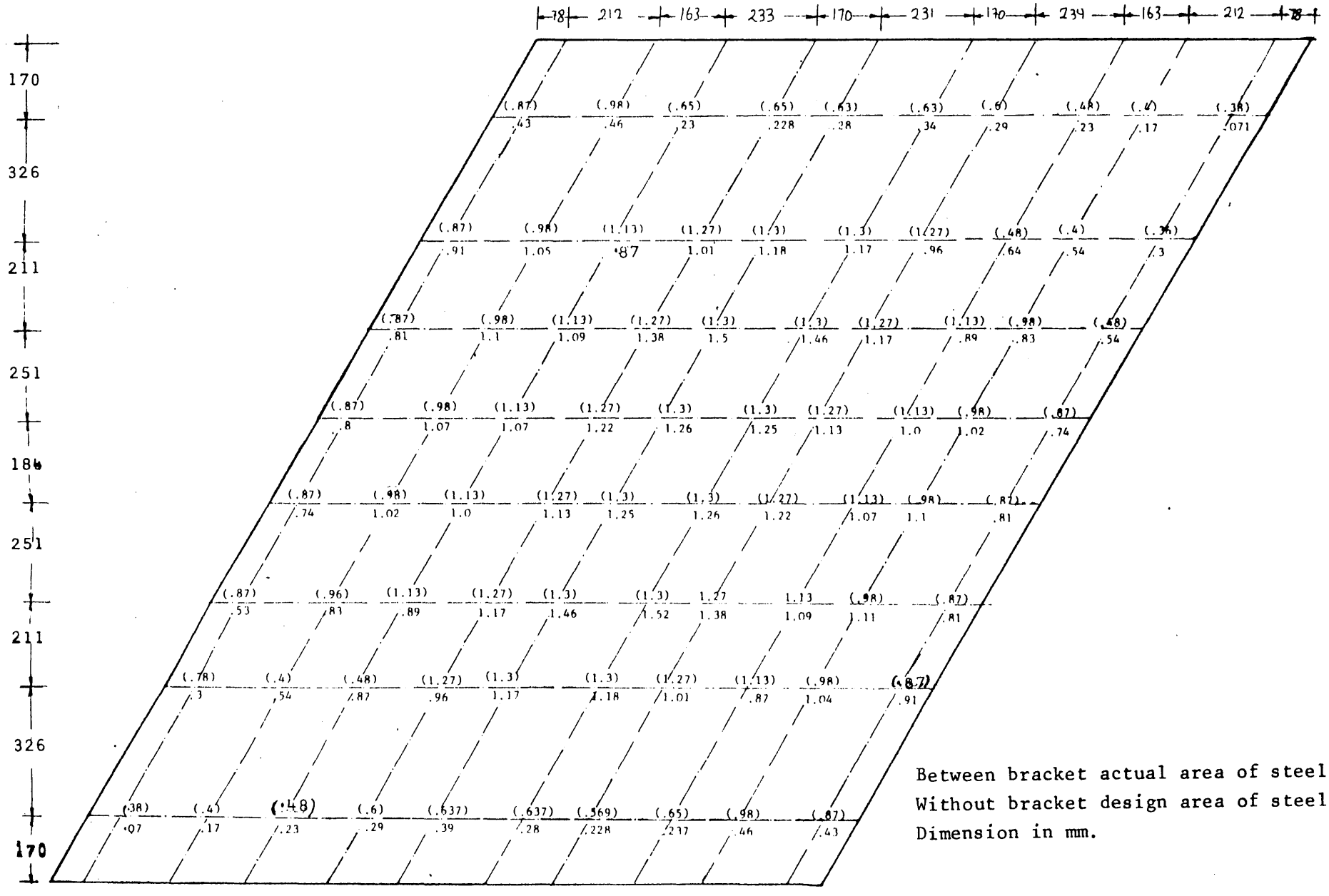

Fig.(6.3.2) MODEL SKEW SLAB NO.(2) Bottom Longitudinal area of steel per unit width of slab (mm^2/mm)

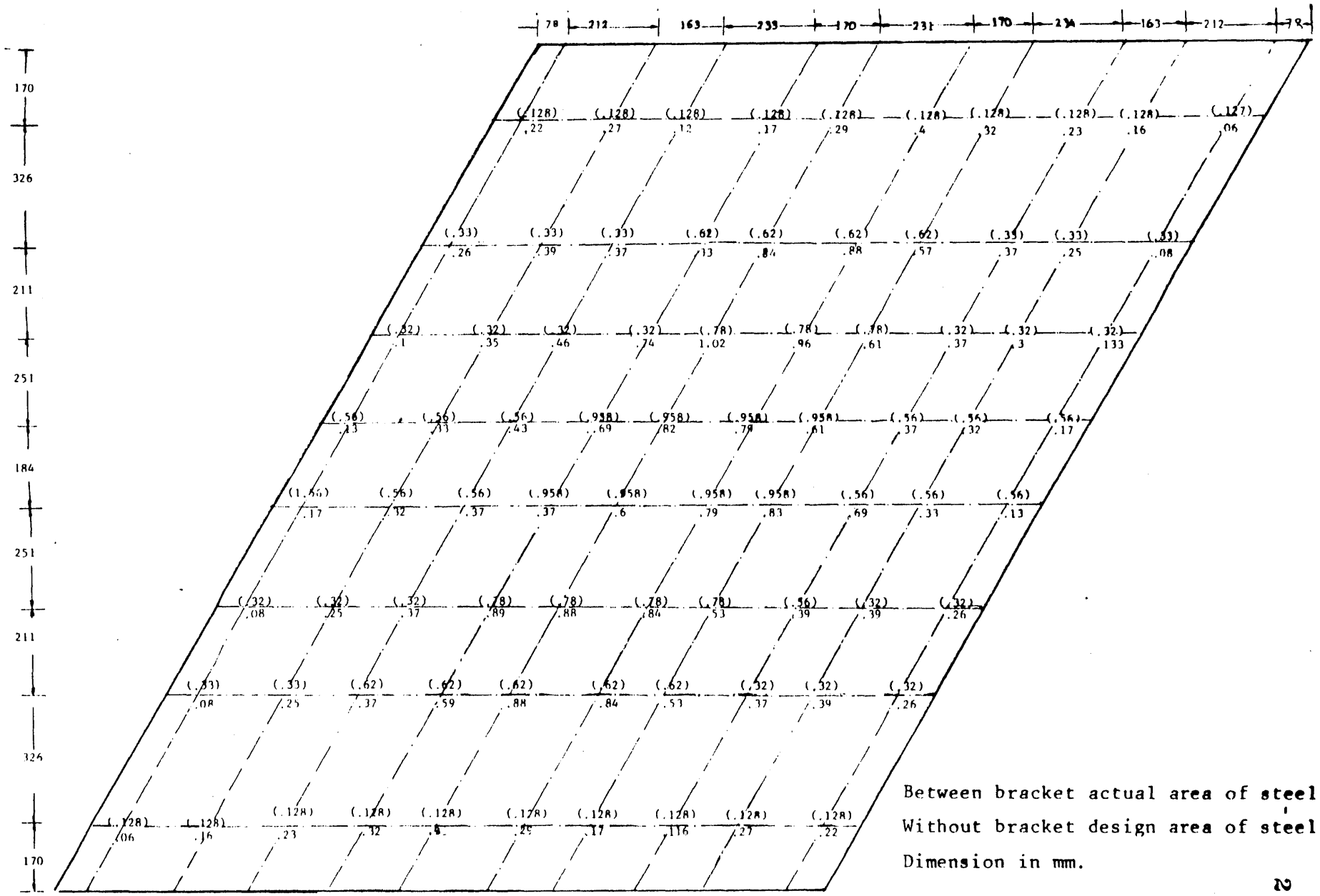

Fig. (6.3.2) MODEL SKEW SLAB NO.(2) Bottom Transverse area of steel per unit width of slab (mm^2/mm)

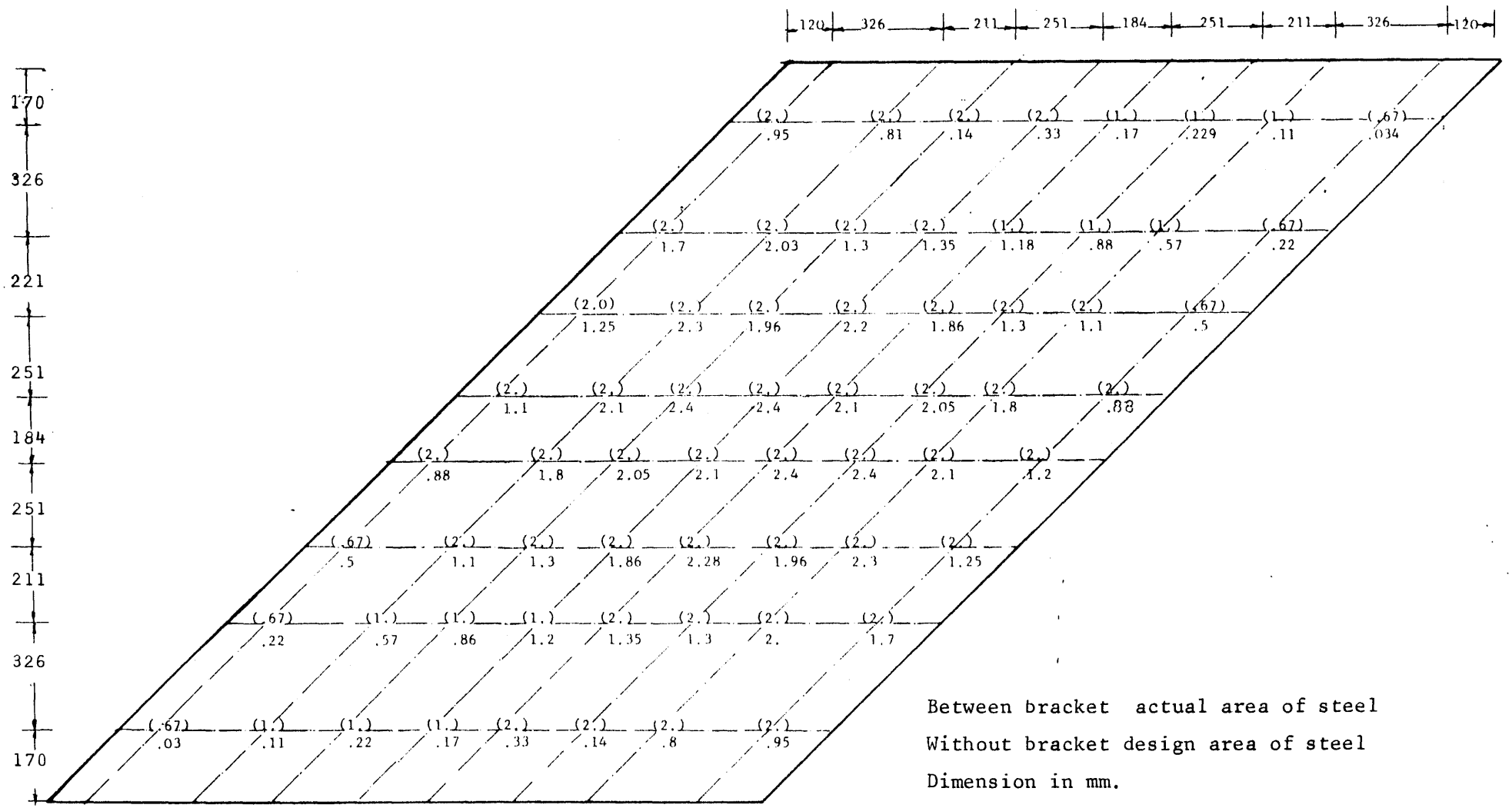

Fig.(6.3.1) MODEL SKEW SLAB NO.(3) Bottom Longitudinal area of steel per unit width (mm^2/mm)

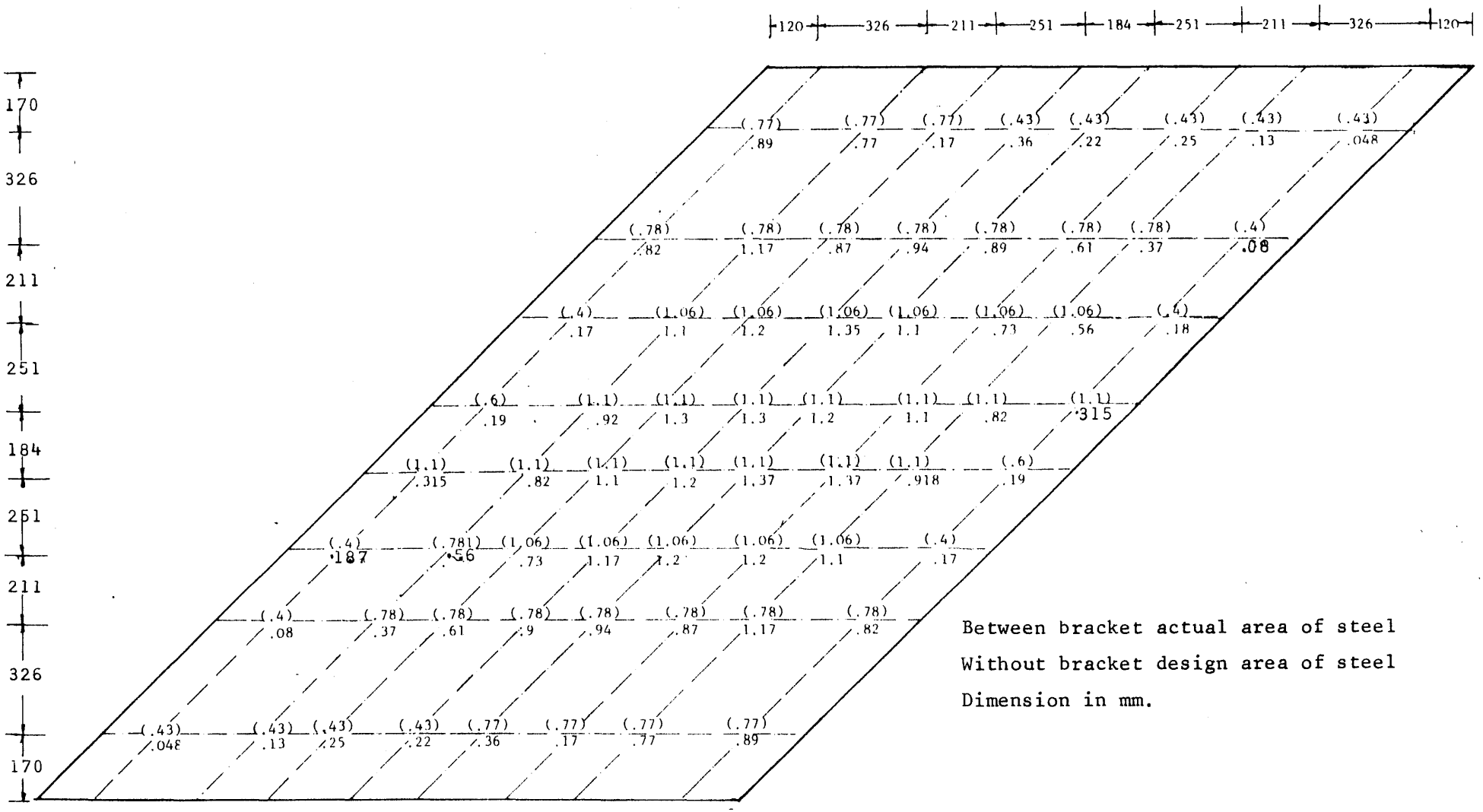

Fig. (6.4.2) MODEL SKEW SLAB NO. (3) Bottom Transverse area of steel per unit width (mm^2/mm)

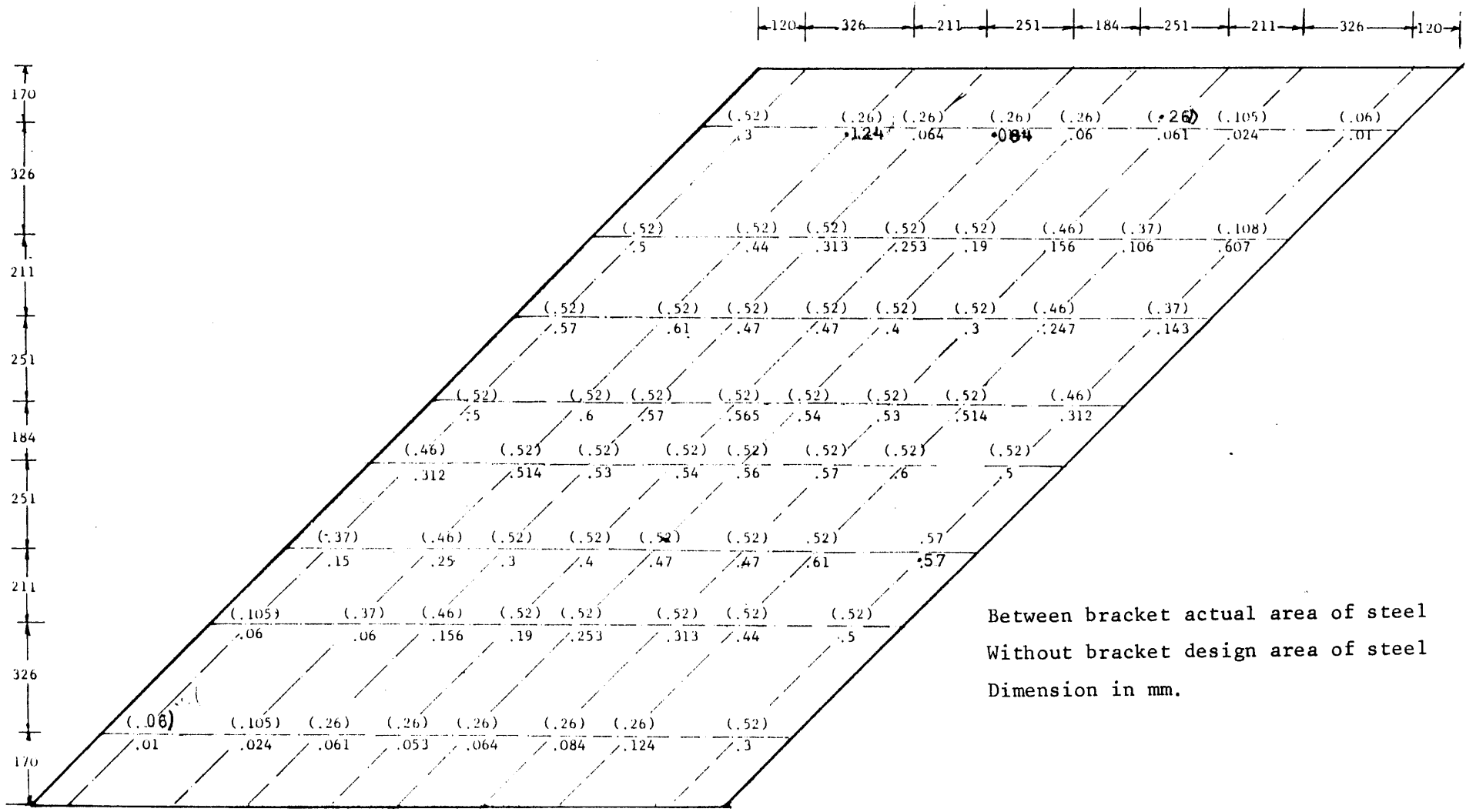

Fig(6.5.1) MODEL SKEW SLAB NO.(4) Bottom Longitudinal area of steel per unit width (mm^2/mm)

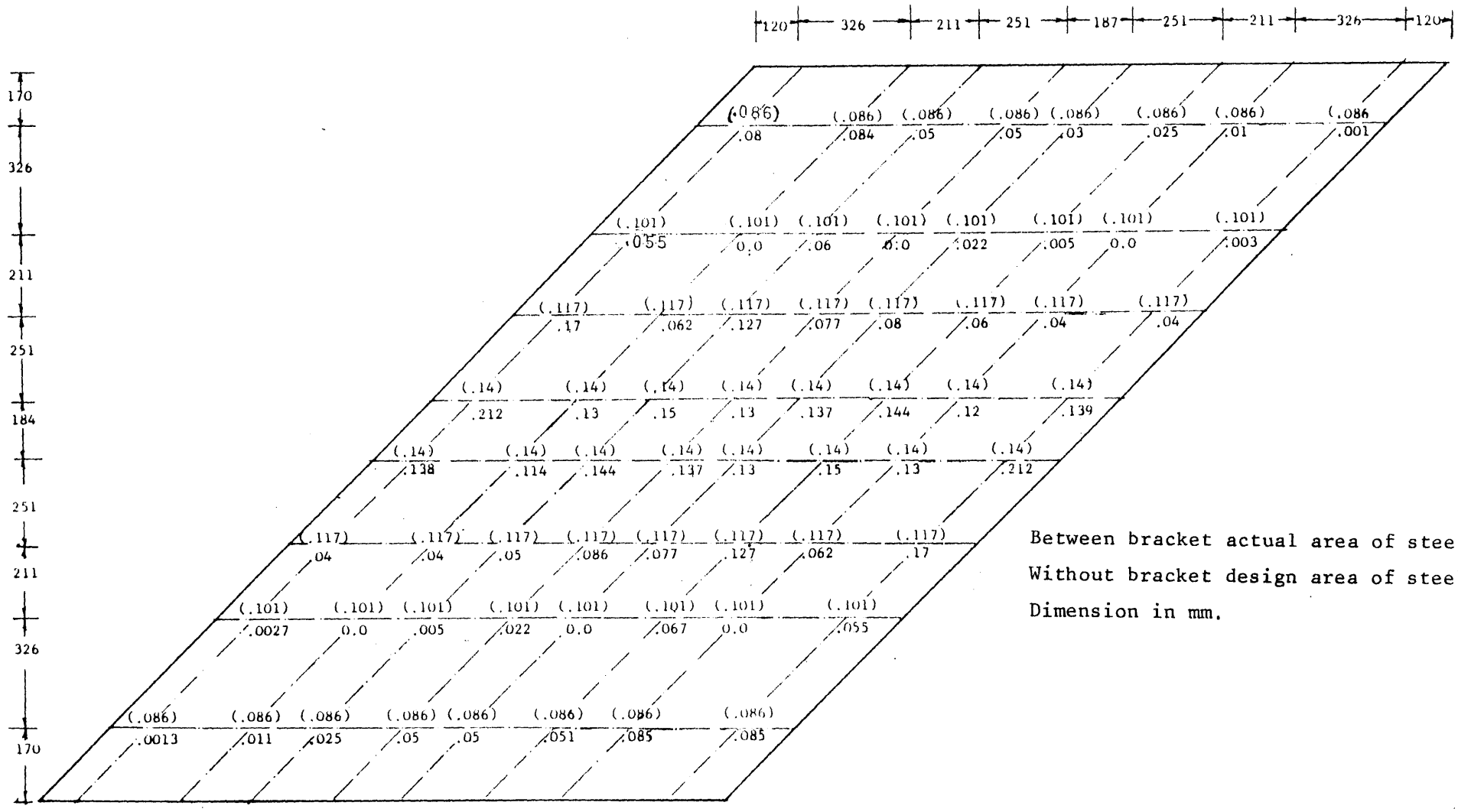

Fig.(6.5.2) MODEL SKEW NO.(4) Bottom Transverse area of steel per unit width (mm^2/mm)

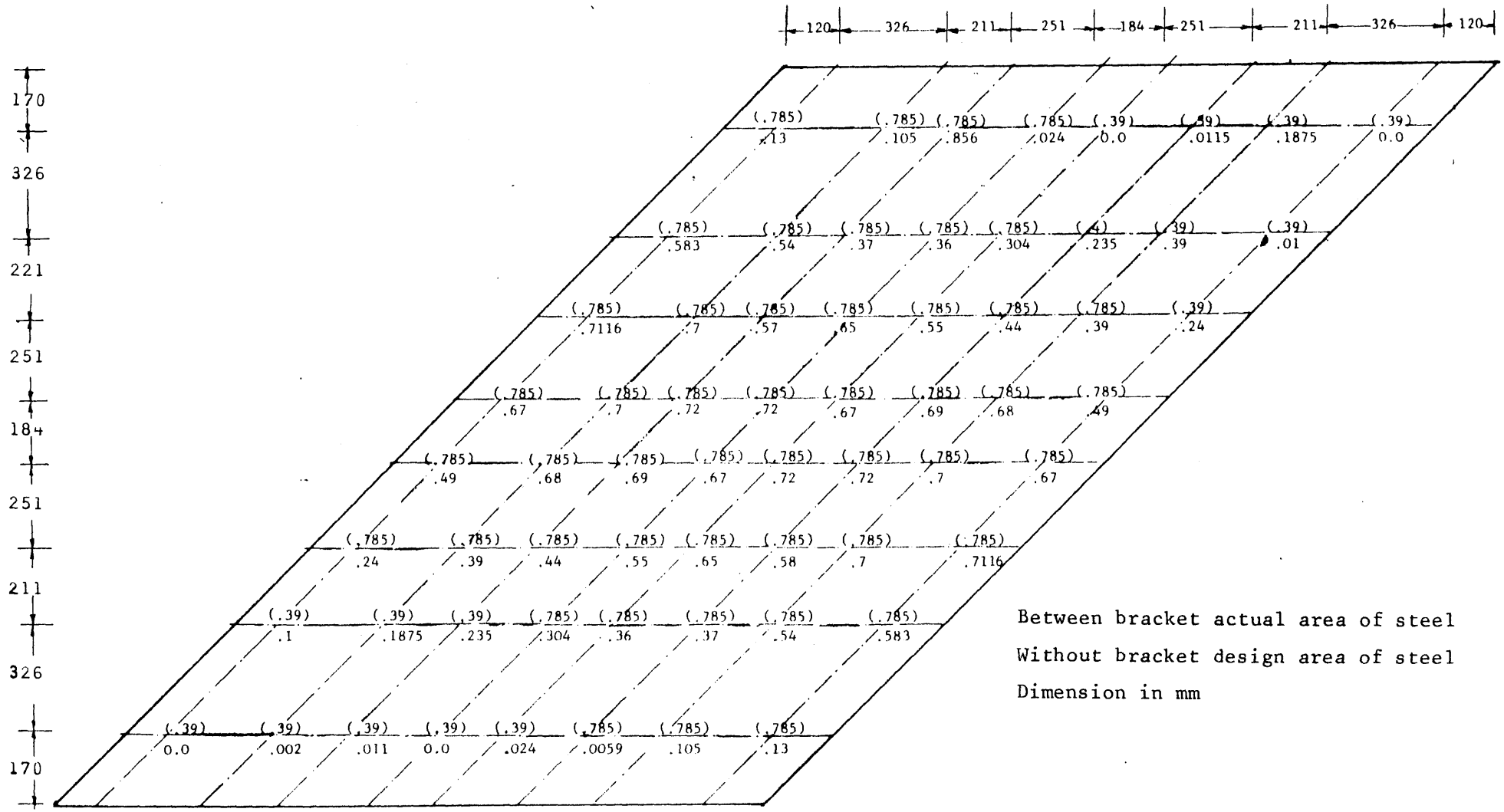

Fig.(6.6.1) MODEL SKEW SLAB NO.(5) Longitudinal area of steel per unit width (mm^2/mm)

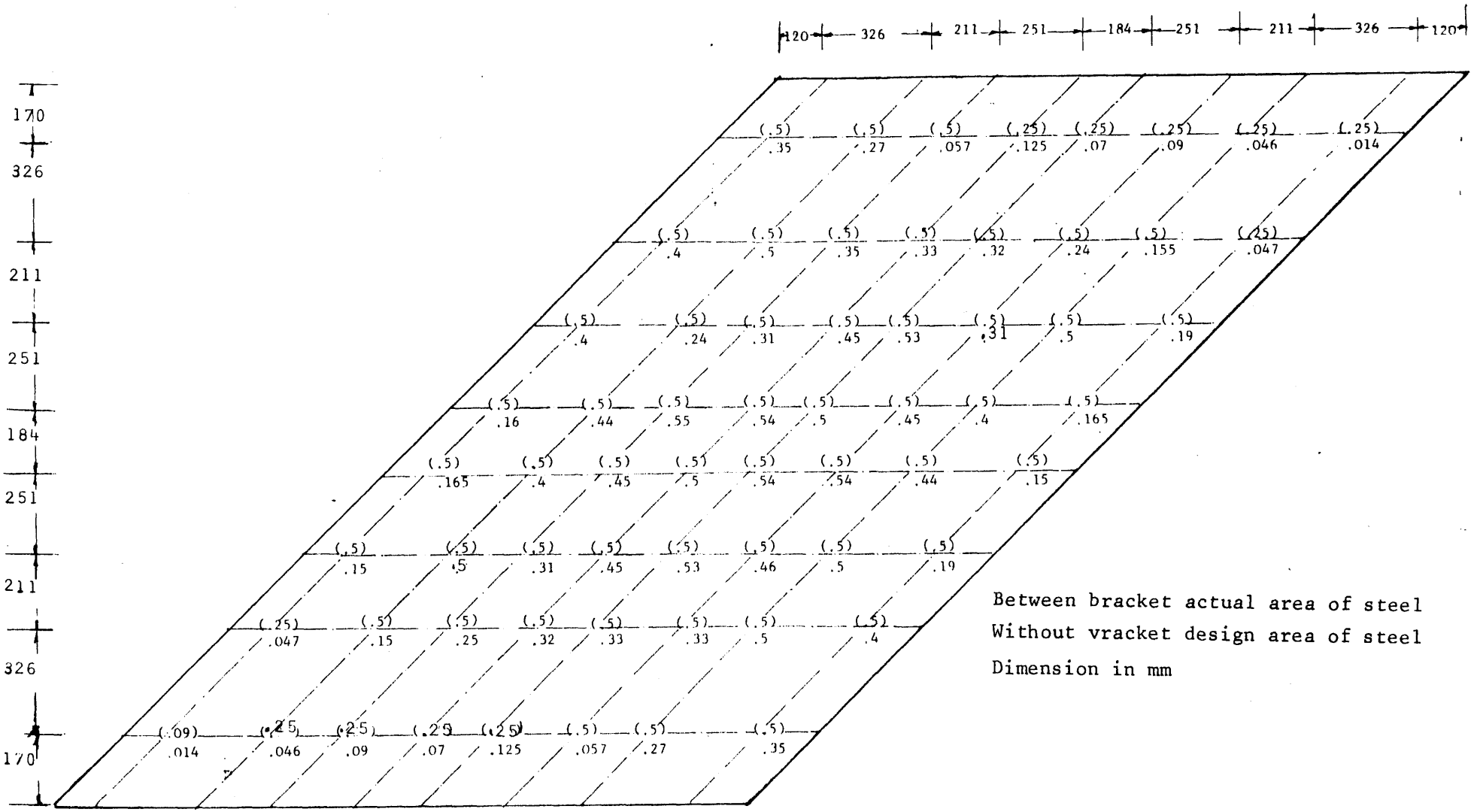

Fig.(6.6.2) MODEL SKEW SLAB NO.(5) Transverse area of steel per unit width (mm²/mm)

provided for each model. To prevent crack widths from becoming excessive, CP110 (30) states that longitudinal bar spacing and the transverse bar spacing should not exceed 150 mm and 300 mm respectively. These rules were adhered to in designing the models. Fig. (6.7.1) to Fig. (6.12.6) show the reinforcement details for each model.

Table (6.2) The comparison between the total design volume and the total actual volume

Model No.	Design total volume of steel (M^3) XE+03		Actual volume/design volume	
	Longitudinal	Transverse	Longitudinal	Transverse
1	3.46	1.7	1.36	1.27
2	3.08	1.55	1.26	1.27
3	4.70	2.70	1.54	1.2
4	1.19	0.03	1.33	1.65
5	1.47	1.13	1.40	1.52

Note: Model six is considered in Chapter Seven

6.3 LOADING RIG

The loading rig is shown in Figs. (6.13a) and (6.13b) the rig was adopted from an earlier research programme involving tests on rectangular reinforced slabs at maximum dimensions 3000mmX 2000mm. The 2000mm span is fixed but the other dimensions may vary from 1000mm to 3000mm. By using this facility, slabs with different angles of skew can be tested. The rig allows 1500mm headroom under the slab so that the bottom surface of the models can be examined during the test. The rig was designed to support a safe load

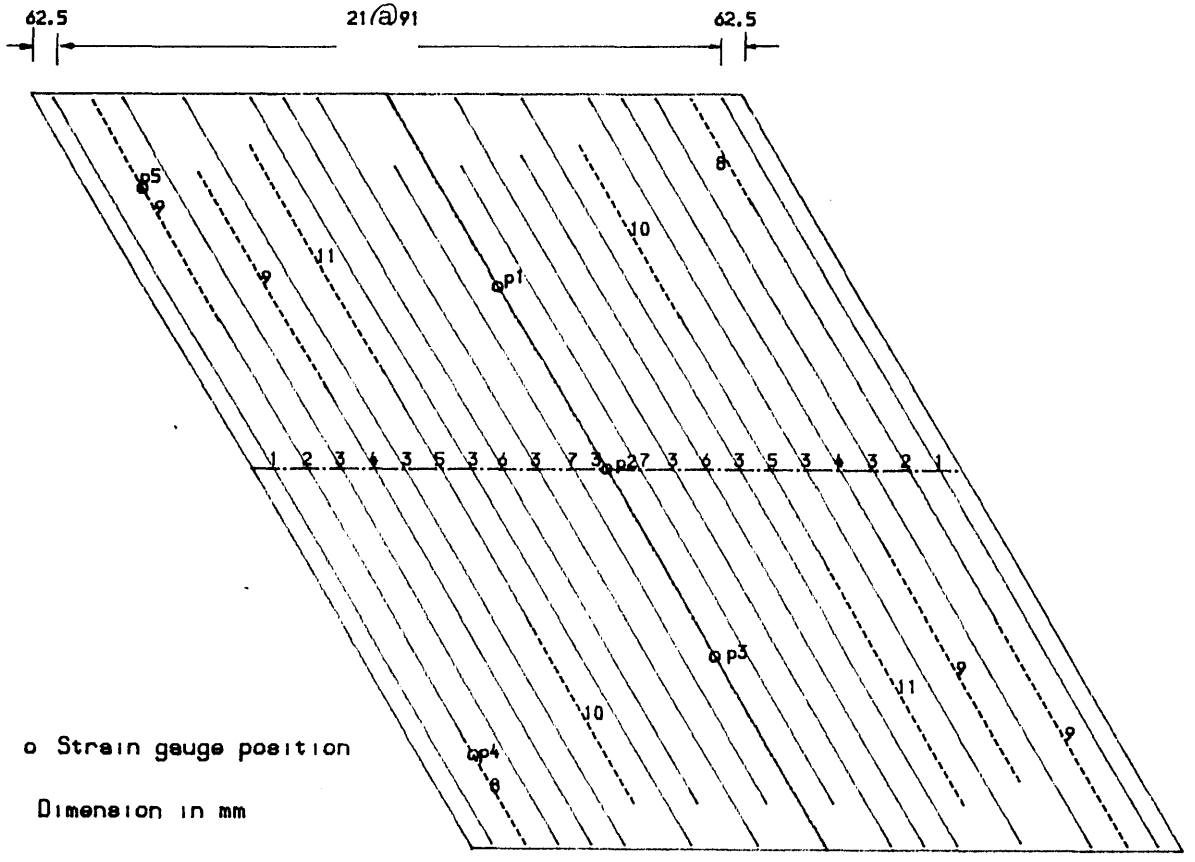

Mark	Lenght	No.	Dia.
1	2395	2	8
2	1355	2	12
3	2395	8	12
4	1475	2	12
5	820	2	12
6	2215	2	12
7	2045	2	12
8	330	2	10
9	710	2	10
10	560	2	10
11	570	2	10

All bars hooked at both ends except the welded ends.
Cover 15.0 mm

Fig. (6.7.1) MODEL SKEW SLAB NO. (1) Details of bottom longitudinal steel parallel to the free edge and position of strain gauges.

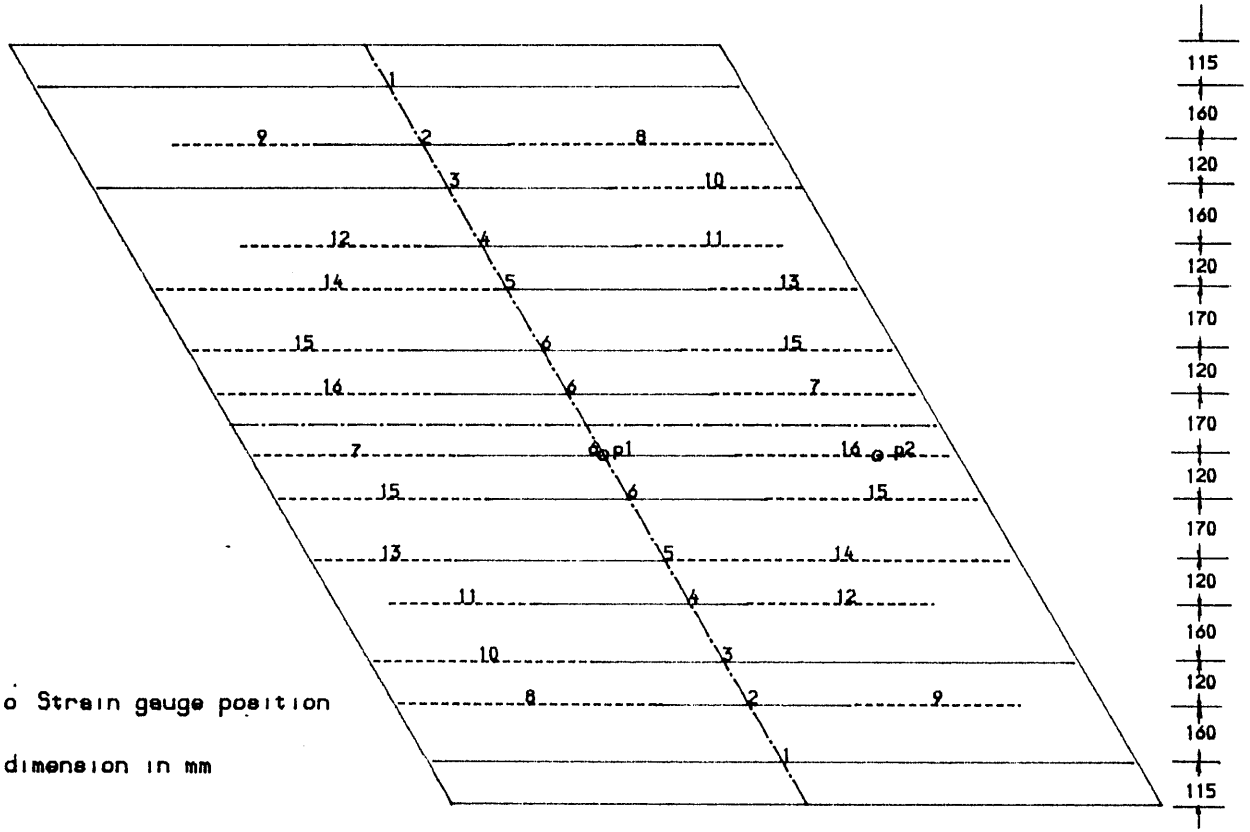

Mark	Lenght	No.	Dia.
1	2395	2	8
2	1355	2	12
3	2395	8	12
4	1475	2	12
5	820	2	12
6	2215	2	12
7	2045	2	12
8	330	2	10
9	710	2	10
10	560	2	10
11	570	2	10

All bars hooked at both ends except the welded ends.
Cover 15.0 mm

Fig. (6.7.2) MODEL SKEW SLAB NO. (1) Details of bottom transverse steel parallel to the supported edge and position of strain gauges.

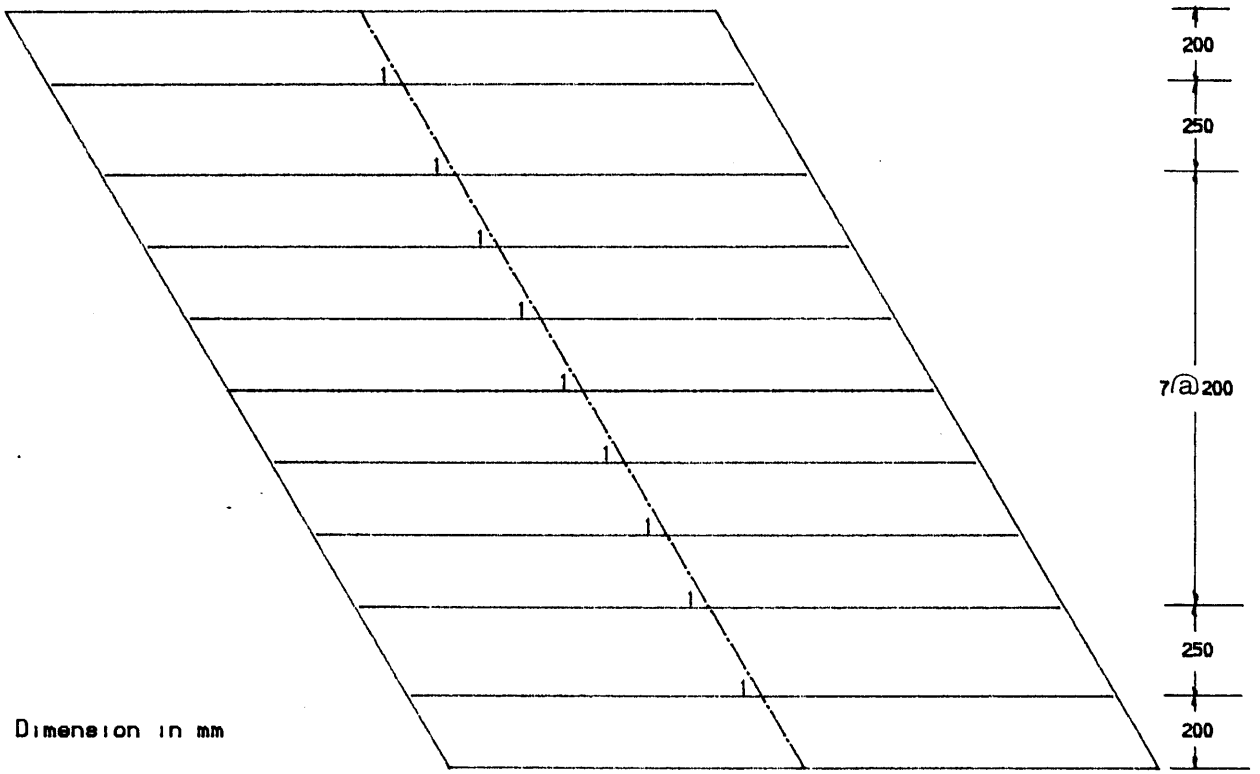

Mark	Lenght	No.	Dia.
1	1915	9	6

All bars hooked at both ends
Cover 10 mm

Fig. (6.7.3) MODEL SKEW SLAB NO. (1) Details of top transverse steel parallel to the supported edge.

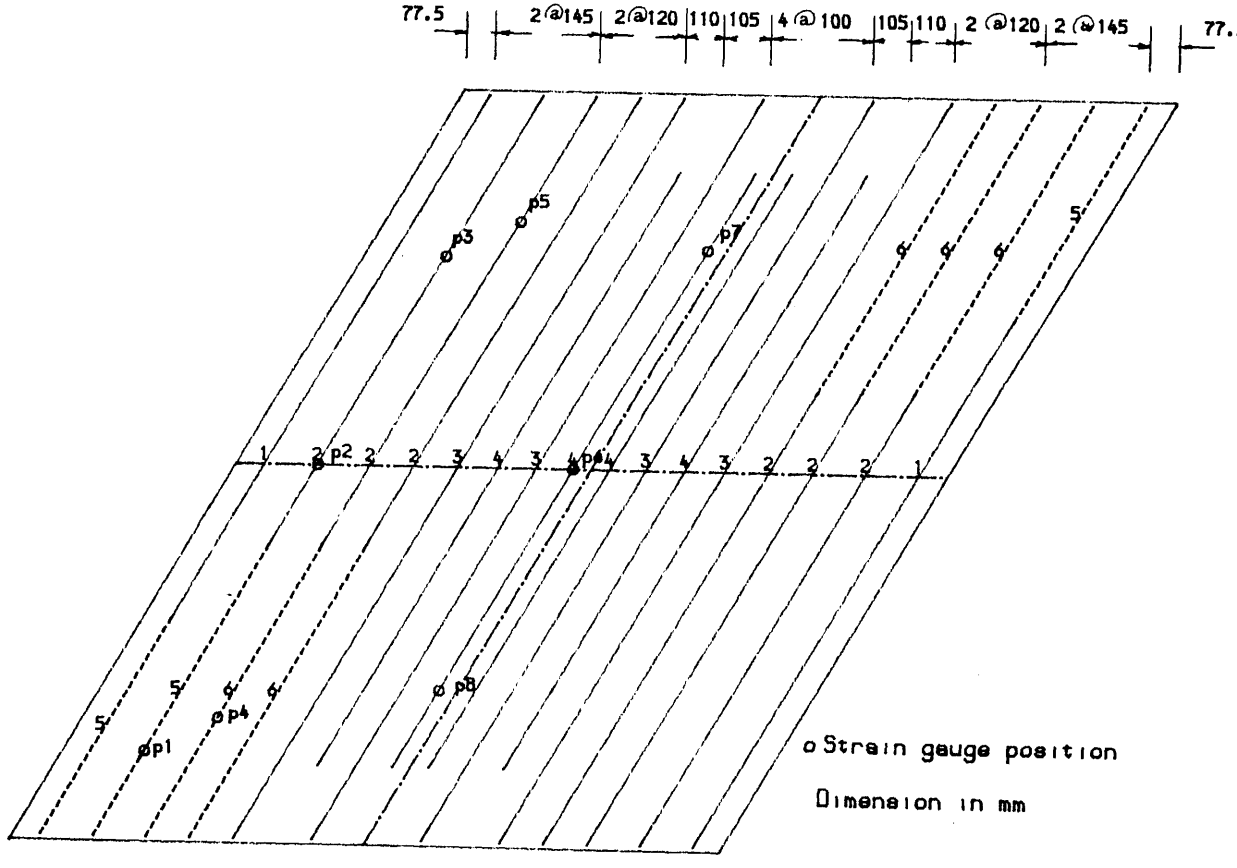

Mark	Lenght	No.	Dia.
1	1700	2	12
2	1455	6	12
3	2395	4	12
4	1925	4	12
5	695	2	8
6	940	6	8

All bars hooked at both ends except the welded ends.
Cover 15.0 mm

Fig. (6.8.1) MODEL SKEW SLAB NO. (2) Details of bottom longitudinal steel parallel to the free edge and position of strain gauges.

Mark	Lenght	No.	Dia.
1	1915	5	10
2	1915	2	12
3	1010	6	10
4	1915	2	8
5	1915	2	6

All bars hooked at both ends

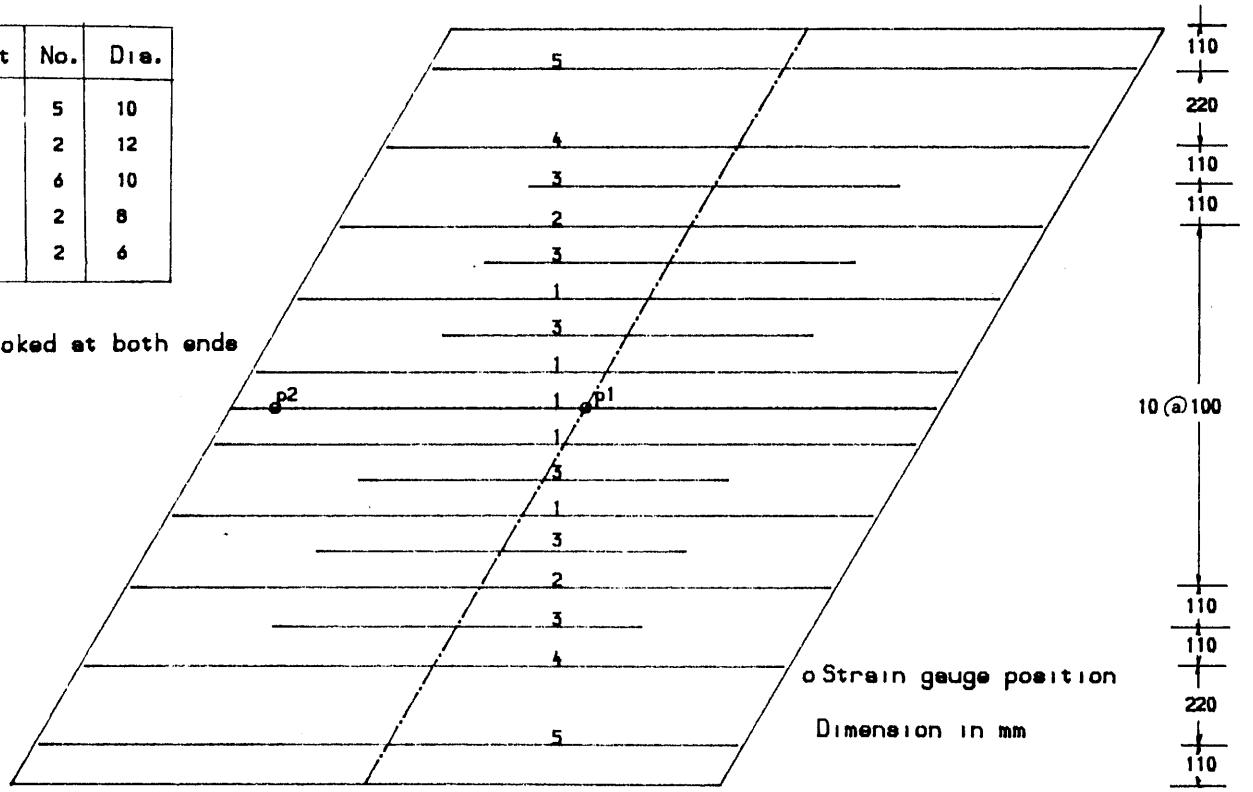

Fig. (6.8.2) MODEL SKEW SLAB NO. (2) Details of bottom transverse steel parallel to the supported edge and position of strain gauges

Mark	Lenght	No.	Dia.
1	2940	12	12
2	2240	10	12
3	1940	2	12
4	1000	2	8

All bars hooked at both ends except the welded ends.
Cover 15.0 mm

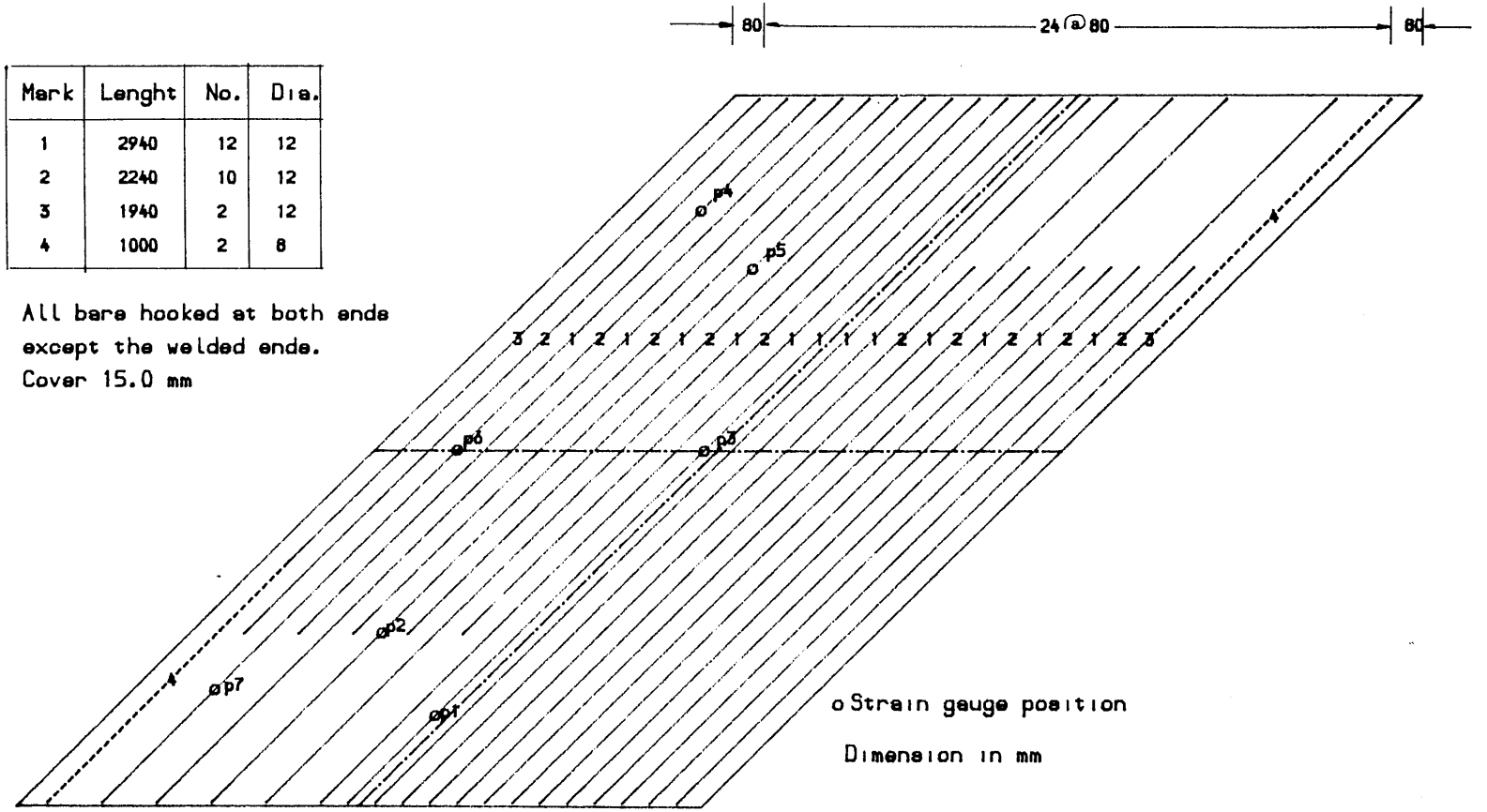

Fig. (6.9.1) MODEL SKEW SLAB NO. (3) Details of bottom longitudinal steel parallel to the free edge and position of strain gauges

Mark	Lenght	No.	Dia.
1	1970	6	10
2	905	2	12
3	1545	4	10
4	1675	6	12
5	1970	2	12

All bars hooked at both ends

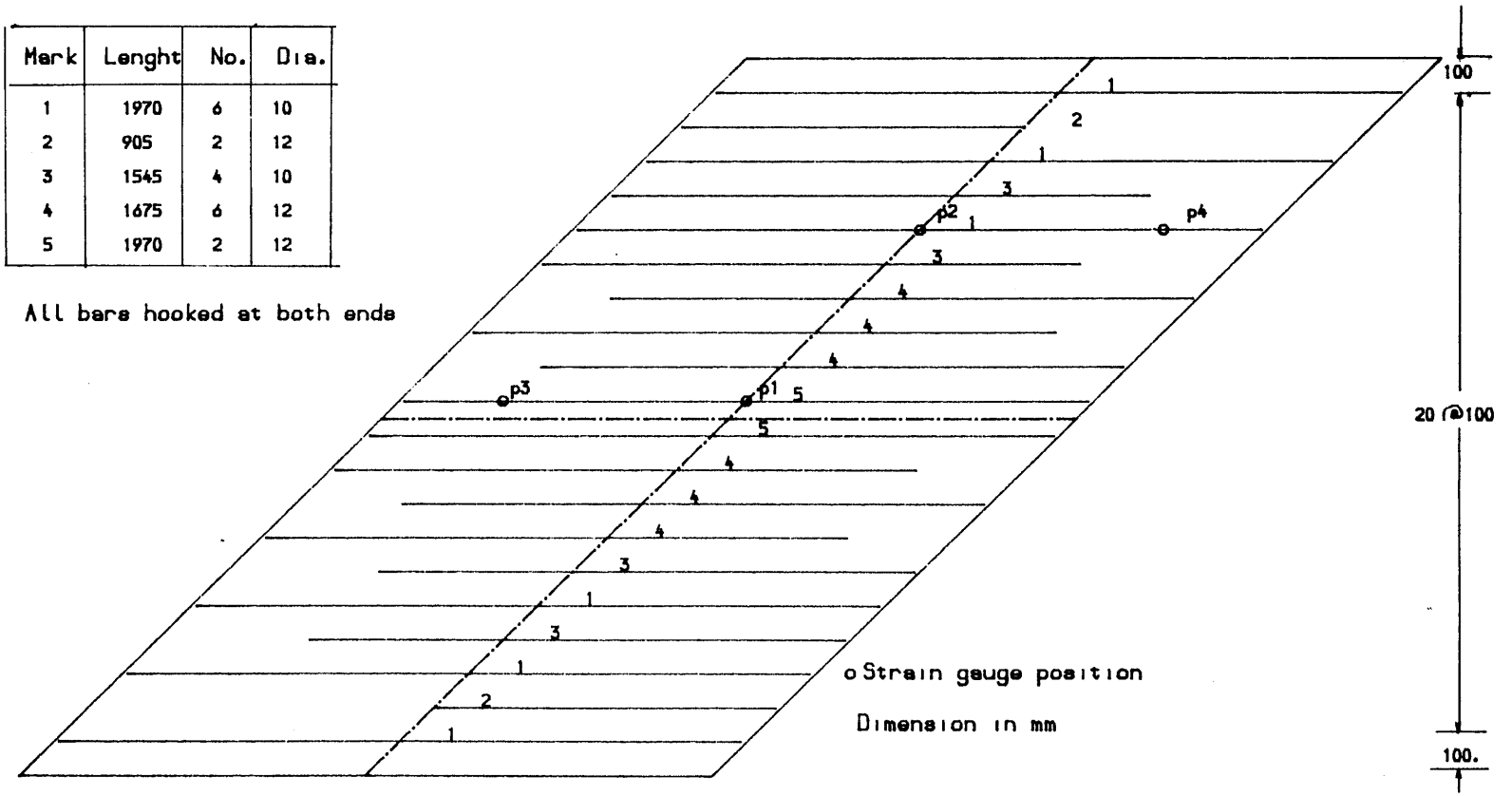

Fig. (6.9.2) MODEL SKEW SLAB NO. (3) Details of bottom transverse steel parallel to the supported edge and position of strain gauges

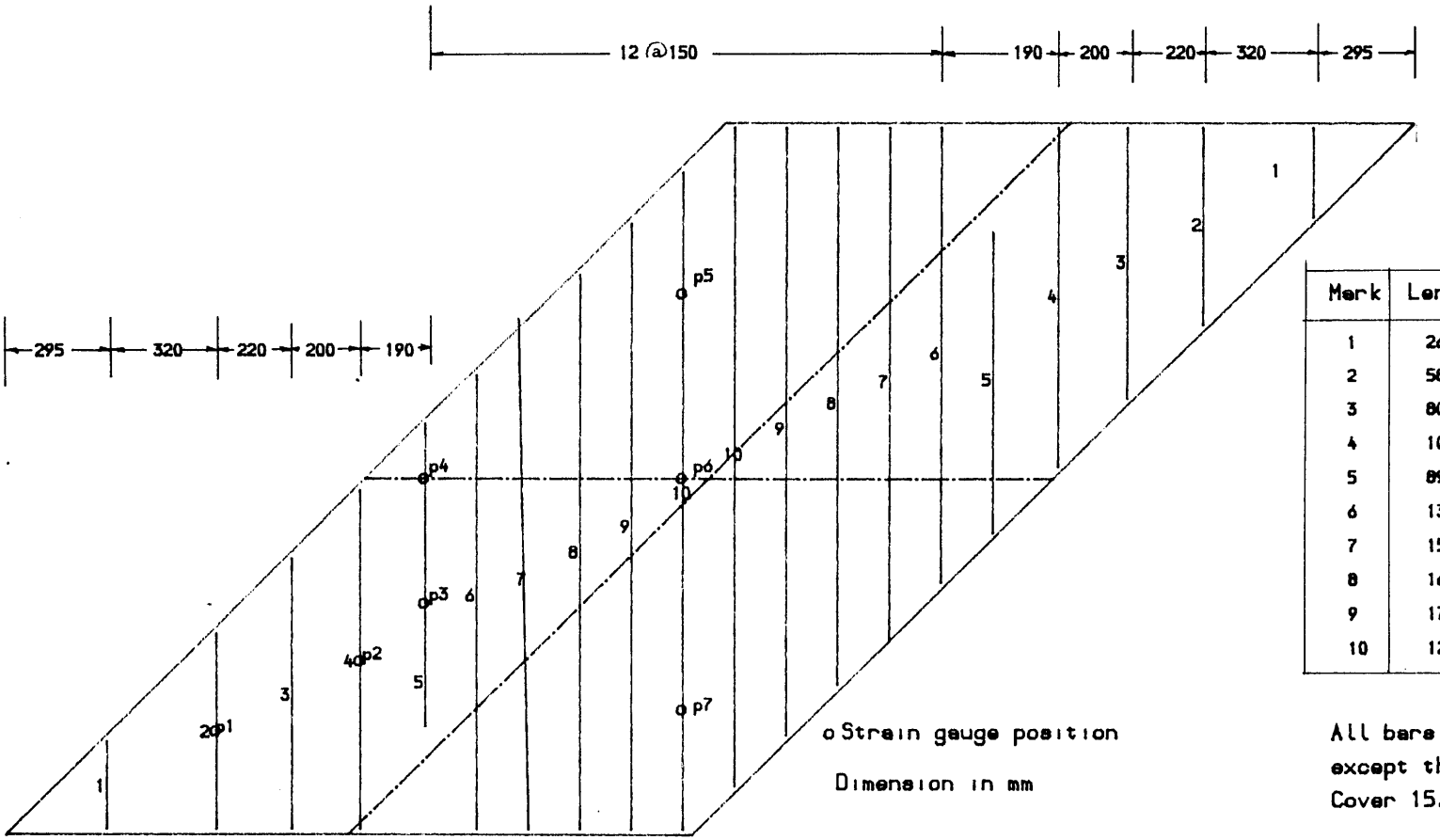

Mark	Lenght	No.	Dia.
1	260	2	6
2	580	2	6
3	800	2	6
4	1000	2	8
5	890	2	10
6	1340	2	10
7	1510	2	10
8	1640	2	10
9	1790	2	10
10	1240	2	10

All bars hooked at both ends except the welded ends.
Cover 15.0 mm

Fig. (6.10:1) MODEL SKEW SLAB NO. (4) Details of bottom longitudinal steel orthogonal to the supported edge and position of strain gauges.

Mark	Lenght	No.	Dia.
1	1970	8	6

All bars hooked at both ends

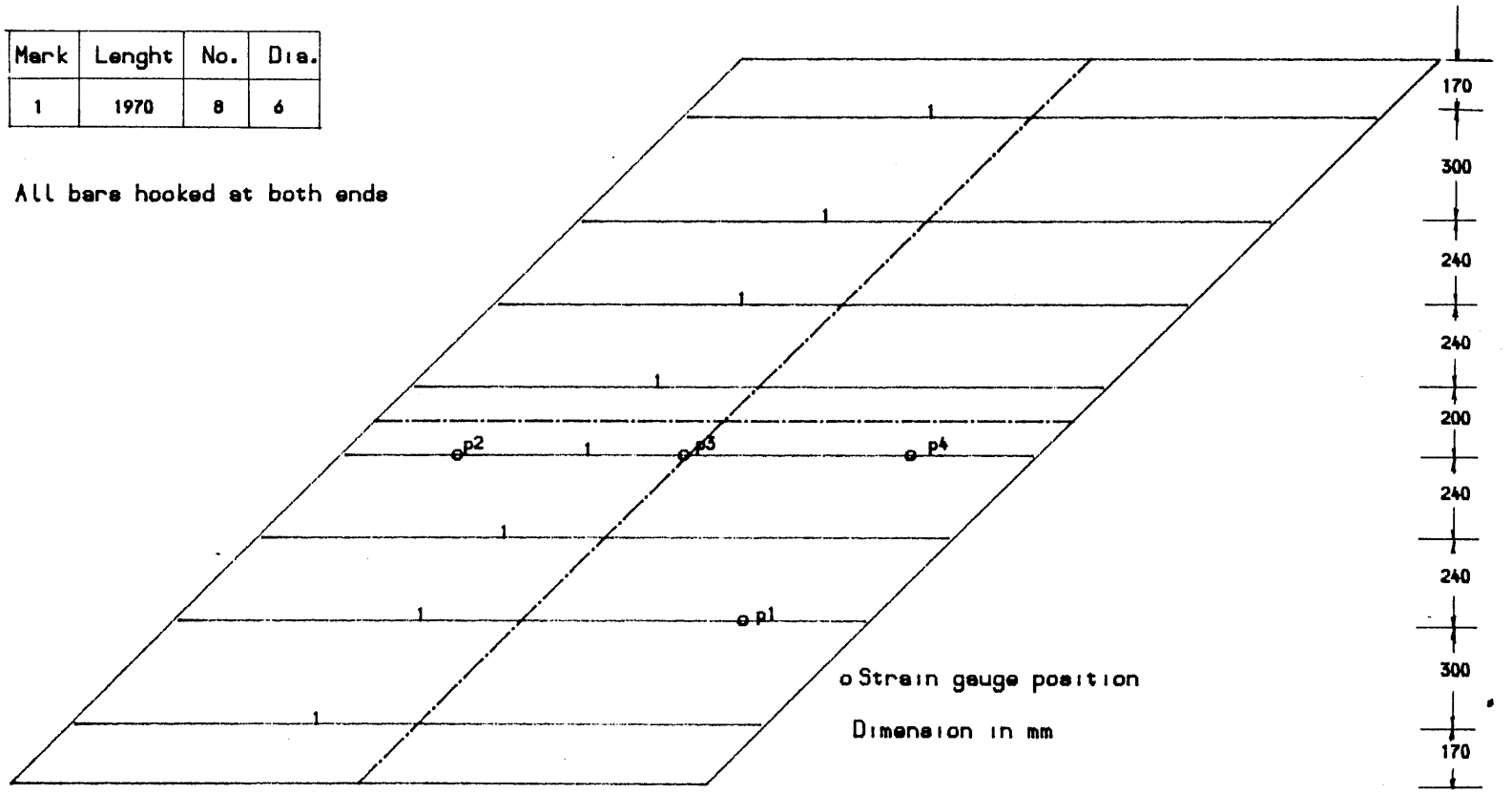

Fig. (6.10:2) MODEL SKEW SLAB NO. (4) Details of bottom and top transverse steel parallel to the supported edge and position of bottom strain gauges

Mark	Lenght	No.	Dia.
1	2940	2	12
2	1940	2	10
3	2940	5	10
4	2240	2	10
5	1840	2	10

All bars hooked at both ends
Cover 15

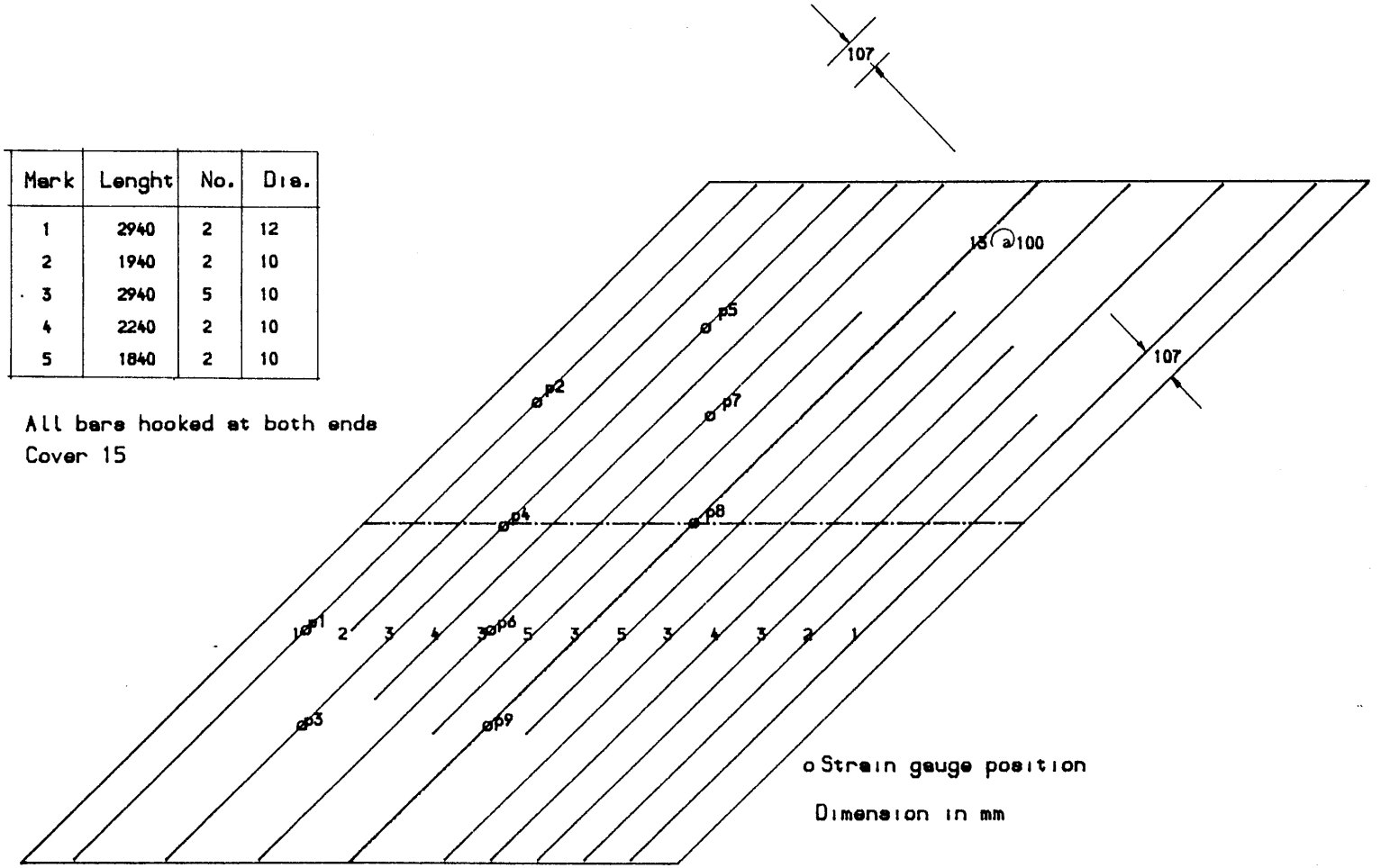

Fig. (6.11.1) MODEL SKEW SLAB NO. (5) Details of bottom longitudinal steel parallel to the free edge and position of strain gauges.

Mark	Lenght	No.	Dia.
1	2940	5	6
2	800	4	6

All bars hooked at both ends

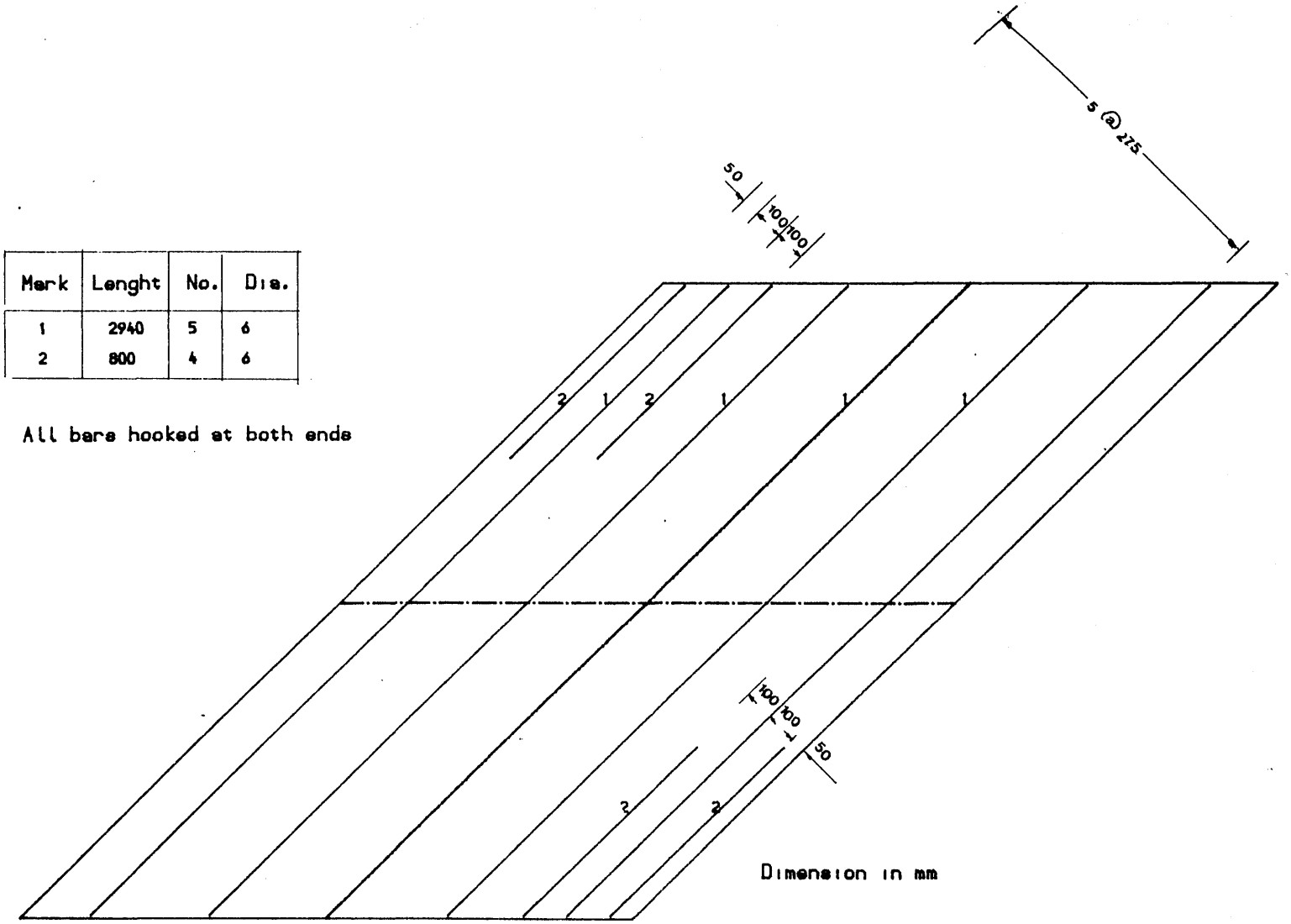

Fig. (6.11.2) MODEL SKEW SLAB NO. (5) Details of bottom longitudinal steel parallel to the free edge.

Merk	Lenght	No.	Dia.
1	340	2	8
2	590	2	8
3	790	5	8
4	990	2	8
5	1190	2	8
6	1290	2	8
7	1380	18	8

All bars hooked at both ends

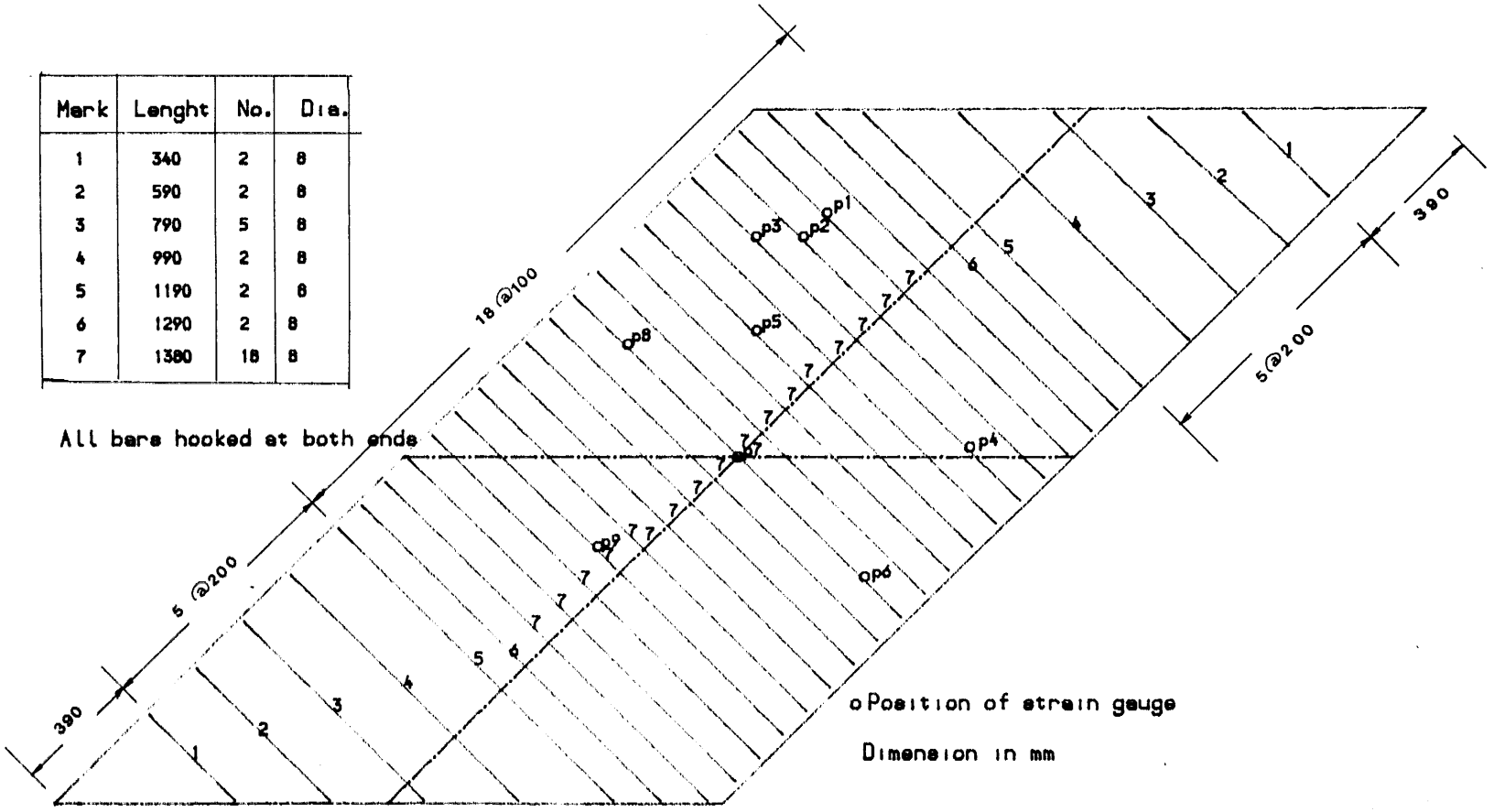

Fig. (5.11.3) MODEL SKEW SLAB NO. (5) Details of bottom transverse steel orthogonal to the free edge and position of strain gauges.

Mark	Lenght	No.	Dia.
1	960	2	6
2	1290	2	6
3	1380	5	6
4	500	4	6

All bars hooked at both ends

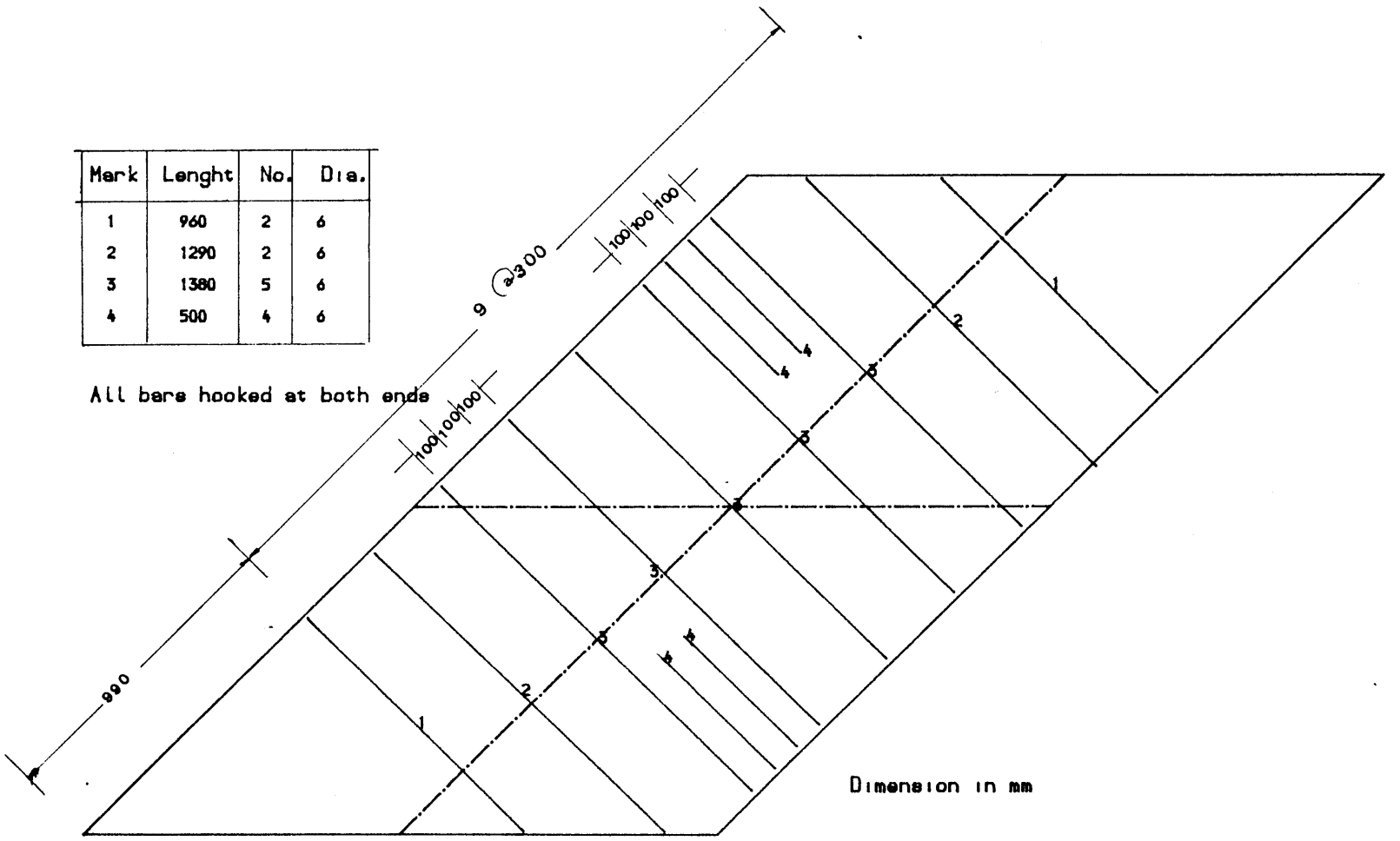

Fig. (6.11.4) MODEL SKEW SLAB NO. (5) Details of top transverse steel orthogonal to the free edge.

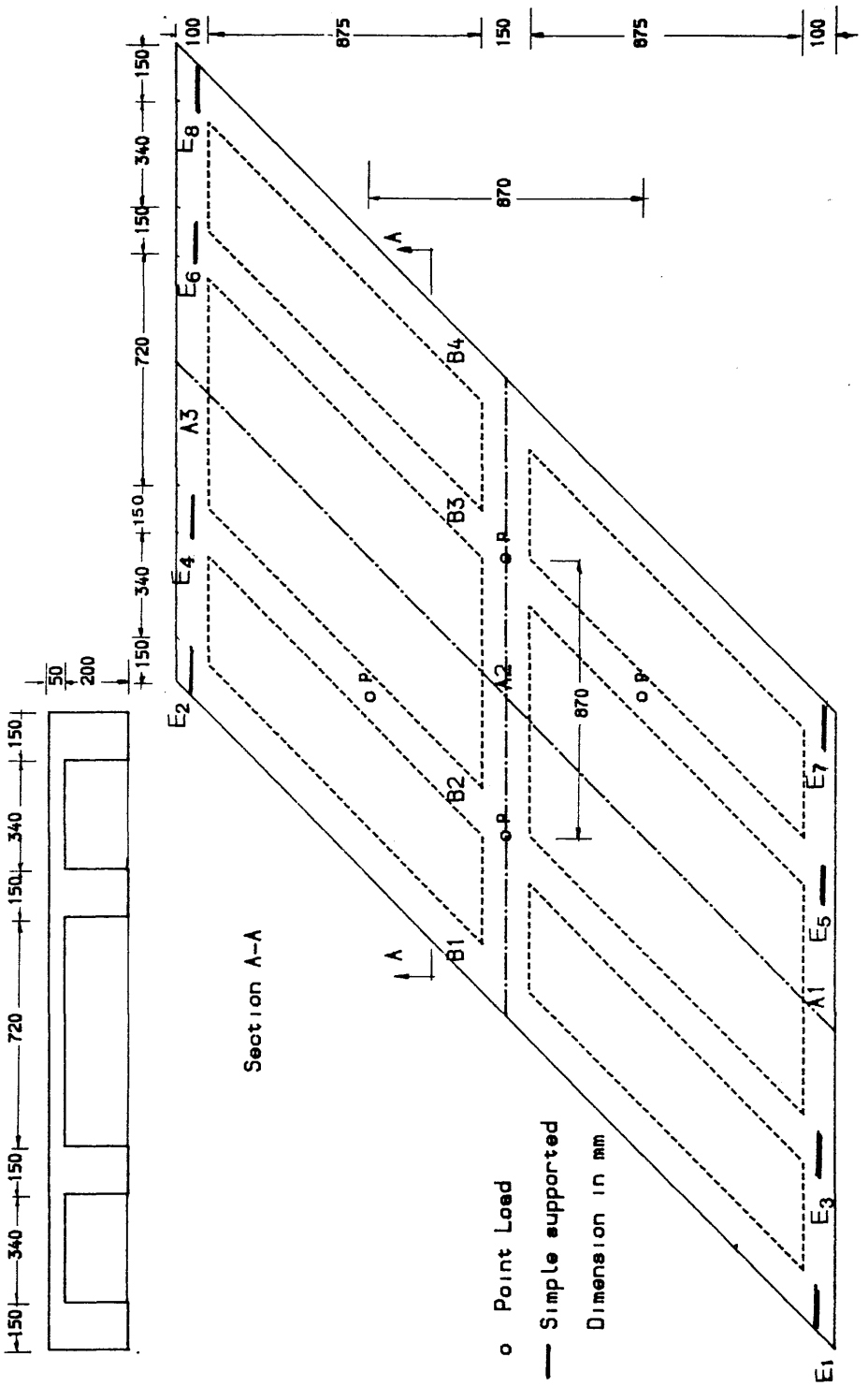

Fig. (6.12.1) Ribbed Skew Slab Model No. (6)

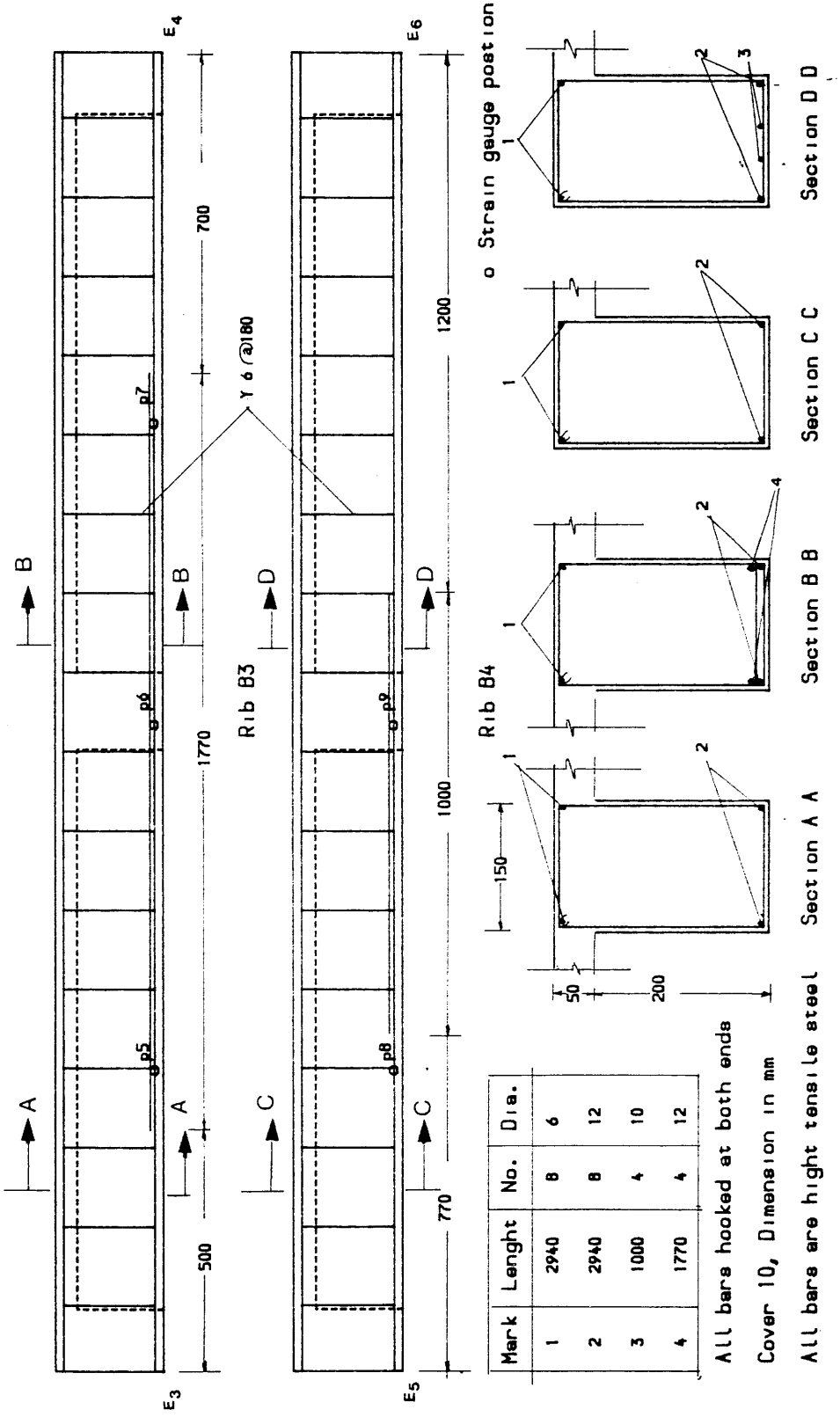

Mark	Lenght	No.	Dia.
1	2940	8	6
2	2940	8	12
3	1000	4	10
4	1770	4	12

Fig. (6.12.3) MODEL RIBBED SKEW SLAB NO. (6) Details of the steel and strain gauges position in the longitudinal ribs (B3 & B4)

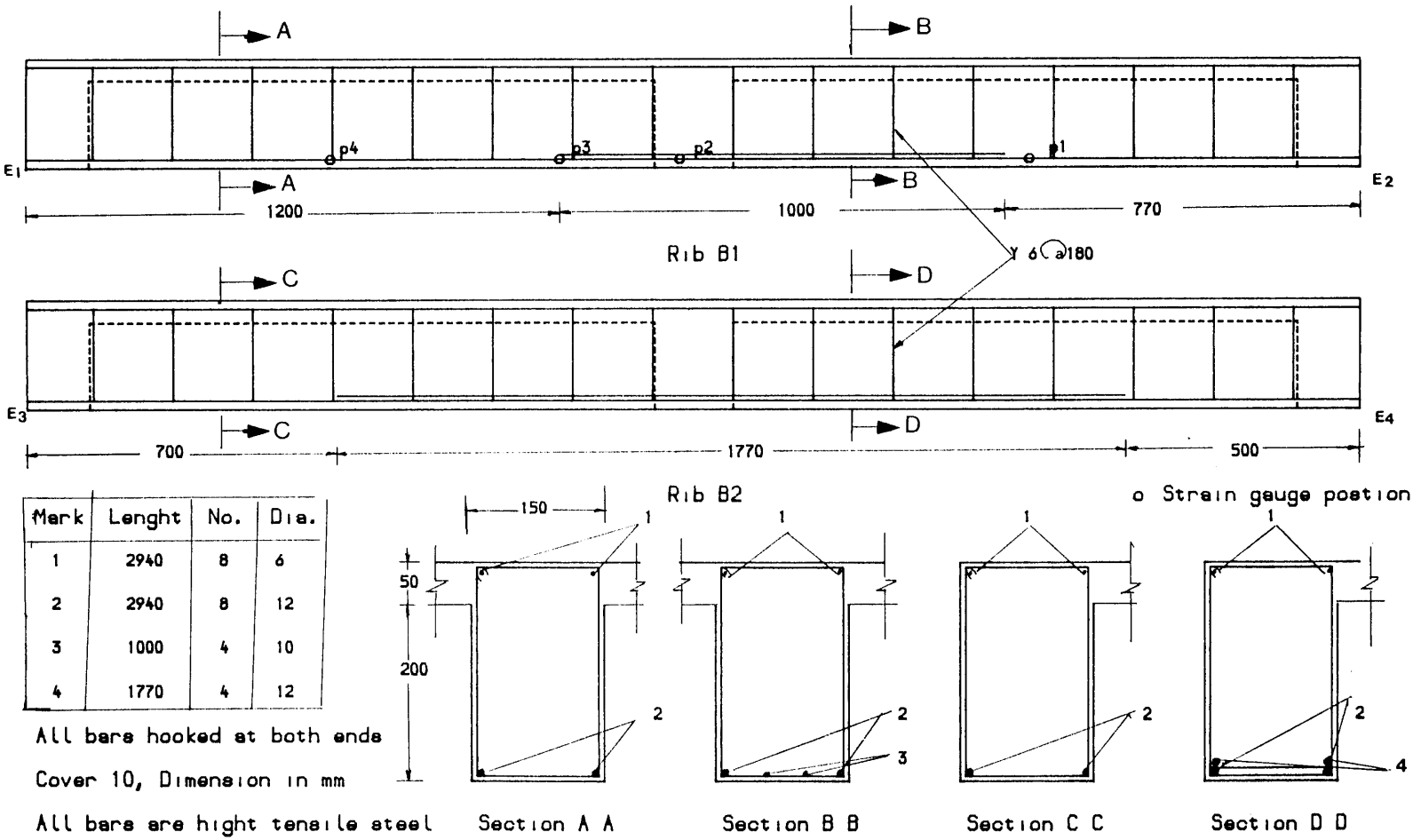

Mark	Lenght	No.	Dia.
1	2940	8	6
2	2940	8	12
3	1000	4	10
4	1770	4	12

All bars hooked at both ends

Cover 10, Dimension in mm

All bars are hight tensile steel

Fig. (6.12.2) MODEL RIBBED SKEW SLAB NO. (6) Details of the steel and strain gauges position in the longitudinal ribs (B1 & B2)

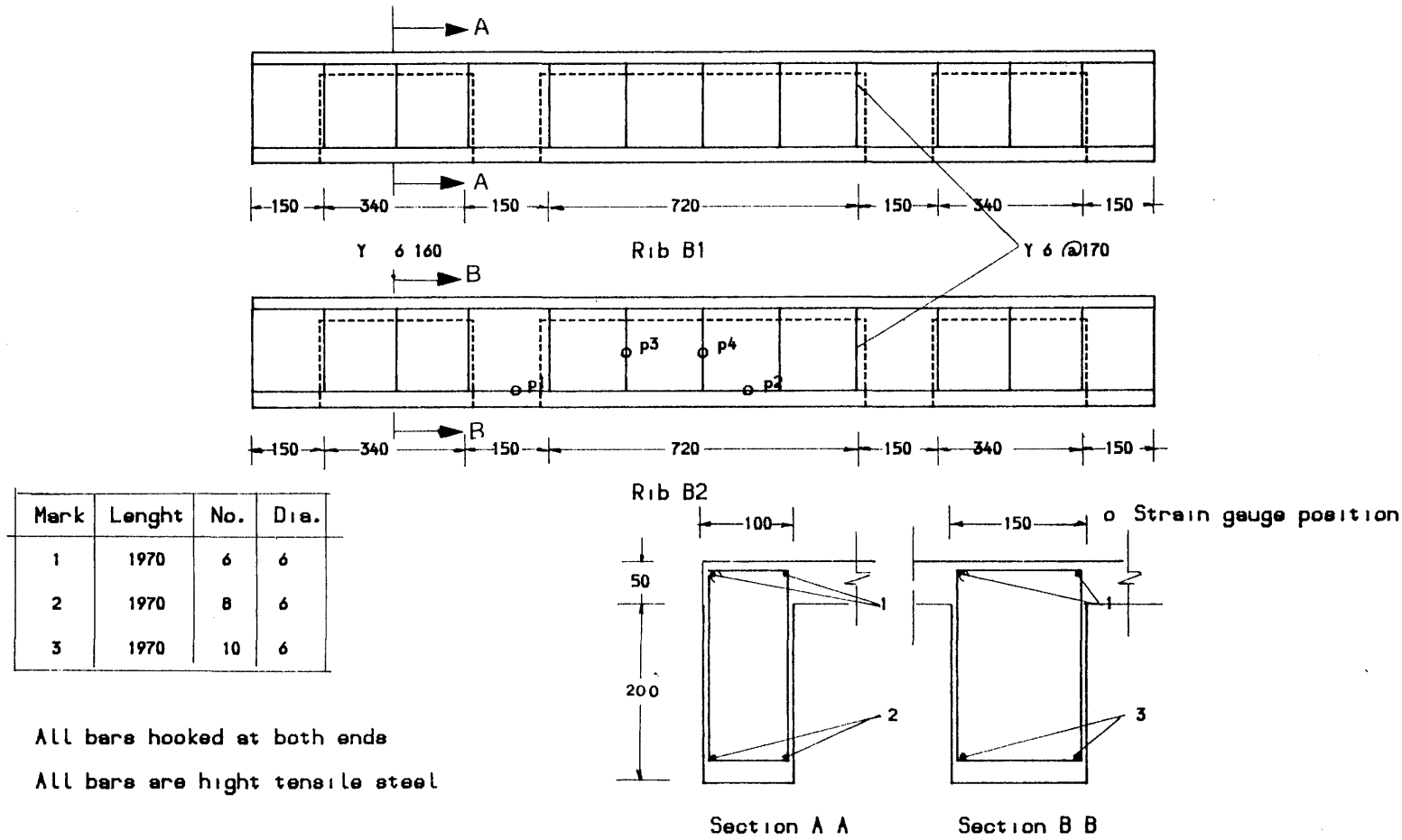

Mark	Lenght	No.	Dia.
1	1970	6	6
2	1970	8	6
3	1970	10	6

All bars hooked at both ends

All bars are hight tensile steel

Fig. (6.12.4) MODEL RIBBED SKEW SLAB NO. 6 Details of the steel and the strain gauges position in the transverse ribs (A1 & A2)

Mark	Lenght	No.	Dia.
1	2940	12	6

All bars are hight tensile steel

All bars hooked at both ends

Cover 10

Dimension in mm

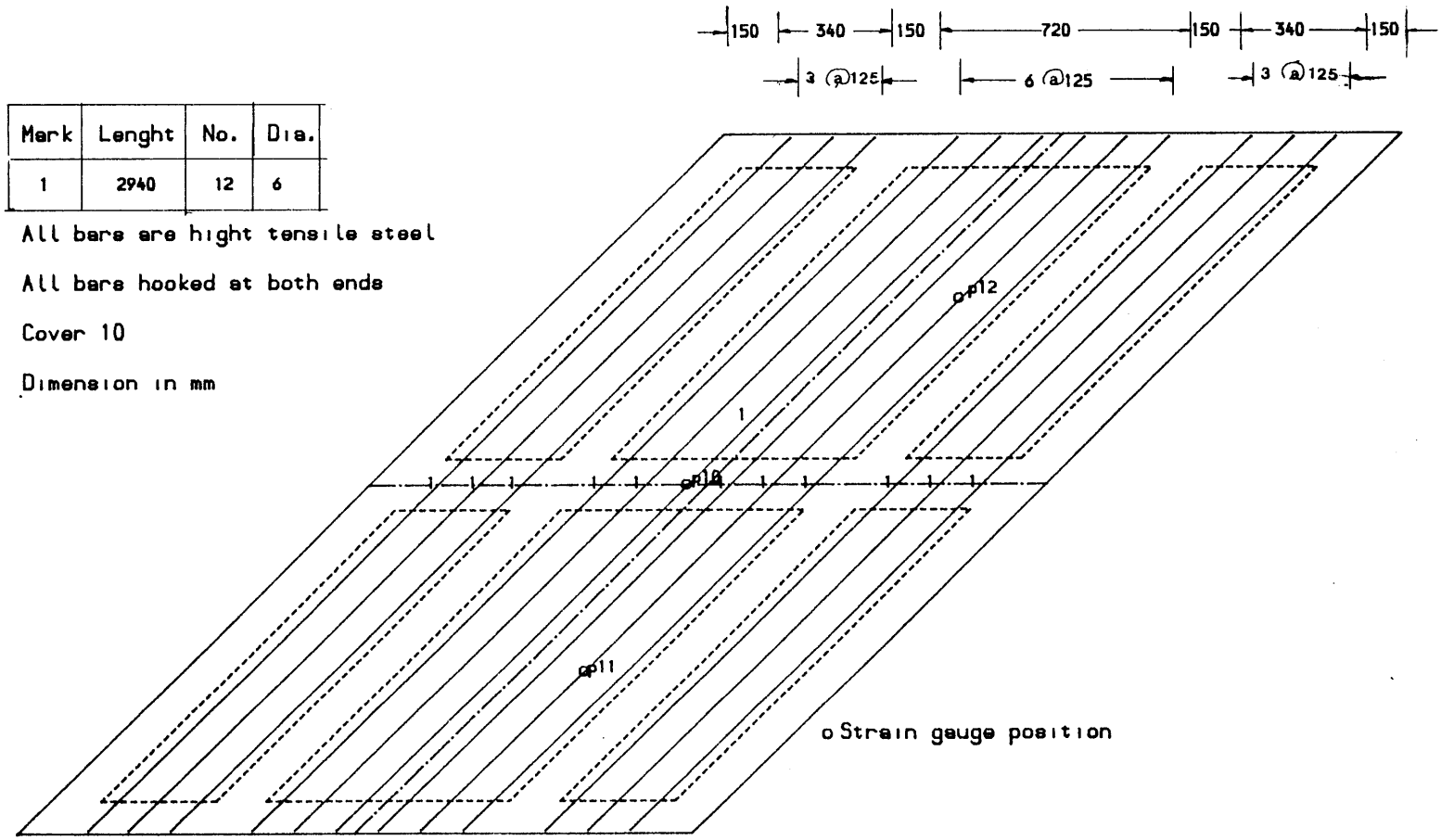

Fig. (6.12.5) MODEL RIBBED SKEW SLAB NO. (6) Details of bottom longitudinal steel and strain gauges position in the slab

Mark	Lenght	No.	Dia.
1	1970	14	6
2	1970	2	8

All bars hooked at both ends

Dimension in mm

All bars are hight tensile steel

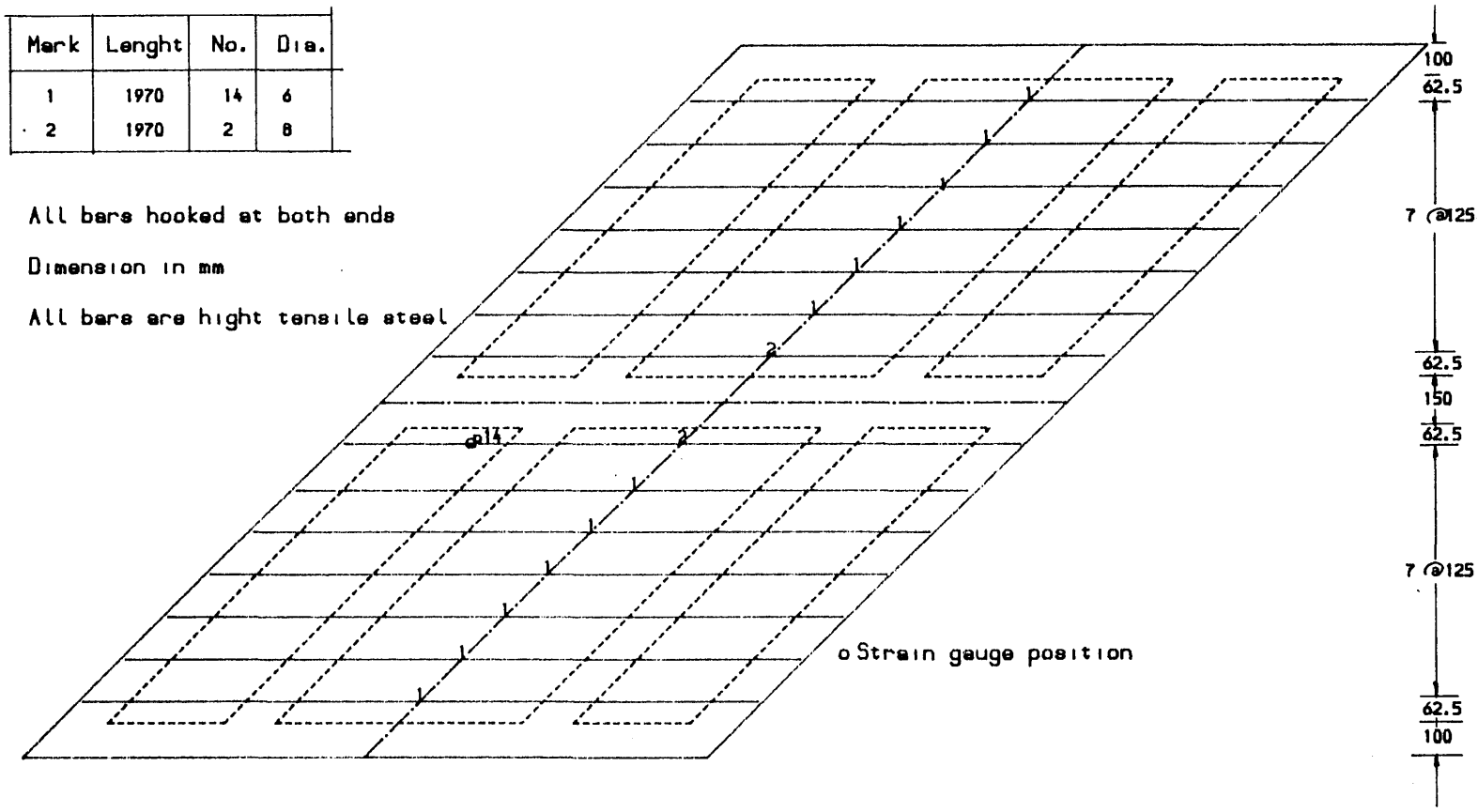

Fig. (6.12.6) MODEL RIBBED SKEW SLAB NO. (6) Details of the bottom transverse steel and strain gauges position in the slab.

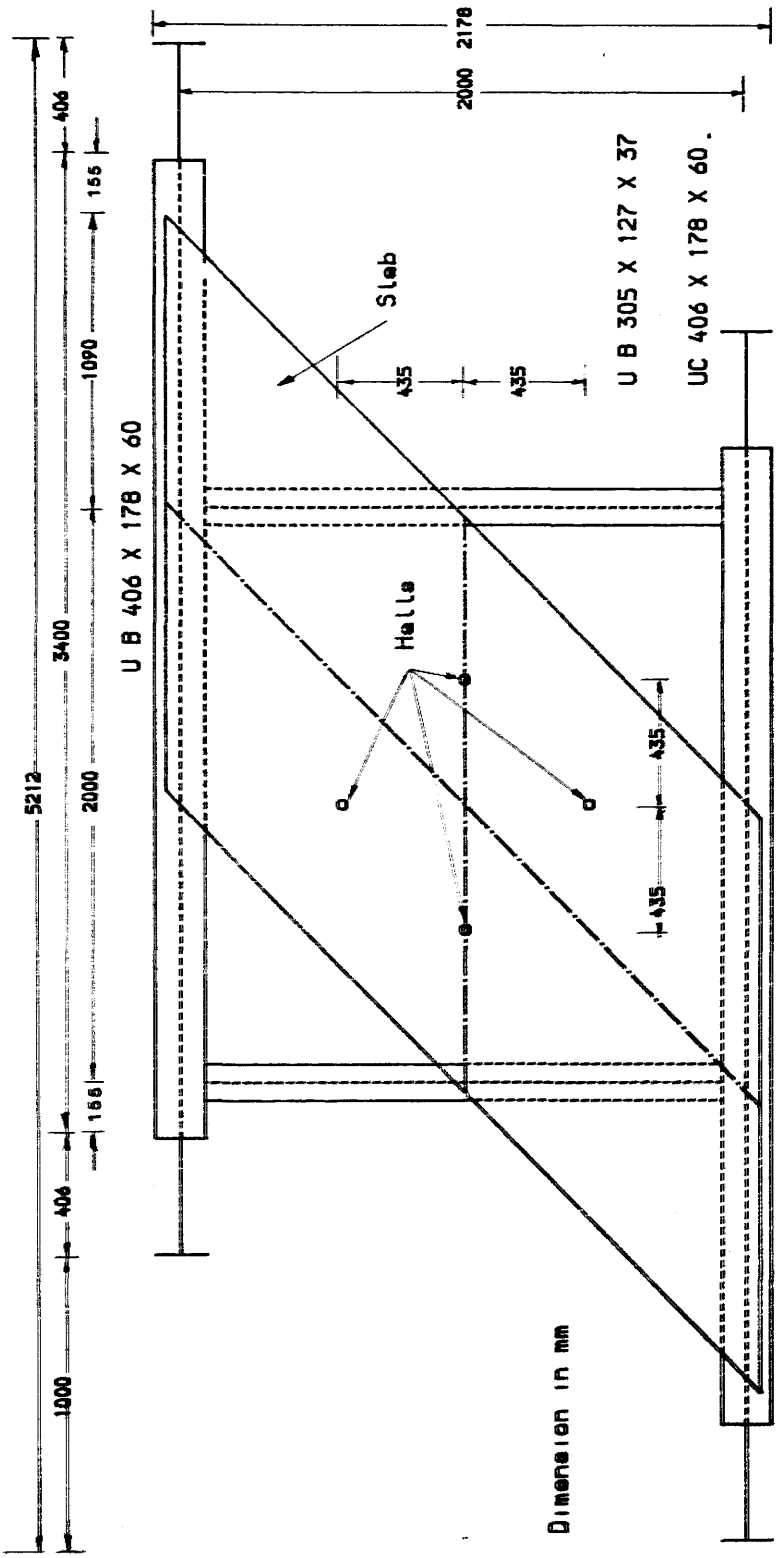

Fig. (6.13a) Loading Rig

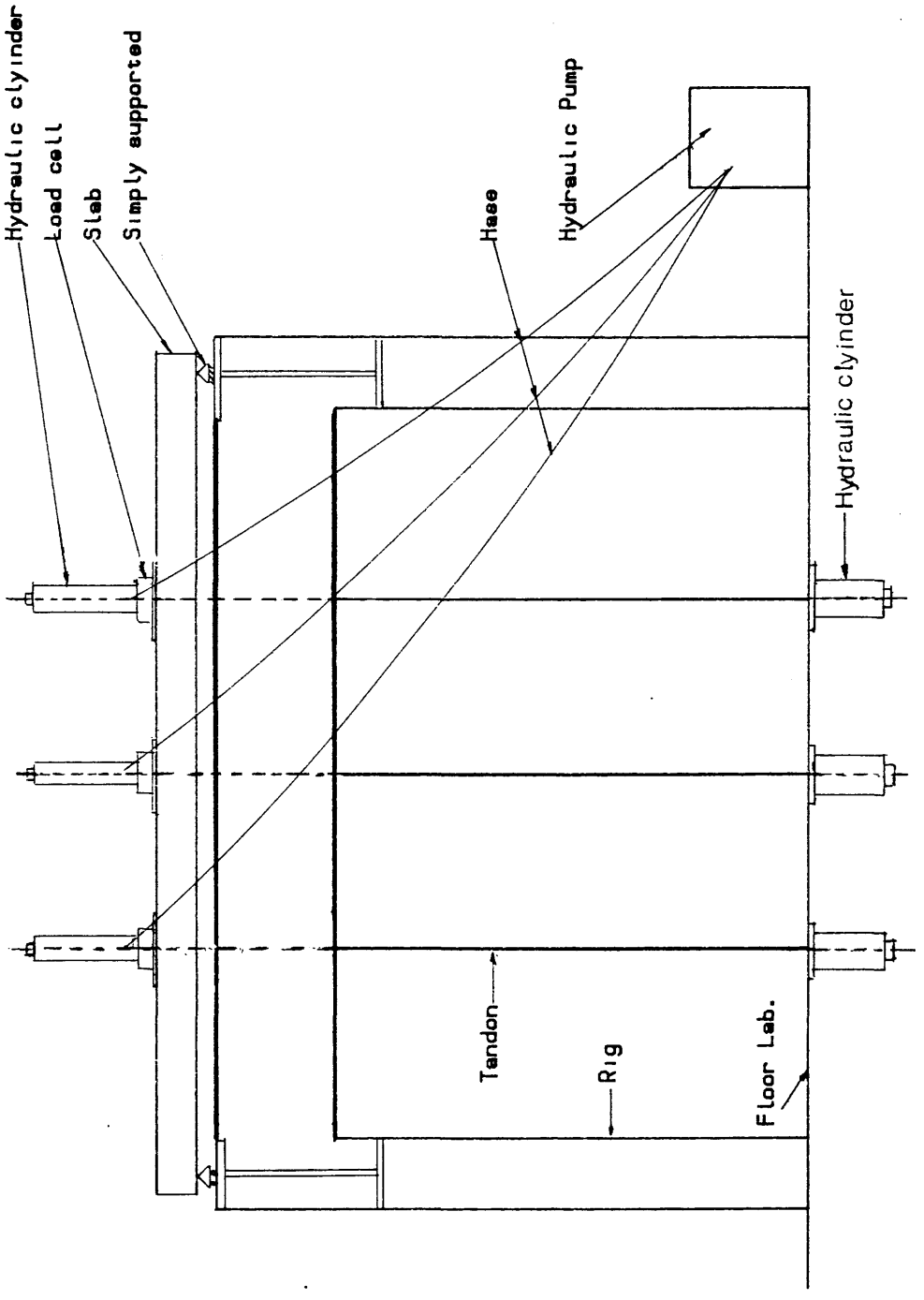

Fig. (6.13b) The Loading Rig

of 600 kN.

6.4 THE SUPPORT SYSTEM

The simple support system used for all the models consisted of two steel flats 12mm thick and 100mm wide separated by 25mm diameter steel roller Fig. (6.14.1). This support system extended over the whole length of the slab except near the acute angle corner for models 1 and 2. Since uplift forces are expected at acute corner, these acute corners were held down using a separate " corner supports " in the case of models one and two only. A load cell was used to measure the uplift force at one corner. The uplift force was found to be negligible so the acute corners were not held down for the rest of the models. The corner support with a load cell to measured the uplift force is as shown in Fig. (6.14.2). The corner support consisted of a system of orthogonal flats and rollers to provide an equivalent spherical support. A 5mm diameter high tension steel bar which passes through the load cell, through a hole in the slab corner and then through a set of orthogonal flats-rollers system was finally anchored to the loading rig. In model 6 which was a ribbed slab, the individual longitudinal beams were simply supported, as Fig. (6.14.2). Proper seating of the slab on the supports was effected by applying a thin layer of gypsum plaster between the flats and slab. Each slab had a overhang of (100 * cosec(angle of skew)mm beyond the centre line of the support.

6.5 THE LOADING SYSTEM

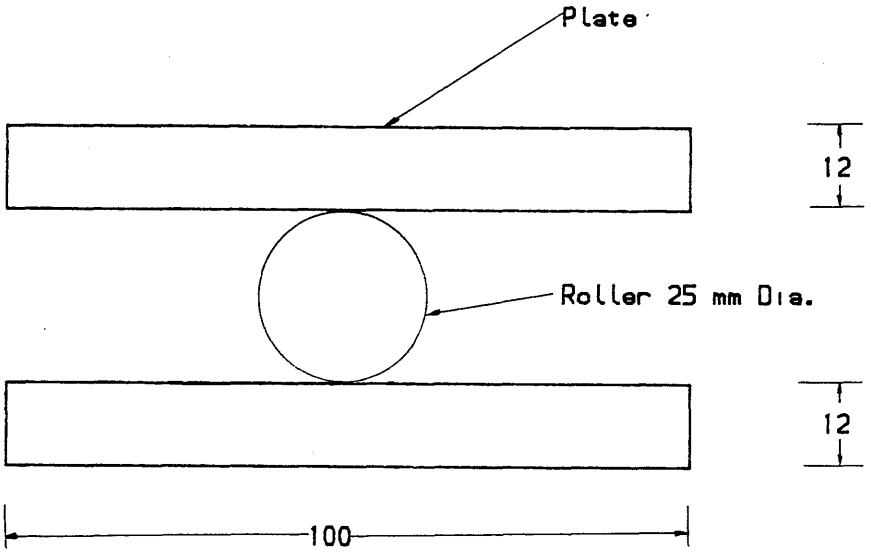

Dimension in mm

Fig. (6.14.1) The edge support system

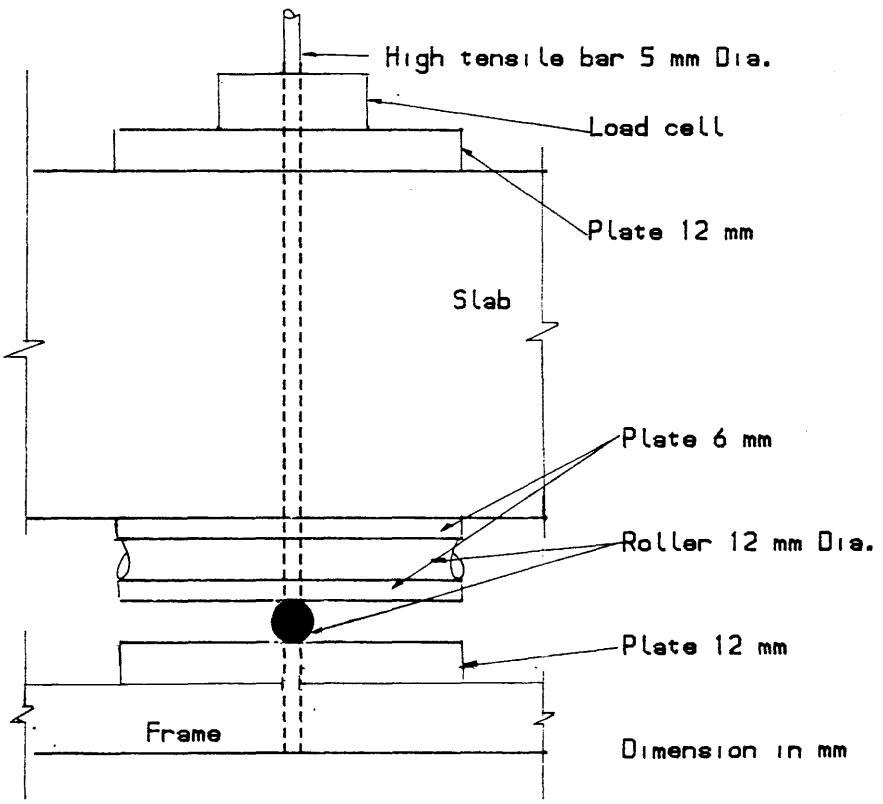

Fig. (6.14.2) The corner support system

Two different systems were used for applying concentrated loads.

6.5.1 Indirect - Point Load System

6.5.1.1 Four Points Load - Beam System: This was used for the first model only and the load was applied through a 30mm diameter high tensile rod passing through a central hole in the slab and a corresponding hole in the floor of the laboratory. The rod transmits equal load to the slab at four points by a system of simply supported spreader beams as shown in Fig. (6.15A). The total applied load was measured at one point by 50-ton load cell and the actual load at each point was measured by combination of 10-ton and 5-ton load cells. The loading rod is tensioned by a 60 ton hydraulic jack reacting against the bottom surface of the strong floor of the laboratory. The jack was operated by a hand pump.

6.6.1.2 Two Points Load - Beam System: This was used for the second model only. This system is similar to the four point load-beam system except that the rod transmits load equally to slab at two points 1000mm apart as shown in figure (6.14B).

6.5.2 Direct Load System

6.5.2.1 Four - Points Load System: This was used for the rest of models three to six. In this case four prestressing cables symmetrically placed about the model centre line were passed through four holes in the slab, as shown in Fig. (6.13b) and Fig. (6.15c). The cables were anchored on the top surface of the model and a spreader plate 200x200x10 mm was used to distribute the load at each

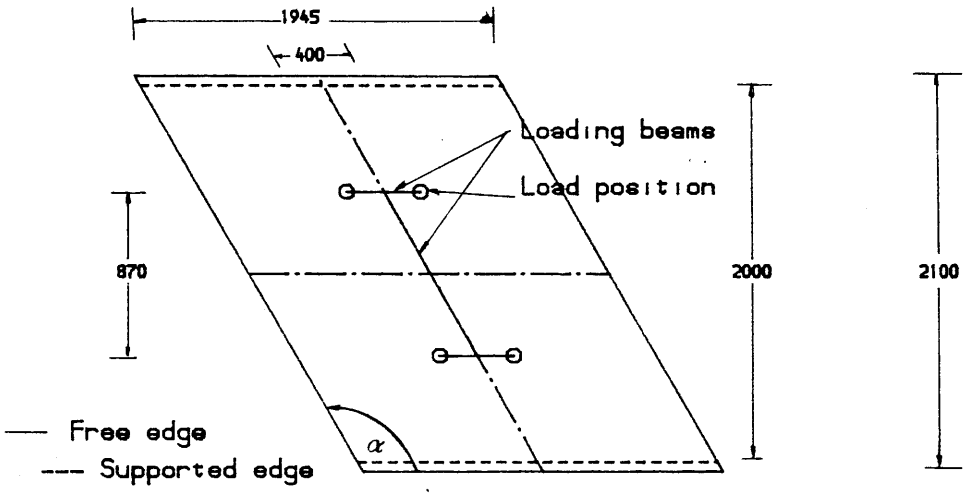

(a) Indirect four points beam system

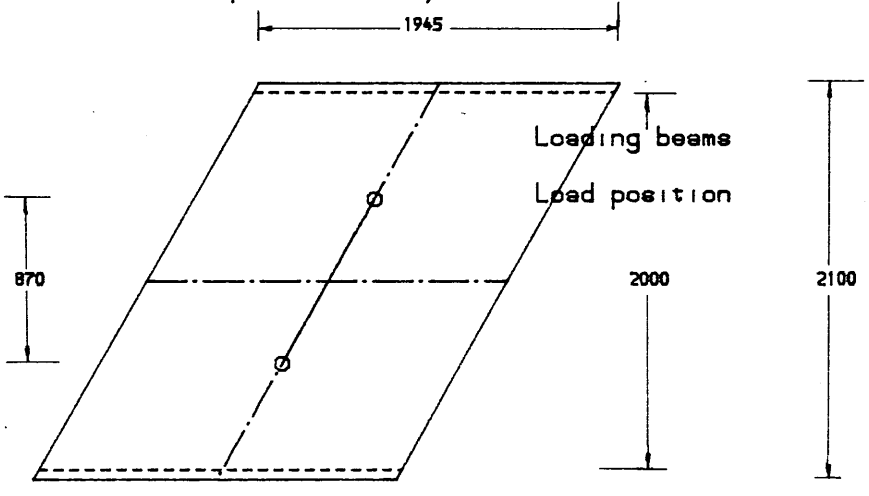

(b) Indirect two points beam system

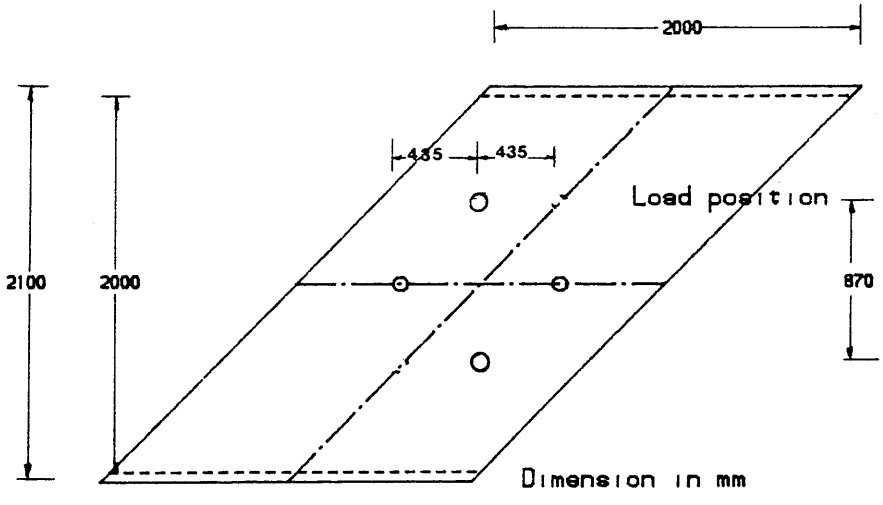

(c) Direct four points

Fig. (6.15) The loading system

point. Each loading cable is tensioned by two 20 ton - hydraulic jack at each end of the cable. One of the jacks rested against the bottom surface of the floor of the laboratory and the another on the top surface of the slab. The bottom jacks were connected by hoses to a regulating electric pump capable of sustaining a maximum of 1000 psi oil pressure. The four hoses were connected to the pump at one point using a distributor. This arrangement would ensure equal pressure distribution in the four jacks. However due to the varying frictional effects in the jack, the load was not equally distributed. and the top surface jacks which were connected to individual hand pumps, were used to adjust the load applied at each point. The load at the slab surface was measured by using a mix of 10 ton and 5 ton load cells. The load cells, measure to a minimum of 10 N with an accuracy of 0.25% of the total the applied load.

6.6 MATERIAL

6.6.1 Concrete: The concrete mix consisted of ordinary portland cement, Hynford sand (max. size of uncrushed gravel was 10mm and grading was in zone (2)). The mix proportions by weight were 1 : 1.5 : 2.6 (i.e cement : sand : gravel) with a water/cement ratio 0.48. For each model, control specimens included 6- 100mm cubes and 4- 150X300 mm cylinders. The compressive strength was measured by standard cube test and the tensile strength was measured by cylinder splitting tests according to British standard NO. BS 1881. 1970.

Typical stress-strain curve of concrete in

compression is shown in Fig. (6.16). Details of material properties are presented with the test results in Chapter Seven.

6.6.2 Reinforcement: 6mm, 8mm, 10mm and 12mm diameter high yield deformed bars were used for all the models. Three samples for each diameter of bar were tested in an OLSEN testing machine fitted with a S-type electronic extensometer. The testing procedure followed the manufacture's instruction manual. The yield stress of the bar was taken as the stress at which a line starting from 0.2% strain and parallel to the initial slope of the curve intersects with the curve stress-strain. The yield strain was assumed to be that given by treating the material as an elastic-perfectly plastic material as shown in Fig. (6.17). Typical stress-strain curves are presented in Fig. (6.18.1) to Fig. (6.18.4).

6.7 CASTING AND CURING

The formwork needed for fabrication was made from 18mm thick plywood sheet. All formwork was oiled for easy removal. Reinforcement cage was properly positioned in the formwork such that 15mm concrete cover is maintained. Because of small size of the laboratory mixer, 12-14 mixer loads were required to cast each slab and the standard control specimens. The concrete was placed in the shuttering and compacted by a poker vibrator. The cubes and cylinders were compacted by a vibrating table. The concrete was cured for three days under wet sacks. Formwork was removed after seven days and the slab and control specimens

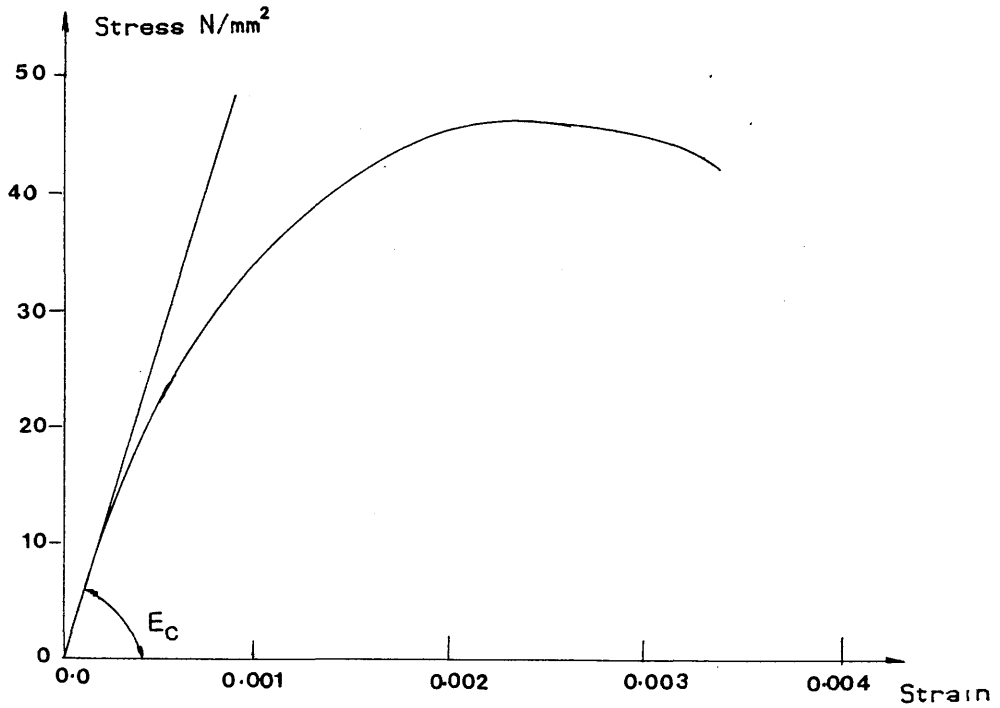

Fig. (6.16) Typical stress-strain curve for concrete

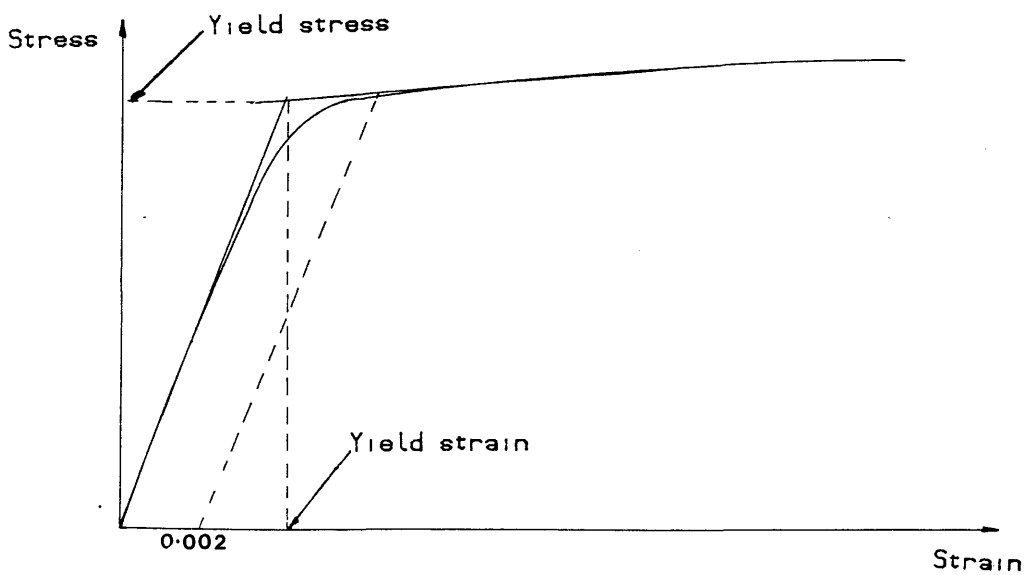

Fig. (6.17) Definitions of yield stress and strain for steel reinforcement

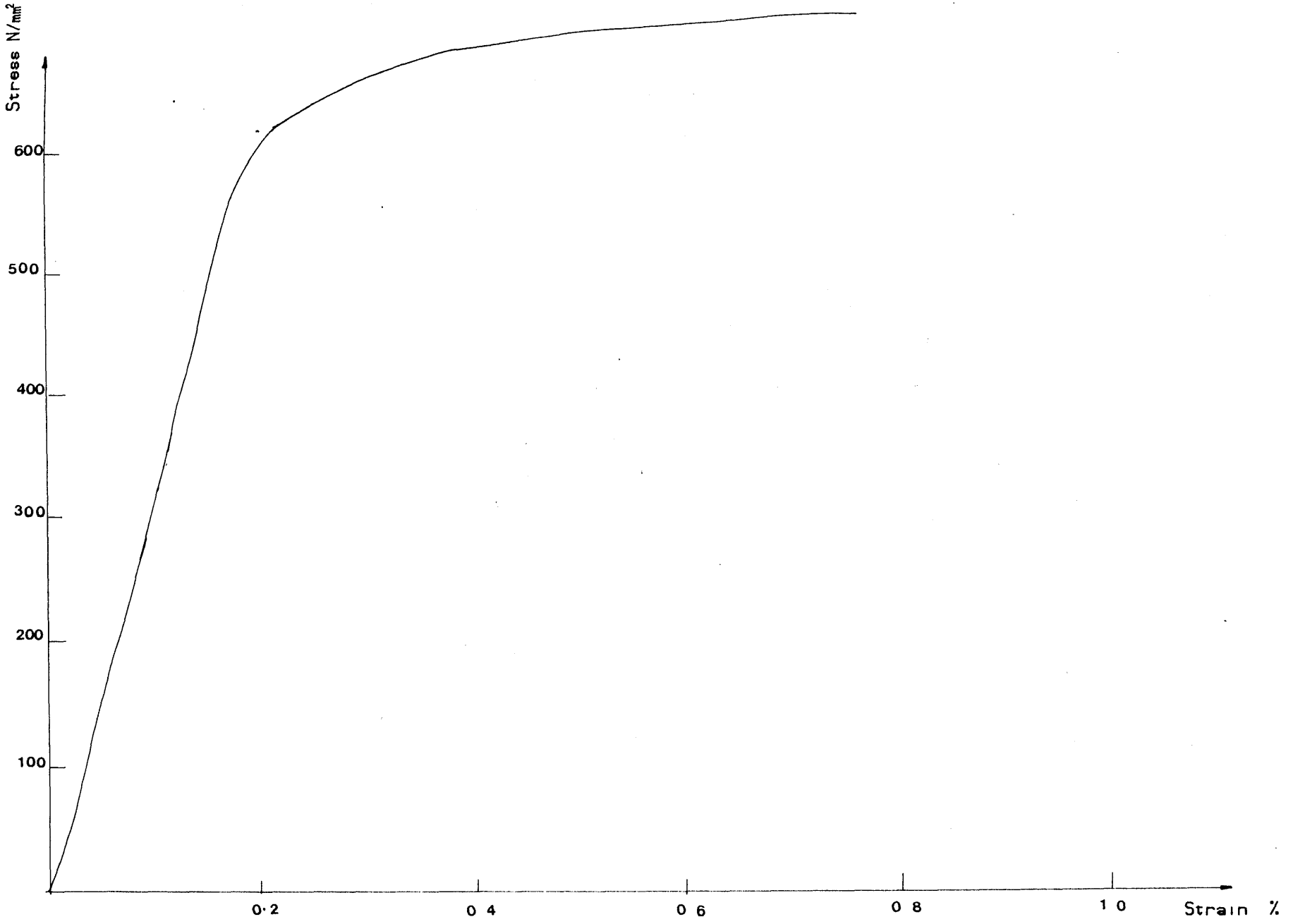

Fig. (6.18.1) Typical stress-strain curve for a bar of 6 mm diameter

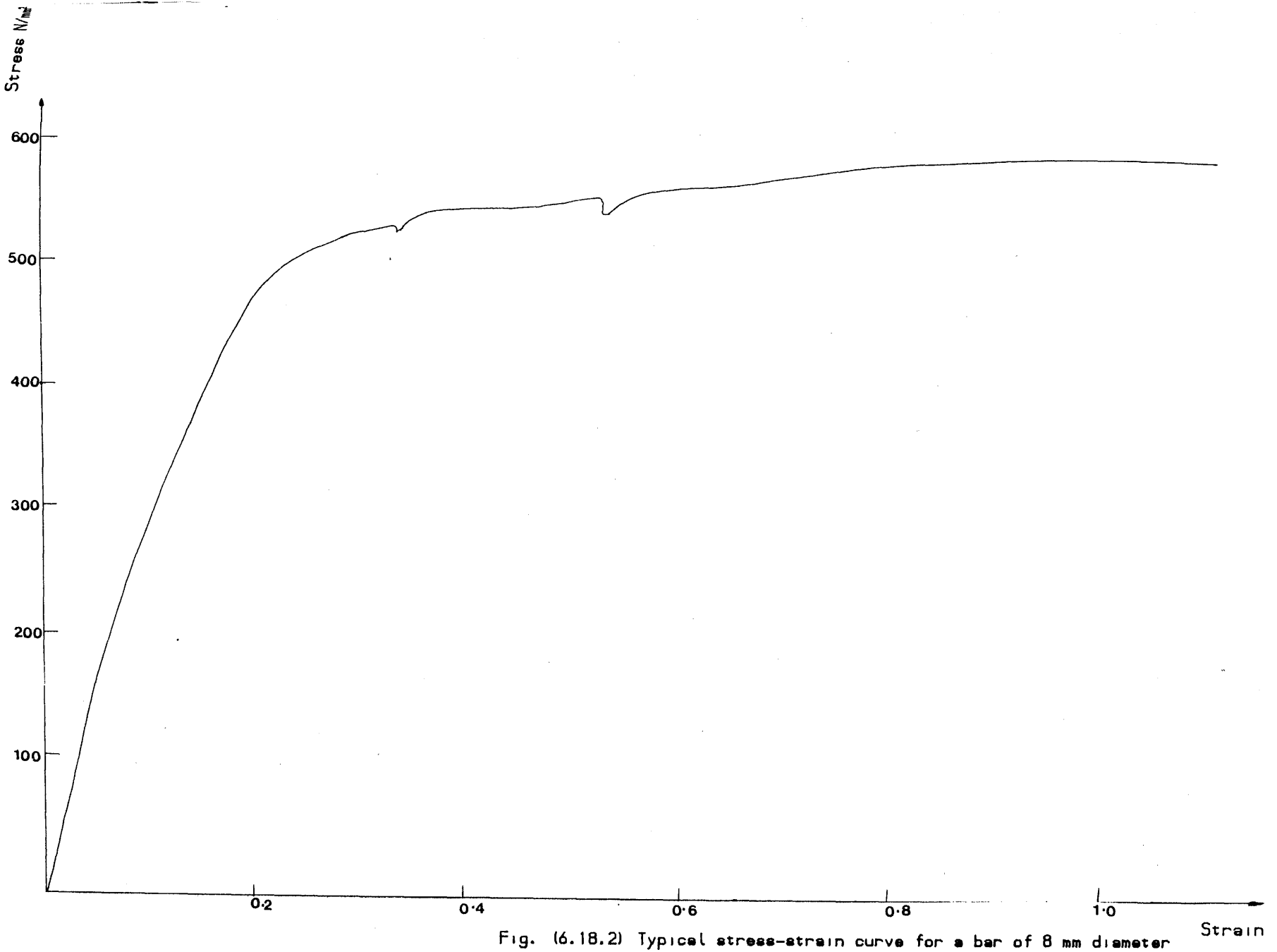

Fig. (6.18.2) Typical stress-strain curve for a bar of 8 mm diameter

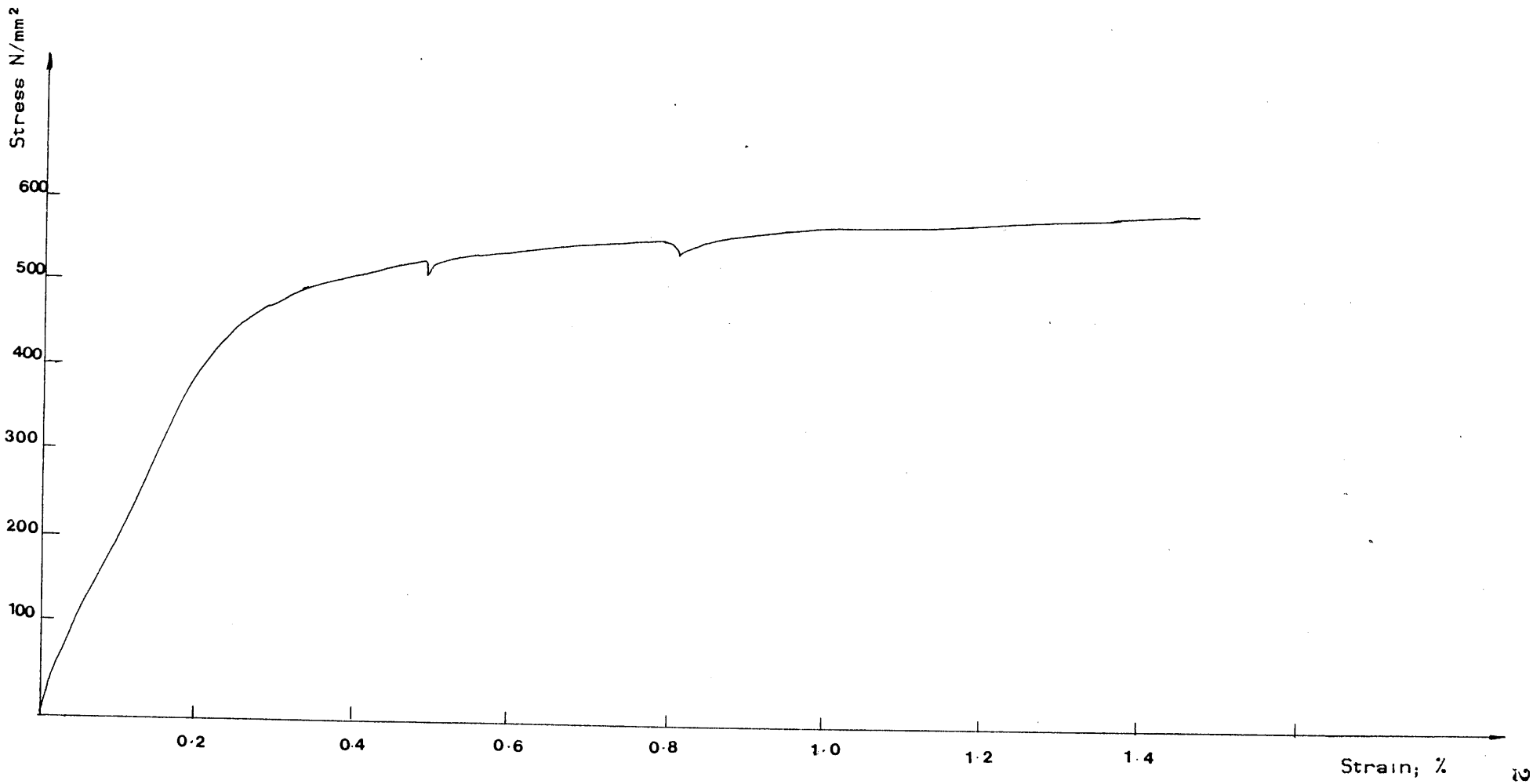

Fig. (6.18.3) Typical stress-strain curve for a bar of 10 mm diameter

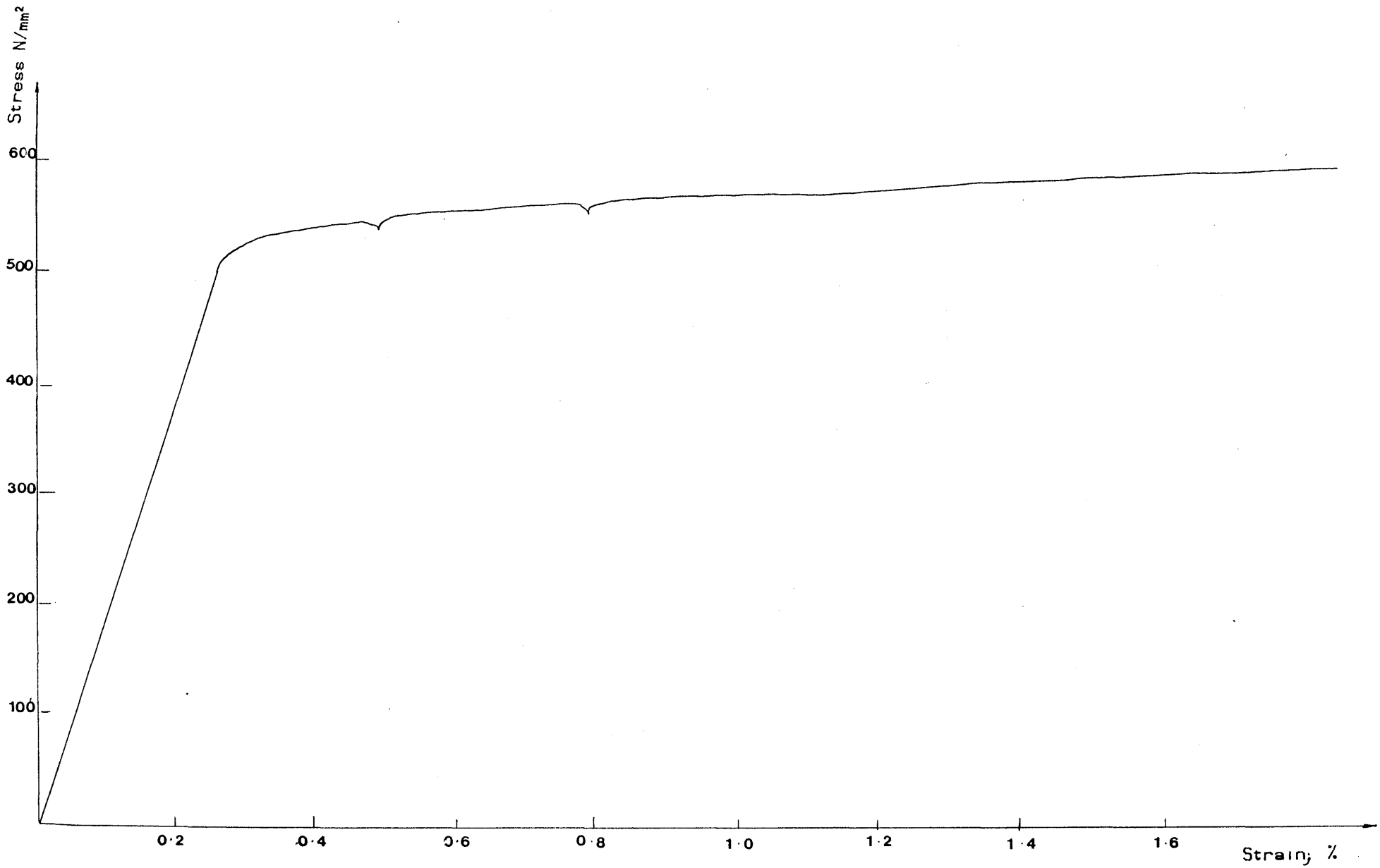

Fig. (6.18.4) Typical stress-strain curve for a bar of 12 mm diameter

were left to 'cure' in the laboratory. In general, slabs were tested 4 week after casting except model five which was tested three weeks after casting because rapid hardening cement had been used for that model.

6.8 INSTRUMENTATION

6.8.1 Deflection

Deflections were measured by means of electrical displacement transducers at the top surface and dial gauges at the bottom surface so as to have a cross check on the transducers. The transducers were used in conjunction with an automatic data storing and processing system. Fig. (6.19.1) to Fig. (6.19.6) shows the transducers locations on the top surface of the models.

6.8.2 Strains

6.8.2.1 Steel Strain: Strain in steel was measured by 6mm gauge electrical resistance strain gauges. The location of strain gauges was chosen at maximum stress positions. Two strain gauges were fixed on diametrically opposite faces of the bar and the average value of two gauges at each position was used to calculate the axial strain in the bar. Fig. (6.7.1) to Fig. (6.12.5) shows the strain gauge locations on the steel bars of the models.

For fixing strain gauges on steel, the bar surface at the required location was filed and smoothened with emery paper. The surface was then treated with M-prep conditioner A and M-prep neutraliser 5 to remove dirt and grease (74).

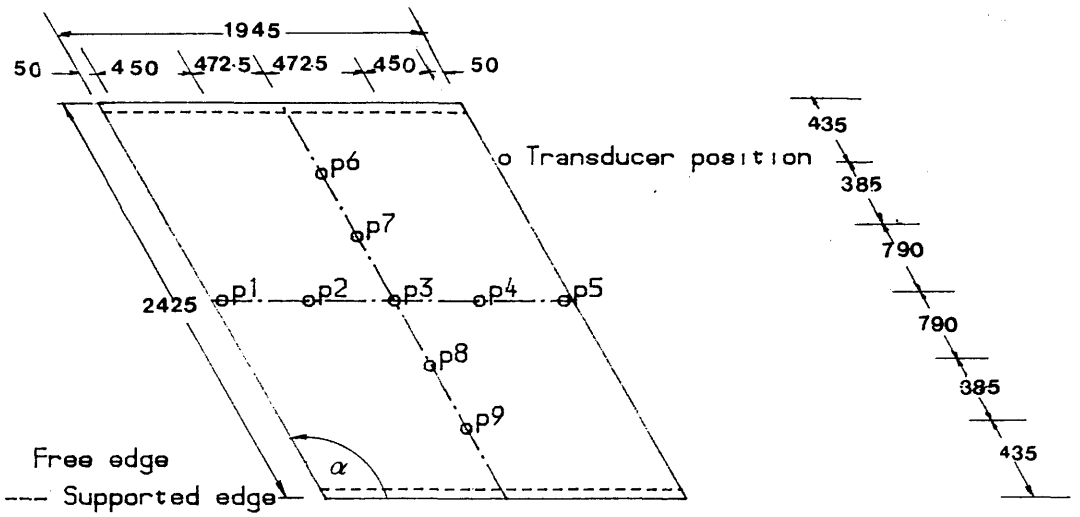

Fig. (6.19.1) MODEL SKEW SLAB NO. (1) Location of transducers on upper surface

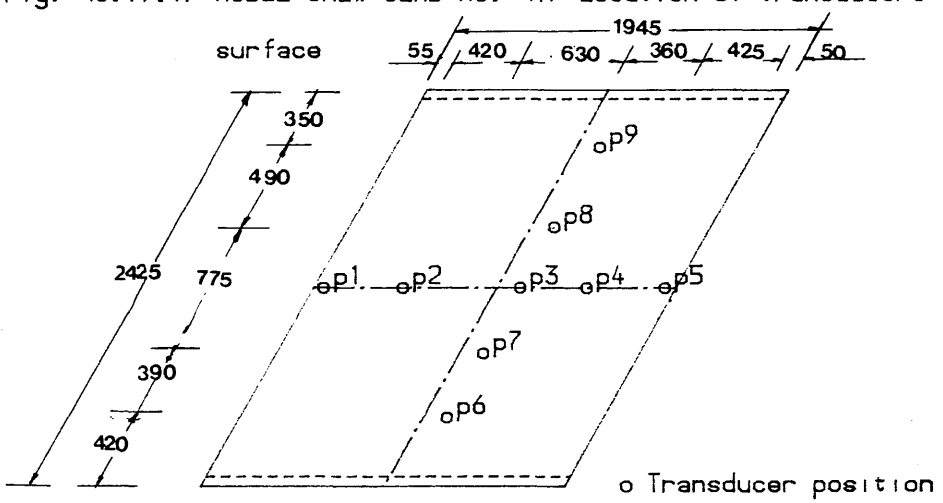

Fig. (6.19.2) MODEL SKEW SLAB NO. (2) Location of transducers on upper surface

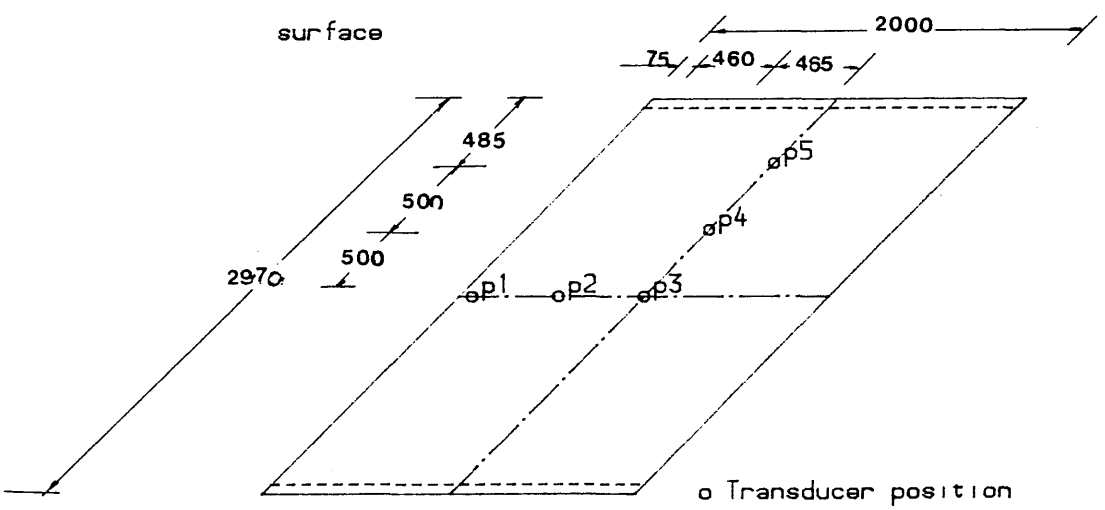

Fig. (6.19.3) MODEL SKEW SLAB NO. (3) Location of transducers on upper surface

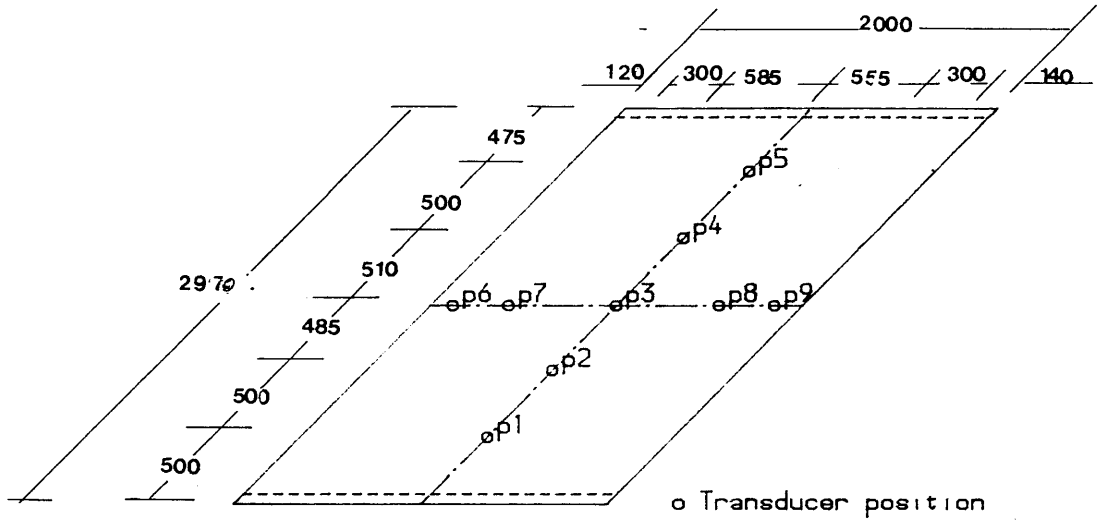

Fig. (6.19.4) MODEL SKEW SLAB NO. (4) Location of transducers on upper surface

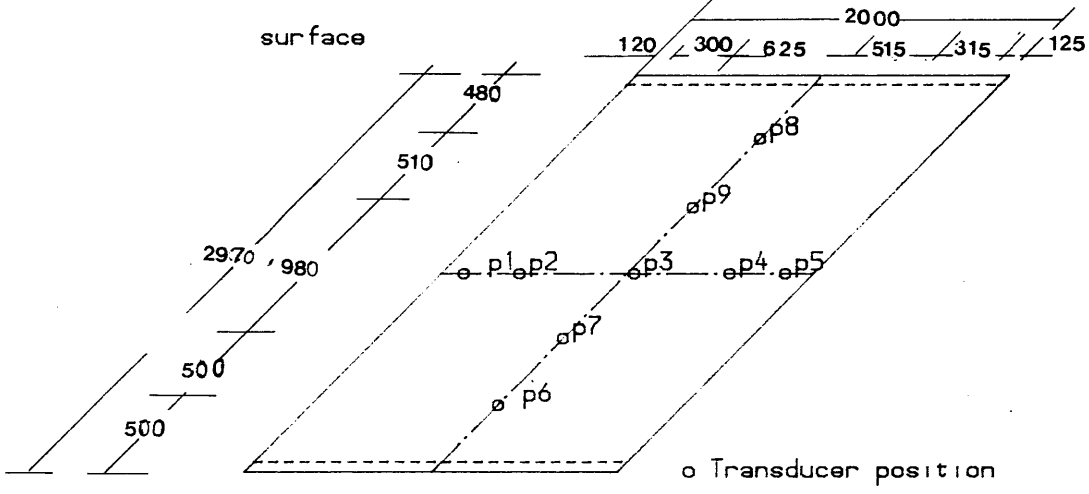

Fig. (6.19.5) MODEL SKEW SLAB NO. (5) Location of transducers on upper surface

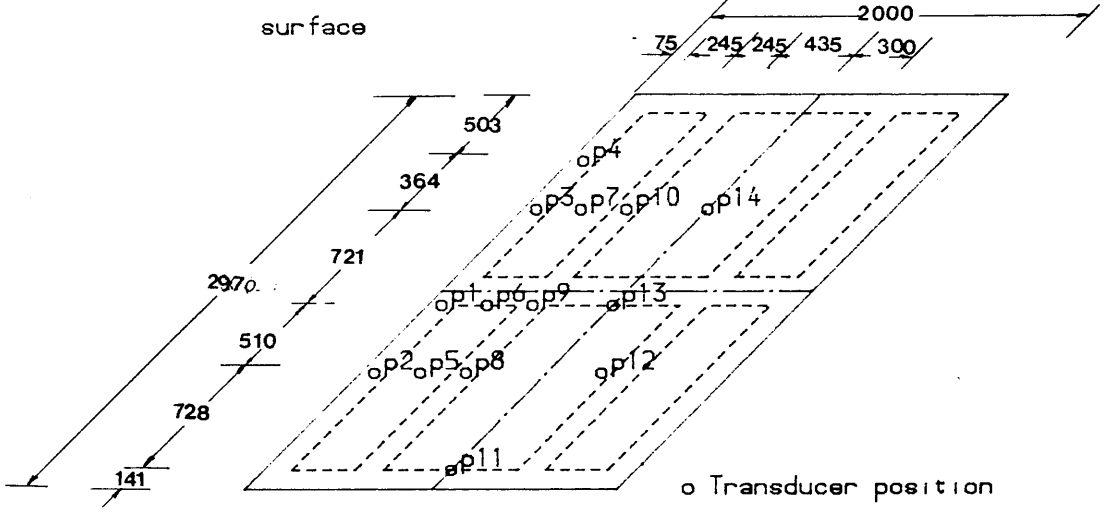

Fig. (6.19.6) MODEL RIBBED SKEW SLAB NO. (6) Location of transducers on upper surface

M-bond 200 adhesive was employed to cement the strain gauges to the bar. The lead wires were soldered to the strain gauge. Protective coating (M-coat D) was also applied. After the connection was thoroughly checked, epoxy resin was applied for further protection of the gauges . All strain gauges were connected to a linear voltage processing mini-computer.

6.8.2.2 Concrete Strains: Strains in concrete were measured using 10mm long electrical resistance strain gauges for the top concrete surface and 50 mm long demountable mechanical gauges (DEMEC) for the bottom surface. The location of these gauges was at ' critical points' along the longitudinal steel direction. For fixing the electrical resistance and Demec gauges, the concrete surface was cleaned and smoothened by grinding using a grinding stone and then followed by a fine sand paper. Carbon tetrachloride was used to remove the dirt and grease. For the demec gauges, a thin coat of M-bond 200 adhesive was employed to cement the gauge to the concrete. A thin coating of a mixture of adhesive type PR 9244/01 and hardener type PR 9244/02 was applied to the cleaned surface to bond the electrical resistance strain gauge the bending was effected by pressing the gauge firmly with the thumb for about two minutes. After 24 hours, the lead wires were soldered to the gauge. Protective coating (white M-coat D) was the applied to the strain gauge. Fig. (6.20.1) to Fig. (6.20.6) shows the strain gauges locations on the upper surface of the models.

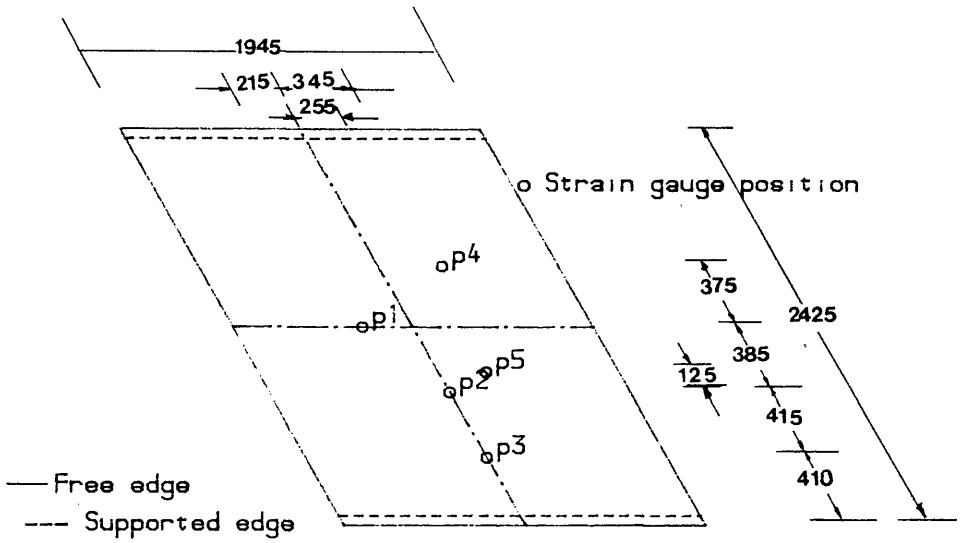

Fig. (6.20.1) MODEL SKEW SLAB NO. (1) Location of strain gauges on upper surface

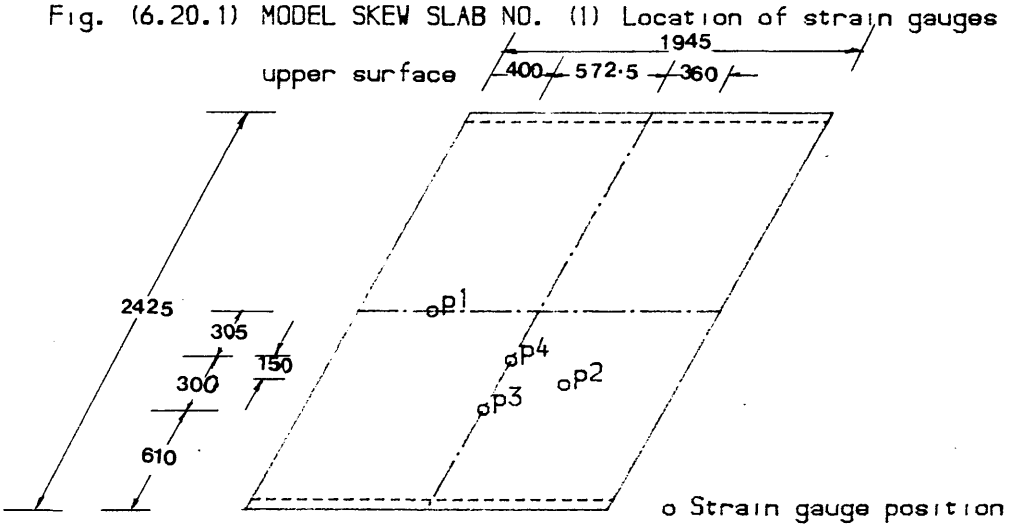

Fig. (6.20.2) MODEL SKEW SLAB NO. (2) Location of strain gauges on upper surface

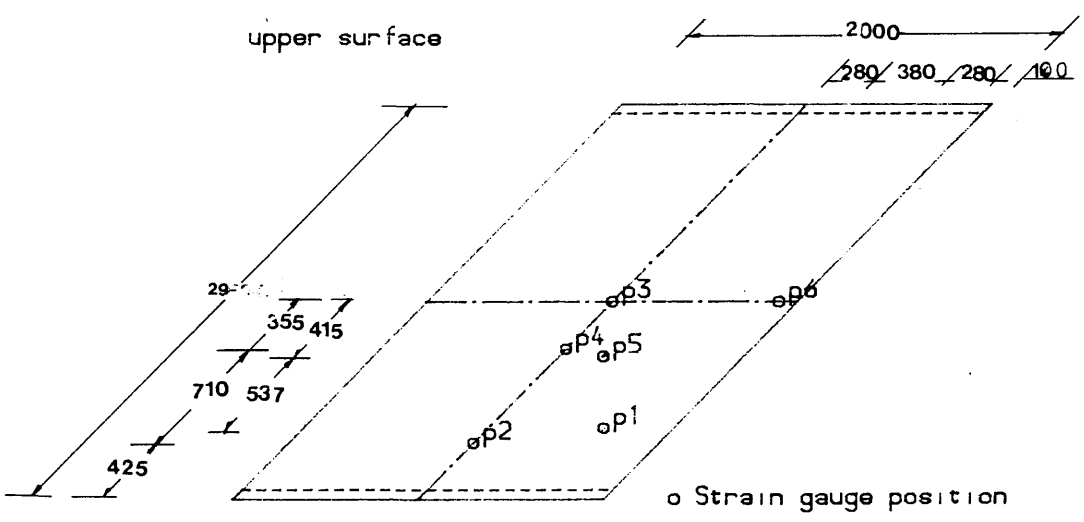

Fig. (6.20.3) MODEL SKEW SLAB NO. (3) Location of strain gauges on upper surface

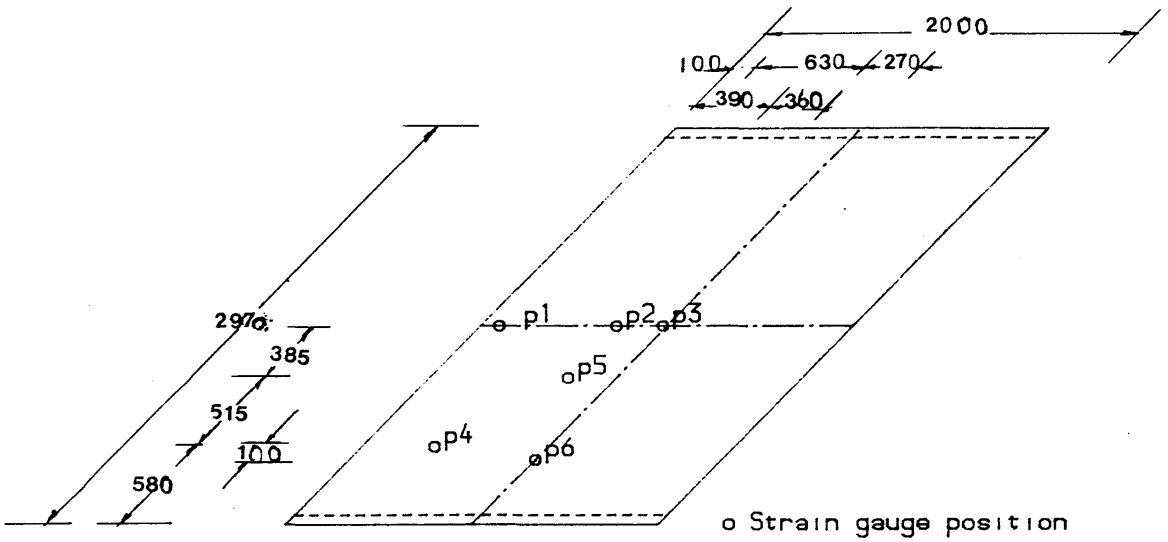

Fig. (6.20.4) MODEL SKEW SLAB NO. (4) Location of strain gauges on upper surface

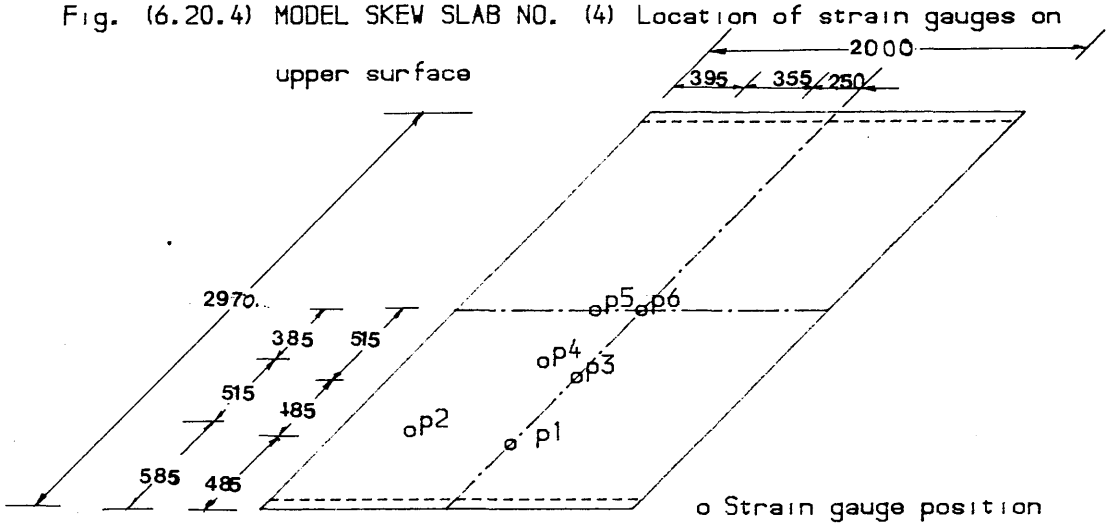

Fig. (6.20.5) MODEL SKEW SLAB NO. (5) Location of strain gauges on upper surface

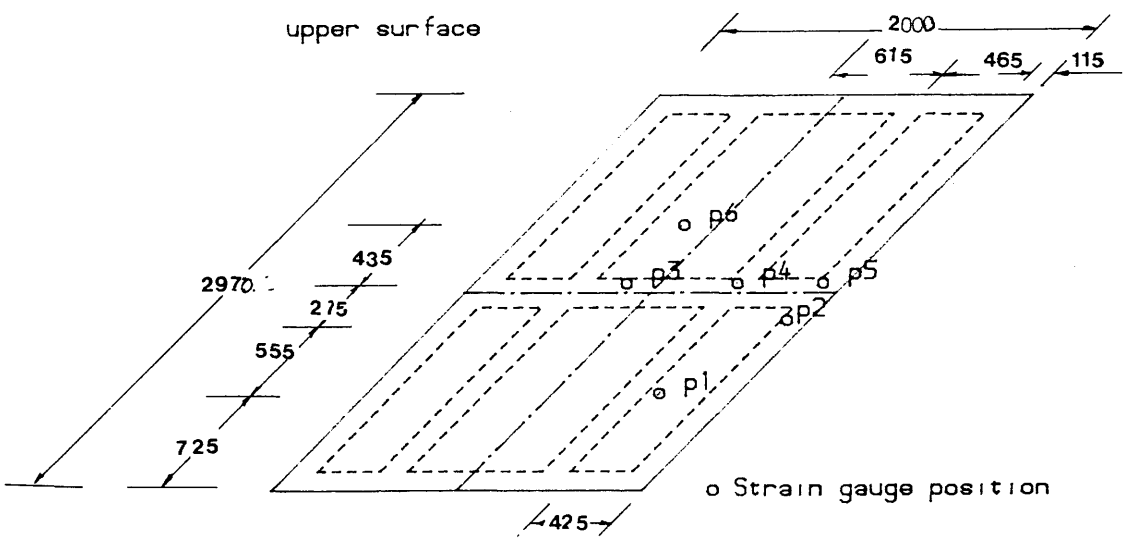

Fig. (6.20.6) MODEL RIBBED SKEW SLAB NO. (6) Location of strain gauges on upper surface

6.9.3 Crack widths

The under side of the slabs was illuminated using four powerful light sources. Cracks on the bottom surface of the slab were monitored with the aid of a magnifying glass. At each increment, if any crack appeared, the crack was traced and the increment number was written beside the crack mark. Two methods were used to measure crack widths.

(a) At certain positions where a large crack width was expected, transducers were fixed so as to measured the displacement normal to the crack. These were fixed after the cracks appeared. The transducers were connected to the data logger.

(b) Crack widths were measured at certain position using a crack measuring microscope reading to .01mm.

6.9 TEST PROCEDURE

All electrical connections were first checked thoroughly by the computer. Deflection transducers were then checked to ensure that they were vertical and they would operate properly during the test. The strain gauges were also checked and defective ones were disconnected. The load cells were also checked by applying a small load to the slab and unloading. Any leaks on the hoses and jacks which may appear during the initial test loading were remedied. When all the primary checks had been made, initial zero load readings were taken of all load cells, transducers, strain gauges. The test was started by applying the load in increment of .04 design load. The data logger recorded the

loads on the load cells and when the desired load level was reached, the computer was started for a complete scan. Results for the load increment were printed. During the test, Load vs the reading of transducer, strain gauge in longitudinal steel and centre demec gauge at the centre of the slab were plotted to check the behaviour of the slab. The loading was maintained for about 10 minutes while the under side of slab was examined for crack. After that a new load increment was applied and the whole procedure was repeated. This was repeated until failure load was reached.

CHAPTER SEVEN

EXPERIMENTAL INVESTIGATION

7.1 INTRODUCTION

This Chapter presents the experimental results of six large reinforced concrete skewed slabs described in Chapter six. The tests were designed to:

(a) Check the validity of the proposed design procedure with respect to service and ultimate load behaviour.

(b) Provide information on the detailing problems associated with this method and the resulting effects on the slab behaviour. Table (7.1) identifies the figures and the tables of Chapter six as they refer to specific models.

In each test, the following data were recorded:

1- Deflections normal to the plane of slab.

2- The load at each increment and the failure load.

3- Surface strains on concrete.

4- Steel strains.

5-Cracks widths.

7.2 TEST RESULTS

7.2.1 Model Skew Slab Number One

7.2.1.1 The Properties of The Slab: The effective dimensions of reinforced concrete slab are 1945mm X 2310mm X 100mm. The angle of skew measured anticlockwise between the support edge and free edge was 120^{o}. The two short

parallel edges of the slab were simply supported and the other two longer edges were free with the acute corners held down. The loading system was the indirect four-point system as shown in Fig. (7.1). the live load was 150 kN and the total design load including dead load was 159.6 kN as shown in Table (7.2). The reinforcement was orientated parallel to the edges. The material properties of the slab are shown in Table (7.2).

7.2.1.2 Response of The Slab: Unfortunately this slab was not tested with an incrementally increasing load to failure. During loading, the loading rod failed at a load 0.8 of the design load. The loading rod was changed and the test was restarted. Cracking was first observed on the bottom surface at the centre of the slab near to the loading points at a load of 0.22 of the design load. The cracks were dominant in the bottom surface midspan area and they propagated from the centre towards both the free edges at spacing of 100 mm and roughly parallel to the support lines. At 0.4 of the design load, additional cracks at an angle of approximately 80 to the free edges appeared. At 0.52 of the design load, inclined cracks propagating from the bottom surface penetrated through the depth of the slab and could be observed at the free edges. At 1.05 of the design load, the cracks extended towards the obtuse corners on bottom surface. At 1.13 of the design load, steel in the longitudinal direction at the centre started to yield. At this stage, the width of the cracks started to increase near the free edges. At 1.39 of the design load, a large shear crack near and parallel

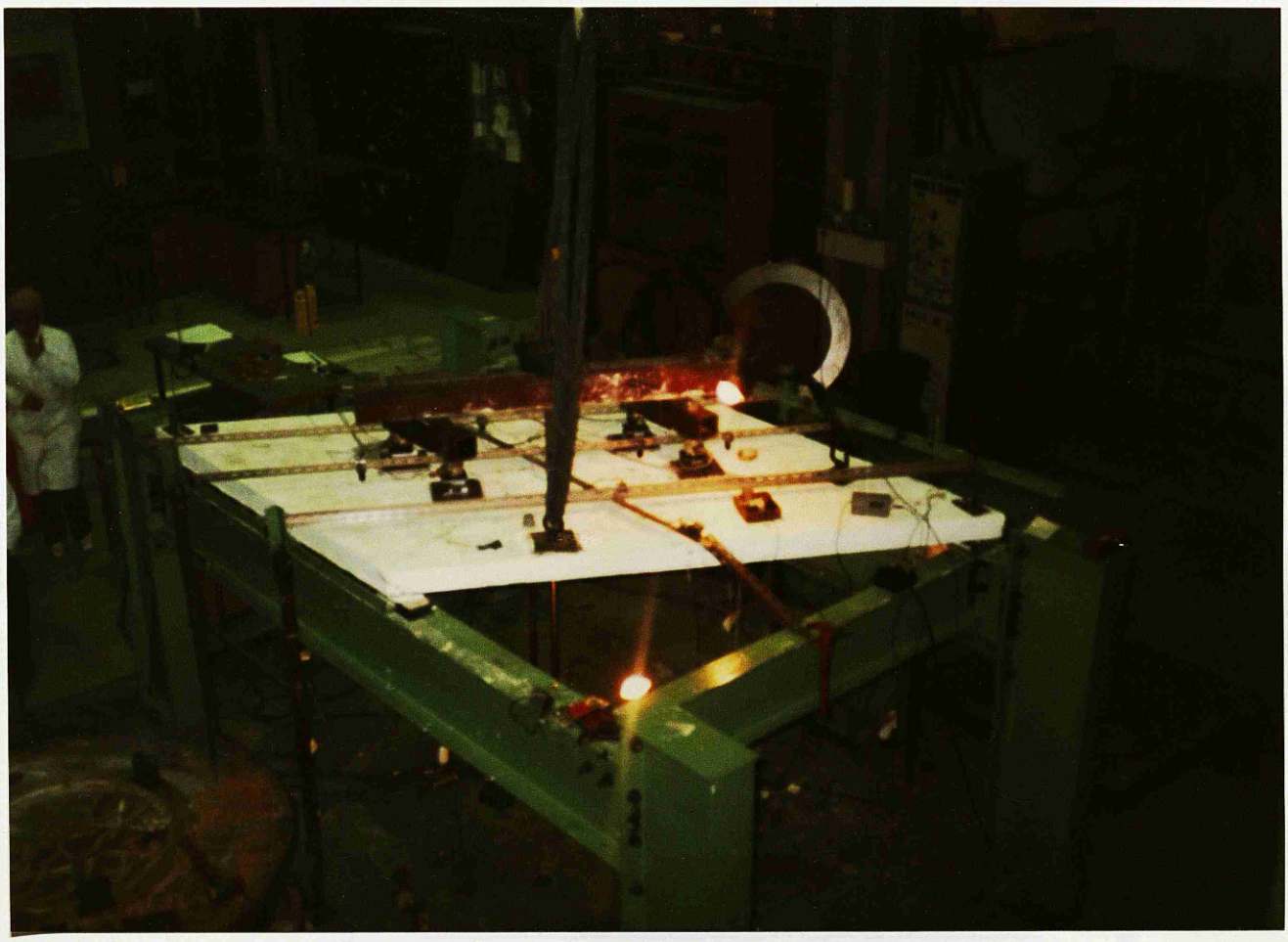

Fig. (7.1) Test set-up for MODEL NO. ONE (system of one centre rod with spreader beams)

Table (7.1) Summary of Tables and Figures Including Properties, Loading System, Steel Areas and Steel Distribution for all Tested Models.

Model No.	Table No. of slab properties	No. of fig. of loading system	Table No. of steel volume	Fig. No. of design actual steel		Fig. No. of steel distribution in the bottom		Fig. No. of steel distribution in the top	
				Longi-tudinal	Transverse	Longi-tudinal	Transverse	Longi-tudinal	Transverse
1	(6.1)	(6.15a)	(6.2)	(6.2.1)	(6.2.2)	(6.7.1)	(6.7.2)	-	(6.7.3)
2	(6.1)	(6.15b)	(6.2)	(6.3.1)	(6.3.2)	(6.8.1)	(6.8.2)	-	-
3	(6.1)	(6.15c)	(6.2)	(6.4.1)	(6.4.2)	(6.9.1)	(6.9.2)	-	-
4	(6.1)	(6.15c)	(6.2)	(6.5.1)	(6.5.2)	(6.10.1)	(6.10.2)	-	(6.10.2)
5	(6.1)	(6.15c)	(6.2)	(6.6.1)	(6.6.2)	(6.11.1)	(6.11.2)	(6.11.3)	(6.11.4)
6	(6.1)	(6.12.1)	(6.2)	*	*	From Fig. (6.12.2) to Fig. (6.12.6)			

* For ribbed slab see Fig. (7.57) to Fig. (6.60).

Table (7.2) Design Loads, Material Properties and Dimensions of the Tested Models.

Model No.	Design Load			f_{cu} N/mm^2	f_t N/mm^2	Cylinder Comp. Strength N/mm^2	E_c kN/mm^2	f_y N/mm^2	E_s kN/mm^2		Hardening Number %	Effect Dimension in mm
	Live Load	Dead Load	Total Load									
1	150.	9.6	159.6	45.0	2.94	35.0	29.25	500.	210.	.0023	6	1945x2300.x100.
2	140.	9.6	149.6	45.0	3.3	39.0	29.25	500.	210.	.0023	0.0	1945x2300.x100.
3	100.	9.6	109.6	41.6	3.52	40.0	28.69	473.	200.	.0024	3	2000x2830.x100.
4	80.	9.6	89.6	44.0	3.5	40.0	29.25	519.	220.	.0023	-	2000x2830.x100.
5	100.	9.6	109.6	44.0	3.5	40.0	29.25	480.	218.	.0022	0.0	2000x2830.x100.
6	288.7	11.3	300.	44.0	3.3	40.0	29.25	460.	230	.002	-	*

* The dimension of model 6 can be seen in Fig. (6.12.1).

to the support edge started from the obtuse corner running to opposite corner (acute corner) causing the concrete cover on the bottom surface of the slab to spall. The slab failed suddenly in shear at this load.

7.2.1.3 Deflections: Measured centre line deflections during loading are presented in Figs (7.2) and (7.3). The load deflection curves indicate the initiation of the nonlinearity at 0.2 design load, which is slightly lower than the load at which the first crack was observed. At a load 0.5 design load, the central deflection was 9 mm. This represents the lower permissible service deflection according to CP110. The load deflection curves indicate that the failure was a brittle failure due to the fact that shear failure occurred.

7.2.1.4 Reactions: The measured reaction at the acute angle was too small to be properly recorded using a 50 KN load cell.

7.2.1.5 Concrete Strains: The lower surface strains were very low except in one gauge at the centre of the slab where a tension strain of 0.02 was recorded near failure load. Fig. (7.4) shows curves of recorded load vs concrete strain in the direction of the longitudinal steel at the top surface at different positions. The general behaviour is similar to the overall behaviour of the slab as indicated by the load-deflection curves. It gives the same cracking load at 0.2 design load The general behaviour is as expected with high strains at the central area (positions 1 and 2), less significant strains near to

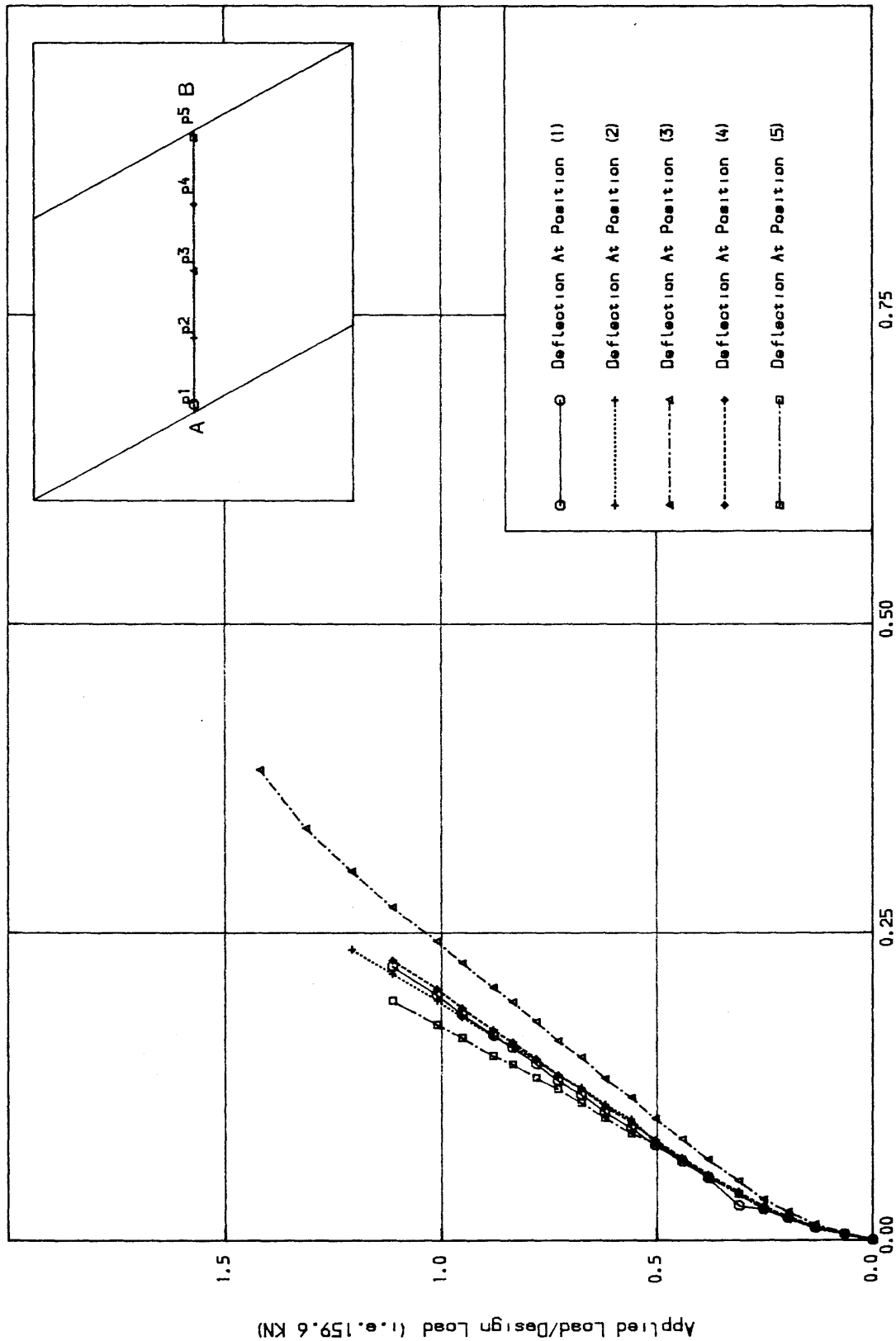

Fig. (7.2) Load-Deflection along the centre line A-B for MODEL NO. ONE

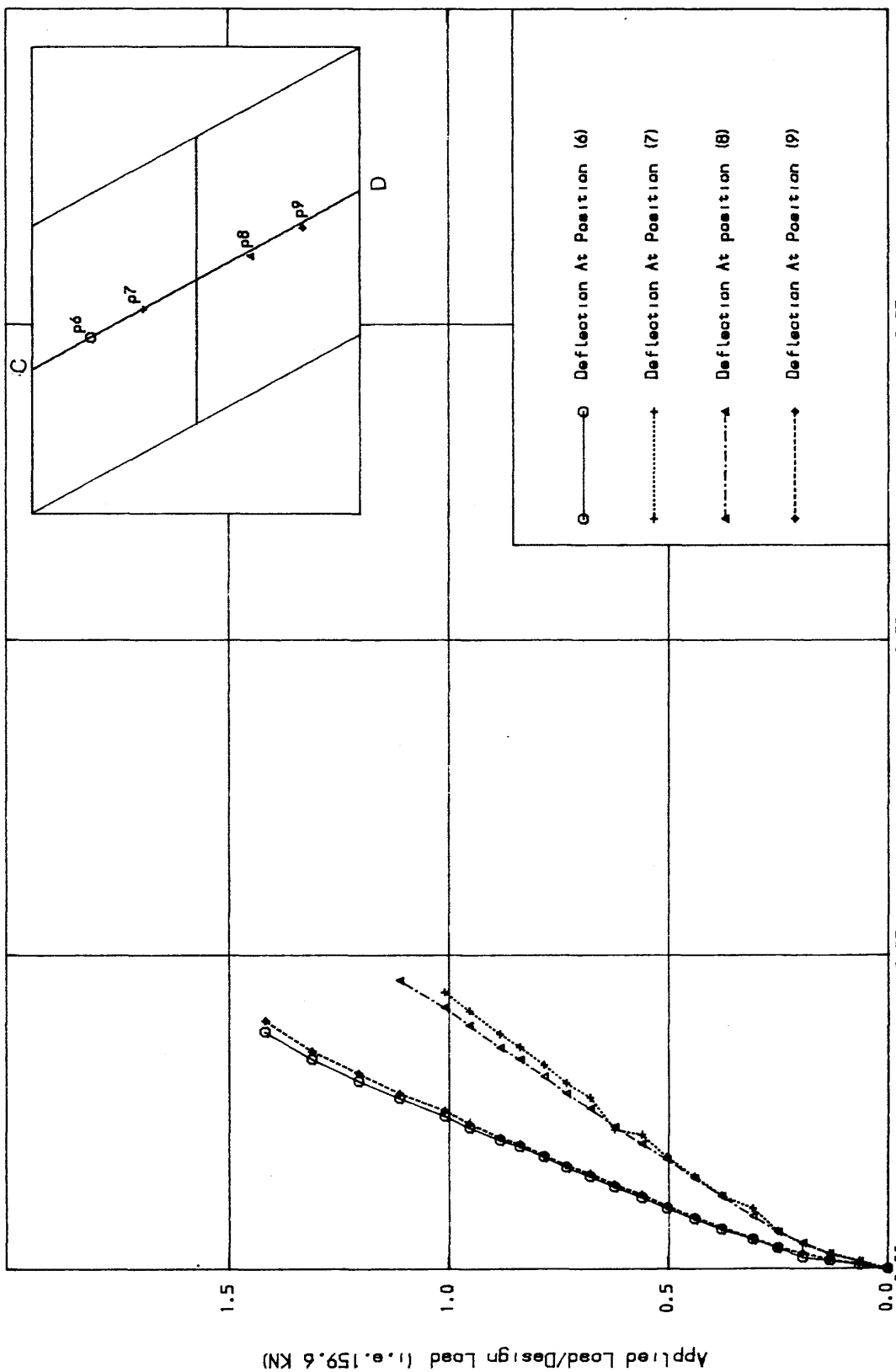

Fig. (7.3) Load-Deflection alonge the centre line C-D for MODEL NO. ONE

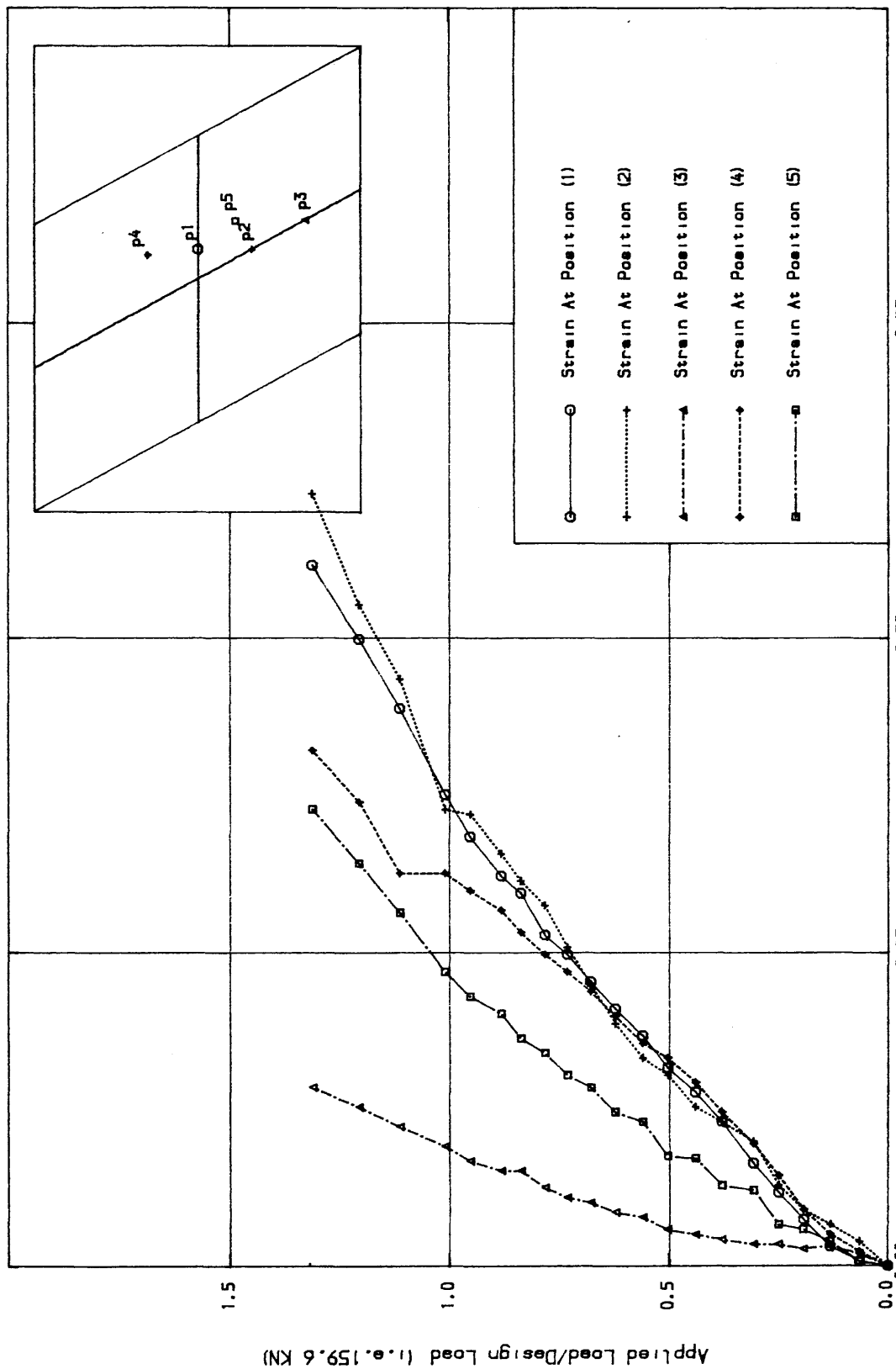

Fig. (7.4) Load-Concrete Strain curves at top surface for MODEL NO. ONE

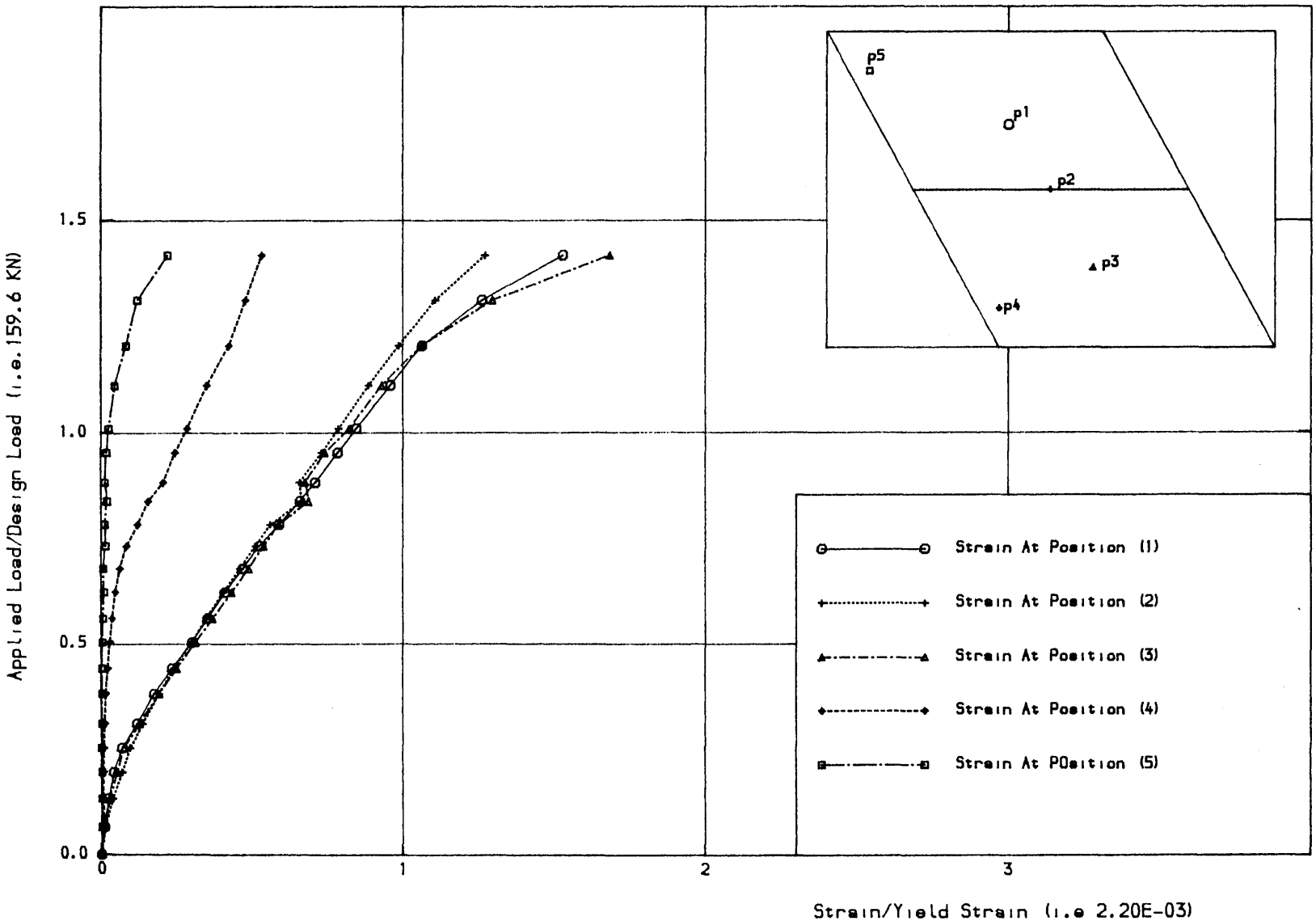

Fig. (7.5) Load-Steel Strain curves in the longitudinal direction for MODEL NO. ONE

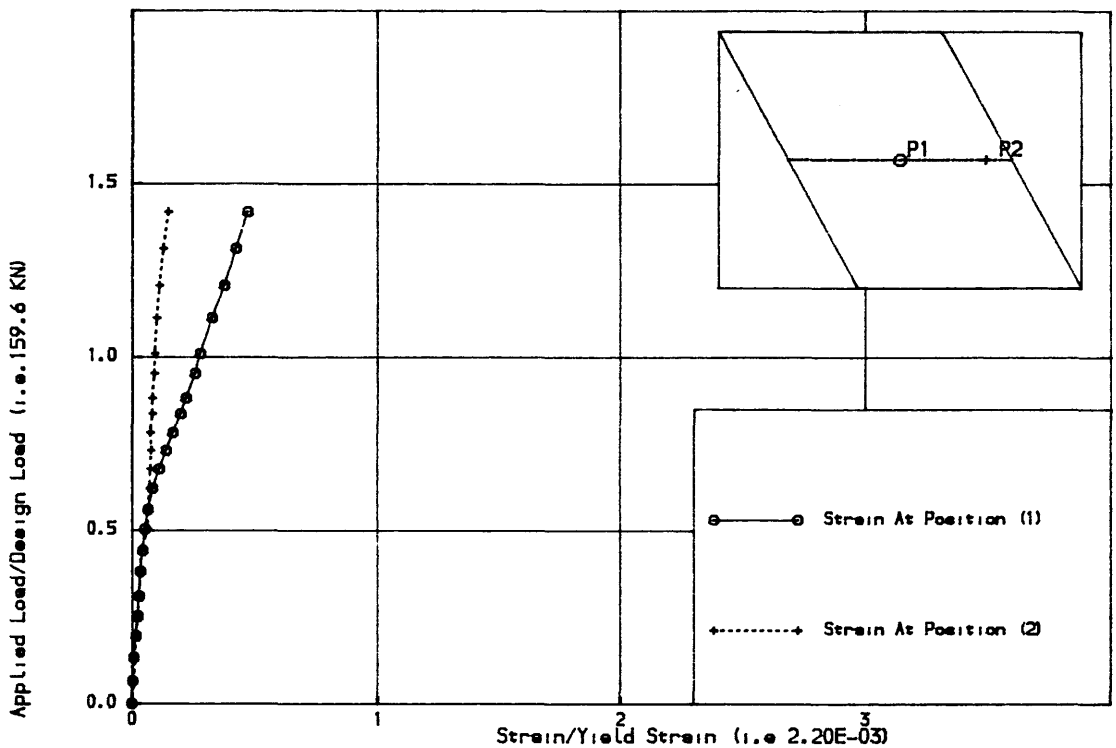

Fig. (7.6) Load-Steel Strain curves in the Transverse direction for MODEl NO. ONE

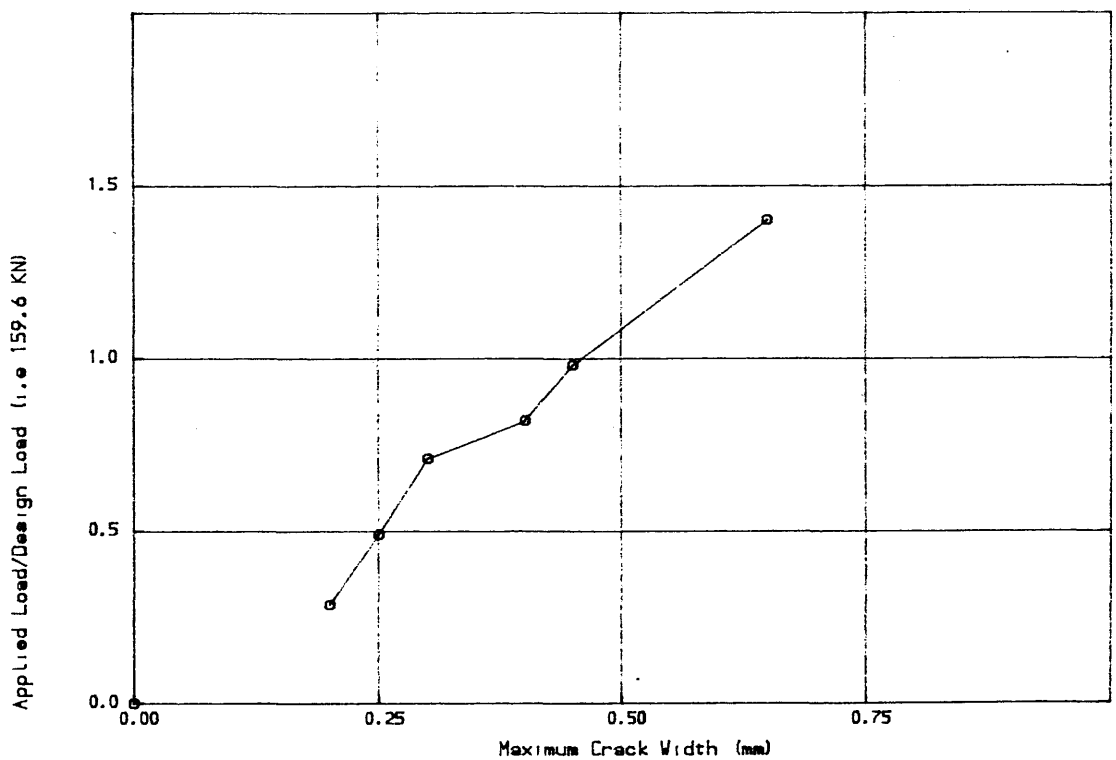

Fig. (7.7) Load-Maximum crack width for MODEL NO. ONE

the obtuse corners (position (4)) and negligible strains near to the the supported edge (position 3).The maximum concrete strain at failure was 0.6 the crushing strain of concrete.

7.2.1.6 Steel Strain: The measured steel strains are shown in Figs (7.5) and (7.6). It can be seen from Fig. (7.5) that the steel in the longitudinal direction at the central area yielded at 1.125 of design load but the steel at the obtuse corner (position (4)) reached only 0.6 the yield strain of steel. The steel at the acute corner (position (5)) carried a negligible stress. Fig. (7.6) shows that the transverse steel at the centre of the slab carried significant stresses but did not yield and the steel near the free edge carried negligible stresses.

7.2.1.7 Soffit Crack Widths: Fig. (7.7) gives approximate maximum crack width measured during the test. The limit service load of cracking was 0.71 of design load and the maximum crack width near the failure load was 0.7 mm.

7.2.1.8 Summary of Results: At 0.2 design load, the nonlinearity was indicated by initial cracking as can be observed from load deflection and load-strain curves see Figs (7.2) to (7.5). The model failed in a brittle fashion. The deflection serviceability limit was attained at about 0.5 design load and a limiting crack width of 0.3 mm was attained at 0.71 design load. At 1.125 design load, the strain gauges on longitudinal steel at centre yielded but transverse steel was still in the elastic

stage. The maximum concrete compressive strain at top surface at the centre of the slab was 0.6 of the concrete crushing strain at failure. The ultimate shear failure load was 1.39 design design load.

7.2.2 Model Skew Slab Number Two

7.2.2.1 The Properties of The Slab: Table (7.1) gives the numbers of the Tables and the Figures which describe the slab properties as given in Chapter six. This model is similar to the previous model except the angle of skew was 60 and the loading system was an indirect two point-beam system, Table (7.2) shows the slab material properties.

7.2.2.2 Response of The Slab: The first crack was observed parallel to the supported edge and near to the load position at 0.31 of the design load. As the load increased, the extent of bottom surface cracking spread towards the slab central area and there was considerable loss of stiffness as can be seen from Figs (7.9) and (7.10). At 0.8 of the design load, inclined cracks progressed from the bottom surface through the slab depth at the edge. At 0.97 of the design load, minor soffit cracks were observed at the obtuse corner. As the load increased, the width of the cracks increased due to the yielding of steel, as shown in Figs (7.13) and (7.14). At 1.18 design load, a large bottom surface crack parallel to the supported edge appeared, at the centre line of the free edge and extending the whole width of the slab as shown in Fig. (7.8). Failure occurred due to yielding of the

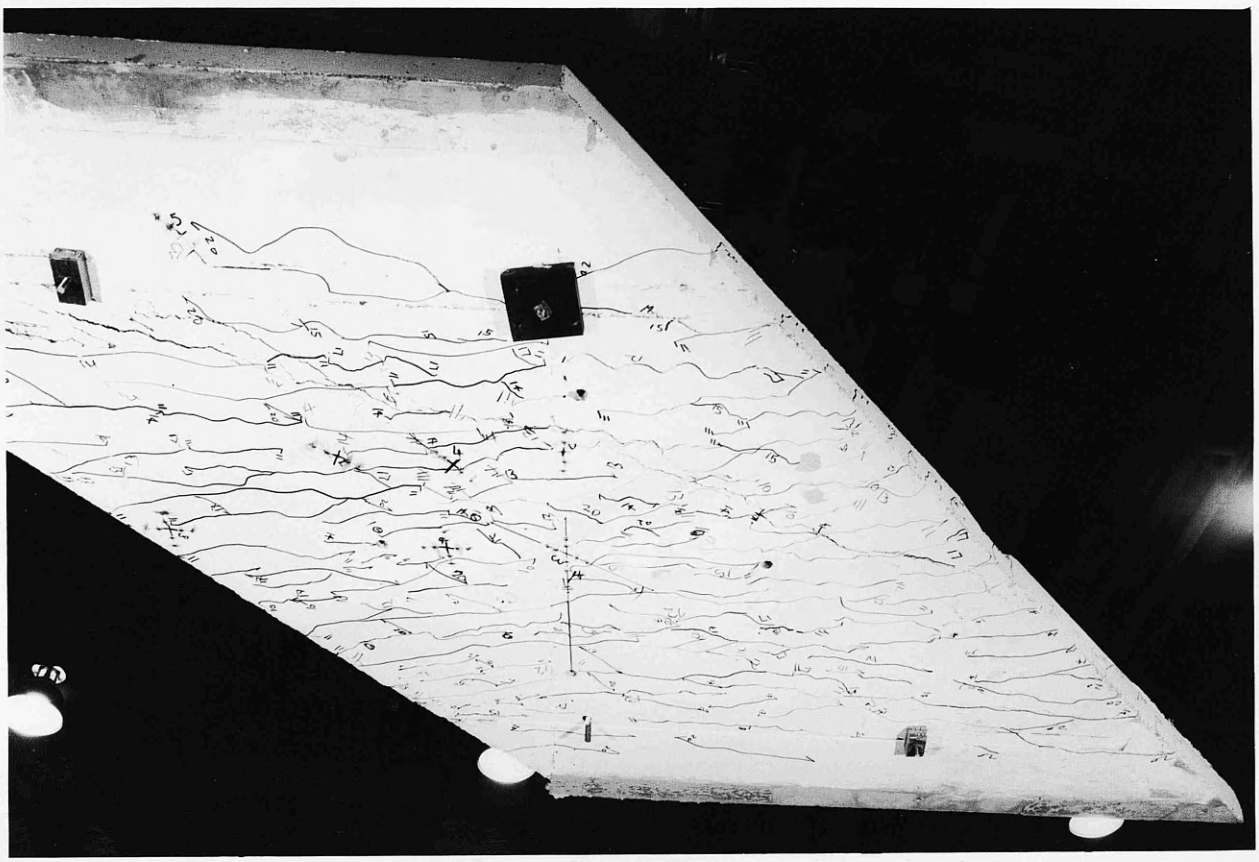

Fig. (7.8) MODEL SKEW SLAB NO. (2) Soffit crack pattern to failure

steel.

7.2.2.3 Deflection: Measured centre line deflections are shown in Figs (7.9) and (7.10). They indicate that the initiation of nonlinearity was at load 0.3 of the design load, which was confirmed by visual inspection. At a load 0.45 of the design load, the central deflection was 9.0 mm . This represents the permissible service deflection according to CP110 (30).

7.2.2.4 Concrete Strain: The concrete strains at top and bottom surfaces are shown in Figs (7.11) and (7.12) respectively. The bottom surface strains are affected by the presence of cracks. The maximum strain was 0.53 of the crushing strain of concrete. The general trend of the concrete strain at the top is similar to the overall behaviour of the slab as measured by deflections.

7.2.2.5 Steel Strain: Steel strains in the longitudinal direction are shown in Figs (7.13) and (7.14). They show that the first yield occurred at the obtuse corner near the free edge (Position 3) at 0.81 of the design load. At 1.18 of the design load, all steel had yielded except one at position (7) near to the acute corners. The load-steel strain curves in the transverse direction in Fig. (7.15) show that the transverse steel did not yield.

7.2.2.6 Soffit Crack Widths: Fig. (7.16) gives approximate maximum crack width in mm. It can be seen from Fig. (7.16) that the limit crack width of 0.3mm was

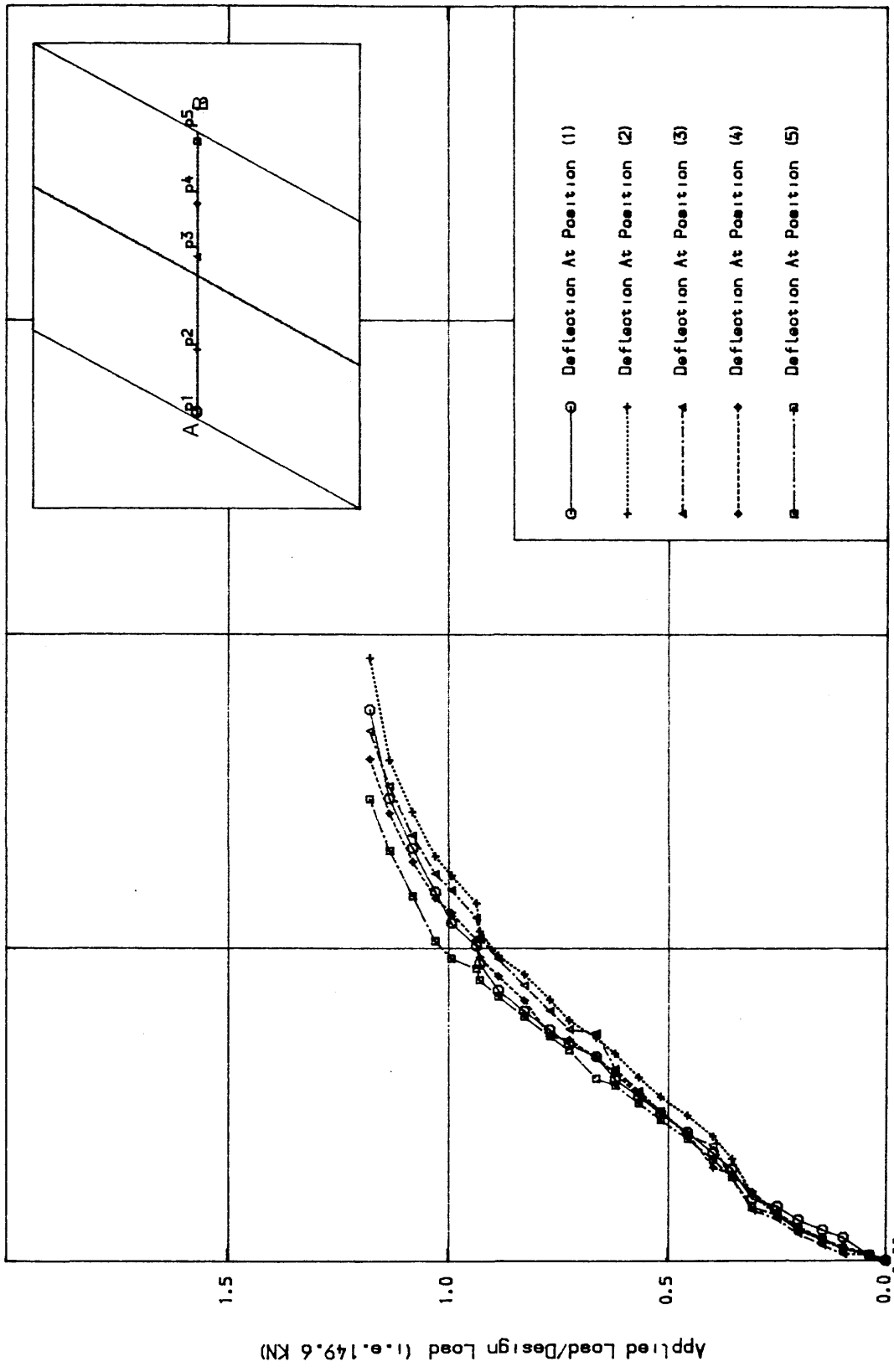

Fig. (7.9) Load-Deflection curves along the centre line A-B for MODEL NO. TWO

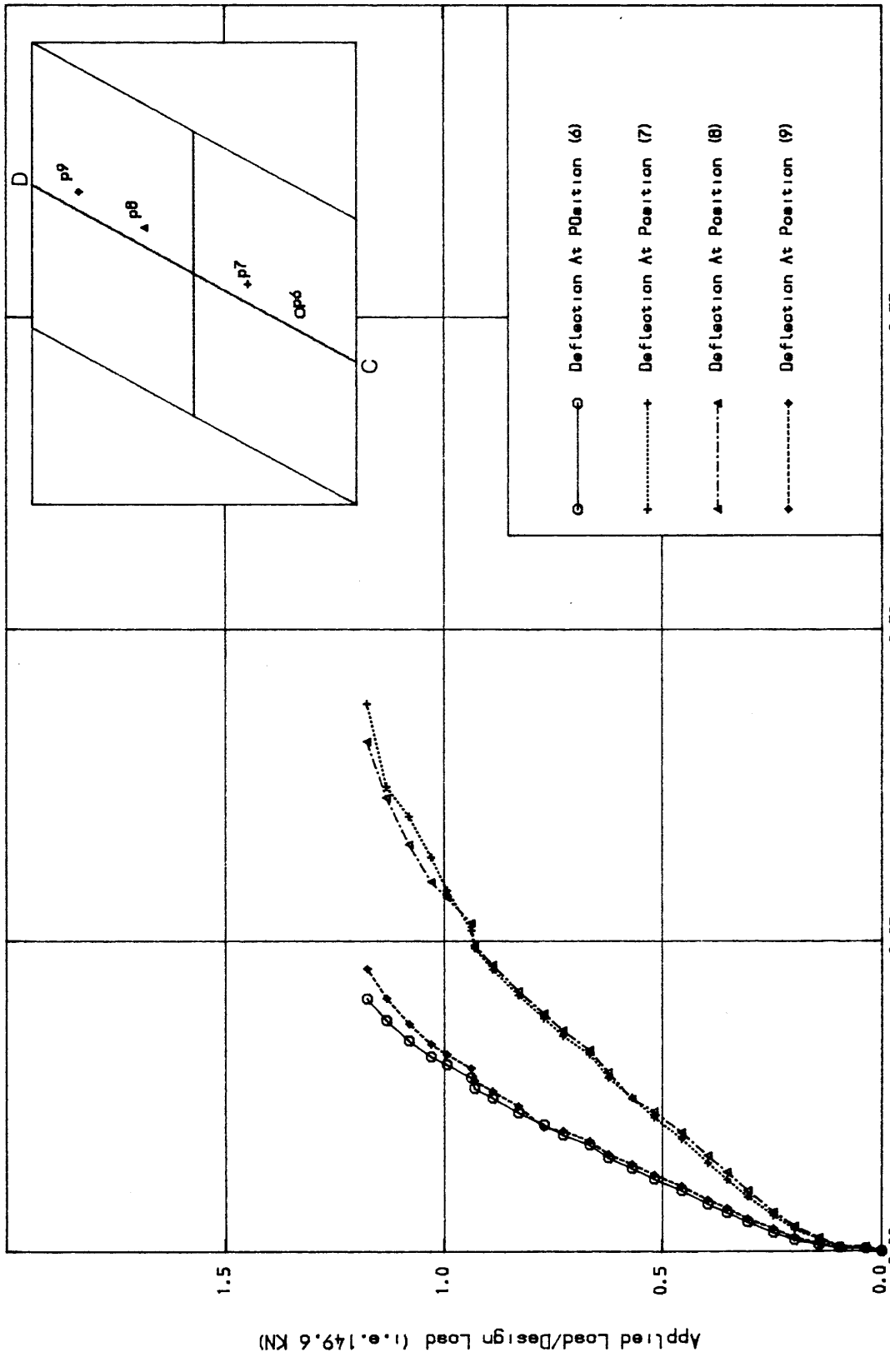

Fig. (7.10) Load-Deflection curves along the centre line C-D for MODEL NO. TWO

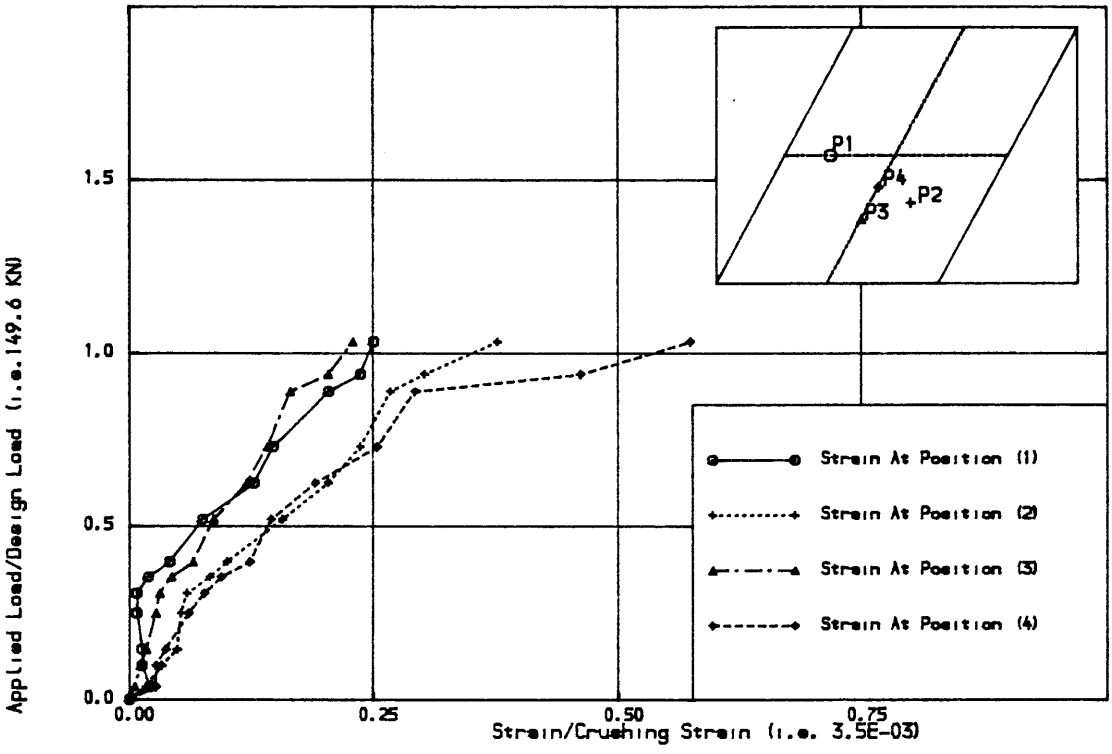

Fig. (7.11) Load-Concrete Strain curves at top surface for MODEL NO. TWO

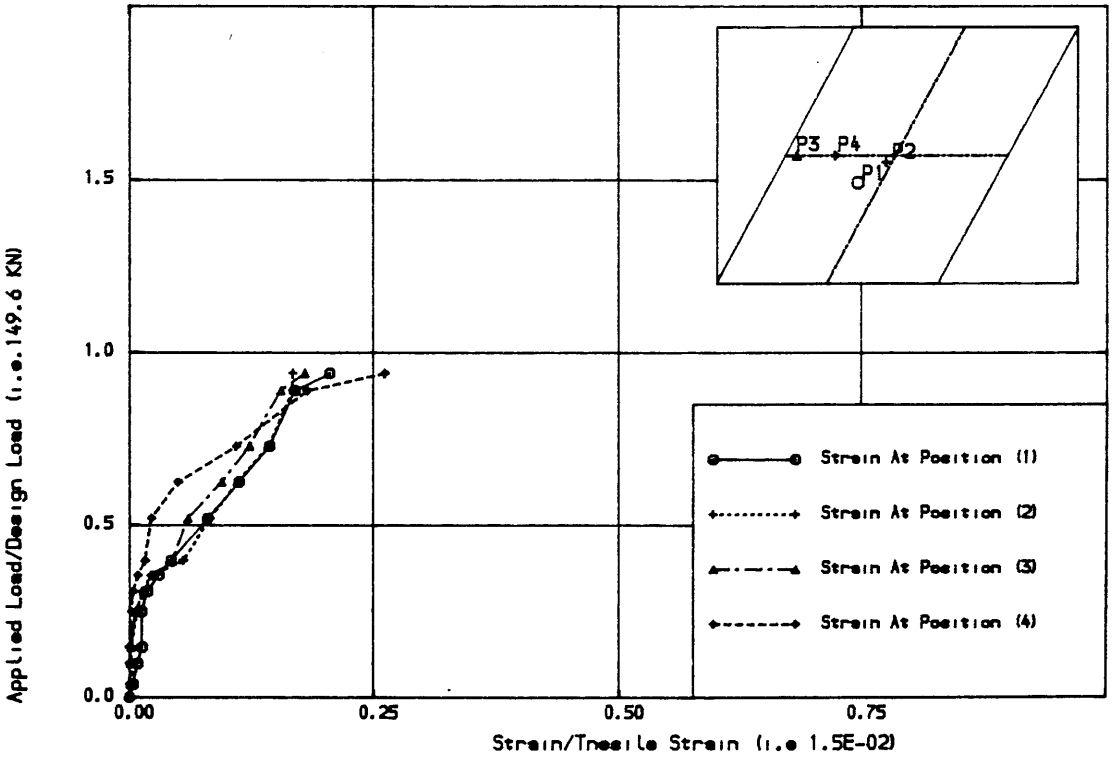

Fig. (7.12) Load-Concrete Strain at bottom surface for MODEL NO. TWO

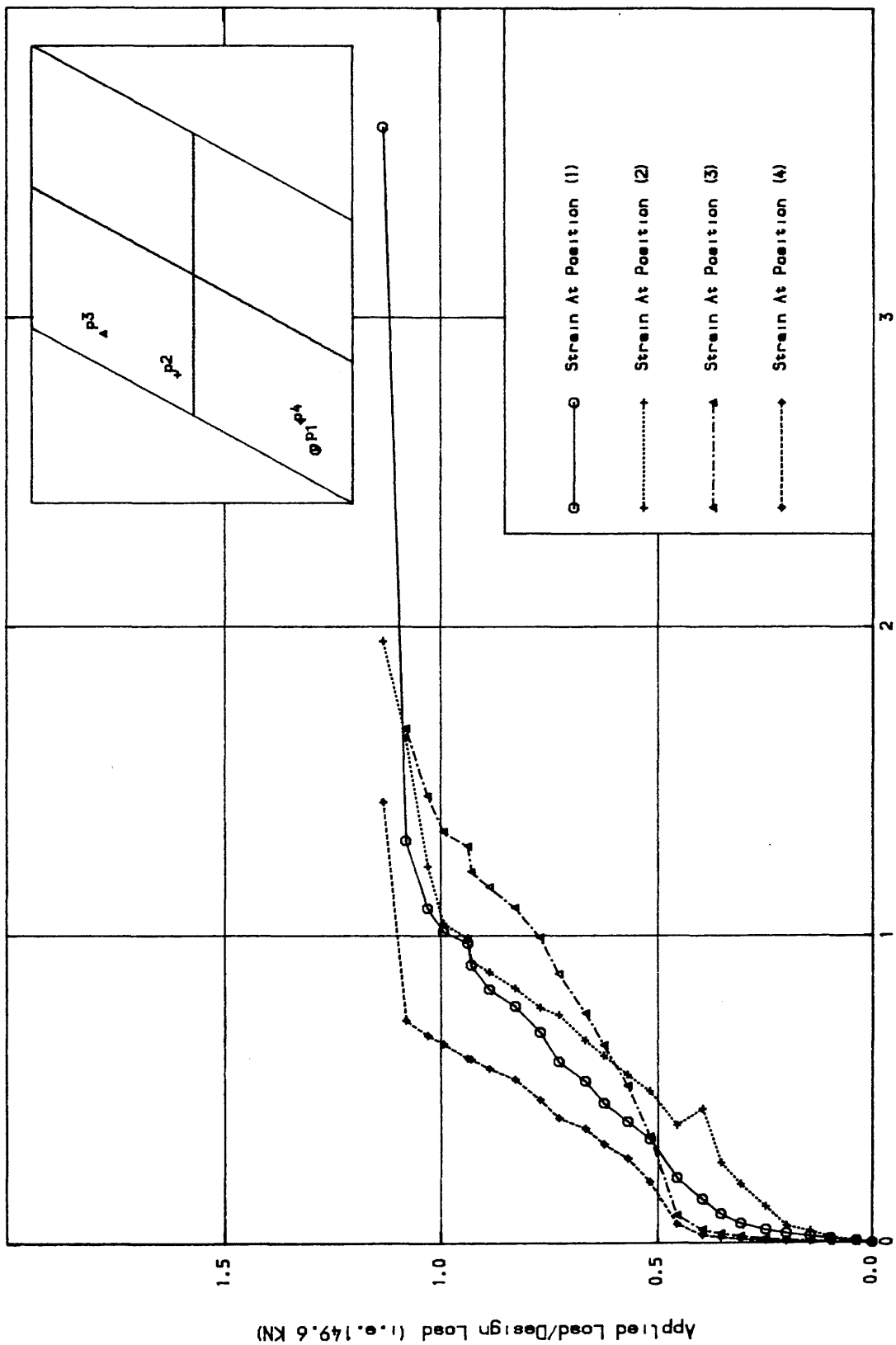

Fig. (7.13) Load-Steel Strain curves in the longitudinal direction for MODEL NO. TWO

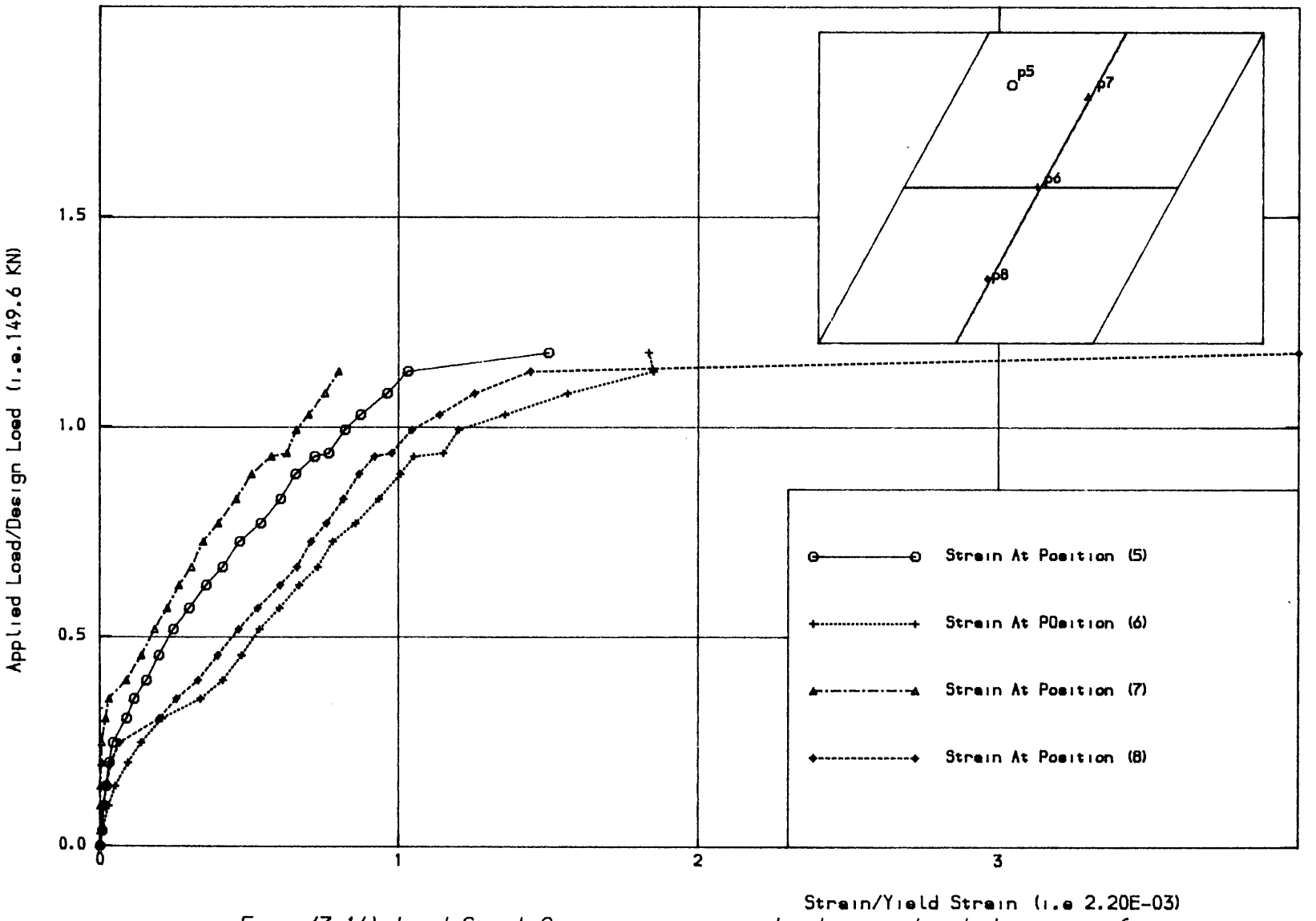

Fig. (7.14) Load-Steel Strain curves in the longitudinal direction for MODEL NO. TWO

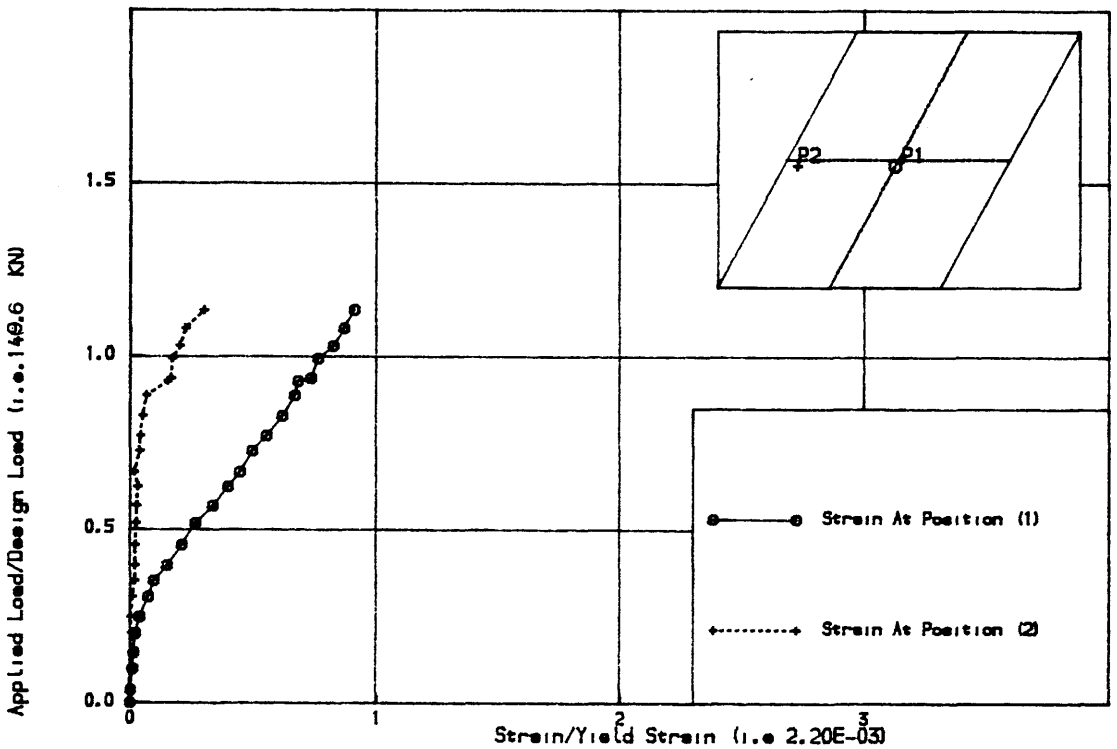

Fig. (7.15) Load Steel Strain curves in the transverse direction for MODEL NO. TVO

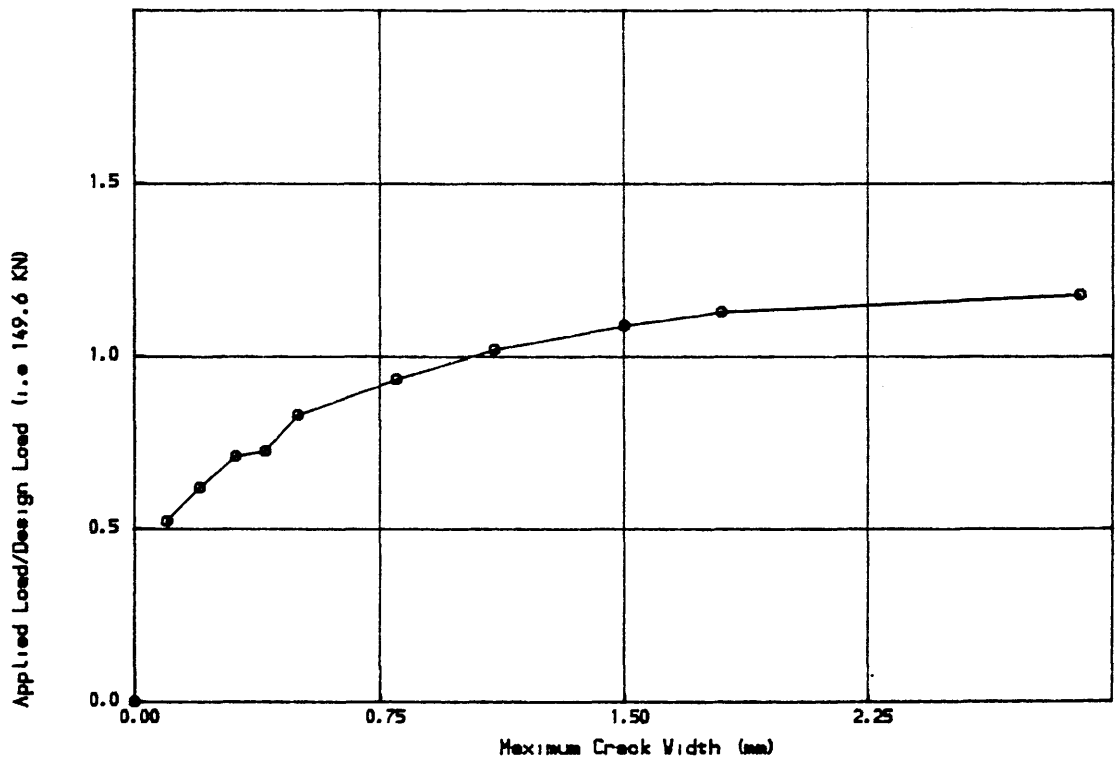

Fig. (7.16) Load-Maximum crack width for MODEL NO. TVO

reached at 0.62 of the design load. Near failure, the maximum crack width was 2.9 mm.

7.2.2.5 Summary of Results: The load at serviceability deflection limit was 0.45 of the design load and crack width limit load was 0.71 of the design load. The steel in the longitudinal direction yielded at 0.81 of the design load. The serviceability deflection limit load is lower than that recommended by the Code. The slab failed in a ductile fashion at 1.18 of the design load.

7.2.3 Model Skew Slab Number Three

7.2.3.1 The Properties of The Slab: Table (7.1) shows the numbers of the Tables and the Figures which discribe the slab properties. The angle of skew was 45. the loading system was a direct four points load system. Steel reinforcement was parallel to the edges. Table (7.2) gives the slab material properties. The test set up is shown in Fig. (7.17).

7.2.3.2 Response of the slab: Initial cracks were observed on the bottom surface at the centre of slab at a load of 0.41 the design load and cracks were dominant in the midspan area. They propagated from the centre of the slab towards the free edges and were roughly parallel to the supported edge at a spacing of about 70 mm. Inclined cracks penetrated to the depth of the slab at free edges at 0.82 design load. Additional cracks at approximately 80 to the free edge developed at 0.82 design load. As the load increased more inclined cracks were observed. At 1.83

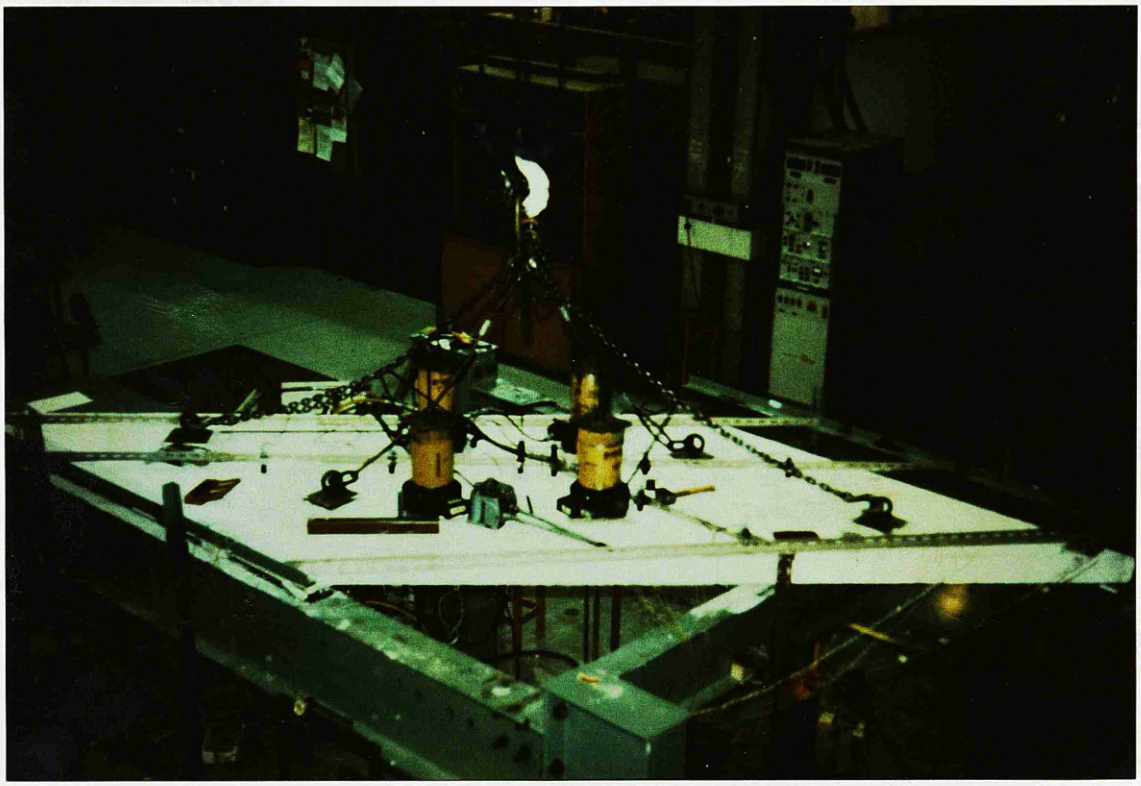

Fig. (7.17) Test set-up for MODELS NO. THREE, FOUR, FIVE and SIX

design load, just before failure, small cracks were observed at the bottom surface at obtuse corners. At 1.96 design load, a very big crack at the centre of the slab near the free edge was observed penetrating the depth of the slab. Fig. (7.18) shows the cracks pattern at the bottom and top surfaces. Failure occurred due to yielding in the steel.

7.2.3.3 Deflection: Fig. (6.19) shows the load-deflection relationship at different locations in the slab. It can be seen from these curves that the response is nonlinear after 0.3 of the design load is exceeded. The deflection limit of span/250 was reached at load 0.5 of the design load. At failure, the deflection at the centre of the slab equal to 0.8 of the slab thickness.

7.2.3.4 Concrete Strain: The concrete strains are shown in Figs (7.21),(7.22) and (7.23). At the top surface Figs. (7.21) and (7.22) show that at the centre of the slab (position (3)), the general behaviour is similar to the overall behaviour of the slab as measured by deflection. Also at position (2) (on the centre line parallel to the free edge near the supported edge) the recorded strain is significant since more or less the exact steel was provided at position. At other positions (4), (5) and (6) near the centre area significant strains are recorded, while at position (1) near to the obtuse corner the strain was not significant because too much steel had been provided. Measured bottom surface strains are presented in Fig. (7.23). The effect of cracking can be seen clearly

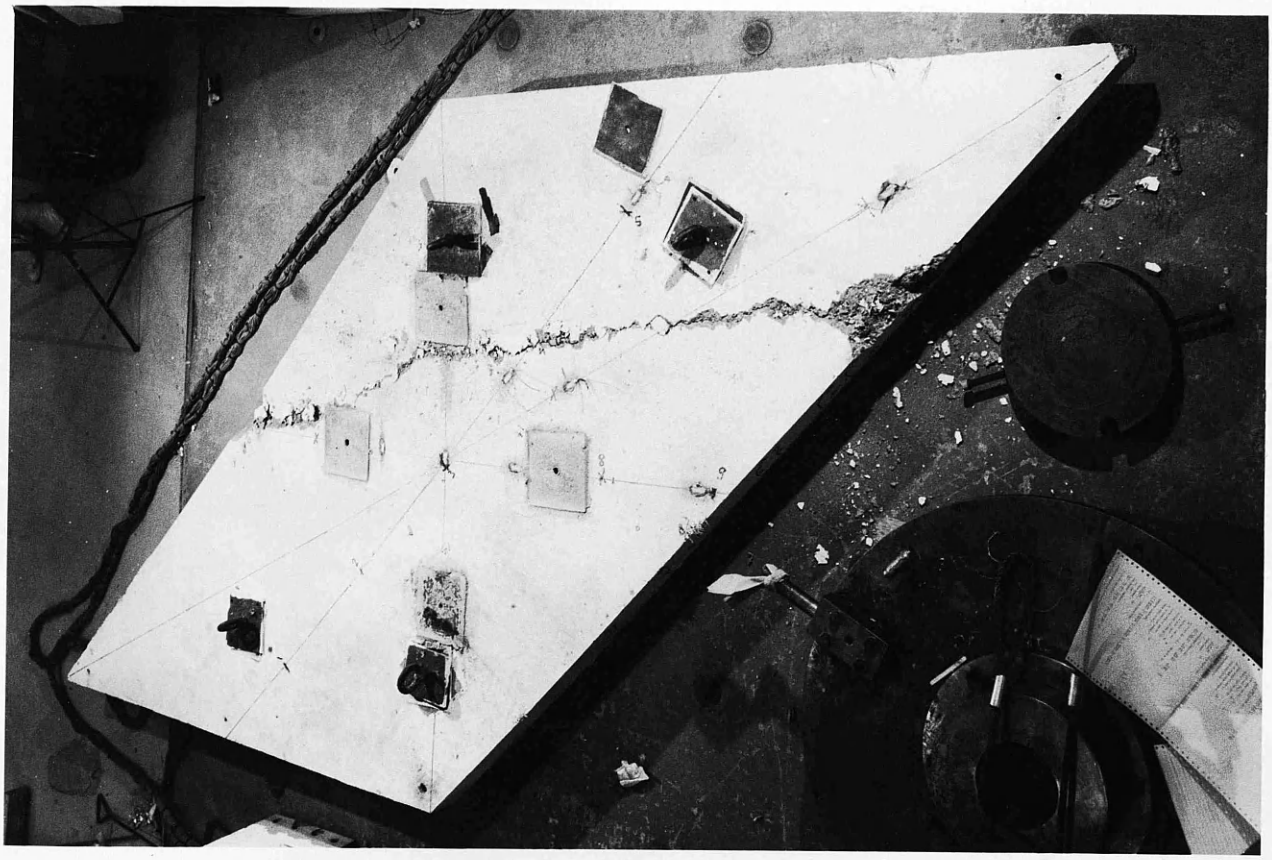

(a) Top surface after failure

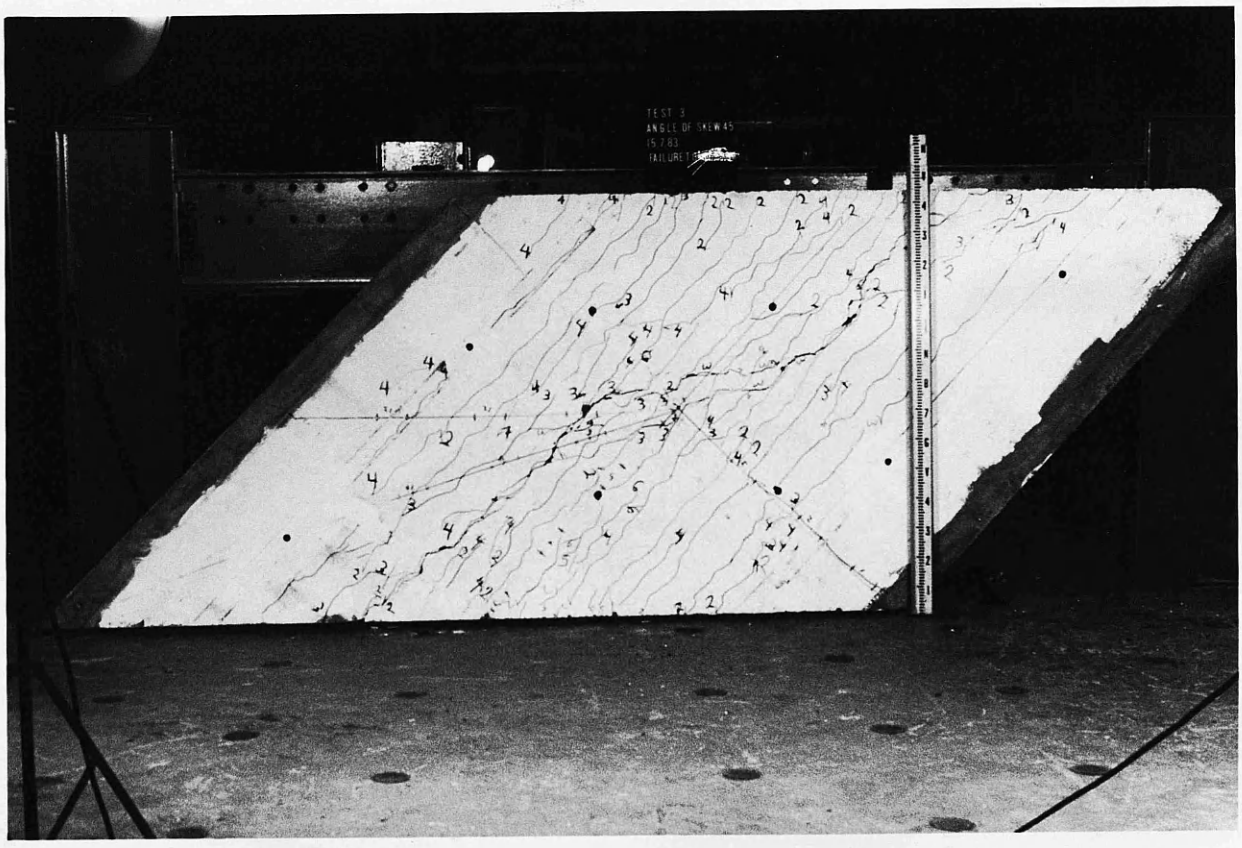

(b) Soffit crack pattern after failure

Fig. (7.18) SKEW SLAB NO. THREE

from these curves.

7.2.3.5 Steel strains: Fig. (7.24) shows the load vs strain curves in the longitudinal direction. It can be seen from these curves that at the centre of the slab (position (3)) the steel yielded at 1.4 of the design load. At positions (6) (near the free edge) and (5) (near to the obtuse corner) steel yielded at 1.68 of the design load. At positions (4) and (2) steel yielded at failure. At positions (1) (at the centre near the supported edge) and (7) (close to the acute corner) the steel did not yield. In the transverse direction, the steel carried significant stresses (up to 0.75 f_y at failure load) as it can be seen from Fig. (7.25).

7.2.3.6 Soffit crack widths: Fig. (7.26) shows maximum bottom surface crack width in mm measured during the test. The service crack width limit of 0.3 mm was reached at 1.25 of the design load.

7.2.3.7 Summary of results: The deflection limit of span/250 was reached at 0.81 of the design load and the crack width limit of 0.3 mm was reached at 1.25 of the design load. The first yield occurred at 1.4 of the design load. Finally the ultimate load was much higher than the design load. This is because more steel had bean used than required. This is may be due to the defect in the approximation method (see section (6.2)) to get the actual area of steel from the design area of steel, see Figs (6.4.1) and (6.4.2). Further discussion on

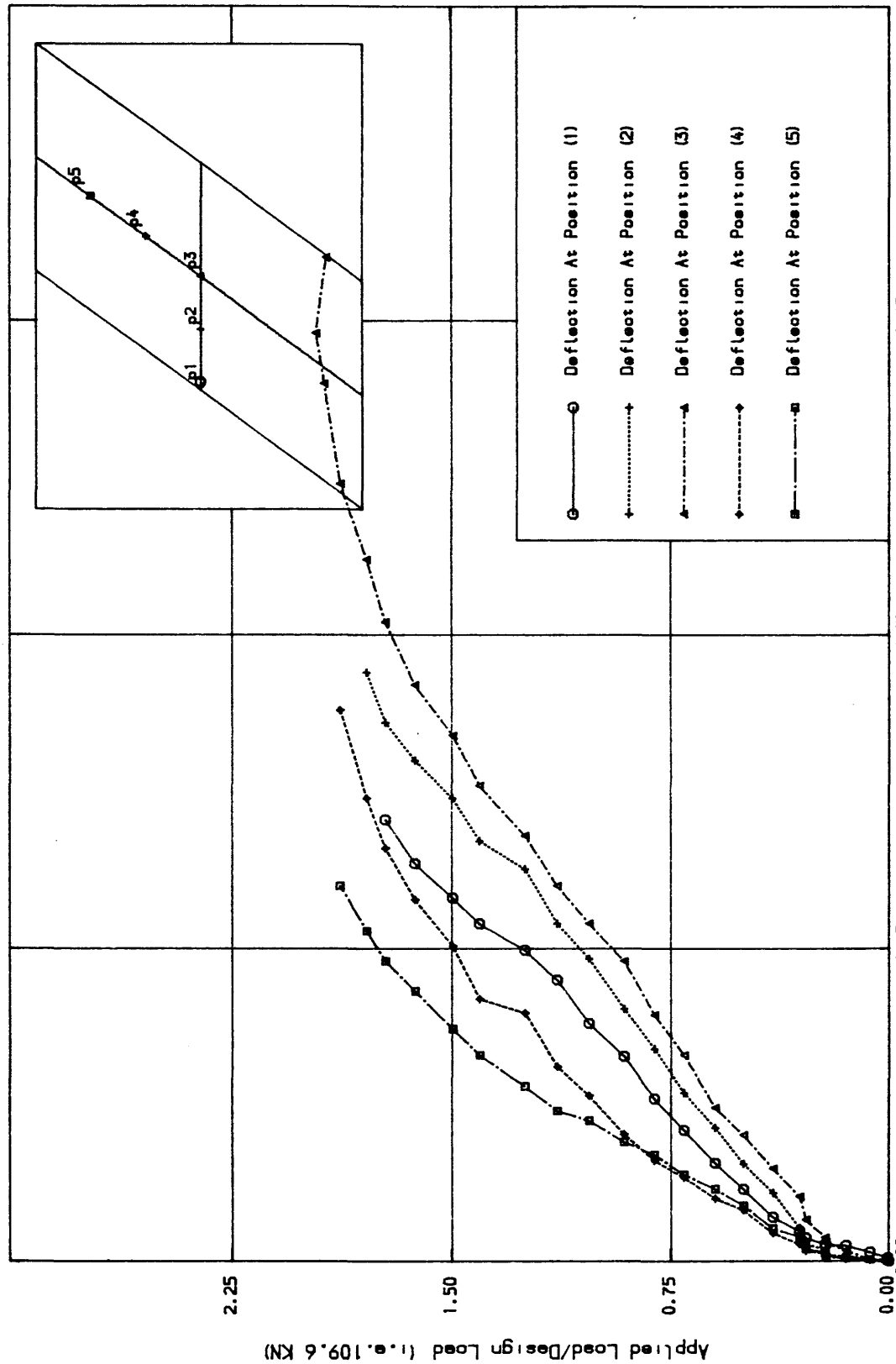

Fig. (7.19) Load-Deflection curves for MODEL NO. THREE

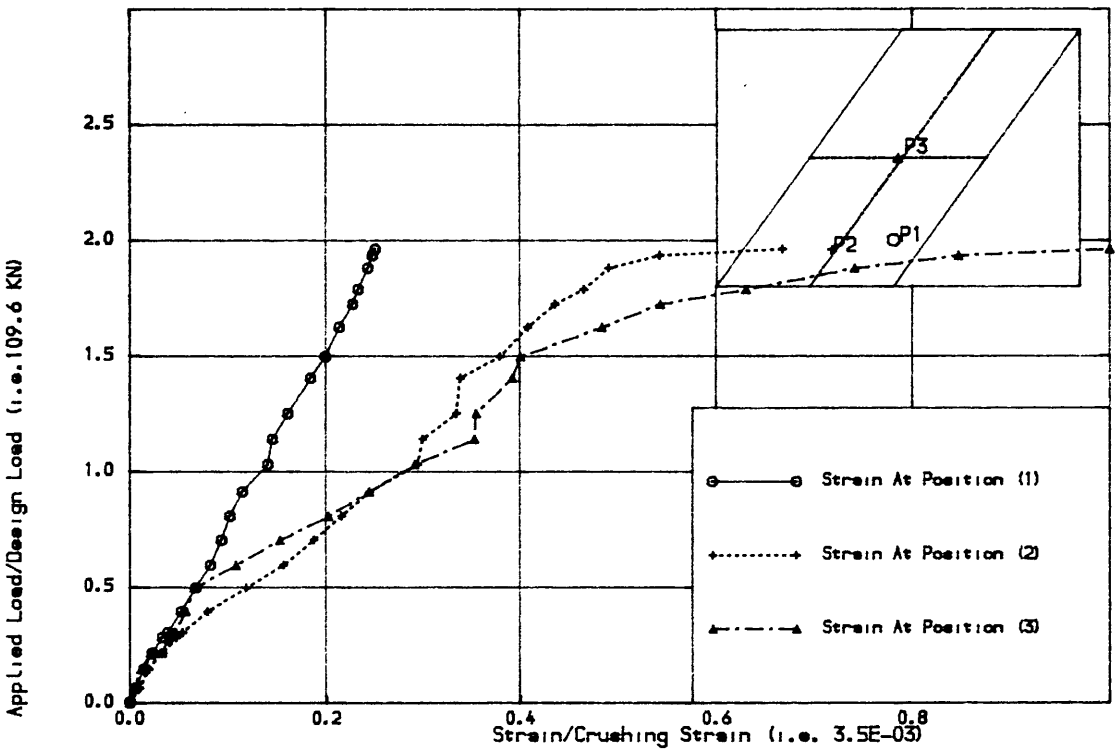

Fig. (7.21) Load-Concrete Strain curves at top surface for MODEL NO. THREE

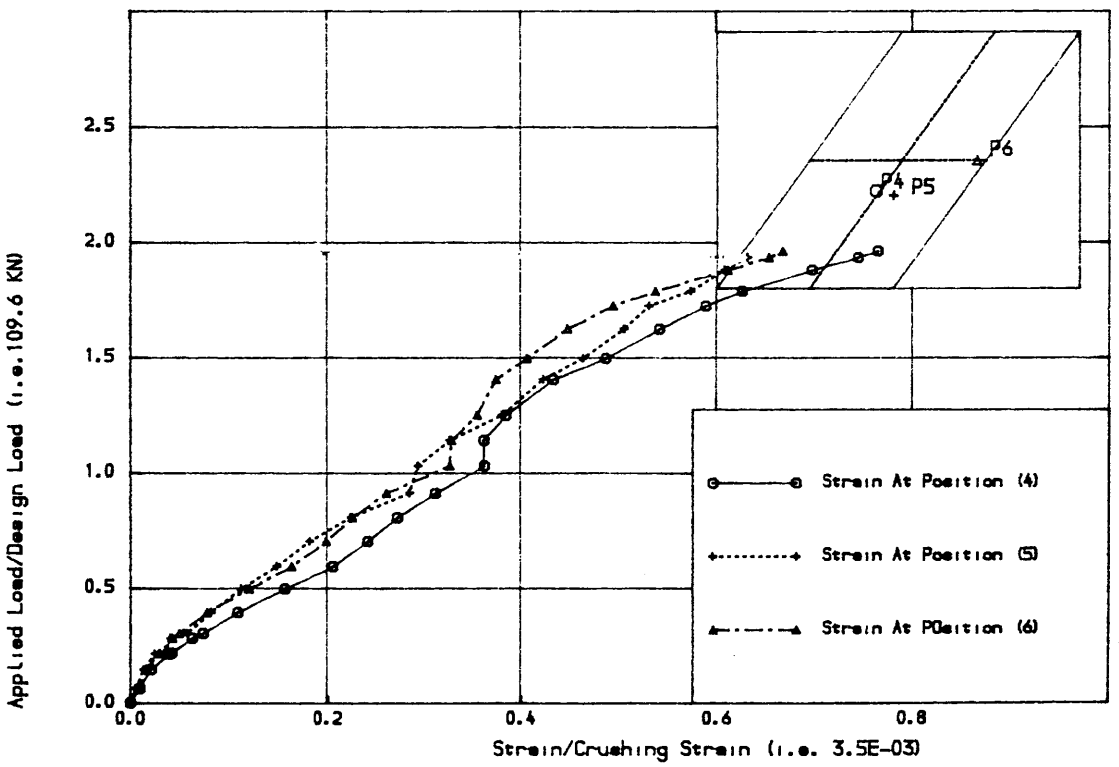

Fig. (7.22) Load-Concrete Strain curves at top surface for MODEL NO. THREE

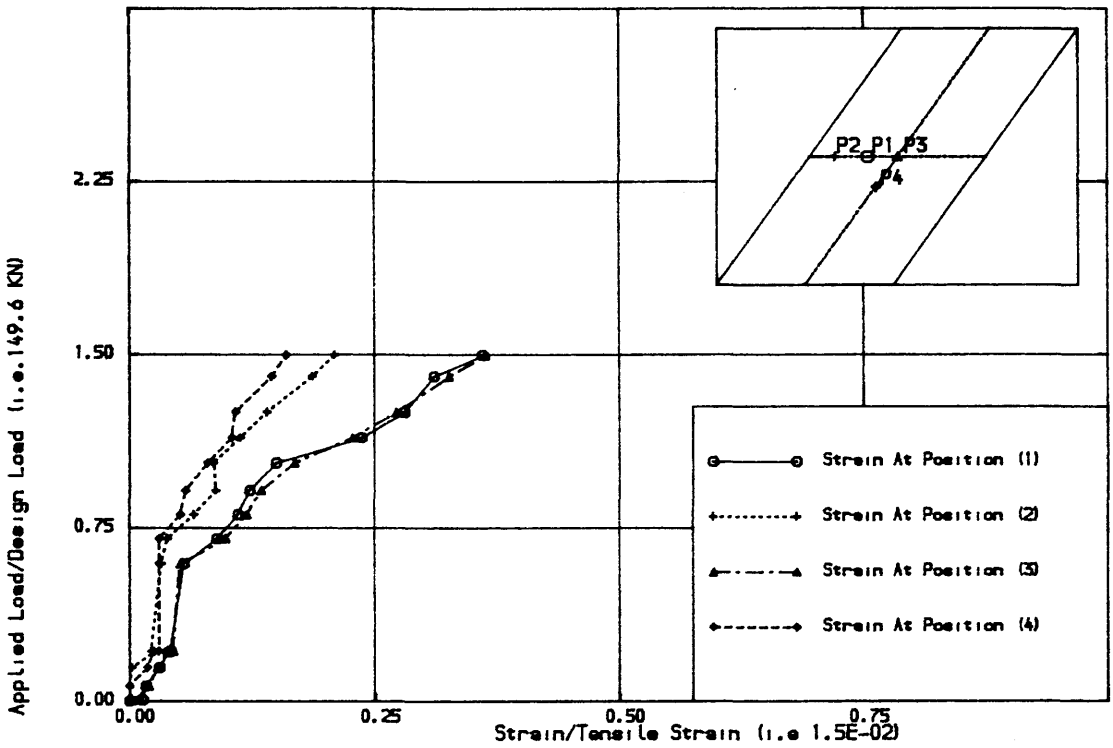

Fig. (7.23) Load-Concrete Strain curves at bottom surface for MODEL NO. THREE

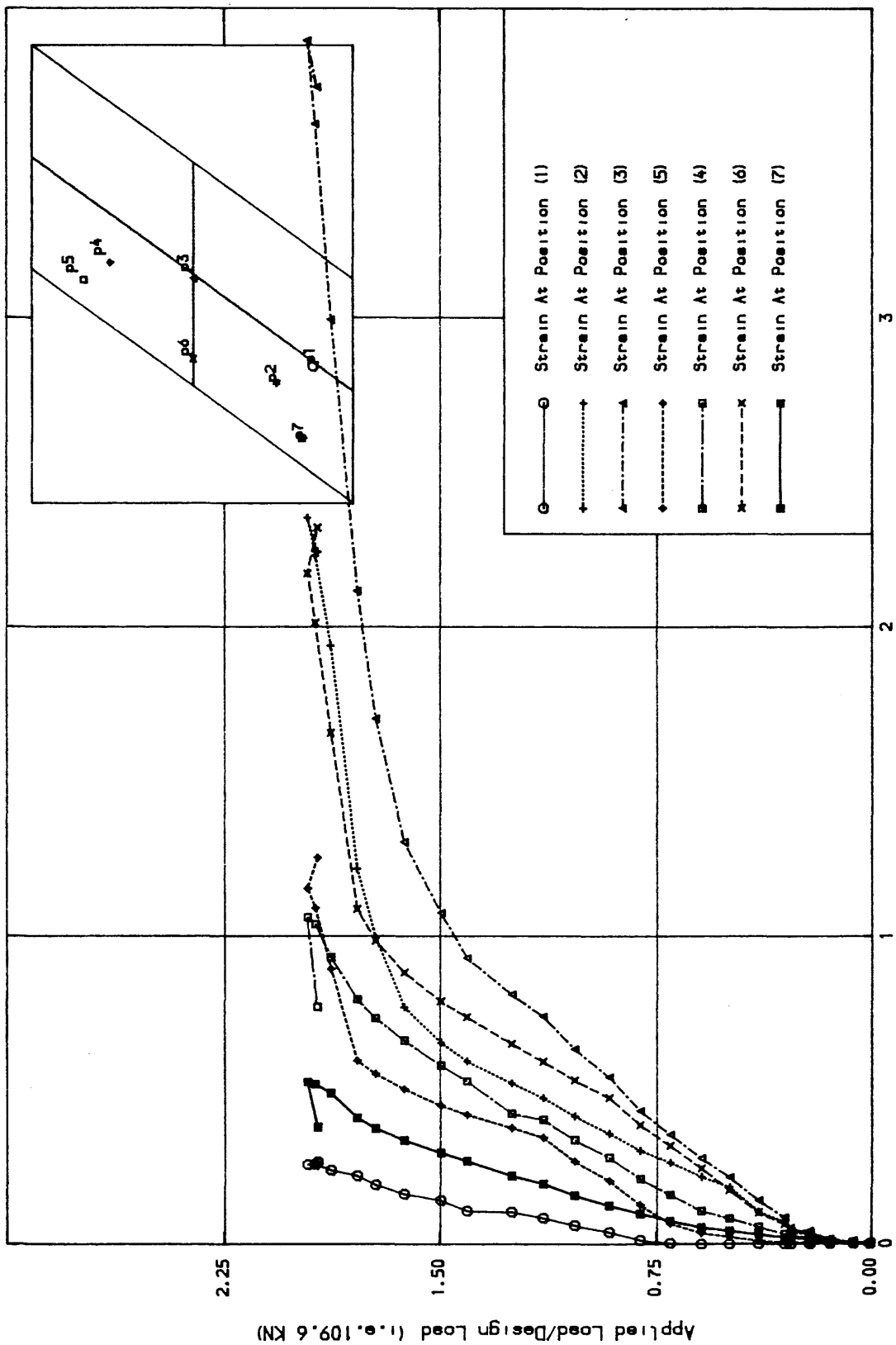

Fig. (7.24) Load-Steel Strain curves in the longitudinal direction for MODEL NO. THREE

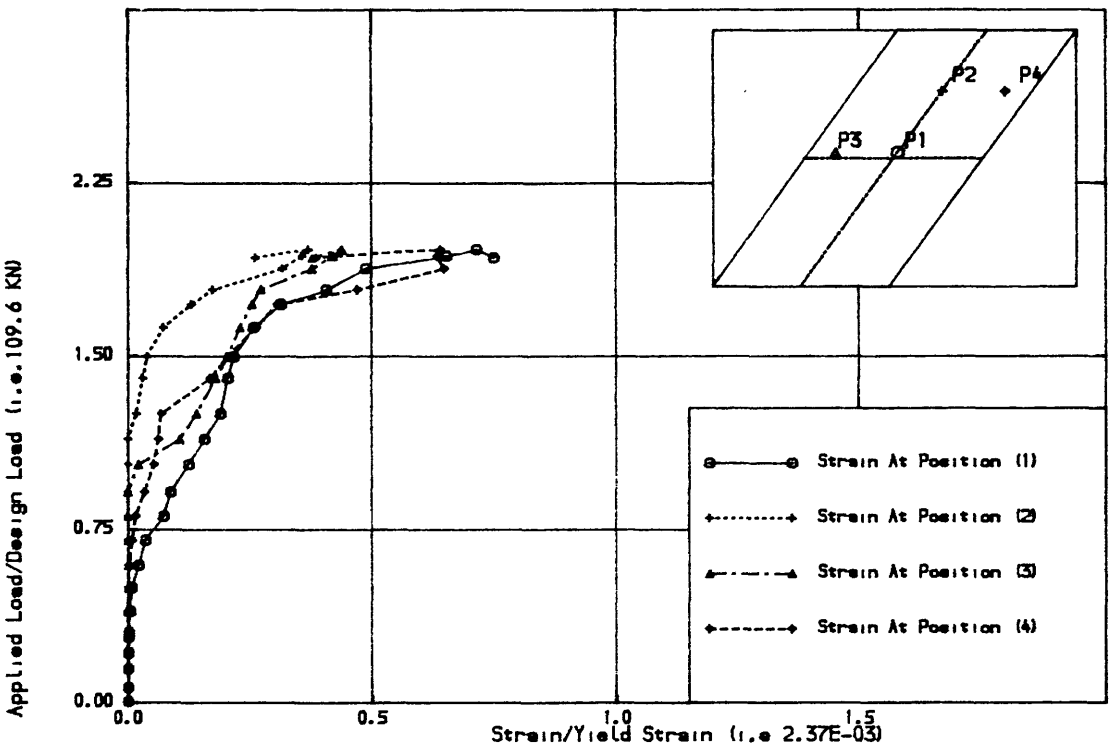

Fig. (7.25) Load-Steel Strain curves in the transverse direction for MODEL NO. THREE

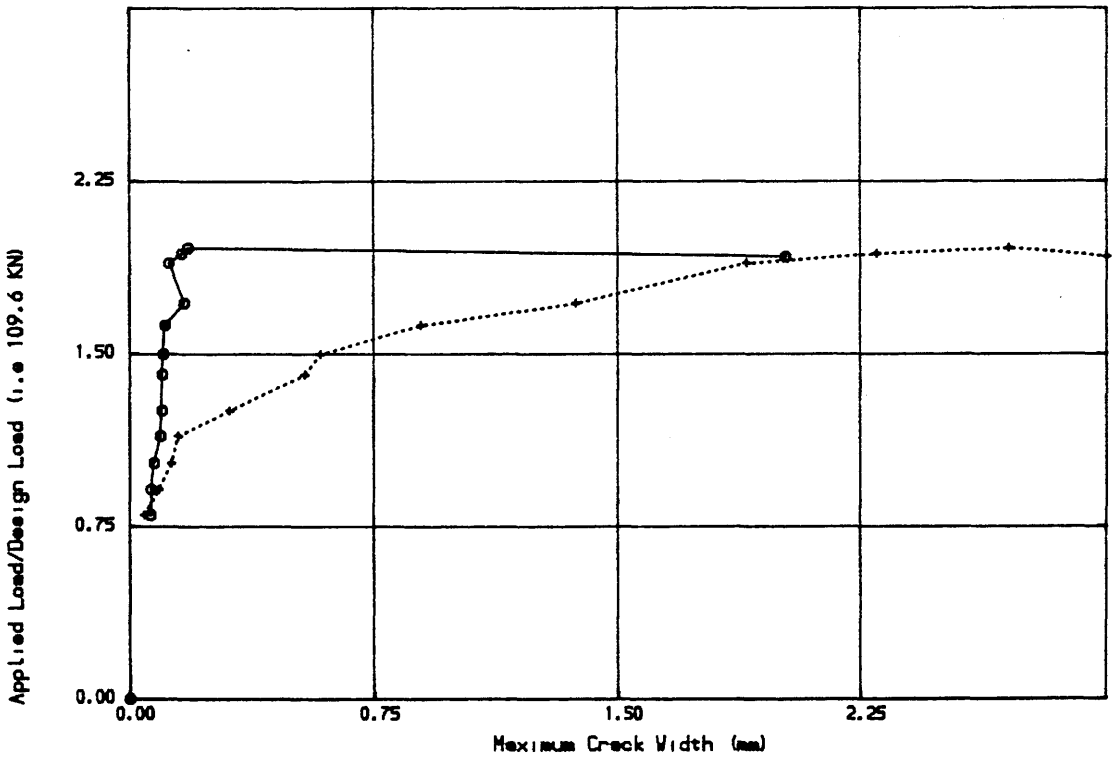

Fig. (7.26) Load-Maximum crack widths at various points for MODEL NO. THREE

this aspect will be given in Chapter eight section (8.3).

7.2.4 Model Skew Slab Number Four

7.2.4.1 Slab Properties: This model was similar to the previous model (model number three) except that the longitudinal steel and the transverse steel were orthogonal and parallel to the supported edges respectively. Table (7.1) identifies the Tables and Figures which define the slab geomety and configuration. Table (7.2) gives the slab material properties.

7.2.4.2 Response of the slab: Initial cracks were observed at the centre bottom surface of slab at 0.29 of the design load. A series of parallel cracks at 15^{o} to the supported edge and at spaced of 90 mm were dominant on the bottom surface at midspan and propagated from the centre towards both the free edges. As the load increased the bottom surface cracking spread towards the slab middle area. Minor cracks appeared near the obtuse corners at 0.45 of the design load. At 0.58 of the design load, cracks at the top face at obtuse corner were observed. Further loading caused one of these cracks to extend to the opposite corner near to the obtuse corners. At 0.65 of the design load, minor inclined cracks propagated from the bottom surface through the depth of the slab at the free edge . At 0.9 of the design load, the large crack at top face suddenly extended to the form shown in Fig. (7.28). This signified the failure of the slab. Although the actual steel was slightly higher than

the design steel,(see Figs (6.4.1) and (6.4.2)) shear strength using CP110 rules had been checked indicating no need shear for reinforcement, the slab still failed to reach the ultimate load. Soffit crack pattern is shown in Fig. (7.27) and the top surface crack pattern is shown in Fig. (7.28).

7.2.4.3 Deflection: Measured centre line deflection at different positions are shown in Fig. (7.29). It can be seen that the nonlinearity started at 0.24 of the design load and the serviceability limit of deflection was reached at 0.57 of the design load.

7.2.4.4 Concrete strains: Figs (7.30) and (7.31) show respectively concrete strains at top, and bottom surface. The maximum concrete strain occurred at positions (1), (2) and (4) (in the centre area) was 0.55 of the concrete crushing strain.

7.2.4.5 Steel Strain: Load-Strain in the steel for longitudinal direction is shown in Fig. (7.32). The maximum strains were at the centre of the slab and near the obtuse corner. The steel started to yield at 0.6 of the design load. At other positions the steel did not yield. The load- steel strain curves in the transverse direction is as shown in Fig. (7.33), the steel at positions (1) near the obtuse corner and at (3) near the centre steel yielded at 0.8 design load. At position (1) due to the large crack which started to appear at 0.79 of the design load, a large strain occurred indicating the imminence of failure.

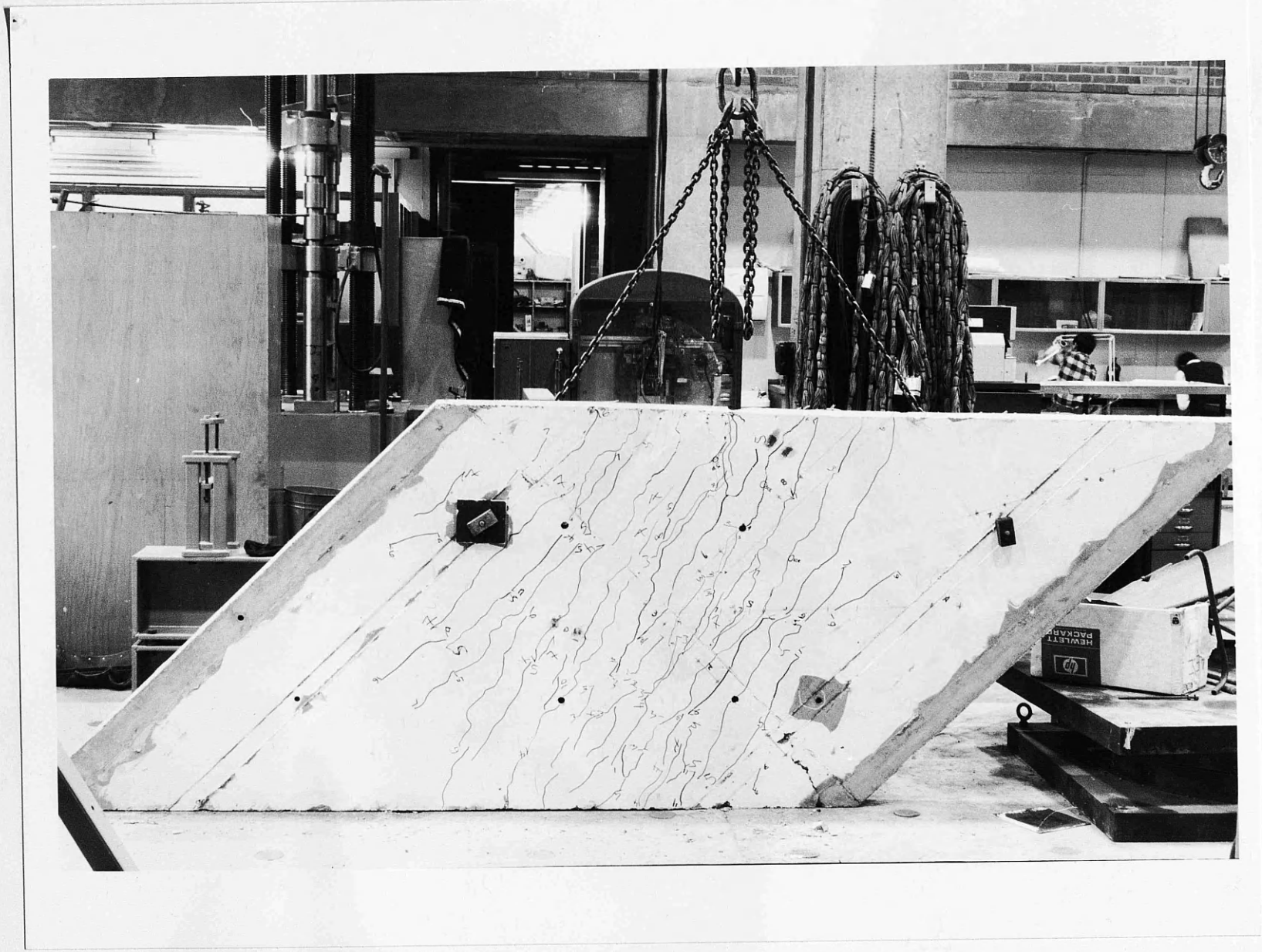

Fig. (7.27) MODEL SKEW SLAB NO. (4) Soffit crack pattern after failure

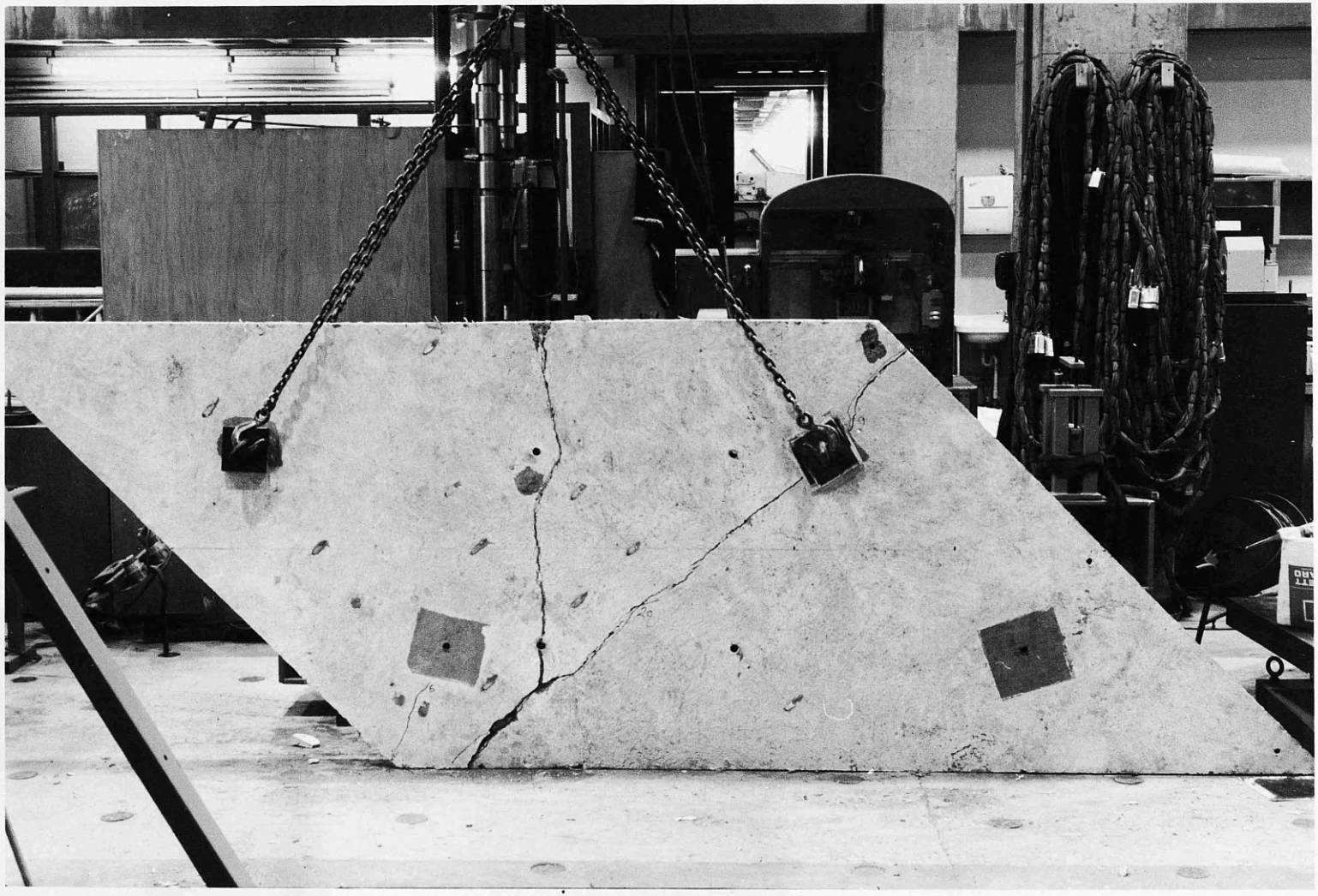

Fig. (7.28) MODEL SKEW SLAB NO. (4) Top surface after failure

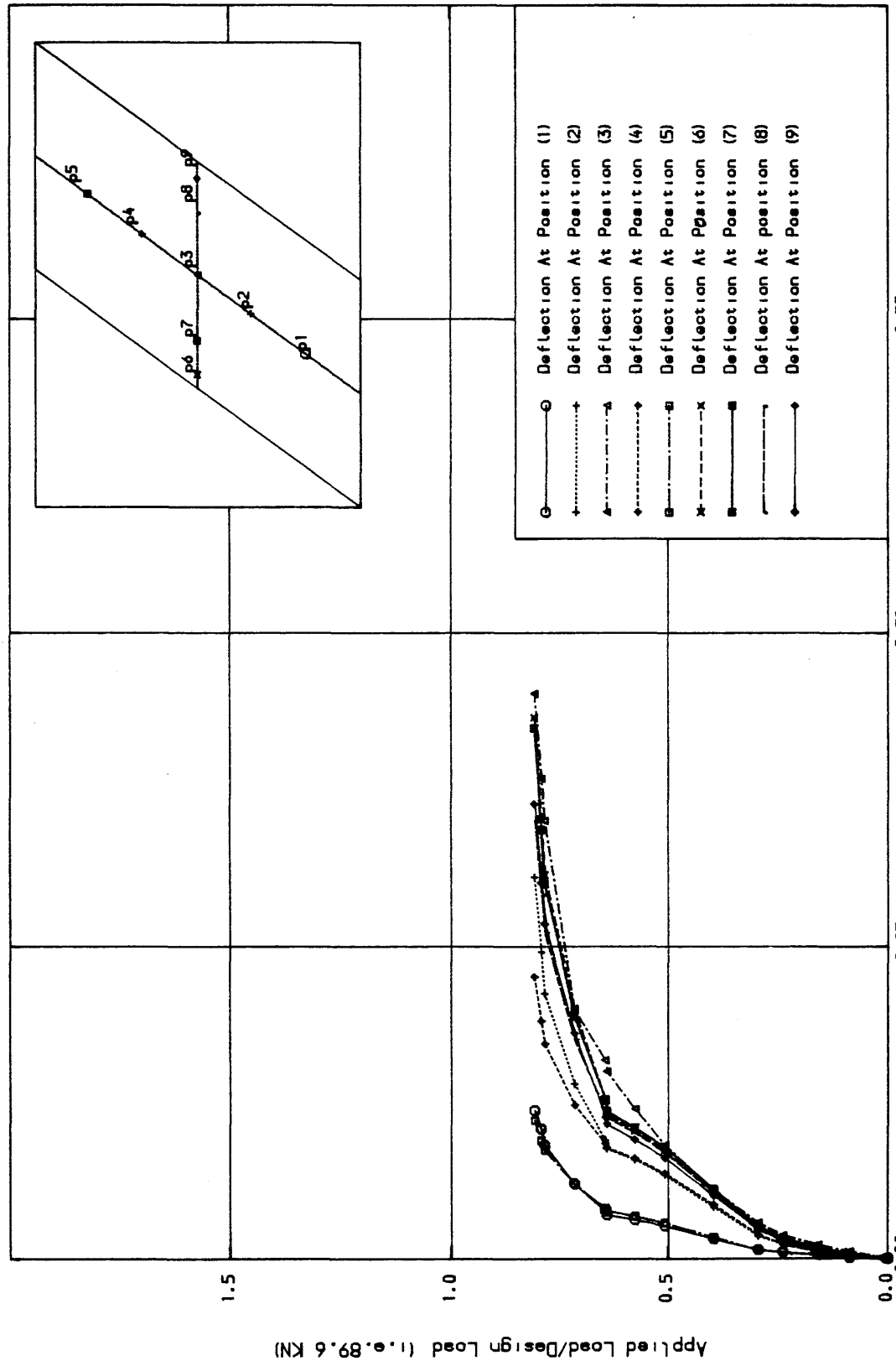

Fig. (7.29) Load-Deflection curves for MODEL NO. FOUR

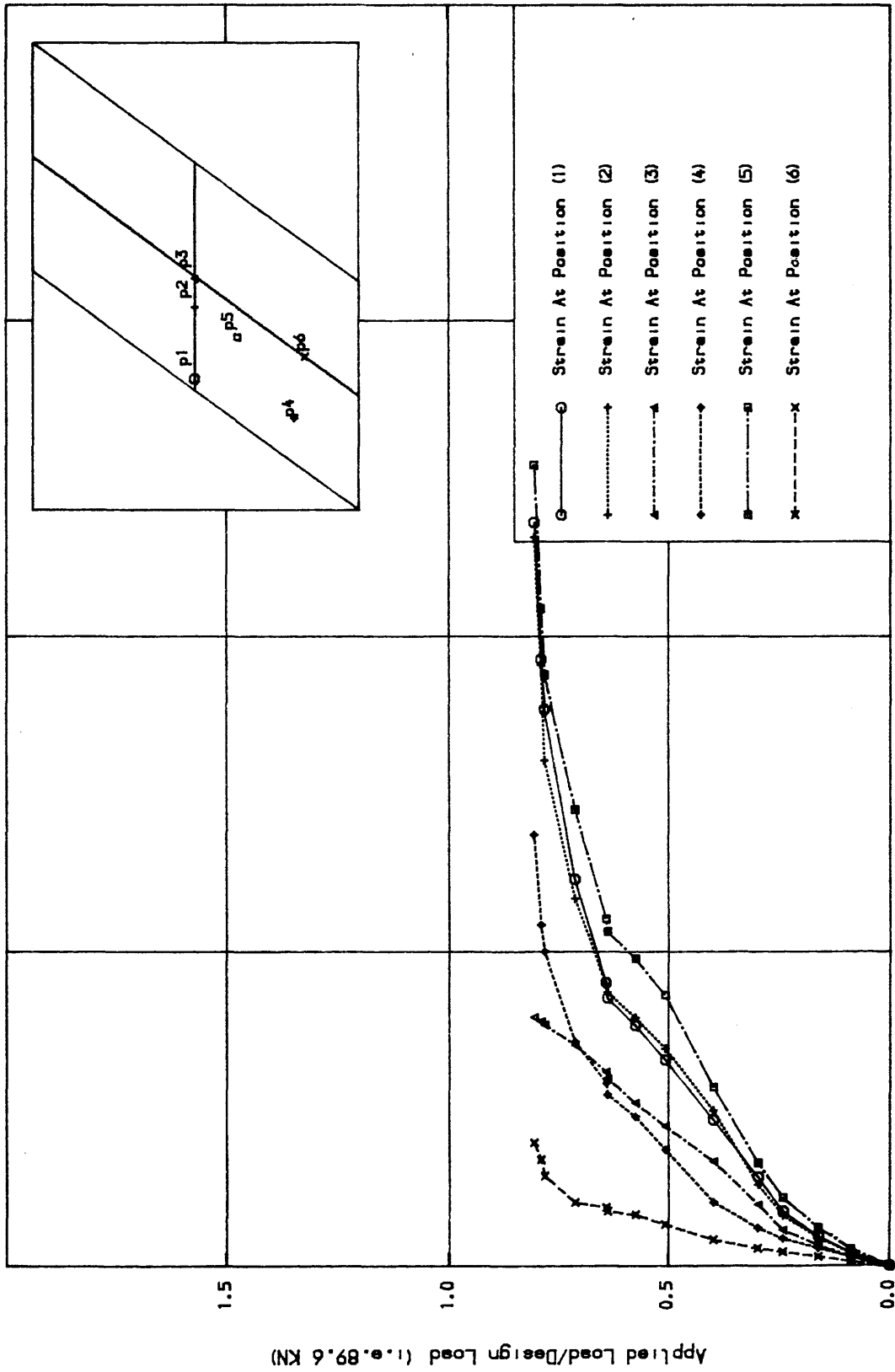

Fig. (7.30) Load-Concrete Strain curves at top surface for MODEL NO. FOUR

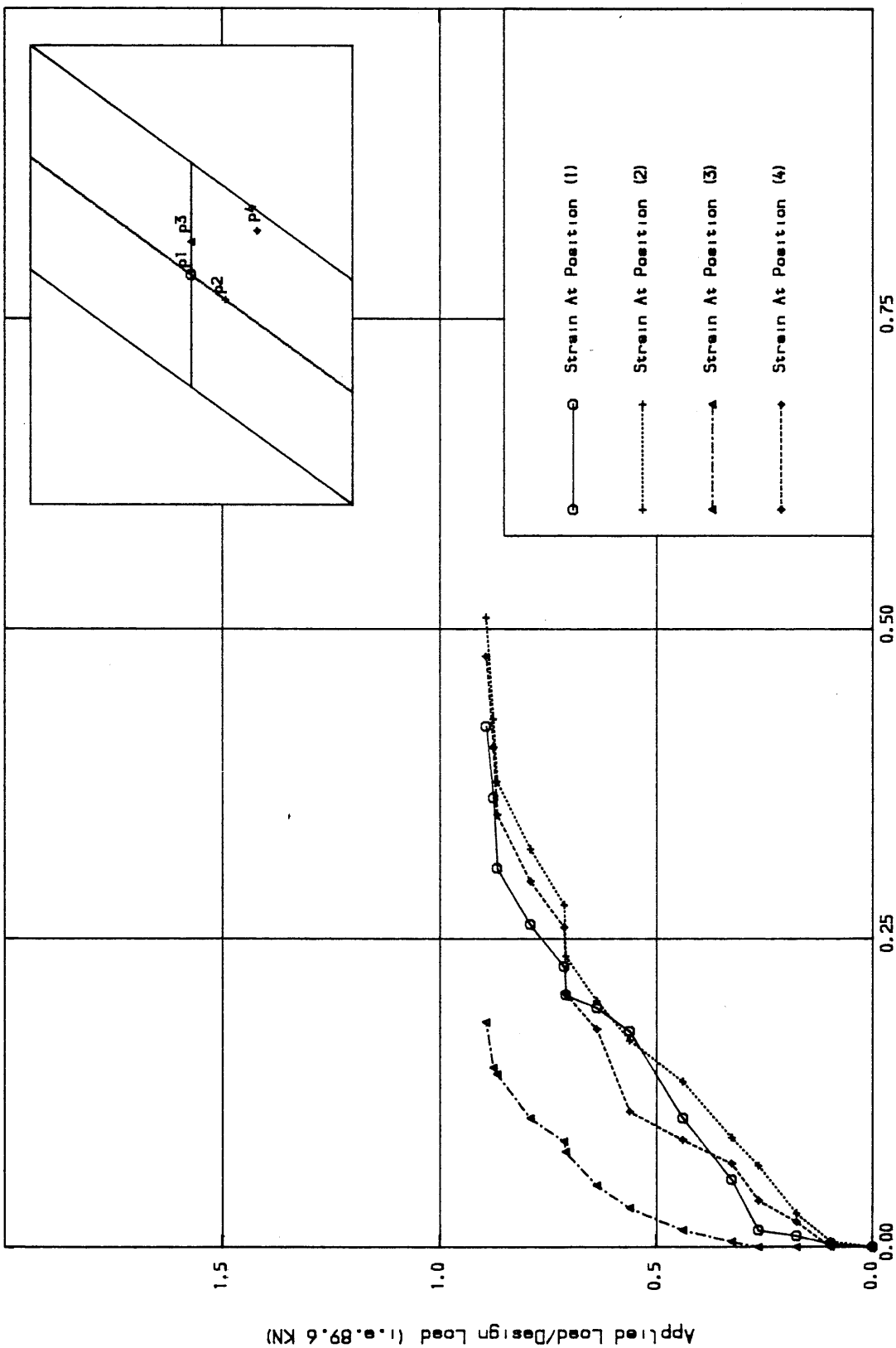

Fig. (7.31) Load-Concrete Strain curves at the bottom surface for MODEL NO FOUR

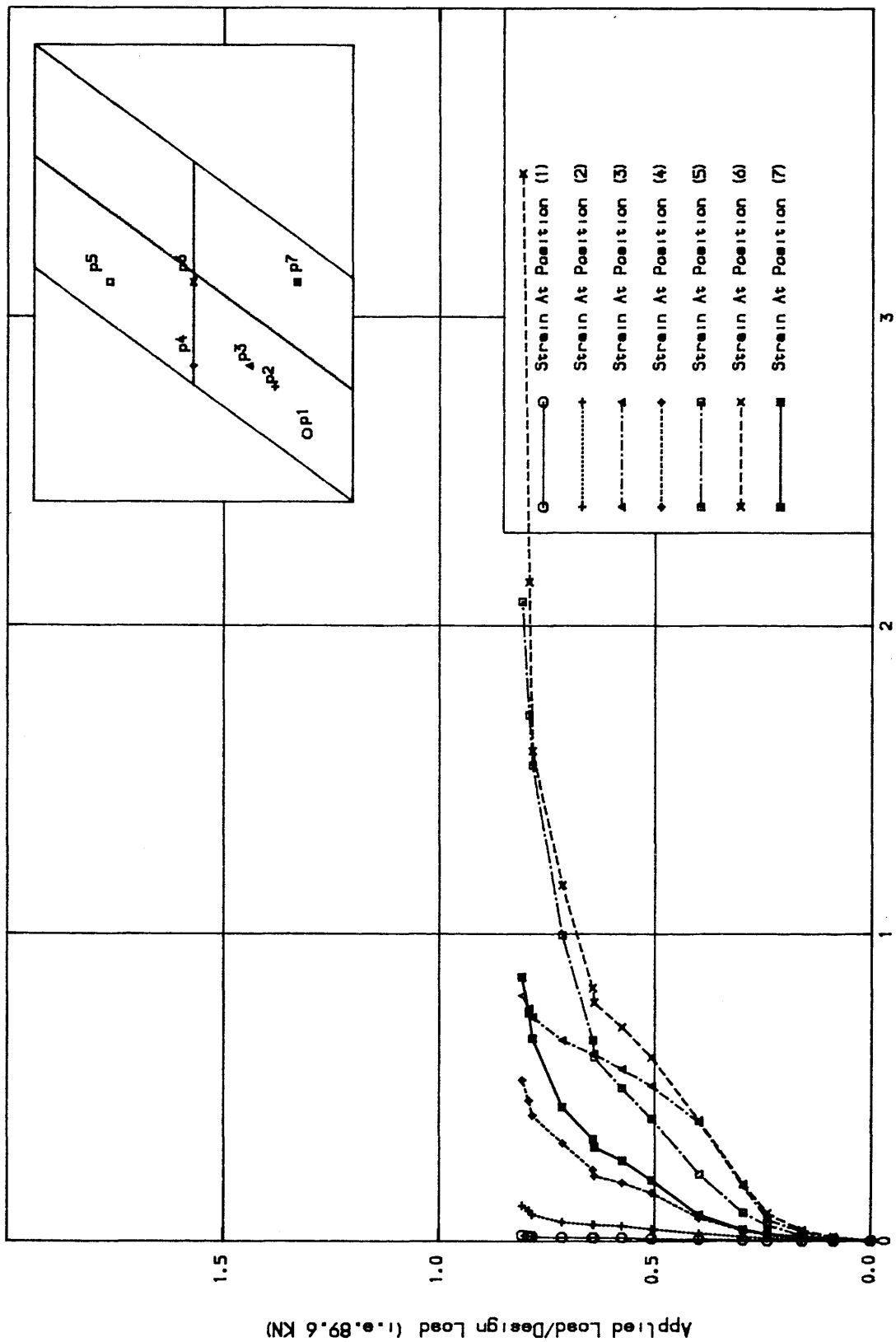

Fig. (7.32) Load-Steel Strain curves in the longitudinal direction for MODEL NO. FOUR

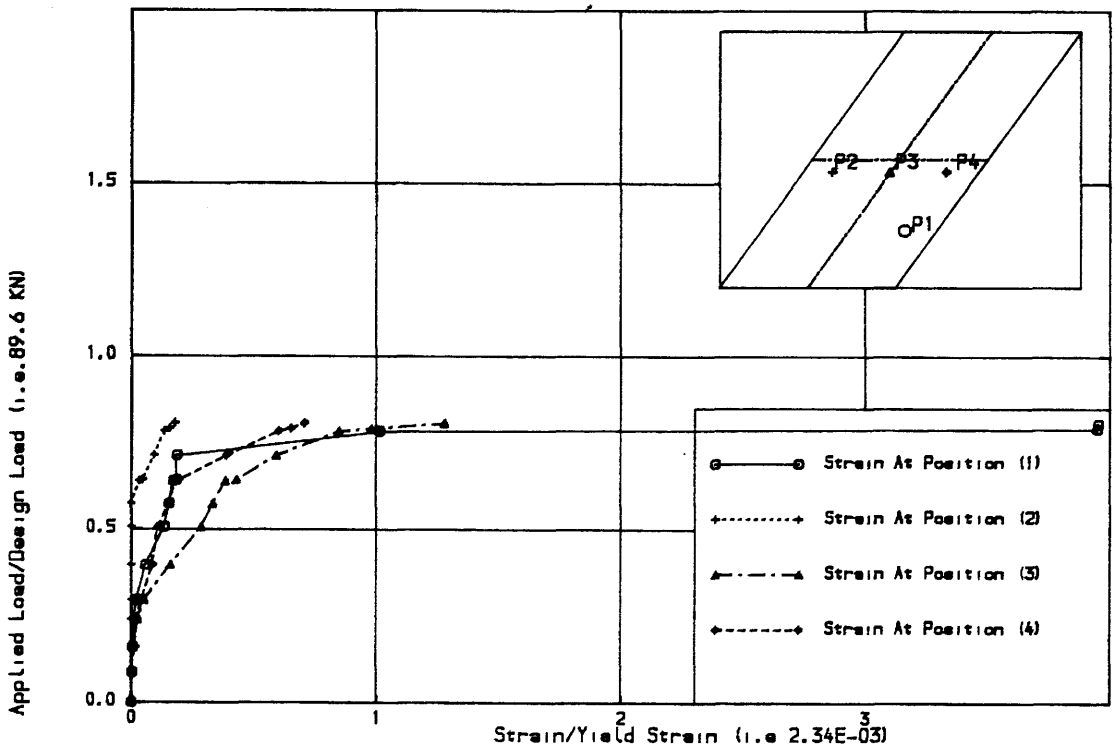

Fig. (7.33) Load-Steel Strain curves in the transverse direction for MODEL NO. FOUR

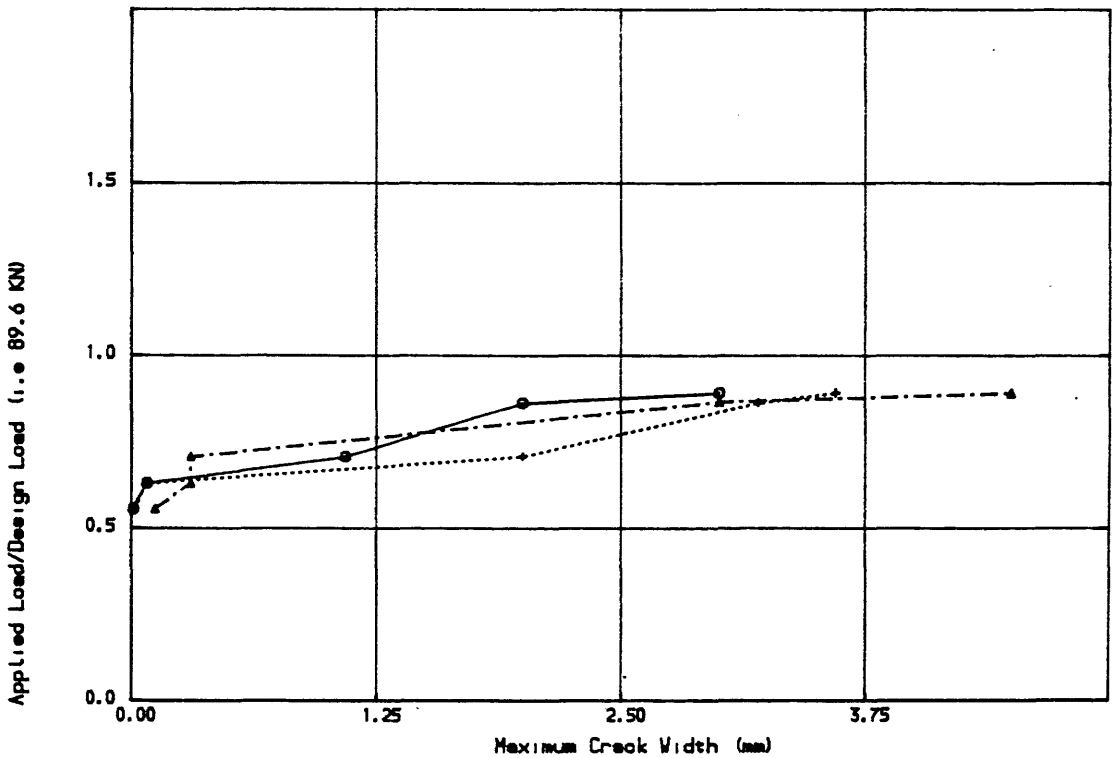

Fig. (7.34) Load-Maximum crack widths at various points for MODEL NO. FOUR

7.2.3.6 Soffit Crack Width: Fig. (7.34) gives the approximate maximum crack width. It can be seen from Fig. (7.34) that the service limit crack width of 0.3 mm was reached at 0.63 of the design load.

7.2.4.7 Summary of Results: The serviceability limit of deflection of span/250 was reached at 0.57 of the design load and the service crack width of 0.3 mm was reached at 0.63 of the design load. The steel yielded in the longitudinal direction at 0.6 of the design load. Unexpected type of failure, may be due to failure in bound.

7.2.5 Model Skew Slab Number Five

7.2.5.1 The properties of the slab: This model was similar (see Table (6.1) Chaptre six) to the previous two models (number three with skew steel and number four with orthogonal steel parallel and orthogonal to the supported edge) except that the longitudinal steel and transverse steel were parallel and orthogonal to the free edge. Table (7.1) identifies the Tables and Figures which define the slab geomety and configuration. Table (7.2) gives the slab material properties.

7.2.5.2 Response of The Slab: Initial cracks were observed on the bottom surface at centre of the slab at 0.24 of the design load. Parallel cracks were dominant on the bottom surface at midspan area and propagated from centre towards both free edges roughly parallel to the

lines of support and at a spacing of about 75.0 mm. As the load increased, more bottom surface cracking appeared near the centre of the slab. Inclined cracks progressing from the bottom surface through the depth of slab could be observed at the free edges at 0.38 of the design load. Short lengths of cracks initiated at 0.4 of the design load and grew parallel to the initially established cracks in the centre area. At 0.49 of the design load, the bottom surface cracking spread towards the obtuse corners. At 0.6 of the design load, cracks in the top surface near the obtuse corners were noticed. At 0.96 of the design load bottom surface cracks began to spread towards the acute corner when more cracks were observed on the top surface at the obtuse corners. The slab behaved as expected up to 1.1 of the design load and it appeared that the slab was about to fail. As the slab deformed a shear crack opened suddenly at one of the obtuse corners right through the depth of the slab, and the slab failed. Figs (7.35) and (7.36) show respectively soffit crack pattern and top surface crack.

7.2.5.3 Deflection: It can be seen from Figs (7.37) and (7.38) that at 0.27 of the design load, the nonlinearity was induced by initial cracking. In the subsequent three load increments, the curves remained horizontal indicating that additional material damage was relatively large. After that, the slab stiffened due to the reinforcement participating in the resistance. Deflection equal to span/250 was reached at 0.52 of the design load. The distribution of the midspan deflections is as shown in Fig. (7.37) which indicate clearly that the slab

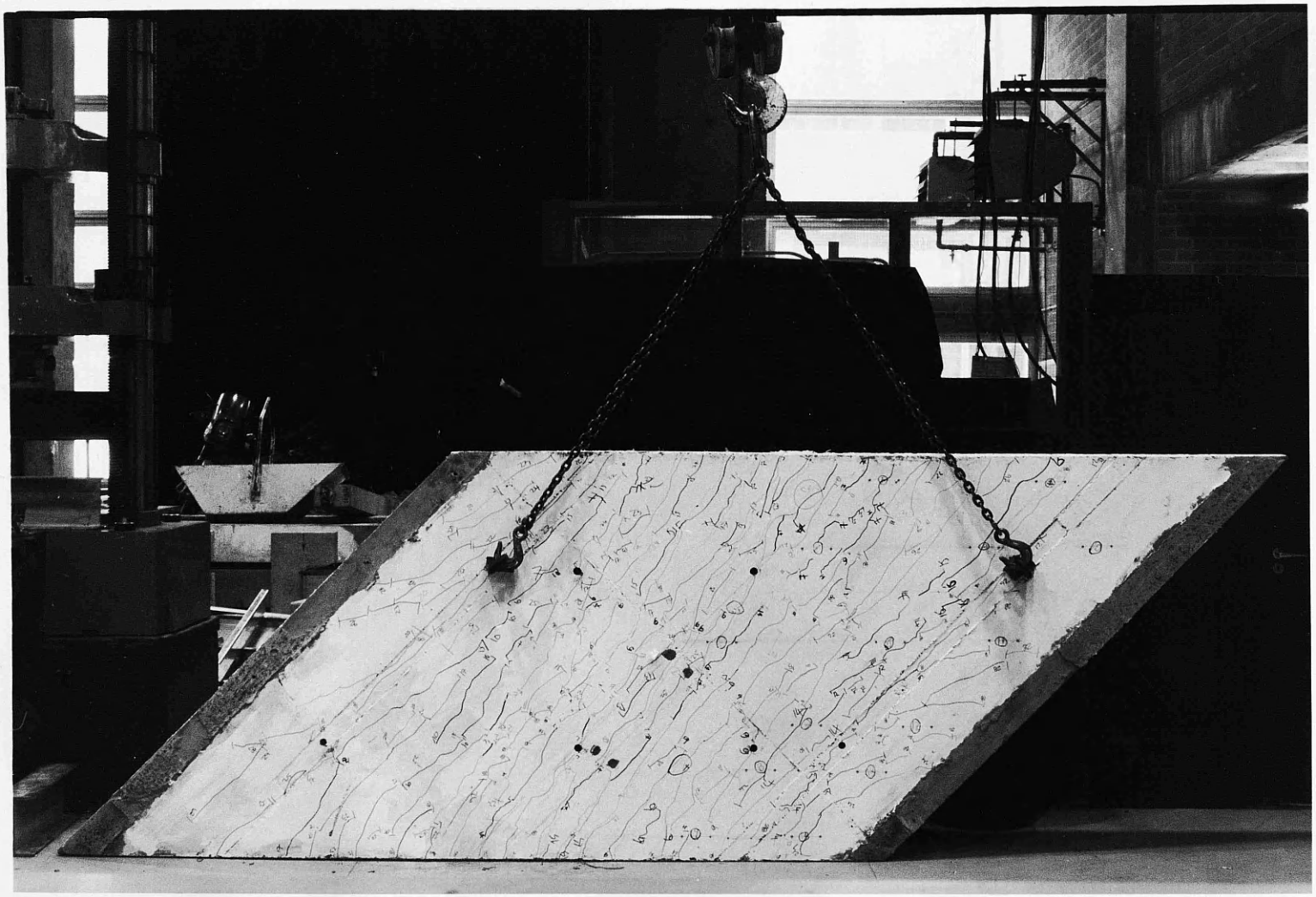

Fig. (7.35) MODEL SKEW SLAB NO. (5) Soffit crack pattern after failure

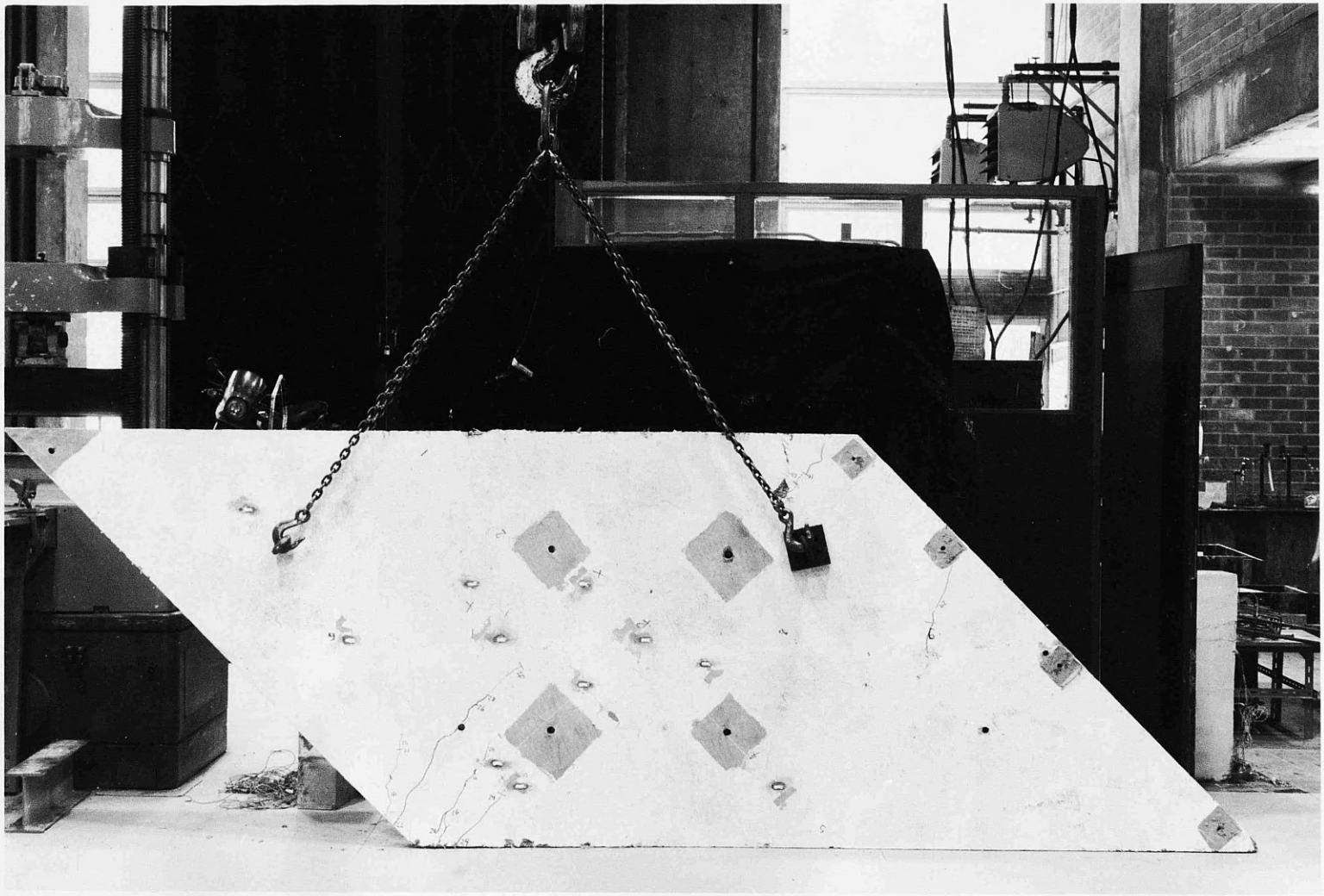

Fig. (7.36) MODEL SKEW SLAB NO. (5) Top surface after failure

behaved as a simply supported beam. In general, the load-deflection curves indicate that the slab behaved in a ductile manner up to failure.

7.2.5.4 Concrete Strain: Measured bottom surface strains in the concrete in the direction of the longitudinal steel are represented in Fig. (7.40). It can be seen from these curves that the general behaviour was similar to the overall behaviour of the slab as indicated by deflection. Also the general behaviour was as expected viz maximum strains occurred near the centre line A-B of the slab and strains were less significant near the obtuse corners. The measured top surface strains during load are represented in Fig. (7.39). At failure, the maximum compression strain at the centre of the slab was 0.94 of the crushing strain.

7.2.5.5 Steel Strains: Measured strains in longitudinal and transverse steel are shown in Figs (7.41), (7.42) and (7.43). It can be seen from Fig. (7.41) that the general behaviour of longitudinal steel was similar to the overall behaviour of the slab. The nonlinearity started at 0.35 of the design load. At 0.78 of the design load, the steel at locations (2, 4, 6 and 8) in the centre area of the slab yielded. As the load increased, steel at other positions (1,5 and 9) yielded. Just before failure the steel yielded everywhere except near the acute corners where steel did not yield but still recorded significantly large strains. The measured steel strains in transverse direction during load

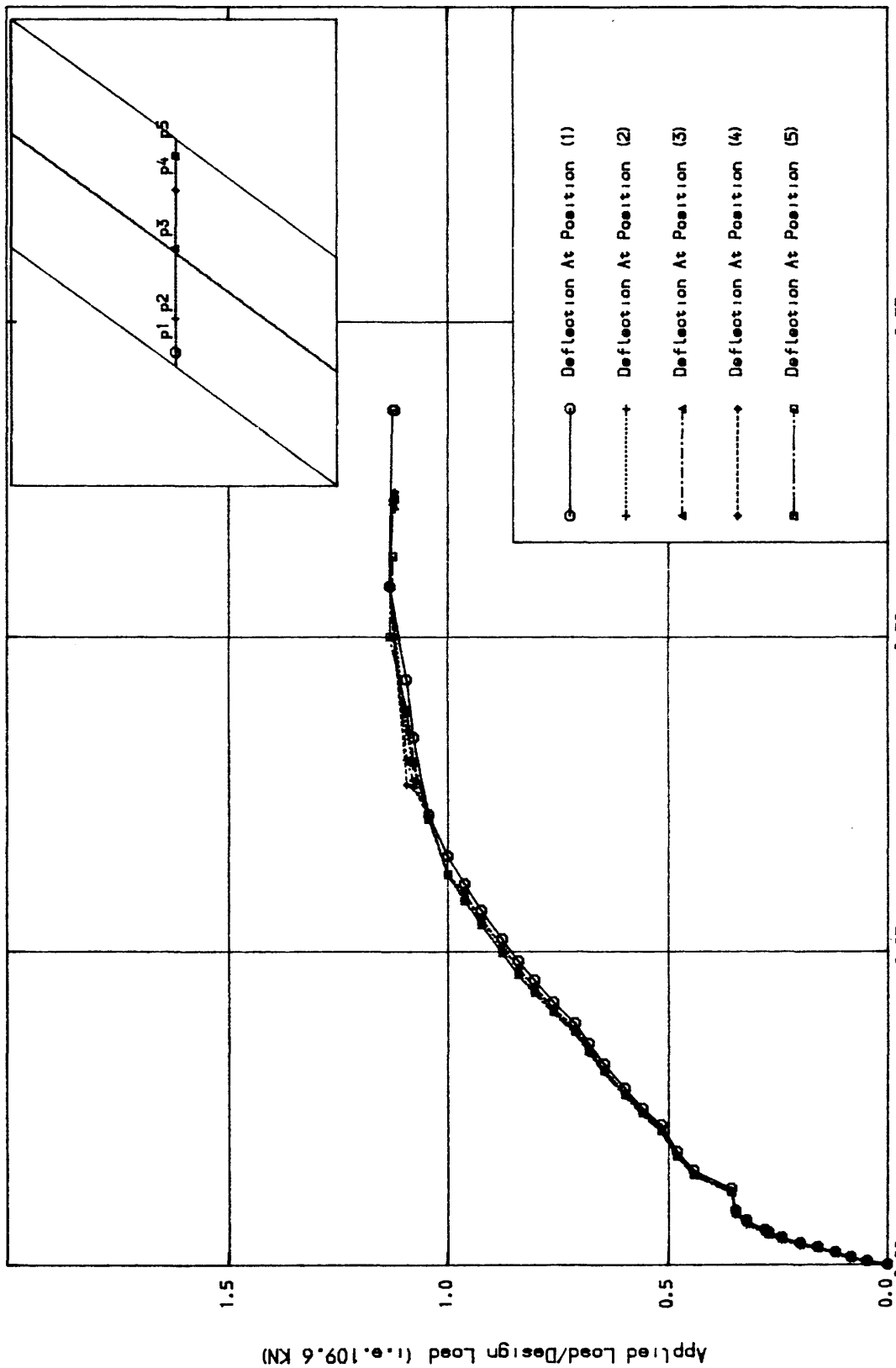

Fig. (7.37) Load-Deflection curves along the centre line A-B for MODEL NO. FIVE

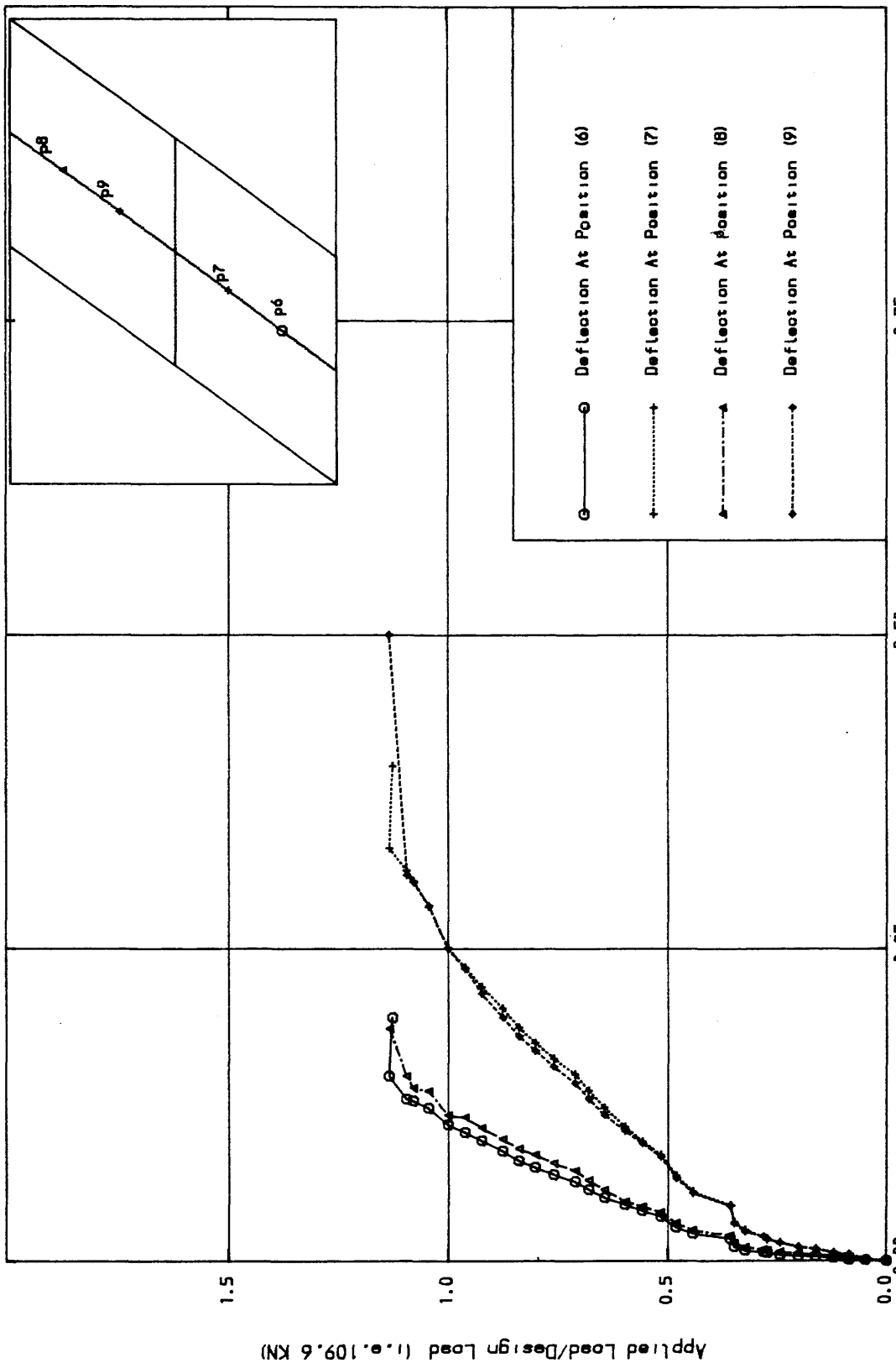

Fig. (7.38) Load-Deflection curves along the centre line C-D for MODEL NO. FIVE

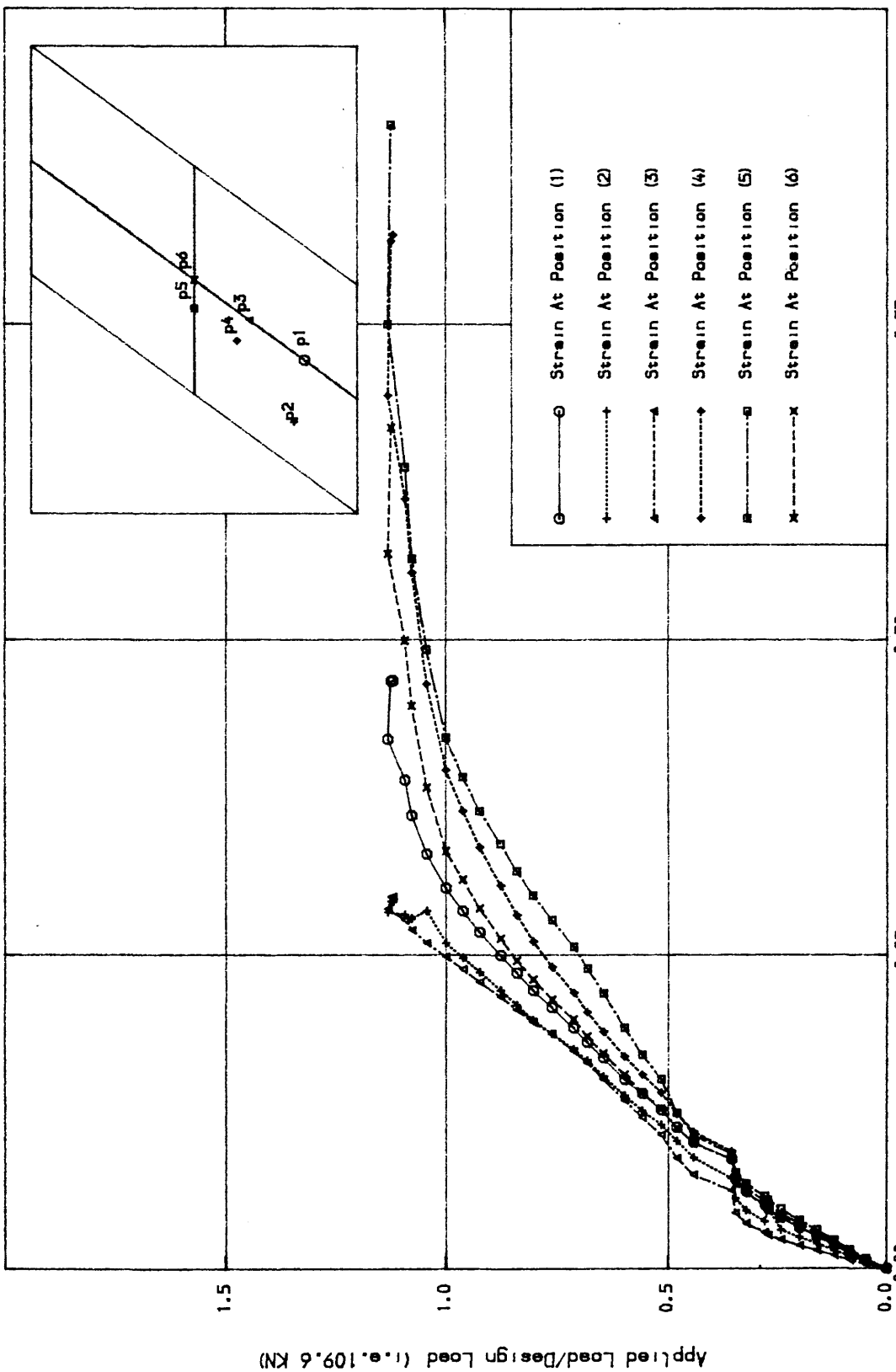

Fig. (7.39) Load-Concrete Strain curves in the longitudinal direction at top surface for MODEL NO. FIVE

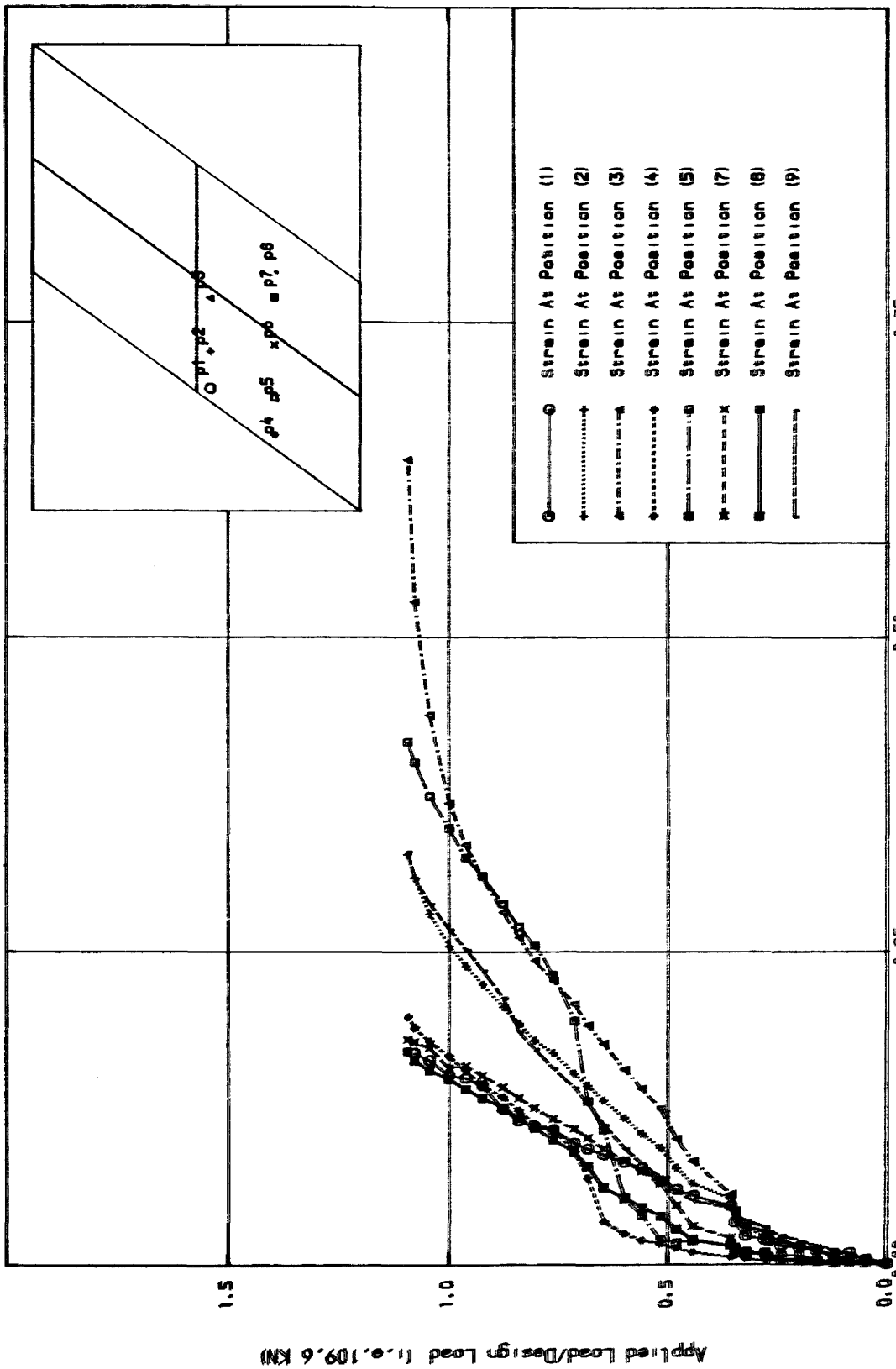

Fig. (7.40) Load-Concrete Strain curves in the longitudinal direction at bottom surface for MODEL NO. FIVE

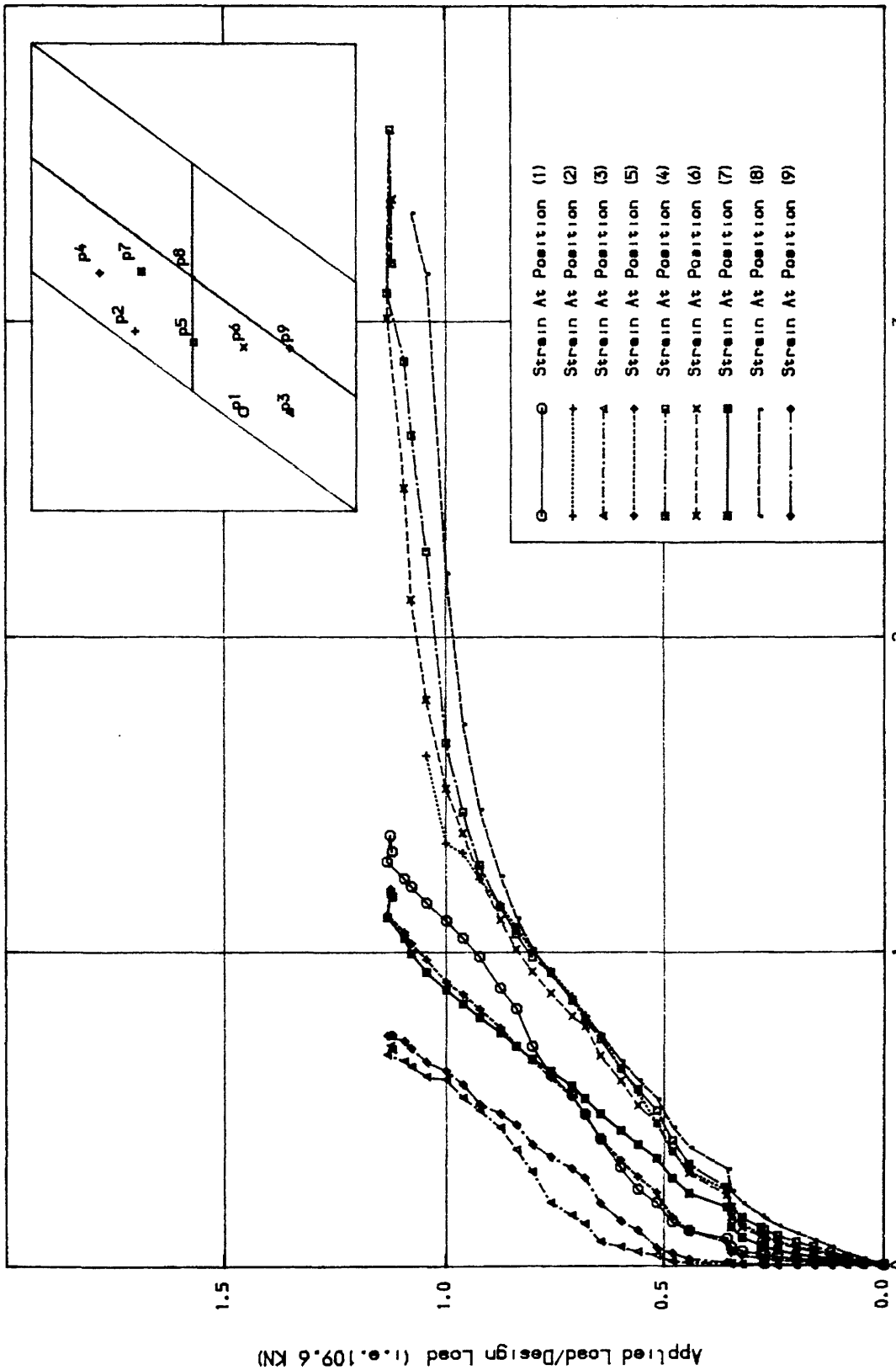

Fig. (7.41) Load-Steel Strain curves in the longitudinal direction for MODEL NO. FIVE.

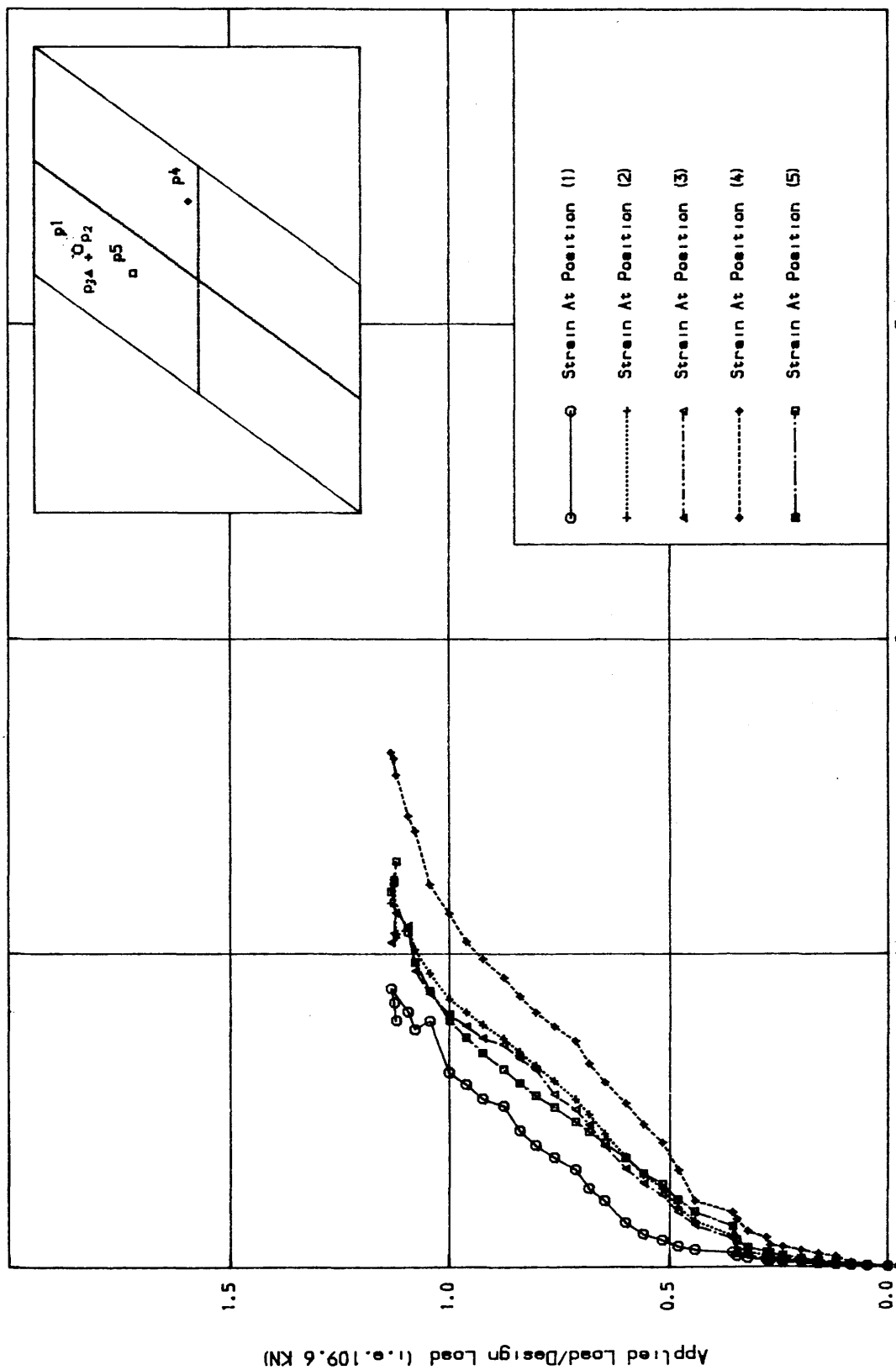

Fig. (7.42) Load-Steel Strain in the transverse direction for MODEL NO. FIVE

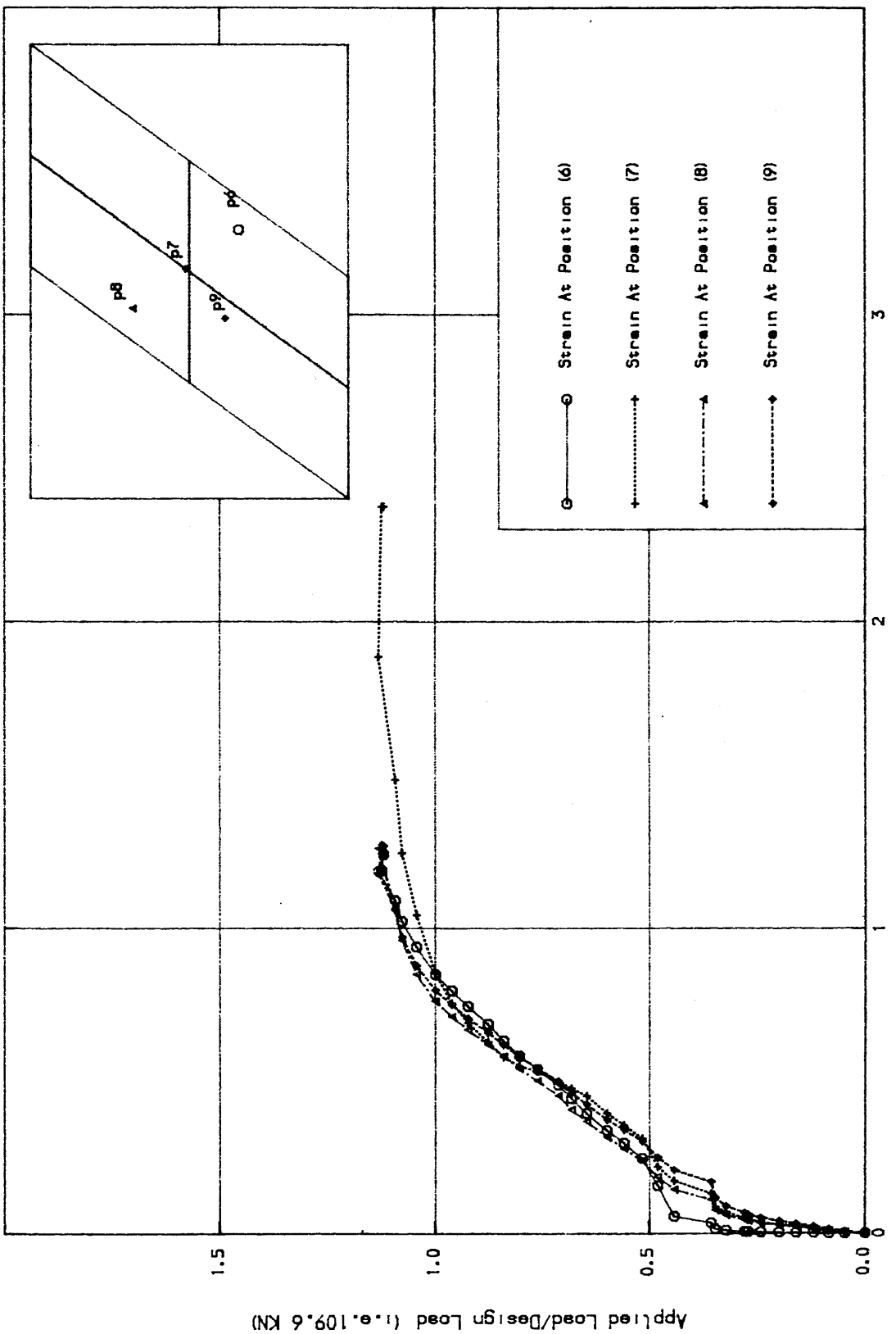

Fig. (7.43) Load-Steel Strain curves in the transverse direction for MODEL NO. FIVE

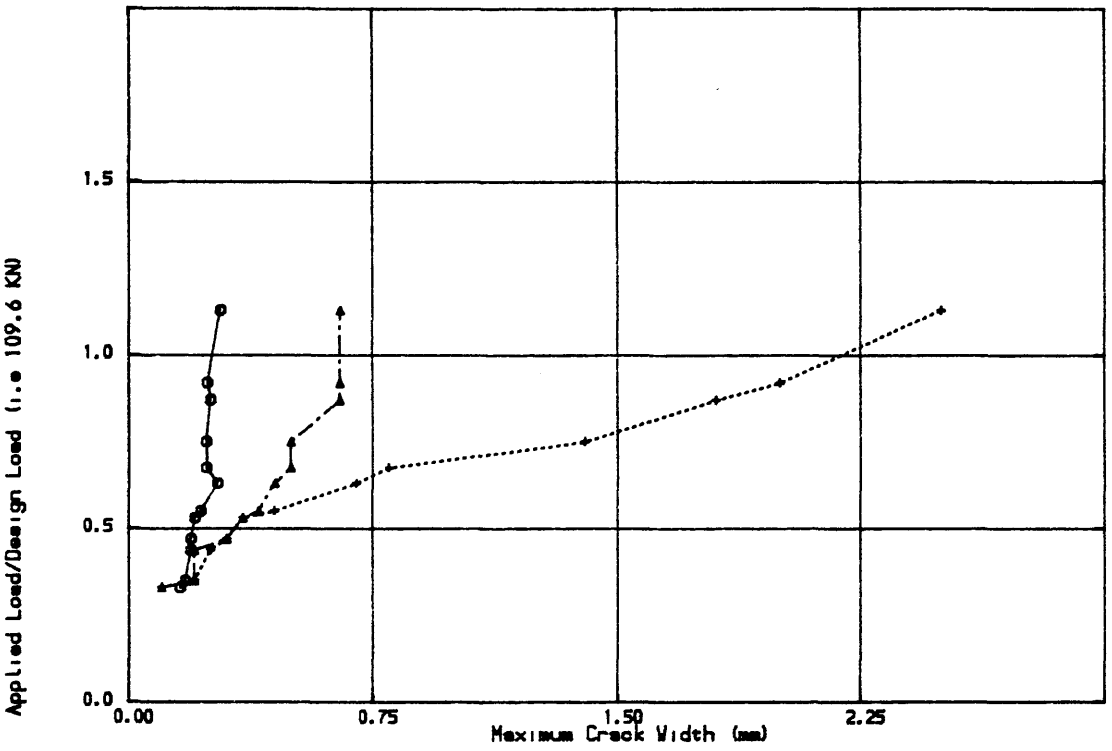

Fig. (7.44) Load-Maximum crack widths at various points for MODEL NO. FIVE

are shown in Fig. (7.42) and (7.43). It can be seen from these curves that all the steel at all locations except at position (1) near the obtuse corner, yielded just before failure.

7.2.5.5 Bottom Face Crack Widths: Fig. (7.44) shows approximate maximum crack widths. Crack width limit of 0.3 mm was reached at 0.52 of the design load.

7.2.5.6 Summary of Results: At 0.24 design load, initial cracking occurred. As the load increased the rate of nonlinearity increased. The deflection limit of span/250 and limiting crack width of 0.3 mm was reached at 0.52 of the design load. The first yield occurred at 0.78 of the design load. In general the slab behaved in a ductile manner.

7.2.6 Model Ribbed Skew Plate Number Six

7.2.6.1 Slab-Beam Properties: Slab-beam structural systems are frequently encountered in practice. Beams are either of reinforced concrete as in some floor systems and bridge decks or of steel as in composite bridges. The general geometrical shape of this model was chosen so as to be similar to the practical bridges. Fig. (6.12.1) show the layout of the model ribbed skew reinforced concrete plate, its cross-sectional geometry, the support conditions and the loading system. The slab thickness was 50 mm. All the ribs had the same overall depth of 250. mm. The breadth of the longitudinal ribs, the support transverse ribs and the inner transverse ribs were 106,

100 and 150 mm respectively. The longitudinal ribs were simply supported at the end. The system of loading was a four-point direct load system. The reinforcement arrangement of the slab was parallel to the edges.

7.2.6.2 Design Procedure: The elastic analysis was used to predict the stress resultants (N_x, N_y, N_{xy}, M_x, M_y, M_{xy}, Q_{xz}, Q_{yz}). The finite element mesh is given in Chapter eight Fig. (8.6). The mesh dimension depened on the breadth of the ribs and on the system of loading. Five layers of 10 mm thickness were used to represent the slab thickness and ten layers of 25 mm thickness were used to represent the ribs. To represent the eccentric rib stiffeners, a reference plane at which all degrees of freedom are defined must be chosen. The reference plane was chosen to coincide with the middle surface of the plate and all the stress resultants were referred to this plane. For design purposes, these forces were referred to the mid plane of each element. The total design load was 300 kN to give a reasonable amount of steel and to remain within the capacity of the available load cells.

(a) Design of reinforcement; This model was designed in two different ways viz fristly, considering the inplane effect (N_x, N_y, N_{xy}) using Clark's equations, section (3.4.3.3) Chapter three and secondly ignoring inplane effects and using Wood and Armer equations, section (3.4.3) Chapter three. This is because from an overall design point of view, the external ribs will be designed as a L-beam, the internal ribs will be designed as a T-beam, the slab will be considered as the flange of the

ribs. The width of the flange in the two sections (L, T) depends on the distance between the ribs. Considering a lateral load case, the inplane overall stress resultant (N_x, N_y, N_{xy}) must be equal to zero if L and T sections with correct flange width are used. In the finite element analysis, a rectangular section is used for the slab as well as for the ribs. To explain the effect of modelling of the cross section on the stress resultant, Fig. (7.45a) shows the stress distribution on a L-section due to a pure positive bending moment. Imagining that the web is separated from the flange, the flange will be under inplane compressive force and a moment, while the web will be under inplane tensile force and a moment. These inplane forces are created due to the neutral axis of the flange and the web not coinciding with the neutral axis of the L section. This is what actually happens in the analysis of the model as shown in Fig. (7.45b). The different reinforcement envelopes are shown in Figs (7.47), (7.48), (7.49) and (7.50) for sections of the model when the effect of the inplane foreces are indicated or neglected. The actual steel was chosen close to the case which ignored the inplane effect as can be seen from Fig. (7.47) to Fig. (7.50).

It should be noted that the actual shear flow due to torsion in the case of this slab is shown in Fig. (7.46a). When a portion is taken from the slab (remote from the corners), the shear flow will be as shown in Fig. (7.46b). This is Wood and Armer (77) and Clark (35) assumed (see Chapter three). The shear flow in the case of

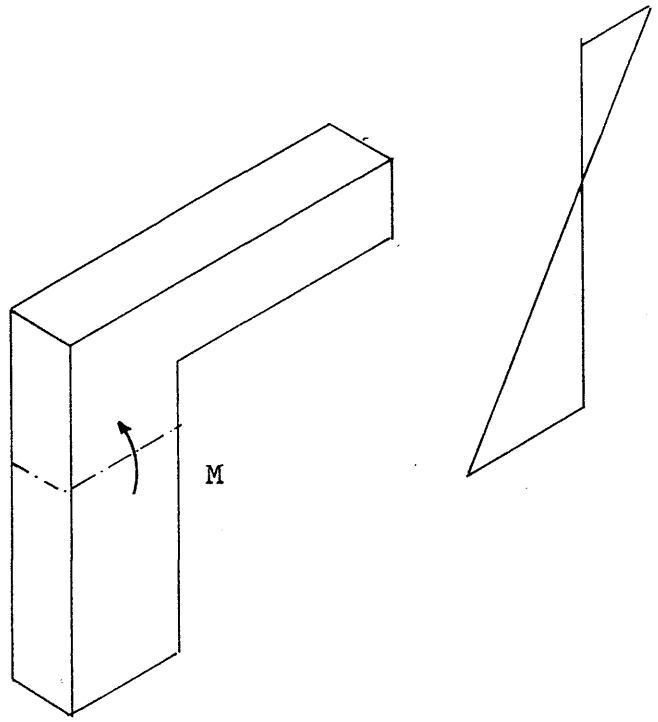

(a) Stress distribution before separation

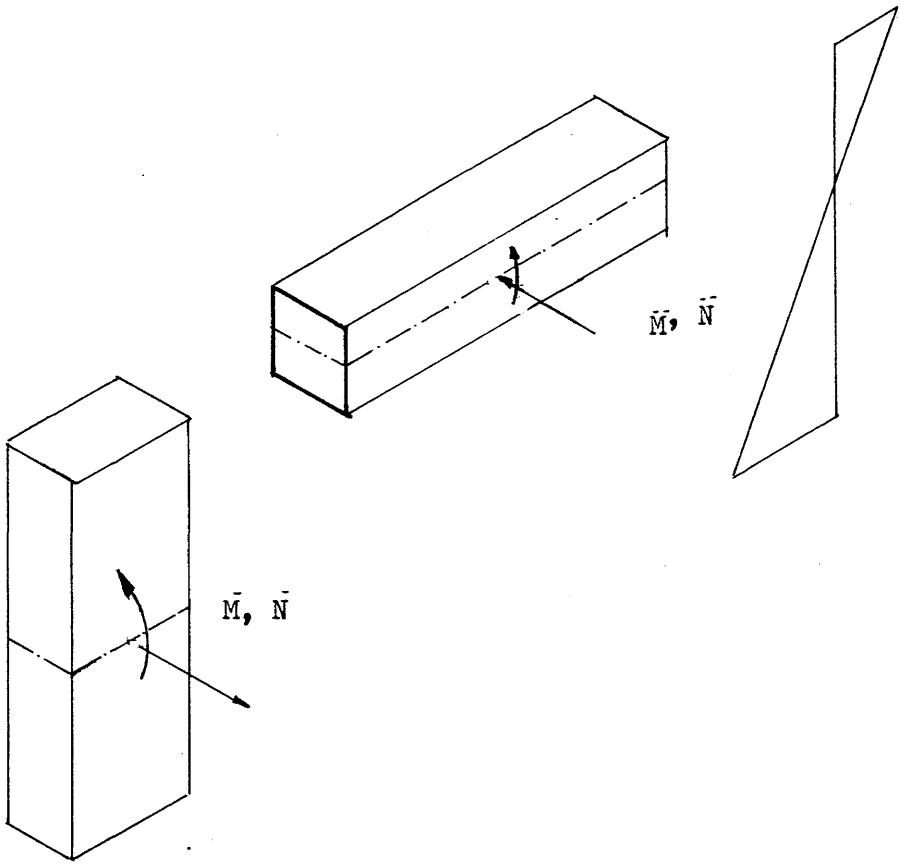

(b) Stress distribution after separation

Fig. (7.45.) L- setion under pure moment (M)

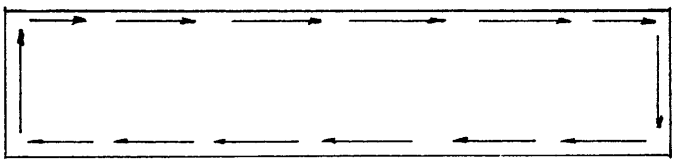

(a) Slab section

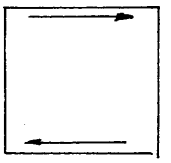

(b) A part from the slab remote from the corner

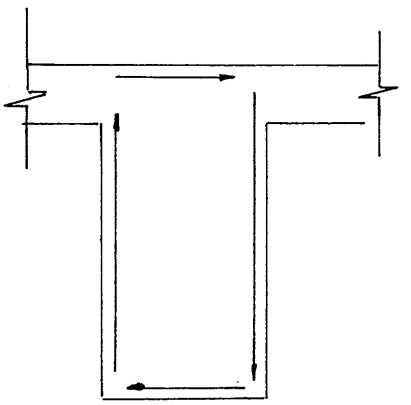

(c) Beam section

Fig. (7.46) The shear flow due to torsion

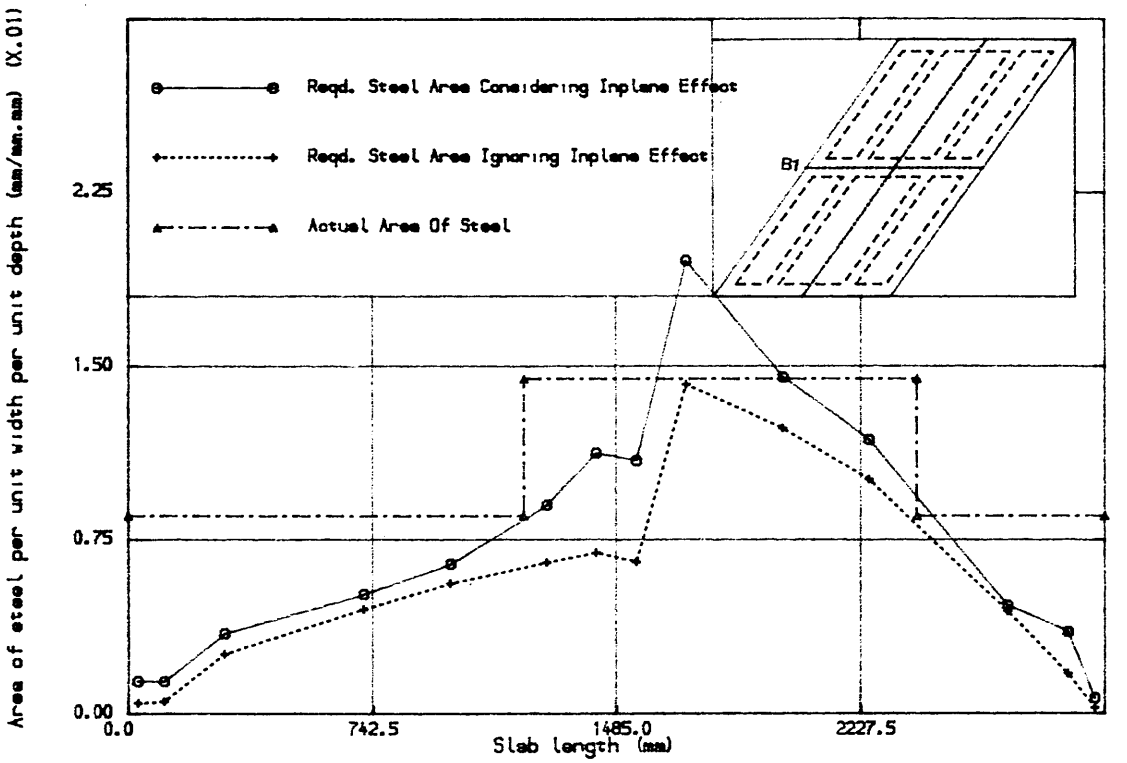

Fig. (7.47) Envelopes for steel area at the bottom of rib B1 for MODEL NO. SIX

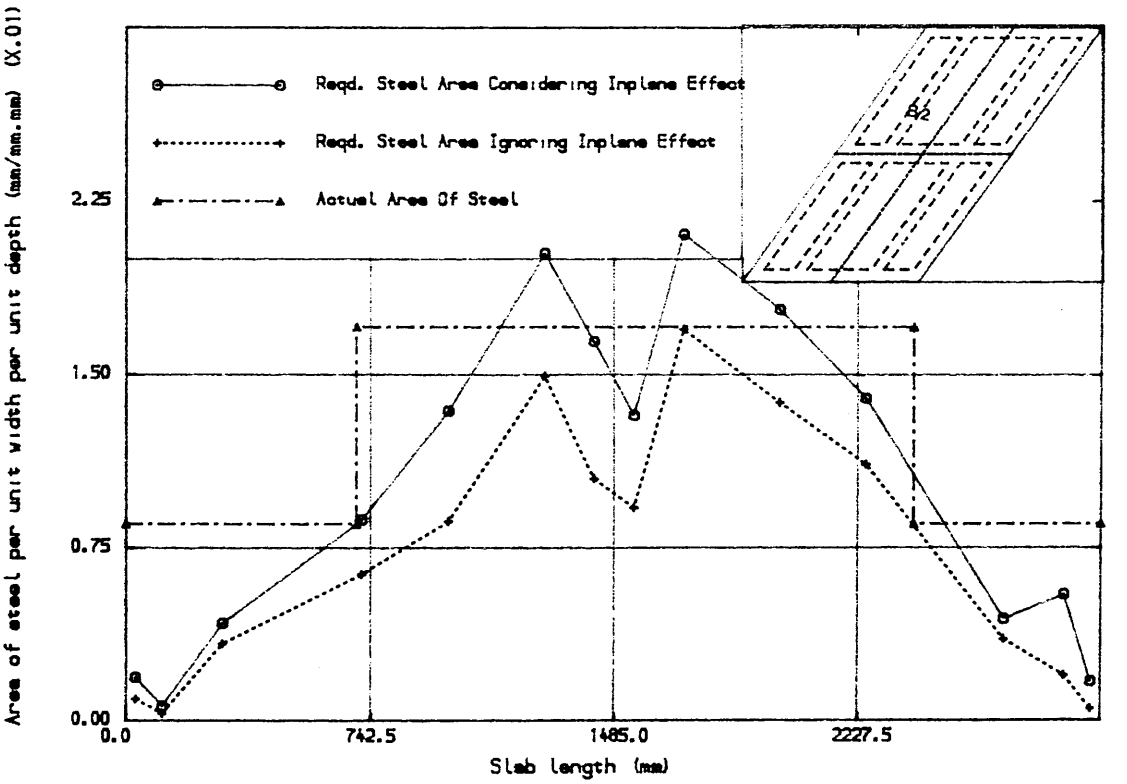

Fig. (7.48) Envelopes for steel area at the bottom of rib B2 for MODEL NO. SIX

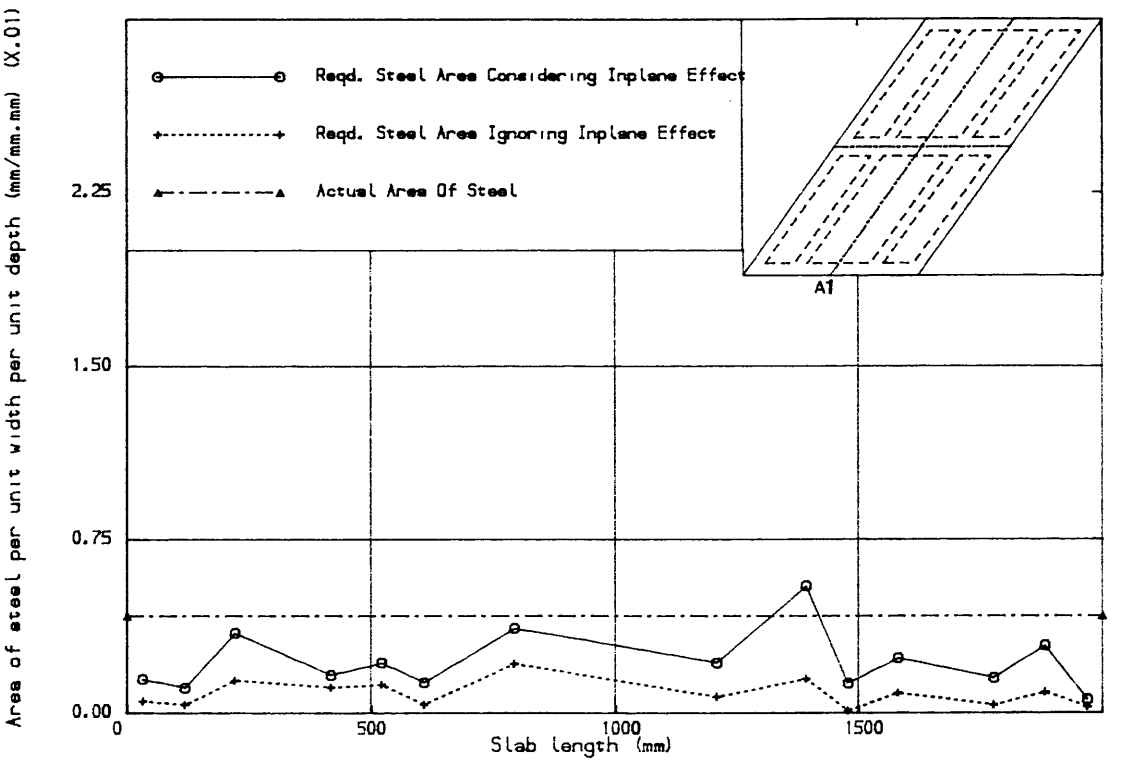

Fig. (7.49) Envelopes for steel area at the bottom of rib A1 for MODEL NO. SIX

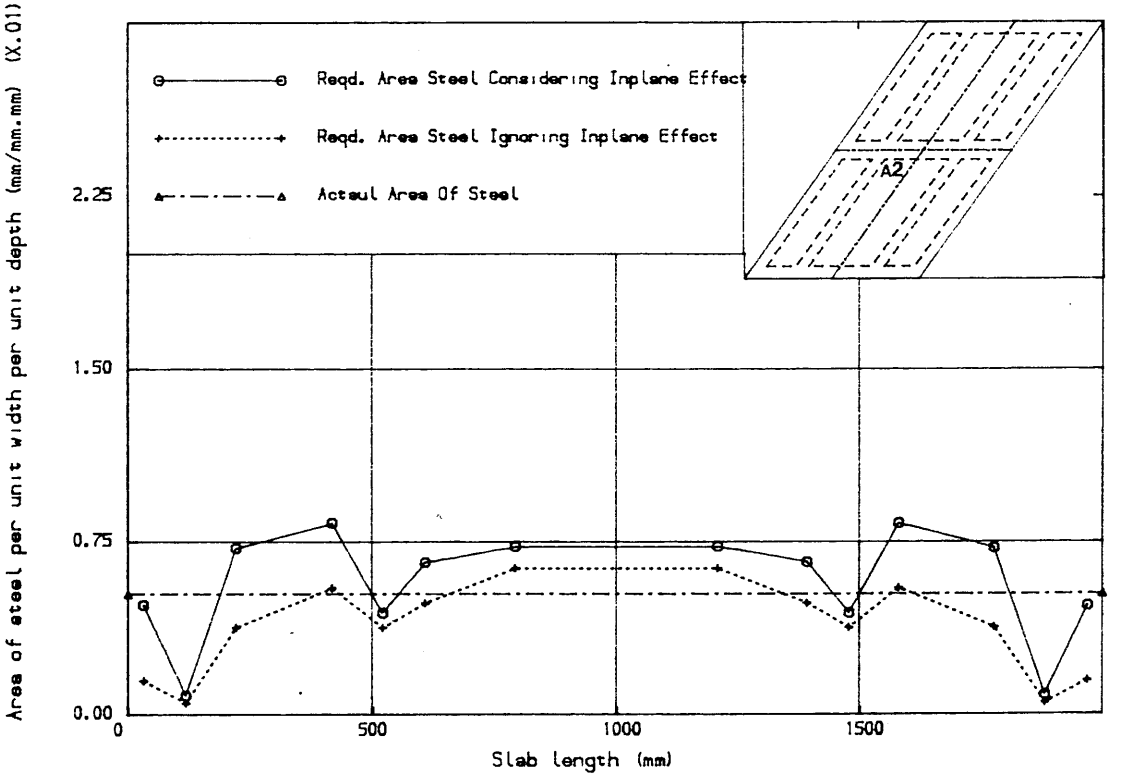

Fig. (7.50) Envelopes for steel area at the bottom of rib A2 for MODEL NO. SIX

beams is shown in Fig. (7.46c). In such a case using Wood and Armer (77) equations to the design of the ribs for flexural will overestimate the flexural reinforcement. Care must be taken when designing for shear reinforcement. (b) Shear reinforcement: Nominal stirrups fabricated from 6 mm high tensile bars were provided along the ribs at 180 mm centres. These stirrups were designed according to BS5400 (34) for 1.25 of the design load (the design shearing force incloudes the effect of half of the tosison moment). Fig. (6.12.2) to Fig. (6.12.6) show the distribution of the reinforcement for different parts of the model and strain gauges position.

7.2.6.3 Response of The Slab: Initial cracks were observed on the bottom face of the longitudinal ribs near the load points at 0.30 of the design load. At 0.37 of the design load, cracks were observed at the intersection of the longitudinal ribs with the inner transverse rib. Short lengths of cracks appeared at the intersection of the longitudinal ribs with the inner transverse rib at 0.37 of the design load. At 0.39 of the design load, at the midspan of the outer ribs, inclined cracks progressed from the bottom face up 0.7 of the rib depth. These cracks made an angle of 80^{o} to the horizontal. At 0.5 of the design load, cracks were well developed in the bottom of the longitudinal ribs. As the load increased, the cracks progressed near to the obtuse corners remaining roughly parallel to the transverse ribs and at a spacing of 50 mm. Inclined cracks similar to the other in the outer longitudinal ribs were also observed in the longitudinal inner ribs. At 0.63 of the design load, cracks in the

the longitudinal ribs near the obtuse supports, similar to the cracks near the midspan were observed. At this stage, inclined cracks were observed in the longitudinal ribs near the acute corners as well. At 0.68 of the design load, vertical cracks spread in the inner transverse rib. At 0.75 of the design load, initial cracks were observed on the bottom surface of the slab at the centre near the load points. At 1.05 of the design load, near the obtuse supports, initial cracks progressed diagonally from the bottom surface through the depth of the longitudinal ribs and further up through the depth of the slab as shown in Fig. (7.53). At 1.12 of the design load, cracks at the intersection of the longitudinal ribs with the inner transverse rib and also the diagonal cracks in the longitudinal ribs near to the obtuse corners became very wide. Also the concrete at the top surface at the intersection of the longitudinal ribs with the inner transverse rib began to crush. During loading to failure (1.12 design load) at the support transverse ribs diagonal cracks were observed near to the obtuse supports corners (see Fig. (7.55)) and the deflection became excessive (about 60 mm at the centre of the model). Several views of the failed model are shown in Figs (7.51) and (7.56). Bottom face crack pattern is shown in Figs (7.52) and (7.53). The extent of additional cracks at a later stage of loading and the cracks at the intersection of the inner transverse rib with the longitudinal ribs which developed at the later load stages can be clearly seen in Fig. (7.52). Fig. (7.51) shows the inclined diagonal tension cracks pattern at the outer longitudinal

rib. Fig. (7.54) shows the inclined shear crack pattern at the outer transverse rib near to the supports. Fig. (7.56) shows the damage in the top surface at failure.

7.2.6.4 Deflection: Load-Deflection curves at different positions are shown in Figs (7.57), (7.58), (7.59) and (7.60). From these curves it can be seen that:

(a) The behaviour of model is in general linear up to 0.21 of the design load.

(b) The deflection limit of span/300 was reached at 0.85 of the design load.

(c) The failure mode was ductile.

7.2.6.5 Steel Strain: Steel strains in the longitudinal ribs, the transverse ribs and the slab are shown in Fig. (7.61) to Fig. (7.65). From these curves it can be seen that;

(a) The influence of cracking on the measured strains of the steel the longitudinal ribs at different positions is clearly indicated in Figs (7.61) and (7.60) . The cracking load was about 0.21 of the design load.

(b) The steel at the middle of the inner longitudinal rib B3 yielded at 0.8 of the design load as shown in Fig. (7.62). The steel near to the obtuse corner (position 5) yielded at 0.94 of the design load. The steel near to the acute corner (position 7) yielded at 1.14 of the design load.

(c) The variation of the strain along the length of the outer longitudinal rib (B1) is shown in Fig. (7.61). The steel near the obtuse corner of the rib (position (1))

yielded at load 0.87 of design load. At the midspan of the rib (position (4)), steel yielded at 0.98 design load. The steel near to the acute corner of the rib (position (3)) yielded at load 1.04 of the design load. Close to the acute corner of the rib (position (2)), the steel yielded at failure. It can be seen from these results that the strains in the steel along the length of the rib decreases as one moves away from the obtuse corner.

(d) Fig. (7.63) shows the strain in the steel of the inner transverse rib (A2) at two positions. In general the steel did not contribute much up to 0.9 of the design load. The steel near to the middle of the rib (position (9)) yielded at 1.10 of the design load and the steel near to the edge of the rib (position (8)) did not yield at all.

(c) Fig. (7.64) shows the steel load strain curves at different positions in the slab. It can be seen that as expected the steel in the two directions showed negligible compressive strains up to 0.80 of the design load.

At load 0.9 of the design load, at the centre of the slab the steel in the longitudinal direction showed tensile strains indicating that the neutral axis shifted in to the slab. At the same position, steel yielded at 1.14 of the design load just before failure, indicating that the neutral axis had shifted to the surface of the slab and the ductile failure was taking place.

(e) The strains in the stirrups were measured by using strain gauges, their locations are shown in Fig. (6.11.4). The measured strains during loading were

obtuse corner

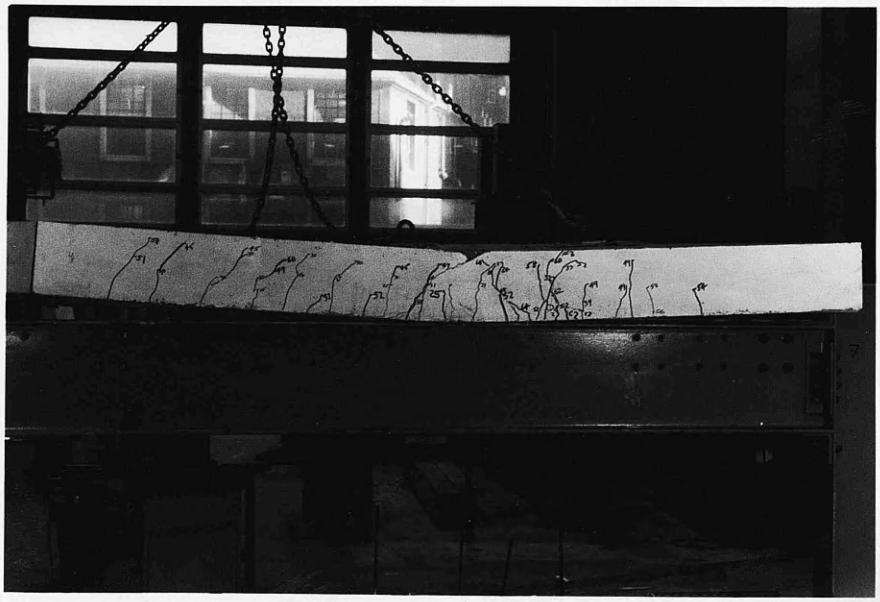

acute corner

Fig. (7.51) MODEL RIBBED SKEW SLAB NO. (6) Crack pattern in the outerside rib (B1) after failure

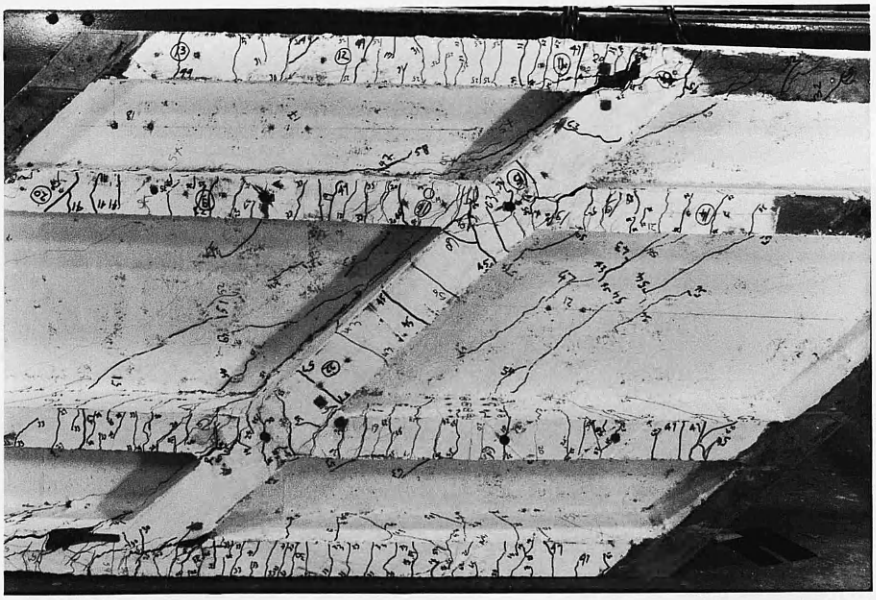

Fig. (7.52) MODEL RIBBED SKEW SLAB NO. (6) Crack pattern at the bottom surface after failure (close up view to the model)

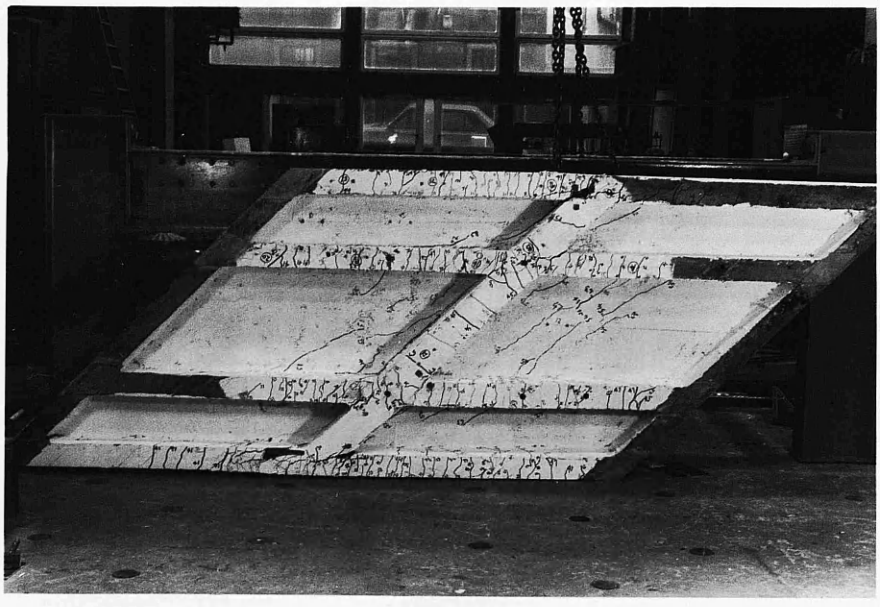

Fig. (7.53) MODEL RIBBED SKEW SLAB NO. (6) Crack pattern at the bottom surface after failure

Fig. (5.54) MODEL RIBBED SKEW SLAB NO. (6) Crack pattern at the transverse rib (A1)

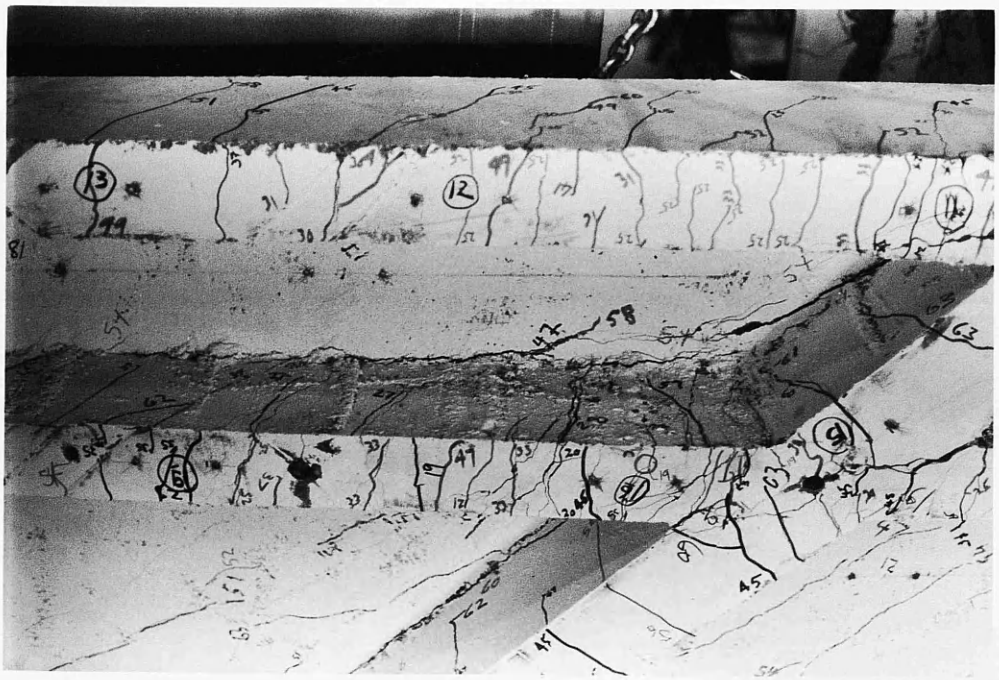

Fig. (7.55) MODEL SKEW SLAB NO. (6) Damage in the midside transverse rib (A2) after failure

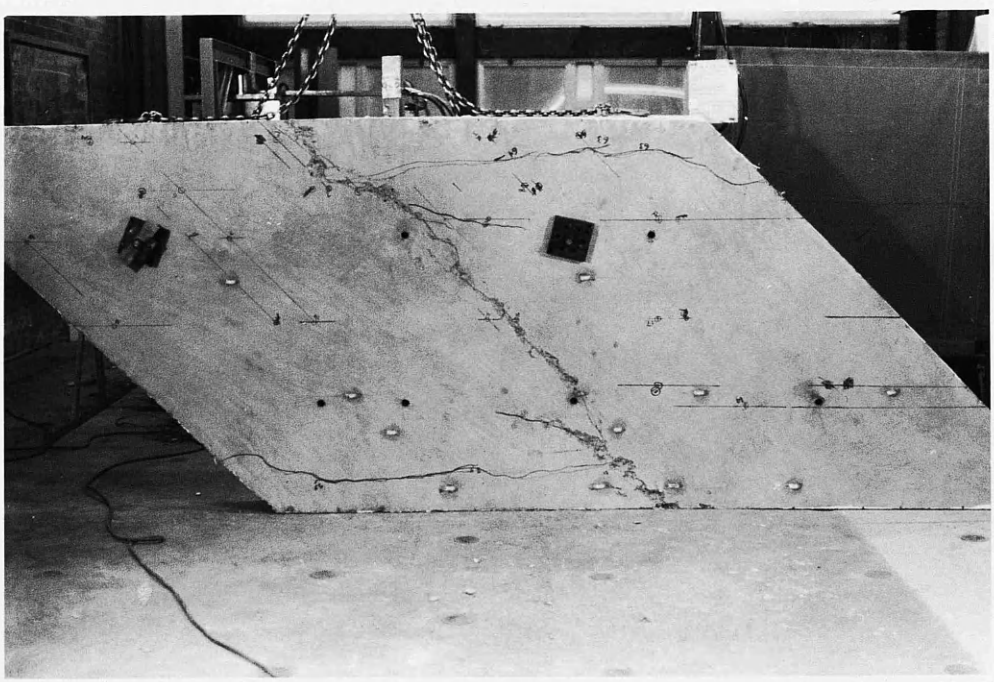

Fig. (7.56) MODEL RIBBED SKEW SLAB No. (6) Damage at the top surface of the model after failure

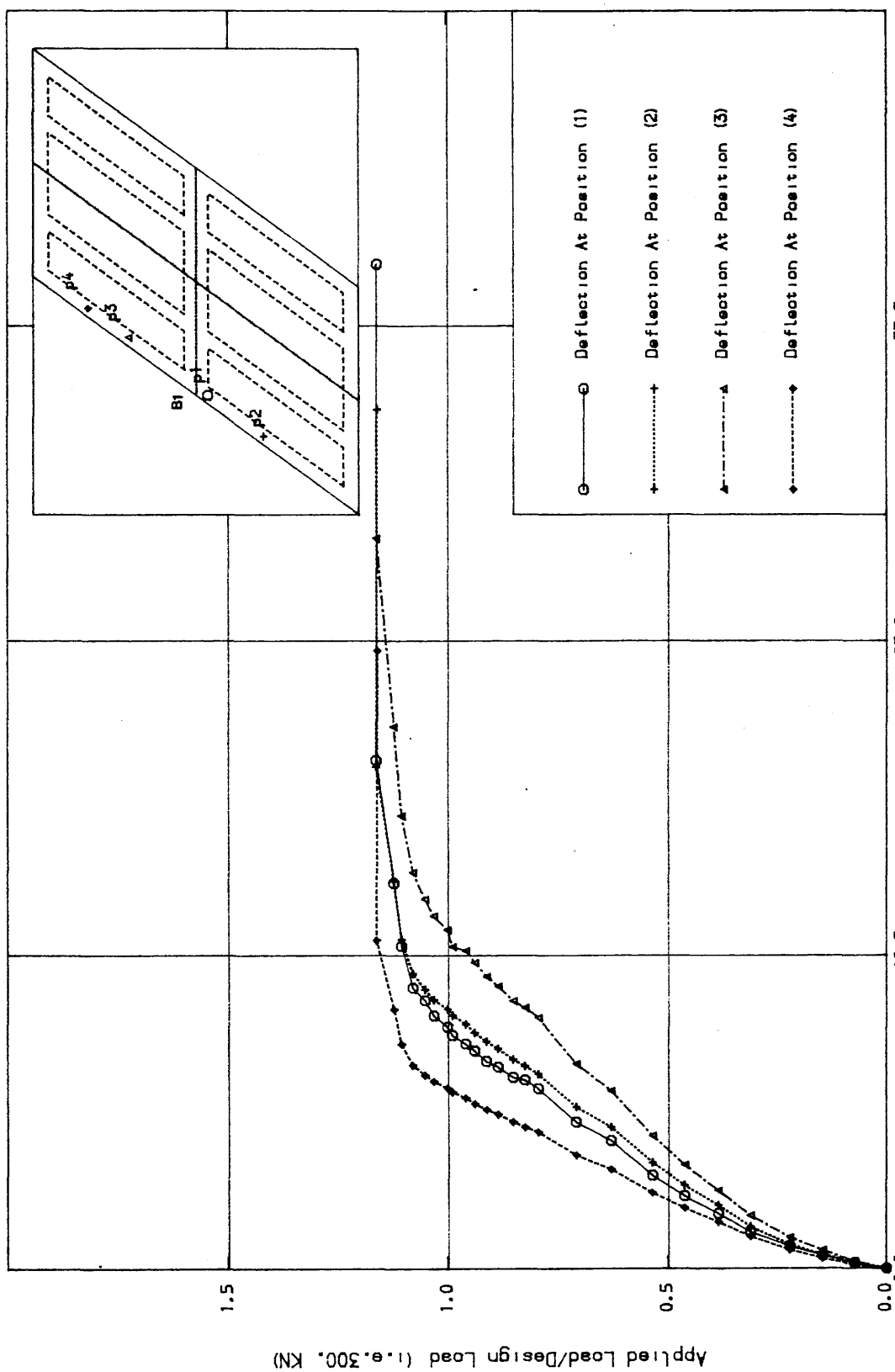

Fig. (7.57) Load-Deflection curves in the longitudinal direction at rib B1 for MODEL NO. SIX

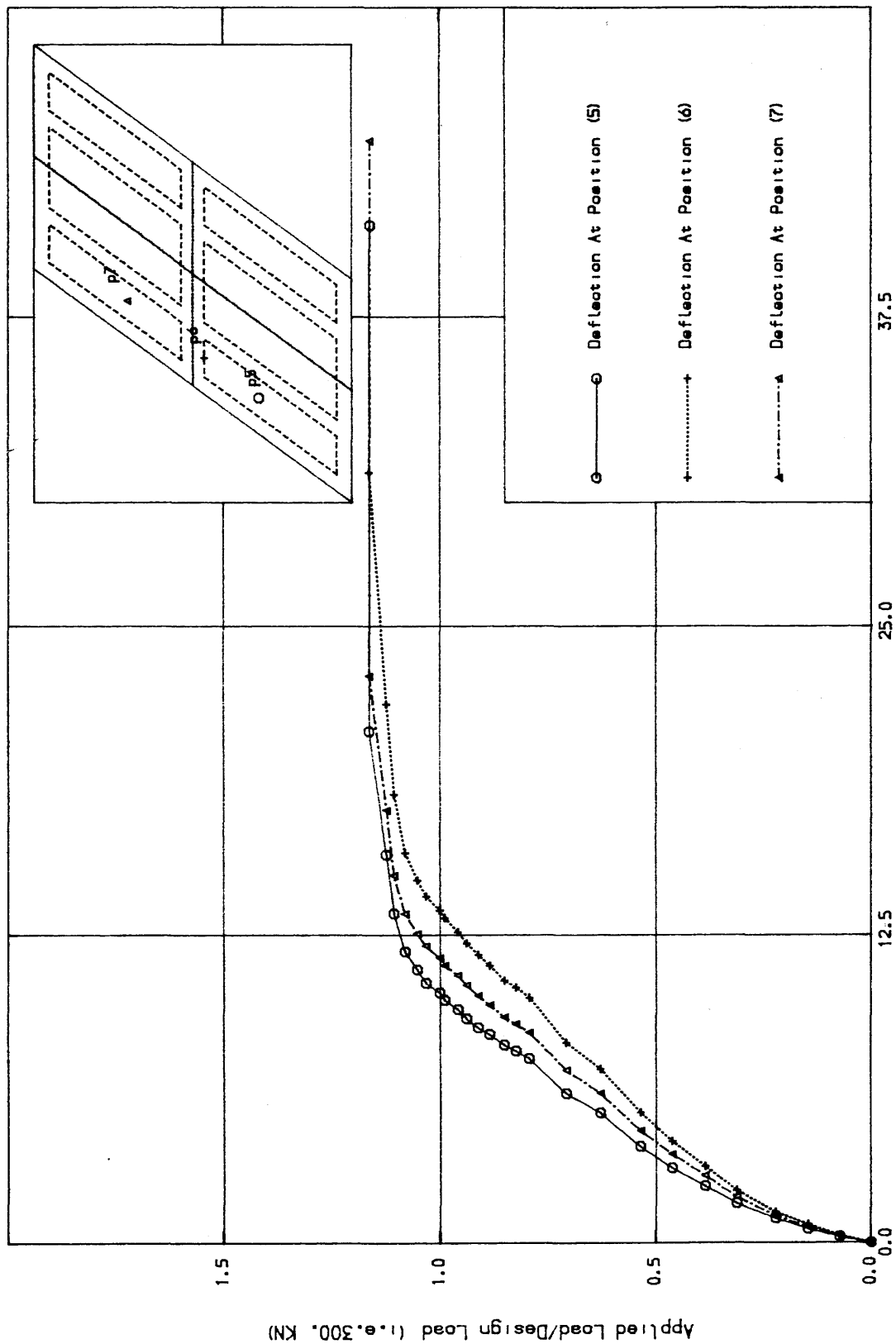

Fig. (7.58) Load-Deflection curves in the longitudinal direction on the slab for MODEL NO. SIX

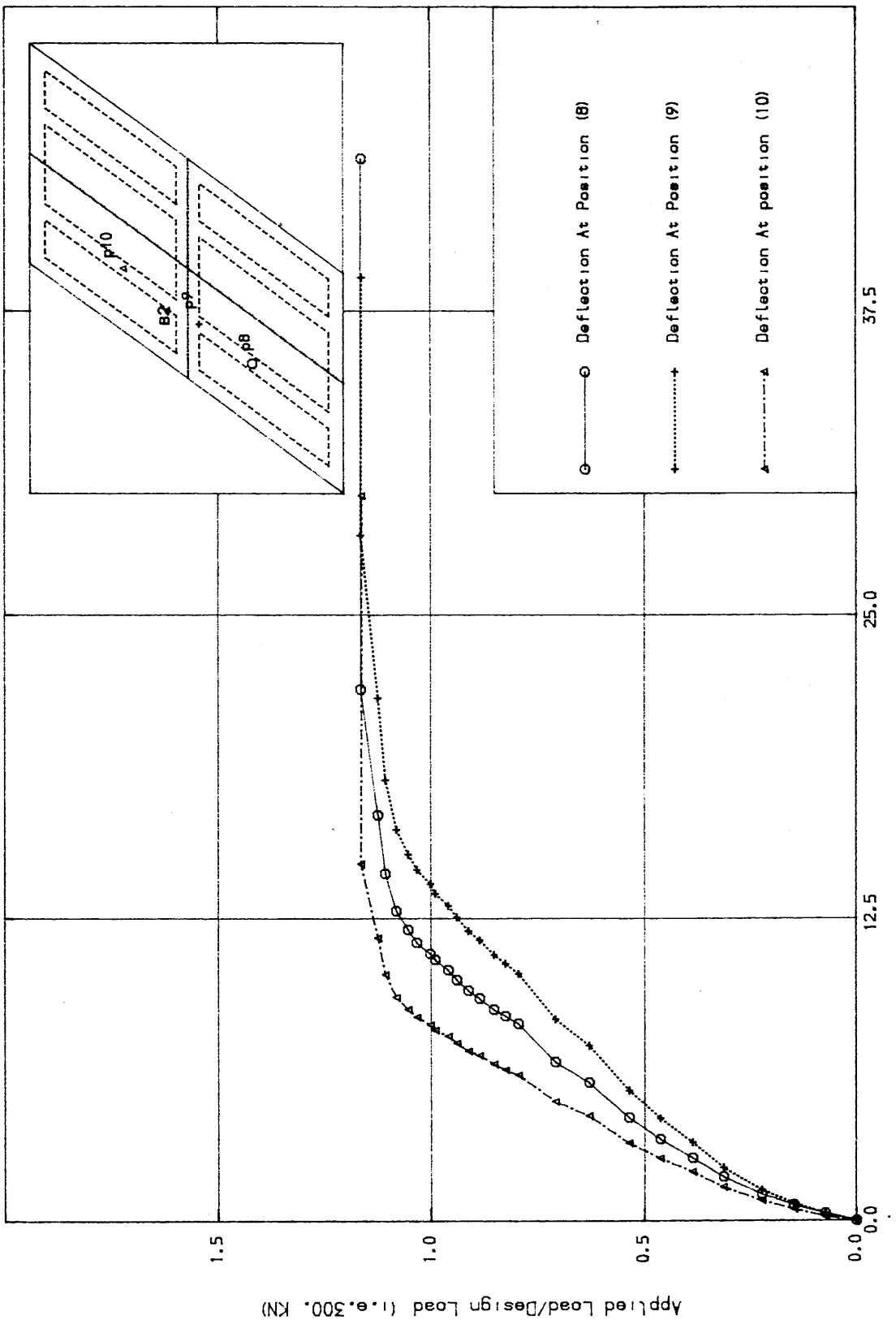

Fig. (7.59) Load-Deflection curves in the longitudinal direction at rib B2 for MODEL NO. SIX

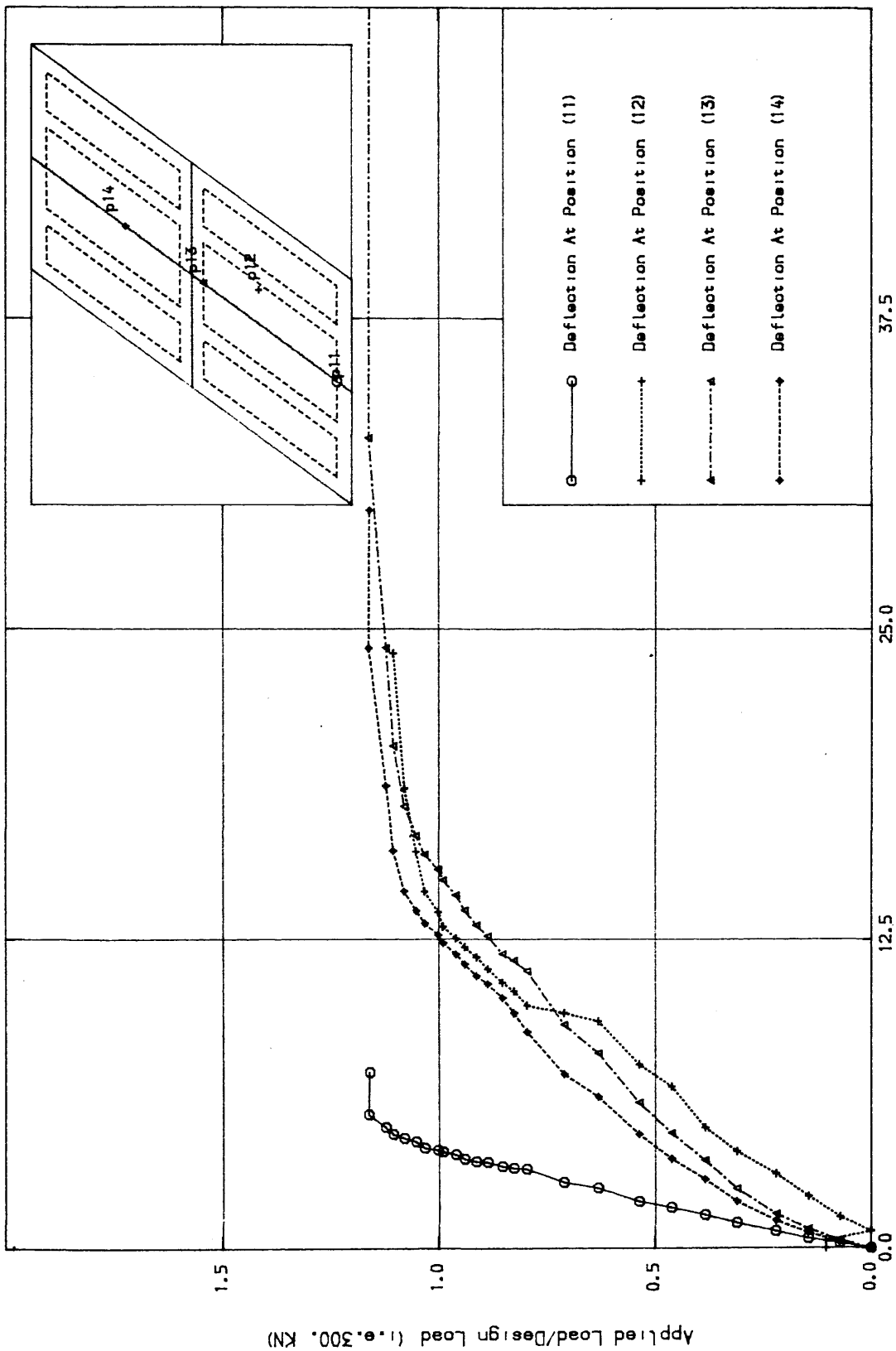

Fig. (7.60) Load-Deflection curves in the longitudinal direction at the slab for MODEL NO. SIX

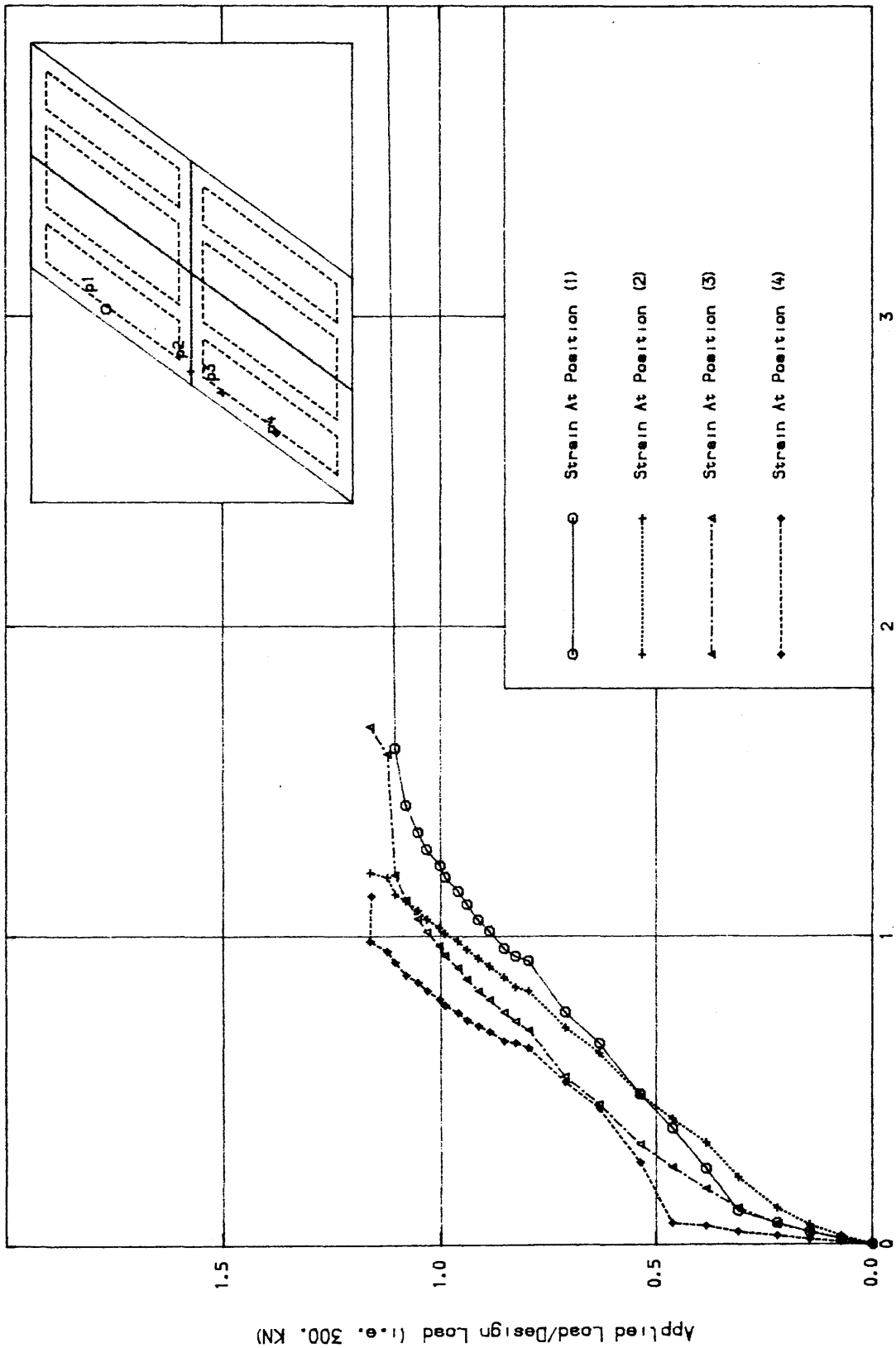

Fig. (7.61) Load-Steel Strain curves in the longitudinal direction along rib B1 for MODEL NO. SIX

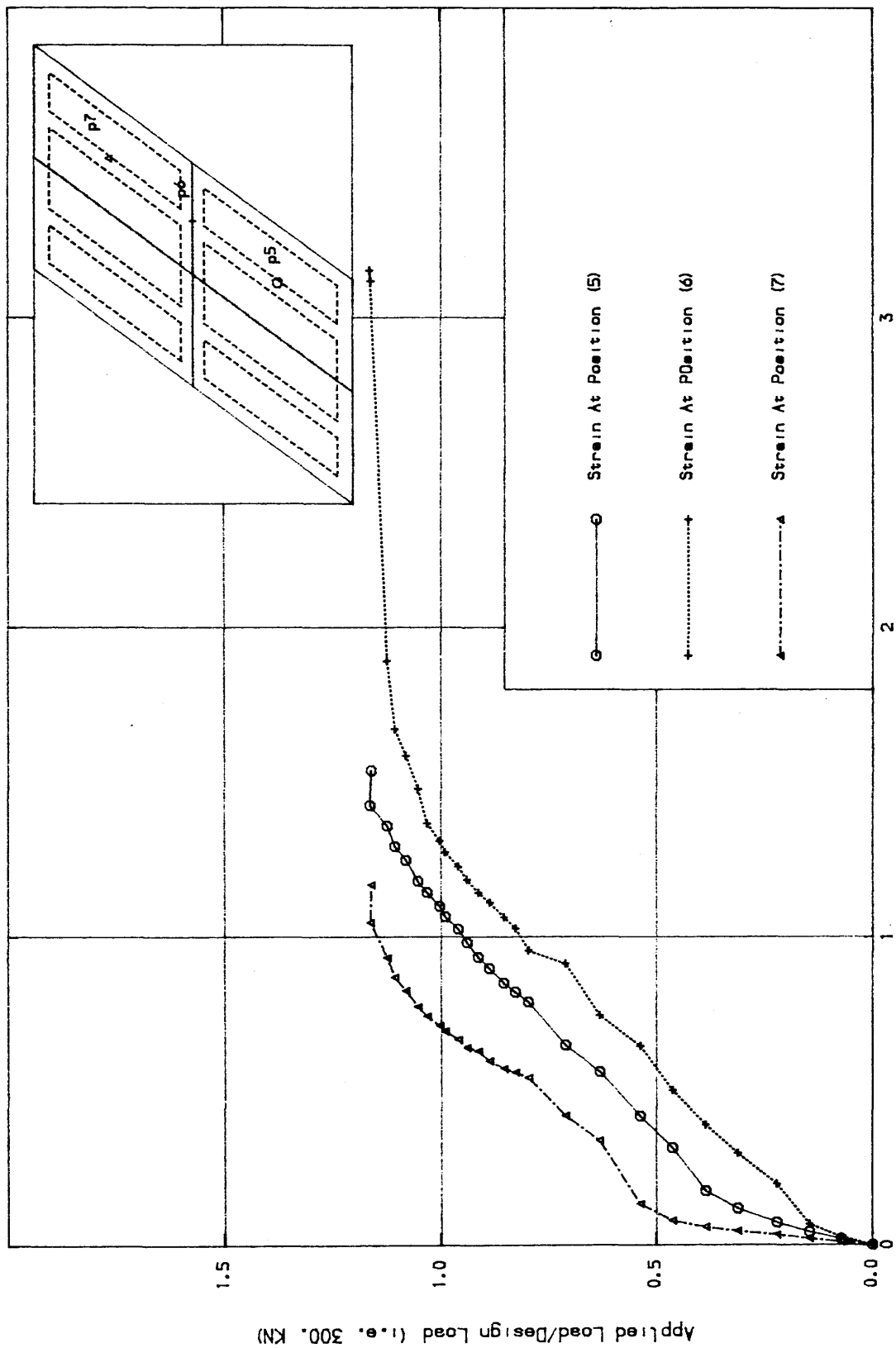

Fig. (7.62) Load-Steel Strain curves in the longitudinal direction along rib B3 for MODEL NO. SIX

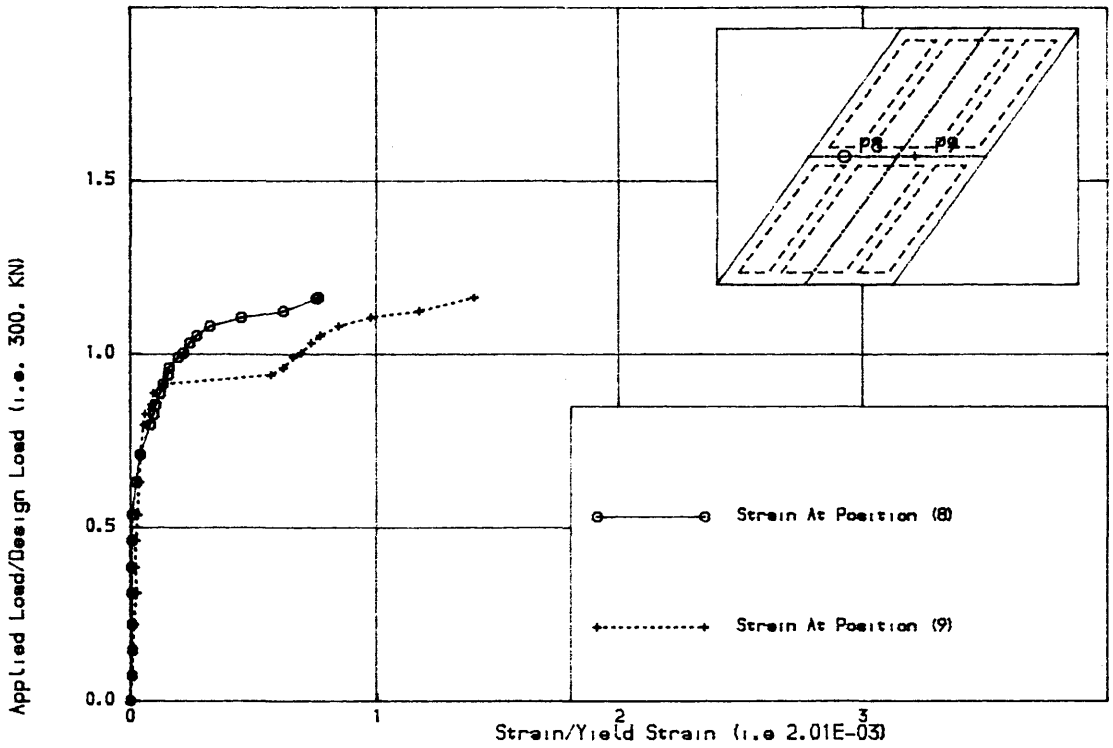

Fig. (7.63) Load-Steel Strain curves in the transverse direction along rib A2 for MODEL NO. SIX

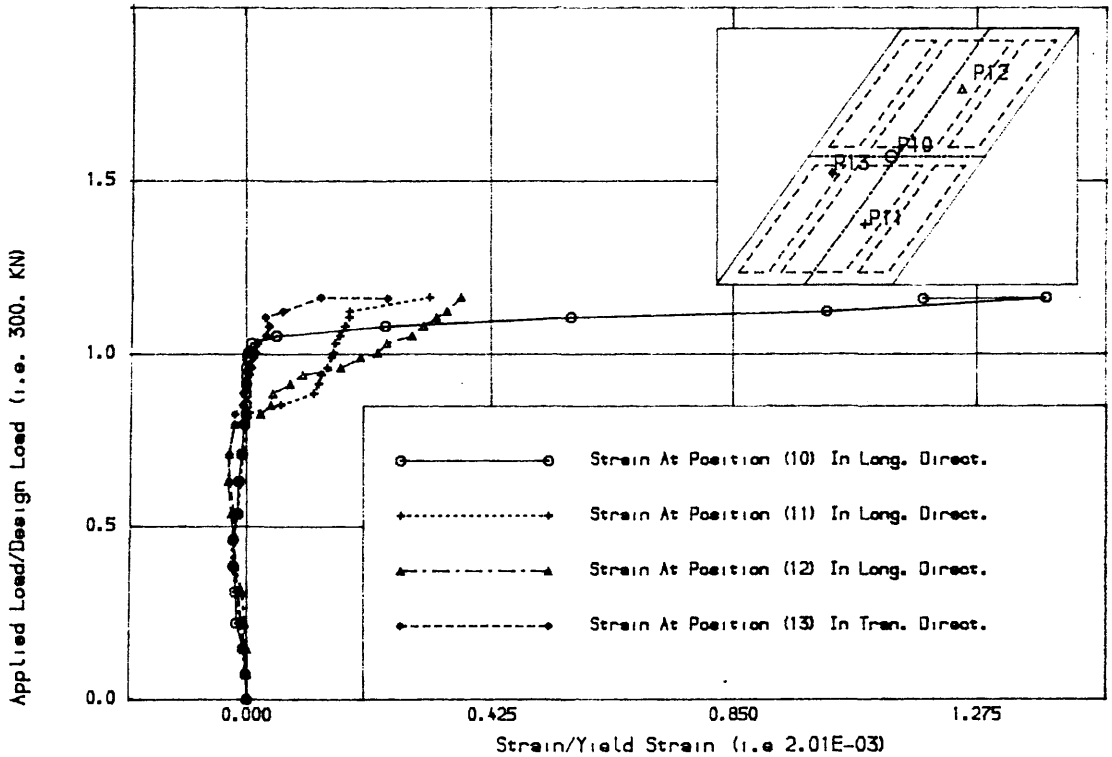

Fig. (7.64) Load-Steel Strain curves in the slab for MODEL NO. SIX

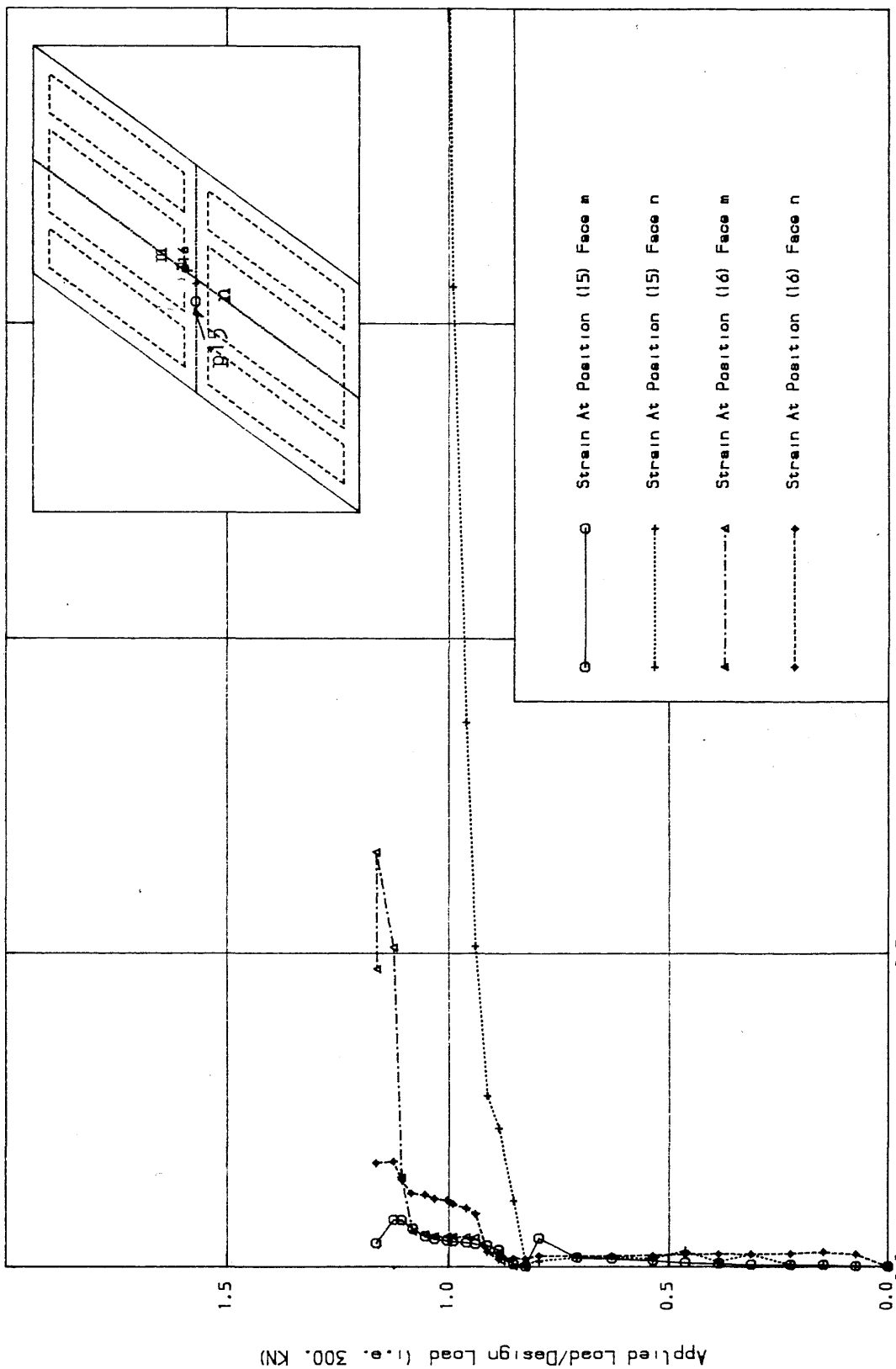

Fig. (7.65) Load-Steel Strain in the stirrups at the transverse rib A2 for MODEL NO. SIX

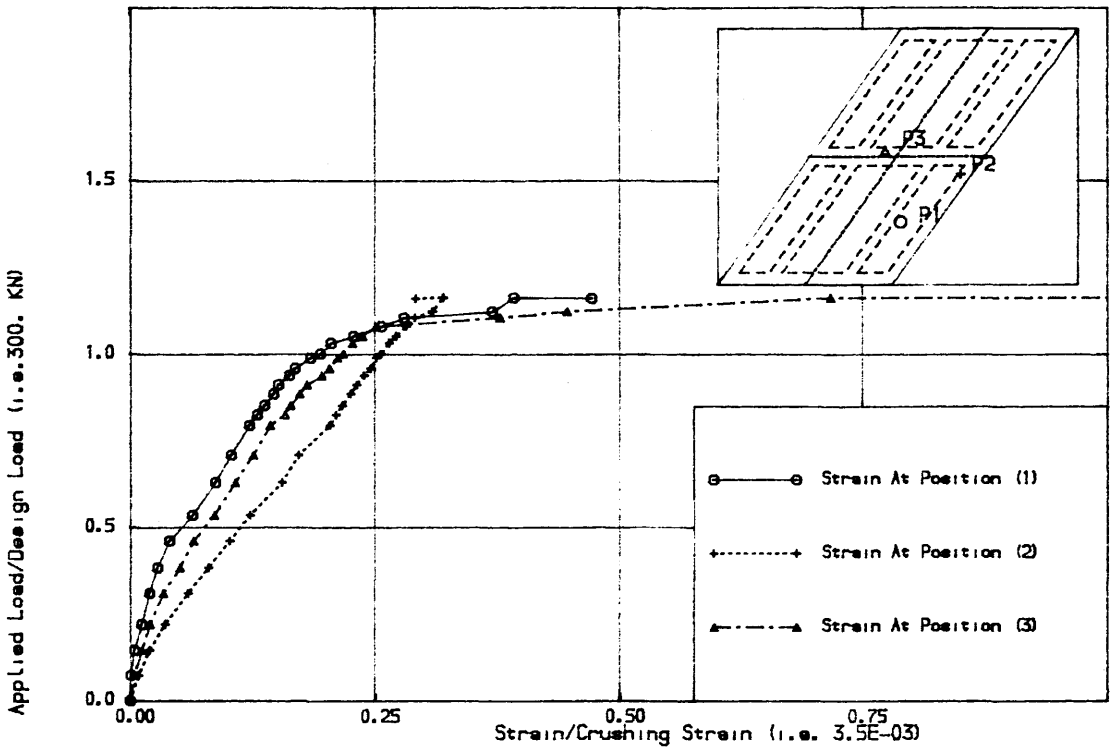

Fig. (7.66) Load-Concrete Strain curves at top surface for MODEL NO. SIX

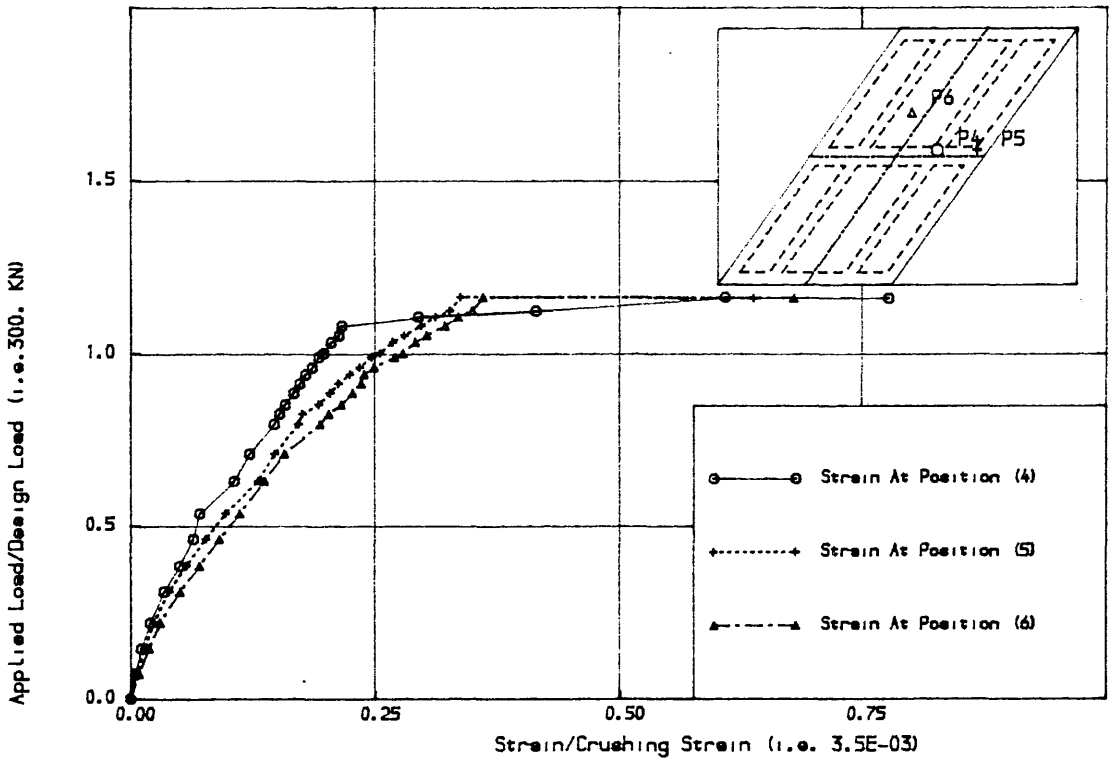

Fig. (7.67) Load-Concrete Strain curves at top surface for MODEL NO. SIX

negligible except at positions 1 and 2 in the transverse rib A2. In general strains on one face were much larger than the strains in the other face, possibly due to torsion.

7.2.6.6 Concrete Strain: Figs (7.66) and (7.67) measured concrete strains at top surface during load. The location of the strain gauges is shown in Fig. (6.20.6), Chapter Six. These curves reveal a similar behaviour to the overall behaviour of the model.

5.2.6.7 Soffit Crack Widths: Fig. (7.68) shows approximate maximum crack widths. Limit crack width of 0.3 mm was reached at 0.90 of the design load.

5.2.6.8 Summary of Results: At 0.15 of the design load, the nonlinearity was induced by the initial cracking. The deflection limit equal to span/300 was reached at 0.85 of the design load and the crack limit of 0.3 mm was reached at design load. At failure the model behaved in ductile manner. The failure load was 1.16 of the design load. The failure was initiated by the yielding of the steel.

7.3 DISCUSSION OF TEST RESULTS

7.3.1 Serviceability Limit states

Skew plates are used in bridges and buildings. In the design of bridges using BS5400 (35), it is necessary to check for crack width. This means that there is an indirect check on reinforcement stresses under service

load. It is desirable that steel remains elastic under all serviceability conditions, so that cracks which open under the application of an occasional overload will close when the loading is removed. A specific criterion in terms of absolute limiting deflection, is not given in the bridges code BS5400 (35). However it is obviously necessary to calculate the deflection in order to ensure that clearance specifications are not violated and adequate drainage is obtained. Deflection calculations are also important where the method of construction requires careful control of levels and for bearing design. In addition in bridge design it is necessary to calculate the flexibility of the structure for vibration using dynamic analysis. In general the service load is taken as the minimum of three values satisfying:

(a) deflection limit of span/250.

(b) maximum crack width of 0.3 mm.

(c) steel stress limit of 0.8 the yield strength.

It must be noted that the thickness of all designed slabs was chosen to comply with the limiting span/depth ratios specified by section (3.3.8) of CP110 (30) and the span is taken as the one which is orthogonal to the supported edge not the incline span.

Table (7.3) summarizes all the test results. The general conclusion to be drawn from the table is that;

(a) Considering models 1,2,3, and 5, the average load at service limit deflection is of 0.4 of the ultimate, which represent a low service load. This is due to the effect of using the orthogonal length to the supported edge in

Table (7.3) Service and Ultimate Behaviour of Tested Slabs.

Model No.	Live Load kN	Dead Load kN	Design Load kN	P_{cr}/P_d	P_{si}/P_u	P_{scr}/P_u	P_y/P_u	P_u/P_d	$0.8P_y/P_u$	Remarks
1	150	9.6	159.6	0.22	0.36	0.51	.92	1.39	0.73	Shear failure
2	140	9.6	149.6	0.3	0.38	0.6	0.69	1.178	0.552	Ductile failure
3	100	9.6	109.6	0.3	0.41	0.47	0.71	1.96	0.57	Ductile failure
4	80	9.6	89.6	0.29	0.63	0.7	0.9	0.9	0.56	*
5	100	9.6	109.6	0.35	0.46	0.46	0.7	1.28	0.68	Ductile failure
6	288.7	11.3	300.0	0.21	0.73	0.86	0.69	1.16	0.552	Ductile failure

P_d Total design load

P_{cr} Cracking load

P_{scr} Limit service load at cracking

P_{si} Limit service load of deflection

P_y First yield load

P_u Ultimate load

* Earlier failure due to oversight during fabrication.

limiting/span ratio specified by CP 110 (30) on the thickness of the slab. Model 4 is excluded from consideration because of early failure due to oversight during fabrication. The service limit deflection of model 6 (ribbed slab) is 0.69 of the ultimate is satisfactory. (b) The average load where the limiting crack width of 0.3 mm was reached is equal 0.51 of the ultimate failure load when models 1, 2, 3 and 5 considered. For model 6 the the limiting crack width of 0.3 is equal 0.86 of the ultimate failure load. (c) Steel Stress limit is average of value of 0.62 of the ultimate load for all the models (excluding model 4) is satisfactory.

7.3.2 Ultimate Limit State

Table (7.3) summarizes the results concerning the ultimate behaviour. The failure load of all the models exceeded the design load except model four. The results of models two and five show clearly that shear failure occurred near the obtuse corners. This happened in model two after the slab reached its design load and in model five when the ductile failure was taking place. Also it has been shown from the recorded measurements that high strain gradients occur near the obtuse corners and this high stress gradient could decrease the shear capacity of the slab. This type of failure will be discussed in Chapter Eight. For models two, five and six an average enhancement of 15% in the design load is observed. The first model recorded 39% load enhancement. The failure load of model three was 1.96 of the design load. This may be be due to the difference between the design steel and

the actual steel. Finite element nonlinear analysis is used to calculate the ultimate load for all models expect model 4 and the results are shown in Chapter Eight.

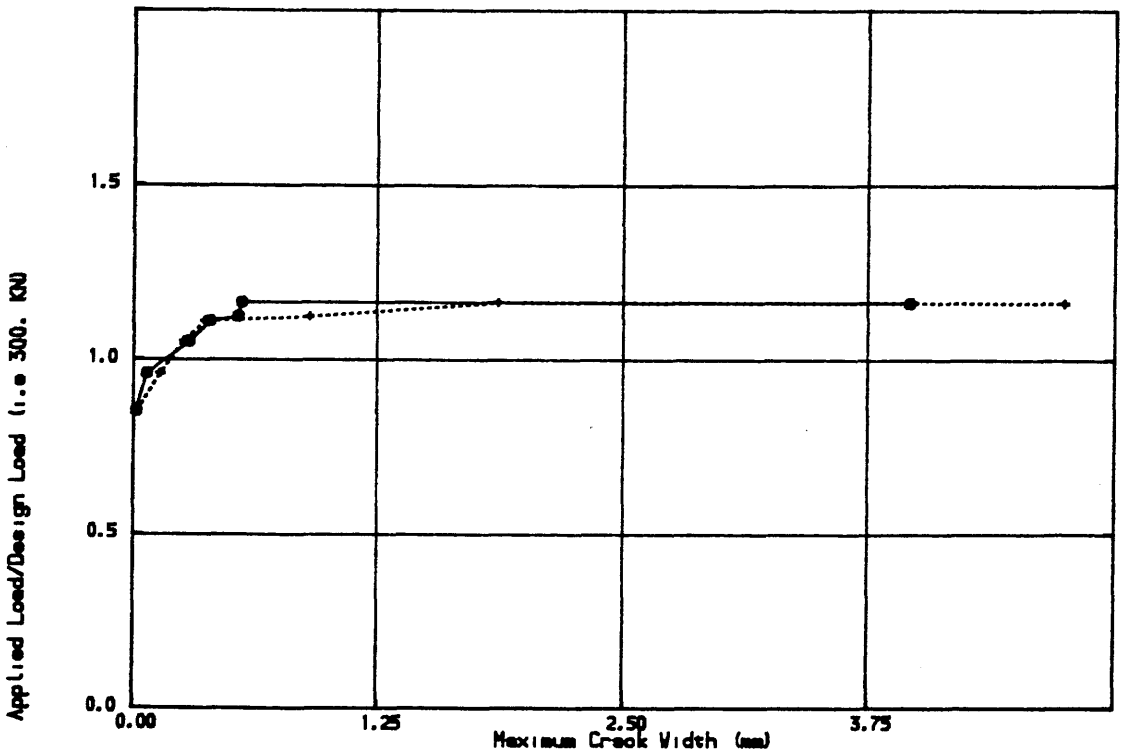

Fig. (7.68) Load-Maximum crack widths at various points for MODEL NO. SIX

CHAPTER EIGHT

THEORETICAL INVESTIGATION

8.1 INTRODUCTION

In Chapter Four, a computer program LAYER was described for the nonlinear finite element analysis of reinforced concrete plates. In this Chapter the program LAYER is used to analyse the experimental models described in Chapter Seven.

The object of this Chapter is to:

(a) Use the programme to carry out the theoretical analysis of the experimental models in order to obtain a better understanding of the stress redistribution and progressive yielding of steel and concrete.

(b) Estimate the serviceability limits of the tested models using the approximate methods given in Chapter Two to check their validity against experimental observation.

8.2 NONLINEAR ANALYSIS

8.2.1 Parameters which affect the numerical solution

The parameters which have an effect on the numerical solution can be summarized as follows;

(a) Mesh size.

(b) Number of concrete layers.

(d) Tension stiffening.

(c) Tensile strength of concrete.

(e) Angle of crack.

(f) Shear retention factor of cracked concrete.

(g) The norm of convergence tolerance.

The influence of the b, d, c, e and g factors except (a) and (f) factors on numerical solution is investigated in Chapters Four and Five. Therefore the influence of factors (a) and (f) will be investigated.

The analysis has been carried out considered using the fixed crack analysis in spite of its limitation as discussed in Chapter Five. For all the analyses which are considered in this Chapter, the convergence tolerance was taken at 5%. This tolerance was reduced to 2% for model two only because the failure load for the skew angle of 60 degrees was sensitive to the value of the norm of residual force adopted. The maximum number of iterations was limited to 20. The material properties used in the nonlinear analysis are shown in Table (8.1). Table (8.2) shows the number of concrete and steel layers adopted in the analysis.

Table (8.1) The Material Properties of the Tested Models Used in the Nonlinear Analysis

Model No.	E_c kN/mm^2	f_{cu} N/mm^2	f_t N/mm^2	E_s N/mm^2	f_y N/mm^2	ε_y	H'
1	29.25	45	2.95	210.0	500.	.0024	0.006
2	29.25	45	3.4	211.6	500.	.0026	0.0
3	28.69	41.6	3.52	205.6	473.	.0023	0.003
4	29.25	44	3.5	213.0	500.	.0023	0.0
5	29.25	44	3.5	230.0	460.	.002	0.0
6	29.25	44	3.3	230.	460.	.002	0.0

Table (8.2) Number of Concrete and Steel Layers Adopted in the Analysis

Model No.	No. of concrete layer	No. of Top Steel layers		No. of Bottom Steel layers		Total No. of layers
		Long.	Trans.	Long.	Trans.	
1	7	-	1	1	1	10
2	8	-	-	1	1	10
3	8	-	-	1	1	10
4	7	-	-	1	1	10
5	8	1	1	1	1	12
6*						

* In model six (ribbed slab) the concrete web section is represented by 8 layers and the concrete flange is represented by 5 layers. The upper and the lower steel bars of the web, the horizontal legs of the stirrups in the webs and plus the slab reinforcement are represented by smeared steel layer. The vertical legs of the stirrups is ignored.

8.2.1.1 Mesh Size:

Model number five was used to study the effect on the behaviour of using twenty four and forty nine elments as shown in Fig. (8.1). These analysis are shown in Fig. (8.2) to Fig. (8.4). As can be seen, the results from the two analysis are almost indistinguishable. The failure load for the 49 element mesh is slightly lower than that for the 24 element mesh by 4%. The cost of analysis increased linearly with the increase in the number of

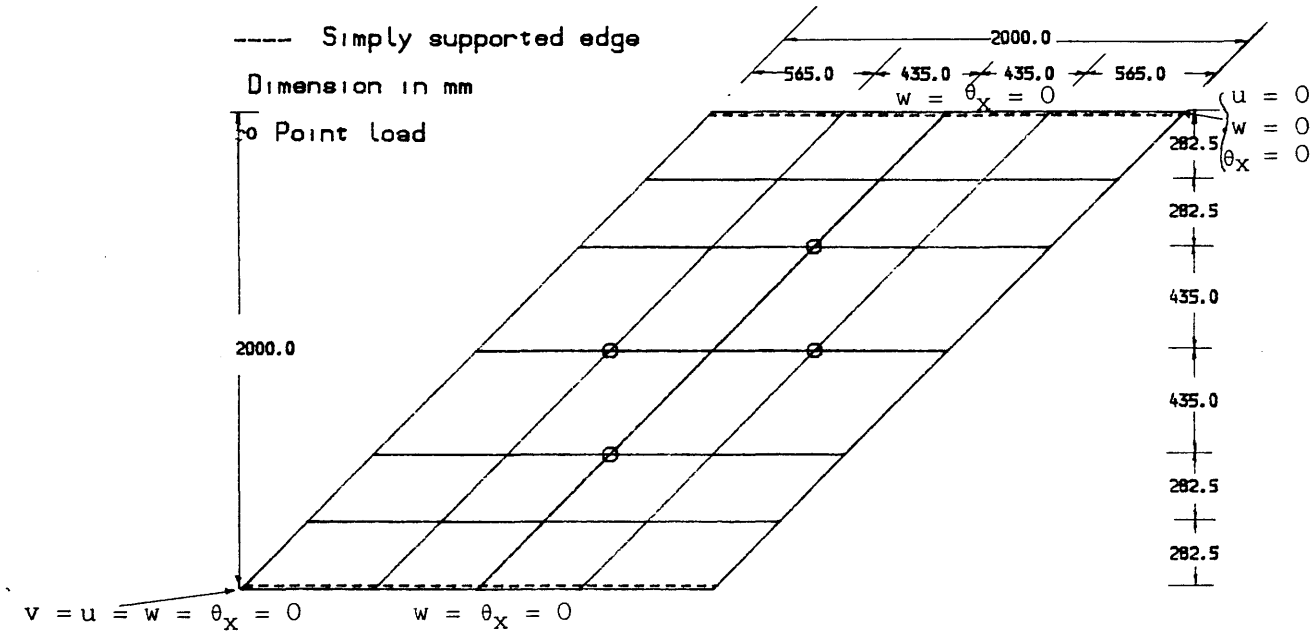

(a) Twenty four element used for models three, four and five

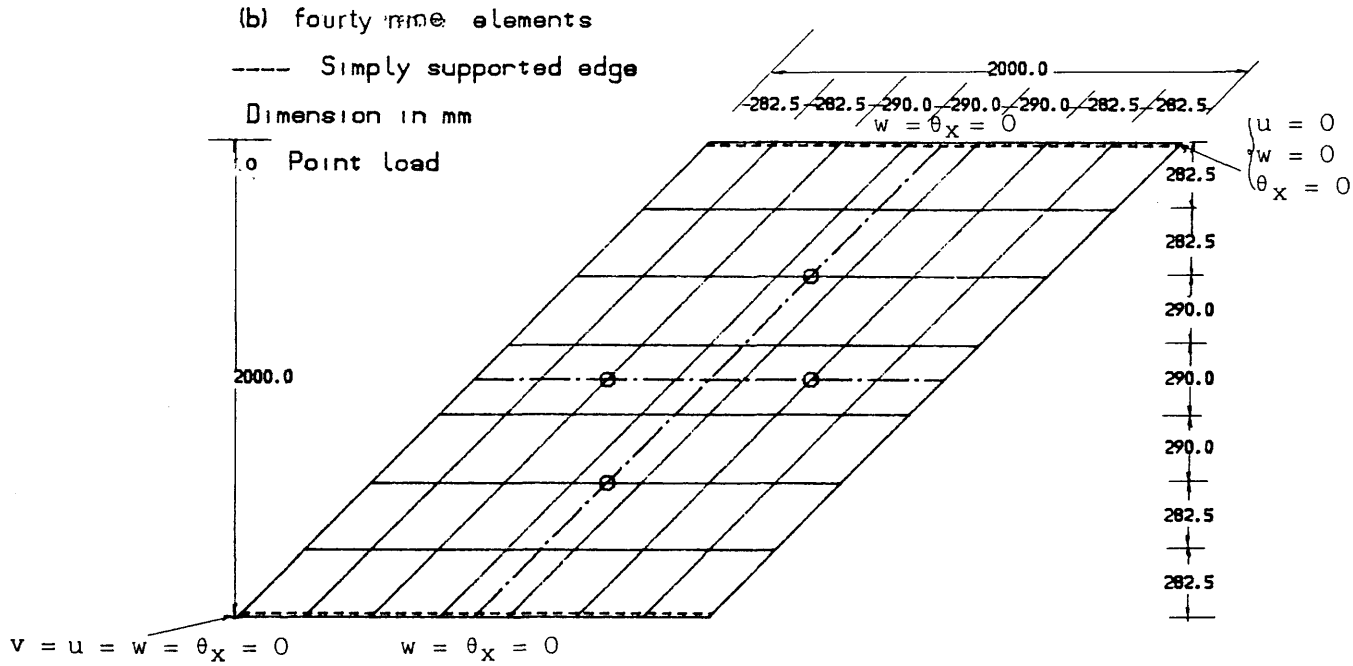

Fig. (8.1) Finite element mesh with boundary conditions and loading system

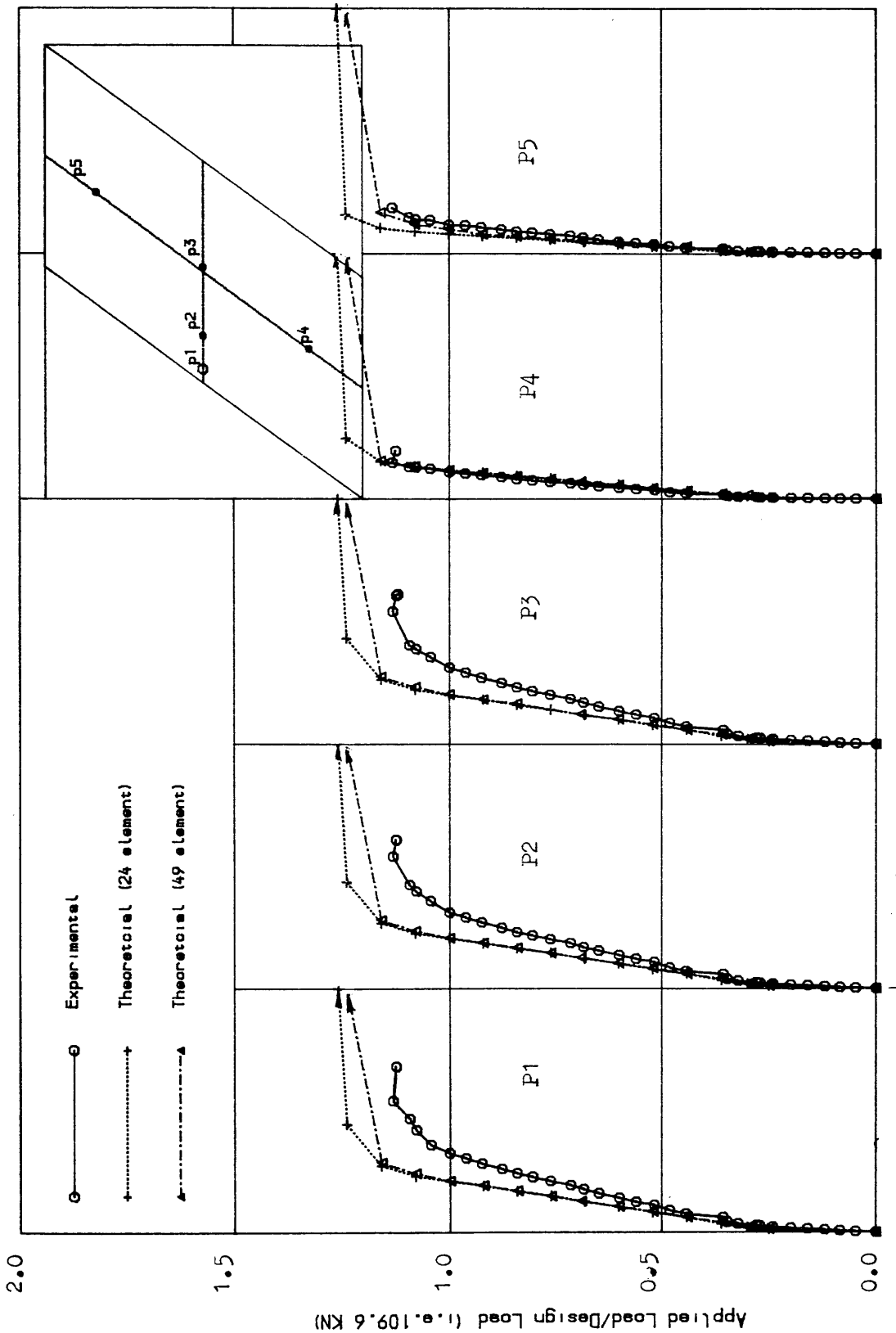

Fig. (8.2) Load-Deflection curves for MODEL NO. FIVE for different type of meshs

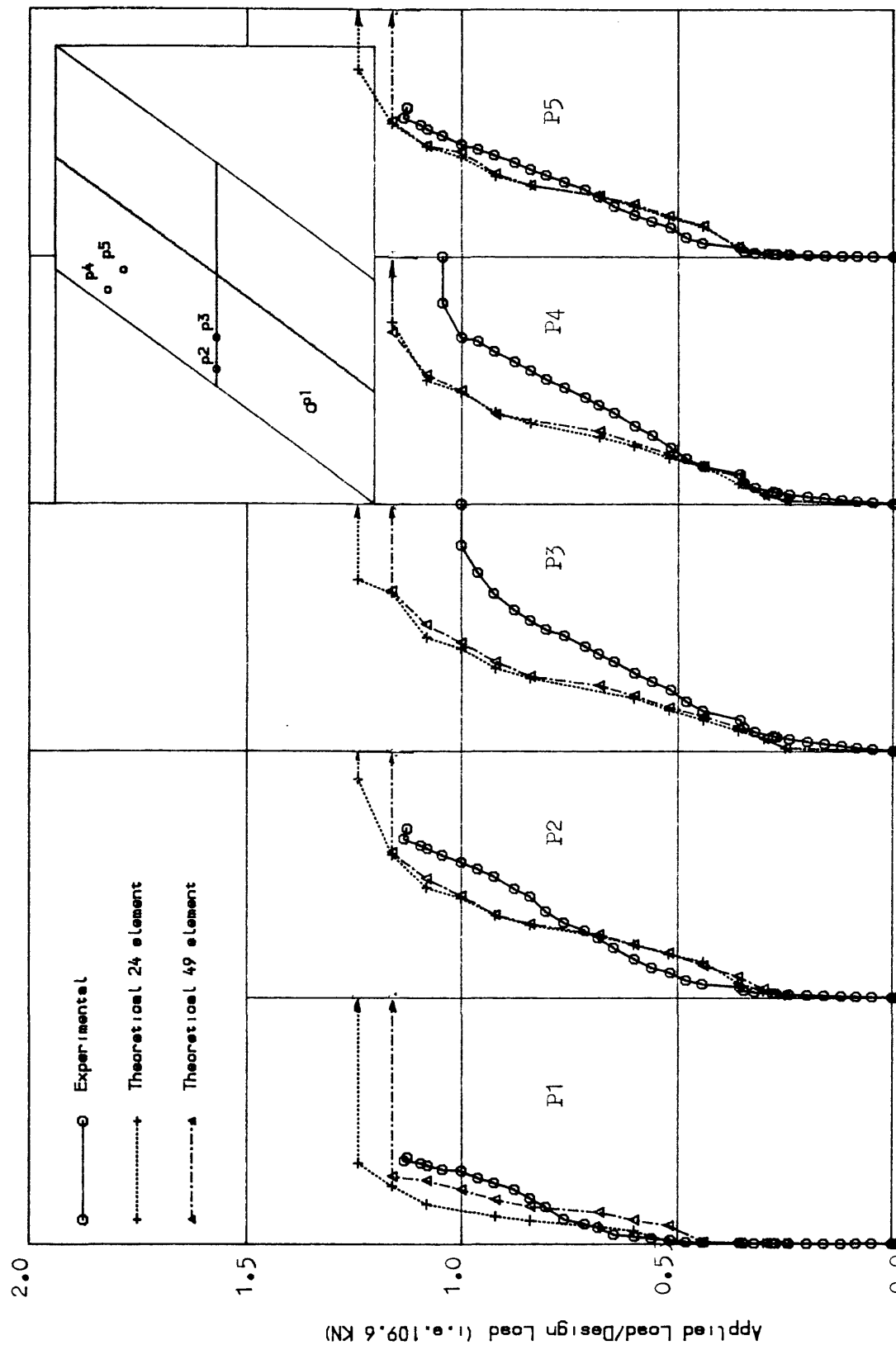

Fig. (8.3) Load-Steel Strain curves in the longitudinal direction for MODEL NO. FIVE for different type of meshs

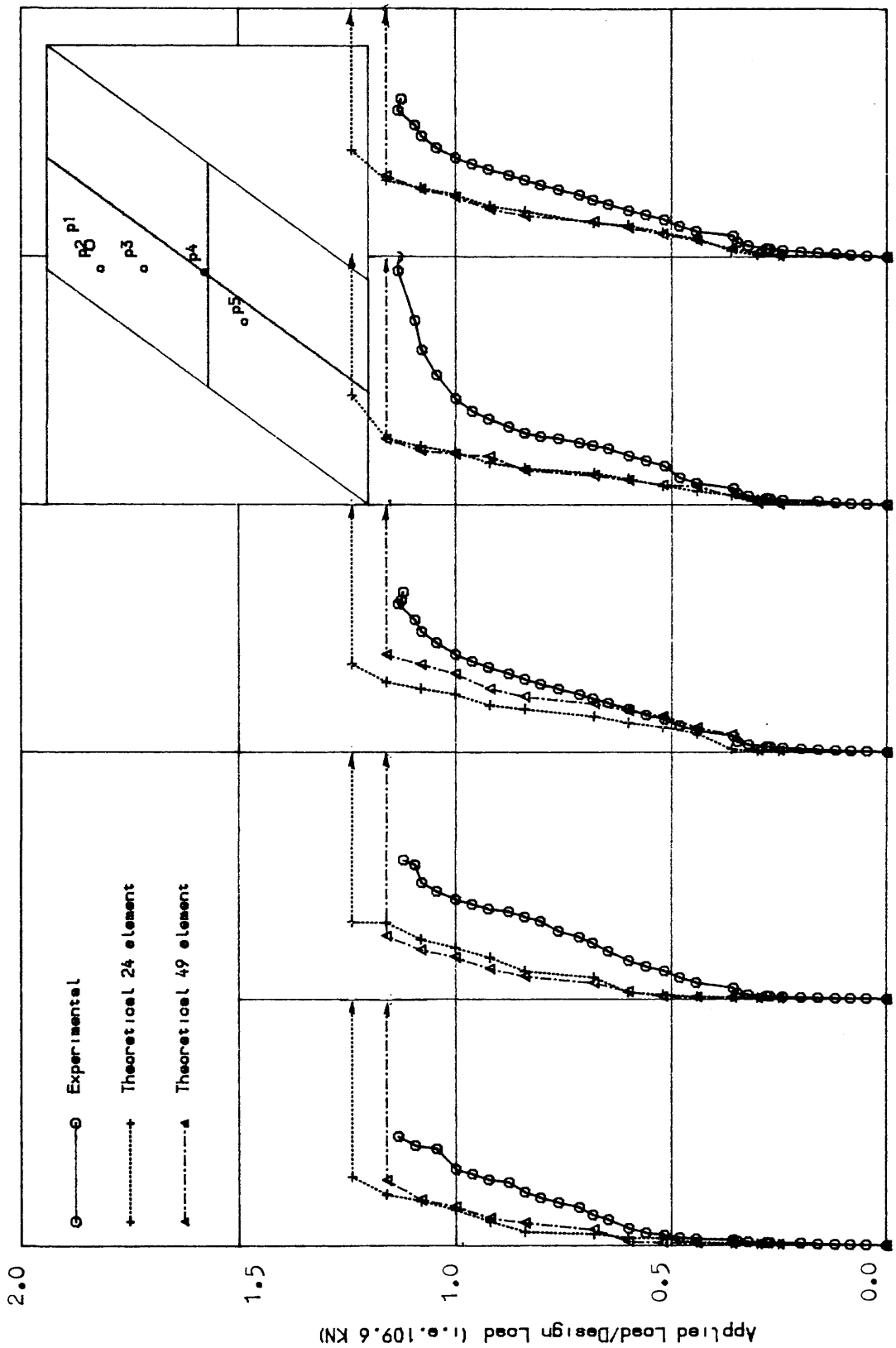

Fig. (8.4) Load-Transverse Steel Strain curves for MODEL NO. FIVE for different type of meshs

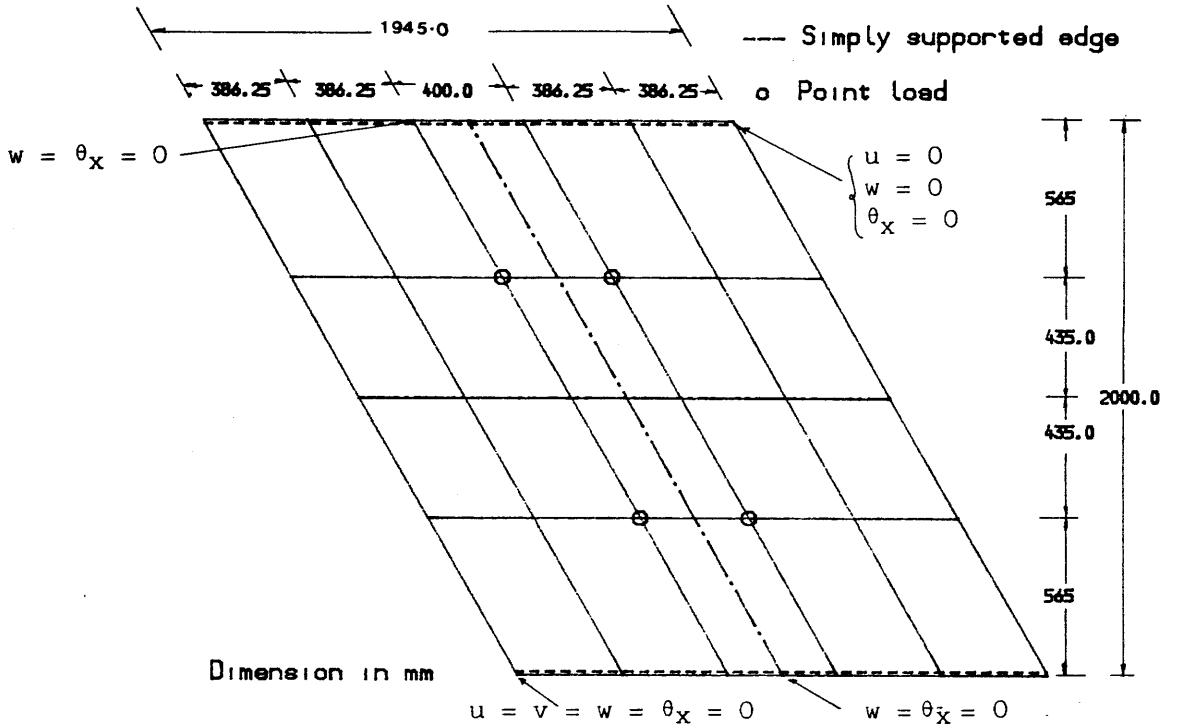

(a) Twenty elements used for MODEL NO. ONE

(b) Thirty element used for MODEL NO. TWO

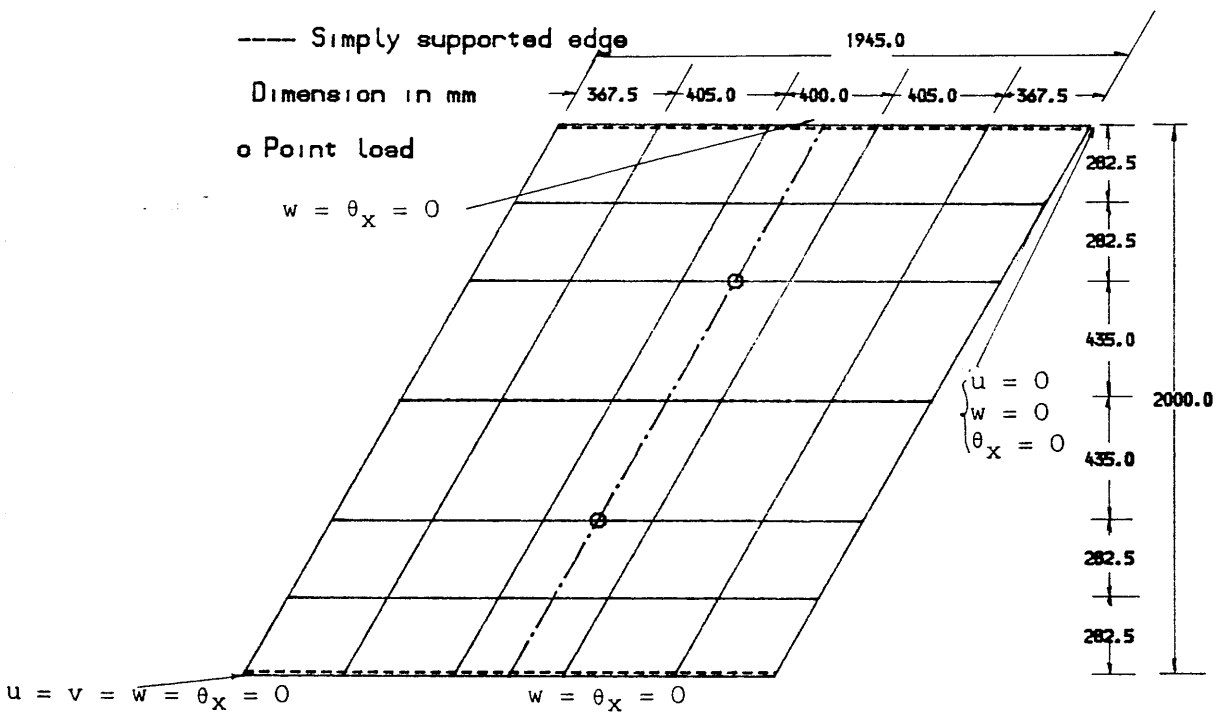

Fig. (8.5) Finite Element mesh with boundary conditions and loading system

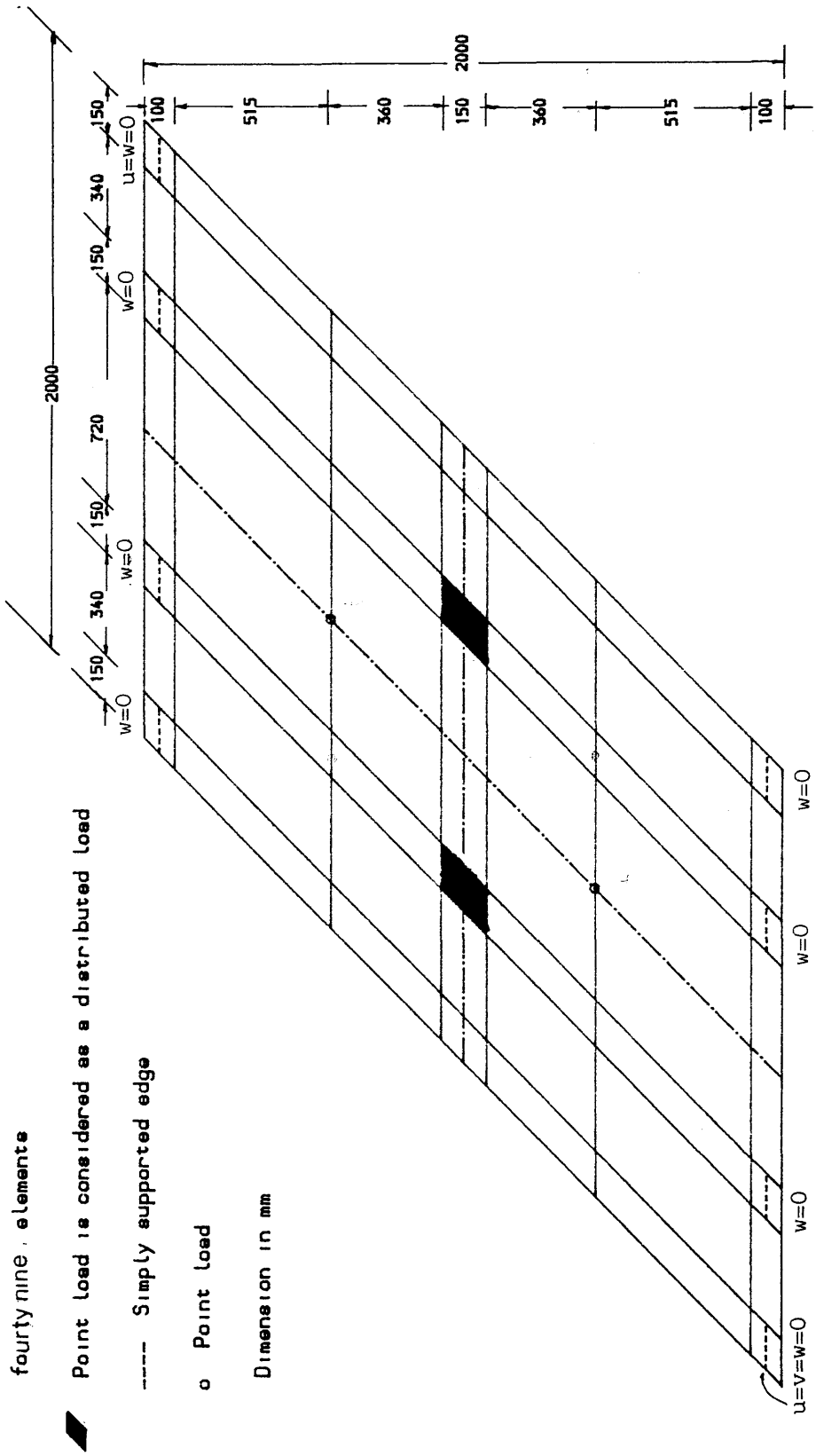

Fig. (8.6) Finite element mesh with boundary conditions and loading system for MODEL NO. SIX

elements used. Therefore a twenty four element representation suffices for this type of slab. The number of elements can be reduced to twenty if the degree of orthotropy of reinforcement and load condition allow, This was possible in model one. In model two thirty elements were used because of the degree of orthotropy of reinforcement. In model six a total of forty nine elements were adopted because of the shape of the model and the load condition. Fig (8.1a) and Figs (8.5) and (8.6) show the different meshs adopted for different models.

8.2.1.2 Shear Retention Factor

It has been shown in Chapter Five that when fixed crack analysis is considered, the predicted ultimate load depends on the tensile strength of the concrete and the value of shear retention factor β. In these analyses, the tensile strength of concrete was taken as the one obtained from tests on control specimen. Al-Mahaidi's formula (66) was used to evaluate B with slight modification:

$$\beta = 0.4 \,/\, cl \quad \text{with} \quad \beta \nless C \qquad (8.1)$$

where $cl = \varepsilon_f / \varepsilon_{cr}$

ε_{cr} is the concrete tensile strain

ε_f is the fictitious strain normal to the crack

C is the constant less than 0.4.

The constant C was used to study the effect of β on the ultimate behaviour of models one ($\alpha = 120^{o}$), two ($\alpha = 60^{o}$) and five ($\alpha = 45^{o}$). In Fig (8.7) to Fig (8.12) comparisons are presented for the load-deflection and load-longitudinal steel strain obtained experimentally and

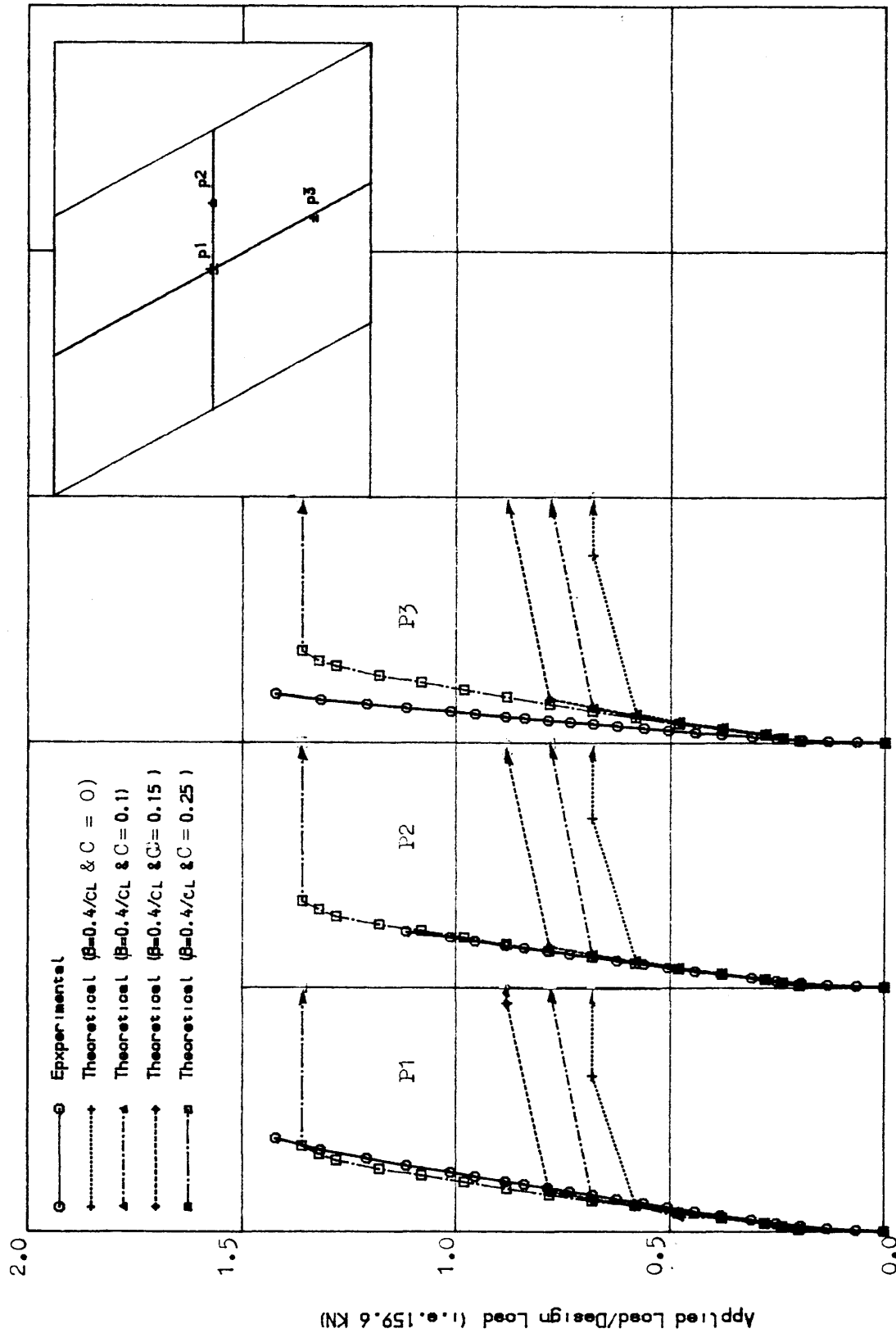

Fig. (8.7) Load-Deflection curves for MODEL NO. ONE using different values of shear retention factor B

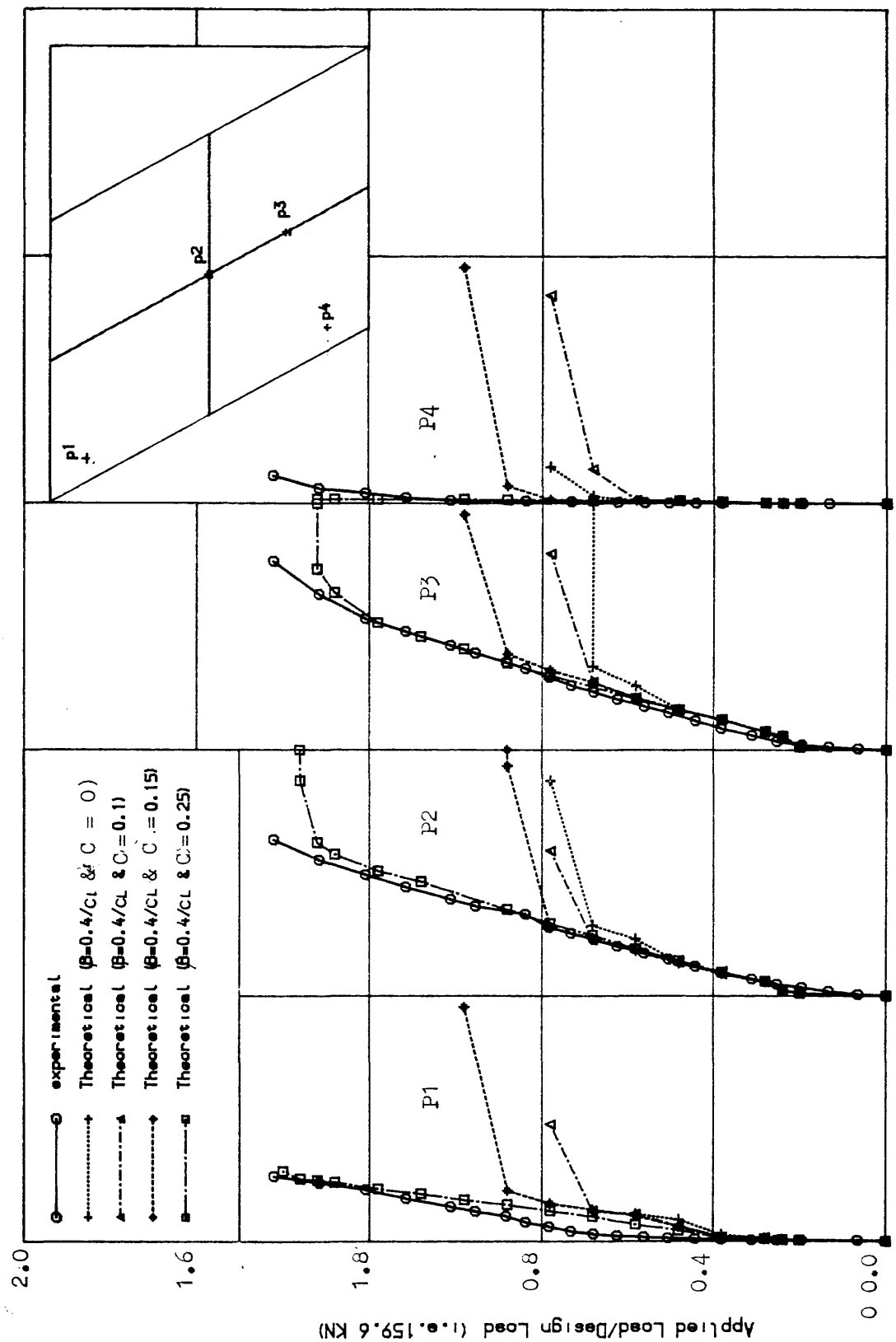

Fig. (8.8) Load-Longitudinal Steel Strain curves for MODEL NO. ONE for different values of shear retention factor B

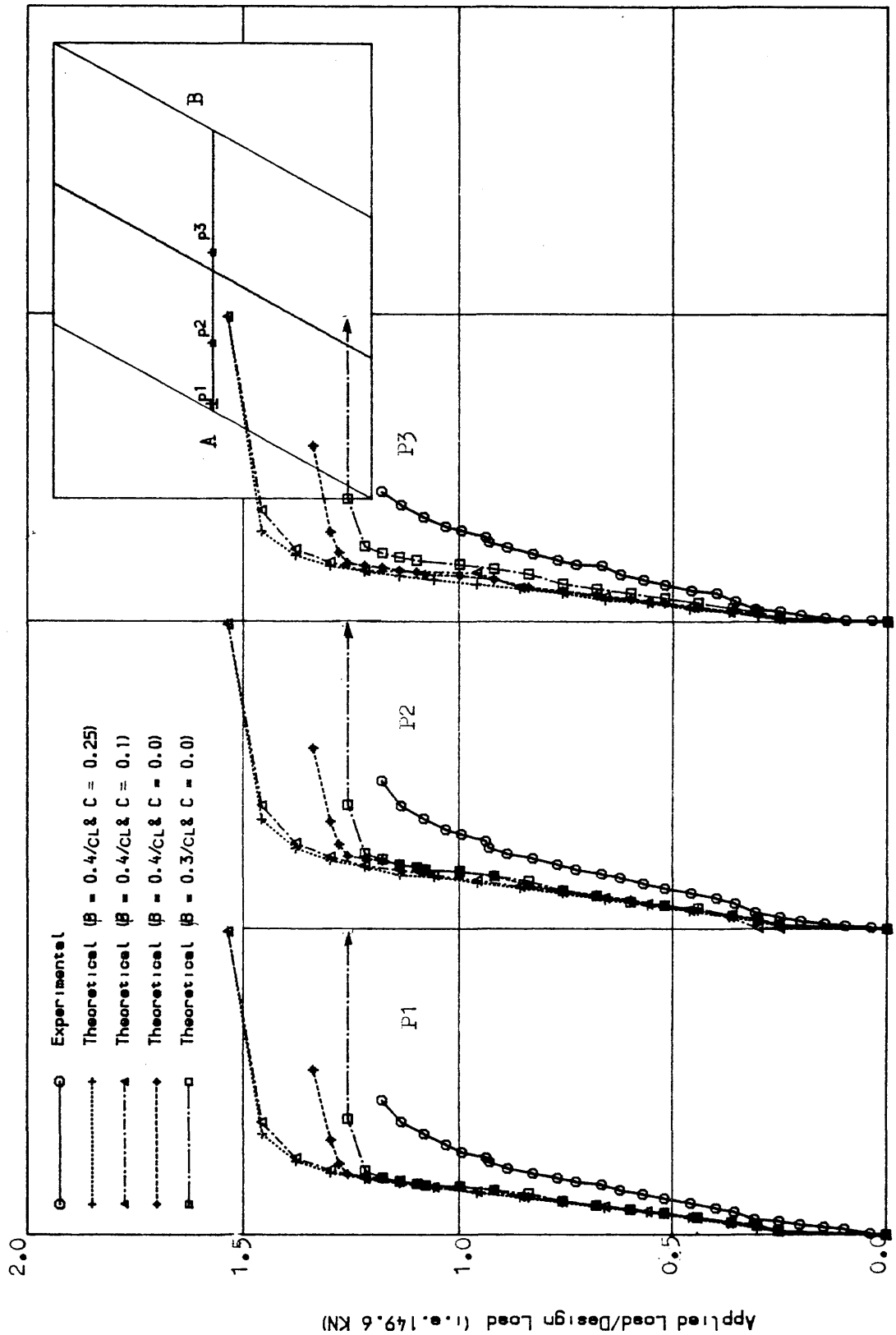

Fig. (8.9) Load-Deflection curves along the centre line A-B for MODEL NO. TWO for different values of shear retention factor B

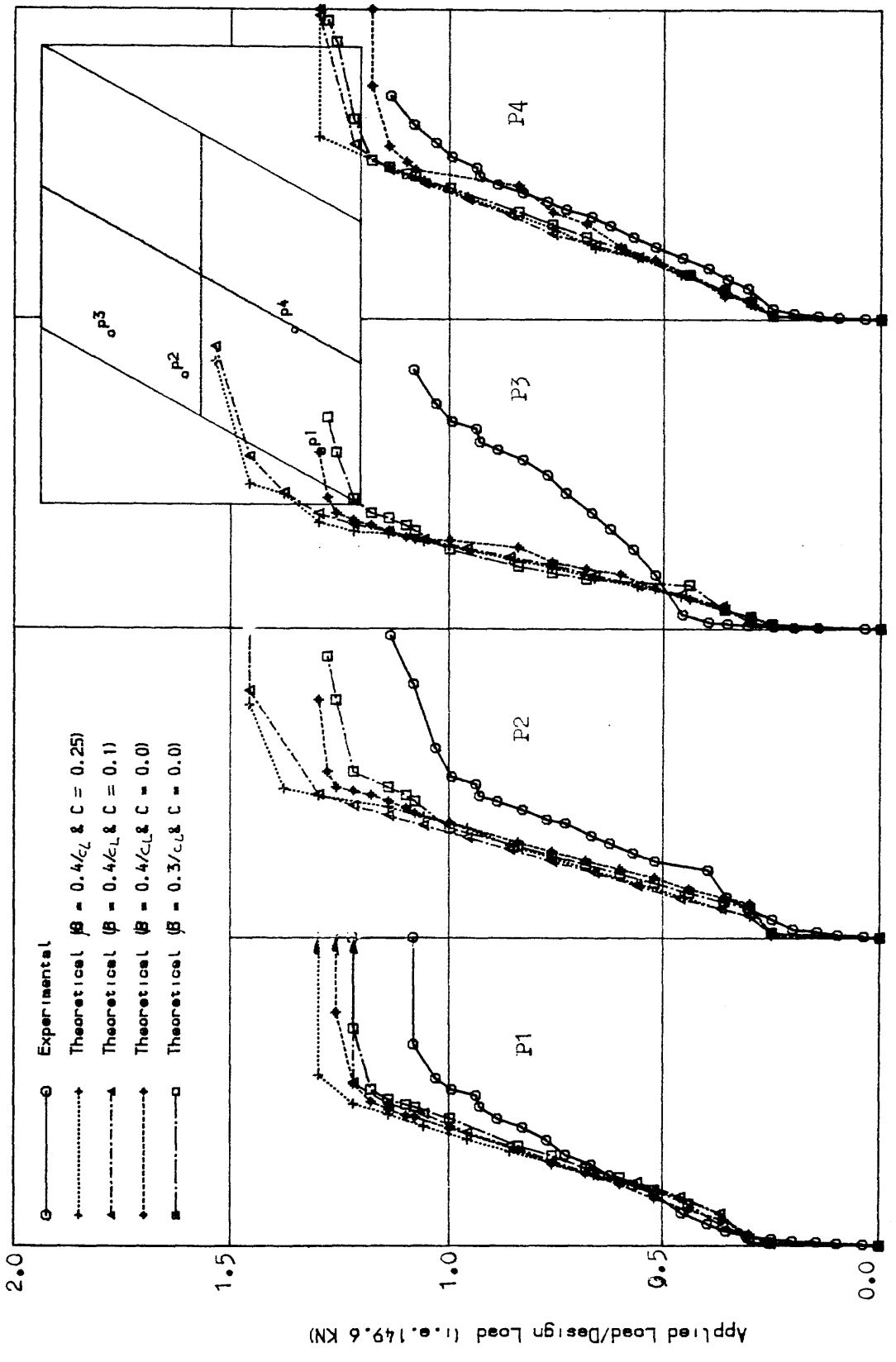

Fig. (8.10) Load-Longitudinal Steel Strain for MODEL NO. TWO for different values of shear retention factor B

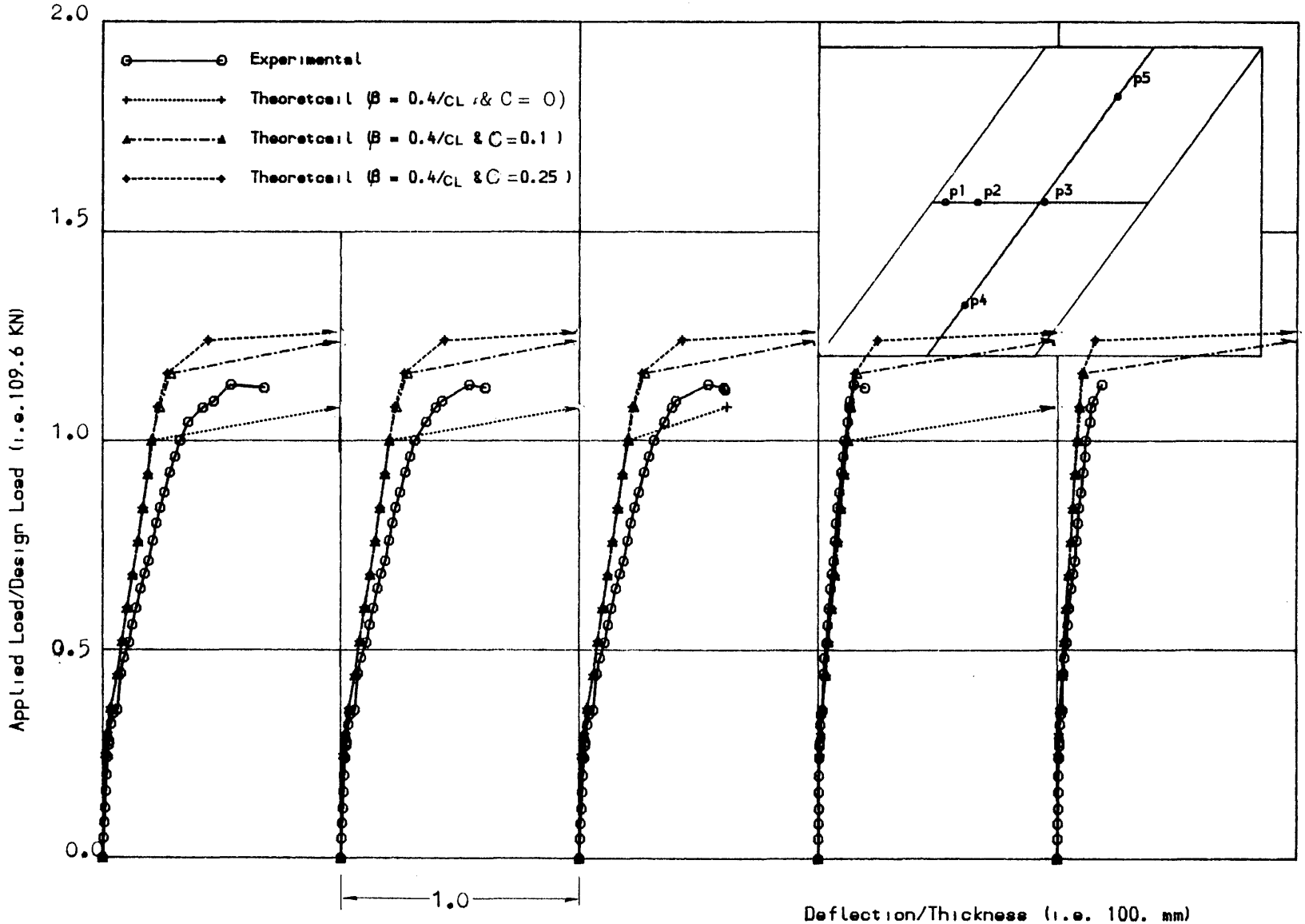

Fig. (8.11) Load-Deflection curves for MODEL NO. FIVE using different values of shear rentention factor B

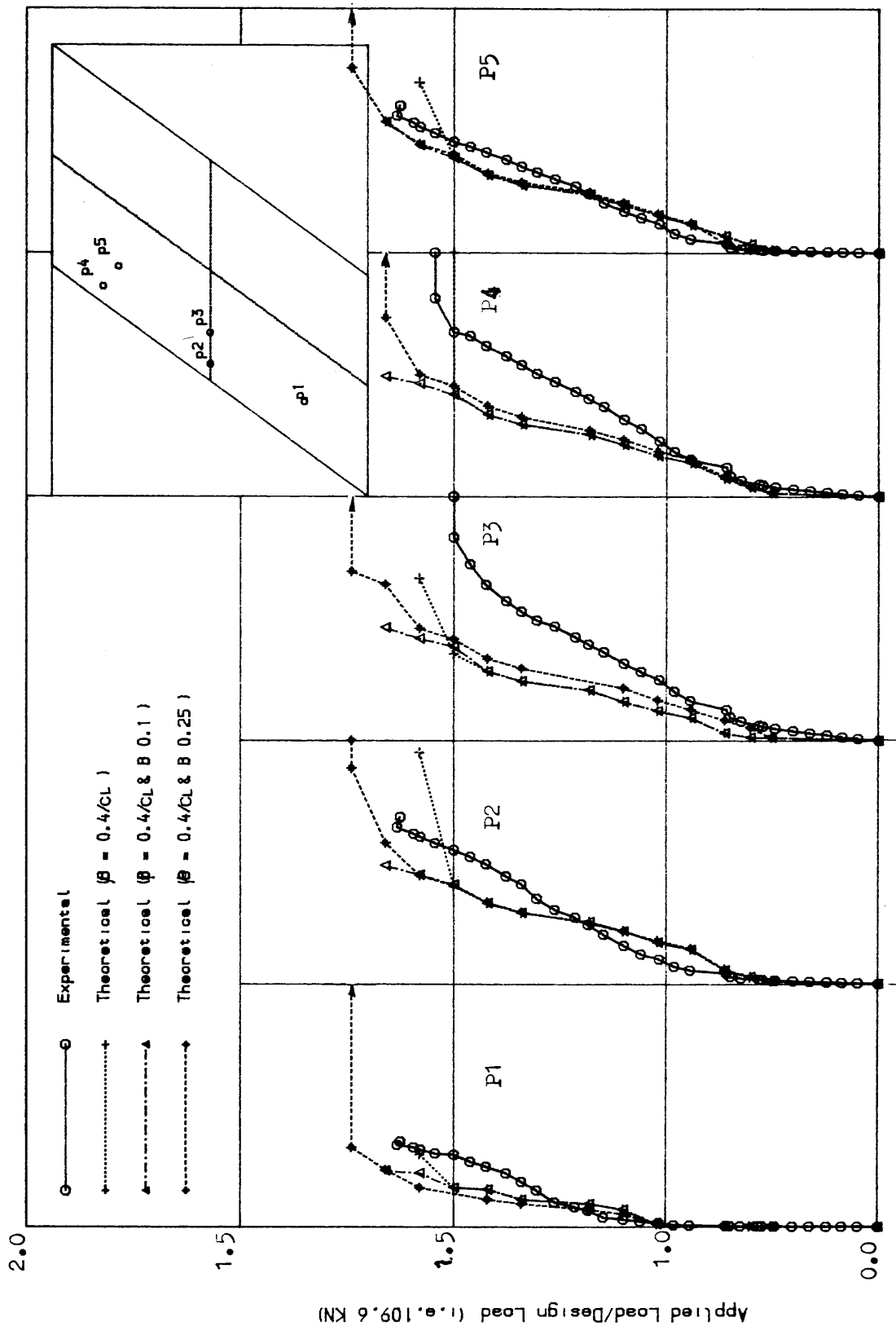

Fig. (8.12) Load-Longitudinal Steel Strain curves for MODEL NO. FIVE for different values of shear retention factor B

those obtained in the present study using different shear retention values. It can be seen that, the effect of Beta on the theoretical failure load was dependent on the angle of skew as follows;

(i) The failure load of the first model ($\alpha = 120^{o}$ is very much affected by the value of C. For C values 0.0, 0.1, 0.15 and 0.25 the ultimate failure loads were 0.56 and 0.56 and 0.71 and 0.97 of the experimental failure load.

(ii) For the second model ($\alpha = 60^{o}$) the failure loads were 1.14, 1.3 and 1.3 of the experimental failure load for C values 0.0, 0.1 and 0.25 respectively. When B = $0.3\varepsilon_f / \varepsilon_{cr}$ is used with C equal 0.0, better comparisons with the experiment values were obtained.

(iii) For model 5 ($\alpha = 45^{o}$) the failure loads were 0.98, 1.06 and 1.12 of the experimental failure load for C values of 0.0, .1 and 0.25 respectively.

It can be concluded from these results that, in general, the best agreement with the experiment was obtained using Eqn (8.1) with C = 0.25. This was used for all the models except for model two for which B = $0.3\ \varepsilon_f / \varepsilon_{cr}$.

8.2.2 Analysis and Comparisons

Table (8.3) summarizes the comparisons between the experimental results and theoretical results for all the models. In Fig (8.13) to Fig (8.27) Comparisons between experimental and $theoretical results are presented for the load-deflection and load-longitudinal steel strain curves.

Table (8.3) Summary of comparison between the experimental results and the theoretical results

Model No.	Theor. crack load / Exper. crack load	Load at first yield of steel (theor.) / Load at first yield of steel (exper.)	Theor. failure load / Exper. failure load	Theor. service load / Exper. service load (at 5.8 f_y limit load)	Defl. at service load (theor.) / Defl. at service load (exper.)	Theor. type of failure	Exper. type of failure
1	1.1	0.98	0.95	0.98	1.05	Initiated by yielding of steel	Initiated by yielding of steel and finished by shear
2	0.83	1.15	1.06	1.1	0.9	Initiated by yielding of steel	Ductile failure
3	1.06	1.32	0.95	1.2	0.86	Initiated by yielding of steel	Ductile failure
5	.90	1.375	1.15	1.08	0.90	Initiated by yielding of steel	Ductile failure combined with punching shear at the obtuse corner
6	1.05	0.98	1.017	1.0	0.96	Initiated by yielding of steel	Ductile failure combined with diagonal shear failure

It should be noted that the data points beyond the range of the of the scale which is noted by (⟶) have not be plotted.

8.2.2.1 Model Number One

(a) Load vs Deflection Curves

Table (8.3) shows the comparisons between the theoretical results and the experimental results. Fig (8.13) shows the comparisons between the experimental load-deflection curves at different locations and the corresponding theoretical values considering the actual steel and the design steel. Referring to the actual steel analysis, it can be seen that the theoretical cracking load was 1.1 of the experimental cracking load. The theoretical ultimate load was 0.97 of the experimental failure load. It is noted from these comparisons that the predicted results compare reasonably well with the experiment. Similar comparisons can be seen from the longitudinal steel strain curves in Fig. (8.14)

8.2.2.3 Model Number Two

(a) Load vs Deflection Curves

In Table (8.3) the experimental results are compared with those obtained numerically. Also in Fig (8.15) comparisons are presented for the load-deflection curves at different locations obtained experimentally and those obtained numerically. These curves show that the theoretical values are smaller than the experimental values. This is probably due to the effect of the fixed angle of crack on the stress redistribution. The

theoretical cracking load was 0.83 of the experimental cracking load and the ultimate theoretical load is 1.10 of the experimental failure load.

(b) Load vs Steel Strain curves

Fig (8.16) shows a comparison of experimental and theoretical results for load-longitudinal steel strain at different locations. From these curves it can be seen that there is a good agreement between the two results at all positions except near the obtuse corner again emphasizing the steep strain gradient at that position. The theoretical yield load is 1.2 of the experimental load. This overestimation is probably due to the effect of fixed crack analysis, as has been discussed in Chapter Five. Similarly Fig. (8.17) shows the results for transverse steel strains.

8.2.2.3 Model Number Three

(a) Load vs Deflection Curves

Considering the actual steel results it can be seen from Table (8.3) that the ratio of the theoretical cracking load is 1.06 of the experimental cracking load. From Fig. (8.18) it can be seen that there is good agreement between the two results for positions near the edges. However there are somewhat stiffer results at positions near the centre area. The theoretical failure load is 0.95 of experimental failure load.

(b) Load vs Longitudinal Steel Strain

Fig (8.19) shows the comparison between the experimental Load vs Longitudinal steel strain curves and

the corresponding theoretical values considering actual steel and design steel. Referring to the actual steel, it can be seen that the predicted results compare well with the experimental results. The theoretical yield load was 1.3 of the experimental yield load.

(c) Load vs Transverse Steel strains.

Fig (8.19) shows the comparisons between the experimental load vs longitudinal steel strain curves and the corresponding theoretical values considering actual steel and design steel. Although the experiment shows that the steel in the transverse direction carried significant (0.7 of f_y) tensile stress, the theoretical results shows the transverse steel carried a negligible compression stress. This is due to the effect of the assumption of fixed crack analysis on the stress redistribution as explained in Chapter Five.

8.2.2.4 Model Number Five

(a) Load vs Deflection Curves

In Fig (8.21) comparisons are presented for the load-deflection curves obtained experimentally and those obtained numerically. It can be seen that the theoretical cracking load is 0.90 of the experimental cracking load. The theoretical results compare reasonably well with the experimental results at positions near the support edges. Slightly stiffer theoretical results are obtained in the region of the midspan of the slab. The theoretical failure load is 1.15 the experimental failure load.

(b) Load-Longitudinal Steel Strain

In Fig (8.21) shows the longitudinal steel strain values obtained experimentally and theoretically. It can be noted from these comparisons that the predicted theoretical results compare well with experimental results at all positions except for positions 3 and 4 which were affected by the presence of cracks at these locations. The theoretical yield load is 1.3 of the experimental yield load.

(c) Load vs Transverse steel strains

Fig. (8.23) shows Load vs transverse steel strains. It can be seen that the theoretical values are smaller than the experimental values.

8.2.2.5 Model Number Six

(a) Load vs Deflection Curves

Figs (8.24) and (8.25) show the load-deflection curves. In general the correlation is reasonably good. The theoretical cracking load is 1.05 of the experimental cracking load. The theoretical failure load is 1.02 of experimental failure load.

(d) The Load-Longitudinal Steel Strain

Figs (8.26) and (8.27) shows the load-longitudinal steel strain curves. It can be seen that on the whole, the theoretical analysis reflects the true behaviour of the model.

8.2.3 General Discussion of results

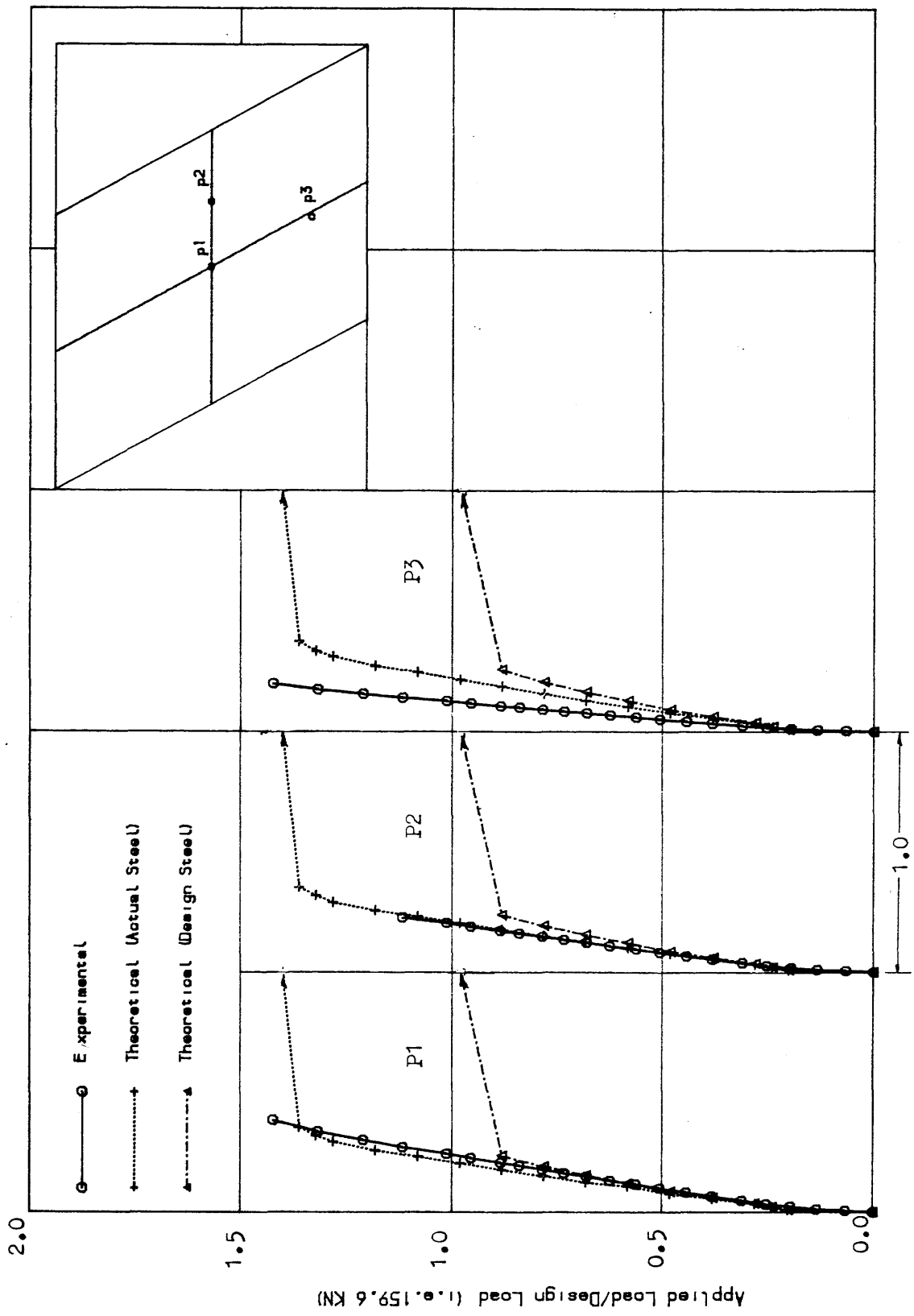

Fig. (8.13) Comparsions of Load-Deflection curves for MODEL NO. ONE

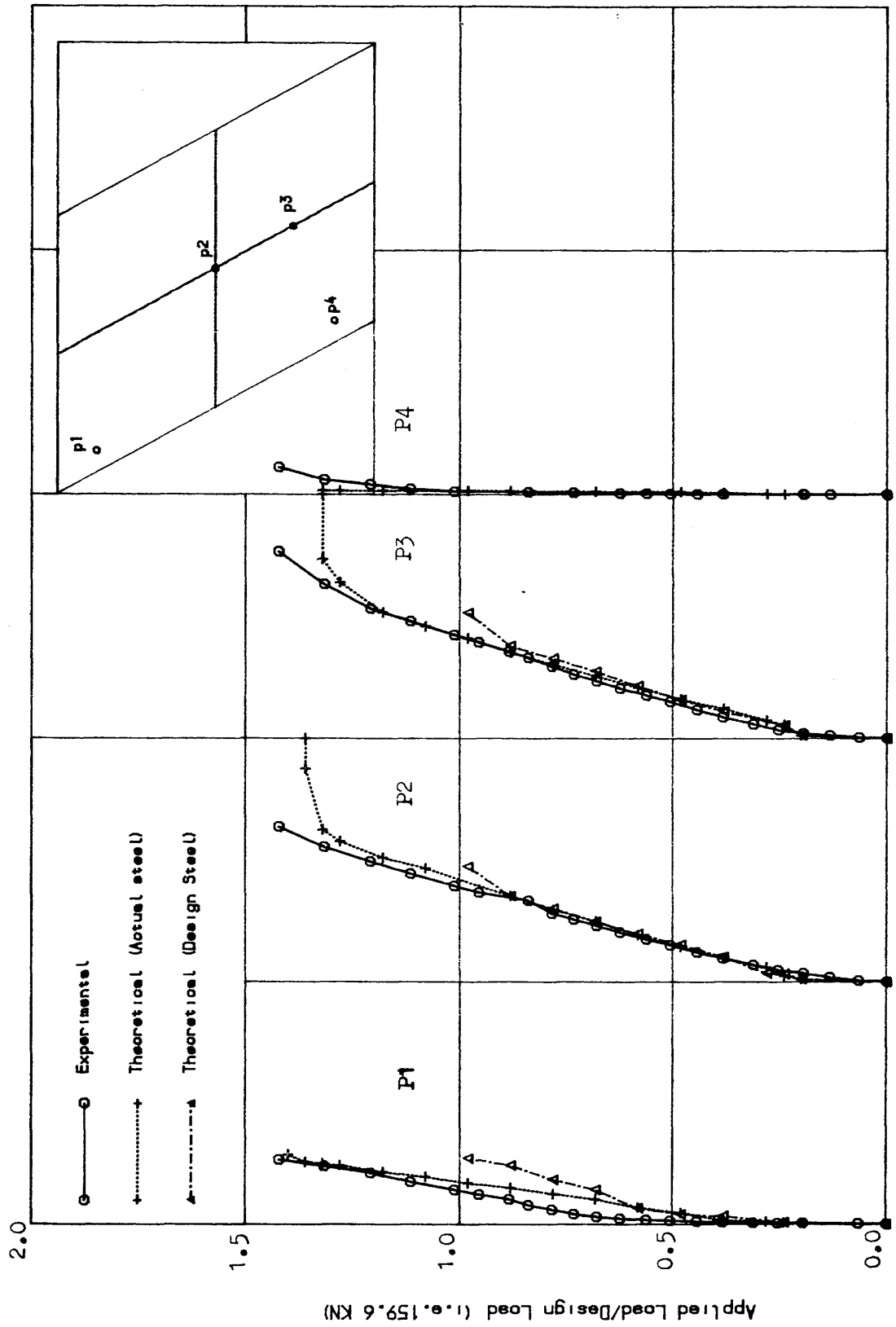

Fig. (8.14) Comparsion of Load-Longitudinal Steel Strain curves for MODEL NO. ONE

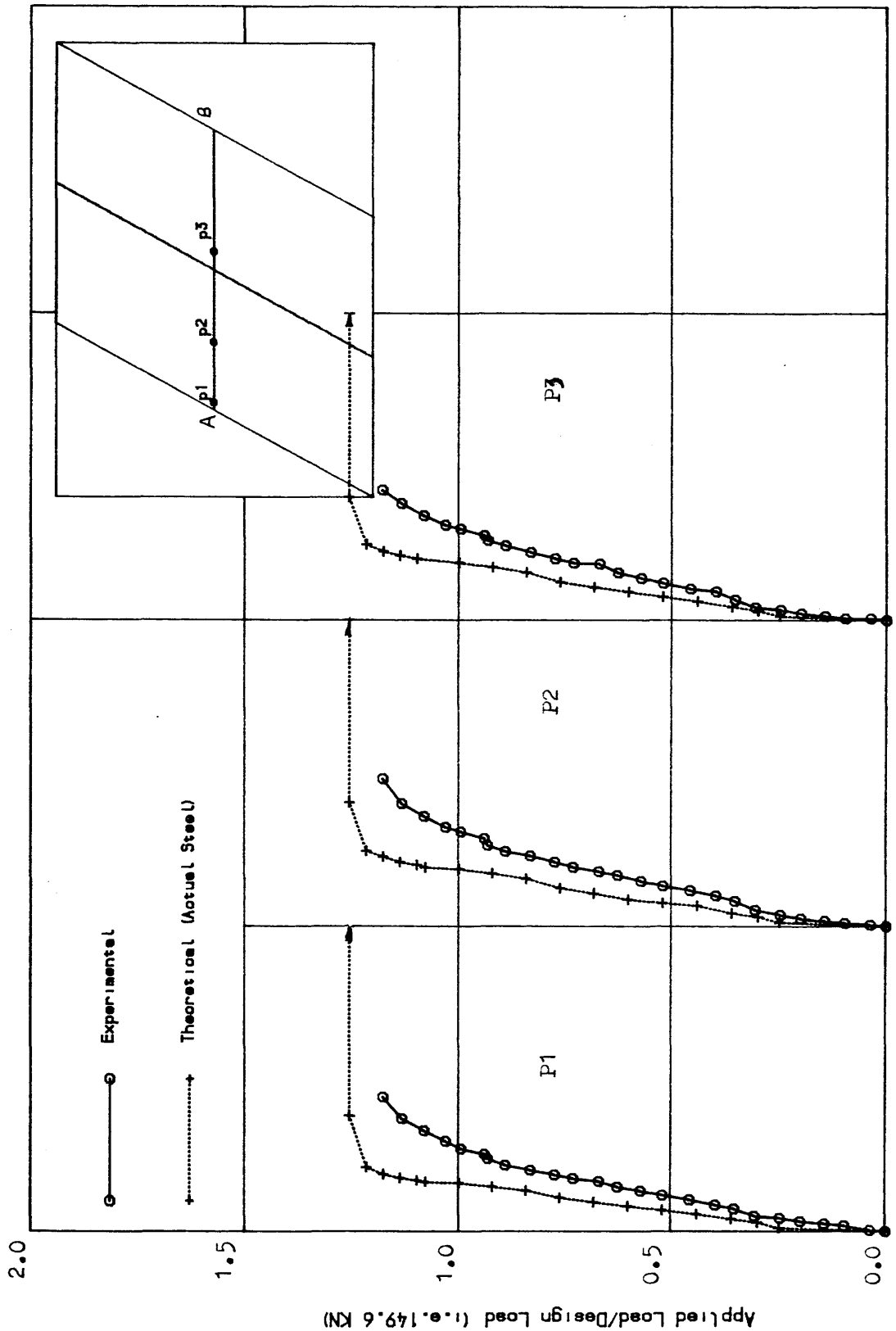

Fig. (8.15) Comparisons of Load-Deflection curves along the centre line A-B for MODEL NO. TWO

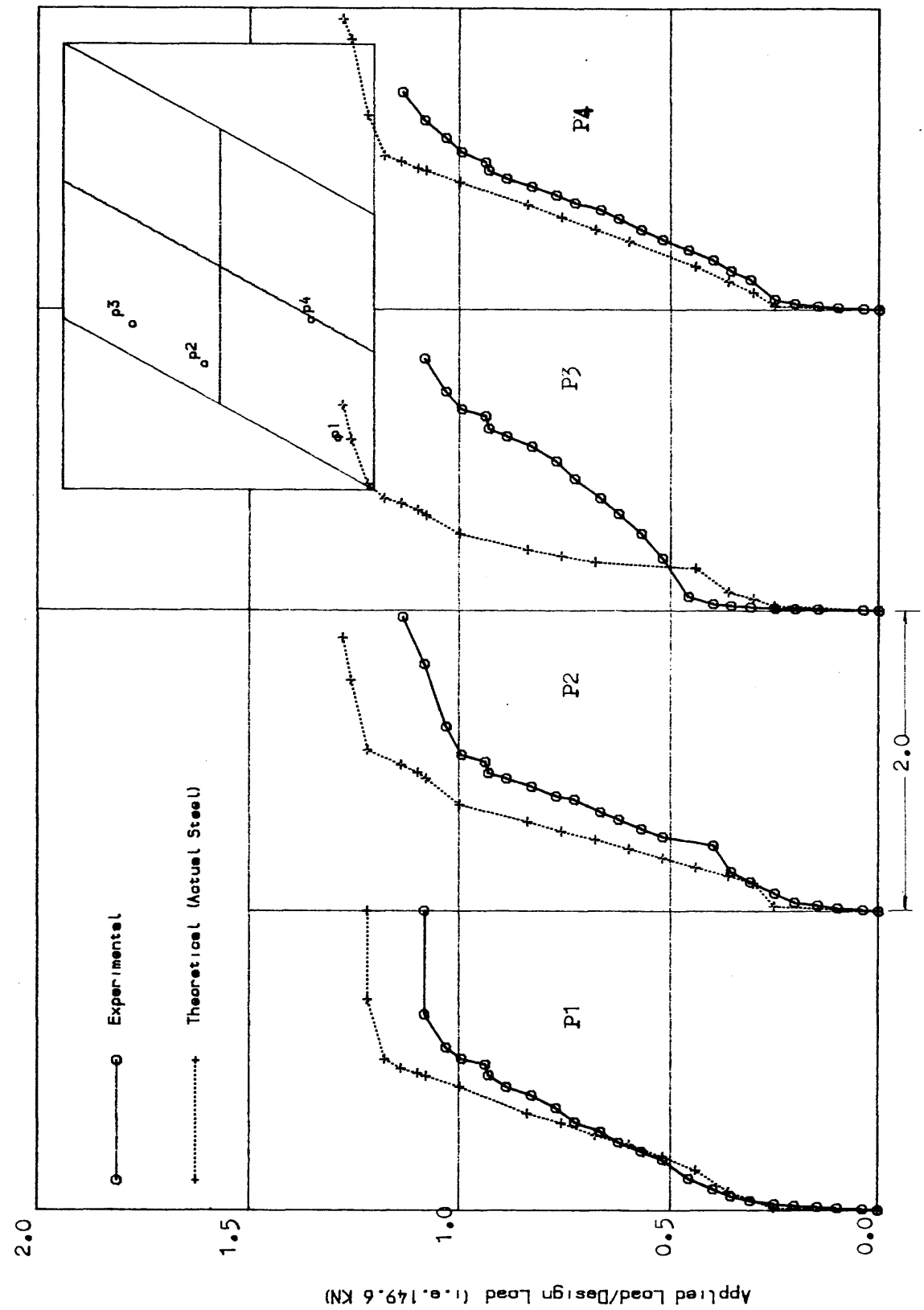

Fig. (8.16) Comparsions of Load-Longitudinal Steel Strain curves for MODEL NO. TWO

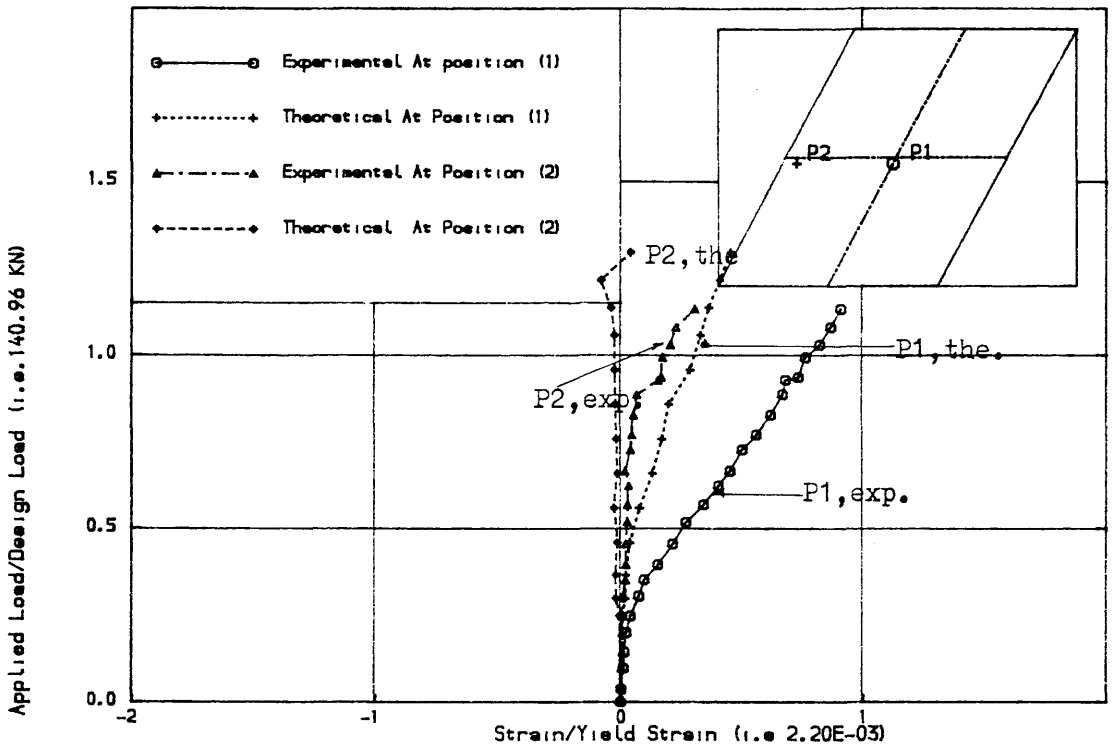

Fig. (8.17) Comparsions of Load-Transverse Steel Strain for MODEL NO. TWO

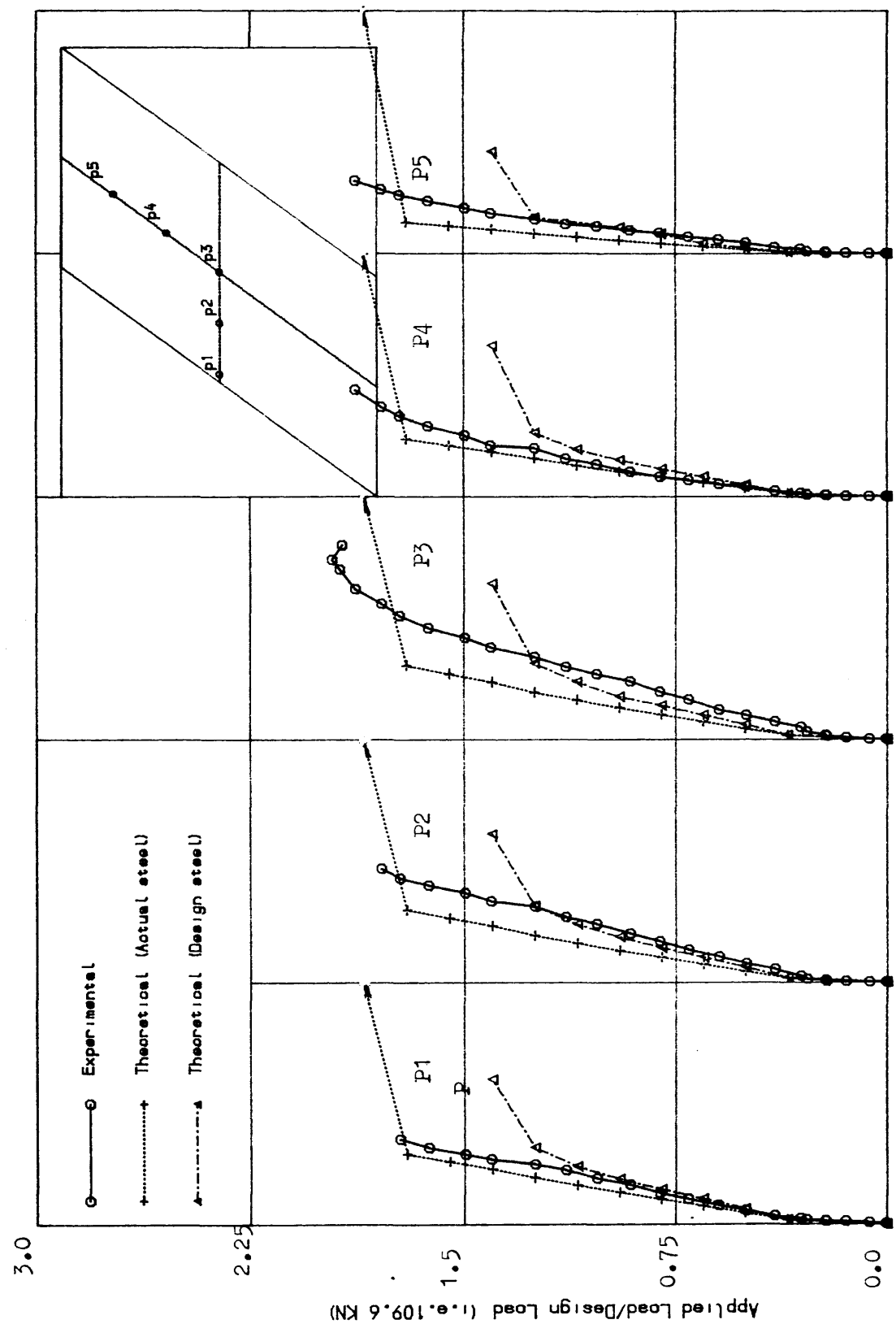

Fig. (8.18) Comparsions of Load-Deflection curves for MODEL NO. THREE

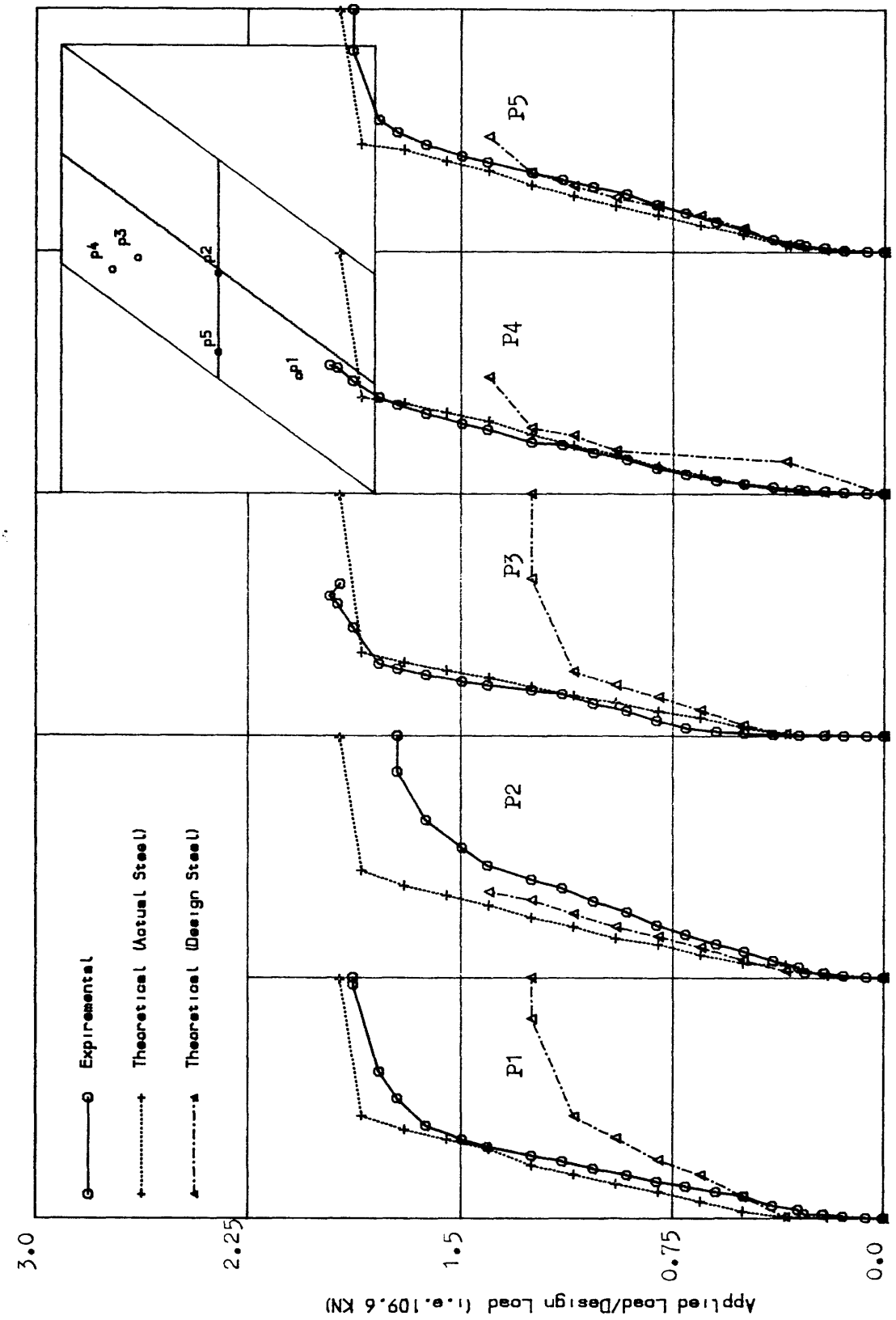

Fig. (8.19) Comparsions of Load-Longitudinal Steel Strain curves for MODEL NO. THREE

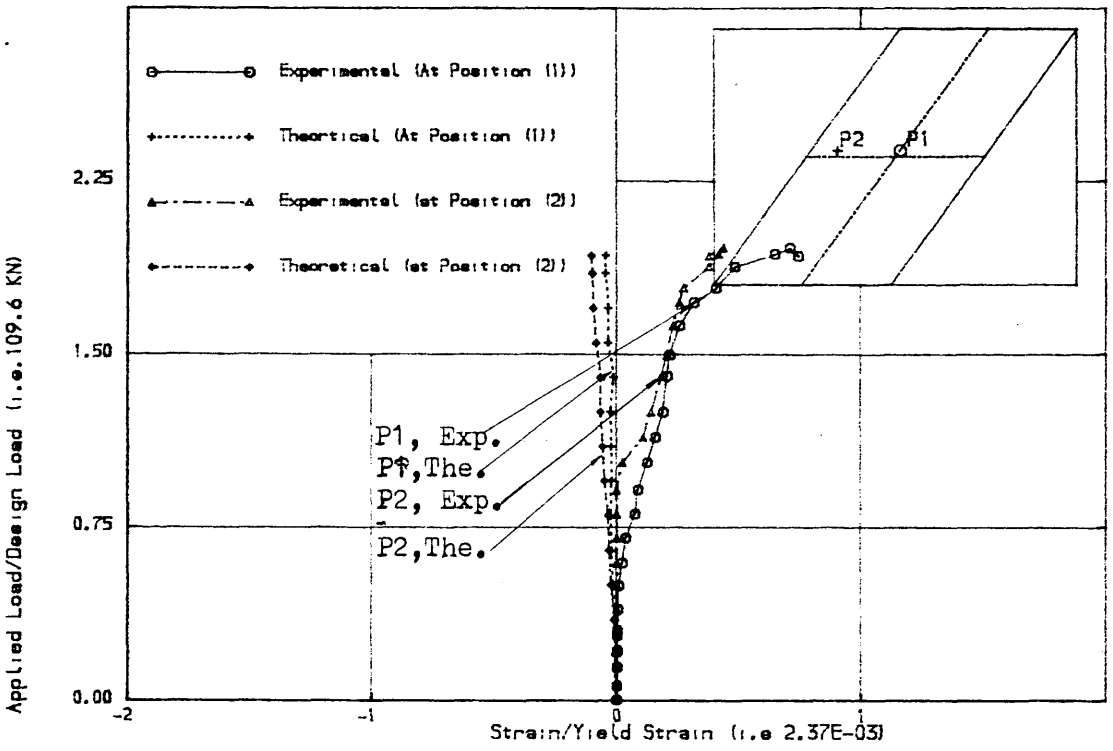

Fig. (8.20) Comparsion of Load-Transverse Steel Strain curves for MODEL NO. THREE

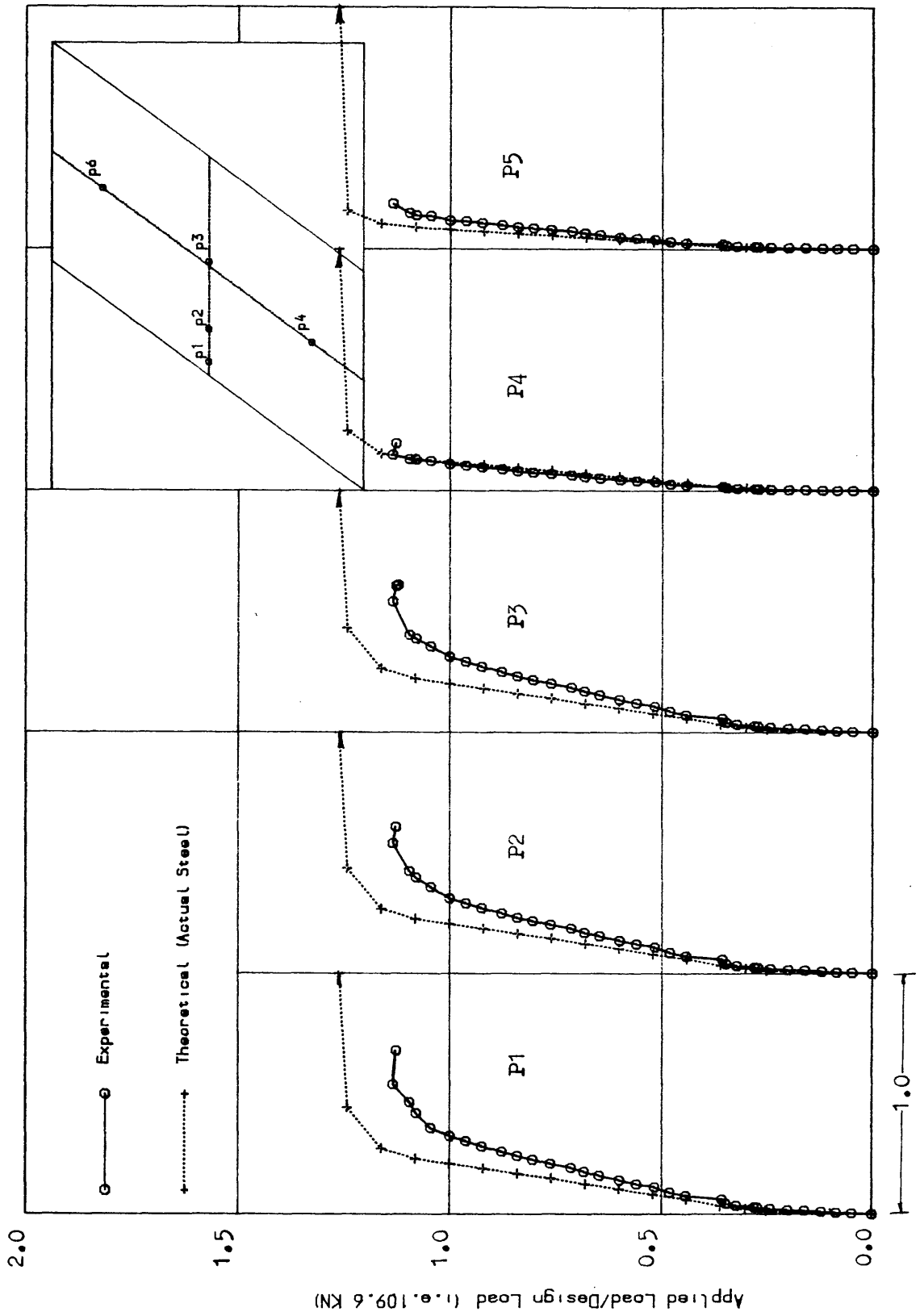

Fig. (8.21) Comparsions of Load-Deflection curves for MODEL NO. FIVE

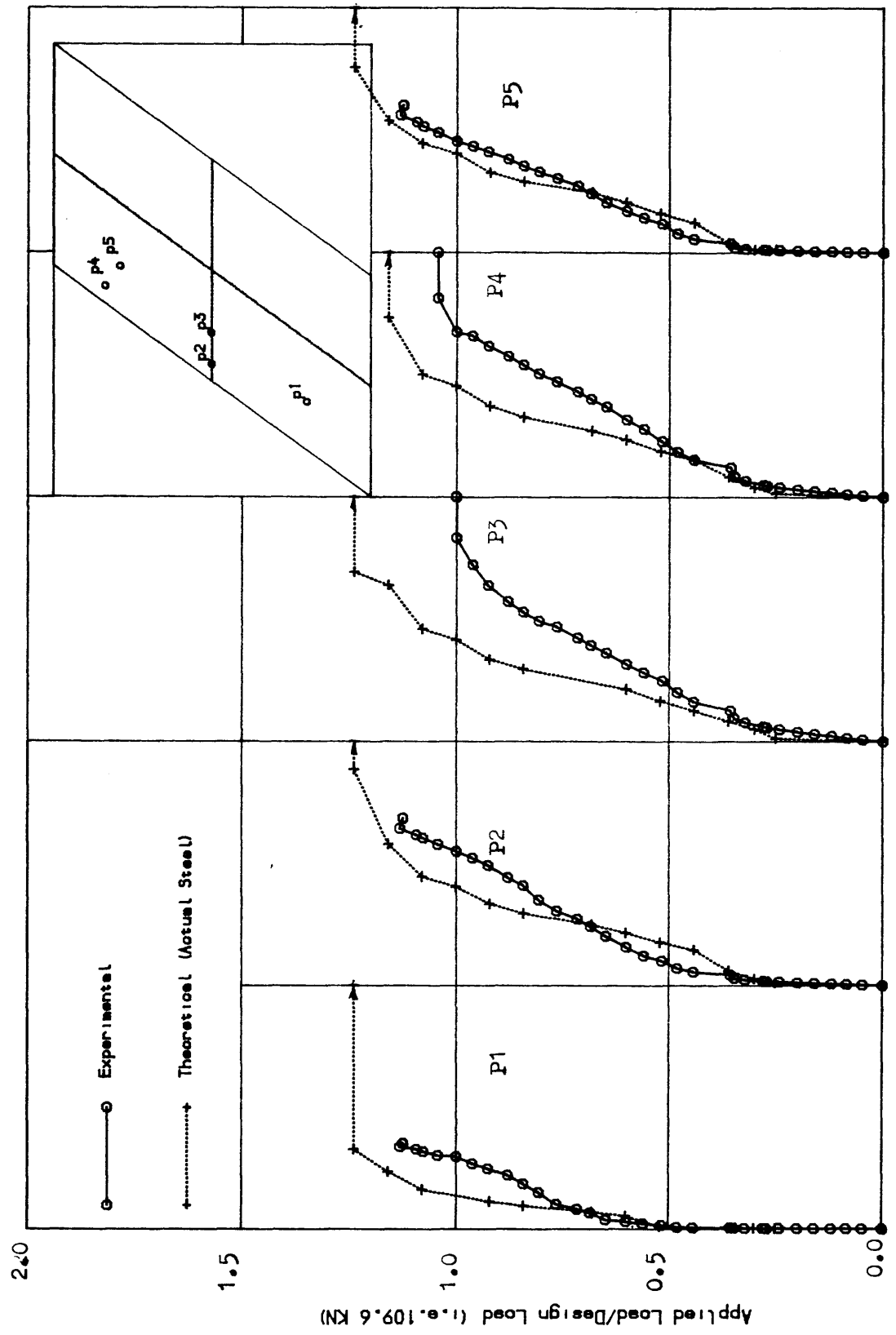

Fig. (8.22) Comparsions of Load-Longitudinal Steel Strain for MODEL NO. FIVE

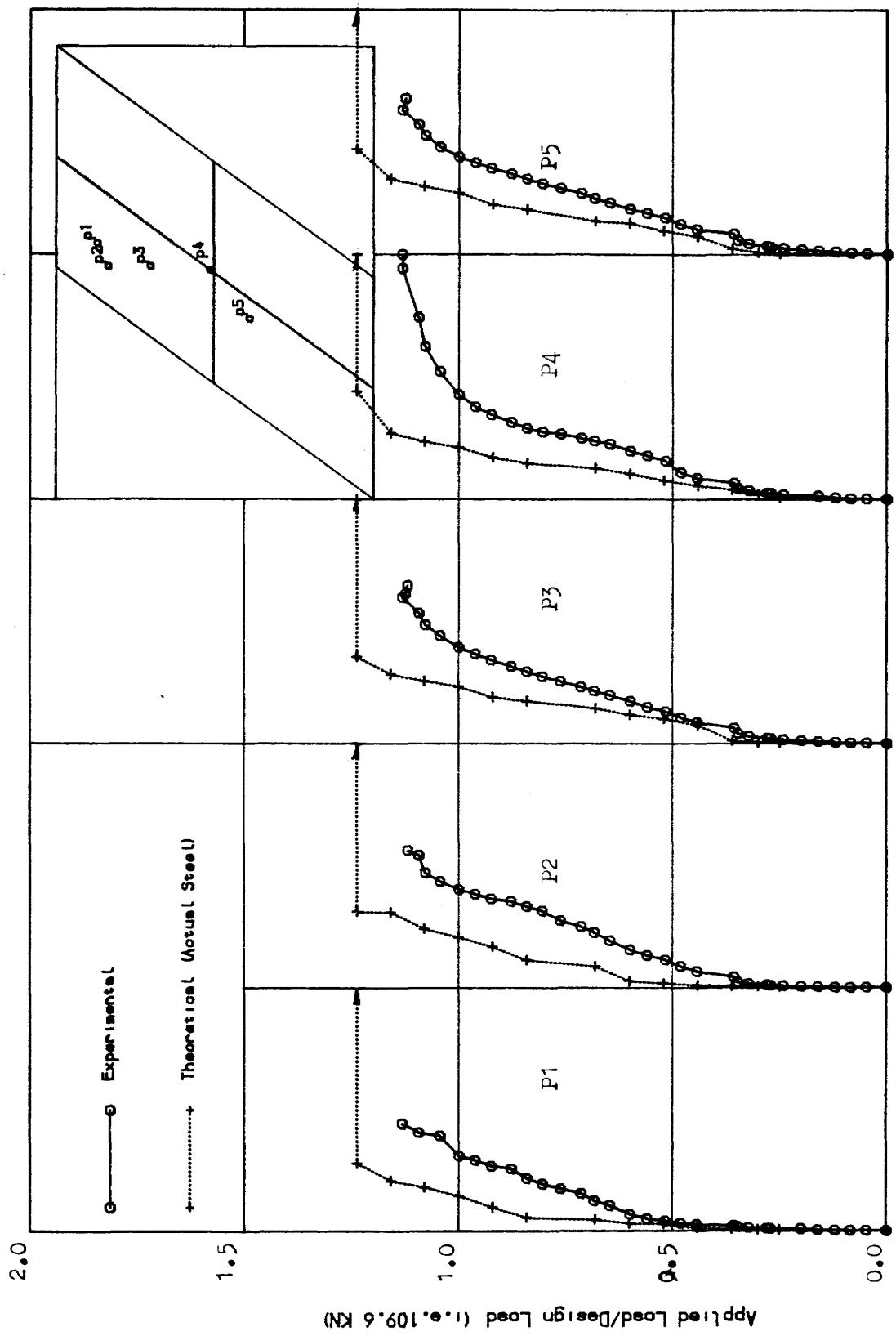

Fig. (8.23) Comparisons of Load-Transverse Steel Strain curves for MODEL NO. FIVE

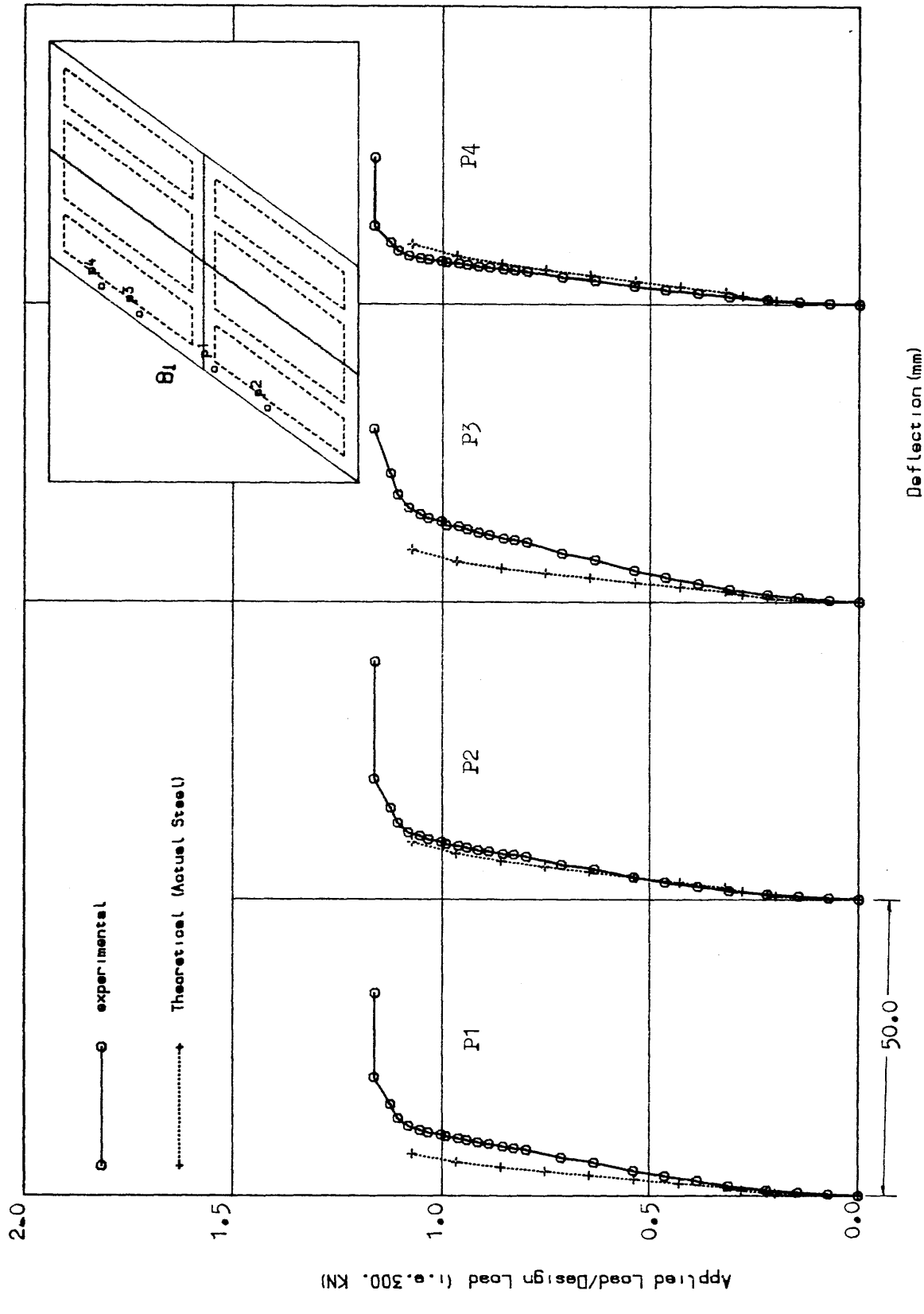

Fig. (8.24) Comparsions of Load-Deflection curves in the longitudinal direction along rib (B1) for MODEL NO. SIX

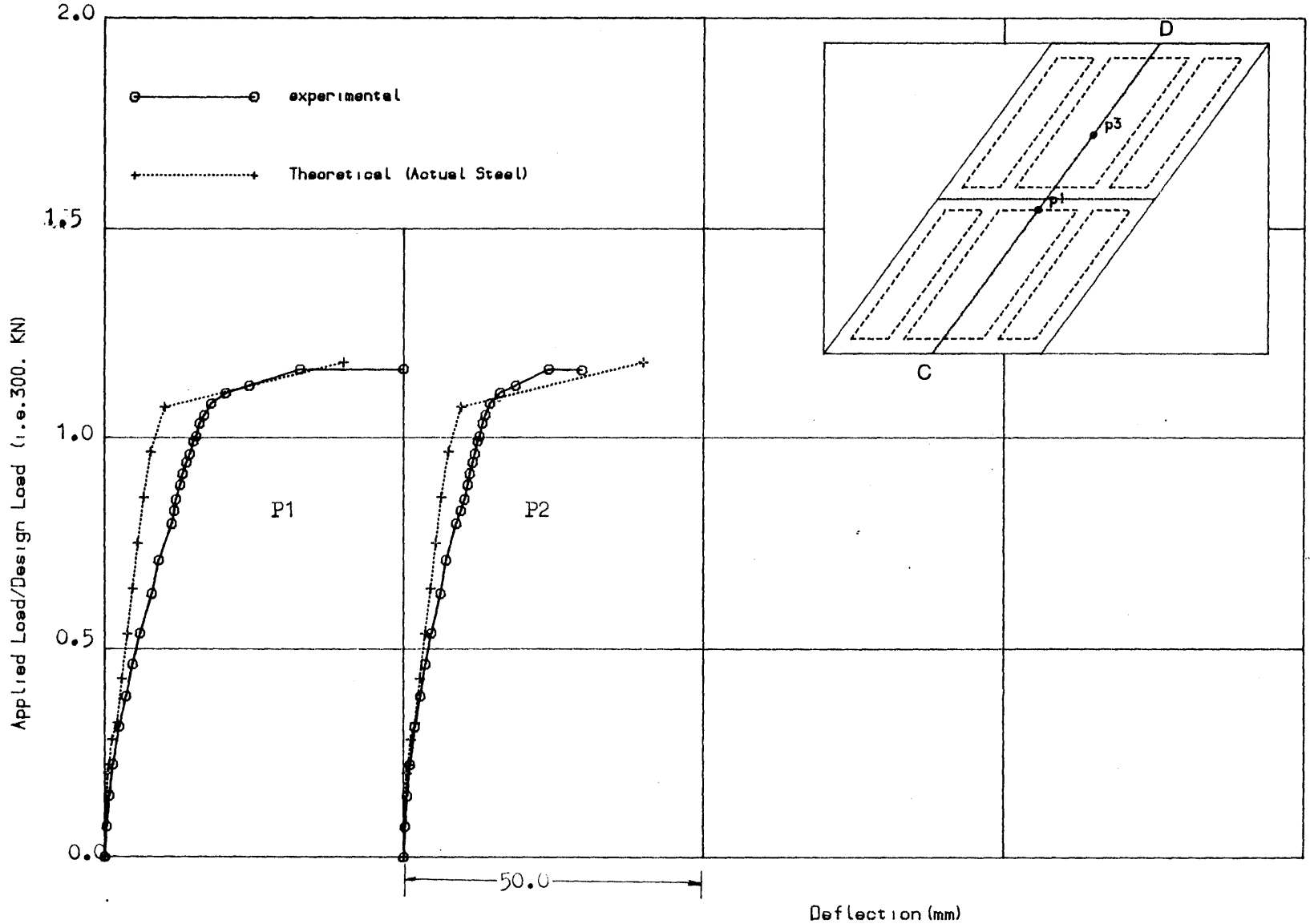

Fig. (8.25) Comparsions of Load-Defelection curves in the longitudinal direction along centre line D-C for MODEL NO. SIX

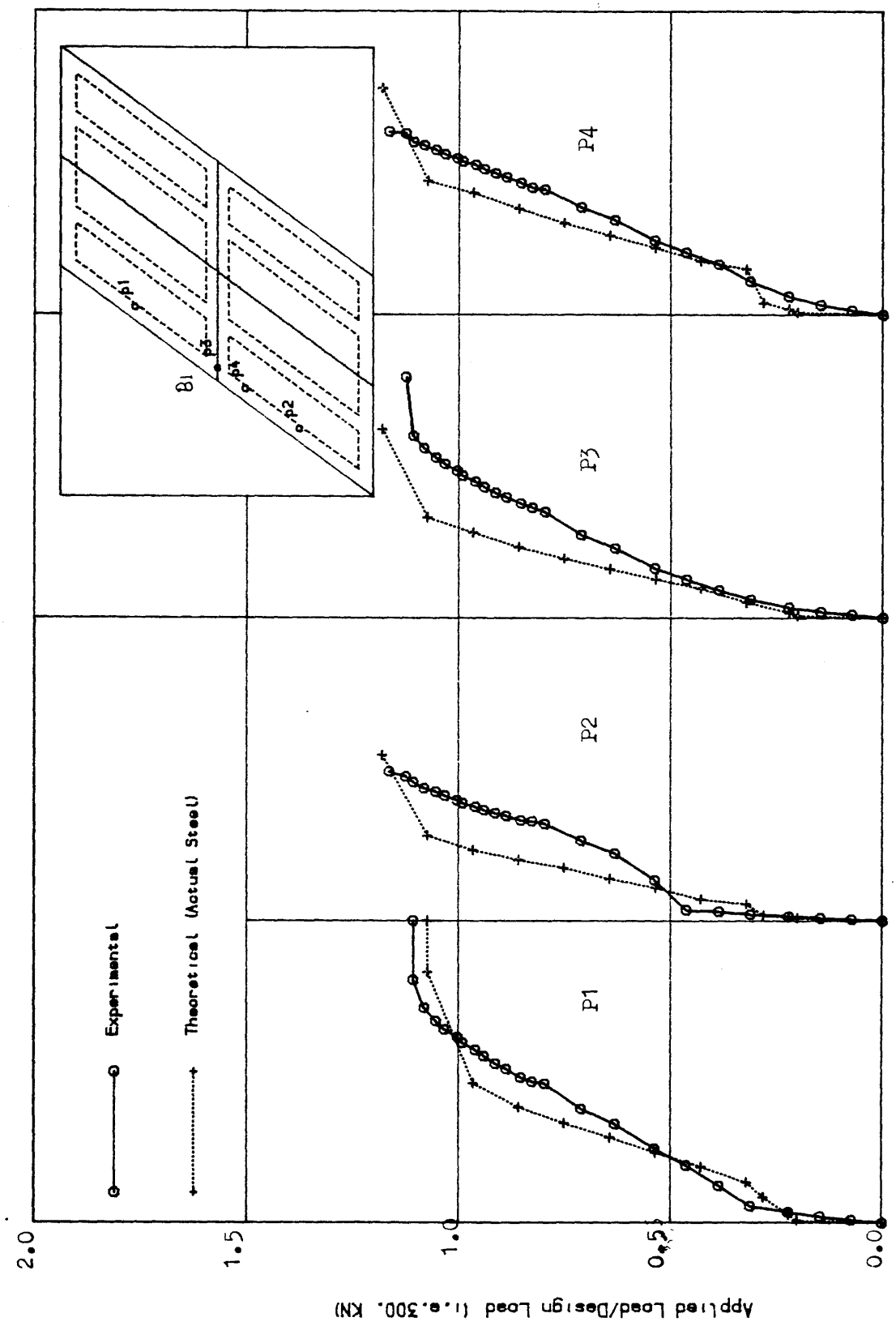

Fig. (8.26) Comparsions of Load-Longitudinal Steel Strain curves along rib (B1) for MODEL NO. SIX

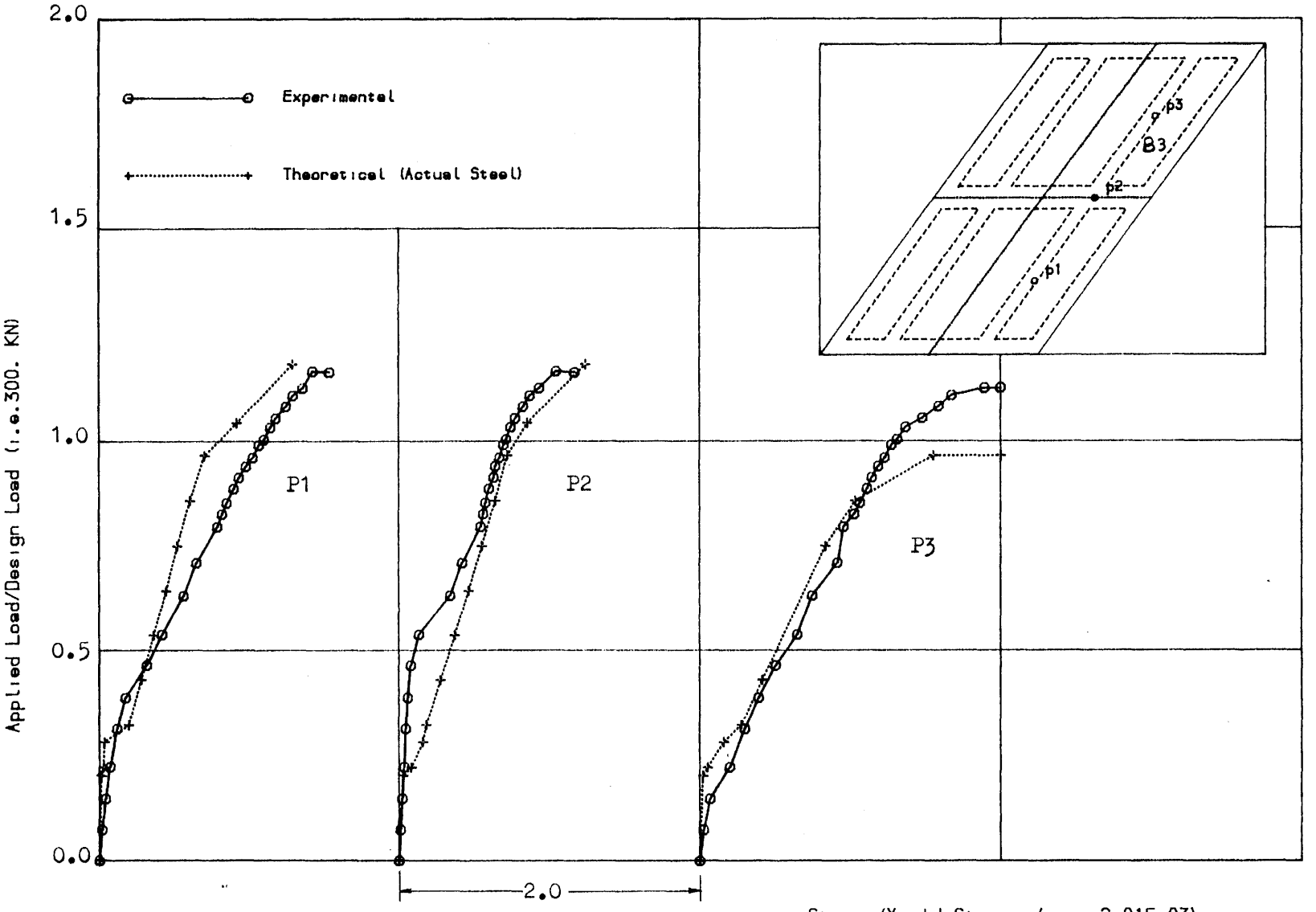

Fig. (8.27) Comprasions of Load-Longitudinal Steel Strain along rib (B3) for MODEL NO. SIX

The theoretical cracking load is not affected by the use of fixed crack analysis. The average ratio of theoretical cracking load to experimental cracking load is 0.99. Excluding model four which failed locally, the fixed crack analysis shows that: the average theoretical service load when the maximum steel strain is 0.8 of the yield strain, is 1.07 of the experimental service load. At this same load, the average theoretical deflection is 0.94 of the experimental defection. The average theoretical load at the first yield load is 1.17 of the experimental yield load. The average theoretical ultimate load is 1.03 of the experimental ultimate. It is noted from these comparisons that the predicted results compare well with the experimental values. It was shown in Chapter Seven that the experimental failure load of model one is 1.39 of the design load. This is due to the difference between the actual steel and the design steel. The theoretical analysis was carried out using design steel to show this effect. Fig (8.13) and (8.14) show the comparisons between the experimental load-deflection and load-longitudinal steel strain curves and the corresponding theoretical ones considering the actual steel and the design steel. These curves show that when the design steel is considered, a flexural behaviour is obtained and the ultimate theoretical load is 0.98 of the design load. In Model three the ultimate experimental load is 1.96 of the design load (see section (7.2.3)). In fact there is not much difference between the design steel and the actual steel except near the free edges. Using the theoretical a steel, nonlinear analysis was carried out to

study this effect. The results are presented in Figs (8.18) and (8.19) The load-deflection curves shows that there is a similar behaviour between using actual steel and design steel except that the failure load in the case of the design steel is 1.40 of the design load. The first yield in the actual steel case was obtained at 1.32 of the design load. The first yield in design steel is occurs at 1.05 of the design steel. The theoretical type of failure is initiated by yielding in the steel.

Factors contributing to this enhancement in the ultimate load are;

(a) Concrete strength: The effect of concrete strength on the ultimate moment capacity is in significant. However compressive strength influences shear capacity and the serviceability limit by its effect on tensile strength, aggregate interlock capacity and the strength of compressive block.

(b) The increase in the provided area of steel rather than the designed area of steel affects both the service and the ultimate behaviour of the slab. In the former case, providing extra stiffness to the slab leads to improved deflection characteristics. This factor does not affect the crack spread over the slab surface, but it does have the desirable influence of restricting crack depth. As a consequence crack width are smaller and hence the stiffness degradation is slower. The total effect is an overall improvement in the serviceability behaviour. Increasing the amount of steel delays the initiation of yield. The effect of this factor on the experimental work

can be seen from the results of models one and three.

(d) Strain hardening of steel: Table (7.2) lists the properties of steel used in the experiments. Typical steel-strain curves are given in Fig. (6.18.1) to Fig. (6.18.4) of Chapter Six. As can be seen from Table (7.2), in Chapter Seven, the type of steel used had a good reserve of strength after the yield. This factor definitely does not affect the serviceability behaviour but in general contributes to the ultimate strength.

(c) Membrane forces: Inplane forces resulting from edge restraints in laterally loaded slabs can be compressive or tensile. The compressive membrane action can be developed at a low deflection due to the friction at the support points. In practice it is difficult to have a friction free action between the roller and the plates (see Fig.(6. 14 a)). The compressive membrane action contributes to the increase in the ultimate load. For all tested models probably this factor is not as significant as has been shown from the numerical results. The tensile membrane action develops at large deflections, and happens at high loads. At this stage, bottom surface cracks would run through the whole of the slab thickness, and the load will be carried by the tension bars with slab acting as a catenary. Prak and Pauley (59) show that this action occurs when the deflection is approximately equal to the slab thickness. This situation could not be achieved in all models tested, due to the limitation of loading apparatus. The present LAYER program can deal with the compressive membrane action (cause the effect of inplane

displacement is considered in the formulation of the element). However this program cannot treat the tensile action, since it ignores large displacement effects.

8.2.4 Shear Resistance at the Obtuse Corner

From the experimental results presented in Chapter 7 for model one, it can be seen that shear failure occurred at the obtuse corner. In model four top face cracks initiated at the obtuse corners at 0.5 of the design load and as the load increased, one of these cracks propagated towards the middle of the slab causing the slab to fail. Similarly in model five, local punching shear failure took place at the obtuse corner. The failure loads of the three models were 1.39, 0.9 and 1.15 of the design load for models one, four and five respectively. It has been shown in Chapter Seven that from the recorded measurements, steep strain gradients occurred near the obtuse corners.

A check against shear failure using the reaction near the obtuse corner from the linear analysis at the design load and applying CP110 (30) rules for slabs (see Chapter Six section (6.2) for more detail) shows that no shear reinforcement was required (see table (8.3)). A similar check against shear failure was carried out using BS 5400 for beams showed that at the design load, shear reinforcement should be provided (see Table (8.4)). Cope (116) has shown that it is unsafe to use CP110 (30) for slabs to check against shear failure. Cope (116) also points out that the steel ratio normal to the cracks

(suggested by Clark (34)) should be involved in the calculation of the shear resistance of the obtuse corner. Table (8.4) shows that the shear resistance of the obtuse corner, when the steel ratio normal to the crack is used in the calculation of the shear resistance, is less than the shear resistance of the corner when the longitudinal steel ratio is considered.

Table (8.4) Shear Strength of the tested models

Model No.	$\nu_d = \frac{V_d}{bd}$ N/mm²	$\nu_u = \frac{V_u}{bd}$ N/mm²	$\frac{100A_s}{bd}$	$\frac{100A_n}{bd}$	ν_{bAn}	ν_{bAs}	ν_b	$\frac{\nu_u}{\nu_b}$	$\frac{\nu_u}{\nu_{bAs}}$	$\frac{\nu_u}{\nu_{bAn}}$
1	0.86	1.19	1.70	0.952	0.74	0.92	1.19	1.0	1.3	1.6
2	0.82	0.959	1.10	0.734	0.65	0.79	1.03	0.87	.93	1.2
3	0.83	1.62	2.35	1.326	0.85	0.97	1.26	1.28	1.67	1.9
4	0.60	0.54	0.45	0.34	0.45	0.51	0.66	0.81	1.05	1.2
5	0.83	0.92	0.93	0.585	0.58	0.73	0.95	0.96	1.26	1.58

ν_d Shear stress at design load,

V_d Shearing force at design load near the obtuse corner

ν_u Shear stress at the ultimate load

V_u Shear force ultimate load at the obtuse corner

A_s Longitudinal steel ratio at obtuse corner

A_n Steel ratio normal to the cracks near the obtuse corner

ν_{bAs} Shear resistance considering longitudinal steel ratio (for beams)

ν_{bAn} Shear resistance considering steel ratio normal to the cracks (for beams)

ν_b Shear resistance for slabs

Note. In model six checking against shear failure had been

done using BS5400 (34)

In fact A_n is more meaningful and more safe than the longitudinal area of steel, because the A_n is represented . the component of reinforcement orthogonal to the crack.

8.3 Serviceability Limit State Calculation

In direct design procedure, use has been made of the elastic stress distribution at the design load by the finite element method. Such an analysis predicts "elastic" deflection under the design load. Since elastic uncracked stiffnesses has been used in the analysis, such elastic deflection would be a serious underestimation of true deflection under service load. A proper design procedure should satisfy not only the ultimate limit state but also the serviceability criteria.

As was shown before, the bridge code BS 5400 (34) does not require crack widths to be checked under all possible load combinations. However BS 5400 (34) states that the stress in steel should not exceed more than 0.8 of the yield strain in steel and the stress in concrete should not exceed more than 0.5 of the cube strength of concrete at service load. In the present design procedure the elastic stresses cannot be directly used to check for serviceability, but they can be useful if the properties of an effective partially cracked section can be established. The elastic stresses have been used with the equations suggested by Clark's (34). If Mser is the elastic moment at service load, the stress in the i_th

steel layer is given by

$$f_i = M_n/I_{cr}\ x_1 \cos \alpha_{ni} \qquad (8.2)$$

where I_{cr} is the second moment of inertia of a cracked section considering A_n in the calculation (A_n is the component of the reinforcement in the direction normal to the crack)

x_1 is the distance between the steel layer and the neutral axis.

α_{ni} is the angle between the normal to the crack and the steel layer i.

M_n the moment at service load in the normal direction to the crack.

The method is fully described in Appendix (B).

A summary of the predicted behaviour of all models using the above procedure is given in table (8.5). The service load has been taken as the experimentally measured one at 0.8 f_{sy}.

As can be seen from Table (8.5), except for model four which failed locally, the approximate procedure gives a reasonable prediction of the stresses in the steel at service limit load. The stress is underestimated by 10% in model two, because at not many points the steel strain reached $0.8f_y$ at the same time . While in models one, three and five because several points reached 0.8fy at the same time, the approximate calculation of the steel stress is the same as the measured experimental value.

Table (8.5) Predicted and Experimental Steel Stress of Tested Models in Accordance with BS5400(34).

Model No.	σ_x / σ_1 N/mm^2	σ_y / σ_2 N/mm^2	σ_{xy} / θ_{cr}	α_α / $\alpha_{n\alpha}$	α_x / α_{nx}	M_x x10^3 N.mm/mm	M_y x10^3 N.mm	M_{xy} x10^3 N.mm	M_n x10^3 N.mm	A_α / $A_{n\alpha}$	A_x / A_{nx}	A_n mm^2/m	d_n mm	m= E_s/E_c	I_{cr} x10^4	f_n N/mm^2	f_α N/mm^2	f_x N/mm^2	$f_\alpha/.8\ f_y$
1	2.69 / 10.35	10.23 / 2.57	.96 / -7.16	120 / -37.2	0.0 / 82.8	5.58	20.5	.77	20.5	1.07 / .433	.494 / .0001	.433	20.4	7.18	1.5	605.	384	9.4	.96
2	.468 / 4.59	4.3 / .174	1.1 / 15.88	60 / -134	0.0 / -74	.89	8.34	-2.	8.87	.63 / .1456	.695 / .004	.1495	12.8	7.56	6.6	734.	355	55.	.89
3	1.68 / 10.11	10.11 / 1.68	-.068 / -.46	45 / -134	0.0 / -89.	3.84	18.2	.83	18.23	1.27 / .308	.7 / 0.0	.308	17.3	7.16	1.2	746.	367	.05	.97
4	.058 / 5.44	5.057 / -.33	1.44 / -15.	90 / -15.	0.0 / 75.	.071	10.5	2.7	11.14	.52 / .456	.14 / 0.0	.456	20.7	7.3	1.7	312.	291	20.9	.73
5	3.31 / 9.31	6.28 / .19	4.36 / -9.2	45 / 35.8	135 / -52.	6.63	13.4	-8.1	18.8	.72 / .311	.5 / .068	.378	20.1	7.86	1.6	603.	396	222.	1.1
6	4.24 / 11.58	7.175 / -1.67	5.68 / -37.7	45 / 7.25	0.0 / 52.2	60.3 / .015*	89.2 / .027*	73.8 / .023*	15.0 / .034*	2.83 / 2.75	.67 / .094	2.84	70.	7.86	57	338. / 2.9*	333 / 2.9*	127 / 1.1*	.91 / .008*

f_n the stress in the normal direction to the crack, f_α the stress in the α steel, f_x the stress in x steel.

Note: stress; N/mm^2; moment N.mm/mm; moment of inertia; mm^4/mm, angles in degrees.

* The inplane effect

Although there is no a specific criterion in terms of deflection given in the code of practice (30), it is obviously necessary to calculate deflection in order to ensure that clearance specifications are not violated and adequate drainage will be obtained . Accordingly in the present design procedure, since the elastic deflection cannot directly be used to check a specified given value of deflection, they can be useful if the properties of an effective partially cracked section can be used. In this study, the deflection at $0.8f_y$ limit is considered as service limit. The elastic deflection has used with Branson's method in section (2.3.3) under service load (the load at 0.8fy limit). So if is the elastic deflection under the design ultimate load, the service deflection will be

$$\delta_{ser} = \delta_{elser} \; Ig/Ieff$$

where δ_{ser} the predicted deflection

δ_{elser} the maximum elastic deflection at service load (in these models the maximum deflection was at the centre of the model)

I_g gross moment of inertia in the longitudinal direction at the same point which gives maximum described

I_{eff} effective moment of inertia of the section at the same point of maximum deflection considering a steel area normal to the crack direction as it is given in Appendix (B)

A summary of the predicted behaviour of all the models is given in Table (8.6). Deflection have been

Table (8.6) Comparison Between the Predicted Experimental Deflection Load of 0.8 f_y with the Analytical Values.

Model No.	$m=\frac{E_s}{E_c}$	A_s mm^2/mm	I_g mm^4/mm_4 x10	A_n mm^2/mm	d_n	I_{cr} mm^4/mm_4 x10	$\frac{P_{cr}}{P\ (at\ .8f_y)}$	I_{eff} mm^4/mm_4 x10	δ ther.at design load mm	$\frac{P(at\ .8f_y)}{P\ design}$	δ exp. at .8f mm	δ ser. ther. mm	$\frac{\delta\ ser.(ther.)}{\delta\ exp.}$
1	7.18	1.296	9.3	.72	24.9	2.38	.21	2.45	4.6	1.004	20.	18.24	.912
2	7.56	1.30	9.37	.44	20.6	1.66	.42	2.23	4.3	0.71	15.	12.8	0.85
3	7.16	2.0	9.83	.827	26.37	2.65	.217	2.72	4.836	1.24	28.	29.	1.035 *
4	7.28	.44	8.67	.48	21.	1.72	.517	2.68	3.93	.57	12.	7.25	.604
5	7.86	.77 **	9.0	.372	18.9	1.41	.356	1.75	4.84	.785	19.	19.45	1.02
6	7.86	2.833	152.756	2.83	70.1	56.92	.328	60.30	3.75	.785	7.5	7.45	0.99

m modular ratio, A_s longitudinal steel ratio and A_n steel ratio in the normal direction to the crack, P_{cr} cracking load

* model four field locally

** total area of steel (top and bottom)

calculated , using the simplifying assumptions for cracked sections (Appendix E).

As can be seen from Table (8.6), there is good agreement between the experiment results and the analytical values except for model two, stiffer results are predicted. Accordingly, the adoption of elastic deflection, modified by cracked transformed section properties, will yield acceptable checks on the specified deflection limit.

CHAPTER NINE

CONCLUSIONS AND RECOMMENDATIONS

9.1 Conclusions

From the theoretical analysis and the experimental investigation reported on this thesis, the following conclusions may be drawn.

9.1.1 Direct Design Method

1- From the theoretical and experimental investigations it can be concluded that the direct design approach is valid as a lower bound approach for different angles of skew and for different arrangements of reinforcement and for plane and stiffened slabs. However in model 3 with for 45 angle of skew when the reinforcement is placed parallel to the edges for plane slab, the ultimate load was grossly underestimated . No rational explanation can be put for this behaviour at present.

2- All the slabs designed by the direct design approach behaved satisfactorily under working loads (see Chapter section (7.3)). All the slabs designed by the direct design approach recorded failure loads close to their design loads expect for a skew angle of 45 when the steel was placed parallel to the edges.

3- Checks against shear strength using CP110 (30) for skew slabs lead to unsafe results. A more appropriate check against shear strength can be carried out using BS4500 (34) considering A_n (the effective area of steel normal to the crack direction) rather than the

longitudinal steel area

4- As the angle of skew decreases, the structure becomes more flexible and it is important to use the inclined length when CP110 (30) length/depth ratio rules are used to check deflection.

5- For the serviceability limit state, the approximate procedure suggested by Clark (34) is an acceptable check on the stresses in the steel at service limit load. The adoption of elastic deflection modified by cracked transformed section properties (31), (34) yields acceptable checks on the specified deflection limit.

6- One important lesson learnt from the fixed and variable crack analysis is taht, just because theoretical results agree clearly with experimental results, it may not be wise to use the theoretical results for design prupose. The reason for this is that the agreement between experiment and theory might involve parameters like tensile strength of concrete etc. where it may not be wise to rely up-on for long term design purposes.

9.1.2 The theoretical analysis

1- The proposed layered model is capable of providing a good prediction of the overall behaviour of plane and ribbed reinforced concrete slabs failing in flexure.

2- The mesh refinement for this particular element has little influence on the predicted behaviour, but has a great influence on the cost of analysis (the cost of the analysis increases linearly with the increase in the number of the elements).

3- The predicted behaviour and the cost of analysis is not significantly influenced by the number of concrete layers adopted and a total of 8 concrete layers is sufficient.

4- The deflection values are sensitive to the value used for the tensile strength of concrete.

5- The deflection values are sensitive to the amount of tension stiffening adopted in the analysis especially at service load.

6- The deflections and the ultimate failure loads are affected to a certain extent by the value of the convergence tolerance. 5% tolerance is recommended and near the failure this tolerance should be reduced to 2%.

7- Shear retention factor is an important parameter in the analysis when skew reinforcement is considered. A value of ($\beta = .4/(\varepsilon_f/\varepsilon_{cr})$ with $B \leq C$) for the shear retention factor of concrete is recommended , with C = 0.25.

8- A value of $0.15P_{cr}$. load increment size should used for highly nonlinear parts of the loading curve (onset of cracking and at failure) and this may be increased up to $0.25P_{cr}$. when nonlinearity is not too great.

9- Fixed crack analysis may be suitable when the orthogonal reinforcement is used but may be misleading in the case of skew reinforcement.

10- Analysis based on concrete as No-Tension material reflected the the design assumptions and helped to

clarify the short-comings of fixed crack analysis.

9.1.3 Ribbed Slabs

1- The present layer model overestimates the torsional stresses and underestimates the stiffness of the beams due to neglecting the vertical shear components in the torsion.

2- In the ribbed slab systems, consideration of membrane forces in the design of the reinforcement can lead to misleading results. Great care is needed in the proper modelling of the slab. Also care must be taken in the designing shear reinforcement (see section (7.2.6.2)).

9.2 SUGGESTIONS FOR FUTURE WORK

The suggestions are as follows:

(a) All the experimental and theoretical (No-Tension analysis) results presented in this thesis show that the initial angle of crack is different from the final angle of crack and in dependent on the angle of reinforcement (α). Experimental study can be carried out on small slab specimens for different unixial loading cases (N_x, N_y ,N_{xy}) for different angles of skew. The variation in the direction of the crack can be measured and used to establish a theoretical cracking model.

(b) In the meantime the cracking model as suggested by Gupta and Akbar (98) can be introduced into the LAYER program.

(c) To reduce the cost of the analysis skew symmetry can

be introduced into the LAYER program by changing the solution subroutine.

(d) All the slabs designed by the direct design approach recorded failure loads close to their design loads, expect for a skew angle of 45 when the steel was parallel to the edges. This problem needs to be studied in great detail.

(g) All the experimental and theoretical work carried out in this thesis was concerned with single load case. Work should be extended to study multiple load cases subjected to different load history.

APPENDIX (A)

Calculation of the steel required for a certain design moment (M^*) per unit width

Using the ultimate limit state theory, it can be assumed that the stress distribution in the section will have the form shown in the Figure below:

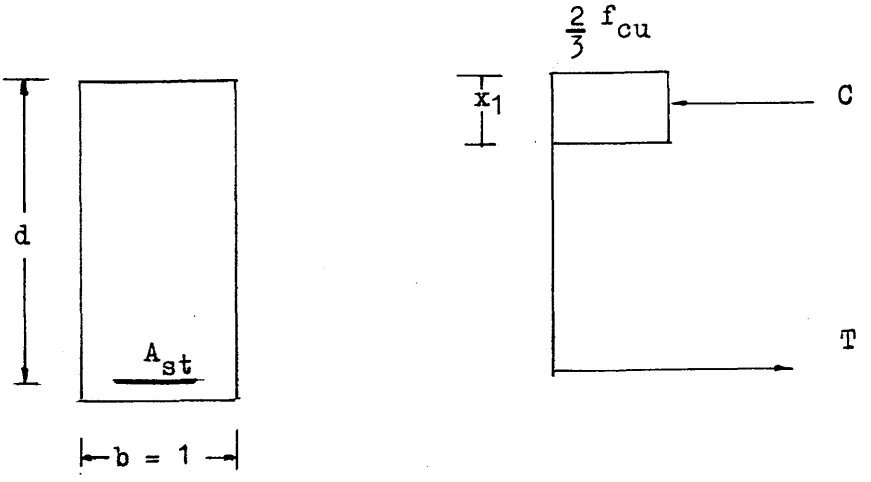

Taking the partial safety factors on both concrete and steel as equal to unity, and by considering the horizontal equilibrium of the section:

then $C = T$ (1)

Using the stress distribution at ultimate

$$\frac{2}{3} f_{cu}\, x_1 = A_{st}\, f_y \qquad (2)$$

$$x_1 = 1.5\, A_{st} \frac{f_y}{f_{cu}} = 1.5\, d\, \rho \frac{f_y}{f_{cu}}$$

where: $\rho = \frac{A_{st}}{d}$ = Reinforcement ratio

Taking moments about the resultant compression force and equating external and internal moments, then

$$M^* = T \left(d - \frac{x_1}{2} \right)$$

$$= A_{st} f_y \quad (d - 1.5 \rho f_y/(2 f_{cu})$$

$$= \rho d^2 f_y \left(1-1.5 \rho \frac{f_y}{f_{cu}} \right)$$

$$= \rho d^2 f_y - 0.75 \rho^2 d^2 \frac{f_y^2}{f_{cu}} \qquad (4)$$

rearranging we get :

$$(0.75 \frac{f_y}{f_{cu}})\rho^2 - \rho + \frac{M^*}{d^2 f_y} = 0 \qquad (5)$$

Solving for ρ and substituting $A_{st} = \rho d$

$$A_{st} = \frac{f_{cu} d}{1.5 f_y} \left[1 - \sqrt{\left(1 - \frac{3 M^*}{d^2 f_{cu}} \right)} \right] \qquad (6)$$

APPENDIX (B)

Calculation for stresses at serviceability limit states

Assumptions: Under the service load the following assumptions are made:

1- Tension stiffening in cracked concrete is ignored.

2- Linear strain distribution across the depth of the section.

3- Materials are linearly elastic.

4- Only uniaxial behaviour is considered.

5- Longitudinal steel (A_s) is considered in the calculation of the gross moment of inertia (I_g).

6- The effective steel area (A_n) to be defined in this Appendix is used in the calcutation of the neutral axis depth and the moment of inertia for fully cracked section (I_{cr}).

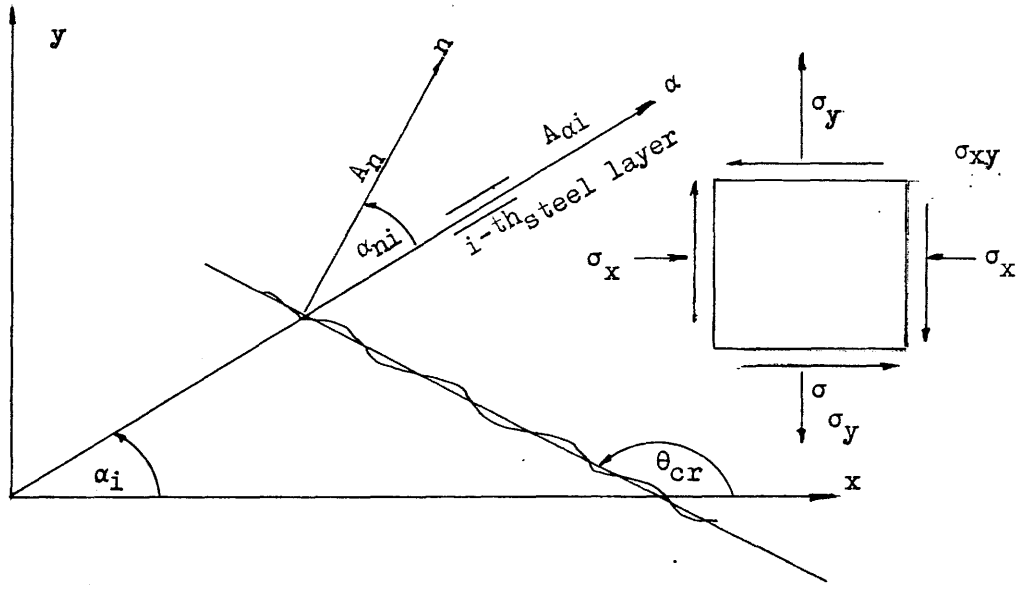

The following steps are followed:

(i) Calculate the principal stresses.

$$\sigma_{1,2} = \frac{\sigma x + \sigma y}{2} \pm \sqrt{\left(\frac{\sigma_x + \sigma_y}{2}\right)^2 + \tau_{xy}^2)} \qquad (1)$$

If $\sigma_1 \geq f_t$

where $f_t = 0.45 \sqrt{f_{cu}}$ N/mm^2

where f_{cu} the concrete cube strength.

(ii) Calculate the inclination of the principal stress.

$$\tan 2\theta = \frac{-2 \tau_{xy}}{\sigma_x - \sigma_y} \qquad (2)$$

(iii) Calculate the normal stress to the prancipal stress.

$$\sigma_n = \sigma_x \cos^2\theta + \sigma_y \sin^2\theta + \tau_{xy} \sin\theta \cos\theta \qquad (3)$$

$$\begin{aligned} &\text{If } \sigma_n = \sigma_1, \text{ then} && \theta_{cr} = \theta \\ &\text{If } \sigma_n = \sigma_2, \text{ then} && \theta_{cr} = \theta + 90 \end{aligned} \qquad (4)$$

where θ_{cr} is the angle of crack. If $\theta_{cr} < 0$, $\theta_{cr} = \theta_{cr} + 180$

(v) Calculate the inclination of the i^{-th} layer bar to the normal to the crack.

$$\alpha_{ni} = \theta_{cr} - \alpha_i - 90 \qquad (5)$$

where α_i the angle of inclination of i^{-th} steel layer to X - axis.

α_{ni} the angle of inclination of i^{-th} steel layer to the normal to the crack.

(vi) Calculate the effective steel area (A_n)

$$A_n = \sum_{i=1}^{N} A\alpha i \cos^4\alpha_{ni} \qquad (6)$$

where $A_{\alpha i}$ the steel area of i^{-th} steel layer in the direction.

N the total number of steel layers.

A_n the total equivalent area normal to the crack.

(vii) Using A_n, the neutral depth dn can be calculated from Appendix (C) Eqn (5) and the moment of inertia of cracked section I_{cr} can be calculated from Eqn (7) Appendix (C).

(viii) Calculate the stress in the direction n.

$$fn = -\frac{M_n}{I_{cr}} \quad (d - d_n) \ (m) \tag{7}$$

where M_n the moment at service limit load in the n-dircetion and is calculated using the following equation.

$$M_n = M_x \sin^2\theta_{cr} + M_y \cos^2\theta_{cr} - 2.0\ M_{xy} \sin\theta_{cr} \cos\theta_{cr} \tag{8}$$

M_x, M_y, M_{xy} are the applied moments.

d the cross section depth.

f_n the stress in the equivalent area of reinforcement (A_n) in the n-direction.

m modular ratio.

(ix) Calculate the stress in the concrete.

$$f_c = \frac{M_n}{I_{cr}} \quad d_n \tag{9}$$

where F_c the compressive stress at in the concrete.

(x) Calculate the stress in the inclined layers.

$$f_i = f_n \cos^2\alpha_{ni} \tag{10}$$

f_i is the stress in i-th layer inclined at an angle α_{ni} to the prependicular direction to the cracks.

APPENDIX (C)

Calculations for Defection Serviceability Limit State

All the assumptions in Appendix (B) are vaild

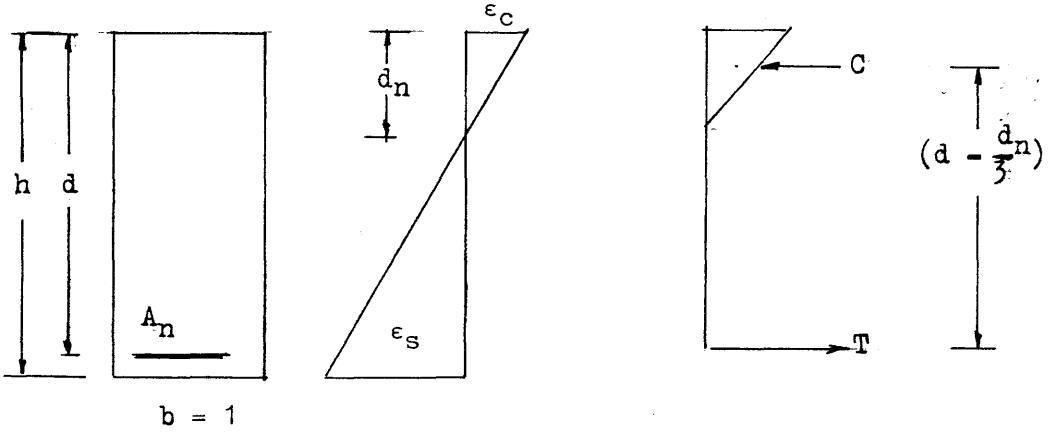

For equlibirium C = T

$$\frac{1}{2} \epsilon_c E_c d_n = A_n E_s \epsilon_s \quad (1)$$

$$d_n = 2 \frac{E_s}{E_c} \frac{\epsilon_s}{\epsilon_c} A_n = 2 m A_n \frac{\epsilon_s}{\epsilon_c} \quad (2)$$

where m = modular ratio = E_s/E_c.

but from the strain diagram

$$\frac{\epsilon_s}{\epsilon_c} = \frac{d - d_n}{d_n} \quad (3)$$

$$d_n = 2 m A_n \left(\frac{d - d_n}{d_n} \right) \quad (4)$$

rearranging

$$d^2_n + 2 m A_n d_n - 2 m A_n d = 0$$

solving gives

$$d_n = (- m A_n + \sqrt{(m A_n)^2 + 2(m A_n) d} \qquad (5)$$

Th gross moment of inertia is

$$I_g = \frac{bh^3}{3} + (m - 1) A_n (d - \frac{h}{2})^2 \qquad (6)$$

and the fully cracked transformed section gives

$$I_{cr} = \frac{bd^2}{3} n + m A_n (d - d_n)^2 \qquad (7)$$

then using the Branson's method, an effective moment of interia is calculated from

$$I_{eff} = I_g \left[\frac{P_{cr}}{P} \right]^3 + I_{cr} \left[1 - \left[\frac{P_{cr}}{P} \right]^3 \right] \qquad (8)$$

in which P_{cr} the cracking load

P the service load

The deflection under the service load is found from the elastic deflection as

$$\delta_{ser} = \delta_{elser} \frac{I_g}{I_{eff}} \qquad (9)$$

wher δ_{elser} is the elastic deflection at service load.

REFERENCES

1- Timoshenko S. and Woinosky-Krieger S.; Theory of plates and Shells. McGraw-Hill, New York, Second Edition 1959.

2- Szilard R.; Theory of Analysis of Plates, Classical and Numerical Methods. Prentic Hall, 1974.

3- Robinson K. E.; The Behaviour of Simply Supported Skew Bridge Slabs Under Concentrated Load. Cement Concrete Association Research Report No. 8, 1059, 1959.

4- Cook R. D. ; Concepts and Application of Finite Element Analysis. Second Edition, Wiley 1981.

5- Owen D. R. Y. and Hinton E.; Finite Element in Plasticity Theory and Practice. Pineridge Press Limited Swansea, U. K., 1980.

6-Park R. and Gamble W. L. Reinforced Concrete Slabs. Wiley 1980.

7- Hillerborg A ; Strip Method of Design. A View Point Publication, 1975.

8- Industrial Processes Building and Civil Engineering; Eurocode No. 2: Common Unified Rules for Concrete Structures; Report Eur 8848 DE, EN, FR

9- Hago A. W. Direct Design of Reinforced Concrete Slabs Ph.D thesis, Glasgow University, 1982.

10- Quinlan P. M. The λ- Method For Skew Plates. Proc. of the 4th U. S. National Congress on applied Mechanics,

A.S. M.E. Vol. 2, 1962.

11- Kennedy J. B. and Huggins M. S.; Series Solution of Skewed Stiffened Plates. Journal of the A.S.C.E., Engineering Mechanics Division Vol. 90 July 1964.

12- Morley L. S. D.; Skew Plates and Structures. Pergamon press, 1963.

13- Coull A. ; The Theoretical Analysis of Orthotropic Skew Bridge Slabs. The Structural Engineering., No 7, Vol. 42, July 1964.

14- Coull A. ; Stress in Skew Slabs. Concrete, April 1967 PP135-139.

15- Jensen V. P.; Analysis of Skew Slabs. University of Illinois Bulletin station Sept. NO. 332, 1941.

16- Zienkiewicz O. C. The finite Element Method in Engineering Science. Third Edition, McGraw-Hill, New York, 1977

17- Ergatoudis, J. G., Irons B. M. and Zienkiewicz O. C. ;Curved Isoparameteric Quadrilateral Elements for Finite Element Analysis, International Journal of solids and structures. Vol 4, 1968 PP31 - 42.

18- West R.; The Use of a Grillage Analogy for The Analysis of Slab And Pseudo-slab Bridge Decks. Cement and Concrete Association 1973 Research report 21.

19- Kennedy ,J. B.; On The Bending of Clamped Plates Under Pressure. Journal of The Royal Aeronautical Society, London, England, Vol. 69 May, 1965, PP. 352-359.

20- FLASH Package, GEC 4070 Version Edition 1 April, 1981 Glasgow University.

21-CP 110 Hand Book on the Unified Code for Structural Concrete 1972. Cement and Concrete Association, 52 Grosvenor Gardens, London SW1W OAQ

22- Morley C. T.; Yield Line Theory for Reinforced Concrete Slabs At Moderately Large Deflection. Magazine of Concrete Research, Vol. 19, NO. 22, 1967 PP 211.

23- Hillerborg R. A; Equilibrium Theory for Concrete Slabs. Betong. Vol. 41 No. 41, 1956 PP 171-182.

24- Hillerborg, A.; Strip Method of Design View Point. Publication, Slough , 1975.

25- Fernando J. S. and Kemp, K. O.; The Strip Method: of Slab Design Unique or Lower-Bound Solution ; Magazine of Concrete Research, Vol. 24, 1975 PP9-23.

26- Hillerborg A.; The Advanced Strip Method, A Simple design Tool. Magazine Concrete Research Vol. 34, 1982, PP 175.

27- Fernando J. S. and Kemp K. O.; A Generalized Strip Deflection Method of Reinforced Concrete Slab Design. Proceedings of the International Civil Engineering, Part 2 Vol. 65 No. 2 1978, PP 163-174.

28-Hayes, B. and Taylor R.; Some Tests on Reinforced Concrete Beam-Slab Panels. Magazine of Concrete Research, Vol.12, No. 67, June 1969, PP113-120.

29- Irons, B. M., A Frontal Solution Program for Finite Element Analysis. Int. J. Num. Meth. Eng., Vol.2, 1970 PP2-32.

30- CP 110 Part 1 1972 The Structural use of concrete. B. S. I. London, 1972.

31- Branson D.E.; Deformation of Concrete Structures. McGraw-Hill, New York, 1977.

32- ACI Building Code Requirements for Reinforced Concrete. American Concrete Institute, Detoit Vol. 77 No. 318, 1977 PP 103.

33- ACI Committee 318, Analysis and Design of Reinforced Concrete Bridge Structures. American Concrete Institute, Detroit, ACI Report Vol.77, No343 1977, PP116.

34- Clark L. A. Concrete Bridge Design to BS 5400. Construction Press, London, 1983, PP 86-88.

35- Desayi P. and Prabhakara A. Load_Deflection Behaviour Of Restrained R/C SKEW Slabs, Journal of the Structural Division, Proceedings of the American Society of Civil Engineers, Vol. 107, No. ST5, May, 1981, PP 873-888.

36- Gerstle, K. H.; Material Modelling of Reinforced Concrete. Introductory Report, IABSE Collopuium on Advanced Mechanics Of Reinforced Concrete , Delft, June 1981 PP41-61.

37- Clark, L.A.; The Provision of Tension and Compression Reinforcement to Resist In-Plane Forces. Magazine of Concrete Research, . Vol. 28, No. 94, March 1976.

38-Beeby A. W.; An Investigation of Cracking in Slabs Spanning One Way. Technical Report Cement and Concrete Association RTA433 May, 1970, PP 31.

39-Orenstein G. S.; Crack Width Control in Reinforced Concrete Two-Way Slabs Subjected to Distributed Load. Journal of American Concrete Institute, Vol. 67, No. 1, Jan 1970, PP57-61.

40-Nawy E. G. and Orenstein G.S.; Crack Width Control in Reinforced Concrete Two-way Slabs. Journal of the Structural Division, Proceedings of the American Society of Civil Engineers, Vol. 96, No. ST3, March 1970, PP701-721.

41-Desayi P. and Kulkarni A. B. Determination of Maximum Crack Width in Two-way Reinforced Concrete Slabs. Proceedings of the Institution of Civil Engineers, Part 2, Vol. 61, June 1976, PP343-349.

42-Desayi P. and Prabhakara A.; Determination of Maximum Crack Width in Reinforced Concrete Skew and Rectangular Slabs. Proceedings of the Institution of Civil Engineers, Part 2, Vol. 67, December 1979, PP1077-1090.

43-Bhaumik A.K. and Hanley J.T. Elasto-plastic Analysis by Finite Difference Method. Journal of the Structural Division, Proceedings of the American Society of Civil Engineers, Vol. 93, No. ST5, October 1967, PP279-294.

44- May G.W. and Gerstle K.H.; Elasto-plastic Bending of Rectangular Plates. Journal of the Structural Division,

Proceedings of the American Society of Civil Engineers, Vol. 97, No. ST7, July 1971, PP1863-1878.

45-Jofriet J.C. and McNeice G.M.; Finite Element Analysis of Reinforced Concrete Slabs. Journal of the Structural Division, Proceedings of the American Society of Civil Engineers, Vol. 97, No. ST3, March 1971, PP785-806.

46- Bell J. C. and Elms D. G.; Nonlinear Analysis of Reinforced Concrete Slabs. Magazine of Concrete Research, Vol. 24, No. 79 June 1972, PP63-70.

47-Bell J.C. and Elms D.G.; A Finite Element Approach to Post-Elastic Slab Behaviour. ACI Special Publications SP30-15, March 1971, PP325-344.

48-Kupfer H., Hilsdorf J. K.; Behaviour of Concrete Under Biaxial Stresses. Proceedings of the American Institute, Vol. 66, No. EM4, August, 1969 PP656-666.

49-Jain O.P., Trikha D.N. and Agarwal S.; A Finite Element Solution of Post Cracking Behaviour of Reinforced Concrete Slabs; Advances in Concrete Slab Technology, Proceedings of the International Conference on Concrete Slabs, Dundee University, 1979, PP129-139, Pergamon Press, Edited by Dhir and Munday.

50-Wegmuller A.W.; Elasto-plastic Finite Element Analysis of Plates. Technical Note TN99, Proceedings of the Institution of Civil Engineers, Part 2, Vol. 57, September 1974, PP535-543.

51-Wegmuller A.W.; Full-Range Analysis of Eccentrically Stiffened Plates. Journal of the Structural Division,

Proceedings of the American Society of Civil Engineers, Vol. 100, No. ST1, January 1974, PP143-159.

52-Hand F.R., Peckhold D.A. and Schnobrich W.C.; Nonlinear Layered Analysis of Reinforced Concrete Plates and Shells. Journal of the Structural Division, Proceedings of the American Society of Civil Engineers, Vol. 99, No. ST7, July 1973, PP1491-1505.

53-Johnarry T.; Elasto-Plastic Analysis of Concrete Structures Using Finite Elements. Ph.D. Thesis, University of Strathclyde, May 1979.

54- Cope R. J. and Rao P. V.; Nonlinear Finite Element Analysis of Concrete Slab Structures. Proceedings of the Institution of Civil Engineers, Part 2, Vol. 63, March 1977, PP159-179.

55-Dotreppe J. C.; Schnobrich W. C. and Pecknold A. Layered Finite Element Procedure for Inelastic Analysis of Reinforced Concrete Slabs. Publications of the International Association for Bridge and Structural Engineers, Vol. 33, No. 2, 1973, PP53-68

56- Abdel Rahman H.H., Hinton E. and Zienkiewicz O.C.; Computational Models for Reinforced Concrete Systems. in Advanced Mechanics of Reinforced Concrete - Final Report, IABSE Colloquium, Delft, 1981, PP 303-313

57- Mathies H. and Strang G. The Solution of Nonlinear Finite Element Equations. International Journal of Numerical Methods in Engineering. Vol. 14, 1979, PP1613-1626.

58- Clark, L. A. and Cranston W. B.; The Influence of Bar Spacing on Tension Stiffening in Reinforced Concrete Slabs. Proceedings of the International Conference on Concrete slabs, Dundee, 1979 PP25-38, Pergamon Press, Edited by Dhir and Munday.

59- Park R. and Paulay T.; Reinforced concrete structures New York. Wlley, 1975.

60- Fenwick, R. C., and Pauley, T.; Mechanisms of shear Resistance of Concrete Beam. Journal of the Structural Division ASCE, Vol. 94, No. ST10, Proceedings, Paper, 2325, October 1968, PP2325-2350

61- Houde T. and Mirza M. S.; A Finite Element Analysis of Shear Strength Of Reinforced Concrete Beams. In Reinforced Concrete. Vol. 1 Special Publication SP-42, American Concrete Institute, Detroite, Michigan 1974.

62- Jimenez, R., White R. N. And Gergely P.; Bond and Dowel Capacities of Reinforced Concrete. Journal of American Concrete Institute, Vol. 76 No. 1, Jan. 1979 PP 73-92.

63- Mindlin R. D. Influence of Rotary Inertia and Shear on Flexural Motions of Isotropic Elastic Plates. J. Appl. Mech. Vol, 18 1951 PP 31-38.

64-Duncan W. and Johnarry T.; Further Studies on the Constant Stiffness Method of Nonlinear Analysis of Concrete Structures. Proc. of the Institute. of Civ. Eng. , Part 2, Vol. 67, DEc. 1979, pp 951- 969.

65- Phillips D.V.; Nonlinear analysis of structural Concrete of Finite Element Method. Ph. D. Thesis, Univ. of Wales, Swansea 1973.

66- Al-Mahaidi, R. S. H. ; Non-Linear Finite Element Analysis of Reinforced Concrete Deep Members. Report No. 79-1, Dept. of Structural Engineering, Cornell University, January 1979.

67- Sinisalo H. S., Tuomala M.T.E. and Mikkola M.J.; Nonlinear Finite Element Analysis of Reinforced Concrete Slabs Subjected To Transient Impulsive Loading. Advances in Concrete Slab Technology, Proceedings of of International Conference on Concrete Slabs, Dundee University. April 1979, PP140-148, Pergamon Press, Edited by Dhir and Munday.

68- Liu T. C-Y, Nilson A. H. and Slate F. O.; Stress-Strains Response and Fracture of Concrete in Uniaxial and Biaxial Compression. Proceedings of the American Concrete Institute, May 1972, PP291- 295.

69- Tasuji M. E., Nilson A.H. and Slate F. O.; Biaxial Stress-Strain Relationships for Concrete, Magazine of Concrete research, Vol. 31, No. 109, Dec., 1979, PP217-224.

70-Kupfer H., Gerstle K. H.; Behaviour of Concrete Under Biaxial Stresses. Journal of Engineering Mechanics Division, Proceedings of the American Society of Civil Engineers, Vol. 99, No. EM4, Aug., 1973 pp853-866.

71- Ngo D. and Scordelis A. C.; Finite Element Analysis of

Reinforced Concrete Beams. Journal of the American Concrete Institute Vol. 64, No. 3, March 1967 PP152-163.

72- Pauley T. and Loeber, P. S.; Shear Transfer by Aggregate Interlock Shear in Reinforced Concrete. American Concrete Institute, Detroit, Special Publication SP-42, Vol. 1, 1974.

73-Chen W. F.; Plasticity in Reinforced Concrete. McGrow-Hill, New York, 1982.

74- Kui Harald, Strain Gauges; Theory and Handling. Phillips Elektronik Industries Gmbh-Hamburg, 1982.

75- Wood, R.H; The Reinforcement of Slabs in Accordance With a Pre-determined Field of Moments. Concrete Vol. 2, No 2. February 1968. PP 69-76.

76- Nielsen, M. P.; Limit Analysis of Reinforced Concrete Slabs. Acta polytechnica Scandinavica, Civil Engineering Construction Series, No. 26, Copenhagen 1964

77- Armer, G.S.T Discussion of Reference 75. Concrete Vol. 2, No. 8. August 1968. PP 319-320.

78- Wood R H.; Slab Design Past, Present and Future. American Concrete Institute International Sympsoium on Slabs, Denver, Marach 1971, and is reprinted from Cracking, Deflection and Ultimate Load of Concrete Slab Systems, ACI Publication SP-30 PP203-221.

79- Kemp K.O; The Yield Criterion for Orthotrpically Reinforced Concrete Slabs. International Journal of Mechanical Sciences, Vol. 7, 1965, PP737-746.

80- Lenschow R. and Sozen M. A. A Yield Criterion for Reinforced Concrete Slabs. Proceedings of the American Concrete Institute, Vol. 64, May 1967, PP273-273.

81- Save M. A Consistent Limit-Analysis Theory for Reinforced Concrete Slabs, Magazine of Concrete Research, Vol. 19, No. 58, March 1967, PP3-12.

82- Cardenas A.E. and Sozen M. A. Flexural Yield Capacity of Slabs. Proceedings of the American Concrete Institute. Vol.70, Feb. 1973, PP124-126.

83- Lenkei P.; Contribution to the Discussion of Ref. 80. Proceedings of The American Concrete Institute, Vol. 64, Nov. 1967, PP786-789.

84- Jain S. C. and Kennedy J. B.; Yield Criterion for reinforced Concrete Slabs. Journal of the Structural Division, Proceedings of the American Society of Civil Engineers, Vol. 100, No. ST3, March 1974, PP631-644.

85- Morley C. T. Yield Criteria for Elements of Reinforced Concrete Slabs. International Conference on Plasticity, International Association for Bridge and Structural Engineers, Copenhagen 1978, PP35-47.

86- Kemp. K O.; Optimum Reinforcement in a Concrete Slab Subjected to Multiple Loading. Publications of the International Association for Bridge and Structural Engineering, Vol. 31, 1971, PP93-105.

87-Brondum-Nielsen T.; Optimum Design of Reinforced Concrete Shells and Slabs. Structural Research Laboratory-Tecnical University of Denmark, Report, NR R44-1974,

PP190-200.

88- Chen W. F. and Ting E. C.; Constitutive Models for Concrete. Journal of the Engineering Mechanics Division, Proceedings of the American Society of Civil Engineers, Vol. 106, No. EM1, Feb. 1979, PP1-19.

89- Morley C. T.; Optimum Reinforcement of Concrete Slab Elements Against Combinations of moments and Membrane Forces. Magazine of Concrete Research: Vol.22, No. 72, Sept. 1970, PP155-162.

90- Morley C. T. and Gulvanessian H.; Optimum Reinforcement of Concrete Slab Elements. Proceedings of the Institution of Civil Engineers, Part 2, Vol. 63, June 1977, PP441-454

91- Nielsen M.P.; Same as Ref. 76

92- Clark L. A.; Tests On Slab Elements and Skew Slab Bridges Designed in Accordance With the Factored Elastic Moment Field. Cement and Concrete Association Technical Report 42.474 September 1972.

93- Hinton, E. and Owen, D. R. J.; An Introduction to Finite Element Computations. Pineride Press, Swansea, U. K. 1979.

94- Hinton, E. and Owen, D. R. J.; Finite Element Programming. Academic Press, 1977.

95-State-Of-The Art Report on finite Element Analysis of Reinforced Concrete. By the task Committee on Concrete and

Masonry Structures ASCE April 1981.

96-Wanhoo M. K. Cracking Analysis of Reinforced Concrete Plates. Journal of Structural Division Proceedings of the American Society of Civil Engineers, Vol. 101, No.ST1, Jan. 1975, PP201-215.

97- Lin C. S. and Scordelis A. C.; Nonlinear Analysis of Reinforced Concrete Shells of General Form. Journal Of the Structural Division, Proceedings of the American Society of Civil Engineers, Vol. 101, No.ST3, March 1975, PP 523-538.

98- Gupta A. K. and Akbar H; Cracking in Reinforced Concrete Analysis. Journal of Structural Engineering, Vol. 110 No 8. August, 1984, PP 1735-1746.

99- Buyukoztur, K O.; Nonlinear Analysis of Reinforced Concrete Structures. Computers and Structures, Vol. 7, 1977, PP149-159.

100- Tasuji M. E., Nilson A. H. and Slate F. O.; Biaxial Stress-Strain Relationships for Concrete. Magazine of Concrete Research, Vol.31, No. 109, Dec. 1979, PP217-224.

101- Liu T. C-Y, Nilson A. H. and Slate F. O.; Stress-Strain Response and Fracture of Concrete in Uniaxial and Biaxial Compression. Proceedings of the American Concrete Institute, May 1972, PP291-295.

102- Clark, L. A., Speirs, D. M.; Tension Stiffening in Reinforced Concrete Beams and Slabs Under Short Term Loads. Technical Report 42.521 Cement and Concrete Association London, 1978.

103- Cope. J; Material Modelling of real Reinforced Concrete Slabs. Proceedings of the International Conference on Computer Aided Analysis and Design of Concrete Structures. Part 1. (Edited by: Damjanic' F., Hinton E., Owen R. D. J., Bicanic N. and Simovic' V.) Pineridge Press Swansea, U. K.

104- Cedolin, L. and Deipoli S.; Finite Element Studies of Shear Critical Reinforced Concrete Beams. Journal. of Engineering Mechanics Division Proceedings, ASCE, Vol.103, No. EM3 June 1972 PP 359-410.

105- Mirza, S. A. and MacGregor, J. G.; Variability of Mechanical properties of Reinforcing Bars. J. Struc. Div., ASCE., Vol. 105 ST5, 1979 PP 921-937.

106- Zienkiewicz, O. C., Taylor, R. L. and Tool, J. M.; Reduced Integration In General Analysis of Plates and Shells, International Journal Numerical Methods Engineering., Vol. 3 1971 PP. 775-290.

107- Fried, I.; Finite Element Analysis of Incompressible Material by Residual Energy Balancing. Int. J. Solids & Structures, Vol. 10, 1974 PP993-1002.

108- Al-Manaseer, A. A.; A Nonlinear Finite Element Study of Reinforced Concrete Beams. Ph. D. Thesis, 1983 Glasgow University.

109- Cope, R. J., Rao, P. V., Clark, L. A.; Non-linear Design of Concrete Bridges Using Finite Elements. University of Waterloo Press, 1980 PP 379-408.

110- Clark, L. A.; Flexural Cracking in Slab Bridges,

Cement and Concrete Association Technical Report 42. 479, London 12PP, 1973.

111- Wood R. H. and Armer, G. S. T.; Theory of strip method for design of slabs, Proc. Inst. Civil Eng. Part 2 Vol. 41 1968 PP 285-311.

112- Kemp, K. O. A; Strip Method of Slab Design With Concentrated Loads or Supports, Struct. Eng. Vol. 49, 1971.

113-Jofriet, J. C.; Short Term Deflections of Concrete Flat Plates, Jou. of The Struct. Div., ASCE Vol. 99, 1973 167-82

114- Beeby A. W.; The Prediction of crack widths in hardened Concrete. Struct. 57 A 1979, PP 9-17 .

115- Beeby, A. W.; The Prediction and Control of Flexural Cracking Reinforced Concrete Members Cracking, Deflection and Ultimate Load of Concrete Slab Systems, ACI SP-30 American concrete Institute, Detroit, 1971, PP55.

116- Cope R. J.; Flexural Shear Failure of Reinforced Concrete Slab Brides. Proc. Instn Civ. Engrs, Part 2, 1985, 79, Sept., PP559-583.